AD783278

RADC-TR-74-104
Final Technical Report
May 1974

RADIATION FIELD COMPRESSION BY DISPERSIVE BROADBAND ANTENNAS

Braddock, Dunn, and McDonald, Incorporated

Approved for public release;
distribution unlimited.

Rome Air Development Center
Air Force Systems Command
Griffiss Air Force Base, New York

DDC
RECEIVED
AUG 13 1974
D

Reproduced by
NATIONAL TECHNICAL
INFORMATION SERVICE
U S Department of Commerce
Springfield VA 22151

387

UNCLASSIFIED

SECURITY CLASSIFICATION OF THIS PAGE (When Data Entered)

REPORT DOCUMENTATION PAGE		READ INSTRUCTIONS BEFORE COMPLETING FORM
1. REPORT NUMBER RADC-TR-74-104	2. GOVT ACCESSION NO.	3. RECIPIENT'S CATALOG NUMBER AD-783278
4. TITLE (and Subtitle) RADIATION FIELD COMPRESSION BY DISPERSIVE BROADBAND ANTENNAS		5. TYPE OF REPORT & PERIOD COVERED Final Report 17 Jan 73 - 17 Nov 73
		6. PERFORMING ORG. REPORT NUMBER BDM/A-186-73-TR
7. AUTHOR(s) C.M. Wiggins Dr. J.S. Yu		8. CONTRACT OR GRANT NUMBER(s) F30602-73-C-0110
9. PERFORMING ORGANIZATION NAME AND ADDRESS Braddock, Dunn, and McDonald, Incorporated 5301 Central Avenue N.E. Albuquerque, NM 87108		10. PROGRAM ELEMENT, PROJECT, TASK AREA & WORK UNIT NUMBERS PE 62702F JO 45060181
11. CONTROLLING OFFICE NAME AND ADDRESS Rome Air Development Center (OCTS) Griffiss Air Force Base, New York 13441		12. REPORT DATE May 1974
		13. NUMBER OF PAGES 176
14. MONITORING AGENCY NAME & ADDRESS(if different from Controlling Office) Same		15. SECURITY CLASS. (of this report) Unclassified
		15a. DECLASSIFICATION/DOWNGRADING SCHEDULE N/A

16. DISTRIBUTION STATEMENT (of this Report)

Approved for public release; distribution unlimited.

17. DISTRIBUTION STATEMENT (of the abstract entered in Block 20, if different from Report)

Same

PRICES SUBJECT TO CHANGE

18. SUPPLEMENTARY NOTES

RADC Project Engineer:
Paul Van Etten (OCTS)
AC 315 330-4437

Reproduced by
NATIONAL TECHNICAL
INFORMATION SERVICE
U S Department of Commerce
Springfield VA 22151

19. KEY WORDS (Continue on reverse side if necessary and identify by block number)

Antennas
Pulse Compression
Electromagnetic Fields

Details of illustrations in this document may be better studied on microfiche

20. ABSTRACT (Continue on reverse side if necessary and identify by block number)

This technique employs an antenna as a waveform compression device. A coded waveform from the transmitter will be spatially compressed during radiation. The primary consideration of this report is to determine the limitations of time-bandwidth products versus bandwidth both from a theoretical and practical viewpoint. It is shown that present-day antennas have time-bandwidth products exceeding 2000. It is shown that the electromagnetic fields can be increased over conventional spatial antenna concepts.

DD FORM 1 JAN 73 1473 EDITION OF 1 NOV 65 IS OBSOLETE

UNCLASSIFIED

SECURITY CLASSIFICATION OF THIS PAGE (When Data Entered)

RADIATION FIELD COMPRESSION BY DISPERSIVE BROADBAND ANTENNAS

C. M. Wiggins
Dr. J. S. Yu

Braddock, Dunn, and McDonald, Incorporated

Approved for public release;
distribution unlimited.

DDC
AUG 19 1974
D

FOREWORD

This Final Report was prepared by Braddock, Dunn and McDonald, Incorporated, 5301 Central Avenue N.E., Albuquerque, New Mexico, as part of a study under Contract F30602-73-C-0110, Job Order 45060181, between 17 January and 17 November 1973, for Rome Air Development Center, Griffiss Air Force Base, New York. Contractor's report number is BDM/A-186-73-TR. Mr. Paul Van Etten (OCTS) was the RADC Project Engineer. Mr. Van Etten provided some of the measured dispersion data analyzed in this report.

Major contributors to this study are Mr. C.M. Wiggins and Dr. J.S. Yu. Valuable assistance was provided in areas of computation by Mr. B.D. Boitnott and in antenna measurements by Mr. J.A. Myers. The report was reviewed and approved by Mr. D.T. Bailey, Director of BDM Applied Sciences, Western Operations.

This report has been reviewed by the RADC Information Office (OI) and is releasable to the National Technical Information Service.

This technical report has been reviewed and is approved.

APPROVED: Paul Van Etten

PAUL VAN ETTEN
Project Engineer

APPROVED: William T. Pope

WILLIAM T. POPE
Assistant Chief
Surveillance & Control Division

FOR THE COMMANDER: Carlo P. Crocetti

CARLO P. CROCETTI
Chief, Plans Office

DDC

ABSTRACT

This is a feasibility study program on the radiation compression concept. The objective is to produce intensified radiation fields using matched-filter techniques. The approach is to investigate candidate antennas that are capable of radiation-pulse compression. Since no antenna is known to possess linear FM characteristics, this program is focused on log-periodic (LP) antennas.

Radiations of an LP antenna driven by an "impulse" source have been measured. Transfer-function characteristics are obtained for six (6) LP antennas. They are all found to be represented by elemental radiation cells with certain percentage bandwidths.

Analytical models are developed for the LP antennas as consisting of fundamental radiation cells with $0.707\ \pi^2$ in directive gain. The mathematical models are verified by measurements to provide precise specifications on transmitter requirements that are necessary for applying matched-filter techniques.

Mechanisms of near-field compression are analyzed to establish the upper and lower bounds for compressed field strengths. It is concluded that no air breakdown would take place before the existing power-handling capabilities are exceeded. A 33-dB compression gain is analytically established under practical contraints for an LP antenna occupying $4.2\ m^3$ and being operated up to 15 GHz. General compression gain is found to increase with the electrical volume of an antenna.

The space-time compression of the radiation field has also been extended to the array of a number of broad band dispersive antennas. A coherent volumetric array is briefly studied and is recommended as a future effort to product the maximum radiation gain.

EVALUATION

This study is part of a continuing effort of the Signal Radiation and Processing Section of the Techniques Branch, Surveillance and Control Division at RADC. Historically, the dispersive properties of antennas have been measured under the In-House Project Number 45060186 entitled "Impulse Technology". The concept of enhancing the electromagnetic field intensity by temporal-spatial compression was developed under the RADC Laboratory Directors Fund Number 01707209 entitled "Electromagnetic Effects".

Considerable technical effort on this report has been expended on developing theory, concepts, measurements, etc. to analyze and predict the time-bandwidth products of present design broadband antennas. The results of the formulation, parametric studies, etc. provide design information valuable to the practical antenna designer to select an appropriate large time-bandwidth antenna system. In addition, a detailed study was performed on antenna breakdown and shows the breakdown problem is eased by employing temporal-spatial compression.

Most of the study effort was directed toward the temporal-spatial distribution on the antenna boresight. It is anticipated that future work will expand to off-boresight radiated fields hopefully giving rise to some exciting discoveries in temporal-spatial antenna patterns. This work is in support of TPO-5, "EM Generation and Control".

Paul VanEtten
Project Engineer/OCTS

TABLE OF CONTENTS

Section		Page
I	INTRODUCTION AND SUMMARY	I-1
	1. PROGRAM OVERVIEW	I-1
	2. STUDY OBJECTIVE	I-3
	3. OUTLINE OF APPROACH	I-4
	4. SIGNIFICANT RESULTS	I-4
	5. SUMMARY OF REPORT	I-6
II	FUNDAMENTALS OF FIELD COMPRESSION	II-1
	1. INTRODUCTION	II-1
	2. RADIATION-FIELD COMPRESSION ANTENNAS	II-1
	3. FREQUENCY-INDEPENDENT ANTENNAS	II-4
	4. LINEAR AND NONLINEAR FILTERS	II-6
	5. EXAMPLE ON FIELD-COMPRESSION RADIATION	II-7
III	VERIFICATION OF FIELD DISPERSION AND COMPRESSION BY MEASUREMENTS	III-1
	1. INTRODUCTION	III-1
	2. TRANSFER FUNCTION MEASUREMENT CONCEPT	III-1
	3. MEASUREMENT SYSTEM	III-2
	4. MEASURED RESULTS: TRANSFER FUNCTIONS AND BT PRODUCTS	III-3
	a. Transfer Function of Cavity-Backed Spiral Antenna ASN-1232A	III-7
	b. Transfer Function of Cavity-Backed Spiral Antenna ASN-117AA	III-9
	c. Transfer Function of Cavity-Backed Spiral Antenna ASN-116A	III-9
	d. Transfer Function of Crossed Planar Log-Periodic Dipole Antenna APX-254A	III-12
	e. Transfer Function of Planar Log-Periodic Dipole Array Antenna APN-995B	III-12
	f. Transfer Function of Pyramidal Log-Periodic Antenna APN-502A	III-15
	5. SUMMARY OF MEASURED RESULTS	III-15
	6. REQUIREMENTS FOR FIELD COMPRESSION	III-18
IV	FIELD COMPRESSION ANTENNA MODEL BY ELEMENTAL REGION FORMULATION	IV-1
	1. INTRODUCTION	IV-1
	2. PHYSICAL DESCRIPTION OF AN ACTIVE REGION OF A LOG-PERIODIC ANTENNA	IV-1
	3. ELEMENTAL MODEL FOR LOG-PERIODIC ANTENNAS	IV-6
	4. ELEMENTAL MODEL FOR QUADRATIC-PHASED ANTENNAS	IV-13

TABLE OF CONTENTS (Continued)

Section		Page
V	PRACTICAL AND THEORETICAL MAXIMUM BANDWIDTH-TIME PRODUCTS OF LOG-PERIODIC ANTENNAS	V-1
	1. INTRODUCTION	V-1
	2. MAXIMUM BT PRODUCTS OF PRACTICAL ANTENNAS	V-1
	3. THEORETICAL BT PRODUCT LIMITS	V-6
	4. LIMIT OF BT PRODUCT - ANOTHER VIEW	V-13
VI	NEAR FIELD COMPRESSION AND POWER HANDLING CAPACITY OF ANTENNAS	VI-1
	1. INTRODUCTORY COMMENTS	VI-1
	2. PEAK AMPLITUDE VARIATION IN THE NEAR FIELD	VI-2
	3. ALLOWABLE PEAK COMPRESSED FIELD AMPLITUDE	VI-4
	4. ESTIMATES OF ANTENNA CURRENTS	VI-11
	5. POWER LIMIT AND FIELD LIMIT	VI-12
VII	GAIN OF FIELD-COMPRESSION RADIATION	VII-1
	1. RADIATION CELL	VII-1
	2. SPATIAL ANGLE-COMPRESSION GAIN	VII-3
	3. TEMPORAL WIDTH-COMPRESSION GAIN	VII-4
	4. SPACE-TIME COMPRESSION GAIN	VII-9
VIII	CONCLUSIONS	VIII-1
	1. ANTENNA DISPERSION AND COMPRESSION	VIII-1
	2. TRANSFER FUNCTIONS AND TRANSMITTER DESIGNS	VIII-5
	3. MAXIMUM POWER-DENSITY GAIN OF A DISPERSIVE ANTENNA	VIII-5
	4. GAIN OF AN ARRAYED DISPERSION ANTENNA	VIII-6
	5. ELECTRIC FIELD INTENSITY AND POWER INPUT	VIII-7
	6. NEAR-ZONE FIELD AND POWER-HANDLING CAPACITY	VIII-7
IX	RECOMMENDATIONS	IX-1
	1. LOG-PERIODIC ANTENNAS AS RADIATION-FIELD COMPRESSORS	IX-1
	2. INTENSIVE R&D EFFORTS ON RETARDATION-RADIATION CELLS	IX-2
	3. EXPONENTIAL DISTRIBUTION FOR TRANSMITTER SPECTRUM	IX-4
	4. VOLUMETRIC ARRAY OF DISPERSIVE ANTENNAS	IX-4

TABLE OF CONTENTS (Concluded)

Section		Page
	5. EXPERIMENTAL VERIFICATION OF FIELD COMPRESSION USING CONJUGATE-MATCHED LOW POWER SOURCE	IX-6
	6. APPLICATIONS IN ADVANCED RADARS AND COMMUNICATION	IX-7
	7. FEASIBILITY OF BUILDING A FIELD COMPRESSION SYSTEM HAVING A BT PRODUCT OF 2000	IX-7
X	REFERENCES	X-1
APPENDIX A	FIELD COMPRESSION BY ANTENNAS	A-1
APPENDIX B	DISPERSED PULSE MEASUREMENTS	B-1
APPENDIX C	TRANSFER FUNCTION AND COMPRESSED PULSE OF DISPERSIVE ANTENNAS	C-1
APPENDIX D	ANALYTICAL FORMULATION OF RADIATION ELEMENTS	D-1
APPENDIX E	WAVE PROPAGATION ALONG PERIODICALLY LOADED STRUCTURES	E-1
APPENDIX F	COMPARISON OF KNOWN FREQUENCY INDEPENDENT ANTENNAS	F-1
APPENDIX G	NUMERICAL AND ASYMPTOTIC EVALUATION OF BT PRODUCTS	G-1
APPENDIX H	MAXIMUM BANDWIDTH-TIME PRODUCTS OF FREQUENCY INDEPENDENT ANTENNAS	H-1
APPENDIX I	A NEAR-ZONE EVALUATION PROCEDURE AND SOME OF ITS RESULTS	I-1
APPENDIX J	AIR-BREAKDOWN BY COMPRESSED PULSES AND BREAKDOWN LAG TIME	J-1

LIST OF ILLUSTRATIONS

Figure		Page
I-1	Radiation-Field Intensification by Space-Time Compression	I-2
II-1	Time-Domain Concept of Field Compression	II-3
III-1 (a)	Experimental Setup Used to Measure the Transfer Function for the ASN-117AA Cavity-Backed Serial Antenna	III-4
III-1 (b)	Experimental Setup Used to Measure the Transfer Function for the ASN-117AA Cavity-Backed Serial Antenna	III-5
III-2	Cavity-Backed Spiral ASN-1232A; (a) Dispersed Pulse; (b) Transfer Function Amplitude; (c) Transfer Function Phase	III-8
III-3	Cavity-Backed Spiral ASN-117AA; (a) Dispersed Pulse; (b) Transfer Function Amplitude; (c) Transfer Function Phase	III-10
III-4	Cavity-Backed Spiral ASN-116A; (a) Dispersed Pulse; (b) Transfer Function Amplitude; (c) Transfer Function Phase	III-11
III-5	Crossed Planar Log-Periodic APX-254A; (a) Dispersed Pulse; (b) Transfer Function Amplitude; (c) Transfer Function Phase	III-13
III-6	Coplanar Log-Periodic APN-995B; (a) Dispersed Pulse; (b) Transfer Function Amplitude; (c) Transfer Function Phase	III-14
III-7	Pyramidal Log-Periodic APN-502A; (a) Dispersed Pulse; (b) Transfer Function Amplitude; (c) Transfer Function Phase	III-16
IV-1	Wave Propagation Characteristics in the $k_o d$-βd Plane	IV-3
IV-2	Dispersion Curve of the Unmodulated Structure	IV-5
IV-3	Frequency Allocation for Radiation Cells of a Log-Periodic Antenna	IV-8
IV-4	Phase Angles Obtained from Measurements on Dispersed Radiations	IV-12
V-1	Design Parameters of a Conical Spiral Antenna Having Maximum Practical BT Product for an Occupied Volume of 4 Cubic Meters: BT = 2537	V-3

LIST OF ILLUSTRATIONS (Continued)

Figure		Page
V-2	Design Parameters of a Log-Periodic Dipole Array Antenna Having Maximum Practical BT Product for an Occupied Volume of 4 Cubic Meters: BT = 2126	V-4
V-3	Design Parameters of a Cavity-Backed Spiral Antenna Having Maximum Practical BT Product for an Occupied Volume of 4.2 Cubic Meters: BD = 2453	V-5
V-4	Parametric Curves for BT Versus θ_o and BT Versus α for A_N = .00284 Meters and A_1 = 1° Meter for a Conical Spiral Antenna	V-8
V-5	Bandwidth-Time Product as a Function of Antenna Volume for Various Radiation Cell Densities.	V-10
VI-1	Pulse Compressions in the Near-Zone for Log-Periodic Array with Coincident Phase Centers	VI-3
VI-2	Smoothed Spectral Distribution of Theoretical Model Approximating a Cavity-Backed Spiral Antenna Which Compresses Pulses at r = 1.5 cm, 3.5 cm, and 100 cm	VI-5
VI-3	Near-Field Space-Time Pulse Compression for an Antenna Model Possessing a Transverse Time Delay Characteristic	VI-6
VI-4	Compressed Pulse Peaks as Functions of Radiation Distance r(cm)	VI-7
VI-5	When Field Strengths Exceed the Dielectric Strength of Air at a Given Pressure, a Minimum Time is Required Before Breakdown Occurs	VI-9
VII-1	Bandwidth-Time (BT) Products of Dispersive Antennas in Terms of Number of Radiation Cells	VII-8
VIII-1	Transfer Function and Associated Characteristics of General Log-Periodic Antennas	VIII-3
IX-1	Recommended Analytic Description for Radiation Field Compression by Use of Log-Periodic Antennas	IX-3

LIST OF ILLUSTRATIONS (Continued)

Figure		Page
IX-2	Recommended Source Functions for Conjugate-Matching Existing LP Antennas	IX-5
B-1	Experimental Apparatus	B-3
B-2	Measurement Instrumentation	B-6
B-3	Circuit Configurations for TDR Measurements	B-9
B-4	TDR of Circuit with Open Feed	B-11
B-5	Feed Terminated Into 50 Ohms	B-11
B-6	Feed Terminated Into Stub Monopole	B-13
B-7(a)	TDR of System Terminated with Cavity-Backed Spiral ASN 117AA S/N 107	B-14
B-7(b)	Expanded View of Antenna Region	B-14
B-8(a)	TDR of System Terminated Into Cavity-Backed Spiral ASN 117AA SN 108	B-16
B-8(b)	Expanded View of Antenna Region	B-16
B-9	IKOR Pulse Generator Characteristics	B-17
B-10	Stub-Monopole Probe	B-19
B-11	Stub-Monopole Probe Response. (a) Measurement Configuration; (b) Upper Trace is the Input Pulse, Lower Trace is the Receive Probe Response - the Derivative of the Input Pulse	B-20
B-12	Long Wire Over Ground Plane Response. (a) Measurement Configuration; (b) The Input Pulse is Shown in the Top Trace, the Yearly Replica Response of the Receive Probe in the Lower Trace. Comparison Shows the Latter to Lack Some Low Frequency Content Due to the Transmit Probe Center Conductor Length of Only 60 cm	B-21
B-13	Response of a 2 cm Monopole to a Monopole Over Ground Plane. (a) Measurement Configuration; (b) Upper Trace Shows Input Pulse; Lower Trace is the Replica Response of the Receive Probe to a Second Derivative Transmitted Pulse	B-23
B-14	Response of a 2 cm Monopole Over Ground Plant to 2 cm Monopole Antenna Showing Reciprocity. (a) Measurement Configuration; (b) Upset Trace is the Input Pulse; the Lower Trace is the Derivative Response of the Receive Probe. Transmit Stub-Monopole Transmits the Derivative of the Input Pulse	B-24

LIST OF ILLUSTRATIONS (Continued)

Figure		Page
B-15	A View of the Arrangement for One-Way Dispersion Measurements. Antenna-Probe Separation is 1 Meter; Height Above Ground (to Center of Spiral) is 2.6 Meters. (Poor Inside Light Necessitated Outdoor Photograph)	B-26
B-16	Antenna Dispersion Results for (a) Cavity-Backed Spiral (ASN 17AA, S/N107) and (b) Cavity-Backed Spiral (ASN 17AA, S/N108). The Upper Trace in Each Photograph Shows the Input Pulse at -60 dB. The Lower Trace is the Transient Response (Dispersed Pulse) of the Antenna When Measured by a 2 cm Stub-Monopole Probe as Shown in Figure B-15	B-27
B-17	Transmit Antenna APN-995B and Its Dispersion Pulse Received by a Stub-Monopole Sensor	B-29
B-18	Transmit Antenna ASN-1232 and Its Dispersion Pulse Received by a Stub-Monopole Sensor	B-30
B-19	Dispersion Pulse at the Receive-Antenna Terminal When the Transmit Antenna is Excited by a "Unit-Step" Pulse (Two Identical Antennas are Used for Both Transmit and Receive)	B-31
B-20	Transmit Antenna APX-254 and Its Dispersion Pulse Received by a Stub-Monopole Sensor	B-32
C-1	Three 100-ps Pulses with Sidelobes More Than 40 dB Below Peak Value	C-3
C-2	Relative Spectral Distributions of Three 100-ps Pulses with Temporal Sidelobes More Than 40 dB Below Peak	C-4
C-3	"Impulse" Used to Drive Antenna ASN-1232A	C-5
C-4	Spectral Amplitude of the "Impulse" Used to Drive Antenna ASN-1232A	C-6
C-5	Phase Angle Associated with the Spectrum of Figure C-4	C-7
C-6	The Dispersed Radiation $f_d(t)$ of ASN-1232A	C-8
C-7	Spectral Density Amplitude of $F_d(t)$ for Figure C-6	C-10
C-8	Phase Angle $\phi_d(f)$ Associated with Figure C-7	C-11
C-9	Spectral Amplitude of $F_a(f)$ for ASN-1232A Transfer Function	C-13

LIST OF ILLUSTRATIONS (Continued)

Figure		Page
C-10	Phase Angle of $F_a(f)$ for ASN-1232A Transfer Function	C-14
C-11	Impulse Used to Drive Antenna ASN-117AA	C-15
C-12	Spectral Amplitude of the "Impulse" Used to Drive Antenna ASN-117AA	C-16
C-13	Phase Angle Associated with the Spectrum of Figure C-12	C-17
C-14	The Dispersed Radiation $f_d(t)$ of ASN-117AA	C-18
C-15	Spectral Density Amplitude of $F_d(f)$ for Figure C-14	C-19
C-16	Phase Angle $\phi_d(t)$ Associated with Figure C-15	C-20
C-17	Spectral Amplitude of $F_a(t)$ for ASN-117AA Transfer Function	C-21
C-18	Phase Angle of $F_a(t)$ for ASN-117AA Transfer Function	C-22
C-19	Output of a Cavity-Backed Spiral Antenna AN-116A About 1.5 M Away from Another Identical Antenna Driven by Step Pulse	C-24
C-20	Relative Spectral Distribution of the Response in Figure C-19	C-25
C-21	Phas Angle Corresponding the "Unit Step Pulse" Response in Figure C-20	C-26
C-22	Relative Phase Angles of the ASN-116A Cavity-Backed Spiral Antenna	C-27
C-23	Relative Spectral Distribution Estimated for the Reception of a Cavity-Backed Spiral Antenna ASN-116A	C-28
C-24	Compressed Radiation Pulse of an Assumed Amplitude Distribution in Fig. C-23 (Under Matched-Filter Conditions)	C-29
C-25	"Impulse" Used to Drive Antenna APX-254A	C-30
C-26	Spectral Amplitude of the "Impulse" Used to Drive Antenna APX-254A	C-31
C-27	Phase Angle Associated with the Spectrum of Figure C-26	C-32
C-28	The Dispersed Radiation $f_d(t)$ of APX-254A	C-34

LIST OF ILLUSTRATIONS (Continued)

Figure		Page
C-29	Spectral Density Amplitude of $F_d(f)$ for Figure C-28	C-35
C-30	Phase Angle $\phi_d(t)$ Associated with Figure C-29	C-36
C-31	Spectral Amplitude of $F_a(t)$ for APX-254A Transfer Function	C-37
C-32	Phase Angle of $F_a(f)$ for APX-254A Transfer Function	C-38
C-33	"Doublet" Used to Drive Antenna APN-995B	C-39
C-34	Spectral Amplitude of the "Doublet" Used to Drive Antenna APN-995B	C-40
C-35	Phase Angle Associated with the Spectrum of Figure C-34	C-41
C-36	The Dispersed Radiation $F_d(t)$ of APN-995B	C-42
C-37	Spectral Density Amplitude of $F_a(t)$ for Figure C-36	C-43
C-38	Phase Angle $\phi_a(f)$ Associated with Figure C-37	C-44
C-39	Spectral Amplitude of $F_a(f)$ for APN-995B Transfer Function	C-45
C-40	Phase Angle of $F_a(t)$ for APN-995B Transfer Function	C-46
C-41	Dispersion Pulse of APN-99B if it Were Driven by a Perfect Impulse	C-47
C-42	Output of a 2.54 cm Monopole Sensing the Radiation of APN-502A Log-Periodic Antenna Driven by an "Impulse"	C-49
C-43	Relative Spectral Distribution of the Response in Figure C-42	C-50
C-44	Phase Angle Corresponding to the Relative Amplitude in Figure C-43	C-51
C-45	Relative Phase Angle Obtained from Figure C-44	C-52
C-46	Compressed Radiation Pulse Under Matched-Filter Conditions for the Characteristics Shown in Figures C-43 and C-44	C-53
C-47	Input Pulse of a Transmitting Test Probe with 2 cm Center-Conductor Stub	C-54

LIST OF ILLUSTRATIONS (Continued)

Figure		Page
C-48	Spectral Amplitude for the "Impulse" of Figure C-47	C-55
C-49	Phase Angle Associated with the Spectral Amplitude in Figure C-48	C-56
C-50	Received Pulse of an Identical Probe Placed 1 m from the Transmitting Probe Driven by the Pulse in Figure C-47	C-57
C-51	Spectral Amplitude of Figure C-50	C-58
C-52	Phase Angle Associated with the Spectral Amplitude in Figure C-51	C-59
C-53	Spectral Amplitude of $j2\pi f\ H^2(f)$ with H(f) as the Probe's Receiving Function	C-61
C-54	Phase Angle Associated with the Spectral Amplitude of Figure C-53	C-62
D-1	Log-Periodic Phase Angle Plotted Against Linear Frequency	D-18
D-2	Spectral Amplitude Assigned to a Log-Periodic Antenna	D-19
D-3	Phase Angle Assigned Corresponding to the Spectrum in Figure D-3	D-20
D-4	Dispersed Pulse Resulting From Complex Distribution of Figures D-3 and D-4	D-21
D-5	Radiated Pulse of the First Region Assigned to Figures D-2 and D-3	D-22
D-6	Radiated Pulse of the Second Region Assigned to Figures D-2 and D-3	D-23
D-7	Radiated Pulse of the Third Region Assigned to Figures D-2 and D-3	D-24
D-8	Radiated Pulse of the Fourth Region Assigned to Figures D-2 and D-3	D-25
D-9	Radiated Pulse of the Fifth Region Assigned to Figures D-2 and D-3	D-26
D-10	Radiated Pulse of the Sixth Region Assigned to Figures D-2 and D-3	D-27
D-11	Radiated Pulse of the Seventh Region Assigned to Figures D-2 and D-3	D-28
D-12	Radiated Pulse of the Eighth Region Assigned to Figures D-2 and D-3	D-29

LIST OF ILLUSTRATIONS (Continued)

Figure		Page
D-13	Radiated Pulse of the Ninth Region Assigned to Figures D-2 and D-3	D-30
D-14	Radiated Pulse of the Tenth Region Assigned to Figures D-2 and D-3	D-31
D-15	Radiated Pulse of the Eleventh Region Assigned to Figures D-2 and D-3	D-32
D-16	Radiated Pulse of the Twelfth Region Assigned to Figures D-2 and D-3	D-33
D-17	Radiated Pulse of the Thirteenth Region Assigned to Figures D-2 and D-3	D-34
E-1	The k_o-β Diagram Corresponding to a Uniform Lossless Dielectric of Relative Permittivity $\varepsilon_r > 1$ (i.e., Basically a Slow-Wave Structure)	E-6
E-2	The $k_o d$ - βd Diagram for a Periodic Structure of Period d for Small Loading (i.e., Uncoupled Modes. The Grid is Obtained by Plotting $k_o d = \pm \frac{1}{\varepsilon} (\beta_n d - 2\pi n)$ for n = 0, ±1, ±2,..., $\varepsilon_r > 1$ and Therefore Corresponds to a Slow-Wave Structure	E-10
E-3	The Two Types of Mode Coupling: (a) Codirectional Coupling Occurs When Tangents at Point of Intersection Have Same Signs; (b) Contradirectional Coupling Occurs When Tangents Have Opposite Signs	E-11
E-4	Wave Propagation Characteristics in the $k_o d$ - βd Plane	E-14
E-5	Brillouin ($k_o d$ - βd) Diagram for a Basically Slow-Wave ($\varepsilon_r > \varepsilon_o$), Periodically Loaded Structure Which Also Supports Fast Waves. When the Phase of the Slow Fundamental (M = o) Wave Reaches Point 2, it Becomes Complex; the n = -1 Harmonic Simultaneously Grows Into a Dominant Fast Wave	E-15
F-1	Equiangular (or Logarithmic) Spiral Antenna Geometry	F-3
F-2	Conical Log-Spiral Antenna Geometry	F-7
G-1	Parametric Curves for BT Versus θ_o and BT Versus α for A_N = .00284 Meter and A_1 = 1 Meter for a Conical Spiral Antenna	G-3
H-1	Log-Periodic Dipole Array Definition	H-6

LIST OF ILLUSTRATIONS (Continued)

Figure		Page
I-1	Spectral Density $E(r, f, r_o, p, k) \times 1.2$ with r = 100 m, and p = 1/2	I-5
I-2	Compressed Pulse of Spectrum in Figure I-1	I-6
I-3	Spectral Density $E(r, f, r_o, p, k) \times 1.2$ with r = 100 m, and p = 1	I-9
I-4	Compressed Pulse of Spectrum in Figure I-3	I-10
I-5	Spectral Density $E(r, f, r_o, p, k) \times 1.2$ with r = 100 m, and p = 1/4	I-11
I-6	Compressed Pulse of Spectrum in Figure I-5	I-12
I-7	Spectral Density $E(r, f, r_o, p, k) \times 1.2$ with r = 1 m, and p = 1/2	I-13
I-8	Compressed Pulse of Spectrum in Figure I-7	I-14
I-9	Spectral Density $E(r, f, r_o, p, k) \times 1.2$ with r = 1 m, and p = 1	I-15
I-10	Compressed Pulse of Spectrum in Figure I-9	I-16
I-11	Spectral Density $E(r, f, r_o, p, k) \times 1.2$ with r = 1 m, and p = 1/4	I-17
I-12	Compressed Pulse of Spectrum in Figure I-11	I-18
I-13	Spectral Density $E(r, f, r_o, p, k) \times 1.2$ with r = 0.1 m, and p = 1.2	I-19
I-14	Compressed Pulse of Spectrum in Figure I-13	I-20
I-15	Spectral Density $E(r, f, r_o, p, k) \times 1.2$ with r = 0.1 m, and p = 1	I-21
I-16	Compressed Pulse of Spectrum in Figure I-15	I-22
I-17	Spectral Density $E(r, f, r_o, p, k) \times 1.2$ with r = 0.1 m, and p = 1/4	I-23
I-18	Compressed Pulse of Spectrum in Figure I-17	I-24
I-19	Spectral Density $E(r, f, r_o, p, k) \times 1.2$ with r = 0.05 m, and p = 1/2	I-25
I-20	Compressed Pulse of Spectrum in Figure I-19	I-26
I-21	Spectral Density $E(r, f, r_o, p, k) \times 1.2$ with r = 0.05 m, and p = 1	I-27
I-22	Compressed Pulse of Spectrum in Figure I-21	I-28
I-23	Spectral Density $E(r, f, r_o, p, k) \times 1.2$ with r = 0.05 m, and p = 1/4	I-29
I-24	Compressed Pulse of Spectrum in Figure I-23	I-30
I-25	Spectral Density $E(r, f, r_o, p, k) \times 1.2$ with r = 0.02 m, and p = 1/2	I-31

LIST OF ILLUSTRATIONS (Continued)

Figure		Page
I-26	Compressed Pulse of Spectrum in Figure I-25	I-32
I-27	Spectral Density $E(r, f, r_o, p, k) \times 1.2$ with r - 0.02 m, and p = 1	I-33
I-28	Compressed Pulse of Spectrum in Figure I-27	I-34
I-29	Spectral Density $E(r, f, r_o, p, k) \times 1.2$ with r = 0.02 m, and p = 1/4	I-35
I-30	Compressed Pulse of Spectrum in Figure I-29	I-36
I-31	Spectral Density $E(r, f, r_o, p, k) \times 1.2$ with r = 0.01 m, and p = 1/2	I-37
I-32	Compressed Pulse of Spectrum in Figure I-31	I-38
I-33	Spectral Density $E(r, f, r_o, p, k) \times 1.2$ with r = 0.01 m, and p = 1	I-39
I-34	Compressed Pulse of Spectrum in Figure I-33	I-40
I-35	Spectral Density $E(r, f, r_o, p, k) \times 1.2$ with r = 0.01 m, and p = 1.4	I-41
I-36	Compressed Pulse of Spectrum in Figure I-35	I-42
I-37	Pulse Compressions in the Near-Zone	I-48
I-38	Pulse Compression in the Far-Zone ($\gamma > 0.75$ m)	I-49
I-39	Balanced Electric and Magnetic Currents for Axially Symmetric Cardioid Radiation Around the Z-Axis	I-50
I-40	Pure Dipole-Modes Spectral Density as a Function of Distance in Wavelength λ	I-51
I-41	Spectral Amplitudes of Equation I-9	I-52
I-42	Linear Log-Periodic Dipole Array Model	I-53
I-43	Linearly Polarized Planar Array with Broadside Radiation	I-54
I-44	Coordinates of Field Point P and the nth Element	I-55
I-45	Smoothed Spectral Distribution of Theoretical Model Approximating a Cavity-Backed Spiral Antenna Which Compresses Pulses at r = 1.5 cm, 3.5 cm and 100 cm	I-56
I-46	Compressed Pulse at 1.5 Centimeters from Antenna Aperture on Boresight	I-57
I-47	Compressed Pulse at 3.0 Centimeters from Aperture Plane on Boresight	I-58
I-48	Compressed Pulse at 3.5 Centimeters from Aperture Plane on Boresight	I-59

LIST OF ILLUSTRATIONS (Concluded)

Figure		Page
I-49	Compressed Pulse at 3.75 Centimeters from Aperture Plane on Boresight	I-60
I-50	Compressed Pulse at 4.0 Centimeters from Aperture Plane on Boresight	I-61
I-51	Compressed Pulse at 5.5 Centimeters from Aperture Plane on Boresight	I-62
I-52	Compressed Pulse at 7.5 Centimeters from Aperture Plane on Boresight	I-63
I-53	Compressed Pulse at 1.0 Meter from Aperture Plane on Boresight	I-64
I-54	Compressed Pulse at 100 Meters from Aperture Plane on Boresight	I-65
I-55	Near-Field Space-Time Pulse Compression for an Antenna Model Possessing a Transverse Time Delay Characteristic	I-66
I-56	An Advantage of Pulse Compression Antennas Possessing Transverse Time Delay Characteristics, Such as the Cavity-Backed Spiral, is that Peak Pulse Amplitude Occurs at Distances Away from the Aperture Plane	I-67
I-57	Compressed Pulse Peaks as Functions of Radiation Distance r(cm)	I-68
J-1	When Field Strengths Exceed the Dielectric Strength of Air at a Given Pressure, a Minimum Time is Required Before Breakdown Occurs	J-3
J-2	Expansion of Figure J-1 Showing Breakdown Lag Times for Field Strengths in the High Megavolt/Meter Range	J-4

LIST OF TABLES

Tables		Page
III-1	Some Specifications for the Antennas Tested	III-6
III-2	Comparison of Measured and Predicted BT Products	III-17
IV-1	Analytically Obtained BT Products Compared with those Observed from Measured Data	IV-10
V-1	Bandwidth-Time Products for Conical Spiral Antennas of Various Lengths Having Fixed Truncated Cone Diameters	V-11
VI-1	Maximum Allowed Compressed Pulse Durations for Various Field Strengths	VI-10
VI-2	Peak Compressed Fields and Average Powers for the First Radiation Cell of Two Log-Periodic Antenna Models Operated with two Bandwidths	VI-13
VIII-1	Comparison of Field Compression Antennas Designed to Provide Maximum BT Products When Normalized by a Common Set of Constraints. The BT Product Per Unit Volume is Approximately the Same for all Log-Periodic Antennas	VIII-4
D-1	List of Radiative Regions	D-5
I-1	Parameters Used in Near-Zone Compressed Pulses of Broadside Array	I-46
J-1	Maximum Allowed Compressed Pulse Durations for Various Field Strengths	J-6

SECTION I

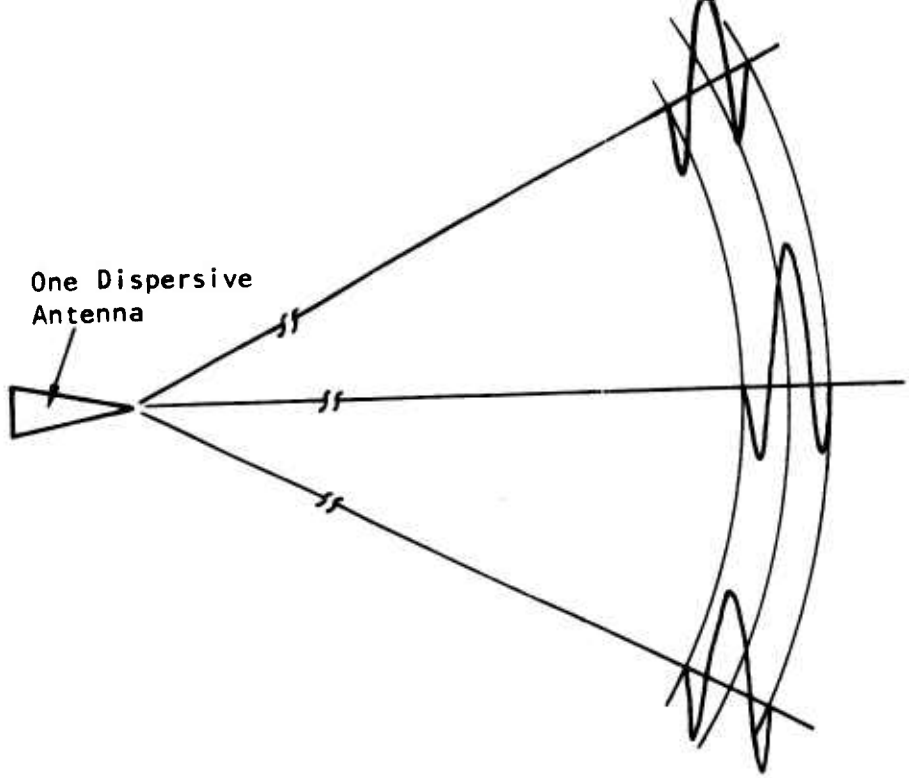
INTRODUCTION AND SUMMARY

Since the discovery of electromagnetic radiation, much effort has been directed toward intensifying the radiation field by designing antennas of various sizes and configurations. The program reported here may be considered as the latest attempt in space-time field compression that will give rise to the maximum compression gain from a given radiation volume.

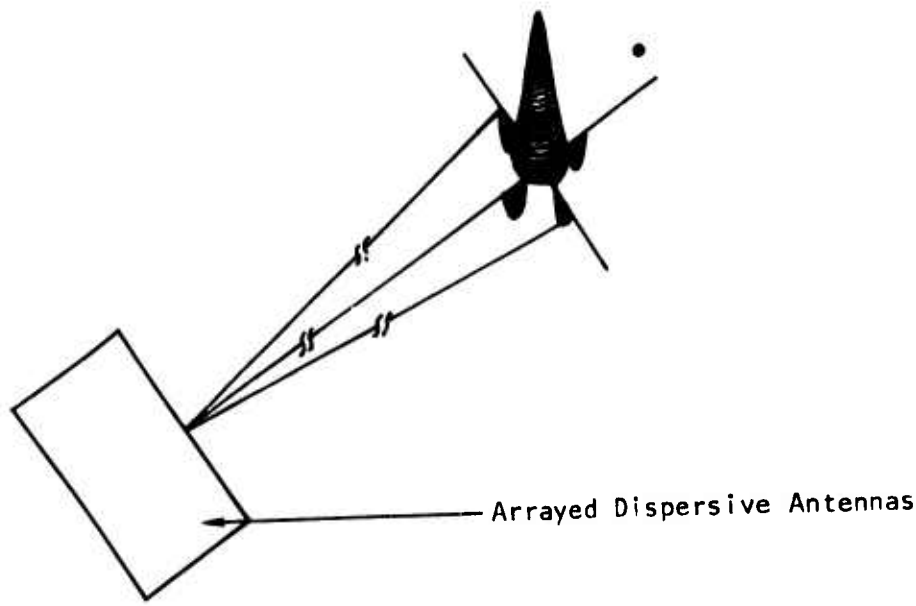
1. PROGRAM OVERVIEW

Field intensification by a large radiation aperture under CW operation is well known. It serves to compress the radiation field in a spatial angle (i.e., the radiated maximum power density increases in inverse proportion to the radiation beamwidth). Analogous to this type of spatial compression is the temporal compression[1-7] that employs conjugate-matched filters to compress a long-duration pulse of low power into a short-duration pulse of high power.

This program has introduced the concept of a radiation cell which constitutes the smallest electrical volume for practical and effective radiation[8-16]. This radiation cell concept can be readily identified with operational log-periodic antennas[17-39]. When these antennas are treated as an array of radiation cells and are conjugate-fed by driving sources, the radiated field compression would take place in a manner sketched in the upper half of Figure I-1. A single dispersive antenna has a relatively large beam angle with moderate directive gain in spatial field compression.



(a) Temporal Compression by An Array of Retarded Radiation Cells



(b) Space-Time Compression by An Array of Dispersive Antennas

Figure I-1. Radiation-Field Intensification by Space-Time Compression

If a number of dispersive antennas are arrayed, the ultimate space-time compression would take place as shown in the lower half of Figure 1-1.

This program can in essence be described as a study effort to quantify the concept of space-time field compression. Both empirical results and analytical developments are combined in this program to arrive at practical design considerations.

2. STUDY OBJECTIVE

The original study objectives as well as the subsequently derived objectives are listed below:

(1) Determine theoretical and practical limits of bandwidth-time (BT) products of dispersive antennas.

(2) Establish transfer-function characteristics through measurements and thus verify the concept of radiation dispersion and compression.

(3) Develop analytical models for dispersive radiations to facilitate specifications of transmitter waveforms.

(4) Quantify ultimate gain in radiation-field compression. (This is, in effect, to evaluate relative gain over the so-called conventional antennas.)

(5) Identify possible limitations on space-time compression applications.

These objectives are considered to have been accomplished through the following technical approach.

3. OUTLINE OF APPROACH

The approach is outlined as follows:

(1) Analyze dispersion characteristics of existing antennas that are broadband in the sense of being frequency independent and are long-duration in the sense of having large retardation in successive radiation elements.

(2) Define elemental radiation cells representing the smallest electrical volume for practical and efficient radiation.

(3) Obtain limits of bandwidth-time (BT) product in terms of geometrical parameters used in antenna designs.

(4) Obtain limits of BT product in terms of electrical parameters used in describing antenna performance.

(5) Formulate total compression gain resulting from a combined space-time field compression.

(6) Evaluate numerically the detailed near-field structures for possible air breakdown [40,41] as a function of pulse intensity and duration.

This program has completed the above technical investigations and has produced the significant results discussed below.

4. SIGNIFICANT RESULTS

(1) "Antennas" with quadratic-phased dispersion or linear FM would have smaller BT products than the log-periodic (LP) phased antennas.

(2) LP antennas have been measured and analyzed to verify the concepts of radiation-field dispersion and compression.

(3) An important concept of radiation cells has been defined for retarded radiations.

(4) Theoretical and practical BT products have been obtained in terms of geometrical parameters used in antenna designs. A practical limit, for example, BT = 2200 for a radiation volume of 4 cubic meters.

(5) Limit of ultimate compression gain has been obtained in terms of electrical parameters used in antenna performance specifications. (The BT product is proportional to total number of radiation cells in a given volume).

(6) Transfer functions of dispersive antennas have been obtained for analytical description of radiation mechanisms.

(7) Analytical models for conjugate-matched driving source have been established for transmitter design specifications.

(8) Near-field compression have been formulated to obtain the upper and lower bounds for compressed peak values.

(9) Conclusions have been made that possible air-breakdown in near-field compression would not take place before the power-handling capacities of antenna structures would be exceeded.

(10) Formulas have been obtained for absolute radiation-field compression gain (relative gain over "conventional" antenna is implicitly given).

5. SUMMARY OF REPORT

This report has been organized by placing most of the technical details in the appendices. Only the following fundamental and significant materials are given in the sections:

(1) Section II gives fundamentals of temporal compression.

(2) Section III describes measurements and analyses of dispersive radiation.

(3) Section IV discusses definition of radiation cells and retardations.

(4) Section V estimates BT-product limits in terms of geometrical parameters.

(5) Section VI investigates near-field compression mechanisms and implications.

(6) Section VII summarizes formulas for space-time compression gain.

(7) Section VIII gives concluding remarks for significant accomplishments.

(8) Section IX lists recommendations for future investigations.

(9) Section X gives reference materials relating to radiation-field compression.

SECTION II

FUNDAMENTALS OF FIELD COMPRESSION

1. INTRODUCTION

Fundamental concepts of field-compression radiation can be discussed by treating antenna transfer functions as that required of conjugate-matched filters. Simple formulations are presented here to lead to the field compression-gain equal to the product of antenna bandwidth (B) and the driving source duration (T). The BT product is well known as the power gain of a conjugate-matched filter operation and is used here directly as the temperal-compression power gain of dispersive antennas used as conjugate-matched filters.

Dispersive antennas may be arbitrarily specified, either having a quadratic phase or a log-periodic phase, or any others. Presently, however, only log-periodic antennas are known to have large operational bandwidths. Although desirable dispersions may be specified under various design considerations, the existing log-periodic antennas do possess larger BT products than a quadratic-phased antenna (refer this comparison to Chapter VII). As a result, there will be more emphasis placed on log-periodic antennas.

After matched-filter concepts are discussed, an example is given to illustrate the gain obtainable in field-compression radiation.

2. RADIATION-FIELD COMPRESSION ANTENNAS

A field compression antenna may be defined as a conjugate-matched filter. That is, if its impulse response is $h(t)$ or $H(\omega)$, then its input, $s(t)$ or $S(\omega)$, is desired to be proportional to time reversal or the complex conjugate of the response,

$$s(t) = k\, h(-t) \qquad \text{(Eq. II-1)}$$

or

$$S(w) = k\, H^*(\omega), \qquad \text{(Eq. II-2)}$$

where the constant of proportionality k is called the matched-filter constant. If h(t) is a relatively long-duration waveform, representing in general a frequency-modulated electromagnetic field, then the output of the antenna will be a compressed field given by the convolution of the driving signal h(-t) with the antenna response k h(t):

$$g(t) = k \int_{-\infty}^{\infty} h(\tau)h(t-\tau)d\tau \qquad \text{(Eq. II-3)}$$

The compressed field g(t) may also be expressed in terms of the inverse Fourier transform of the product of the signal frequency spectrum $H^*(\omega)$ with the antenna frequency spectrum k $H(\omega)$:

$$G(\omega) = S(\omega)\, H(\omega) = k|H(\omega)|^2 \qquad \text{(Eq. II-4)}$$

$$g(t) = \frac{k}{2\pi} \int_{-\infty}^{\infty} |H(\omega)|^2 e^{j\omega t}\, d\omega \qquad \text{(Eq. II-5)}$$

A sketch of the field compression concept is shown in Figure II-1. The field compression ratio is the ratio of the temporal width of the input signal to the temporal width of the compressed field. This ratio is also equal to the product of the dispersed field duration arising from the antenna tranfer function and the spectral bandwidth of the input signals; it will be referred to as the bandwidth-time product or simply the BT product. Since it is known of passive antenna devices, that the total

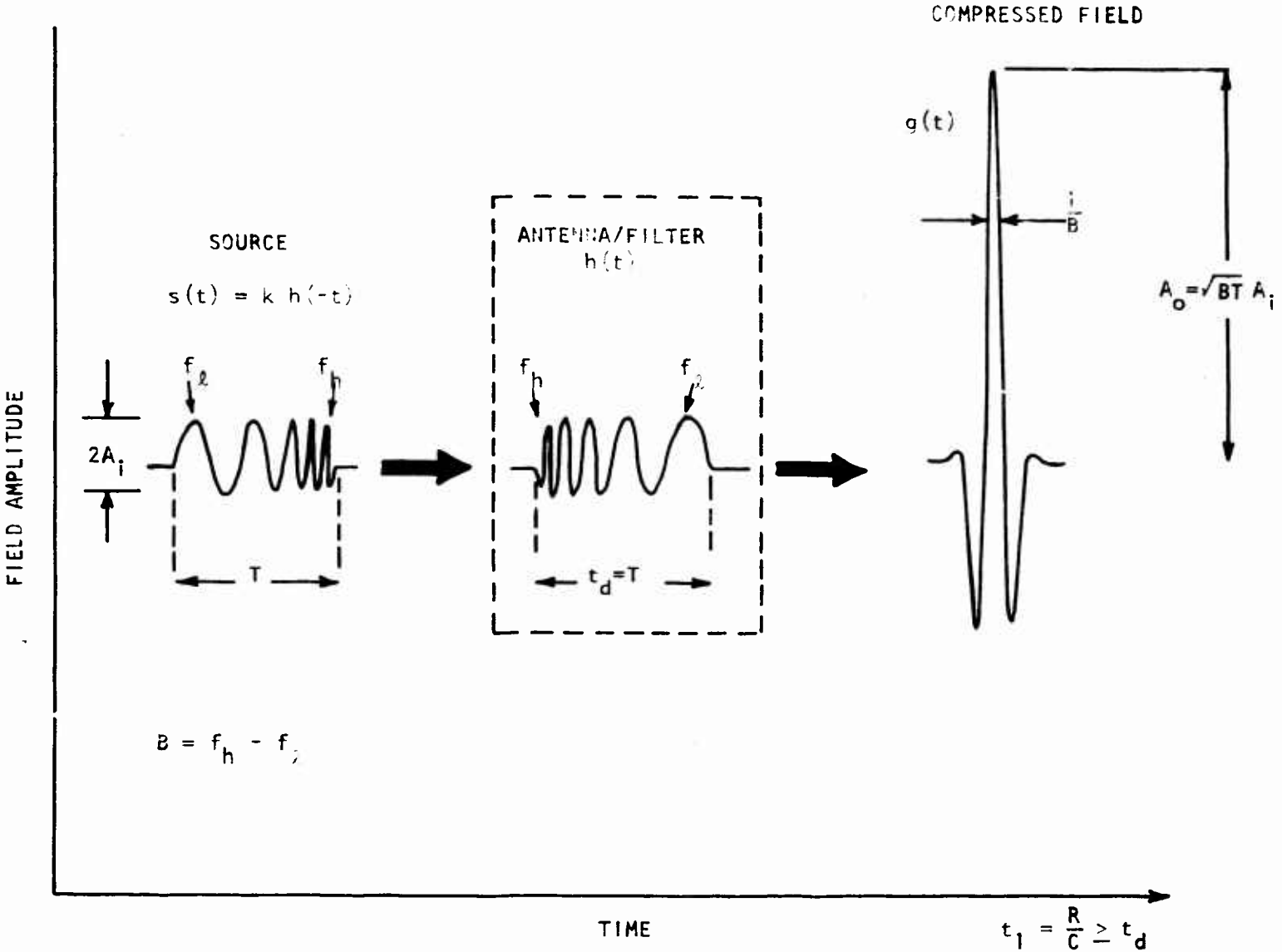


Figure II-1. Time-Domain Concept of Field Compression

energy of the compressed field can be no greater than that of the input or source field, it follows that the amplitude of the compressed field is equal to or less than the product of $\sqrt{BT}$ with the source field amplitude. The maximum power density of the compressed, radiated field relative to the source input power will therefore be proportional to BT as

$$\frac{P_o}{P_i} = KDT \qquad \text{(Eq. 11-6)}$$

where the constant K is related to antenna geometry and field coordinates.

Usually, antennas are described in terms of their radiation characteristics. The criteria such as beam width and sidelobe level are frequently applied as measures of antenna performance. In system applications where an antenna is used as a conjugate-matched filter, additional criteria such as phase or frequency modulation must be considered equally important in terms of overall performance. Clearly, filter parameters must be expressed in terms of those of the antenna if the combined system is to be analyzed according to antenna theory. In its role as a field compression device, the antenna must possess the following properties: the dispersive characteristics of a filter which is conjugate-matched to a source field in order to create maximum signal duration, as large a bandwidth as possible in order to maximize the compression, high directivity, and efficiency as a radiator. In addition, there will be practical characteristics such as small size at the lowest desired frequency of operation and the ability to accept significant input power at the highest operational frequency where antenna geometry is the smallest. These are, therefore, the basic constraints for field compression antennas.

3. FREQUENCY-INDEPENDENT ANTENNAS

There is a certain class of antennas which exhibit both large bandwidth, some greater than 50:1, and high dispersion. These are called frequency

independent antennas. They have been operated to frequencies as high as 12 GHz, hence having relatively small size while maintaining large bandwidth is clearly possible. A study of the properties of this class of antenna as potential field compression devices is considered here.

In order for an antenna to be frequency independent, its geometry must be invariant to a change of scale that is proportional to a change in wavelength. For instance, it can be shown that this invariance under scale change can be equivalent to a spatial rotation which leaves the structure invariant. From this principle, it follows that the class of all surfaces capable of being frequency independent antenna structures are those for which (see geometrical details in Appendix F)

$$\phi - b \ln r = f(\theta) \qquad \text{(Eq. II-7)}$$

where (r, θ, ϕ) are the usual spherical coordinates and $f(\theta)$ is an arbitrary function of θ. Antennas satisfying Equation II-7 are those with log-periodic, geometrical structures, that is, structures having a periodicity which expands at a logarithmic rate. These include the planar log-periodic dipole array, the planar equiangular (or logarithmic) spiral and conical spiral antennas, all of which follow from Equation II-7 under the restriction

$$\theta - \theta_o = F(\phi - b \ln r) \qquad \text{(Eq. II-8)}$$

where $F(\phi - b \ln r)$ is a periodic function of $(\phi - b \ln r)$ and θ_o and b are constants for any given antenna. In principle, there can be an infinite variety of frequency independent antenna geometries depending on the form of F; structure periodicity appears to be only a sufficient condition for an antenna to possess this property.

Any antenna satisfying Equation II-8 is, in principle, no better than any other: they are simply all frequency independent. However, in practice, some antennas have more desirable features for certain applications than others. For example, some are more compact while others possess greater directionality. The point is that for a given application, the best choice of frequency independent antennas cannot be determined without first limiting the infinite class represented by Equation II-7. In the following sections only a known subclass of these antenna structures will be considered: those which derive their frequency independent behavior from Equation II-8 and are therefore called log-periodic structures. There is no theoretical limit on the bandwidth over which these antennas can be designed. In Section IV, it will be seen that the log-periodic scaling property is also the origin of their high dispersion.

4. LINEAR AND NONLINEAR FILTERS

The theory of matched filters has been adequately described by Cook and Bernfield.[2] In general there are two types of FM pulse compression filters: linear and nonlinear. Linear FM filters possess a phase which varies quadratically with frequency. There are no known broadband, dispersive antennas having this phase variation. Nonlinear FM filters characteristic of log-periodic antennas have phases which vary as the logarithm of the frequency. In either case, the filter is a dispersive device and it follows that the antenna used as an FM filter must also be dispersive. For a given antenna, its characteristic design will determine whether its filter characteristics will be linear or nonlinear.

The characteristic dispersion of an antenna can be described by its transfer function, that is, by antenna impulse response. It should be noted that once the antenna transfer function $H(\omega)$ is known, then the source needed to drive the antenna under conjugate matching is in theory described by Equation II-2, or by Equation II-1, if $h(t)$ is determined instead of $H(\omega)$. Therefore, determination of the transfer function for a field

compression antenna provides the essential information necessary to actually construct the source.

In view of the nonexistence of broadband, highly dispersive, quadratic phase antennas, emphasis has been shifted to in-depth studies of log-periodic antennas as being the most promising types for field compression. Nevertheless, the theory of quadratic phase antennas will also be presented in Section IV along with the theory of log-periodic phase antennas.

Measured transfer functions and BT products for a variety of log-periodic antennas are given in Section III.

5. EXAMPLE ON FIELD-COMPRESSION RADIATION

Application of BT product to a radiated field requires simple definition of radiated power density in the far zone. Suppose an antenna is fed by a power, W, which is radiated by an omnidirectional antenna, the power density, at r from the antenna is

$$P_o = W/4\pi r^2$$

If a practical antenna has a directive gain D with perfect radiation efficiency, the radiated power density would be

$$P_a = DP_o = WD/4\pi r^2$$

This last expression for radiated power density is for CW or monchromatic operation. If a dispersive antenna with a BT compression gain is used, this broadband antenna would have a peak-power density gain by an additional factor BT. Therefore, the radiated power density is

$$P_a = (BT)\ P_a = W(D)(BT)/4\pi r^2 \qquad \text{(Eq. 11-9)}$$

For instance, if a log-periodic antenna has $D \approx \pi^2/\sqrt{2}$ (see Chapter VII), $BT \approx 2000$ for an antenna volume of 4 m^3 (see Chapter V), the radiated maximum power density is

$$P_d = W\ (250\ \sqrt{2}\ \pi)/r^2$$

$$= 0.25\ \sqrt{2}\ \pi\ W$$

at a distance 100 m from the antenna. If the directive gain $D = \pi^2/\sqrt{2}$ is used in Equation II-9, the compressed electric field intensity,

$$E = \sqrt{P_d/120\ \pi} \qquad \text{(Eq. II-10)}$$

$$= \frac{\sqrt{BTW}}{r\sqrt{2}}$$

Substitution of BT gain and the input power W, the compressed electric field can be readily obtained for log-periodic antennas. In addition to the gain of a single dispersive antenna, many dispersive antennas can be arrayed to increase total gain further. The most simple way to evaluate this gain is to use the total number of radiation cells available, as will be discussed in Chapter VII. Simply stated here, the compressed power density is

$$P_d = \left(W \sum_{j=1}^{N} (D_j)\ (BT)_j\right)/4\pi r^2$$

where the running index j is to denote various dispersive antennas that may possess various directive gain D_j and temporal compression gain $(BT)_j$.

SECTION III

VERIFICATION OF FIELD DISPERSION AND COMPRESSION BY MEASUREMENTS

1. INTRODUCTION

The purpose of the material presented in this chapter is to demonstrate the validity of the field compression concept by analyzing measured dispersion data. A short pulse is used to excite six log-periodic antennas. Their radiated fields are received in the far zone by a monopole stub. The radiated pulse dispersions are presented to demonstrate required driving-pulse duration if these antennas are to be used for pulse compression.

Frequency-domain characteristics are established for the antenna transfer functions by numerical Fourier transforms. Despite the inadequacy of the driving source (to be discussed), the essential information about phase angle or instantaneous frequency delay has been established for every antenna measured. This information enables analytical formulations of filter-functions for the antenna and gives rise to an accurate prediction of the BT product for each antenna.

Since measured data have verified the desired dispersion characteristics for which analytical models are to be given in Section IV, the concept of field-compression radiation is considered to have been verified by the measured data from which conjugate-matched driving source can be specified.

2. TRANSFER FUNCTION MEASUREMENT CONCEPT

Before antenna field compression can be demonstrated, the antenna transfer function would first have to be determined. This is so because

it contains the necessary information on how to design the conjugate-matched source waveform. The measurement of the antenna transfer function directly provides bandwidth and duration. It thus allows BT product evaluation without the need of driving the antenna with a conjugate-matched source. The field can then be compressed analytically by taking the inverse Fourier transform of $H(\omega)^2$ (recall Equation II-5).

The transfer function is given by the antennas' impulse response

$$H(\omega) = \frac{G(\omega)}{S(\omega)} \qquad \text{(Eq. III-1)}$$

where $S(\omega)$ and $G(\omega)$ are the measured input and output antenna signals. Ideally, the driving source for testing a dispersive antenna is an impulse that would have flat spectral density from dc to an indefinitely high frequency. If this were so, $S(\omega)$ would be constant and $H(\omega) \propto G(\omega)$. Since this source does not exist, the alternative is to provide a source having significant spectral density from dc to the highest frequency of interest. The presently available high voltage pulse generators can only provide significant spectral content up to 1.5 GHz and may be down by -40 dB or more at 4 GHz. (See Appendix C for a discussion of driving source characteristics.) As will be described later, several antennas which were measured have high frequency response up to 4 GHz, and another goes to 10 GHz. The inadequacy of using the presently available pulse generators for these types of measurements makes it necessary to analytically compensate measured results in order to obtain antenna transfer functions.

3. MEASUREMENT SYSTEM

Basically, antenna dispersion was measured using a high voltage, fast risetime, short duration pulse generator to drive the antenna. Both the input signal and the antennas' radiated response were displayed on a sampling oscilloscope and photographed. This information was then digitized and used to determine the complex antenna transfer function, source function and compressed pulse in the frequency and time domains.

Some of the measured data for this analysis have been provided by Paul VanEtten of RADC.

The measurement system used to test the ASN-117AA cavity-backed spiral by BDM is shown in Figure III-1 and is described in detail in Appendix B. The system used at RADC is similar to the one used at BDM. It should be pointed out, however, that some dispersion measurements were made using a receiver antenna identical to the one under test. In these cases, since identical antennas can be as assumed to exhibit the same characteristic dispersion, the dispersion time or pulse duration is doubled. Most of the tests were conducted using a 2 cm stub monopole as the receiver field probe. In this configuration, the one-way antenna dispersion is measured. The differences in responses will be pointed out as the data are presented.

An analysis of the characteristics of the 2 cm stub monopole probe was made to determine its effect on the measured antenna response. In principle, this type of field sensor should provide replica response. The analysis, presented in Appendix C, provides amplitude and phase information indicating a relatively flat probe response to frequencies up to 1.6 GHz. For frequencies higher than 1.6 GHz, probe response becomes noisy. This appears to have been caused by the pulser source energy that has extremely low amplitudes above 1.6 GHz. (See Figure C-48.) By treating the stub as a monopole, the receiver probe should in theory be able to measure frequencies as high as 7.5 GHz.

4. MEASURED RESULTS: TRANSFER FUNCTIONS AND BT PRODUCTS

Six measured antenna responses have been selected for digitization, Fourier transformation and dispersion characterization. All antennas are manufactured by American Electronic Laboratories, Inc. (AEL) and they are briefly summarized in Table III-1. Response measurements of these antennas are described in Appendix B. A complete presentation of the digitized

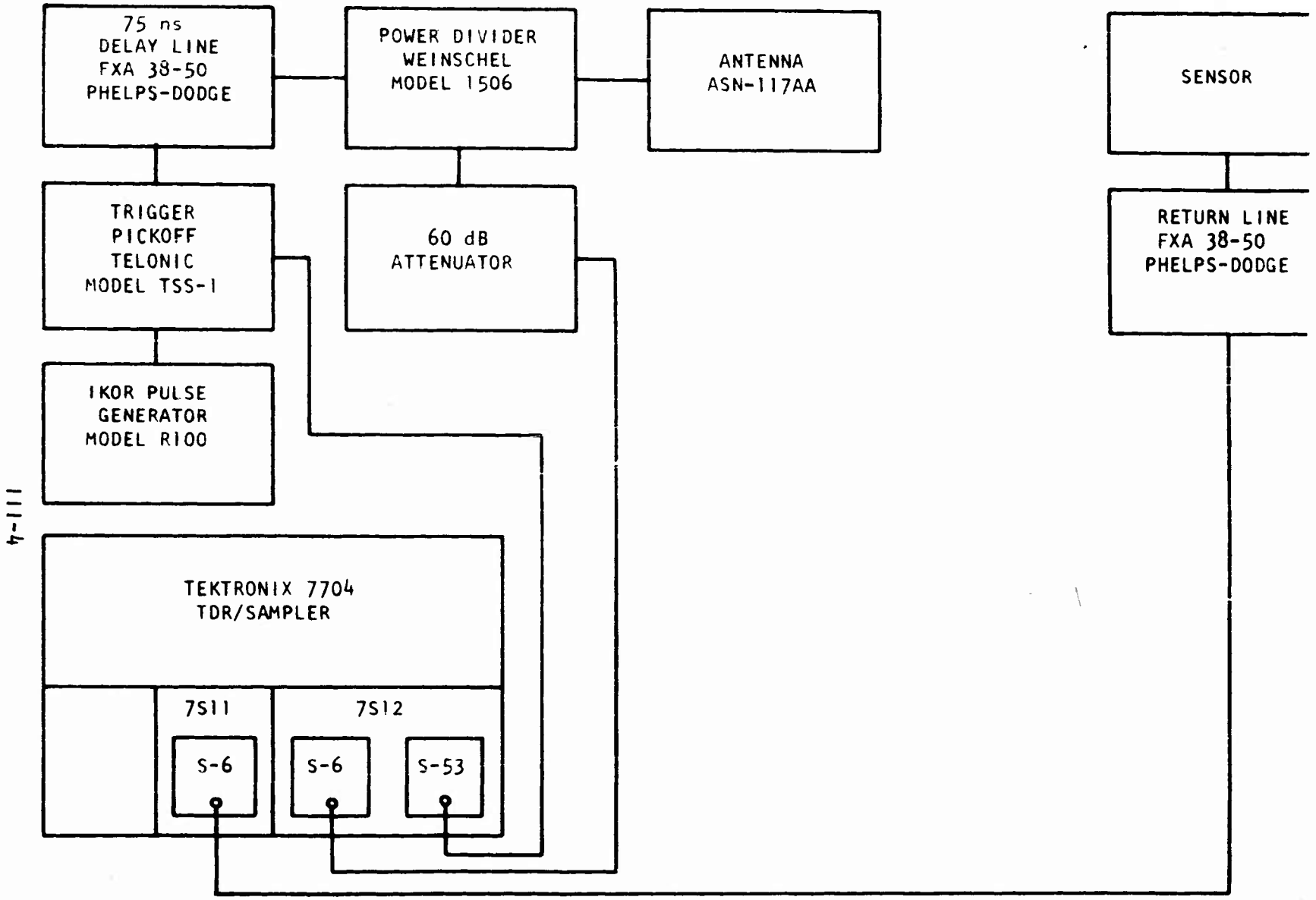


Figure III-1(a). Experimental Setup used to Measure the Transfer Function for the ASN-117AA Cavity-Backed Serial Antenna

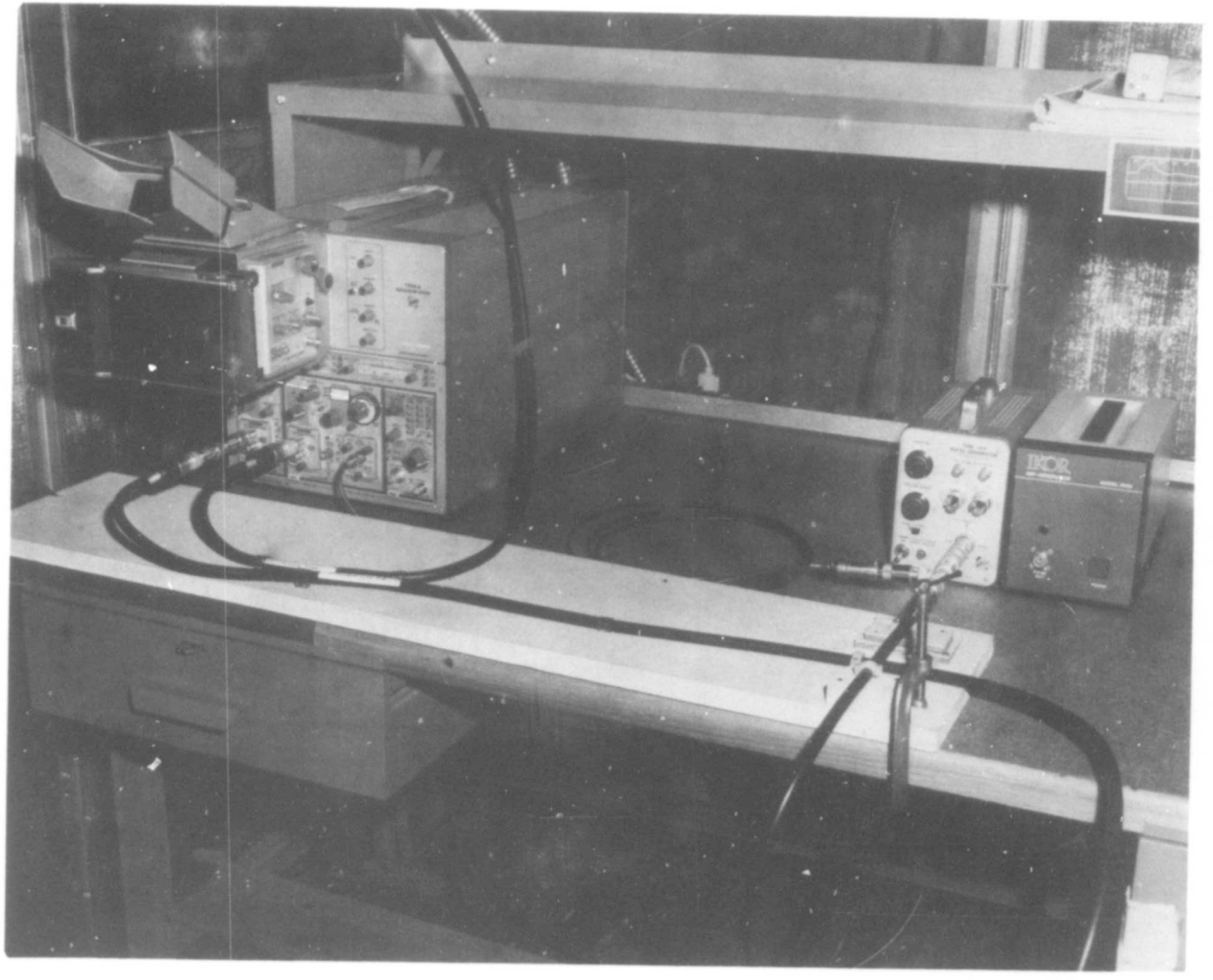


Figure III-1(b). Experimental Setup Used to Measure the Transfer Function for the ASN-117AA Cavity-Backed Serial Antenna

TABLE III-1

SOME SPECIFICATIONS FOR THE ANTENNAS TESTED.

ALL ANTENNAS WERE MANUFACTURED BY AMERICAN ELECTRONIC LABORATORIES, INC.

MODEL BY AEL	ANTENNA TYPE	BANDWIDTH (GHz)	POLARIZATION	CW GAIN (dB)	DIMENSIONS	
					TRANSVERSE (cm)	AXIAL (cm)
ASN-1232A	Cavity-Backed Spiral	0.2 - 4.0	Circular	6	46	27
ASN-117AA	Cavity-Backed Spiral	0.4 - 4.0	Circular	6	30	15
ASN-116A	Cavity-Backed Spiral	1.0 - 10.0	Circular	6	16	8
APX-254A	Crossed Planar Log-Periodic	0.4 - 4.0	Linear	7	41	58
APN-995B	Coplanar Log-Periodic	0.03 - 1.1	Linear	6	503	263
APN-502A	Pyramidal Log-Periodic	0.2 - 3.0	Linear	11	97	79

dispersed pulses, the amplitude and phase distributions, the input functions, and the transfer functions can be found in Appendix C.

a. Transfer Function Cavity-Backed Spiral Antenna ASN-1232A

This antenna, shown in Figure B-18, has a dispersed pulse duration of about 65 ns as seen in Figure III-2(a). The amplitude of the transfer function is shown in Figure III-2(b) and the phase variation is Figure III-2(c). The peak in the transfer function amplitude at 2.1 GHz is noise induced, being caused by a deep null in the source (Appendix C, Figure C-4). The phase shows the characteristic log-periodic behavior only from 0.15 GHz to 0.9 GHz. The reason for this premature cutoff can be seen in Figure C-5 which shows that the phase of the input signal is very irregular between 0.9 GHz and 2 GHz. It is clear that the measured antenna transfer function is source limited. If one ignores the peak at 2.1 GHz, then the amplitude of the transfer function is seen to be fairly flat over a bandwidth of 0.15 GHz to 4 GHz. The rising trend in amplitude above 4 GHz is due to numerical processing which gives very low-level high-frequency components in the source and relatively high level in the antenna response. The transfer function in all the noisy regions should be discarded because of the inadequacy in pulser source.

Because of source limitations, the complex transfer function should only be considered representative of actual antenna characteristics. To obtain a BT product from measured data, the dispersed pulse duration is seen to be about 65 ns and the bandwidth may be obtained from the phase plot as 0.75 GHz over which the transfer function phase angle is nearly log-periodic. Thus

$$BT = (0.75\ \text{GHz})(65\ \text{ns}) = 49$$

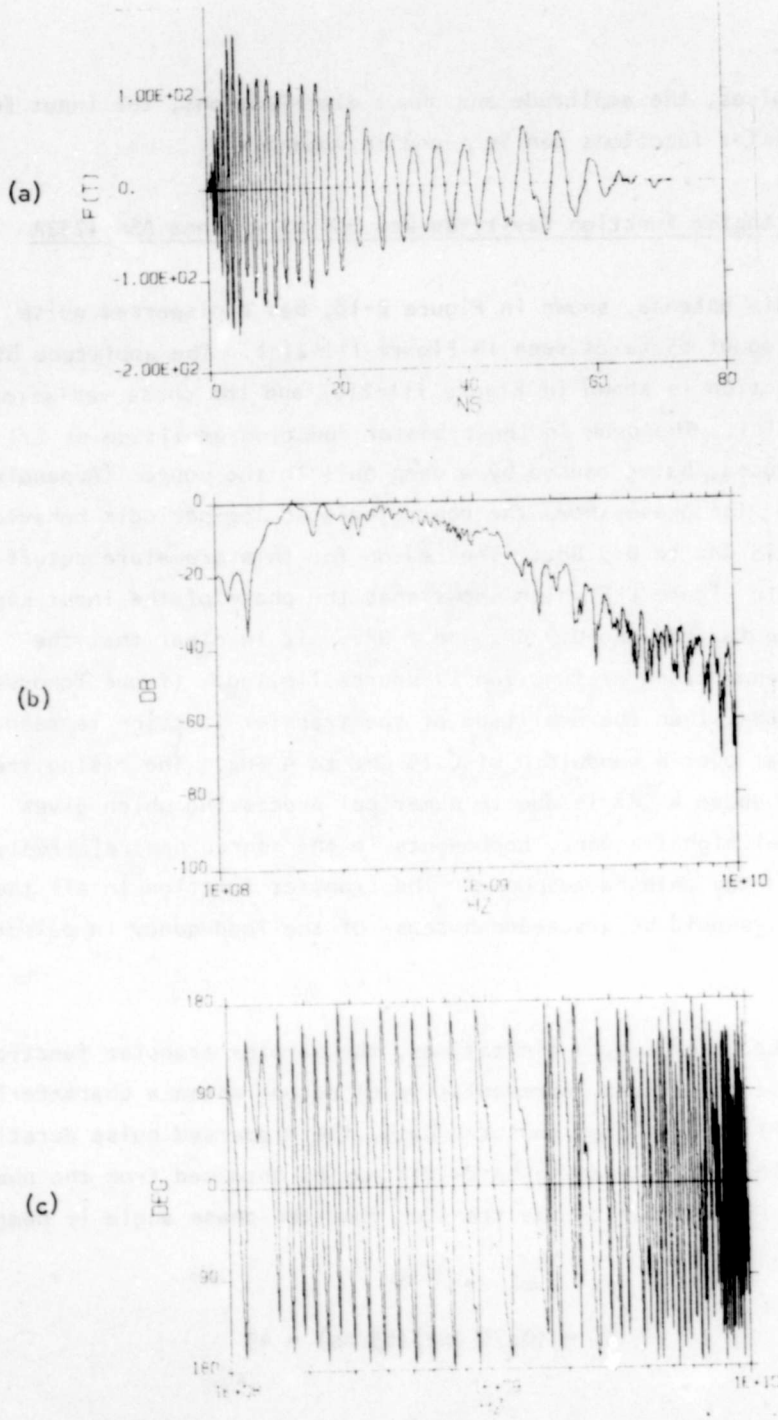


Figure III-2. Cavity-Backed Spiral ASN-1232A. (a) Dispersed Pulse; (b) Transfer Function Amplitude; (c) Transfer Function Phase

which is low because of the source limitations, and should be treated as a preliminary evaluation from measured data. If an adequate source was used to drive this antenna, a BT product of 250 should be realized under the criteria stated above. This will be discussed in greater detail at the end of this chapter.

b. Transfer Function of Cavity-Backed Spiral Antenna ASN-117AA

This antenna is shown in Figure B-15. The dispersed pulse duration is about 15 ns as seen in Figure III-3(a). Transfer function amplitude and phase are shown in Figure III-3(b) and Figure III-3(c), respectively. Significant nulls occurring at 2.7 GHz and 3.3 GHz in the source spectrum (Figure C-12) are responsible for the rising trend in transfer function amplitude. Using the spectral amplitude at 2 GHz as a reference, the -10 dB bandwidth is approximately 0.35 GHz to 3.7 GHz. The phase shows good log-periodicity from 0.28 GHz to 1.8 GHz. Using the bandwidth over which phase is log-periodic as the criteria for measured compression evaluation, the BT product is

$$BT = (1.52\ \text{GHz})(15\ \text{ns}) = 23$$

c. Transfer Function of Cavity-Backed Spiral Antenna ASN-116A

This antenna is shown in Figure B-19. Two identical antennas were used to record the dispersion shown in Figure III-4(a). The input pulse used to drive these antennas was not recorded, hence the output could not be normalized by the input in order to provide an accurate measure of the transfer function. The total duration of the dispersed pulse is about 14 ns and this is using two antennas. Therefore, the actual duration is only 7 ns. Figure III-4(b) and III-4(c) show the amplitude and phase, respectively, of the dispersed pulse. Log-periodic phase is exhibited from about 0.63 GHz to 2.5 GHz. The BT product based

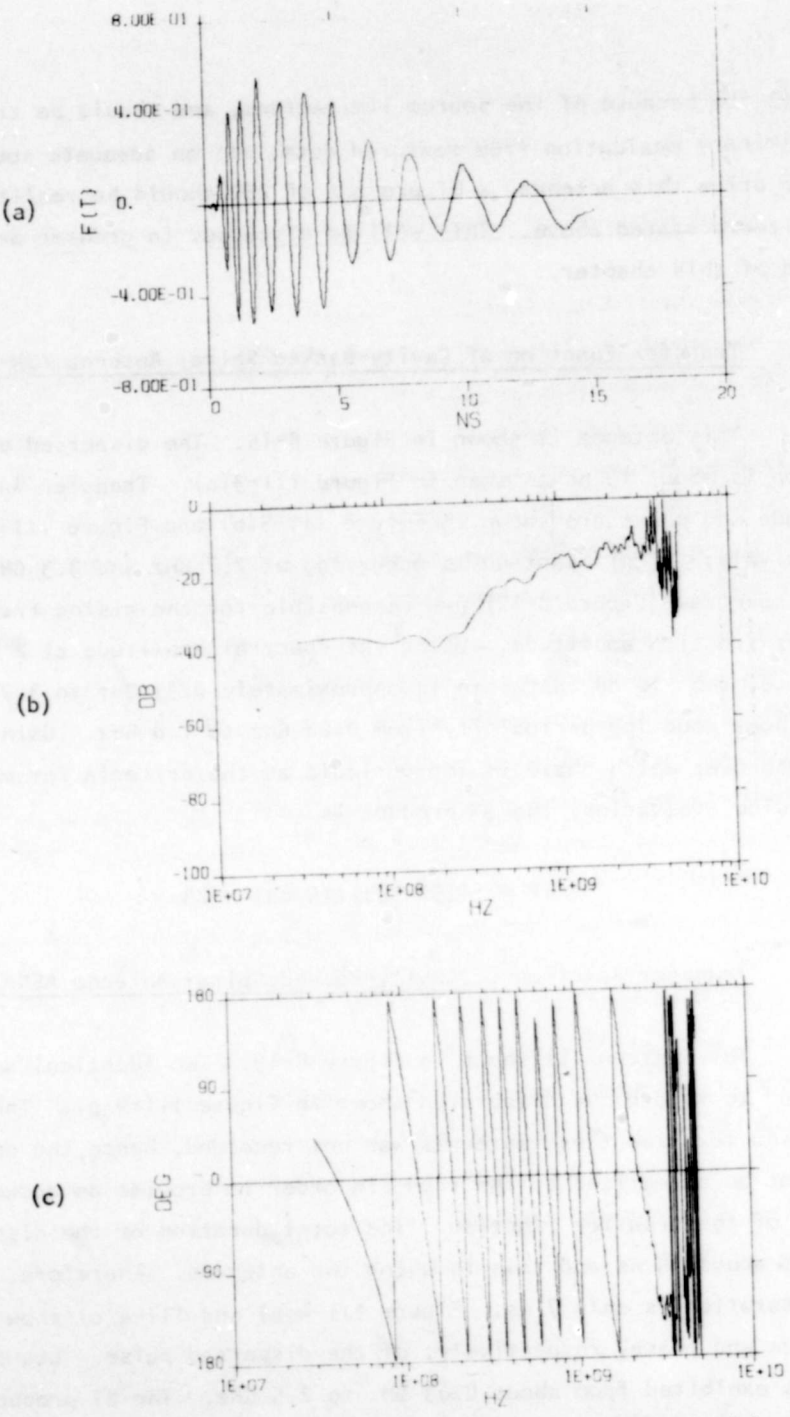


Figure III-3. Cavity-Backed Spiral ASN-117AA. (a) Dispersed Pulse; (b) Transfer Function Amplitude; (c) Transfer Function Phase

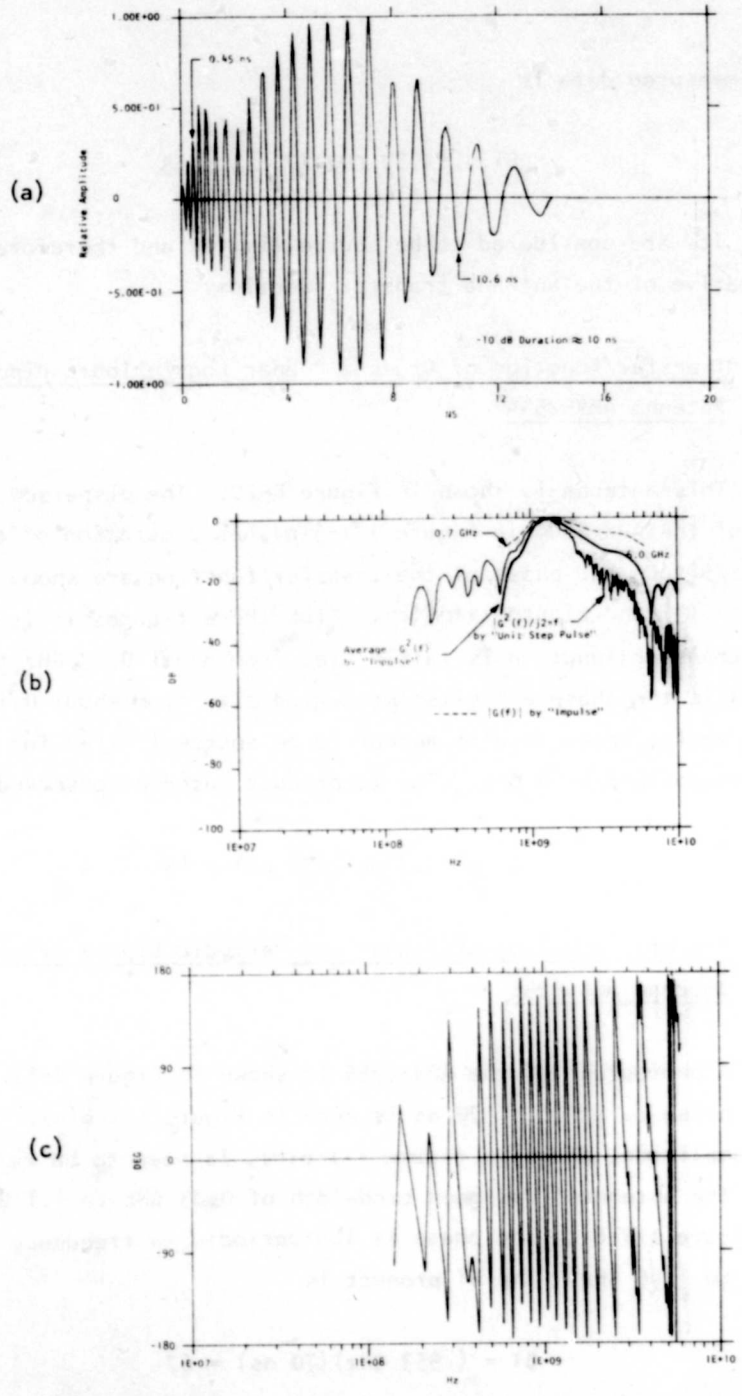


Figure III-4. Cavity-Backed Spiral ASN-116A. (a) Dispersed Pulse; (b) Transfer Function Amplitude; (c) Transfer Function Phase

on these measured data is

$$BT = (1.87\ GHz)(7\ ns) = 13$$

These results are considered to be source limited and therefore not representative of the antenna transfer function.

d. Transfer Function of Crossed Planar Log-Periodic Dipole Antenna APX-254A

This antenna is shown in Figure B-20. The dispersed time response of the APX-254A in Figure III-5(a) has a duration of about 70 ns. Amplitude and phase of the transfer function are shown in Figure III-5(b) and Figure III-5(c). From these figures it is seen that the transfer function is fairly flat from about 0.13 GHz to about 0.8 GHz while the phase exhibits log-periodicity from about 0.1 GHz to 0.8 GHz. Again, these results appear to be source limited for an antenna designed to operate to 4 GHz. The BT product based on observed data is

$$BT = (0.7\ GHz)(70\ ns) = 49$$

e. Transfer Function of Planar Log-Periodic Dipole Array Antenna APN-995B

A photograph of the APN-995B is shown in Figure B-17. A dispersed pulse duration of 70 ns is seen in Figure III-6(a). Transfer function amplitude, shown in Figure III-6(b), is seen to be relatively flat over the antennas' designed bandwidth of 0.03 GHz to 1.1 GHz. As seen in Figure III-6(c) the phase is log-periodic in frequency from 0.097 GHz to 1.05 GHz. The BT product is

$$BT = (.953\ GHz)(70\ ns) = 67$$

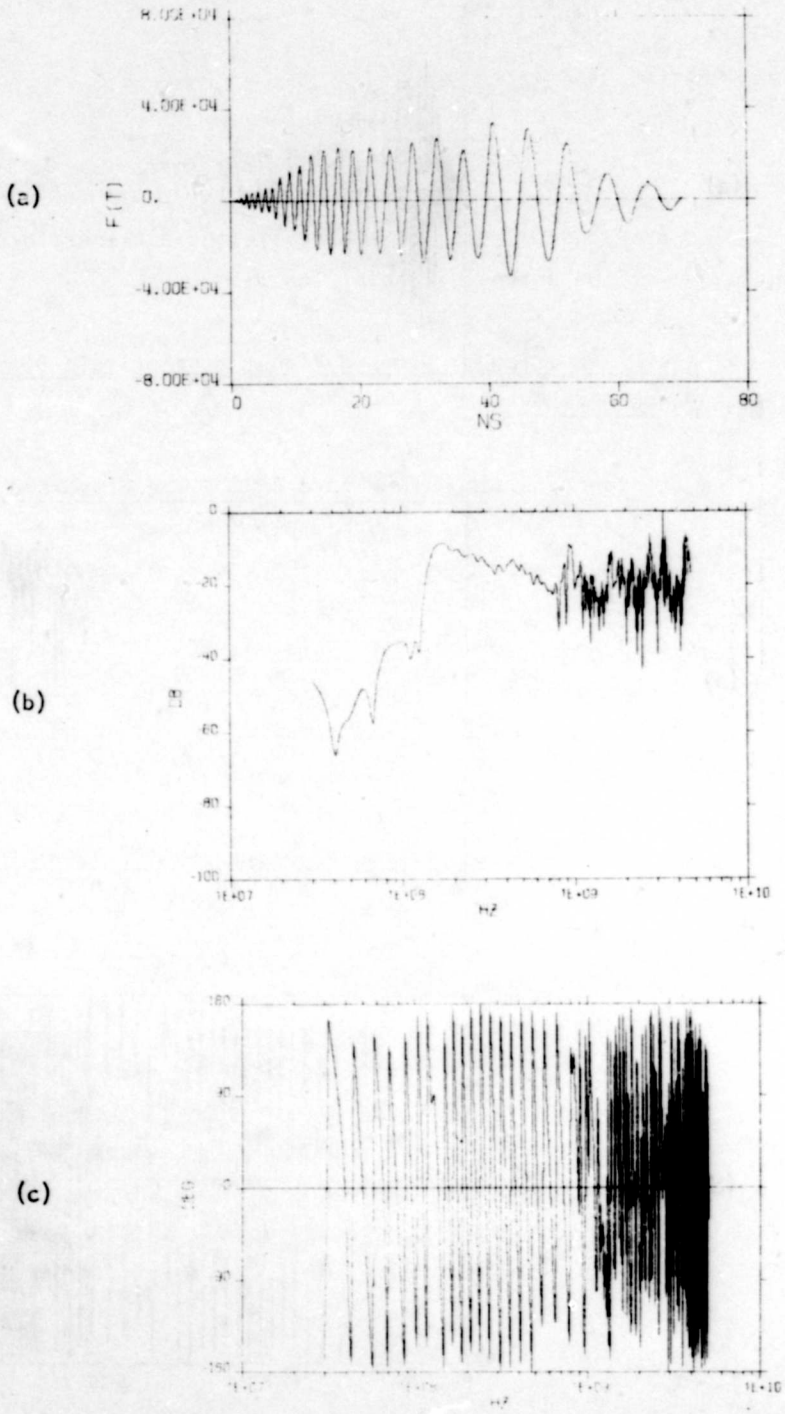
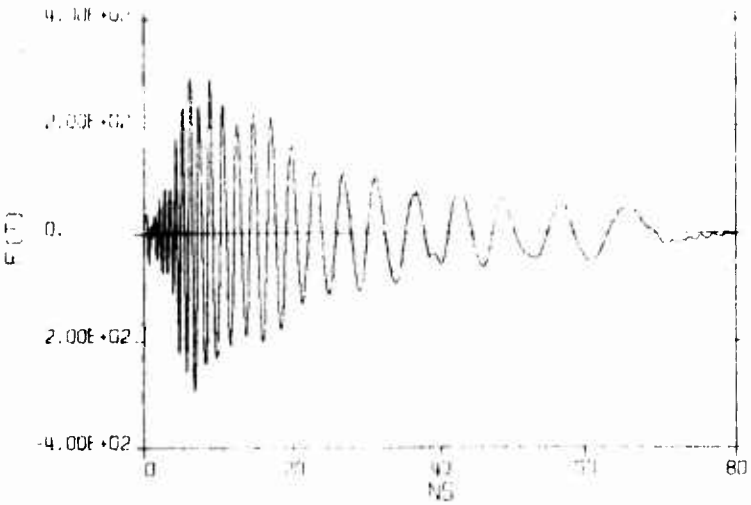
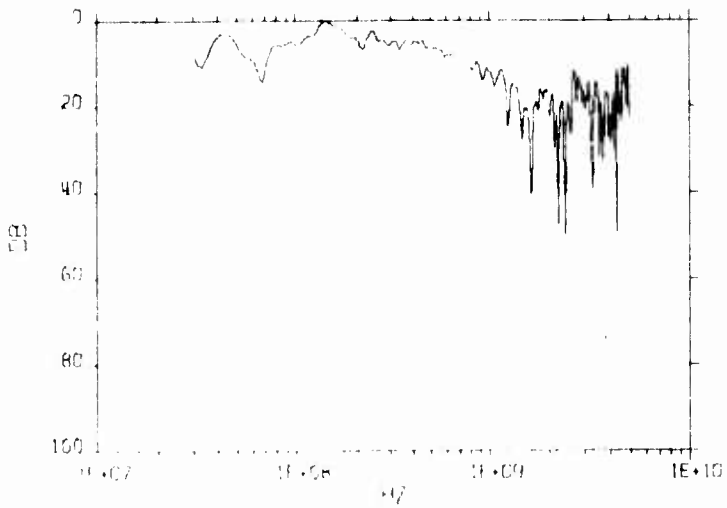


Figure III-5. Crossed Planar Log-Periodic APX-254A. (a) Dispersed Pulse; (b) Transfer Function Amplitude; (c) Transfer Function Phase

(a)



(b)



(c)

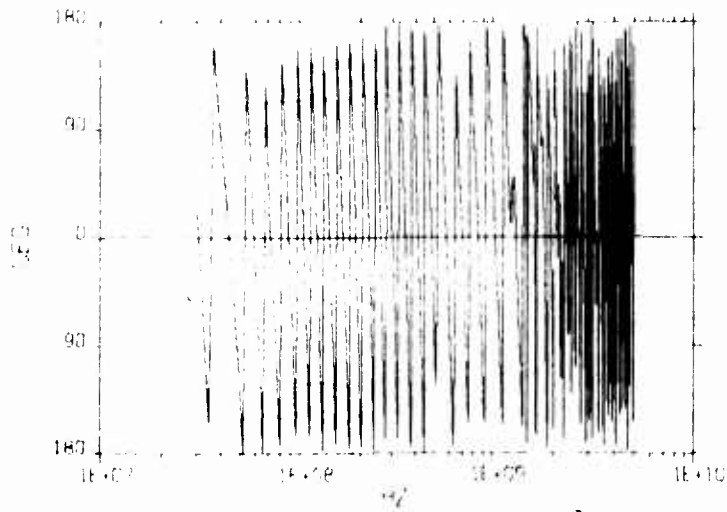


Figure III-6. Coplanar Log-Periodic APN-995B. (a) Dispersed Pulse; (b) Transfer Function Amplitude; (c) Transfer Function Phase

It should be pointed out that this was the only antenna which could be adequately tested over its complete design bandwidth.

f. Transfer Function of Pyramidal Log-Periodic Antenna APN-502A

The dispersed pulse has a measured duration of about 16 ns as seen in Figure III-7(a). The -10 dB bandwidth of the APN-502A is from 0.14 GHz to 1.45 GHz as seen in Figure III-7(b). The 4 GHz component has dropped below -40 dB which again demonstrates the inadequacy of source used to drive the antenna. Figure III-7(c) shows that the phase is log-periodic from 0.17 GHz to 2.0 GHz. The observed BT product of this antenna is

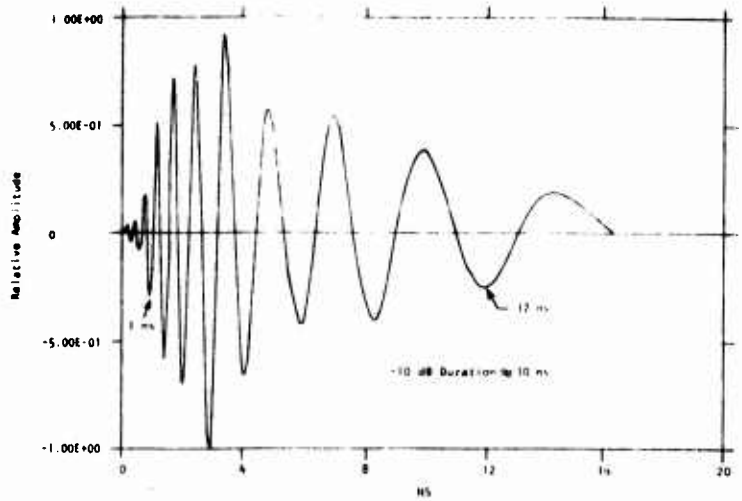
$$BT = (1.83 \text{ GHz})(16 \text{ ns}) = 30$$

5. SUMMARY OF MEASURED RESULTS

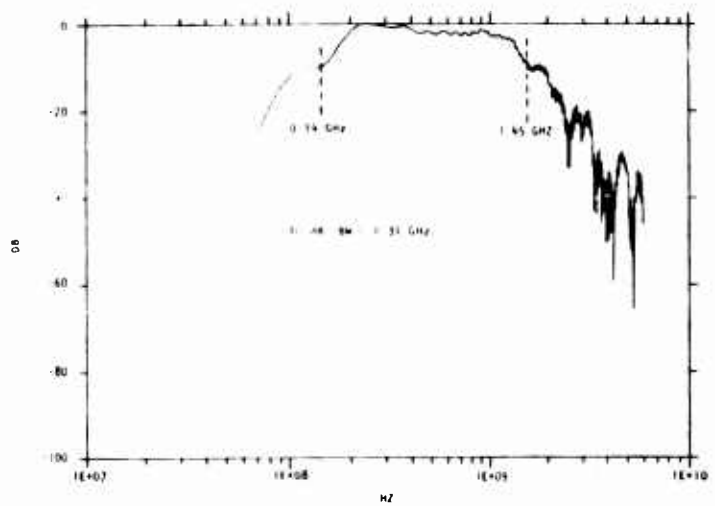
For all antennas tested, the driving source was inadequate to excite their full bandwidth response. (The source was considered adequate for the APN-995B.) As a result, measured BT products are much smaller than they should have been. Table III-2 shows a comparison between measured and predicted results under the assumption of a driving source adequate to excite a g.. tennas' highest frequency response. It can be seen that BT products may prove to be as much as 5 times greater than measured results indicated for these antennas.

Several useful observations of transfer functions of log-periodic antennas may be made. All antennas possess a phase which varies as the logarithm of the frequency. This means that the time delay is inversely proportional to the frequency. The greatest time delay occurs for the lowest frequency, therefore there is a tendency for antennas with lower frequencies of operation to exhibit longer durations. Other design factors can affect this as will be seen in the following chapters.

(a)



(b)



(c)

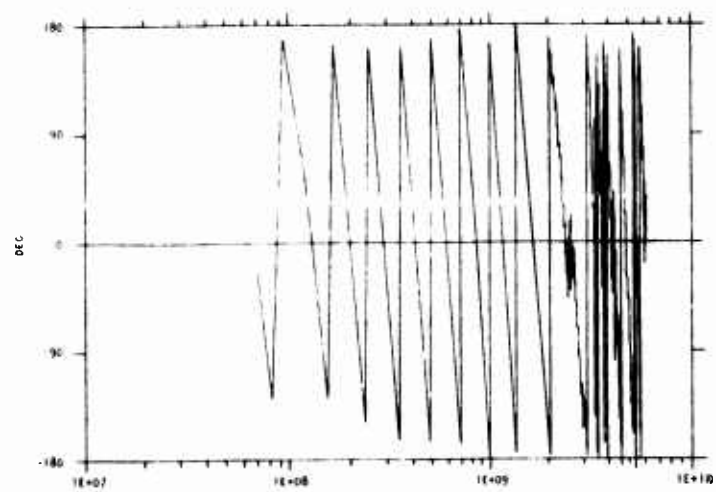


Figure III-7. Pyramidal Log-Periodic APN-502A. (a) Dispersed Pulse; (b) Transfer Function Amplitude; (c) Transfer Function Phase

TABLE III-2

COMPARISON OF MEASURED AND PREDICTED BT PRODUCTS

ANTENNA TYPE	MEASURED[1]			PREDICTED		
	BANDWIDTH (GHz)	DURATION (ns)	BT	BANDWIDTH[2] (GHz)	DURATION[3] (ns)	BT
CAVITY-BACKED SPIRAL ASN-1232A	0.15 - 0.9	65	49	0.15 - 4.0	65	250
CAVITY-BACKED SPIRAL ASN-117AA	0.28 - 1.8	15	23	0.28 - 4.0	15	56
CAVITY-BACKED SPIRAL ASN-116A	0.63 - 2.5	7	13	0.63 - 10.0	7	66
CROSSED PLANAR LOG-PERIODIC DIPOLE APX-254A	0.1 - 0.8	70	49	0.1 - 4.0	70	273
LOG-PERIODIC DIPOLE ARRAY APN-995B	0.097 - 1.05	70	67	0.097 - 1.1	70	70
PYRAMIDAL LOG-PERIODIC APN-502A	0.17 - 2.0	16	30	0.17 - 3.0	16	46

NOTES: [1]The bandwidth has been taken as that over which the measured phase variation is log-periodic. Observed durations have been used without regard to spectral weighting.

[2]Bandwidths have been taken as the difference between the highest designed CW frequency and the measured lowest frequency assuming an adequate impulse source.

[3]Correction for high frequency response is not expected to significantly alter durations.

If the transfer function amplitude were smoothed over the operating bandwidth as if the antenna were driven by a perfect source (consider for example Figure III-6(b), the amplitude distribution could be approximated by a Hamming weighting function.

Also, if the phase angle of the transfer function were log-periodic over the entire CW-specified bandwidth, the complex transfer function of a field-compression antenna could be formulated analytically as described in Section IV.

6. REQUIREMENTS FOR FIELD COMPRESSION

The measured data in time domain have shown sequential delays of instantaneous frequencies from the high-end to the low-end of operational bandwidth. Although the high-end frequency components cannot be easily identified because of the lack of these components in the driving sources, the estimates for dispersed-pulse duration are considered to be good approximations for actual antenna performance. These estimated durations can be considered as those required of respective driving sources with frequency components taking place in reverse order of that measured in this program.

The transfer functions of all antennas have demonstrated well-behaved log-periodic phase angles in the bandwidths where the source has provided adequate excitation. By referring to CW specifications of these antennas, it appears that log-periodic phases can be assured over the entire specified bandwidths. These extrapolated phase functions are analytically formulated and plotted for all six antennas in the Section IV.

To use any of the antennas for field compression, its driving source has to be designed in the frequency-domain to have a conjugate phase angle of the measured dispersion. Although the requirements for driving source

can be stated equivalently in either time or frequency domain, it is important to recognize that a successful source design can best be helped by having information available in both domains.

The measured pulses have shown their spectral densities to have the tendency of decreasing rapidly with lower frequencies. This is expected since the CW-bandwidth of each antenna element decreases exponentially with decreasing frequencies. The observed common tendency is indeed the result of maintaining a constant fractional bandwidth for each element. To design a source to perform pulse compression, there are various choices for spectral density. If spectral distribution of a source is designed to be the same as that of the antenna, the radiated pulse would be compressed symmetric to the pulse peak and yield a definite value for BD gain. Should a source be designed with spectral distribution different from that of the antenna, the compressed pulse shape would be asymmetric with respect to the pulse peak, and the BT gain would vary according to assigned distribution. More numerical results reflecting BT gain with source spectral distribution will be given in Section VII.

SECTION IV

FIELD COMPRESSION ANTENNA MODEL BY ELEMENTAL REGION FORMULATION

1. INTRODUCTION

In order to maximize field compression, it is necessary to develop an analytical expression of the BT product in terms of antenna parameters. This requires an understanding of the radiation mechanism which makes the antenna an effective filter. In this chapter, the mechanism for the dispersive radiation of log-periodic antennas is formulated in terms of active region radiation by slow wave structures. This will be accomplished by first presenting the theory for radiation by a single active region. Then, an analytical model of a log-periodic antenna will be treated as a collection of many active regions. As a result of this analysis, it will be seen that the relative time delay between radiations from adjacent active regions depends upon the slowness of wave propagation along the axis of the antenna and, further, that this can be expressed in terms of the fractional bandwidth per active region. This model will be verified by using it to predict the dispersion durations measured for the six antennas in Section III.

2. PHYSICAL DESCRIPTION OF AN ACTIVE REGION OF A LOG-PERIODIC ANTENNA

Active region radiation by a log-periodic antenna is presently understood in terms of wave propagation along certain slow wave, slightly aperiodic structures. This theory is outlined in Appendix E and will only be summarized here as it applies to log-periodic antennas.

A slow wave structure is one in which the propagation velocity of a wave along the structure is less than that of a free-space wave traveling in the same direction. The ratio of the slow wave phase velocity v_p to the free space phase velocity defines the slowness factor S for a particular structure:

$$S \equiv \frac{v_p}{c} = \frac{k_o}{\beta} = \pm \frac{1}{\sqrt{\varepsilon_r}} \qquad \text{(Eq. IV-1)}$$

where k_o and β are the free space and slow wave propagation constants, respectively, and $\varepsilon_r = \varepsilon/\varepsilon_o > 1$ represents the effective permittivity of the slow wave structure. The most general characterization of active region radiation by a log-periodic antenna is that it can support not only slow waves (S 1) but also fast waves (S > 1). Such structures can be most simply described by Equation IV-1 when ε_r is a spatially periodic function of z with a period d. A convenient representation of the wave properties of this type of structure over one period is shown in Figure IV-1. A point ($k_o d$, βd) on this diagram determines both the slowness and the propagation direction of waves traveling on the structure. A general wave propagating along antenna structures can be expressed in terms of spatial harmonics of which all wave numbers differ by a constant determined by structure periodicity:

$$\beta_n = \beta_o + \frac{2\pi n}{d} \quad , \quad n = o, \pm 1, \pm 2, \ldots \qquad \text{(Eq. IV-2)}$$

From Equations IV-1 and IV-2, it is seen that when $|n|$ is sufficiently large, such that $\beta_n > k_o$ or $v_p < c$, all spatial harmonics become slow waves. Taking $\beta_o > o$, spatial harmonics for $n \geq o$ are considered forward-traveling waves. Those for $n < o$ with either $|n| \gg 1$ or $d \ll \lambda$, would have negative phase velocities and are associated with backward traveling waves. It is important to observe that a backward wave spatial harmonic with n=-1 is allowed provided $d \ll \lambda$. This particular mode is of present concern for log-periodic antennas which predominately involve this spatial harmonic.

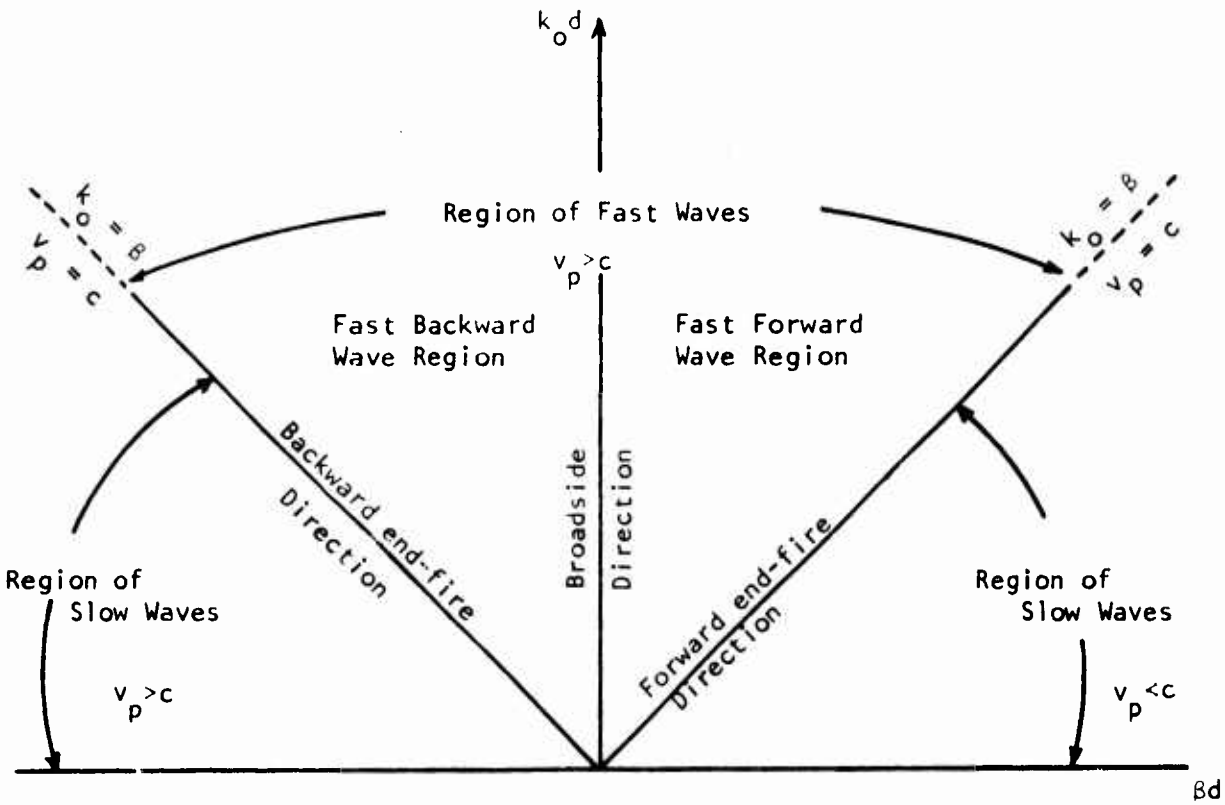


Figure IV-1. Wave Propagation Characteristics in the $k_o d$-βd Plane

The usefulness of the $k_o d - \beta d$ diagram for the description of a single active radiation region of a log-periodic antenna may now be given. When the logarithmic expansion rate of the structure periodicity is slow enough, departure from uniform periodicity is very slight over several spatial periods. Under this condition, a given small region of the antenna is locally periodic. Therefore, this single region may be locally characterized by the dispersion exhibited by a uniformly periodic antenna structure whose geometry is the same as the localized geometry of the log-periodic structure being considered. The slowness S is determined by the periodic structure as

$$S \equiv \frac{v_p}{c} = \frac{1}{\sqrt{\varepsilon_r}} = f \text{ (geometrical structure parameters)} \quad \text{(Eq. IV-3)}$$

where v_p is the axial component of the phase velocity of the fundamental wave feeding the structure and f is a function of the antenna geometry. The $k_o d$-βd diagram which represents a suitable dispersion curve of the unmodulated structure is shown in Figure IV-2. It can be seen that, at a fixed value of k_o and for slowly expanding log-periodic geometry, d is gradually and monotonically increasing so that $k_o d$ will increase proportionately away from the input region of the antenna. Assuming the presence of a dominant mode involving coupling between only the n=o and n=-1 spatial harmonics, the line with n=o representing the feed, will be traversed from low toward increasing values of $k_o d$; hence the $k_o d$-βd diagram may be regarded as a plot of the propagation constant along the log-periodic antenna as a function of the variable antenna element spacing. Near the feed (the small end of the antenna), element spacing and, therefore, the values $k_o d$ are sufficiently small that the structure operates in its slow wave region. The n=o fundamental feed wave continues to be a slow, bound wave until it reaches the backfire boundary of the n=-1 spatial harmonic radiation region. As this happens, the n=-1 harmonic has progressed to the backfire boundary of the fundamental fast wave region. At this point, the traveling feed wave becomes complex with $B_{-1} d = k_o d$

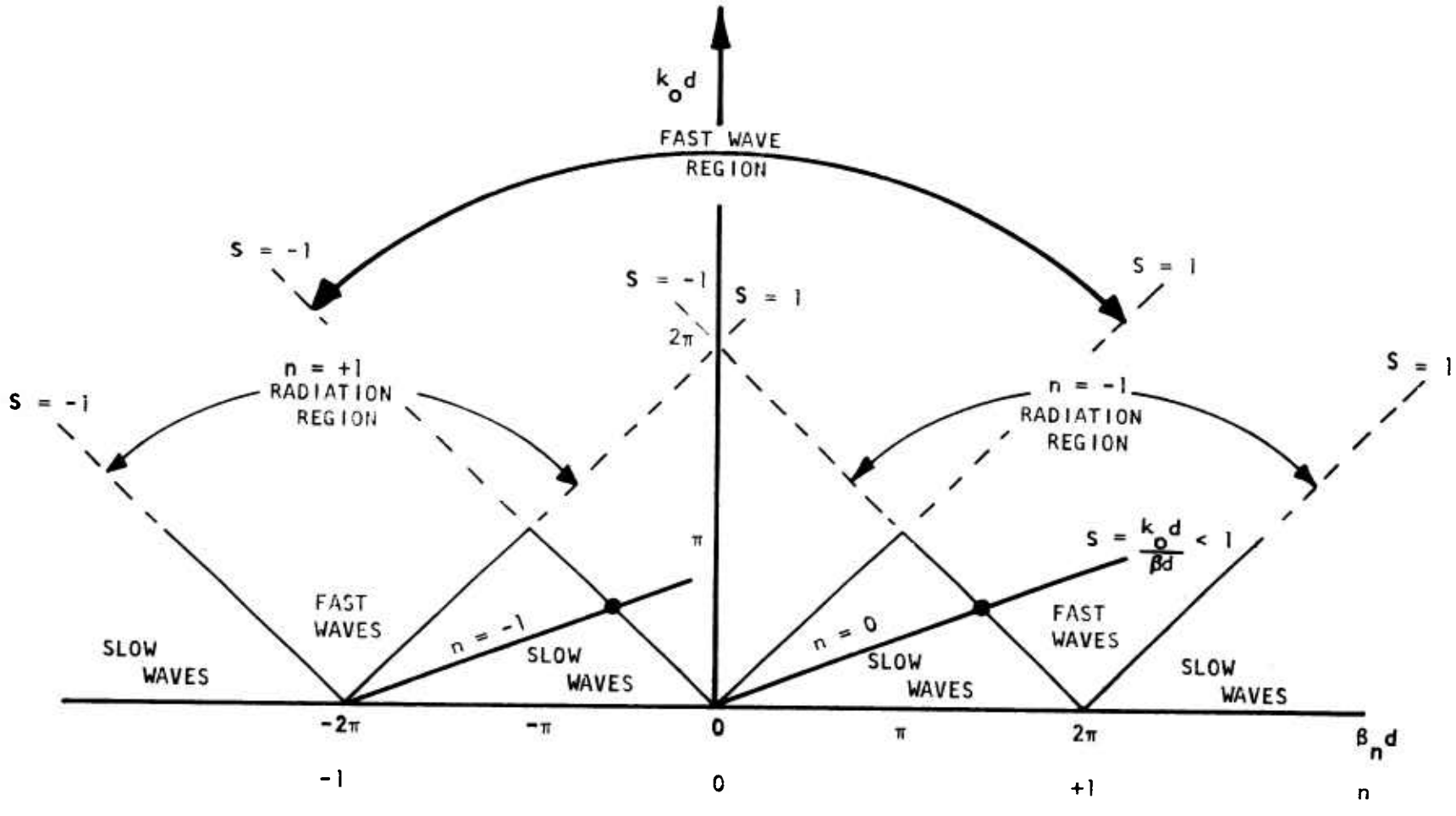


Figure IV-2. Dispersion Curve of the Unmodulated Structure

and radiates energy via the n=-1 spatial harmonic, which has now become a fast wave in the backfire direction. The location on the actual antenna where this radiation occurs at a fixed frequency of operation will define the active region. The element in an active region is designed to be about one-half wavelength of the operating frequency to enhance radiation. It was stated earlier that a condition necessary for a given structure to support a slow wave involving the n=-1 spatial harmonic was that the spatial period of the structure, d, should be much less than the wavelength at a given frequency of operation. Thus, it can be concluded that successful antenna design for backfire radiation, a characteristic of all axially log periodic antennas, is for d to be much smaller than the resonant $\frac{\lambda}{2}$ antenna dimensions.

The complete characterization of the dispersive properties of log-periodic antennas requires the consideration of all active regions of the antenna. Or, equivalently, one may say that the active region in these antennas moves in response to a frequency modulated signal in order to satisfy the scaling condition. As the FM signal travels down the structure, the high frequencies radiate from active regions close to the apex and the lower frequencies from regions farther down the antenna. Therefore, it is the difference in transit time necessary to excite active regions along the complete axial length of the antenna which is responsible for the dispersive characteristic of log-periodic antennas.

3. ELEMENTAL MODEL FOR LOG-PERIODIC ANTENNAS

Log-periodic antennas have been measured in this program to show that, regardless of their geometric appearances, they share a common transfer-function characteristic. That is, their phase angles are log-periodic and each period represents an element that is designed for CW applications. The fractional bandwidth of all elements is observed to be the same for a given antenna. It is quite natural, therefore, to

define each element that has its center frequency and definite bandwidth as a radiation cell of the dispersive antenna.

Analytical models of dispersive antennas are given in Appendix D where a complete illustration of radiation mechanisms is available for a log-periodic antenna. The sequence and nature of pulses radiated by all radiation cells are, therefore, not to be repeated here. Instead, certain antenna parameters are to be emphasized here for the purpose of future design considerations on transmitter waveforms.

Figure IV-3 gives a perspective of how log-periodic antennas perform their sequential radiations when driven by an impulse. The first cell represents the highest-frequency element that is centered at f_{10} and is cut off at $f_{1\ell}$ and f_{1h}. It would extract whatever driving power that is within its bandwidth and radiate into space as the first dispersion pulse. At a certain time later, the second cell would perform in the same way and radiate into space a second dispersion pulse. This process would continue until the last cell centered at f_{No} performs its function and radiates the last dispersion pulse. The resultant pulse is then a combination of all these pulses as have been measured to have a long duration and time-varying instantaneous frequencies. The group delays of the pulses from each cell are derived in Equation D-19 to be

$$t_{no} = 1/2f_{no}\ell n(1+\delta) \qquad \text{(Eq. IV-4)}$$

where δ is the effective fractional bandwidth of the cells. The overall dispersed-pulse duration is equal to the delay time of the last radiation cell. Let T be the duration of a log-periodic antenna, then

$$T = 1/2f_{No}\ell n(1+\delta) = 1/2f_{\ell}\ell n(1+\delta) \qquad \text{(Eq. IV-5)}$$

$$f_{10} = \frac{f_{1h}}{1+\delta} = \frac{f_{1\ell}}{1-\delta}$$

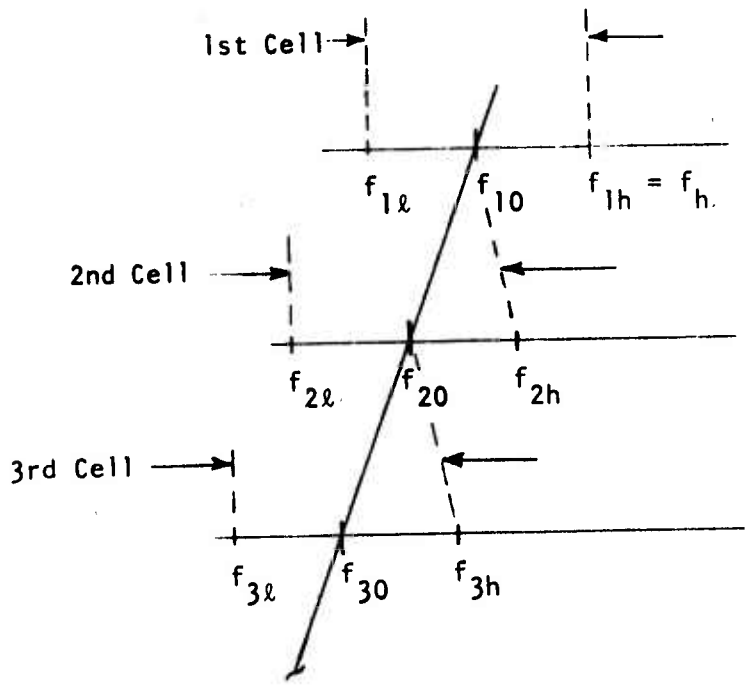
$$f_{20} = \frac{f_{10}}{1+\delta} = \frac{f_{2h}}{1+\delta} = \frac{f_{2\ell}}{1-\delta}$$

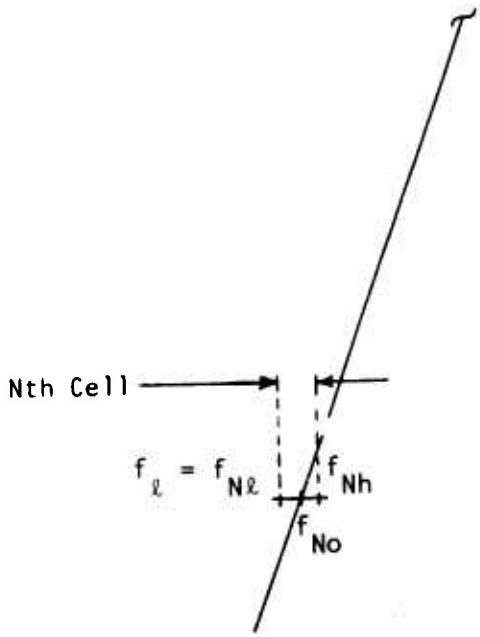
$$f_{30} = \frac{f_{10}}{(1+\delta)^2} = \frac{f_{20}}{(1+\delta)}$$

$$= \frac{f_{3h}}{1+\delta} = \frac{f_{3\ell}}{1-\delta}$$

$$f_{No} = \frac{f_{10}}{(1+\delta)^{(N-1)}} = \frac{f_{(N-1)o}}{1+\delta}$$

$$= \frac{f_{Nh}}{1+\delta} = \frac{f_{N\ell}}{1-\delta}$$





$$f_h = f_{1h} = f_{no}(1+\delta)^n$$

$$f_\ell = f_{N\ell} = \frac{(1-\delta)}{(1+\delta)^N} f_h$$

$$= \frac{(1-\delta)}{(1-\delta)^{N-n}} f_{no}$$

$$N = 1 + \frac{\log\ (f_{10}/f_{No})}{\log\ (1+\delta)}$$

Figure IV-3. Frequency Allocation for Radiation Cells of a Log-Periodic Antenna

If the lowest-frequency f_ℓ and the effective fractional bandwidth δ can be identified for an antenna, the dispersed-pulse duration of the antenna can be readily evaluated. This duration value T is critical in that any transmitter design for pulse compression will have to take it into consideration. For all six antennas measured in this program, their durations are analytically obtained as shown in Table IV-1.

The phase angles of the log-periodic antennas are obtained from measured data by restricting interpretation only into the bandwidths where the driving-source pulser has significant spectral intensity. A general expression that applies to all measured antenna is

$$\phi(f) = \ell n(f_o/f_h)/\ell n(1+\delta), \quad f_\ell \leq f \leq f_h \qquad \text{(Eq. IV-6)}$$

where f_h is the highest cutoff frequency at which the phase angle is chosen equal to zero as reference. For a given antenna, the phase angle may be uniquely established if f_h and the effective fractional bandwidth δ are known. Evidently, the phase slope is a constant determined by δ. Steeper slopes would result from smaller values of δ. The phase slopes of six measured antennas are evaluated as $1/\ell n(1+\delta)$ in Table IV-1 where δ is also given for every antenna to indicate their CW bandwidths. It is of interest to note that $\ell n\ (1+\delta)$ is approximately δ if δ is much less than unity which is the case for most practical LP antennas. As a result, the duration T for an LP antenna can be approximated as the inverse of the product of f_ℓ and δ. By decreasing f_ℓ or δ in antenna design by one-half, one can expect its dispersed pulse duration T to increased by a factor of 2. An increase of T by a factor of 4 can be expected if both f_ℓ and δ are reduced from the original design by one-half.

TABLE IV-1

ANALYTICALLY OBTAINED BT PRODUCTS COMPARED

WITH THOSE OBSERVED FROM MEASURED DATA

ANTENNA MODEL	$\frac{1}{\ell n(1+\delta)}$ [1]	δ	BANDWIDTH		DURATION $(2f_\ell \ell n (1+\delta)^{-1}$ (ns)	BT [2]	T (ns) [3]	BT [3]
			f_h (GHz)	f_ℓ (GHz)				
ASN-1232A CAVITY-BACKED	17.1	0.06	4.0	0.15	57	220	65	250
ASN-117AA CAVITY-BACKED	8.77	0.12	4.0	0.28	15.2	57.2	15	56
ASN-116A CAVITY-BACKED	8.95	0.118	10.0	0.625	7.1	66.6	7	66
APX-254A CROSSED DIPOLE	15.5	0.069	4.0	0.099	78.3	305.4	70	273
APN-995B PLANAR DIPOLE	13.4	0.079	1.1	0.097	69	69.2	70	70
APN-502A PYRAMIDAL	5.6	0.195	3.0	0.17	16.5	46.7	16	46

NOTES: (1) Slope determined from measured phase data
(2) Calculated by analytical model
(3) From Table III-2

After obtaining analytical models of phase angle $\theta(f)$ and the dispersion delay, T, they can be compared to evaluate T based on the lowest frequency, f_ℓ, observed in measured data. As for the highest frequency f_h, the measured data cannot be used because the driving source has inadequate spectral intensity in this region. Therefore, the f_h listed in Table IV-1 are obtained from CW specifications of the antennas. The BT products obtained by analytical models as well as CW specifications are listed for all six antennas. The data in the last two columns are obtained from measured T and CW-specified f_h. Good agreement in BT products can be easily established by comparisons.

Figure IV-4 presents a summary of phase characteristics of all six antennas measured. ASN-1232A is noted to have the steepest slope which indicates in turn that this antenna radiation cell has the smallest fractional bandwidth. Since the retardation time of successive radiation cells is inversely proportional to $\ell n(1+\delta) \cong \delta$, a smaller δ is equivalent to a larger delay if the same antenna volume is imposed on all antennas. Stated in another way, should all six antennas be made to have the same volume, the antenna with smallest δ would have the largest retardation time from one radiation cell to another. Of course, the frequencies involved would have to be the same for a meaningful discussion. Therefore, by assuming the same volume and the same bandwidth, antenna ASN-1232A would require the smallest antenna volume, if a given BT product is required of all the six antennas.

The antenna APN-502A has the largest $\delta = 0.195$ which indicates that each of its radiation cells has about 20 percent bandwidth. In terms of CW operations, this antenna is a very good antenna for generally required broadband CW operations. However, for pulse compression operation, this antenna is considered to be the poorest, because each radiation cell would be driven and radiating with the highest intensity among all the six antennas. In other words, this antenna has the smallest duration and would require the largest bandwidth for a specified BT product.

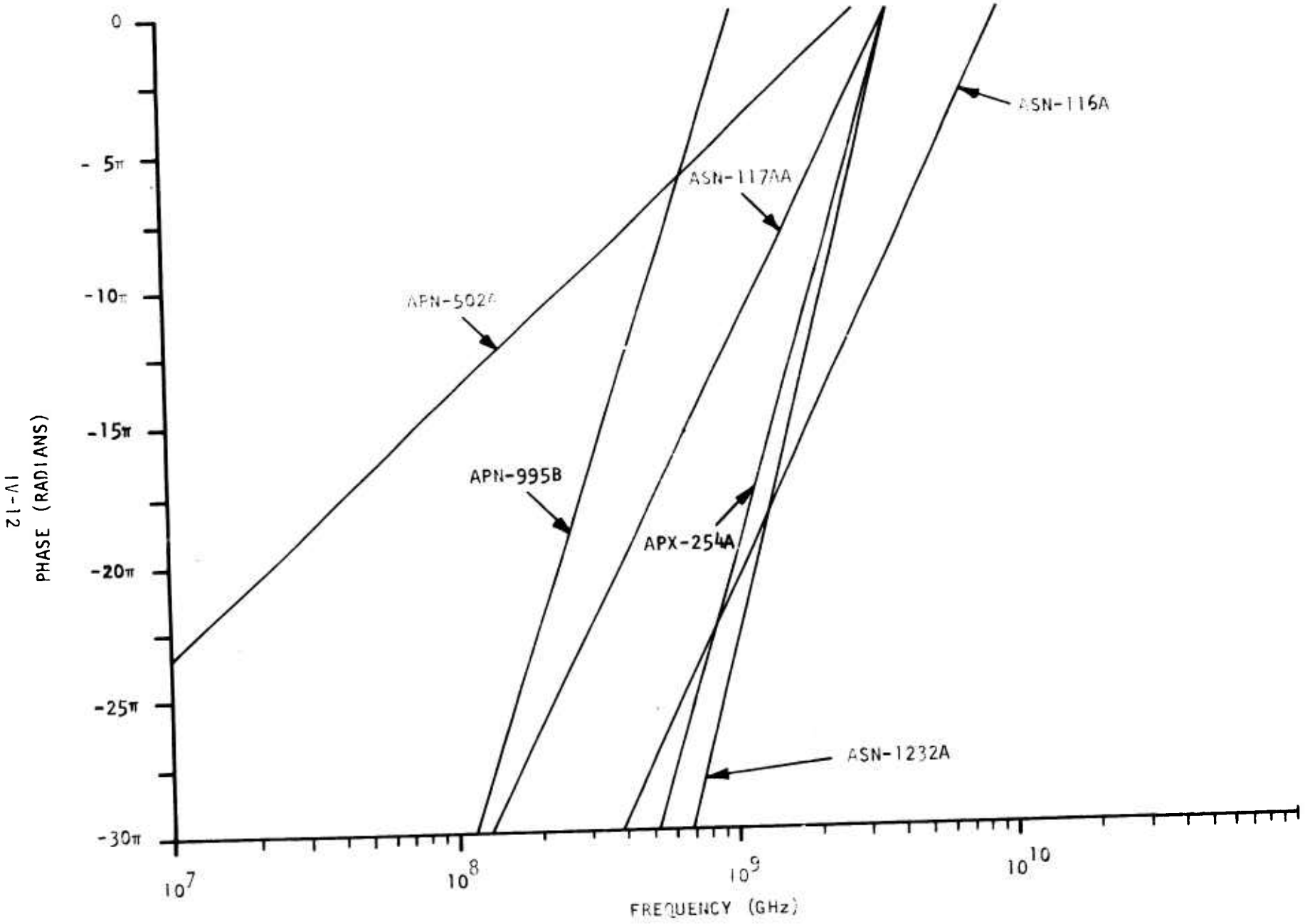


Figure IV-4. Phase Angles Obtained from Measurements

4. ELEMENTAL MODEL FOR QUADRATIC-PHASED ANTENNAS

That no quadratic-phased antenna is known to exist has made any extensive discussion on this antenna type less meaningful. Nevertheless, certain analytical treatments are possible and they are shown in Appendix D.

A simple model for this antenna is to assume that there would be N radiation cells, each of which has the same elemental bandwidth b such that

$$Nb = B \qquad \text{(Eq. IV-7)}$$

where B is the total operational bandwidth. A study on the feasibility of making this type of antenna an effective radiator is beyond the scope of the present program. The overall duration of the type of dispersive antenna has been obtained as

$$T = 1/b \qquad \text{(Eq. IV-8)}$$

Therefore, the BT product of this antenna is N which is used in connection with estimating the overall compression gain of volumetric antennas in Section VII.

SECTION V

PRACTICAL AND THEORETICAL MAXIMUM BANDWIDTH-TIME PRODUCTS OF LOG-PERIODIC ANTENNAS

1. INTRODUCTION

Theoretically, the bandwidth-time (BT) product of an antenna can be indefinitely increased by increasing either the bandwidth (B) or the duration (T) or both. For instance, antenna structures may be fabricated to radiate frequencies of 30 GHz or higher. But the structures would be required to have very fine, high precision elements and would eventually reach the limits of practicality for any given application. These limits will include such things as desired power handling capability and the availability of oscillators with the desired output characteristics.

In an effort to conduct meaningful maximum BT product evaluation, certain arbitrary constraints on antenna power handling capacity and size are imposed. The following section presents realistic estimates of achievable BT products, maximized according to these constraints, for three antennas: the conical log-spiral, the log-periodic dipole array, and the cavity-backed spiral. The details of this analysis, which relates the BT product to antenna parameters are given in Appendix H.

Following this, the analytical expression for the BT product of a conical spiral antenna is examined numerically and in the asymptotic limit in order to demonstrate the effects of varying antenna parameters. These results follow from an analysis given in Appendix G.

2. MAXIMUM BT PRODUCTS OF PRACTICAL ANTENNAS

Since there are no analytical limitations on the bandwidth of log-periodic antennas, the BT product of an antenna must be determined on the basis of practically realizable considerations. It will be assumed

that the smallest feed cable needed for a practical antenna to accept a reasonable amount of input power is one that has an outside diameter of 0.358 cm (.141 inch). Such a cable would typically be capable of delivering an average power ranging from 100 watts at 15 GHz to about 3000 watts at 50 MHz into a 50 ohm antenna. The feed cable diameter determines the highest operating frequency. The diameter of the first or highest frequency active region should be several times larger than the feed cable diameter for a well-defined radiation. To be more specific, maximum allowable antenna dimensions have been set as follows:

(1) Maximum Allowed Axial Length = 4 meters

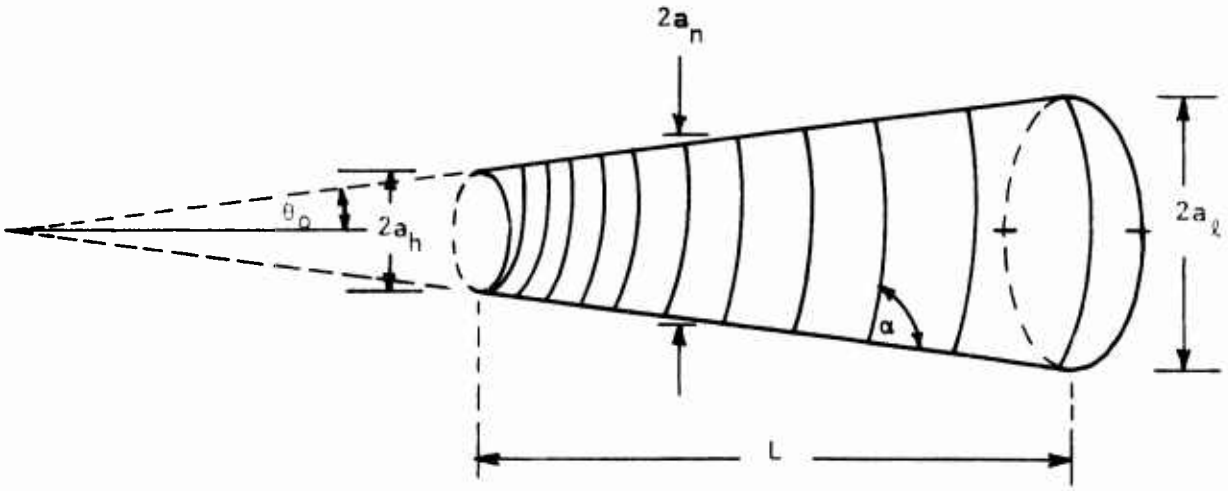
(2) Maximum Allowed Transverse Dimension (Aperture Diameter) = 2 meters

Under these constraints, Appendix H shows that practical antenna bandwidth becomes approximately

$$B \simeq (15 \text{ GHz} - 75 \text{ MHz}) = 14.93 \text{ GHz}$$

a value which fluctuates very little among the three antenna types. Duration ,or time dispersion is determined fundamentally by the amount of time the feed current takes to traverse the antenna structure. In general, maximum T requires maximizing the lengths of current paths along radiating elements relative to the overall geometrical antenna dimensions. This is equivalent to making the number of active regions in a given antenna volume as large as possible.

Figures V-1, V-2, and V-3 show the maximum BT products for practical field compression antennas of the conical spiral, log-periodic dipole array, and cavity-backed spiral type, respectively. It is seen that there is relatively little variation in the BT products of all three types:



θ_o = 14°

α = 85°

S = v/c = $\cos\alpha \cos\theta_o$ = 0.084

L = 4 meters

a_n/λ_n = 0.14

a_h = 0.0028 meters

a_ℓ = 1 meter

f_h = 15 GHz

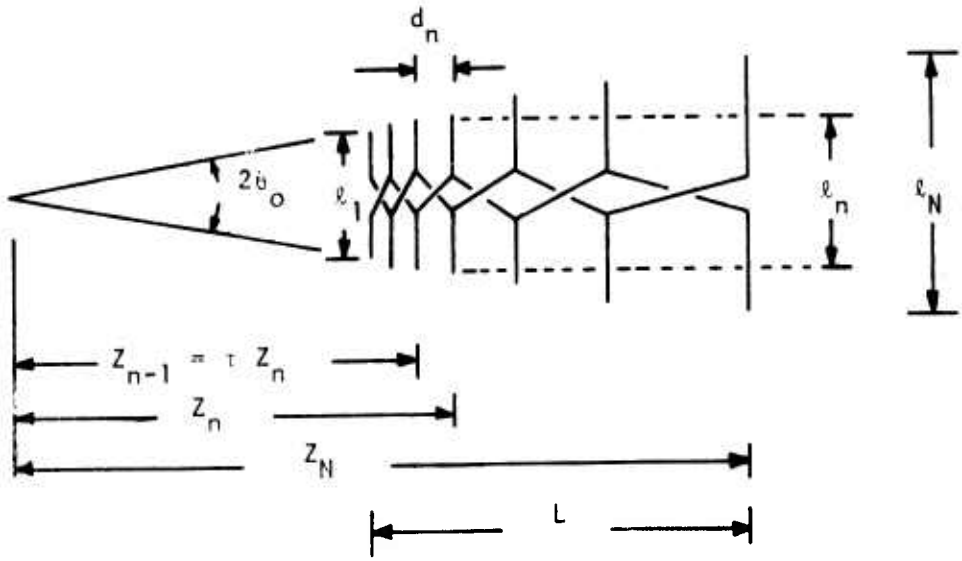
f_ℓ = .042 GHz

B = 14.96 GHz

T = 169.6 ns

BT = 2537

Figure V-1. Design Parameters of a Conical Spiral Antenna Having Maximum Practical BT Product for an Occupied Volume of 4 Cubic Meters: BT = 2537



θ_o = 14°

σ = d_n/ℓ_n = 0.1

S = v/c = 2σ = 0.2

τ = $1-2\sigma \tan\theta_o$ = 0.95

L = 4 meters

ℓ_1 = 0.01 meters

ℓ_N = 2 meters

f_h = 15 GHz

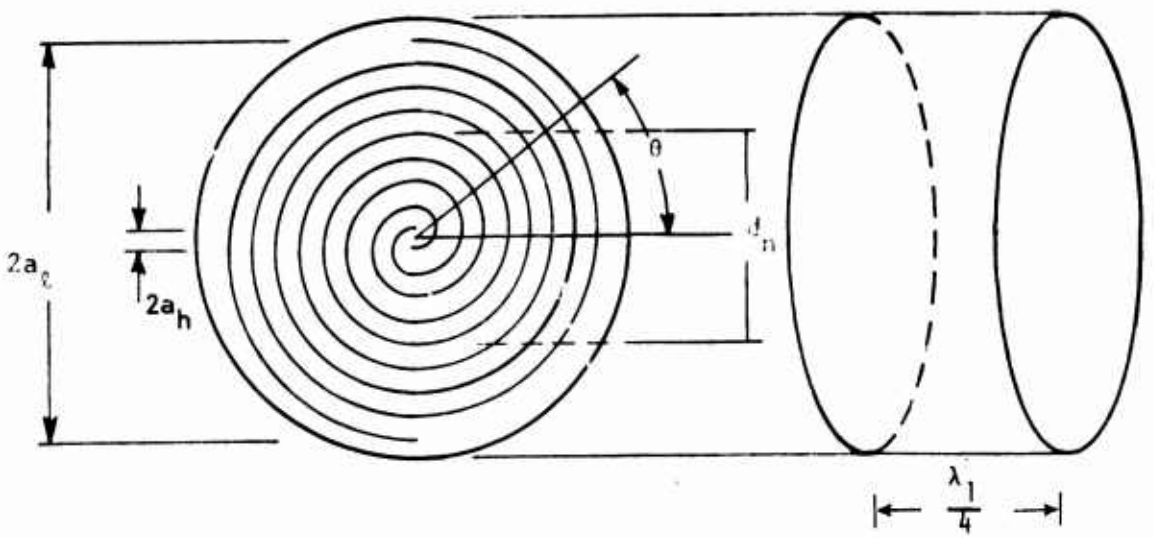
f_ℓ = 0.075 GHz

B = 14.93 GHz

T = 142.4 ns

BT = 2126

Figure V-2. Design Parameters of a Log-Periodic Dipole Array Antenna Having Maximum Practical BT Product for an Occupied Volume of 4 Cubic Meters: BT = 2126



$\phi = \cot^{-1} \frac{a_n(\theta\theta')}{a_n(\theta)}$, $\theta' = \theta + 1$ radian

ϕ = 88° 51'

d_n/λ_h = 0.28

a_h = .0028 meters

a_ℓ = 1 meter

T = Spiral length = 49.3 meters

$S = \frac{v}{c} = \frac{a_\ell - a_n}{T} = 0.02$

f_h = 15 GHz

f_ℓ = 0.042 GHz

B = 14.96 GHz

T = 164 ns

BT = 2453

Figure V-3. Design Parameters of a Cavity-Backed Spiral Antenna Having Maximum Practical BT Product for an Occupied Volume of 4.2 Cubic Meters: BT = 2453

(1) Conical Spiral Antenna: BT = 2537

(2) Log-Periodic Dipole Array: BT = 2126

(3) Cavity-Backed Spiral: BT = 2453

Also, all three antennas occupy essentially the same geometrical volume, (i.e., about 4 cubic meters). It may be concluded that, when normalized to the same unit volume, all log-periodic antennas give approximately the same maximum BT products.

3. THEORETICAL BD PRODUCT LIMITS

By allowing certain antenna parameters to vary, the BT product can approach any desired value. This can be demonstrated using the theoretical expression for the BT product of a conical spiral antenna as derived in Appendix H. In terms of antenna parameters

$$BT\ (A_h,\ L,\ \theta_o, \alpha) = \left(\frac{L \tan \theta_o}{A_h}\right) \left[\frac{1}{2\pi\left(1 + \frac{A_h}{L \tan \theta_o}\right)} \cdot \frac{\tan \alpha}{\tan \theta_o} \right.$$

$$\left. - \frac{1}{\pi \tan \theta_o} \left(\frac{\sin \alpha \cos \theta_o}{1 + \cos \alpha \cos \theta_o}\right) \sinh\left(\frac{\pi \sin \theta_o}{\tan \alpha}\right) \right] \qquad \text{(Eq. V-1)}$$

This product depends, in general, upon four independent parameters:

(1) A_h = The cone radius at the highest frequency active region.

(2) L = Allowed axial length of the conical antenna.

(3) θ_o = The half-cone angle.

(4) α = The spiral wrap rate angle.

The number of independent variables can be reduced as follows. Let the maximum antenna aperture be fixed, this determines A_ℓ. The axial length L may then be expressed as a function of A_h and θ_o

$$L(A_h, \theta_o) = \frac{A_\ell - A_h}{\tan \theta_o} \qquad \text{(Eq. V-2)}$$

Consequently, the number of independent variables has been reduced to three: A_h, θ_o and α. Under the assumption that A_h is also fixed by the size of the input cable driving the highest frequency active region, then

$$L \tan \theta_o = A_\ell - A_h = \text{constant} \qquad \text{(Eq. V-3)}$$

In this case, the BT product depends only on the half-cone angle and on the wrap rate angle of the antenna. The BT product has been numerically evaluated in this case for half-cone angles ranging from $\theta_o = 40^\circ$ to $\theta_o = 0.0167^\circ$ and for wrap rate angles from $\alpha = 60^\circ$ to $\alpha = 89.9833^\circ$. The results are shown as two sets of parametric curves in Figure V-4:

$$BT = BT(\theta_o) \quad \text{for various } \alpha \qquad \text{(Eq. V-4)}$$

and

$$BT = BT(\alpha) \quad \text{for various } \theta_o \qquad \text{(Eq. V-5)}$$

In all cases, A_ℓ = 1 meter and A_h = .00284 meters. For the set of curves described by Equation V-4, the BT products approach infinity asymptotically as $\theta_o \to 0$. For any given α, the axial length of the antenna also approaches infinity as $\theta_o \to 0^\circ$. On the other hand, the curves following

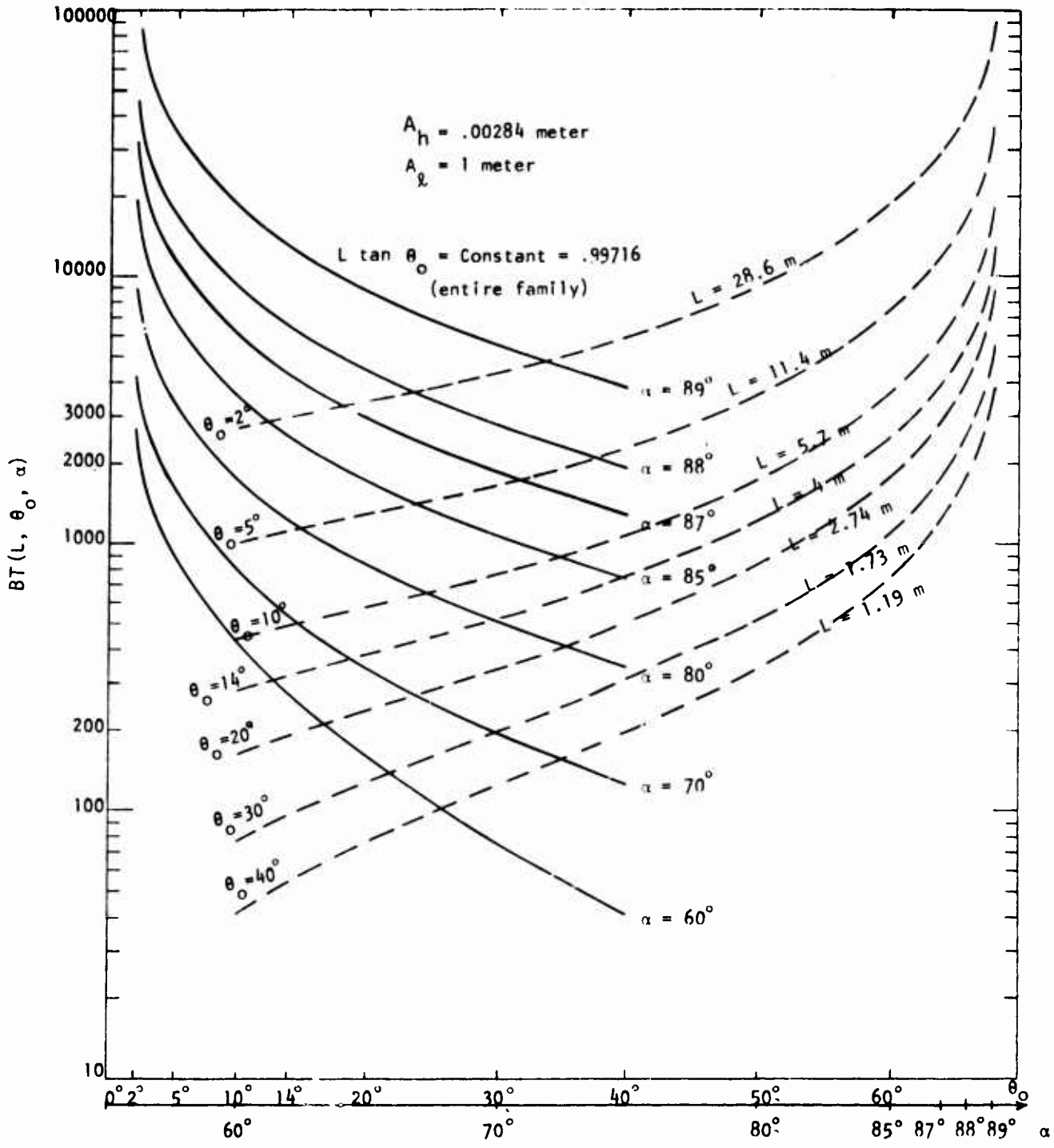


Figure V-4. Parametric Curves for BT Versus θ_o and BT Versus α for A_h = .00284 Meters and A_ℓ = 1° Meter for a Conical Spiral Antenna

Equation V-5 show that L is a constant along one curve. All curves also approach infinite BT product asymptotically as $\alpha \rightarrow 90^{\circ}$.

These curves demonstrate clearly that the BT product increases as θ_o becomes smaller and α becomes larger. As the cone angle decreases and the spiral turns become closer together on the cone, the BT product increases.

Consider the BT versus α curve for $\theta_o = 14^{\circ}$ which corresponds to the antenna design given in Figure V-1. Along this curve, L = 4 meters and the bandwidth is essentially constant (as seen by examining Equation H-66). At $\alpha = 85^{\circ}$ the BT product is 2537 as given in Table V-1. This product is doubled, BT = 5074, when $\alpha = 88^{\circ}$ - a change of only 3° in the wrap rate. Since the bandwidth remains constant, it is observed that the duration has doubled. This is directly related to the fact that the length of spiral conductor has doubled. An important point to realize here is the that bandwidth and duration do not need to change in proportion to each other.

It is shown in Figure V-5 that the BT product increases linearly as the antenna volume increases whenever the wrap rate α is constant and A_h and A_ℓ are fixed. Since each complete spiral turn constitutes one active radiation cell of the antenna and since the number of spiral turns increases as α becomes larger for a given volume, then it is clear that α is proportional to the radiation cell density. Therefore, there are two basic ways of increasing BT products: (1) by increasing the occupied antenna volume while keeping the radiation cell density constant; or (2) by maintaining constant antenna volume and increasing the radiation cell density (e.g., increasing α). The family of curves for BT versus θ_o for various α in Figure V-1 may be interpreted in terms of (1), where as BT versus α curves for various θ_o represent method (2). In order to realize the maximum BT product, the antenna designer would make the antenna volume as large as possible and then increase the radiation cell density within this volume to

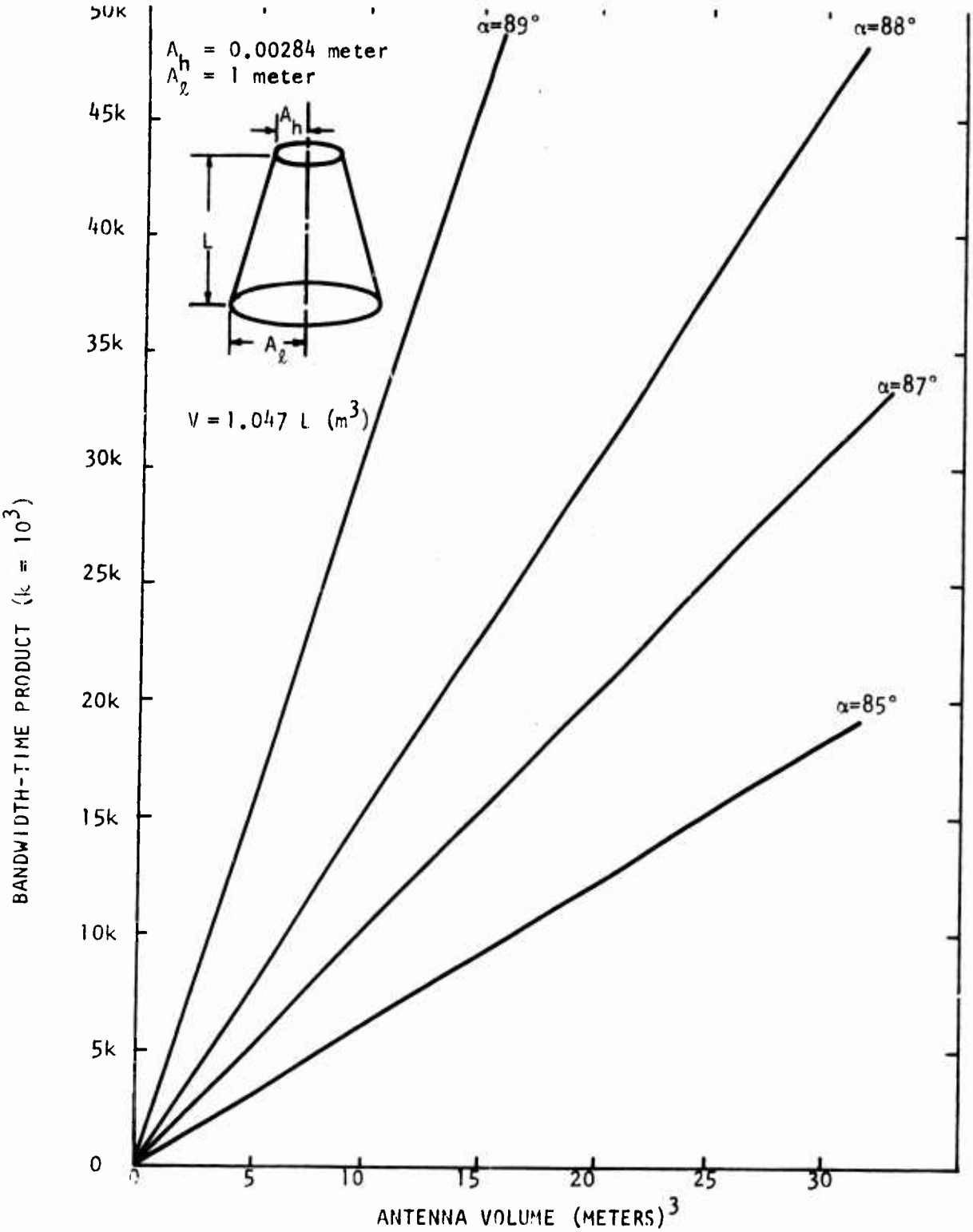


Figure V-5. Bandwidth-Time Product as a Function of Antenna Volume for Various Radiation Cell Densities. (The wrap rate angle α is proportional to the number of active radiation cells per unit volume.)

TABLE V-1

BANDWIDTH-TIME PRODUCTS FOR CONICAL SPIRAL ANTENNAS OF VARIOUS LENGTHS HAVING FIXED TRUNCATED CONE DIAMETERS: A_h = 0.00284 METER AND A_ℓ = 1 METER

	A_h = 0.00284 METER			A_ℓ = 1 METER	
LENGTH L (METERS)	θ_o (DEGREES)	α (DEGREES)	BANDWIDTH B (GHz)	DURATION T (ns)	BT
28.6	2	90	16.75	326,857	5,474,618
		89	16.46	5,552	91,411
		+88	16.18	2,824	45,683
		87	15.90	1,914	30,430
		85	15.35	1,186	18,211
11.4	5	90	16.70	130,882	2,185,173
		89	16.41	2,223	36,483
		88	16.13	1,130	18,227
		87	15.85	766	12,136
		*85	15.31	474	7,252
5.7	10	90	16.50	65,691	1,084,224
		89	16.23	1,115	18,099
		88	15.95	567	9,038
		87	15.68	384	6,013
		85	15.15	237	3,585
4.0	14	90	16.26	47,152	766,773
		89	15.99	800	12,798
		88	15.72	406	6,389
		87	15.46	275	4,248
		85	14.94	169	2,528
2.7	20	90	15.75	33,352	525,257
		89	15.50	566	8,766
		88	15.24	287	4,374
		87	14.99	194	2,906
		85	14.51	119	1,725

+ $\rho = 2^\circ$

* $\rho = 5^\circ$

the maximum achievable value subject to power-handling constraints. These conclusions are general and apply to all log-periodic antennas.

A tabulation of maximum BT products for conical spiral antennas which all have the same truncated cone radii is presented in Table V-1.

In order to analytically establish the limit of the BT product, a convenient asymptotic expression is derived in Appendix G. By allowing the limiting case of small θ_o and large α, that is, in the limit $0 < \rho < < 1$ with

$$\alpha = \frac{\pi}{2} - \rho \qquad \text{(Eq. V-6)}$$

$$\theta_o = \rho \ , \qquad \text{(Eq. V-7)}$$

Equation V-1 reduces to

$$BT\ (\rho;\ A_h,\ L) = \frac{1}{2\pi}\ \frac{\left(\frac{L}{A_h}\right)^2}{\left(1 + \frac{L\rho}{A_h}\right)}\ - \frac{L\rho^2}{A_h} \qquad \text{(Eq. V-8)}$$

There are two subcases of Equation V-8 because $\rho < < 1$ does exclude either $\rho < < A_h/L$ or $\rho > > A_h/L$. These are

$$BT\ (A_h,\ L) = \frac{1}{2\pi}\ \left(\frac{L}{A_h}\right)^2, \quad \rho < < \frac{A_h}{L} \qquad \text{(Eq. V-9)}$$

and

$$BT\ (\delta,\ A_h, L) = \frac{1}{2\pi}\left(\frac{L}{A_h\rho}\right), \quad \rho > > \frac{A_h}{L} \qquad \text{(Eq. V-10)}$$

These limiting cases show clearly that, theoretically, BT can be as large as desired. However, for a given set of finite design parameters (δ, A_h, L), there will always be a definite upper limit on BT. Two examples that give the maximum BT products for various ρ are included in Table V-1. The asymptotic expressions Equations V-9 and V-10, have limited usefulness, in practice, because there will likely always be a constraint on the allowed antenna volume. Since θ_o should always be maximized to these dimensions in order to maximize both bandwidth and duration, and since α should always be made as large as possible regardless of volume, then invariably these two angles will approach limiting values other than would be characterized by Equation V-6 and V-7. The importance of Equations V-9 and V-10 is that they demonstrate, in a simple way, the manner in which the BT product approaches infinity for various cases and may be useful in subsequent theoretical studies.

4. LIMIT OF BT PRODUCT - ANOTHER VIEW

In addition to arriving at BT product limits through geometrical parameters, analytical models based upon electrical parameters can also be used to establish BT product limits. The electrical parameters needed for establishing BT products are the number N of total radiation cells in a dispersive antenna and the effective fractional bandwidth δ of each cell. These two parameters are defined analytically in Appendix D. The expressions for BT products in terms of these two parameters are given in Equations VII-5 through VII-10.

Essentially, the BT products can be obtained independently without stating antenna size by specifying the number of radiation cells to be built into a specified volume. A family of BT curves is plotted in Figure VII-7 with pertinent discussions. These curves are consistent with the results arrived at in the last section using geometrical parameters. This fact is discussed in Section VII by introducing a practically achievable elemental bandwidth $\delta = 0.1$.

SECTION VI

NEAR FIELD COMPRESSION AND POWER HANDLING CAPACITY OF ANTENNAS

1. INTRODUCTORY COMMENTS

It has been recognized that the near-field regions of antennas deserve special consideration as a result of potential high field strengths produced there by field compression. It is possible for peak field strengths in the near-field to exceed the dielectric breakdown strength of air. Potentially, such a situation could lead to quenching of the compressed field and preventing radiation from antennas. The present analysis demonstrates the mechanism of near-field compression and suggests means for avoiding this problem.

In order to set limits on the peak amplitude of compressed fields in the near-field, two analytical antenna models have been used. As described in Appendix I, these include a dipole array and a cavity-backed spiral. Inherently, most of the longitudinal antenna structures designed to radiate in the backward direction, such as typified by the dipole array, maximum field compression occurs at the feed point. This is so because the longitudinal time delays tend to produce a field maximum right on the end of the antenna. On the other hand, a broadside radiating structure, such as a cavity-backed spiral, will produce a peak amplitude at a point some distance away from the aperture plane. Pertinent numerical results are to be given here for the purpose of quantitatively comparing the near-field behaviors of these two types of antennas.

A useful curve relating the maximum allowable field strength as a function of compressed-pulse duration will also be given to establish an important conclusion. That is, the power-handling capacities of existing

antennas will be exceeded before compressed-field intensities could exceed the air-breakdown level.

2. PEAK AMPLITUDE VARIATION IN THE NEAR FIELD

Two analytical antenna models have been used to establish upper and lower bounds on both the magnitude and location of near-field compressed pulse values.

Upper bounds have been established using a dipole array model (Appendix J) to approximate the radiation characteristics of a log-periodic antenna. However, in this model the phase centers of radiating elements are all located at the feed point which, of course forces peak compression to also occur there. For this reason the resulting near-field amplitude variation is considered representative of the worst case to be expected for antennas radiating with longitudinal time delays. The model is designed to radiate over a bandwidth of 0.2 GHz to 10.2 GHz, with a maximum aperture of $D = \lambda/2$ at 0.2 GHz. Using the far-zone criterion $2D^2/\lambda$, the minimum far-field distance is 0.75 meters. Field compression as a function of both time and distance is shown in Figure VI-1 for distances of 1.5 cm to 9.5 cm from the antenna. The compressed pulse amplitudes tend to increase exponentially toward the antenna, the total voltage swing at 1.5 cm being 1300 kV/m. The pulse duration also increases as the aperture plane is approached. This extreme buildup in amplitude and duration results from the coincidence of all phase centers of radiating elements in the present antenna model, and is thus to be treated as the worst possible case. Since no other arrangement can be made to produce higher near-field level, the curves in Figure VI-1 can be used as the upper bounds on near-field compression maxima.

An analytical model approximating the transverse delay characteristics of a cavity-backed spiral antenna has been used in Appendix I to establish

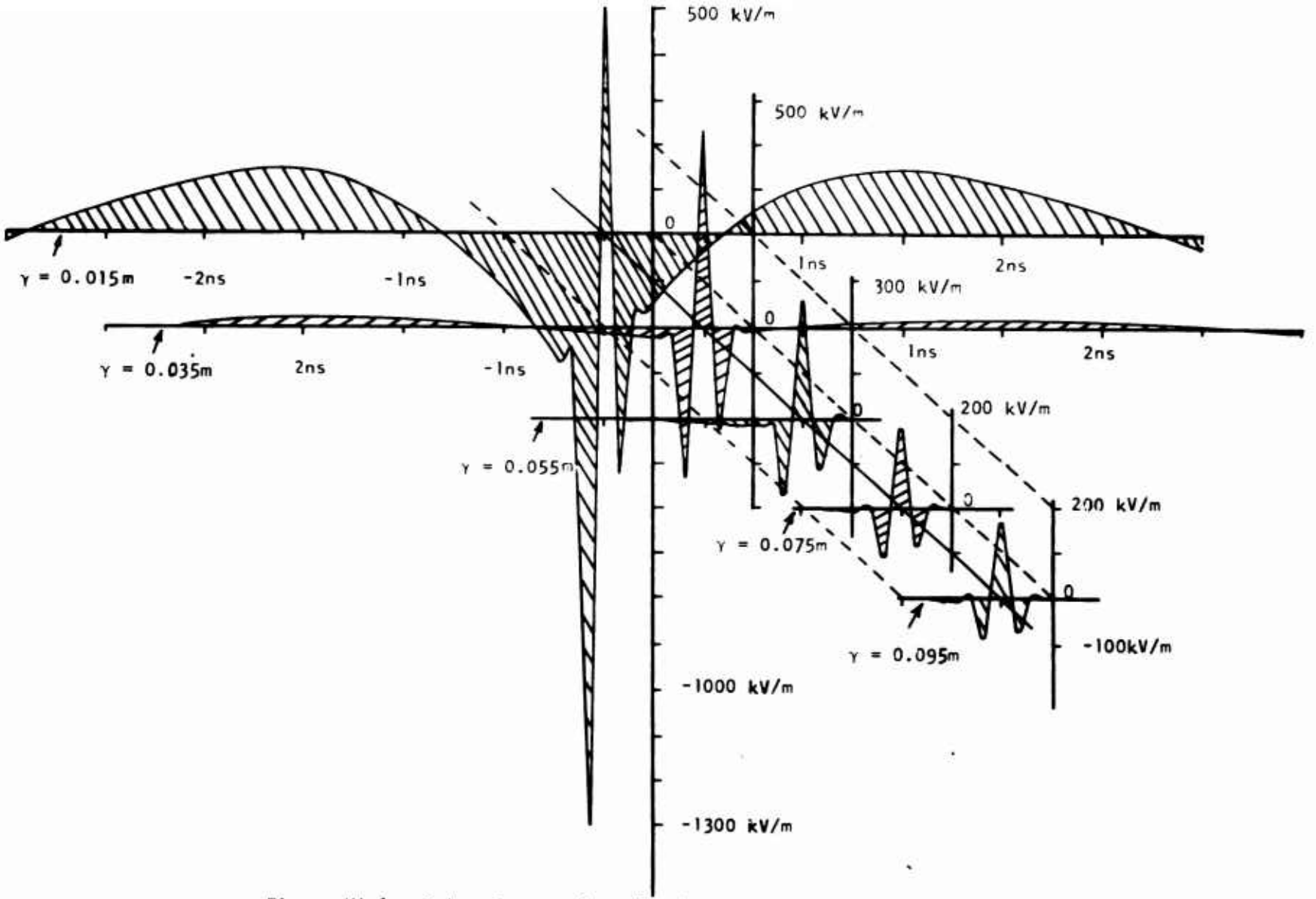


Figure VI-1. Pulse Compressions in the Near-Zone for Log-Periodic Array with Coincident Phase Centers

a lower bound on peak compressed field variation in the near field. This model is designed to operate over the same bandwidth of 0.2 GHz to 10.2 GHz and has a total of 37 active regions displaced log-periodically across the aperture plane. Time delay is therefore in a plane transverse to the radiation direction. The effect of choosing the transverse dispersion on both spectral amplitude and phase angle of the compressed pulse is shown in Figure VI-2. As the on-axis field point moves closer to the aperture plane, the weighting of spectral amplitude shifts toward higher frequencies. In the limit of approaching toward aperture plane the only field contribution would be that of the applied voltage across the antenna feed terminal. As the near-field distance decreases, less and less contribution would be received from the low-frequency radiation cells. As a result, the time-domain compressed pulse amplitude will also decrease. The near-field variation of the compressed pulse amplitudes and durations are shown in Figure VI-3. As the field is sampled along radiation distance the peak amplitude starts at a relatively low level, increases to a maximum at about 3.5 cm, and then begins to fall off as 1/R as the far-field zone is reached. The most significant result of the broadside array is that its near-zone compressed pulses (Figure VI-3) do not increase exponentially toward the aperture center as those shown in Figure VI-1 for coincident-phase-center compression. To give an easier comparison, Figure VI-4 summarizes the peak values of the two compressions. At the distance of 10 cm, the two compressed peak values are about equal. This is not surprising because the same operating bandwidth is used for both antennas. For other distances beyond 10 cm, the peak values decrease approximately in inverse proportion with the distances.

3. ALLOWABLE PEAK COMPRESSED FIELD AMPLITUDE

Using Figure VI-4 as a basis, it is seen that for log-periodic antennas having 10 GHz bandwidth, the near-field compression amplitude may approach 1 MV/m. For antennas possessing a larger bandwidth or

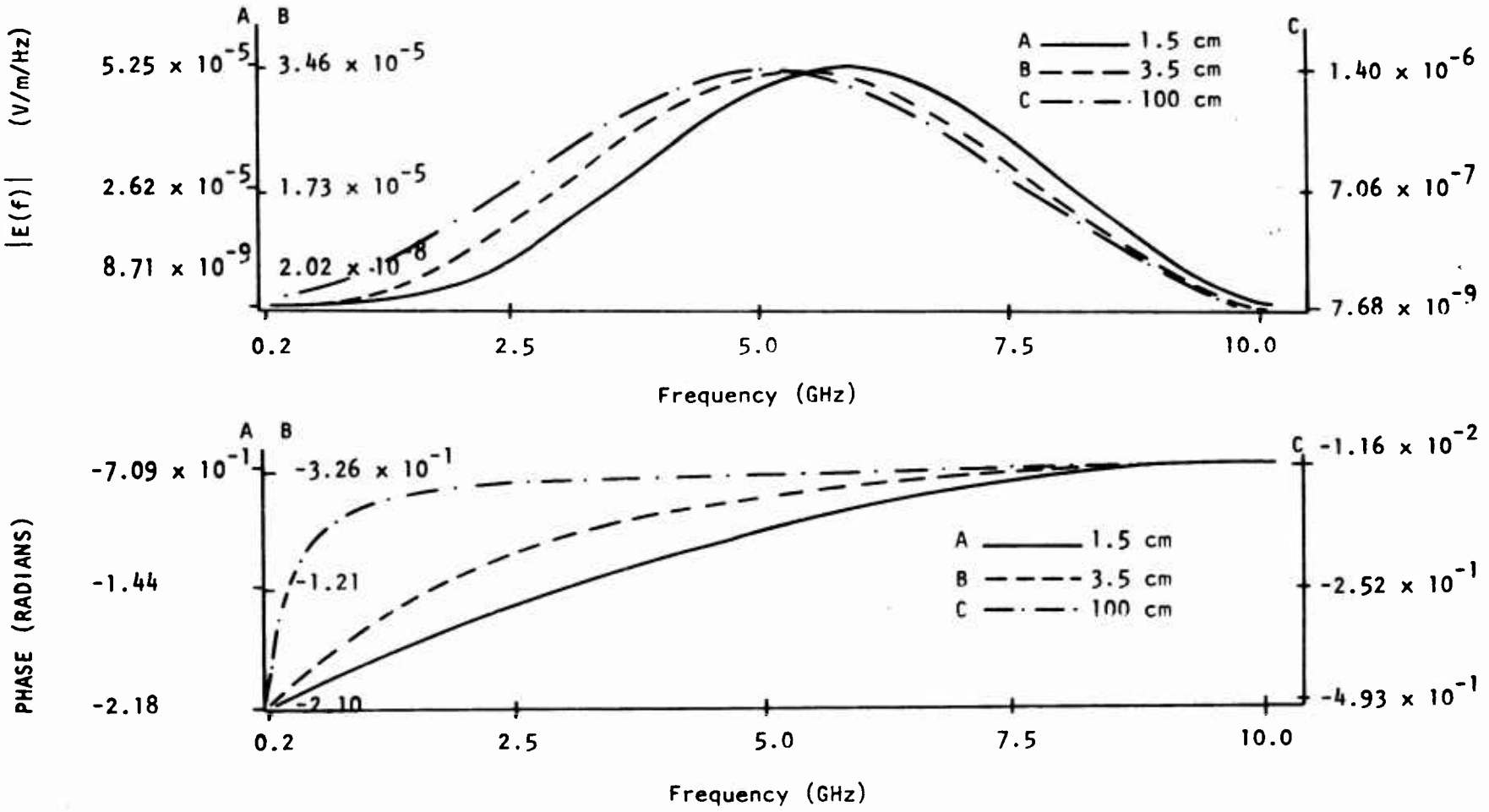


Figure VI-2. Smoothed Spectral Distribution of Theoretical Model Approximating a Cavity-Backed Spiral Antenna Which Compresses Pulses at r = 1.5 cm, 3.5 cm, and 100 cm

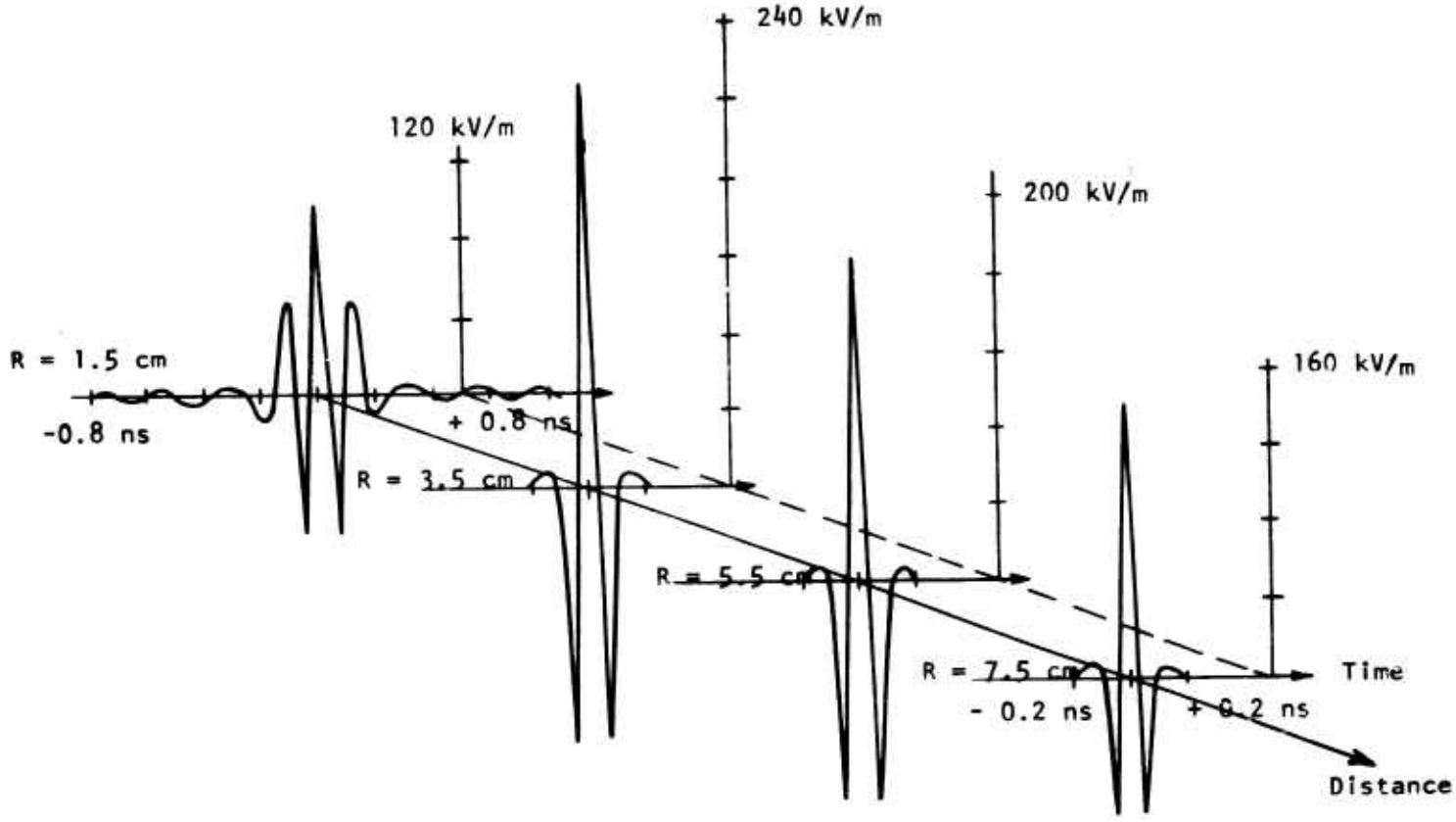


Figure VI-3. Near-Field Space-Time Pulse Compression for an Antenna Model Possessing a Transverse Time Delay Characteristic

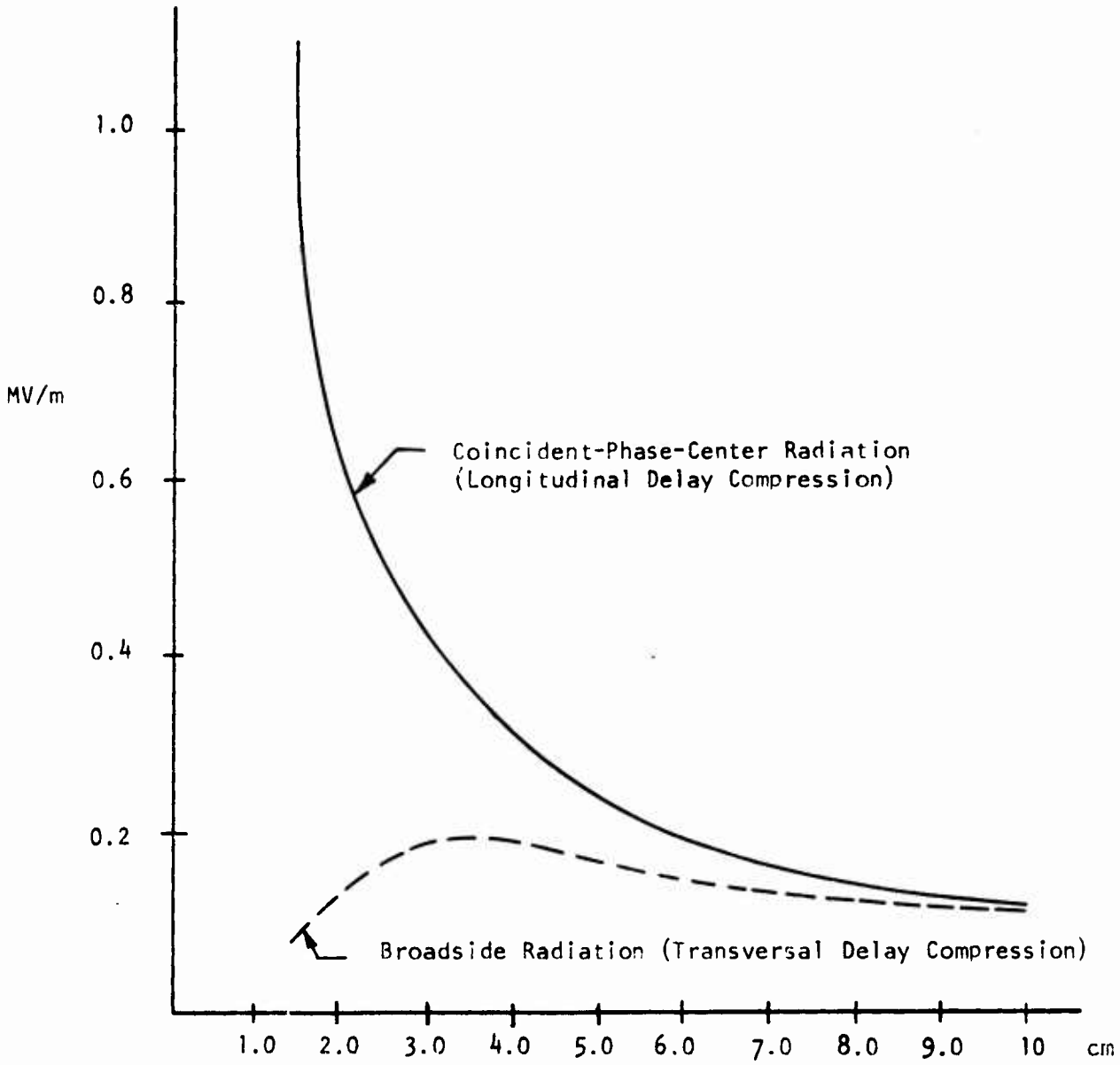


Figure VI-4. Compressed Pulse Peaks as Functions of Radiation Distance r(cm)

radiating with a higher current it is possible for peak compressed fields to exceed the dielectric breakdown strength of air, 3 megavolts/meter. Such a situation could lead to quenching of the compressed field, but these processes do not occur spontaneously. It is discussed in Appendix J that even when an overvoltage condition exists as a result of field compression, no breakdown will occur provided the compressed pulse width is less than its breakdown lag time. This is the time between the onset of electron avalanche and that point at which the process will not quench, that is, it is the minimum time necessary for breakdown to occur. Figure VI-5 shows the variation in breakdown times for field strengths larger than the static breakdown strength of air. As an illustration of the use of this curve, assume a field has been compressed to a duration of 0.1 ns. The maximum compressed pulse that can be radiated without causing breakdown is that whose breakdown lag time just equals 0.1 ns, or about 18 megavolts/meter. Table VI-1 provides some data on allowable pulse durations for various field strengths above the static air breakdown. For example, the practical design examples of Section V have a bandwidth of about 15 GHz. If a uniform distribution is assumed, their far-zone compressed pulse would have a pulse width of about 133 picoseconds. From Table VI-1, the possible breakdown field strength for a pulse duration of 133 ps would be about 17 MV/m. For a design bandwidth of 10 GHz with uniform distribution, the compressed-pulse duration in the far zone would be about 200 ps, and the possible air breakdown would take place if the electric field strength is 15 MV/m or larger. The two examples shown in Figures VI-1 and VI-3 are computed using a 10 GHz bandwidth with Hamming's weighting. Therefore, the compressed pulse width is about 400 ps which would require a field strength of 13 MV/m or larger to cause air breakdown. The next section gives some examples on finding antenna currents when a field intensity is specified.

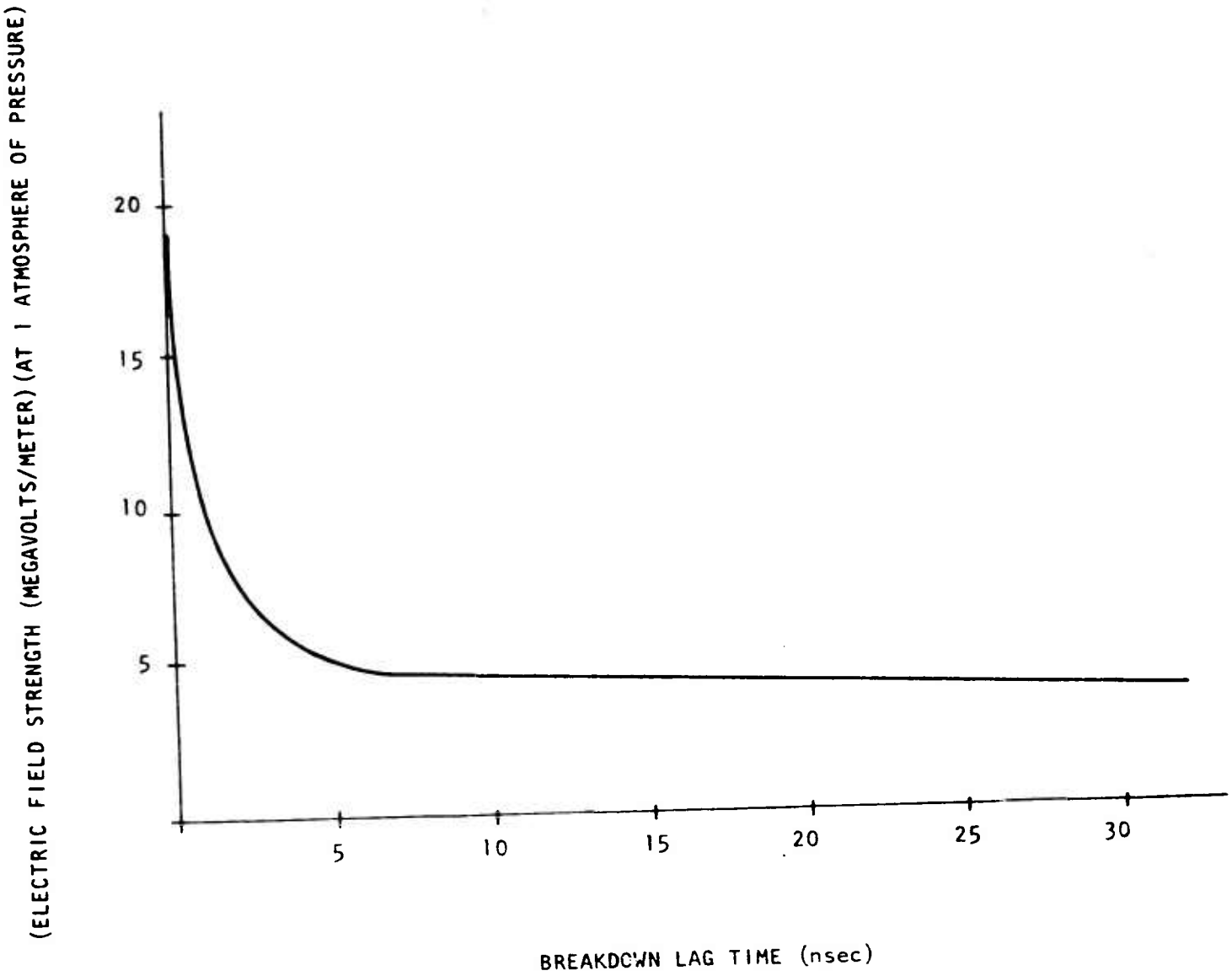


Figure VI-5. When Field Strengths Exceed the Dielectric Strength of Air at a Given Pressure; a Minimum Time is Required Before Breakdown Occurs

TABLE VI-1

MAXIMUM ALLOWED COMPRESSED PULSE DURATIONS
FOR VARIOUS FIELD STRENGTHS

ELECTRIC FIELD STRENGTH (MV/m)	MAXIMUM ALLOWED COMPRESSED PULSE DURATION (ns)
49	.02
34	.04
26	.06
22	.08
18	.1
15	.2
13	.4
11	.6
9.8	1
7.6	2
6.3	3
5.5	4
5.1	5
3.8	30
3 (dc AIR BREAKDOWN)	∞

4. ESTIMATES OF ANTENNA CURRENTS

Suppose log-periodic antennas are operating over a 10 GHz bandwidth with uniform distribution. The two examples given in Figures VI-1 and VI-3 are obtained by assuming the spectral current density of 10^{-8} Amp/Hz as specified in Appendix I. Since the widest elemental bandwidth $f_{no}\delta$ takes place in the highest-frequency radiation cell, the largest current is expected in the highest-frequency element of log-periodic antennas. Consider $\delta = 0.1$ as an example, the current flowing in the first radiating element can be calculated as

$$I_1 = (f_{10}\delta) \times 10^{-8}$$

$$= (9.1 \times 10^9 \times 0.1) \times 10^{-8} = 9.1 \text{ Amperes}$$

where f_{10} is the center frequency of the highest frequency element. This current means that the element would have to be able to handle an amount of average power

$$P_1 = \frac{1}{2} I_1^2 R \approx \frac{1}{2} I_1^2 (70)$$

$$= 2.4 \times 10^3 \text{ watts}$$

where R is taken equal to 70 Ohms as the radiation resistance of the antenna element. If the operating bandwidth is increased to 15 GHz, the current in the first element with $\delta = 0.1$ is

$$I_1 = (f_{10}\delta) \times 10^{-8}$$

$$= (13.6 \times 10^4 \times 0.1) \times 10^{-8} = 13.6 \text{ Amperes}$$

and the average power needed to be handled by this element is

$$P_1 = \frac{1}{2} I_1^2 R \approx \frac{1}{2} I_1^2 (70)$$

$$= 6.5 \times 10^3 \text{ watts}$$

The above two power requirements are listed in the last columns of Table VI-2. For Hamming's weighting instead of uniform distribution, the highest frequency radiation cell has a distribution (see Figure C-2 for example) about 0.1 of the maximum spectral density. Therefore, the power requirements would be reduced by a factor of 100. This factor is very significant in that a given log-periodic antenna with a uniform spectral distribution can be adjusted for its power-handling capability by changing spectral distribution for its compressed pulse. While power level in the highest-frequency radiation is reduced by a factor of 100, the near-field peak would be reduced by a factor of about 10, and the far-field compressed peak would be reduced by a factor of only 2. Therefore, as far as log-periodic antennas are concerned, the limit of power-handling would be determined by the highest-frequency radiation cell, and a reduction of 20 dB in its power would mean 0.1 reduction in its near-field compression and only 0.5 reduction in the compressed far fields.

5. POWER LIMIT AND FIELD LIMIT

Ultimate feasibility of field compression concepts appear to have a limit imposed by either maximum allowable field strength in the air or the maximum allowable power in the antenna. The former limitation has been established by upper and lower bounds of two antenna models. The later limitation is to be imposed by antenna design details for which no complete information is currently available, although the 6.5 kW for 15 GHz in Table VI-2 appears to be far beyond common specifications. A combined application of Tables VI-1 and VI-2, together with the

TABLE VI-2

PEAK COMPRESSED FIELDS AND AVERAGE POWERS FOR THE FIRST RADIATION CELL OF TWO LOG-PERIODIC ANTENNA MODELS OPERATED WITH TWO BANDWIDTHS

			NEAR-FIELD (MV/m)		
DISTRIBUTION	BANDWIDTH (GHz)	FAR-FIELD (V/m at 100 m)	LOWER-BOUND TRANSVERSAL DELAY	UPPER-BOUND LONGITUDINAL DELAY	AVERAGE POWE (kW)
UNIFORM	10	260	≈(0.8, 2.0) at (1.5, 3.5) cm	≈(11.0, 3.7) at (1.5, 3.5) cm	2.9
	15	390	≈(1.2, 3.0) at (1.0, 2.32) cm	≈(16.5, 5.65) at (1.0, 2.33) cm	6.5
HAMMING	10	130	(0.08, 0.2)* at (1.5, 3.5) cm	(1.1, 0.37)* at (1.5, 3.5) cm	0.029
	15	195	≈(0.12, 0.3) at (1.0, 2.32) cm	≈(1.65, 0.565) at (1.0, 2.33) cm	0.065

Effective fractional bandwidth $\delta = 0.1$ is used

Values with ξ is from Appendix J

Values with ≈ are approximately estimated

Values with * are from Figure VI-4

Spectral density of antenna current is 10^{-8} Amp/Hz maximum

upper-bound near-zone compression in Figure VI-3, gives no combination of near-zone field peak and duration that would exceed air breakdown. Therefore, it is reasonable to conclude that, according to current technology, the limit of pulse compression by a single log-periodic antenna would be limited by its power-handling capacity before air breakdown would take place. To overcome this limitation is to employ an array of log-periodic antennas as discussed in the next section.

SECTION VII

GAIN OF FIELD-COMPRESSION RADIATION

Intensification of a radiated field by an antenna is considered here as compression gain. Two types of field compressions may be better known as the directivity gain of a conventional antenna or array under monochromatic radiation, and the pulse-width compression gain of a dispersive broadband antenna.

Spatial angle-compression of planar antennas or arrays will be briefly discussed first to provide certain relationships concerning ultimate gain of a dispersive antenna array. Dispersive antennas are defined as those capable of radiating over large bandwidths with an orderly sequence of subbandwidths. These antennas can compress the radiated pulse width along the direction of propagation and are called temporal field compression antennas.

The objective of formulating the gain of a field-compression radiator is to obtain simple expressions by which both spatial and temporal field compressions can be properly evaluated. A simple concept of a radiation cell will be first defined to facilitate the formulation. Various aspects of compression gains are then developed to lead to the evaluation of maximum possible compression gain for an antenna occupying a specified volume.

1. RADIATION CELL

Fundamental radiation sources are known to be either electric dipole or magnetic dipole. Both of them can be made into efficient radiators when their linear dimensions are on the order of one-half wavelength. Their

gains are approximately $\pi/2$ when defined as the increase in the maximum power density over a fictitious omnidirectional radiator.

For most operational radiators such as log-periodic antennas or an electric dipole placed one-quarter wavelength above a large ground plane, the directivity gains are further increased to about 2π or more as discussed in Appendix A.

A radiation cell is defined for field-compression purposes as the fundamental radiation volume which can radiate effectively over an operating bandwidth. Practical designs have many variations that can cover the operating bandwidth from a few percent to more than 100 percent of the operating center frequency. For log-periodic antennas, the fractional bandwidth is typically from 3 percent to 30 percent of the operating center frequency. The smallest volume of an effective radiation cell is approximately $(\lambda/2)^3$ where λ is the operating wavelength of the radiator.

A practical radiation cell radiates a power-density pattern of an approximately cardioid-shape which is symmetric around the axis of radiation. This type of radiation cell has an approximate directivity gain as

$$D = \eta\ (4\pi A/\lambda^2)\ (4\pi L/\lambda) \qquad \text{(Eq. VII-1)}$$

$$= \pi^2/\sqrt{2} = 7$$

where the value is obtained by assuming $L = \lambda/2$, $A = (\lambda/2)^2$ and $\eta = (1/\sqrt{2})^3$. That is, if the radiation cell is a cube of one-half wavelength on its side and the excitation current is cosinusoidally distributed to have an average value of 0.707 peak value, the directivity gain would be equal to 7 which is approximately the value of most log-periodic antennas. It is quite natural to note that practical antenna gains vary around this value,

because no perfectly balanced electromagnetic radiations can be achieved in actual designs.

2. SPATIAL ANGLE-COMPRESSION GAIN

Practical planar arrays consist of one layer of radiation cells in the transverse extent (i.e., in the plane perpendicular to the direction of radiation). If there are M radiation cells in a planar array, the directive gain of the array is

$$T = 7M = M\pi^2/\sqrt{2} \qquad \text{(Eq. VII-2)}$$

where the gain of each cell is assumed equal to 7 as evaluated in Equation VII-1. It is also assumed here that all the radiation cells are identical and are driven by equal amount of power.

For a very large array of radiation cells, the array's directive gain is also well known by the formula

$$T = 4\pi \text{ (Array Area)}/\lambda^2 \qquad \text{(Eq. VII-3)}$$

$$= 4\pi \text{ (MA)}/\lambda^2$$

$$= M\pi^2/\sqrt{2}$$

where the last expression is given by use of Equation VII-1, and the value of A is to be interpreted as the projected area of a radiation cell. Assuming that all radiation cells are identical and uniformly distributed, the projected area is solved as

$$A/\lambda^2 = \pi/4\sqrt{2} \qquad \text{(Eq. VII-4)}$$

for the radiation cells. This value is in general agreement with most practical planar arrays under monochromatic operations. It is noted,

however, that there are many choices on the effective radiation-cell area. If the area is larger than the above value, there may exist grating lobes and such an array would be desirable. If on the other hand, the radiation cell is made to occupy less area than the above value, the feeder network would encounter excessive reactance, and render the array operation ineffective. Therefore, with minor changes in design, the effective area of a radiation cell for field-compression applications should be designed in the neighborhood of the value given in Equation VII-4.

3. TEMPORAL WIDTH-COMPRESSION GAIN

If radiation cells are arrayed in the longitudinal direction along which radiation is to take place, there would be certain limitations on possible spatial compression under CW operation. A simple-minded arraying with a single frequency would, in fact, prevent the array from radiation. While spatial modulation on array structure can be made to achieve a directive gain in proportion to array length, this type of "line-source" radiation will be excluded from further considerations.

Instead of the monochromatic operation, radiation cells of various frequencies across a wide bandwidth can be designed to form a longitudinal array. A log-periodic dipole array is a practical example for this type of array. Since all cells are radiating with essentially the same directivity, and the gain in radiated power density is achieved by a conjugate-matched filter concept, this type of field intensification results in compressing the radiated pulse width and is called the temporal field compression.

Temporal field compression gain is expressed as the product of total spectral bandwidth (B) and the dispersed pulse duration (T). The BT product varies depending on dispersive characteristics of the antenna. Both

quadratic-phased and log-periodic dispersions are treated in Appendix D. By assuming a quadratic-phased dispersion array has an identical bandwidth for all its radiation cells, the total bandwidth of this antenna is simply the product of elemental bandwidth b and the number of radiation cells N. The duration for dispersed pulse is equal to the inverse of elemental bandwidth (i.e., 1/b). The BT product for this quadratic-phase antenna has a simple expression.

$$BT = (Nb)\ (1/b) = N \qquad \text{(Eq. VII-5)}$$

indicating in direct proportion to the number of radiation cells of the antenna.

The bandwidth of a log-periodic antenna can be obtained by adding all the elemental bandwidths of radiation regions (Appendix D) as

$$B = \sum_{n=1}^{N} f_{no}\delta \qquad \text{(Eq. VII-6)}$$

$$= f_{no}\ \delta(1+\delta)^{N-1} \sum_{n=1}^{N} \frac{1}{(1+\delta)^{n-1}}$$

where f_{no} are the central frequencies of elemental radiation region, δ is the fractional bandwidth of each region, and f_{no} is the lowest central frequency of the antenna. These parameters are discussed in Appendix D which also gives the dispersed-pulse duration as

$$T = 1/2f_{no}\ell n(1+\delta) \qquad \text{(Eq. VII-7)}$$

Making use of the above two equations gives the BT product

$$BT = \left(\delta(1+\delta)^{N-1} \sum_{n=1}^{N} \frac{1}{(1+\delta)^{n-1}}\right) \Big/ 2\ell n(1+\delta) \qquad \text{(Eq. VII-8)}$$

$$\approx \frac{(1+\delta)^{N-1}}{2} \left| 1 + \frac{1}{1+\delta} + \frac{1}{(1+\delta)^2} + \text{----} \frac{1}{(1+\delta)^{N-1}} \right|$$

$$= \frac{1}{2\delta} \left[(1+\delta)^N - 1 \right]$$

where an approximation $\ell n(1+\delta) \approx \delta$ is made by assuming δ is much less than unity which is the case for most practical log-periodic antennas.

If a log-periodic antenna is driven by a source whose phase is a complex conjugate to the antenna phase angle, but where the amplitudes of each radiation cell are distributed to decrease from high-frequency to low-frequency and as $(1+\delta)^{n-N}$, the total bandwidth in Equation VII-6 may be effectively treated as $B \approx N\delta f_{no}$. The resultant BT product for this case is

$$BT \approx N/2 \qquad \text{(Eq. VII-9)}$$

If, on the other hand, the amplitude of the driving source were made to increase as $(1+\delta)^{n-1}$ from the high-frequency to low-frequency end, the effective bandwidth may be treated as $B = f_{no}\delta(1+\delta)^{N-1}$, and the BT product would become

$$BT = \frac{N}{2}(1+\delta)^{N-1} \qquad \text{(Eq. VII-10)}$$

The last two expressions are obtained by evaluating in terms of the "effective" bandwidth by which the compressed field is intensified proportionately. More detailed numerical confirmations on BT products may be needed before actual design considerations are made for the sake of completeness in comparing various BT product possibilities. The above four expressions are plotted as functions of N, the number of radiation cells in a dispersive array. Note that these BT-product curves are plotted independently of design details which have been discussed in Section VI. As long as the number of radiation cells is established in a given volume, the curves in Figure VII-1 will give the maximum possible BT product. For example, for a log-periodic array with a constant amplitude in its transfer function, the BT product is given in Equation VII-8, and Figure VII-1 shows that the value is BT = 2141 for N = 100. This result is in good agreement with the maximum BT product established for a conical spiral antenna like that studied in Section VI.

The plotted BT-product curves make the following conclusions clear:

(1) BT = N for a quadratic-phased dispersive antenna. The experimental bandwidth as discussed in Appendix D does not affect the BT product.

(2) $BT = ((1+\delta)^N - 1)/2\delta$ for a constant amplitude distribution of a log-periodic array. Both of the fractional bandwidths $\delta = 0.05$ and 0.10 are practical values for existing antennas, and they yield BT products higher than the corresponding value by quadratic-phased antennas.

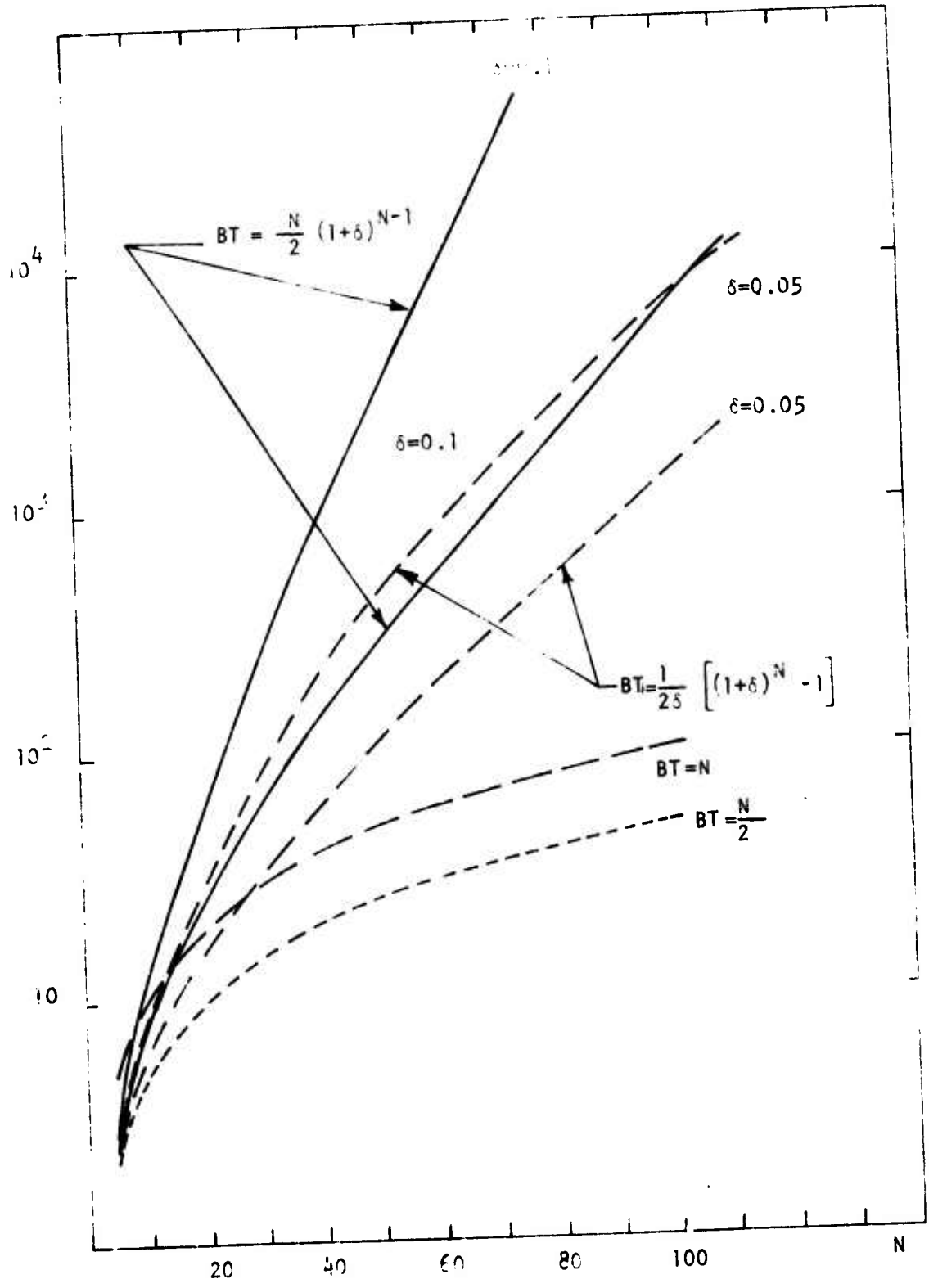


Figure VII-1. Bandwidth-Time (BT) Products of Dispersive Antennas in Terms of Number of Radiation Cells

(3) By using skewed weighting $(1+\delta)^{n-1}$ giving higher excitations for lower frequency cells, the BT product is seen to have further increased the BT product for a given N. The compressed pulse shape for this distribution would also be skewed with respect to the pulse-peak, resulting in significant ringing after the peak. This type of distribution is particularly desirable if higher amounts of low-frequency power are desired in the compressed radiation.

(4) A BT-product of 40 dB with N = 110 can be reached by two curves. If the same bandwidth, B, and the same N are imposed for the constant-amplitude and the skewed-amplitude distributions, the former with $\delta = 0.1$, would require a larger volume when compared with that of the latter with $\delta = 0.05$

4. SPACE-TIME COMPRESSION GAIN

Total field-compression gain is the product of spatial directivity gain and temporal compression gain. Let C be the total field-compression gain

$$C = (\text{Spatial Compression Gain})\ (\text{Temporal Compression Gain})$$

$$= \frac{\pi^2}{\sqrt{2}}\ (M)\,(BT) \qquad \text{(Eq. VII-11)}$$

where M is the number of identical dispersive arrays. If different dispersive arrays with different BT values are used, the total field compression can be written

$$C = \frac{\pi^2}{\sqrt{2}} \sum_{j=1}^{J} (M_j)\ (B_j T_j) \qquad \text{(Eq. VII-12)}$$

The simplest configuration of using M identical quadratic-arrays with the BD product equal to N is given in Equation VII-5, and the total field-compression gain is equal to $MN\ \pi^2/\sqrt{2}$.

The next simplest configuration is to array a number of identical cavity-backed spiral antennas. Consider the example given in Table V-3 where a cavity-backed spiral antenna with a volume of $4\pi/3\ m^3$ has 110 radiation cells. The BT product of this antenna is given as 2453 which is in good agreement with the curve for

$$BT = ((1+\delta)^N - 1)/2\delta \text{ with } \delta = 0.05$$

in Figure VII-1. Use of Equation VII-11 gives

$$C = \pi^2/\sqrt{2}\ (2453)\ M \approx 1.7 \times 10^4\ M \qquad \text{(Eq. VII-13)}$$

If six identical antennas were used, the array would occupy $8\pi\ m^2$ volume and give a field compression gain of 50 dB. This gain would mean a power density of $10^6/4\pi$ watts/m^2 at a distance 100 m from the array, if a total of 10 kW is fed to the six antennas. In terms of electric field intensity, it would be 5.5 kV/m at the distance 100 m from the array. A field compression gain of 60 dB can be achieved by using 12 identical cavity-backed spirals with $\delta = 0.05$ and with the source distribution that gives rise to

$$BT = N(1+\delta)^{N-1/2}$$

in Figure VII-1. If 70 dB gain is needed, 120 antennas can be assembled with a volume of $160\ \pi\ m^2$, and delivering the gain that would give rise to the 55 kV/m electric field at 100 m from the array.

Other types of array arrangements can be made according to the dispersion antennas chosen. For a general type of arrangement, the formula in Equation VII-12 should be used to make compression gain estimations.

SECTION VIII

CONCLUSIONS

This study program on radiation-field compression has covered the dispersion-compression concepts, the experimental verifications, and the development of analytical models. The conceptual studies have treated various dispersive antennas as potential candidates to intensify the radiation fields. The empirical data and their associated analyses have demonstrated radiation mechanisms and compression limitations for log-periodic antennas. Both geometrical parameters and electrical properties have been employed to develop the analytical models for predicting the BT gains and the required driving source functions for conjugate matchings. The following paragraphs will serve to summarize briefly the extent and significance of the results emerged from this program.

1. ANTENNA DISPERSION AND COMPRESSION

There is conceptually no restriction on what dispersion characteristics can be used for field-compression purposes. The well known quadratic-phase dispersion or linear FM have received limited study in this program, but no operational antenna is known to exist at the present. Also, its BT product is found to be less than the log-periodic phased dispersion which is exhibited by many so-called frequency-independent antennas. Therefore, a great portion of this program effort has been concentrated on log-periodic (LP) antennas for field compression.

Six LP antennas have been measured for their dispersion characteristics of radiated fields. Extensive numerical results are obtained in both time- and frequency-domains. Dispersed field durations and bandwidths are tabulated for these antennas to compare their relative merits for BT products. Analytical models for these dispersions have

been formulated in a common form in terms of electrical parameters such as radiation cells and their center frequencies. The complex transfer function of these antennas is summarized as shown in Figure VIII-1 where the effective fractional bandwidth δ, the highest radiation frequency, and the total number of radiation cells are used to completely describe the far-zone dispersive transfer function of all periodic antennas. This program has, thus, in essence, established the transmitter waveform requirements if LP antennas are to be employed to compress radiation fields.

The BT products of LP antennas have been evaluated for their theoretical and practical limits when certain geometrical parameters are imposed. The largest linear dimensions of 2 m in the transverse plane and 4 m along the longitudinal axis of antennas are imposed as upper limits for antenna size, because they serve to give a solid design example and allow further studies by simply changing these parameters. The highest operating frequency of a dispersive antenna is presently imposed at 15 GHz. This limit is set by considering the required antenna structure's precision requirements and power-handling capacities, in addition to the transmitter availability and propagation losses through the air, etc. Even under the restricted parameters, the BT product can still become indefinitely large in theory, if the slowness factor of the antenna structure were allowed to approach zero. This approach leads immediately to many impractical designs as well as operations. Therefore, based on certain practical constraints, the practical BT-product limits are listed in Table VIII-1 with appropriate comments. It shows that the three antenna types have about the same BT-products when their volume is approximately the same.

Complementary to the above conclusion are the results obtained from the analytical model based on electrical properties such as total number of radiation cells and their fractional bandwidth. BT products ar-

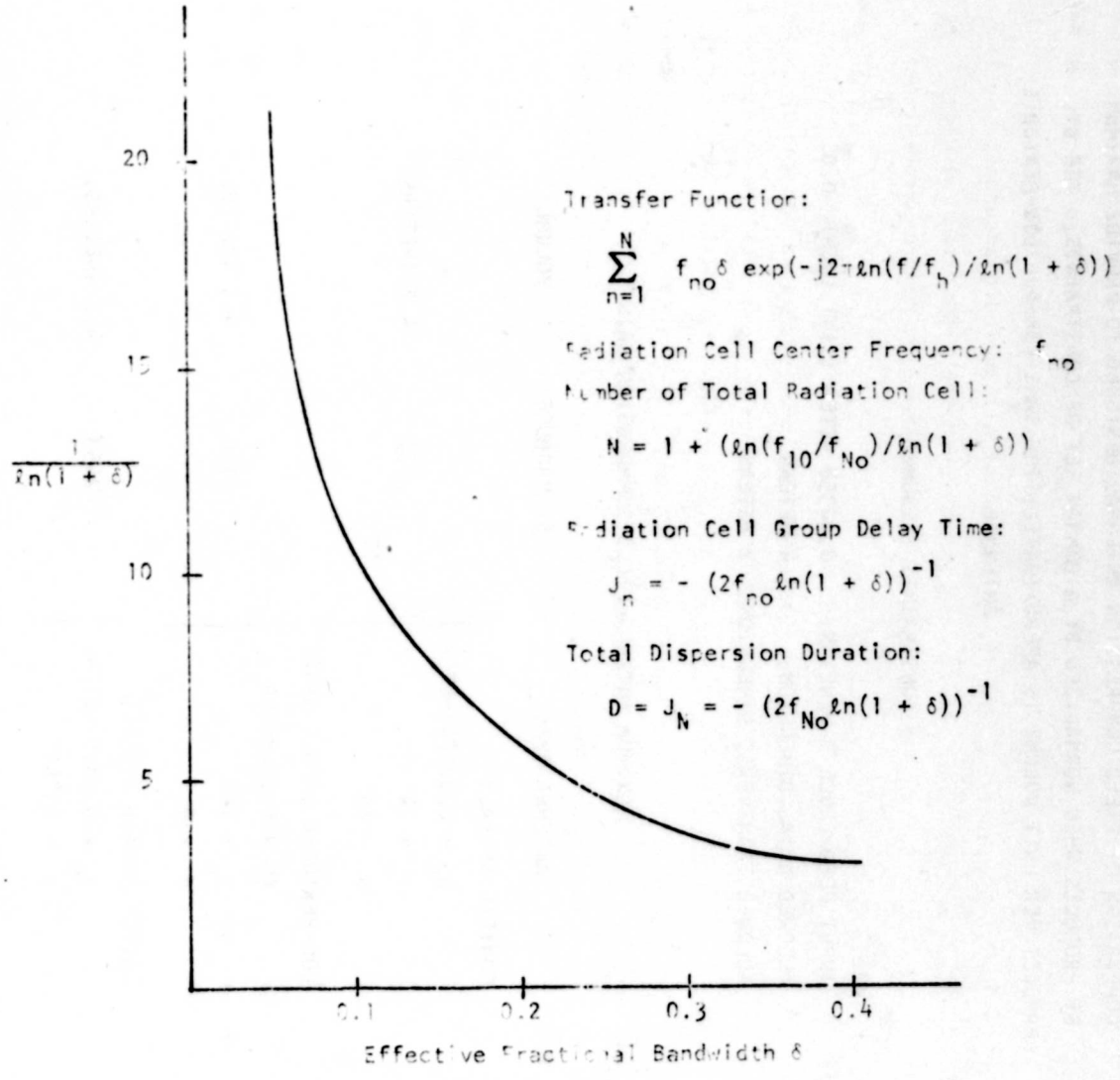


Figure VIII-1. Transfer Function and Associated Characteristics of General Log-Periodic Antennas

TABLE VIII-1

COMPARISON OF FIELD COMPRESSION ANTENNAS DESIGNED TO PROVIDE MAXIMUM BT PRODUCTS WHEN NORMALIZED BY A COMMON SET OF CONSTRAINTS. THE BT PRODUCT PER UNIT VOLUME IS APPROXIMATELY THE SAME FOR ALL LOG-PERIODIC ANTENNAS

CONSTRAINTS (ASSUMED)[1]

INPUT FEED CABLE DIMENSION:	0.00358 METER (.141 INCH) O.D.
ALLOWED AXIAL DIMENSION:	4 METERS
ALLOWED TRANSVERSE DIMENSION:	2 METERS

MAXIMUM ANTENNA FIELD COMPRESSION GAIN

ANTENNA TYPE	BT PRODUCT	VOLUME[2]
CONICAL SPIRAL: a_n = 0.00284 METER, θ_o = 14°, α = 85°	2537	4.2 (METERS)^3
LOG-PERIODIC DIPOLE ARRAY: ℓ_n = 0.01 METER, θ_o = 14°, σ = 0.1	2126	4.2 (METERS)^3
CAVITY-BACKED SPIRAL: a_h = 0.0028 METER, ϕ = 88°51'	2453	4.2 (METERS)^3

[1]These are reasonable, but arbitrary.

[2]Estimated effective radiation volume.

evaluated by the models in Section VII. Should there be a quadratic-phased antenna, its BT product would be equal to the total number of radiation cells in a given volume. Log-periodic dispersive antennas, on the other hand, are shown to have various possibilities in BT products depending on spectral distributions. In general, these BT products increase with total number of radiation cells. When the number is chosen 110, in agreement with the models based on geometrical parameters, the BT product becomes about 2200 as in agreement with those in Table VIII-1.

To summarize, this program has developed two analytical models by which the BT product of LP antennas can be consistently predicted. These models will become useful tools for the system designers of radiation-field compression antennas.

2. TRANSFER FUNCTIONS AND TRANSMITTER DESIGNS

Since dispersion-filter function is a complex conjugate of driving-source function, either of them can be chosen first as the desired function and the other will then be designed for conjugate matching. This program has chosen LP antennas as dispersive filters for field-compression applications, and the driving-source functional characteristics are to be recommended for future developments. To this extent, this program has successfully developed the transfer function as shown in Figure VIII-1. A successful transmitter-function design in the future will be required to produce the driving-source function as the complex conjugate of the LP transfer function.

3. MAXIMUM POWER-DENSITY GAIN OF A DISPERSIVE ANTENNA

This program has analytically determined that radiation-field compression is accomplished by an array of cells which radiate in a sequential manner. The LP antenna radiates the highest-frequency pulse

from the first radiation cell which occupies the largest elemental bandwidth ($f_{10}\delta$). As the time goes on, the successive radiation cells give rise to a series of pulses with time-varying instantaneous frequencies. When the last cell, corresponding to the lowest operating frequency, completes its radiation, the overall dispersed pulse of the antenna is a superposition of N pulses.

The LP antenna has approximately the same directive gain $\pi^2/\sqrt{2}$ for all its radiation cells. This value of gain stays the same for all operational frequencies if the antenna is used for CW or monochromatic radiation. Should a broad-bandwidth and long-duration pulse be conjugate-matched to the antenna transfer function, the resultant radiation field could be intensified beyond the monochromatic directive gain. Depending on the source bandwidth and duration, various compression gain can be achieved for the antenna. Considering the additional compression gain equal to the BT product, a dispersive antenna can intensify its radiated maximum-power density to a value equal to BT $\pi^2/\sqrt{2}$. By referring to the BT curves in Section VII, a dispersive antenna gain can be readily evaluated. For instance, if a dispersive antenna was designed to have BT equal to 2828 or 1414, its overall compression gain would be about 43 dB or 40 dB, respectively. This program has established that a dispersion antenna occupying about 4 m^3 can produce a compression gain of 43 dB or higher.

4. GAIN OF AN ARRAYED DISPERSION ANTENNA

The gain of a single dispersion antenna is enhanced by temporal pulse compression while maintaining a fixed spatial compression gain of about $\pi^2/\sqrt{2}$. Further increase in power-density gain is possible by arraying a number of dispersion antennas. Basically, there may be two ways of arraying: one is to increase the radiation volume by extending transversal coverage, and the other is to extend simply longitudinal

coverage. An appropriate combination of these two basic arrays, the power-density gain of the array would be most properly called a simultaneous space-time compression. By restricting the highest frequency to 15 GHz, this program has established that a radiation volume of 4 m^3 or 400 m^3 can produce a power-density gain of about 43 dB or 63 dB.

5. ELECTRIC FIELD INTENSITY AND POWER INPUT

Let C be the space-time compression gain of an array of dispersive antennas which consist of arrays of radiation cells. The compressed electric field intensity E at a distance r from the array center is expressed as a function of total input power W as

$$E_{array} = \frac{\pi}{r}\sqrt{3WC/\sqrt{2}}$$

If only a dispersive antenna is used, the electric field intensity is enhanced only by the BT product and the radiation cell directivity as

$$E_{antenna} = \frac{\pi}{r}\sqrt{3W(BT)/\sqrt{2}}$$

The above two formulas can be used to estimate required input power W if the field intensity E is specified at a given r. Examples for these evaluations are given in Section VII where it is stated, in effect, that the space-time compression gain is a function of the total radiation volume.

6. NEAR-ZONE FIELD AND POWER-HANDLING CAPACITY

Because of concern over possible air breakdown in the near-zone compression, these near-zone fields have been formulated and computed. Two dispersive antenna models have been used to establish upper and lower bounds for compressed-pulse peaks in the near-zone. The pulse shapes and durations of these two models are demonstrated in Section VI where a

curve relating breakdown field strength and pulse duration was also given. The curve and its associated tabulation have been used to establish that no near-field breakdown would take place outside of the spherical volume enclosing the highest-frequency element. This program has used the near-zone models to predict performances of other antennas under different operating conditions. By estimating the present power-handling capacities of various antennas, it is concluded that no near-zone breakdown would take place before the antenna structures exceed their power-handling specifications. Although more in-depth studies on the state-of-the-art designs for power handling should be conducted, it appears that the limit of the pulse compression by a dispersive antenna will be set by the antenna's power-handling capacity rather than the possibility of a near-field breakdown. In either case, a ready solution is to array a number of dispersive antennas as was discussed earlier.

SECTION IX

RECOMMENDATIONS

As this program completes its experimental verifications of radiated field dispersion and concludes its analytical models for dispersive-antenna transfer functions, it leads naturally to the last area of field-compression elements: the transmitter functions that will conjugate match the dispersive antennas.

The results of this program have made it clear that both analytical developments and practical designs of a transmitter require a definitive knowledge on application potentials as well as operational limitations. The following recommendations will be made on the basis of technical understandings accomplished in this program.

1. LOG-PERIODIC ANTENNAS AS RADIATION-FIELD COMPRESSORS

The log-periodic antennas are recommended for use in radiation-field compressions. Certain obvious reasons for this recommendation are:

(1) Analytically, they have larger BT-product potential than the quadratic-phased dispersion antennas.

(2) Practically, they have been verified to have well behaved dispersion characteristics, while the quadratic-phased antenna is not known to exist.

(3) Both theoretical and practical limits of their BT product have been established in terms of geometrical parameters involved in their designs.

(4) Radiation cells of these antennas have been formulated in terms of their electromagnetic performance parameters.

(5) Their near-zone compressions have been analyzed extensively with numerical results to obtain the upper and lower bounds that can be used to evaluate air-breakdown possibilities.

(6) Formalisms of their dispersion characteristics have been developed (Figure IX-1) to provide precise statements for transmitter requirements.

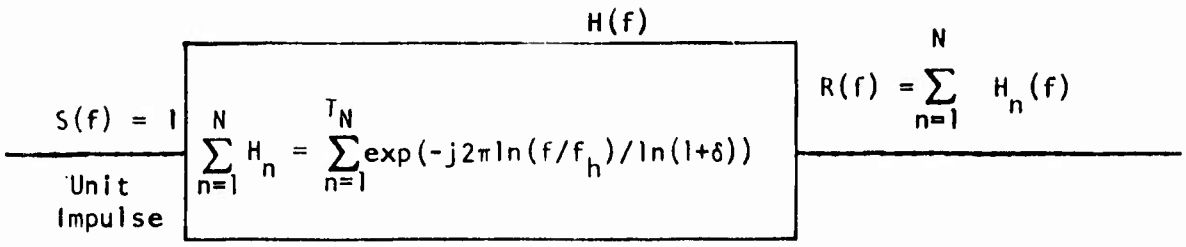
2. INTENSIVE R&D EFFORTS ON RETARDATION-RADIATION CELLS

Operational log-periodic antennas have, in the past, been designed for CW or monochromatic applications. This program has produced the radiation-cell concepts that are describable in terms of both geometrical and electromagnetic parameters. Successful applications of LP antennas for radiation-field compression will require more information pertaining to the following questions:

(1) Is the imposition of 15 GHz realistic as the highest operation frequency? The only meaningful answer to this question requires substantiation by measured data.

(2) What is the maximum power or energy density that a radiation cell can handle? The most adequate answer to this question appears to require a specification of joules per cubic wavelength.

(3) How well must log-periodic-phase characteristics be maintained across the operating bandwidth? Realizable compression gain estimates and practical transmitter designs will be facilitated by the answer.



(a) Dispersive Log-Periodic Filter Driven by an Impulse

$$S(f) = \sum_{n=1}^{N} \sqrt{\frac{D_n}{T_n}}\, H_n^*(f)$$

H(f)

$$R(f) = \sum_{n=1}^{N} \sqrt{\frac{T_n}{B_n}}\, \exp(jo)$$

$$r(t) = \sum_{n=1}^{N} \sqrt{B_n T_n}\, \frac{\sin \pi B_n t}{\pi B_n t} \exp(j2\pi$$

$$r(0) = \sum_{n=1}^{N} \sqrt{B_n T_n} = N$$

(b) Conjugate - Matched Driving Source and the Filter Response

Figure IX-1. Recommended Analytic Description for Radiation Field Compression by Use of Log-Periodic Antennas

(4) What are the slowness factor and effective fractional bandwidth that can be realized by the state-of-the-art design? The answer will set a limit on a realizable compression gain for a dispersion-antenna radiation.

(5) How do you most tightly pack radiation cells into a given volume of a dispersive antenna? This answer will have to be dictated by tolerable reactive-energy storage or conduction loss in the antenna structure.

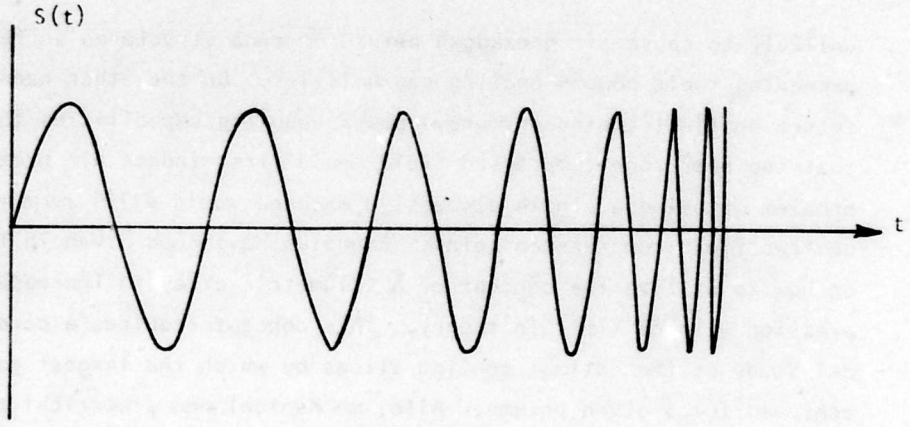
(6) Should the dispersion-pulse bandwidth or duration be increased in order to enhance the antenna's compression gain? The answer will depend on the state-of-the-art design, antenna volume specification, and transmitter-function distribution.

3. EXPONENTIAL DISTRIBUTION FOR TRANSMITTER SPECTRUM

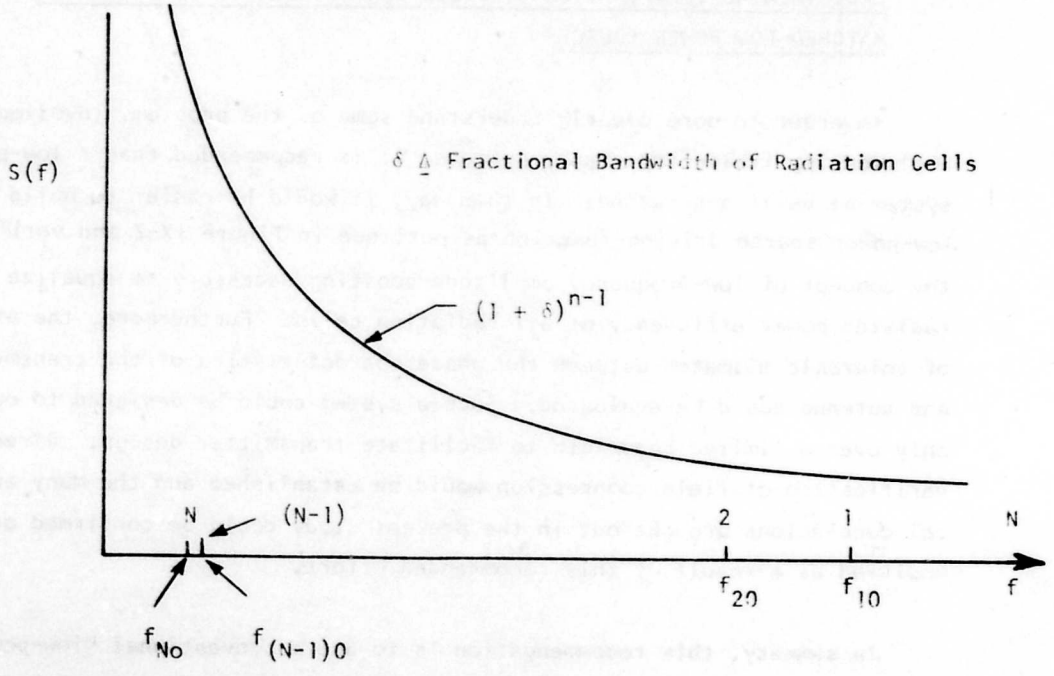
Present design of LP antennas does not give rise to a uniform dispersion gain for all the radiation cells involved. The highest-frequency cell gives the maximum gain because of its inherently largest bandwidth. The lowest-frequency cell occupies the largest fraction of the total radiation volume, although it gives rise to the minimum pulse amplitude. In order to let the antenna radiate its compressed-pulse power in proportion to the volume occupied by its radiation cells, the transmitter spectral distribution is recommended as shown in Figure IX-2 where the corresponding time-domain waveform is also depicted qualitatively.

4. VOLUMETRIC ARRAY OF DISPERSIVE ANTENNAS

This program has indicated that, according to the present CW-specified power capacities, the compressed pulses in either the near- or far-zone are



(a) Time-Domain Source Distribution



(b) Frequency-Domain Source Distribution

Figure IX-2. Recommended Source Functions for Conjugate-Matching Existing LP Antennas

unlikely to cause air breakdown before antenna structures suffer from exceeding their power-handling capabilities. On the other hand, should future design techniques improve power-handling capabilities to the point that the near-zone compressed field would first induce air breakdown, the problem of using a single dispersive antenna would still remain for certain desired field-compression gains. Examples have been given in this program on how to utilize the concept of a volumetric array to increase the compression with no limit in theory. This concept requires a careful analytical study on the optimal configurations by which the largest gain can be achieved for a given volume. Also, mechanical and electrical tolerances of the volumetric array need be conducted in the same way the extremely large parabolic dishes are designed for extremely large gain.

5. EXPERIMENTAL VERIFICATION OF FIELD COMPRESSION USING CONJUGATE-MATCHED LOW POWER SOURCE

In order to more clearly understand some of the problems involved in implementing field-compression systems, it is recommended that a low-power system be built and tested. In this way, it would be easier to build the low-power source driving-function as outlined in Figure IX-2 and verify the concept of low-frequency amplitude boosting necessary to equalize the radiated power efficiency of all radiation cells. Furthermore, the amount of tolerable mismatch between the phase characteristics of the transmitter and antenna could be evaluated. Such a system could be designed to operate only over a limited bandwidth to facilitate transmitter design. Direct verification of field compression would be established and the many analytical conclusions brought out in the present study could be confirmed or modified as a result of this recommended effort.

In summary, this recommendation is to use a conventional "low-power" source to investigate and verify the critical operational parameters. Whether a "new" high-power source would be necessary could become more apparent after this recommended effort.

6. APPLICATIONS IN ADVANCED RADARS AND COMMUNICATION

One of the most readily apparent applications for field compression is in long range, high resolution radar systems. As a result of the very narrow pulse width and high power gain achieved using radiation field compression, both range and resolution would be increased over conventional radar systems using the same input power. A field compression antenna is a passive device and would offer distinct advantages over complicated electronic filters which might otherwise be used to obtain the same results.

There appears to be potential applications for field compression in certain areas of communication. For example, it should be possible for amplitude modulated information to be coded onto a long-duration frequency-modulated pulse without upsetting the conjugate-phase relationship between the transmitter and antenna. Since the same conjugate-matched filter characteristic which exists between the transmitter waveform and the antenna must also be met by a receiving antenna if the original transmitter waveform is to be detected, then any information coded onto the transmitter waveform could only be decoded by using the same conjugate-matched receiving antenna.

In conclusion, it is recommended that potential applications for radiated-field compression be the subject of further investigation.

7. FEASIBILITY OF BUILDING A FIELD COMPRESSION SYSTEM HAVING A BT PRODUCT OF 2000

In an effort to determine the feasibility of field compressors having BT products on the order of 2000, BDM has made a brief survey of some of the problems involved. It appears that the three antenna designs discussed in Section V can be met by the present level of antenna

technology. The basic problem area centers around the design of the source. At present, there is no adequate source of either the impulse type or the dispersed FM type to drive the antenna. An "impulse" source having spectral content up to 15 GHz would be needed to meet the required pulse widths on the order of 67 ps at a level of at least 500 volts and a pulse repetition rate of about 500 pps for high-resolution dispersion measurements using sampling techniques. For direct verification of field compression, it would be more desirable to use a dispersed pulse generator which has the reversal time characteristic to the antenna transfer function. Such a pulser would be required to generate an FM waveform starting at the lowest frequency (about 75 MHz) and proceeding to higher frequencies as time increases. The total sweep time required to reach 15 GHz should equal the dispersion time of the antenna, nominally about 170 ns. Since there would be a compression gain of the radiated pulse of at least 2000 or +33 dB, then an output power level of such a dispersed FM generator of only several mW would be adequate to deliver radiated, compressed pulses on the order of 1 or 2 watts. The pulse repetition rate of this pulser should again be on the order of 500 pps for high-resolution sampling.

Even though neither of these pulse generators is known to exist at present, BDM feels that both types are within the present state-of-the-art in pulse generator technology. Under the assumption that a 15 GHz field compression antenna is to be built, then the construction of both types of pulse generators would be recommended since the "impulse" type would be needed in order to accurately measure the antenna transfer function.

SECTION X

REFERENCES

PULSE COMPRESSION AND MATCHED-FILTER THEORY

1. Cook, C. E., and M. Bernfield. Radar Signals, Academic Press, New York, 1967.

2. Farnett, E. C., et. al. "Pulse - Compression Radar," Chapter 20, Radar Handbook, Edited by Skolnik, McGraw-Hill, 1970.

3. Berkowitz, R. S. Modern Radar, Part IV, John Wiley, New York, 1965.

4. Felsen, L. B. "Asymptotic Theory of Pulse Compression in Dispersive Media," IEEE Trans. Antennas and Propagation, Vol. AP-19, May 1971, pp. 424-432.

5. Cook, C. E. "Pulse Compression - Key to More Efficient Radar Transmission," Proc. IRE, Vol. 48, Pt. 1, March 1960, pp. 310-316.

6. Klauder, J. R., et. al. "Theory and Design of Chirp Radars," Bell Systems Tech. J., Vol. 39, July 1960, pp. 745-808.

7. Klauder, J. R. "The Design of Radar Signals Having Both High Range Resolution and High Velocity Resolution," Bell Systems Tech. J., Vol. 39, July 1960, pp. 809-820.

TRANSIENT ANTENNA RESPONSE

8. VanEtten, P. "Temporal-Spatial Compression Antennas," RADC-TR-73-179 Technical Report, Rome Air Development Center, Griffiss Air Force Base, New York, September 1972. AD764 354

9. Knop, C. M. "On Transient Radiation From a Log-Periodic Dipole Array," IEEE Trans. Antennas and Propagation, Vol. AP-18, November 1970, pp. 807-808.

10. Pulfer, J. K. "Dispersive Properties of Broadband Antennas," Proc. IRE (correspondence), Vol. 49, March 1961, p. 644.

11. Stiefvater, K., et. al. "Preliminary Results of the Transient Response of Broadband Antennas," RADC-TR-69-203, Griffiss Air Force Base, New York, June 1969. AD855 388

12. Cronson, H. M., and J. M. Proud. "Wideband Antenna Development," (IKOR, Inc.), RADC-TR-70-74, Griffiss Air Force Base, New York, May 1970. AD870 224L

13. Ross, G. F., et. al. "Transient Behavior of Radiating Elements," (Sperry Rand Research Center) RADC-TR-66-790, Final Report, Griffiss Air Force Base, New York, February 1967. AD812 886

14. Ross, G. F., et. al. "Transient Behavior of Large Arrays," RADC-TR-64-581, Final Report, Griffiss Air Force Base, New York, June 1965. AD618 701

15. Susman, L., and D. Lamensdorf. "Picosecond Pulse Antenna Techniques," (Sperry Rand Research Center) RADC-TR-71-64, Final Report, Griffiss Air Force Base, New York, May 1971. AD884 646

16. Martins, V. C., and J. L. VanMeter. "Picosecond Pulse Reflector and Antenna Investigation," (Braddock, Dunn and McDonald, Inc.) RADC Contract No. F30602-72-C-0276, Final Report, Griffiss Air Force Base, New York, January 1973. RADC-TR-73-215, AD774 132

FREQUENCY-INDEPENDENT ANTENNAS

17. Rumsey, V. H. Frequency Independent Antennas, Academic Press, New York, 1966.

18. Walter, C. H. Traveling Wave Antennas, McGraw-Hill, New York, 1965.

19. Colin, R. E., and F. J. Zucher. Antenna Theory, pts. 1 & 2, McGraw-Hill, New York, 1969.

20. Jordan, E. C., G. A. Deschamps, J. D. Dyson, R. E. Mayes. "Developments in Broadband Antennas," IEEE Spectrum, April 1964, pp. 58-71.

21. Rumsey, V. H. "Frequency Independent Antennas," IRE National Convention Record, pt. 1, 1957, pp. 114-118.

22. Du Hamel, R. H., and D. E. Isbell. "Broadband Logarithmically Periodic Antenna Structures," IRE National Convention Record, pt. 1, 1957, pp. 119-128.

23. Dyson, J. D. "The Equiangular Spiral Antenna," IRE Trans. Antennas and Propagation, Vol. AP-7, April 1959, pp. 181-187.

24. Dyson, J. D. "The Characteristics and Design of the Conical Log-Spiral Antenna," IEEE Trans. on Antennas and Propagation, Vol. AP-13, July 1965, pp. 488-499.

25. Dyson, J. D. "The Unidirectional Equiangular Spiral Antenna," IRE Trans. on Antennas and Propagation, Vol. AP-7, October 1969, pp. 329-334.

26. Dyson, J. D. "New Circularly-Polarized Frequency-Independent Antennas With Conical Beam or Omnidirectional Patterns," IRE Trans. on Antennas and Propagation, Vol. AP-9, July 1961, pp. 334-342.

27. Kieburtz, R. B. "A Phase-Integral Approximation for the Current Distribution Along a Log-Periodic Antenna," IEEE Trans. on Antennas and Propagation, AP-13, September 1965, pp. 813-814.

28. Greiser, J. W., and P. E. Mayes. "The Bent Backfire Zigzag - A Vertically-Polarized Frequency Independent Antenna," IEEE Trans. on Antennas and Propagation, Vol. AP-12, May 1964, pp. 281-290.

29. Dyson, J. D. "Multi-Mode Logarithmic Spiral Antennas-Possible Applications," 1961 or 1962.

30. Tang, C. H. "A Class of Modified Log-Spiral Antennas," IEEE Trans. on Antennas and Propagation, Vol. AP-11, July 1963, pp. 422-427.

31. Atia, A. E., and K. K. Mei. "Analysis of Multiple-Arm Conical Log-Spiral Antennas," IEEE Trans. on Antennas and Propagation, Vol. AP-19, May 1971, pp. 320-331.

32. Mei, K. K., et. al. "Directive Frequency Independent Arrays," IEEE Trans. on Antennas and Propagation, Vol. AP-13, September 1965, pp. 807-809.

33. Hudock, E., and P. E. Mayes. "Near-Field Investigation of Uniform Periodic Monopole Arrays," IEEE Trans. on Antennas and Propagation, Vol. AP-13, November 1965, pp. 840-855.

34. Mittra, R., and K. E. Jones. "Theoretical Brillouin (k-β) Diagrams for Monopole and Dipole Arrays and Their Application to Log-Periodic Antennas," IEEE Trans. on Antennas and Propagation, Vol. AP-12, September 1964, pp. 533-540.

35. Mittra, R. and P. W. Klock. "A Theoretical Study of the Conical Spiral Antenna," Electromagnetic Wave Theory, pt. 2, ed. J. Brown, Pergamon Press, 1967, pp. 751-765.

36. Kieburtz, R. "Analysis and Synthesis of Aperture Fields of Log-Periodic Antennas," Electromagnetic Wave Theory, pt. 2, ed. J. Brown, Pergamon Press, 1967, pp. 767-784.

37. Oliver, A. A. "Guided Complex Waves on Slow-Wave Periodic Structures," Electromagnetic Wave Theory, pt. 1, ed. J. Brown, Pergamon Press, 1967, pp. 467-476.

38. Oliver, A. A. "Leaky Waves in Electromagnetic Phenomena," Electromagnetic Theory and Antennas, pt. 2, ed. E. C. Jordan, Pergamon Press, 1963, pp. 837-856.

39. Du Hamel, R. H. "Log-Periodic Antennas and Circuits," Electromagnetic Theory on Antennas, pt. 2, ed. E. C. Jordan, pp. 1031-1050.

40. Nesterikhin, Y. E., V. S. Komel'kov, and E. Z. Meilikkov, "Pulsed Breakdown of Small Gaps in the Nanosecond Range," Soviet Physics - Technical Physics, 9, July 1964, 29-39.

41. Felsenthal, P., and J. M. Proud, "Nanosecond Pulse Breakdown in Gases," Physics Rev. 139, A1796-A1804, September 1965.

APPENDIX A

FIELD COMPRESSION BY ANTENNAS

1. INTRODUCTION

Field compression is to increase radiated power density by use of antenna structures. There are great varieties of antennas* developed to serve the purpose of radiation-field compressors. Broadly speaking, one may classify different antenna types into radiators that are driven by line sources, surface sources, and volume sources. Classical treatments on antennas have been concentrated on the former two categories. The present program of achieving a maximum field compression has brought into focus the need of studying volume-distributed sources for high-intensity radiations.

This appendix is intended to serve as an outline on possible antenna gains when elemental sources are distributed over a specified volume. Some fundamental definitions on antenna directivity, antenna array, radiation cell, dispersive radiation, etc. will be discussed in terms of field intensifications. By combining these fundamental concepts, the overall gain of a volumetric dispersive array will be given in terms of the total number of radiation cells involved.

2. GAIN AND DIRECTIVITY

The directivity of a radiator is defined as the ratio of the power density produced by the antenna over the power density produced by an assumed onmi-directional antenna, provided an equal amount of power is radiated by both antennas. In practice, the maximum directivity of an antenna is of principal interest. For the present program, this maximum directivity will be our only concern. That is, the directivity of an antenna is to be understood as the maximum value.

*Antenna Engineering Handbook, Henry Jasik, Editor; McGraw-Hill, New York, 1961.

Practical antennas require feeding networks to provide power for their radiation. Since a feeding network cannot be perfectly matched to an antenna terminal, the radiated power is invariably smaller than the available feeding power. Also, whatever amount of power is transferred to an antenna, it can be distributed in a different manner over the antenna surface so that different radiation intensities would result in the direction of maximum radiation. These two factors, among others such as polarization mismatch, etc., always reduce the practical gain of an antenna to a level less than the theoretically possible value. For the sake of simplicity, all practical factors that reduce an antenna's maximum directivity will not be considered in this appendix. In other words, only directivity will be treated as the intensification factor for radiated power density.

3. RADIATION CELL - ELEMENTAL ANTENNA

Radiation from practical antennas can always be decomposed into small radiation cells whose integrated effects represent the overall antenna performance. There are various ways of characterizing the small radiation elements; some ways may be purely mathematical in nature, others may more closely resemble actual radiation mechanisms. For the present program, a radiation cell is defined as the minimum volume in which a unidirectional and efficient radiation can take place.

Efficient radiation by a small current element is known as being from either an electric or magnetic dipole whose length is in the neighborhood of one-half wavelength. Omnidirectional radiation of a small region is known to be contributed to by proper phasing along the longitudinal direction. The smallest longitudinal depth for efficient radiation is also about one-half wavelength. Therefore, without concerning effective current distributions, the elemental antenna with unidirectional efficient radiation is about a volume occupying $(\lambda/2)^3$.

This radiation cell can be closely identified with a newly verified electromagnetic dipole, an electric dipole with a director and reflector, an electric dipole over a ground plane, and one element of a log-periodic dipole array. For the present program, the last identification is of immediate concern.

4. PLANAR ARRAY - SPATIAL ANGLE COMPRESSION

A planar antenna under monochromatic radiation has the well known directivity as

$$T = 4\pi A/\lambda^2 \qquad \text{(Eq. A-1)}$$

if the source distribution is uniform. . The formula can be used for an array consisting of many elemental radiators. Each element of the array can be treated as a radiation cell with an effective radiation area. For a slot antenna or an electric dipole over ground plane, the projected radiation area is approximately $(\lambda/\sqrt{2})^2$. Therefore, for all practical purposes, an estimate for the elemental directivity is

$$4\pi(\lambda/\sqrt{2})^2/\lambda^2 = 2\pi \qquad \text{(Eq. A-2)}$$

which corresponds to a directive gain of 8 dB for each array element. This value is close to most operational planar arrays depending on their design details.

Since the array consists of elemental areas, an assumption of uniform distribution for these areas gives

$$T = M(2\pi) \qquad \text{(Eq. A-3)}$$

where M is the total number of elemental areas with equal-amplitude excitation. It is noted again that both elemental current distribution as well as the array

total distribution are assumed to be uniform. For a more realistic and commonly used distribution, the above directivity values should be reduced by a factor of 2.

5. DISPERSIVE ARRAY - RETARDATION CELLS

Instead of a planar array whose directivity is in proportion to its projected area, there also exists a longitudinal array whose directivity is proportional to the depth along the direction of propagation. An arraying along the propagation direction can, in theory, be made by using elemental cells as defined earlier. However, because of the intention of intensified radiation instead of supporting a bounded wave without radiation, the longitudinal arraying is seldom accomplished in monochromatic operation.

A radiation cell intended for longitudinal arraying has a directivity of about 4π times the projected length or depth of the cell. For the cell chosen for this program, the projected cell depth is $\lambda/2$ which gives the elemental directivity

$$4\pi L/\lambda = 4\pi(1/2) = 2\pi \qquad \text{(Eq. A-4)}$$

This result is the same as Equation A-2, because the same radiation cell is concerned.

Suppose a volumetric radiation cell is treated directly in terms of volume, instead of in terms of projected area or depth, one can write the radiation cell directivity as

$$(4\pi A/\lambda^2)(4\pi L/\lambda) = (4\pi)^2(V'/\lambda^3) = 7 \qquad \text{(Eq. A-5)}$$

where the value 7 is obtained by allowing the cell to be a cubic volume of equal sides, each of which is $(\lambda/2\sqrt{2})$. The directivity gain is about 8.5 dB which is the value commonly achieved in log-periodic or other types of frequency-independent antennas.

6. VOLUMETRIC DISPERSION ARRAYS

Analytical developments for radiation cells are to be found in Appendix D. Both log-periodic-phase and quadratic-phase distributions are developed there for the bandwidth and duration of dispersive antennas. These antennas are broadband in the sense that in a given volume there are numerous radiation cells across a wide bandwidth. Should there be proper excitation sources to these antennas, all these radiation cells would radiate sequentially with certain amounts of time delay from the first cell to the last cell. There are many operational antennas that are capable of this type of radiation. Some of the measured results demonstrating log-periodic characteristics or inverse delay time for instantaneous frequencies are presented in Appendix C.

Unlike most conventional antennas whose field compression gain is achieved through reducing the spatial angle of radiation, a volumetric dispersion array can be designed to compress its radiated field in time or in the direction propagation. This additional compression gain is proportional to the field bandwidth (B) and the dispersed-pulse duration (T). For the sake of being precise, product of bandwidth and duration is called the BT product of a volumetri volumetric dispersion array.

When a number of volumetric dispersion arrays are again being arrayed for additional field compression, the resultant field compression becomes the product of the temporal BT and the spatial compressions (as defined in Equation A-1 and A-4). Let the overall compression gain be C as

$$C = (\text{Spatial Compression})(\text{Temporal Compression})$$

$$= \left((4\pi A/\lambda^2)(4\pi L/\lambda)\right)(BT)$$

$$= (4\pi)^2 (V/\lambda^3)(BT) \qquad \text{(Eq. A-6)}$$

$$= M\ (7)(BT)$$

where the last expression is obtained by use of Equation A-5 and by assuming that M is the number of radiation cells of the center frequency occupying a transverse extent with an area A and a depth equal to the depth of a cell.

It remains to determine the BT product in terms of radiation cells occupying a retardation region. In Appendix D, for instance, the bandwidth of a dispersive antenna with a quadratic phase is obtained as

$$B = Nb \qquad \text{(Eq. A-7)}$$

where N is the number of retarded radiation cells and b is the elemental bandwidth. It is also shown in Appendix D that the total dispersion pulse duration is

$$T = 1/b \qquad \text{(Eq. A-8)}$$

Subsitution of Equations A-7 and A-8 into Equation A-6 gives

$$C = 7MN \qquad \text{(Eq, A-9)}$$

This is the final expression for a volumetric dispersion antenna whose maximum compression gain is equal to the product of radiation-cell gain 7 and the total number of radiation cells in a given volume, provided the antenna dispersion is of quadratic phase in nature.

7. CONCLUDING REMARKS

An example has been given here to show the maximum compression gain for a quadratic-phased dispersive volumetric array. There are other types of array which have different compression gains. In fact, existing frequency-independent arrays are log-periodic in nature and their BT products have been treated in the main text.

As far as Equation A-9 is concerned, the compression gain states simply that radiated power density in the direction of maximum intensity is directly proportional to the total number MN of radiation cells in a given volume. This conclusion is independent of volume involved. In other words, by a given design procedure and a given set of constraining parameters, the maximum number of radiation cells in a given volume is limited. Thus, a normalization by the volume gives the general expression stating that, when best design considerations are given, the only other way to increase compression gains is to increase the array volume. This conclusion is similar to a planar array whose gain in spatial angle compression is directly proportional to the array area. By excluding the possibility of highly-reactive supergain consideration, the only way to increase the gain of a planar array is to increase its effective area.

Associated with the field compression gain is an array of related problems such as possible air breakdowns, minimum practical pulse duration after compression, antenna power limits of each radiation cell, practical antenna size and arrangement, etc. These problems have been treated to a great extent in appropriate places of the main text and in the following appendicies.

APPENDIX B
DISPERSED PULSE MEASUREMENTS

1. INTRODUCTION

The primary objective of the following antenna measurements is to substantiate theoretical predictions for an antenna known to have large operational bandwidth and radiation dispersion. Generally, the experimental methodology in meeting this objective has been as follows. Taking the theoretical expression for the BT product (which has been given in terms of antenna parameters), a BT product value for an antenna which falls into the class covered by the theory is predicted. The BT product of this antenna is then measured and compared with the theoretical value, thus establishing the credibility of the theory. This procedure is considered as the necessary first step prior to construction of a prototype for maximum BT product (not a specific task of this contract).

It is important to realize that there are two methods by which the BT product for an antenna may be determined from experimental data. One method is to calculate BT directly from the antennas' impulse response. The other method is to compute the antenna transfer function, determine the complex conjugate waveform, and then take the inverse Fourier transform of their product to obtain the compressed pulse. In the latter case, the BT product would be given by the ratio of peak power output to peak power input amplitude. While the first method may be expected to agree more closely with intuitive prediction, the second method should give a more realistic measure of the actual pulse compression. The reason is that the first method ignores amplitude differentials between the maximum of the conjugate matched input signal and the amplitudes at highest and lowest frequencies (i.e., it assumes constant input pulse amplitude). Transfer function determination of BT, as in the latter case, does provide the correct evaluation method. For this reason, it is necessary to be able to accurately determine the antenna transfer function

from measured data. The manner in which this is done, therefore, becomes important. This has been done by BDM with the minimum perturbing influences by using a replica receiving probe and impulsing the antenna. In the past, dispersion has often been measured by using a supposedly identical receive and transmit antenna. This obviously makes the determination of the transmit antenna transfer function more complicated.

Finally, one-way dispersion measurements allow us to evaluate two-way dispersion (i.e., whether the dispersion is, indeed, twice as long).

2. MEASUREMENT SYSTEM

The measuring system to determine antenna transfer function consisted of high-voltage, ultra-fast pulse instrumentation and an antenna range suitable for wideband frequency measurements.

a. Instrumentation

An operational bandwidth of dc to 11.5 GHz has been assumed in specifying the electronic apparatus in order to insure flat system response from 400 MHz to 4 GHz, the range over which measurements were actually made. Circuit operation, shown in Figure B-1, is as follows. Pulses, approximating gaussian distribution, are generated by the IKOR Model R 100 IMP Generator at a rate of 250 pps. These pulses have rise and fall times of less than 100 psec and -3 dB pulse widths of less than 150 psec, hence the highest useful spectral frequency component will be somewhat less than 10 GHz depending on system losses. Peak pulse amplitude is 1 kV into 50 ohms. Since there is no pretrigger available on this pulse generator, the combination of a trigger pickoff followed by approximately 75 nsec of delay line is used to start the sweep on the sampling oscilloscope. The unavoidable use of this technique does degrade pulse fidelity, but judicious choice of these components keeps the distortion to a minimum. The trigger pickoff consists of an

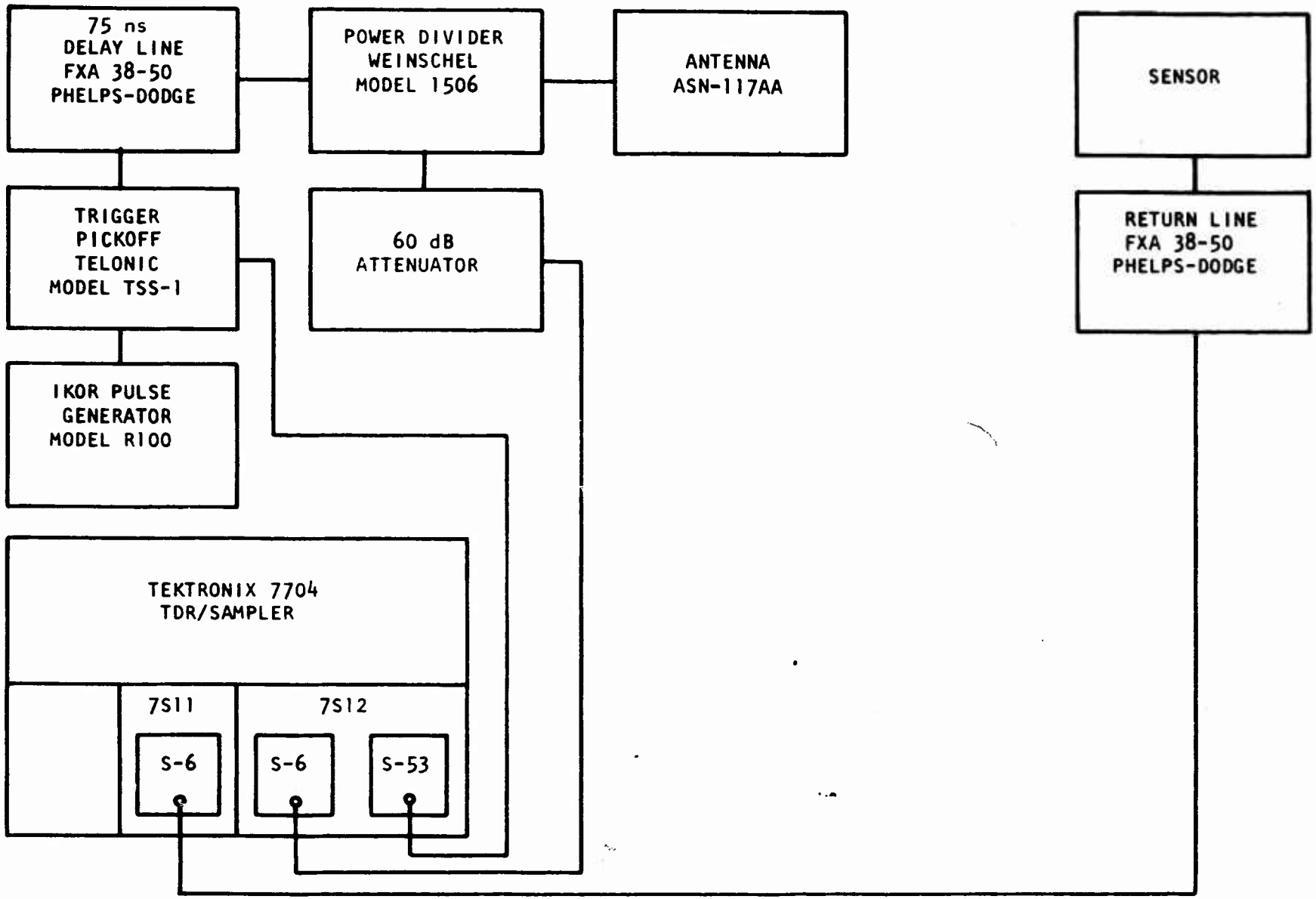


Figure B-1. Experimental Appara us

electrostatic probe which is capacitively coupled to the main line. The amount of coupling is adjustable from less than 10 dB to greater than 40 dB so that perturbation of the main pulse can be made minimal. Insertion loss and frequency range for the Telonic Model TSS-1 are 0.2 dB and 1 MHz to 12.4 GHz, respectively. The delay line is approximately 42 feet of 3/8-inch solid aluminum sheathed, foamed polyethylene dielectric coaxial cable (Cablewave Systems, Inc., FXA 38-50). Cutoff frequency for this cable is 12.5 GHz; it will handle peak voltages of 1.7 kV. Total attenuation is 1.9 dB at 1 GHz and 8.6 dB at 10 GHz. The pulse is then sampled and fed to the antenna. The signal sampler was a 6 dB resistive power divider (Weinschel Engineering, Model 1506) used to provide a replica of the antenna feed pulse. The bandwidth of this device is dc to 10 GHz. The radiated signal was monitored in the far field, 1 to 2 meters downrange from the antenna, by a two-centimeter stub monopole probe. This probe was chosen because of its ability to receive very nearly a replica of the transmitted waveform. Both the input signal and the received signal were displayed simultaneously on the oscilloscope through the use of dual channel sampling, and were photographically recorded. This system was used for both dual channel sampling and time-domain reflectometry measurements. As a sampler, the system consisted of the following Tektronix components: 7704 mainframe, 7S12 combination TDR/Sampler plug-in, 7S11 sampling vertical amplifier, two S-6 sampling heads and an S-53 trigger recognizer head. Overall, this system is capable of displaying pulses having risetimes of the order of 30 psec and bandwidths from dc to 11.5 GHz at -3 dB. The system also doubles as a TDR unit when the S-53 is replaced by an S-52 pulse generator head, having a risetime of 45 psec.

All interconnecting cable was FXA 38-50 (the same as was used for the delay lines) and all connectors were Type N, except the input connectors to the sampling oscilloscope which were Type SMA.

The instrumentation was placed inside a copper screen room adjacent to the antenna range. The actual delay lines were used to connect to the antenna to keep system losses down.

A photograph of the actual instrumentation is shown in Figure B-2 as seen from inside the screen room.

b. Antenna Range

As a result of the lowest measured frequency being 400 MHz, it was possible to construct the antenna range in a cubical volume 5.2 meters on a side. With these dimensions, it was possible to take far-field antenna measurements and eliminate groundbounce interference from the long duration received pulse. (The far-field criteria are established in Section 4 of this appendix.)

The basic relation which must be satisfied in order that the direct signal may be recorded prior to the arrival of any reflections is given by

$$h = \frac{cT}{2}\sqrt{1 + \frac{2s}{cT}}$$

where c is the speed of light in free space; T is the duration of the transmitted pulse; s is the separation distance (on boresight) of the transmit and receive antennas, respectively; and h is the perpendicular distance from the transmit antenna to the nearest reflecting surface, the ground in this case. Since the maximum received pulse duration of the antennas tested was 15 ns and since the antenna-probe separation necessary to satisfy the far-field criteria was found to be 1 meter, h was determined to be 2.6 meters. Thus, the antenna and stub-monopole probe were placed at this height above ground in the working volume.

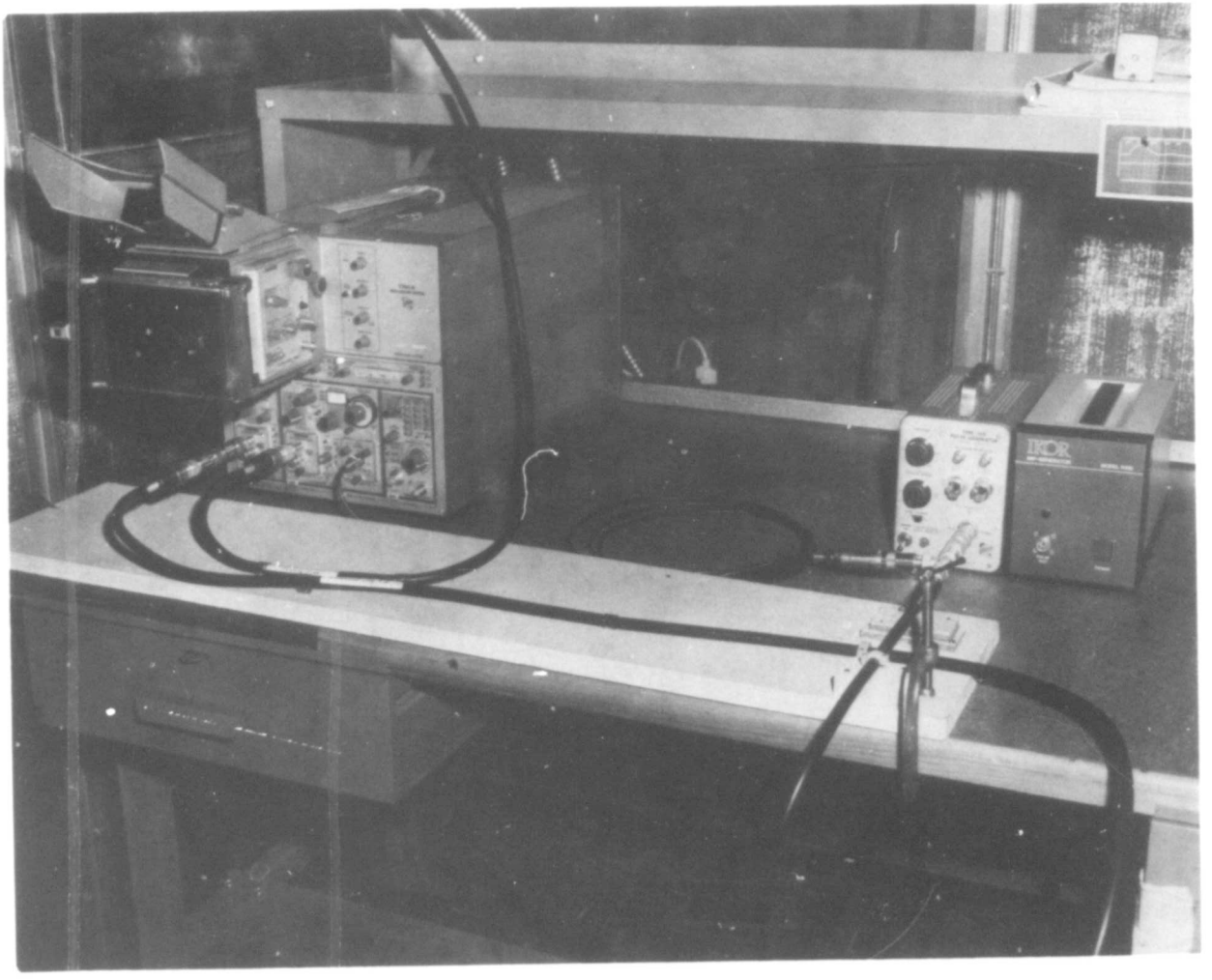


Figure B-2. Measurement Instrumentation

Originally, wooden mounts were used for the antenna and probe, but these caused severe noise problems at gigahertz frequencies: sharp wooden obstructions near the coaxial feedlines were excellent reflectors. To alleviate this problem, these support structures were made of styrofoam.

3. CALIBRATION

In order to insure the quality of measured results which ultimately were used to determine the antenna transfer function, considerable emphasis was placed upon system calibration. Let us examine in some detail the problems involved in accurate experimental determination of the antenna transfer function, since this will clearly show the areas where calibration is most important.

In principle, the antenna transfer function $H(\omega)$ would be given by its impulse response as

$$S(\omega) \longrightarrow \underset{H(\omega)}{\text{ANTENNA}} \longrightarrow G(\omega) = H(\omega)\ S(\omega)$$

or

$$H(\omega) = G(\omega)/S(\omega) = G(\omega)$$

where $S(\omega)$ is the spectral distribution of the unit impulse. In the present set of measurements, $S(\omega)$, being the output of the pulse generator, is certainly not a unit impulse. Furthermore, one does not measure the antenna response $G(\omega)$ directly because of the presence of the probe in the circuit. The actual situation is characterized as follows:

$$S(\omega) \longrightarrow \underset{H(\omega)}{\text{ANTENNA}} \longrightarrow G_1(\omega) \longrightarrow \underset{P(\omega)}{\text{PROBE}} \longrightarrow G_2(\omega)$$

we find that

$$H(\omega) = \frac{G_2(\omega)}{S(\omega)\ P(\omega)}$$

Therefore, correct determination of the antenna transfer function can only be made after the probe transfer function has been determined. This obviously requires that the probe has been calibrated by $S(\omega)$ as

$$P(\omega) = \frac{G_3(\omega)}{S(\omega)}$$

If the probe can be designed to produce an output which is the replica of the input signal, then it would have no effect on the input signal and its presence in the measuring circuit could be ignored. Replica waveform transmission may be approached in practice with a properly designed stub-monopole probe, but this can only be determined by separate tests.

The results of the probe analysis will therefore be presented in c. Drive pulse characteristics will be discussed in b.

Since it is necessary to be able to detect the effect of the antenna alone on the input pulse shape, it is important to know how the rest of the system influences these quantities. In practice, other system components such as interconnecting coaxial cables, connectors, delay lines, and attenuators always degrade pulse shape. Time domain reflectometry was, therefore, used in order to determine system losses and bandwidth limitations so that their influence on overall dispersion could be determined. This is discussed in a.

a. Time Domain Reflectometry (TDR) Circuit Analysis

The measuring circuit was analyzed using TDR techniques to identify and eliminate, where possible, internal component reflections. These measurements were made for the basic circuit configuration of Figure B-3, but with four different types of feed terminations: (1) open feed; (2) feed terminated into 50 ohms; (3) with stub-monopole as the

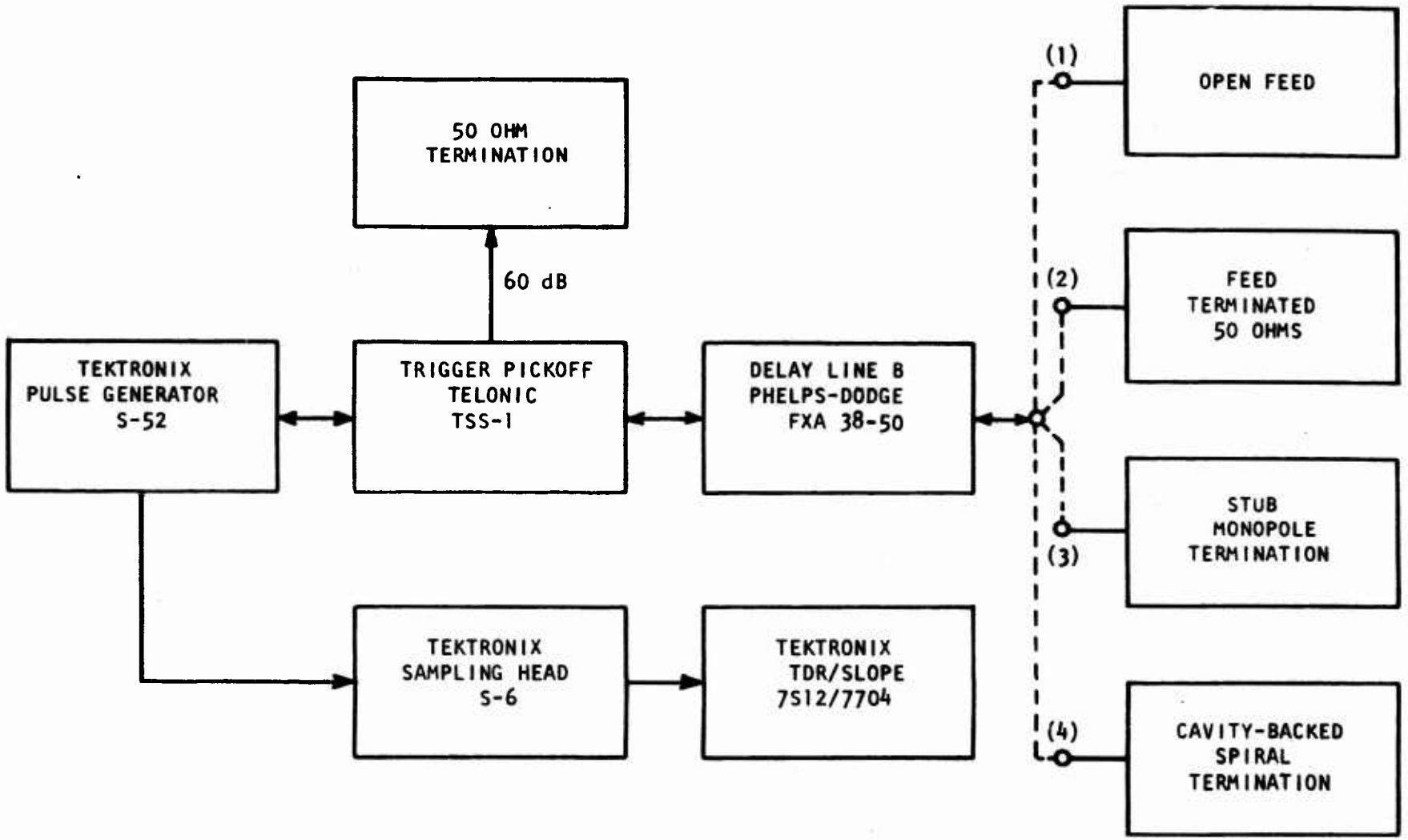


Figure B-3. Circuit Configurations for TDR Measurements

load; and (4) with a cavity-backed spiral antenna as the load. In the last configuration, VSWR and input impedance were measured for both cavity-backed spirals. Finally, delay line losses and overall system dispersion were determined.

(1) Open Feed

Figure B-4 demonstrates the quality of the circuit feed line up to the antenna. There are no noticeable reflections arising from circuit connections up to this point, until the reflection at the open end.[1]

(2) Feed Terminated into 50 Ohms

In Figure B-5(a), it is seen that the system is matched very well at 50 ohms. There is a slight discontinuity at the connector of the 50 ohm termination occurring at 142 ns after pulse initiation. Recalling that this represents the two-way transit time of the feed line, it is understood that the actual time of occurrence is 71 ns. Figure B-5(b) shows a magnification of this region. The mismatch is caused by the reduction in connector size from Type "N" to Type "BNC" on the terminator.

---

[1] This photograph is also used to normalize ρ, the reflection coefficient, as follows. The second step, caused by the reflection at the open feed end, represents $\rho = 1$. Therefore, from the photo one has

$$\rho = k_{100}\, \rho \text{ meas.}$$

where $k_{100} = 4.44$ is the scale normalization factor on the 100 mρ/division range. It has been determined that $k_{100} = k_{50} = k_{20}$, and that $k_{10} = 13.3$.

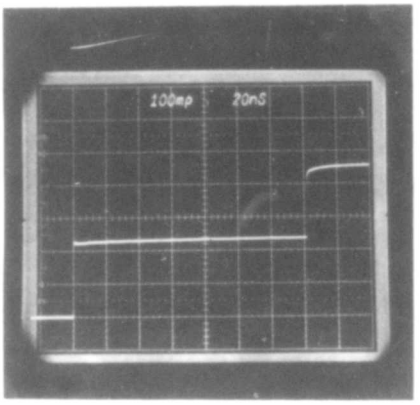
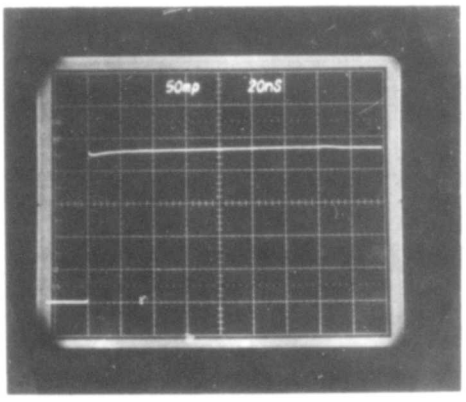
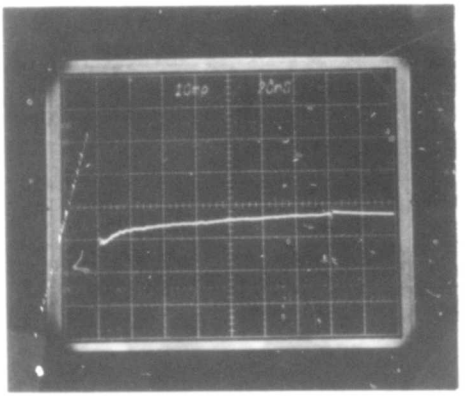


Figure B-4. TDR of Circuit with Open Feed



(a) Feed Terminated into 50 ohms.



(b) Magnification Showing Terminator Reflection

Figure B-5. Feed Terminated into 50 Ohms

(3) Feed Terminated into Stub Monopole

The TDR configuration for the 2 cm stub monopole probe was slightly different from that shown in Figure B-3. Here the actual signal return cable (FXA-38-50) has been used instead of the original delay line. The trigger pickoff has also been removed from the circuit. The reason for this change was to analyze the probe in its actual in-circuit configuration.

That the stub monopole appears little different from the open feed configuration is seen by comparing Figure B-6(a) to Figure B-4. The actual risetime of the signal return circuit containing approximately 45 ns of cable plus the 2.6 meter long probe can be determined from Figure B-6(b). It is seen that the 10 percent to 90 percent return circuit risetime is about 200 ps, indicating a frequency response up to 5 GHz.

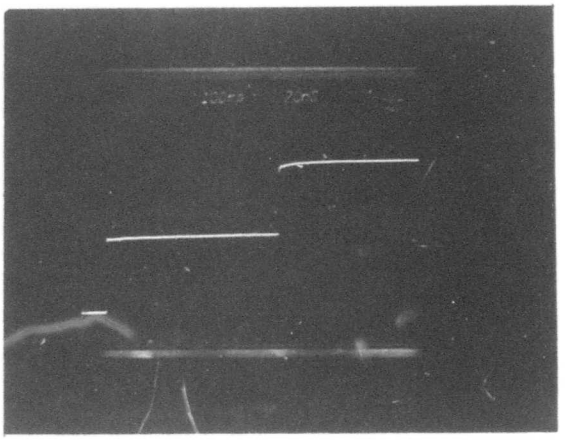
(4) Feed Terminated into Cavity-Backed Spiral Antennas

(a) ASN 117AA S/N 107

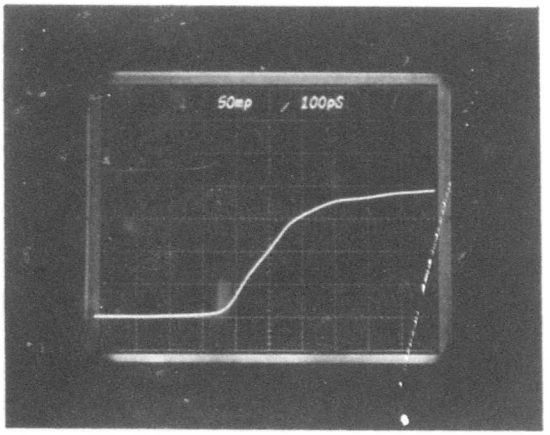
In Figure B-7(a), the first step duration corresponds to twice the delay line transit time, t_{DL}. The second step is the reflection due to the antenna, again twice the antenna transit time, t_{ANT}. It is seen that t_{ANT} = 18 ns, which can be taken as the upper limit in antenna dispersion duration.

Figure B-7(b) shows an expanded view of the antenna region. The discontinuity at 2.5 ns is believed to be due to a reflection from the transmission line termination at feed point on the spiral center.

The voltage standing wave ratio and input impedance of this antenna are found to be



(a) Feed Terminated with 2 cm Stub Monopole Probe



(b) Risetime of Signal Return Circuit to Determine Overall Frequency Response.

Figure B-6. Feed Terminated into Stub Monopole

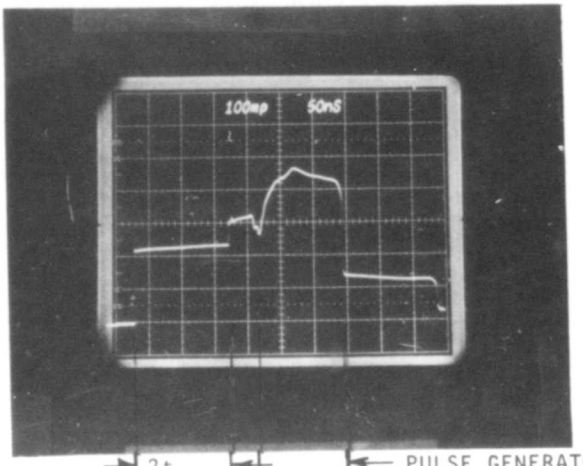


Figure B-7(a). TDR of System Terminated with Cavity-Backed Spiral ASN 117AA S/N 107

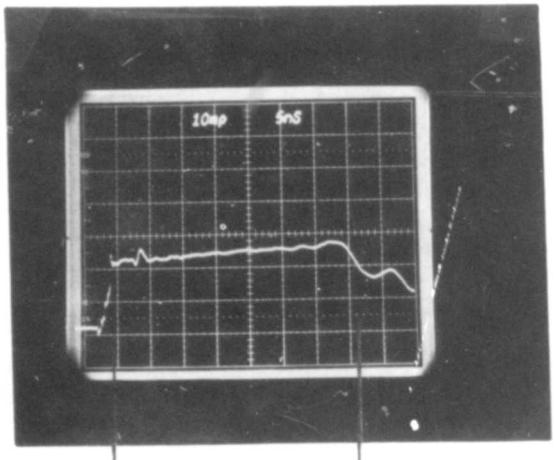


Figure B-7(b). Expanded View of Antenna Region

$$\rho' = k_{10}\ \rho \text{ meas.}$$

$$\text{VSWR} = \frac{1 + |\rho'|}{1 - |\rho'|} = 1.72$$

$$Z_{ANT}\ Z_o \frac{1 + \rho'}{1 - \rho'} = (50)\ (1.72) \text{ ohms} = 86 \text{ ohms}$$

(b) ASN 117AA S/N 108

In Figure B-8(a), the first step duration is twice the return cable transit time t_{L2}. The second step represents the antenna characteristics with t_{Ant} = 17.5 ns. The large, slowly rising pulse in the center of this photograph is due to re-reflection of the incident pulse after high frequency losses.

The antenna region is shown on an expanded scale in Figure B-8(b). This antenna was found to have the following characteristics:

$$\rho' = k_{20}\ \rho \text{ meas.}$$

$$\text{VSWR} = 1.85$$

$$Z_{ANT} = 92.5 \text{ ohms}$$

b. IKOR Pulse Generator Characteristics

The characteristics of the IKOR MODEL R100 IMP Generator were measured from the photographs shown in Figures B-9(a) and (b):

(1) Risetime

(10 percent - 90 percent) tr = 175 ps

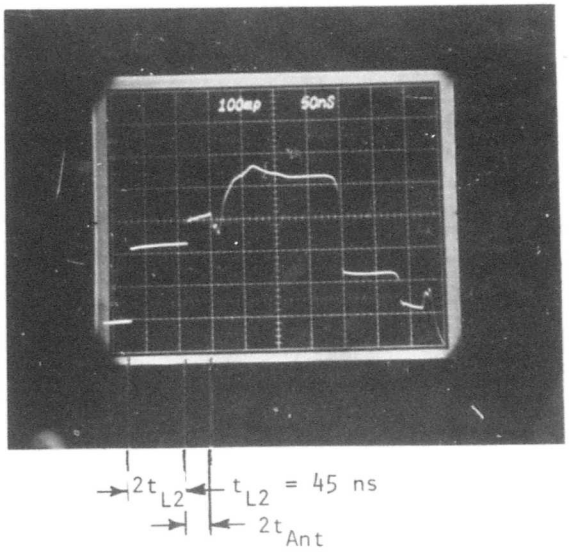


Figure B-8(a). TDR of System Terminated into Cavity-Backed Spiral ASN 117AA SN 108

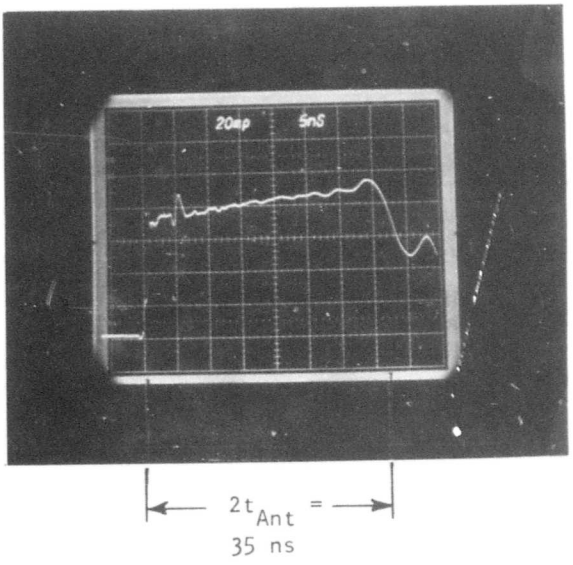
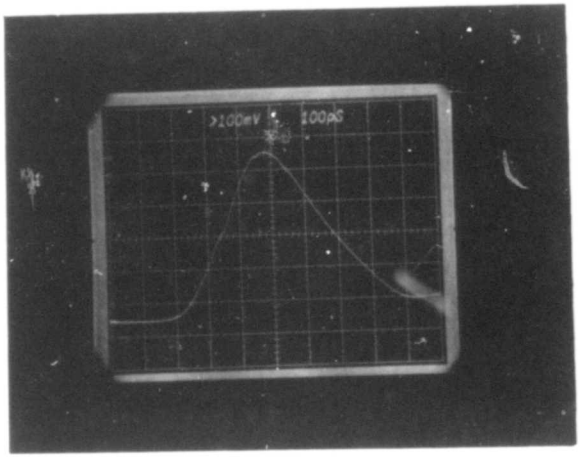
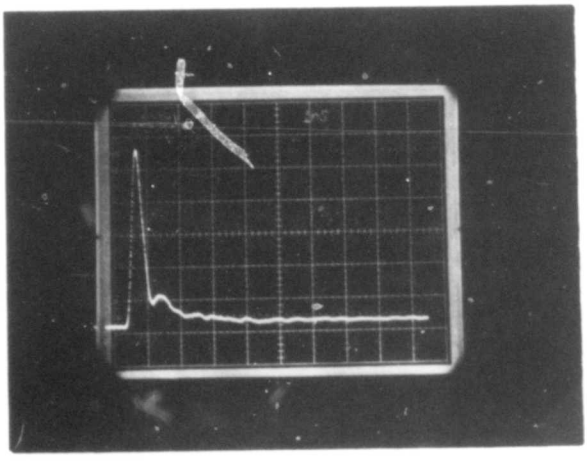


Figure B-8(b). Expanded View of Antenna Region



(a) IKOR Pulse Generator Waveform



(b) Input Pulse Waveform Showing
Comples Structure Following Main Peak

Figure B-9. IKOR Pulse Generator Characteristics

(2) Pulse Width

(-3 dB)	235 ps
(3) Pulse Amplitude	1106 volts (540 mV + 66 dB)
(4) Pulse Repetition Rate	250 pps

As can be seen from Figure B-9(b), this pulse does have a rather complex energy distribution with a secondary maximum of about 12 percent of the peak value. Following this, the amplitude tends toward zero asymptotically over about 7 ns.

c. Stub Monopole Receiving Probe

A considerable experimental effort was made to correctly model and determine the receiving probe characteristics. It is desirable that this field probe should produce an output which is the replica of the transmitted pulse. Two identical probes were made as shown in Figure B-10. The two probes were supported vertically by styrofoam stands at a separation of 1 meter. One probe, used as a transmitting antenna, was impulsed with an IKOR pulse generator and this signal was measured using the record probe as shown in Figure B-11. It is seen that the output signal from the receiving probe resembles approximately the derivative of the input pulse waveform. However, it is not obvious whether this differentiation occurs at the transmitting stub-monopole or at the receiving stub-monopole. Clearly, only one probe is taking the derivative. This problem was resolved as follows. It is known that a long wire over a ground plane transmits a replica of the input pulse. A ground plane consisting of an aluminum disk 30 cm in diameter was attached to the transmitting probe outer coax and wire lengths up to 60 cm were added to the center conductor as shown in Figure B-12. These

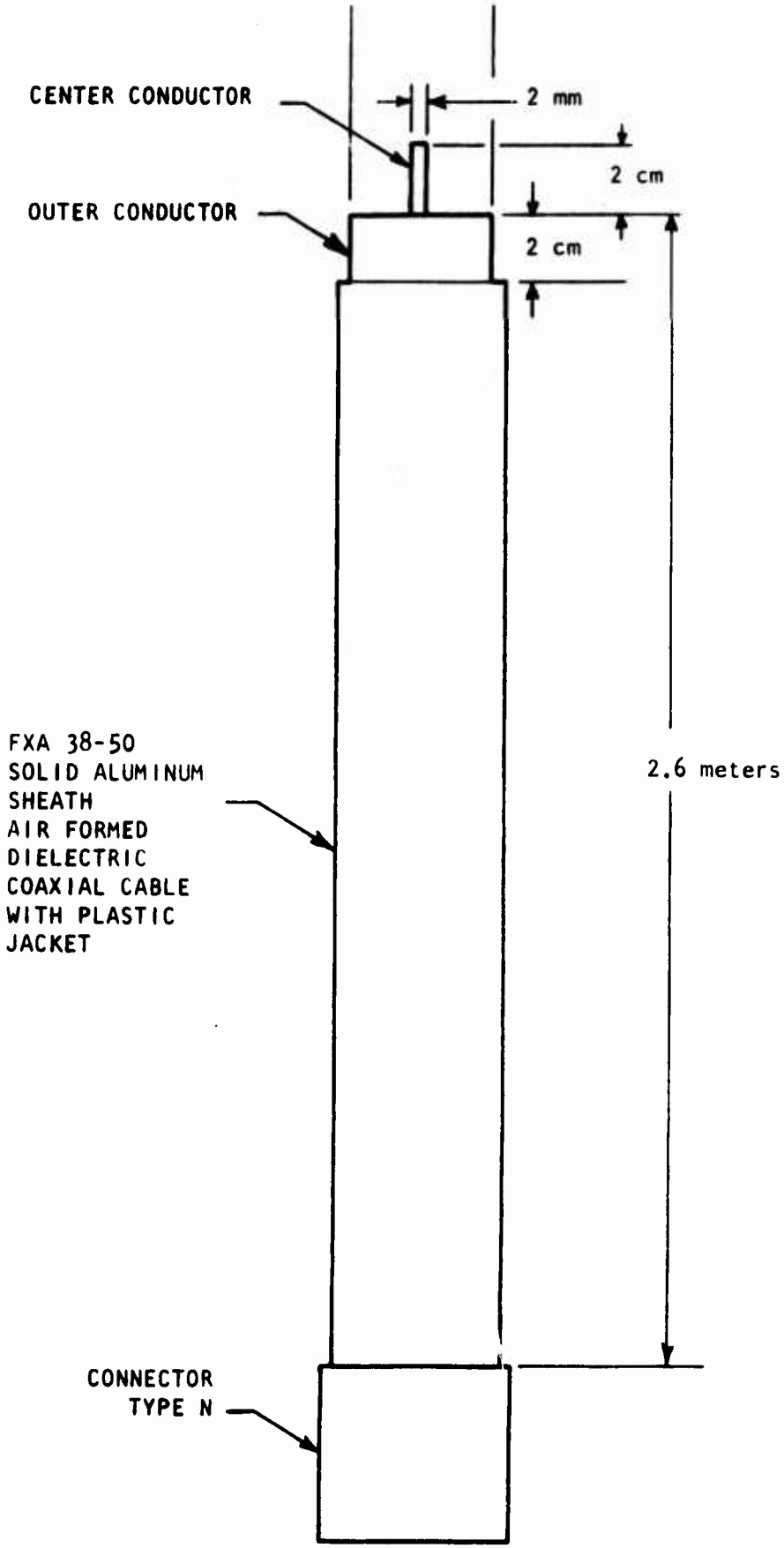
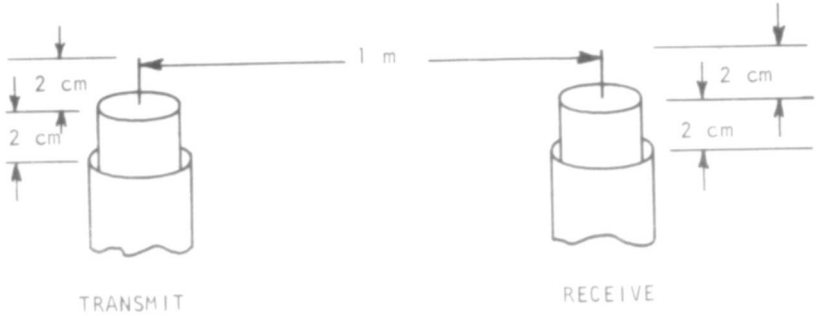
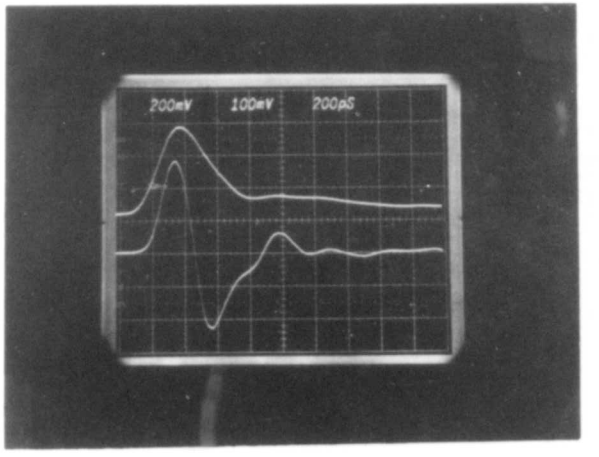


Figure B-10. Stub-Monopole Probe



(a)



(b)

Figure B-11. Stub-monopole probe response. (a) Measurement Configuration; (b) Upper Trace is the Input Pulse; Lower Trace is the Receive Probe Response - the Derivative of the Input Pulse

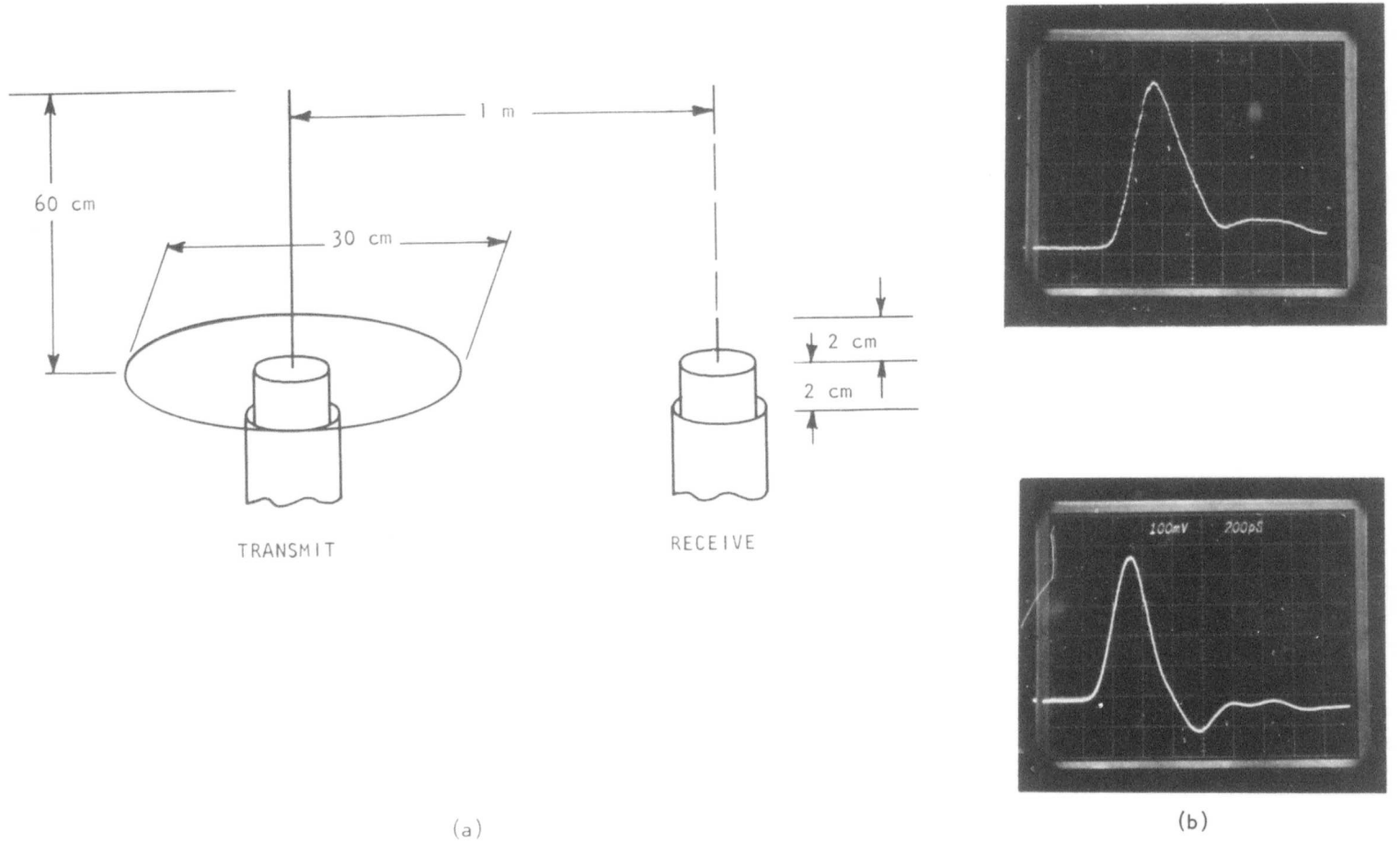


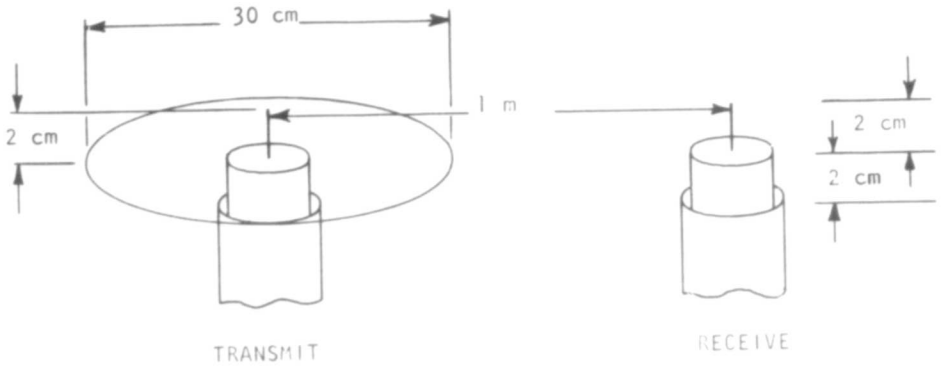
Figure B-12. Long Wire Over Ground Plane Response. (a) Measurement configuration. (b) The input pulse is shown in the top trace, the nearly replica response of the receive probe in the lower trace. Comparison shows the latter to lack some low frequency content due to the transmit probe center conductor length of only 60 cm

measurements clearly show that as the center conductor becomes longer, the output waveform from the receiving probe approaches a replica of the input signal. Furthermore, this means that the receiving probe does indeed receive a replica of whatever signal was transmitted. Conversely, when the ground plane remains on the transmitting monopole and its center conductor is shortened to 2 cm, then the response is as shown in Figure B-13: it now takes two derivatives - one because it is a stub-monopole over ground plane and one because it is used as the transmitting antenna. Reciprocity is seen to hold in Figure B-14 where the transmitting and receiving roles are reversed. Here the stub-monopole takes one derivative on transmit and the stub-over-ground plane, being a derivative sensor, takes an additional derivative upon receive.

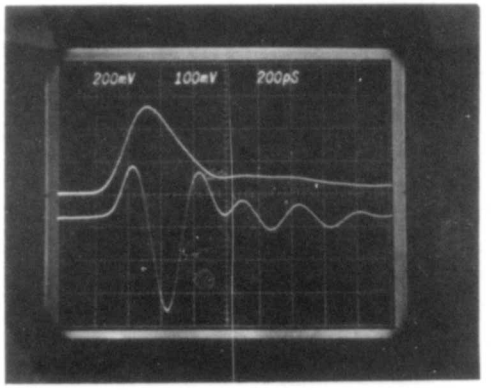
In conclusion, the short stub-monopole probe can receive a replica of the transmitted waveform. The extent to which this probe actually does receive a replica, of course, depends upon its frequency response and, in turn, upon stub length, diameter and capacitance. As indicated in the TDR analysis, this 2-cm stub-monopole has a response to about 5 GHz. In measurements involving several transfer functions such as is always the case in antenna transfer function measurements, the probe transfer function should not be ignored.

4. ANTENNA TRANSFER FUNCTION MEASUREMENTS

Prior to recording the dispersed pulse waveform of the cavity-backed spiral, the far-field region of this antenna was established. This was done by observing the rate of amplitude decay for a low frequency component of the dispersed pulse as a function of the probe - antenna separation distance. The far-field region was taken to be the distance where this amplitude began to fall off as 1/r. This region was found to start at a separation of about 75 cm. The separation distance at which the dispersed pulse measurements were actually made

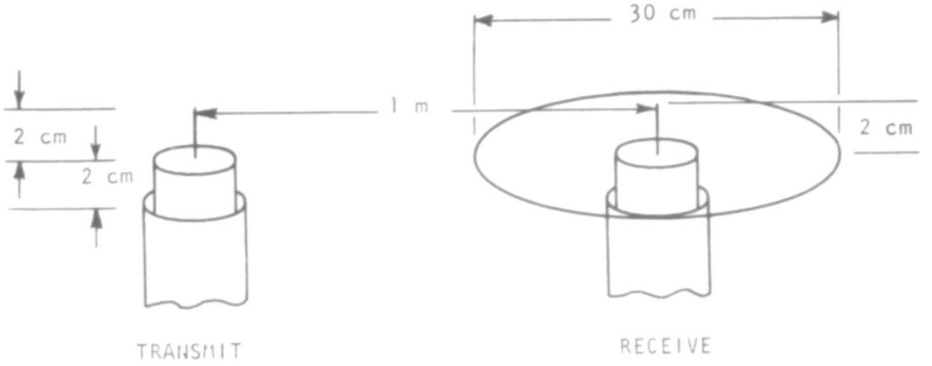


(a)

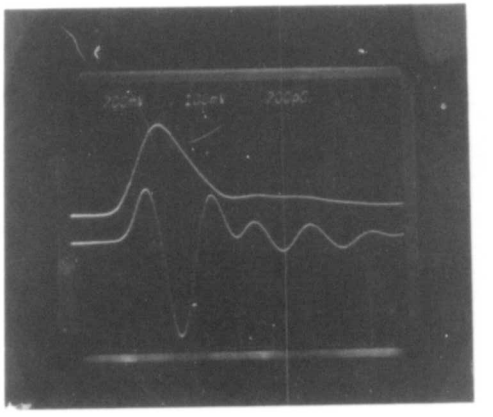


(b)

Figure B-13. Response of a 2-cm Monopole to a Monopole Over Ground Plane. (a) Measurement configuration. (b) Upper trace shows input pulse; lower trace is the replica response of the receive probe to a second derivative transmitted pulse



(b)



(b)

Figure B-14. Response of a 2 cm-Monopole Over Ground Plant to 2 cm Monopole Antenna Showing Reciprocity. (a) Measurement configuration. (b) Upset trace is the input pulse; the lower trace is the derivative response of the receive probe. Transmit stub monopole transmits the derivative of the input pulse.

was chosen to be 100 cm. This separation distance was later increased to 200 cm when using two cavity-backed spirals.

The geometrical arrangement for one-way dispersion measurements is shown in Figure B-15. The results of these measurements on both antennas are shown in Figure B-16(a) and 16(b), for S/N 107 and 108 respectively.

From Figure B-16(a), it can be seen that the period at the beginning of the dispersed pulse is approximately 250 ps corresponding to a highest radiated frequency of about 4 GHz. This pulse has the character of an amplitude and frequency modulated waveform which decreases in frequency as time increases. Total time duration is about 15 ns at which time the frequency has reduced to about 200 MHz at these end points, pulse amplitude is roughly -20 dB.

There is slight variation in the dispersion between the two antennas.

In the past, most measurements of the dispersion have been performed using two identical antennas to transmit and receive the pulse. It has been reported[2] that in this case the pulse is dispersed twice, once by each antenna, and that the pulse duration is therefore twice as long as that given by a single antenna. When two-antenna dispersion was compared with single-antenna dispersion in our measurements, this was indeed found to be true.

---

2 Paul Van Etten, Rome Air Development Center, Griffiss Air Force Base, New York, private communication.

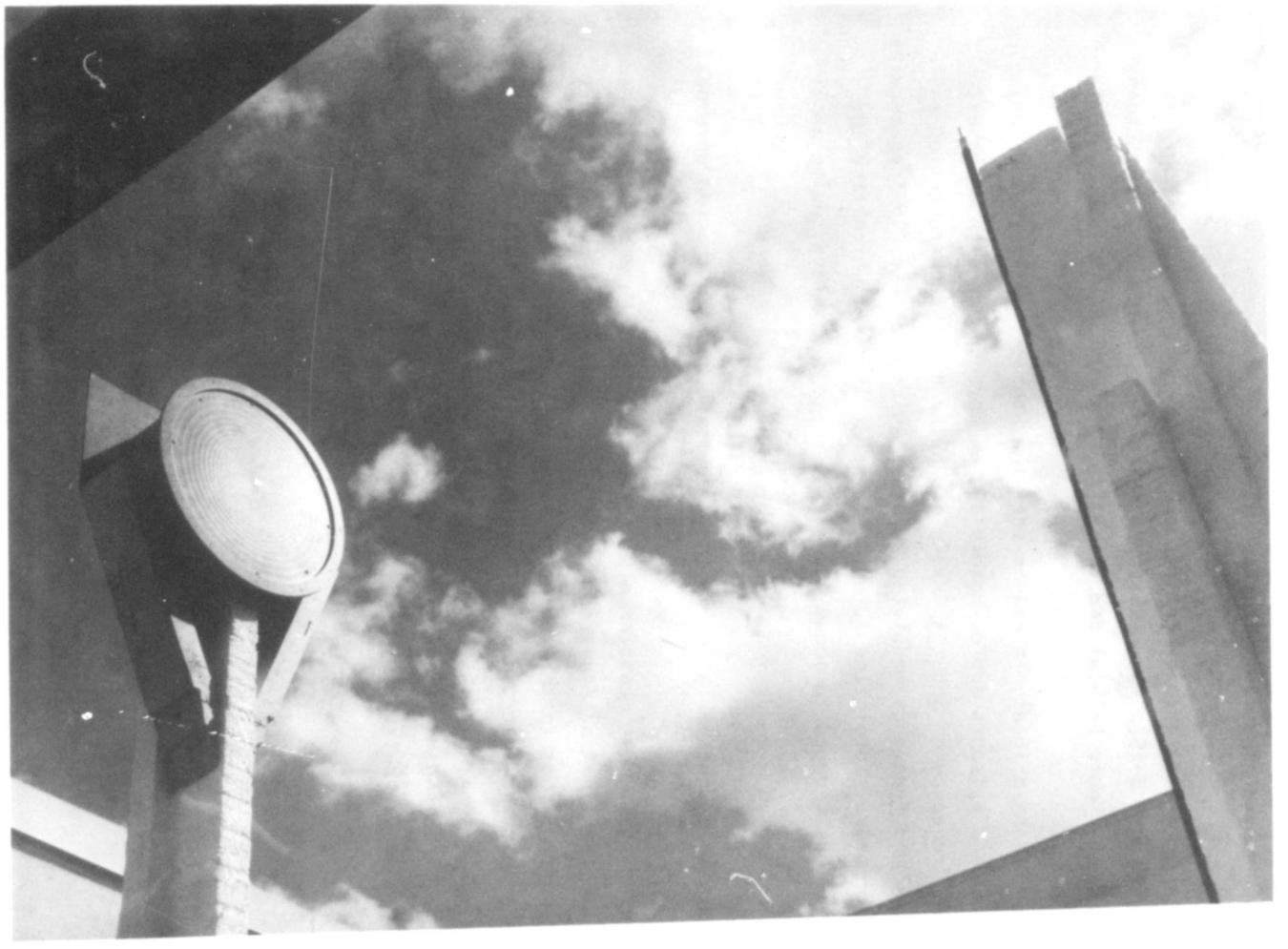
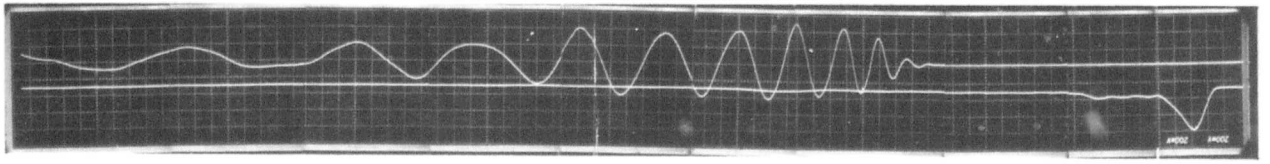
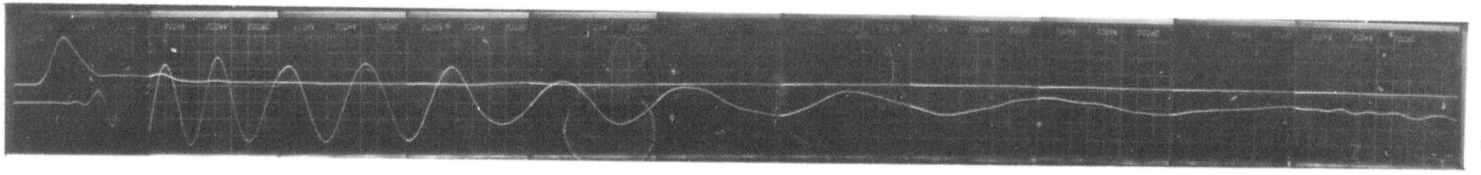


Figure B-15. A View of the Arrangement for One-Way Dispersion Measurements. Anetenna-Probe Separation is 1 Meter; Height Avove Ground (to Center of Spiral) is 2.6 Meters. (Poor inside Light Necessitated outdoor Photograph)



(a)



(b)

Figure B-16. Antenna Dispersion Results for (a) Cavity-Backed Sprial (ASN 17AA, S/N107) and (b) Cavity-Backed Spiral (ASN 17AA, S/N108). The Upper Trace in Each Photograph Shows the Input Pulse at -60 dB. The Lower Trace is the Transient Response (Dispersed Pulse) of the Antenna When Measured by a 2-cm Stub Monopole Probe as Shown in Figure 15

5. OTHER MEASURED RESULTS

In addition to the measurements performed at BDM for ASN-117 AA, Mr. VanEtten of RADC has measured* dispersion pulses of other antennas. Some of his measured data are included here for reference purposes.

Figure B-17 shows the result of dispersion by APN-995B when it was driven by the time-derivative of an "impulse." Dispersive response of this antenna was also measured by use of an "impulse." Except that the highest frequency components are slightly lower than those shown in Figure B-17, the antenna produced almost identical waveforms for both the "impulse" and its time derivative.

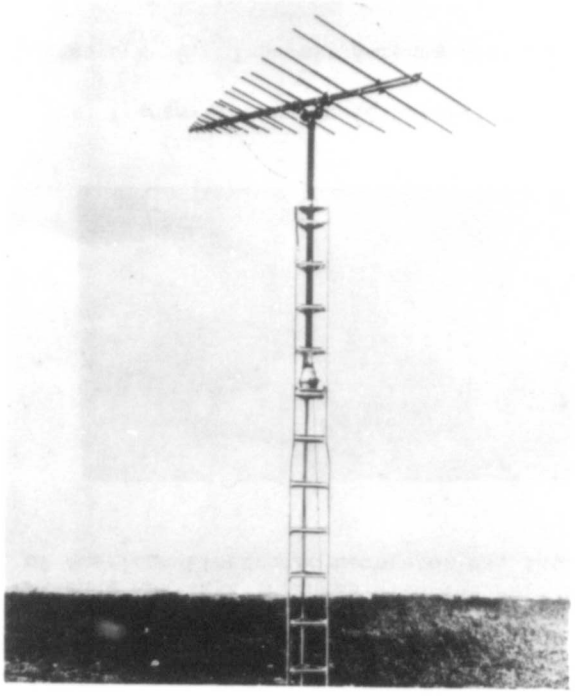
Figure B-18 shows an "impulse" that was applied to the transmitter antenna ASN-1232. The antenna's dispersion pulse was measured by a stub-monopole sensor position at the transmitting-antenna's far zone. Similar measurements for APX-254 are shown in Figure B-20.

Figure B-19 shows dispersion pulses (0.4 ns/div and 1.0 ns/div) of ASN-116 A. The measurements were made by using two identical antennas: one for transmit and the other for receive. The transmit antenna was driven by a "unit-step" pulse instead of an "impulse."

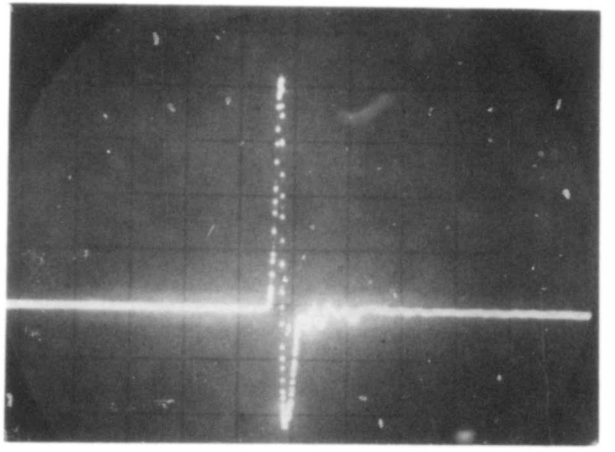
Analyses and transfer functions of these antennas are given in Appendix C.

---

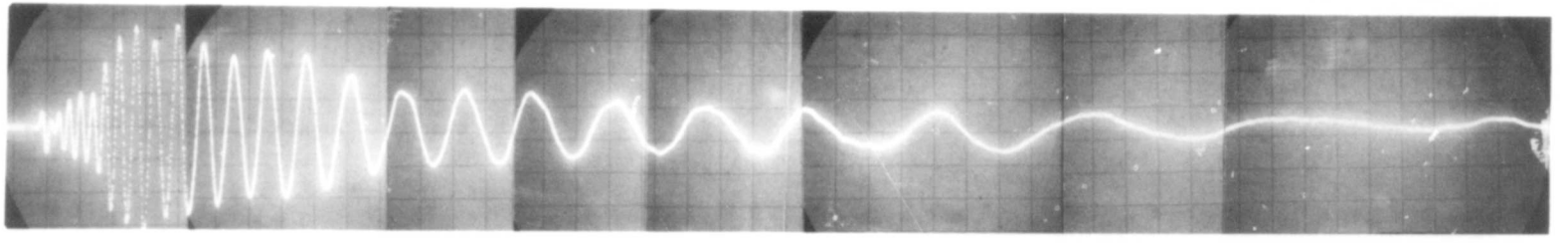
*VanEtten Paul, "Temporal-Spatial Compression Antennas," Technical Report RADC-TR-73-179, Rome Air Development Center, Air Force Systems Command, Griffiss Air Force Base, N.Y., September 1972.



(a) Antenna APN-995B (Printed With the Permission of American Electronic Laboratories Inc.)

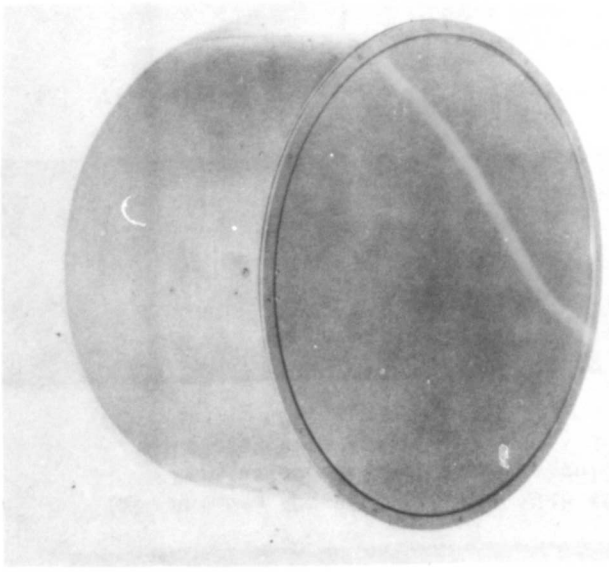


(b) Input Pulse (2 ns/div) to APN-995B (Furnished by RADC)

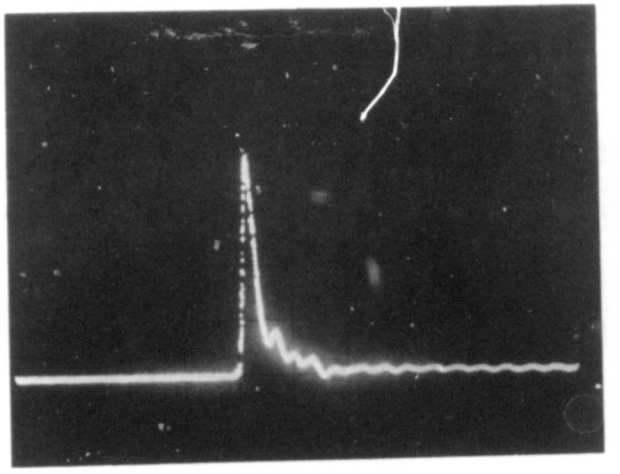


(c) Transmitted Dispersion Pulse (2 ns/div) With Low-Frequency Arms Fully Extended (Furnished by RADC)

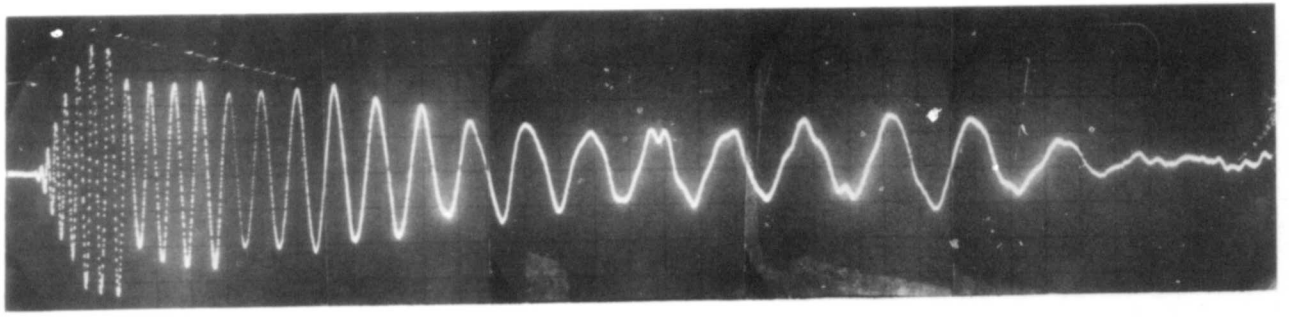
Figure B-17. Transmit Antenna APN-995B and Its Dispersion Pulse Received by a Stub-Monopole Sensor



(a) Antenna ASN-1232 (Printed with the Permission of American Electronic Laboratories, Inc.)



(b) Input Pulse (2 ns/div) (Furnished by RADC)



(c) Transmitted Pulse (2 ns/div) (Furnished by RADC)

Figure B-18. Transmit Antenna ASN-1232 and Its Dispersion Pulse Received by a Stub-Monopole Sensor

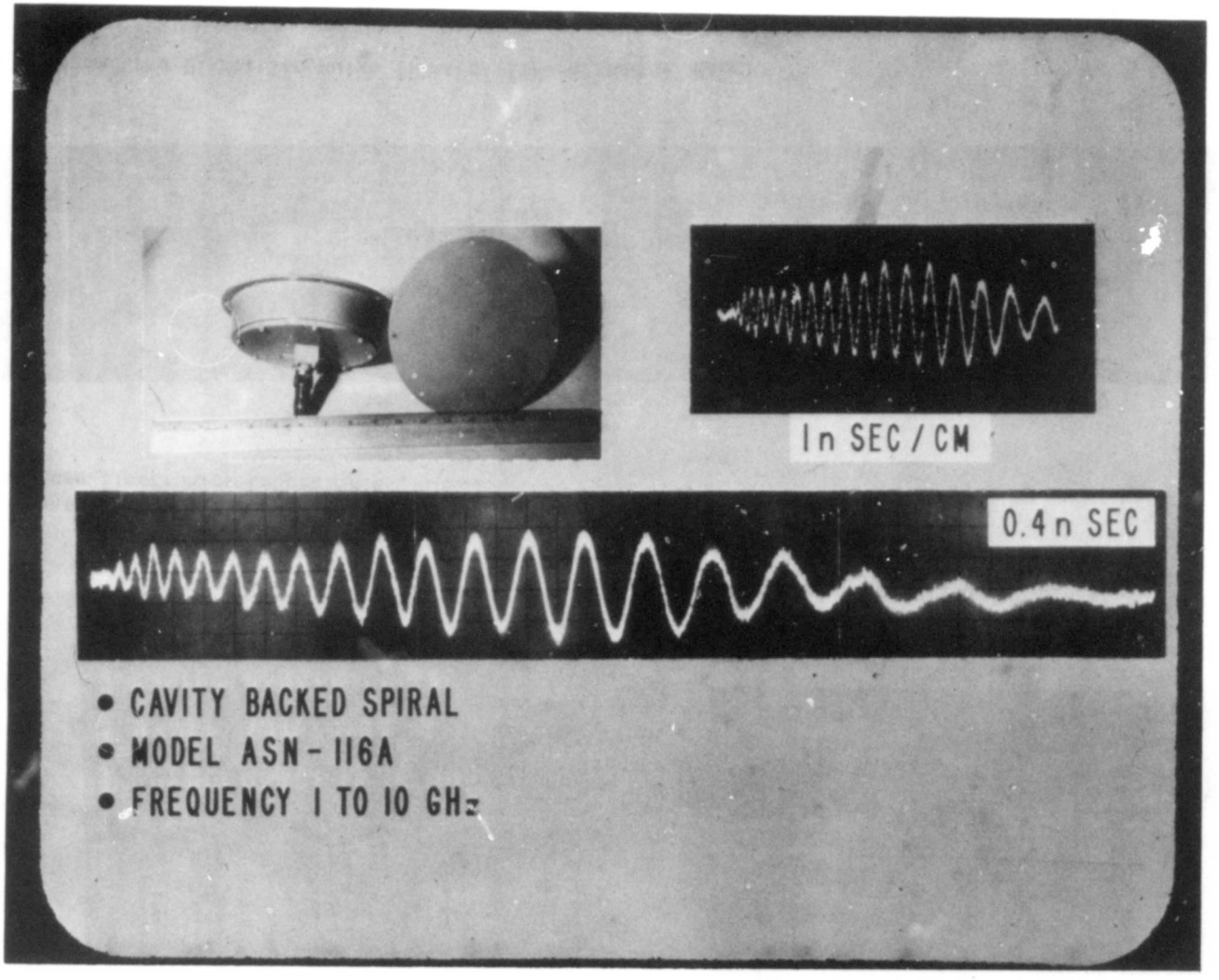
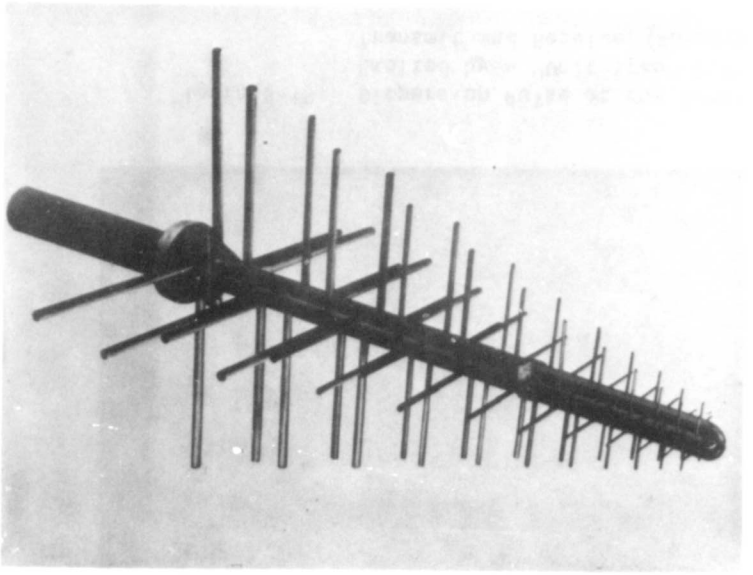
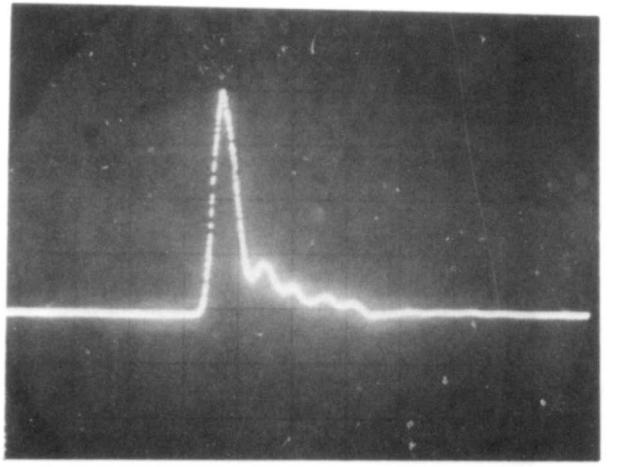


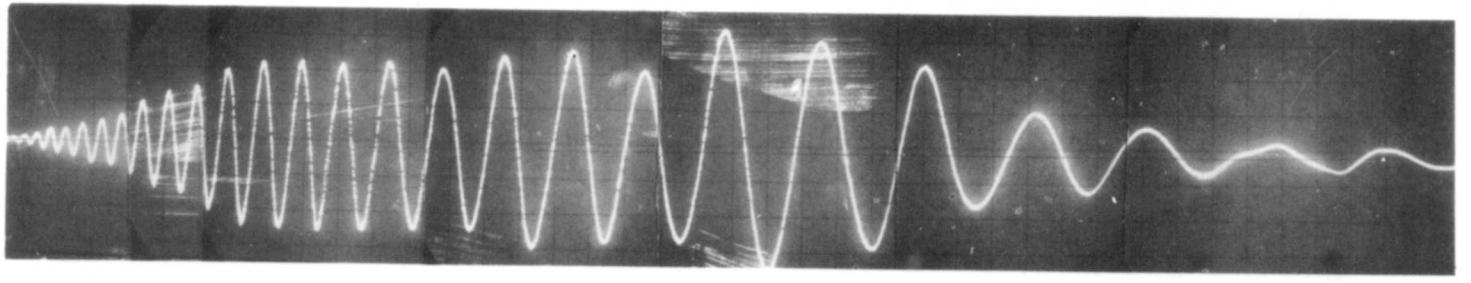
Figure B-19. Dispersion Pulse at the Receive-Antenna Terminal When the Transmit Antenna is Excited by a "Unit-Step" Pulse (Two Identical Antennas are Used for Both Transmit and Receive) (Furnished by RADC)



(a) Antenna APX-254 (Printed With the Permission of American Electronics Laboratories, Inc.)



(b) Input Pulse (1 ns/div) (Furnished by RADC)



(c) Transmitted Dispersion Pulse (1 ns/div) (Furnished by RADC)

Figure B-20. Transmit Antenna APX-254 and Its Dispersion Pulse Received by a Stub-Monopole Sensor

APPENDIX C

TRANSFER FUNCTION AND COMPRESSED PULSE OF DISPERSIVE ANTENNAS

1. INTRODUCTION

Dispersive characteristics of wide band antennas are most easily determined by measuring their responses due to a transient input. This appendix is intended to give analyses on certain measured data so that measured antennas can be characterized for possible pulse compression applications.

Six antenna responses have been selected for digitization, Fourier transformation, and dispersion characterization. These antennas are manufactured by the American Electronic Laboratories, Inc. (AEL) and they are briefly summarized as follows:

MODEL (BY AEL)	TYPE	FREQUENCY	POLARIZATION
APN-502A	Pyramidal Log Periodic	0.2-3.0 GHz	Linear
ASN-116A	Cavity-Backed Spiral	1.0-10.0 GHz	Circular
ASN-1232A	Cavity-Backed	0.2-4.0 GHz	Circular
APN-995B	Coplanar Log Periodic	0.03-1.1 GHz	Linear
ASN-117AA	Cavity-Backed Spiral	0.4-4.0 GHz	Circular
APX-254A	Crossed Planar Log Periodic	0.4-4.0 GHz	Linear

Measurements on the responses of these antennas are described in Appendix B. Only digitized results presented in conjunction with analysis results are in this appendix. Before individual antennas are considered, the ideal "impulse" characteristics are to be discussed. Finally, conclusions will be drawn after a measurement probe is analyzed.

2. "IMPULSE" FUNCTION - DRIVING SOURCE

Ideally, the driving source for testing a dispersive antenna is an impulse that would have flat spectral density from dc to indefinitely high frequency. Since this source does not exist, the next best "impulse" is to have significant spectral density from dc to whatever highest frequency is of interest. Figure C-1 shows one-half of an "impulse" that has a cutoff duration of 100 picosecond (ps) with all the time sidelobes 40 dB or more below its peak value. These impulses have spectral densities as shown in Figure C-2 where the 10 GHz component is about 6 dB below the dc component. If an impulse has a cutoff duration of 1000 ps or 1.0 nanosecond (ns) the -6 dB bandwidth would be approximately from dc to 1.0 GHz.

Figure C-3 shows an actual impulse whose effective cutoff duration is about 1.5 ns. Its spectral density gives a -6 dB bandwidth from dc to 0.6 GHz as shown in Figure C-4. Unlike that of Figure C-2, the actual impulse has phase angles that are changing with the frequency as shown in Figure C-5.

3. TRANSFER FUNCTION OF CAVITY-BACKED SPIRAL ANTENNA ASN-1232A

For the driving source characterized in Figures C-3 to C-5, the dispersed pulse for antenna ASN-1232A is given in Figure C-6 where the cutoff duration is seen to be about 65 ns. Let the dispersed pulse be

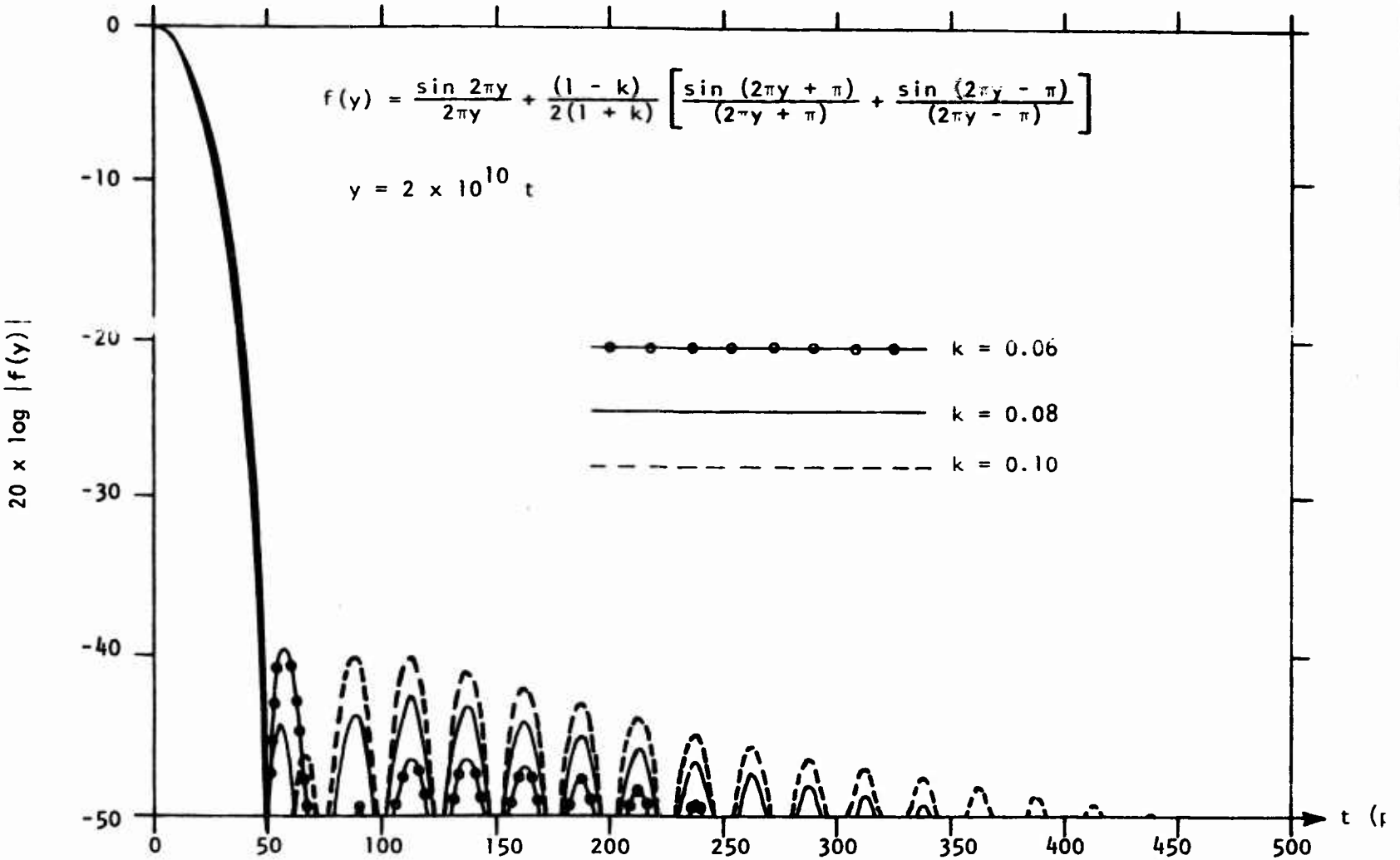


Figure C-1. Three 100-ps Pulses With Sidelobes More Than 40 dB Below Peak Value

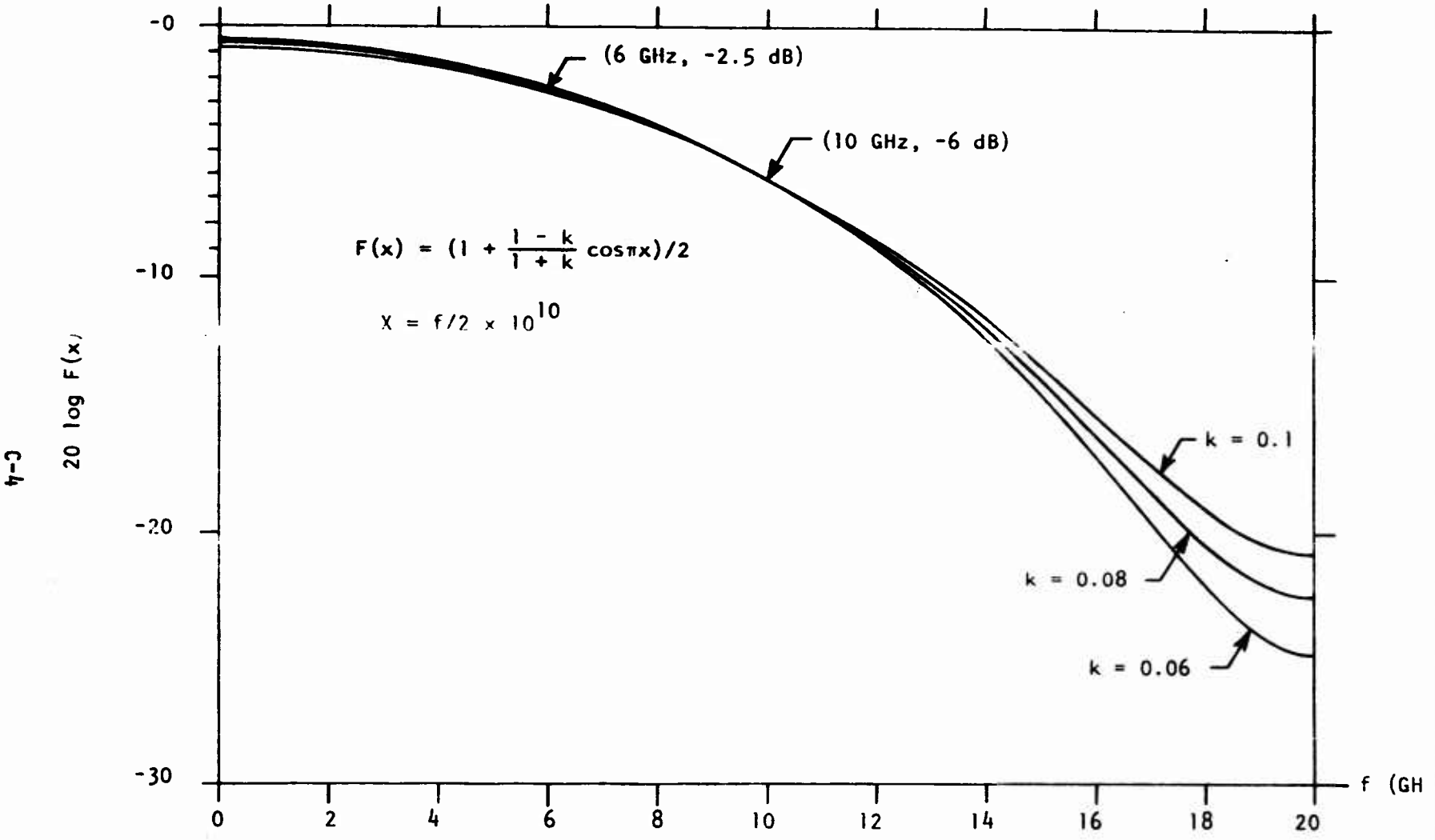


Figure C-2. Relative Spectral Distributions of Three 100-ps Pulses With Temporal Sidelobes More Than 40 dB Below Peak

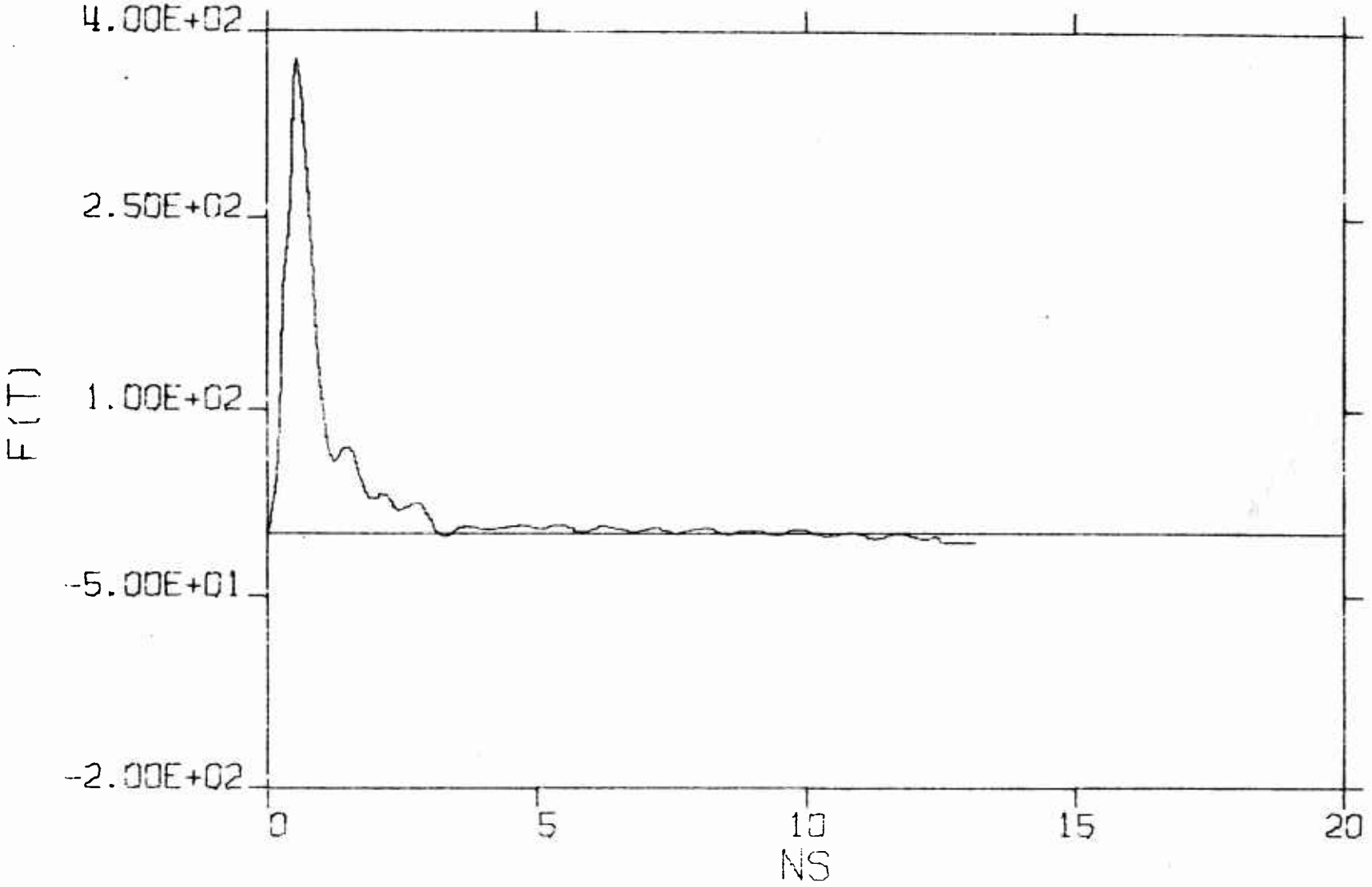


Figure C-3. "Impulse" Used to Drive Antenna ASH-1232A

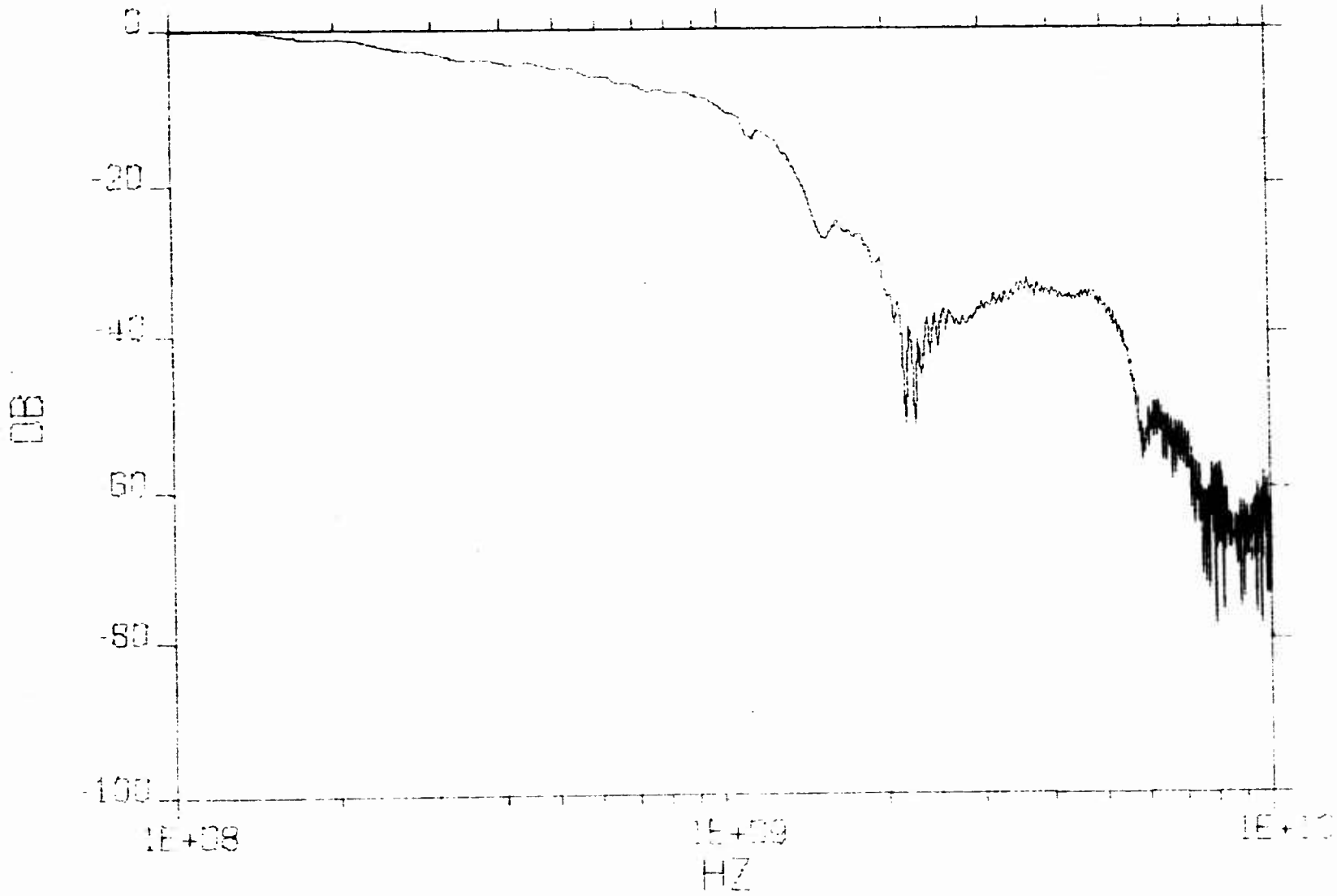


Figure C-4. Spectral Amplitude of the "Impulse" Used to Drive Antenna ASN-1232A

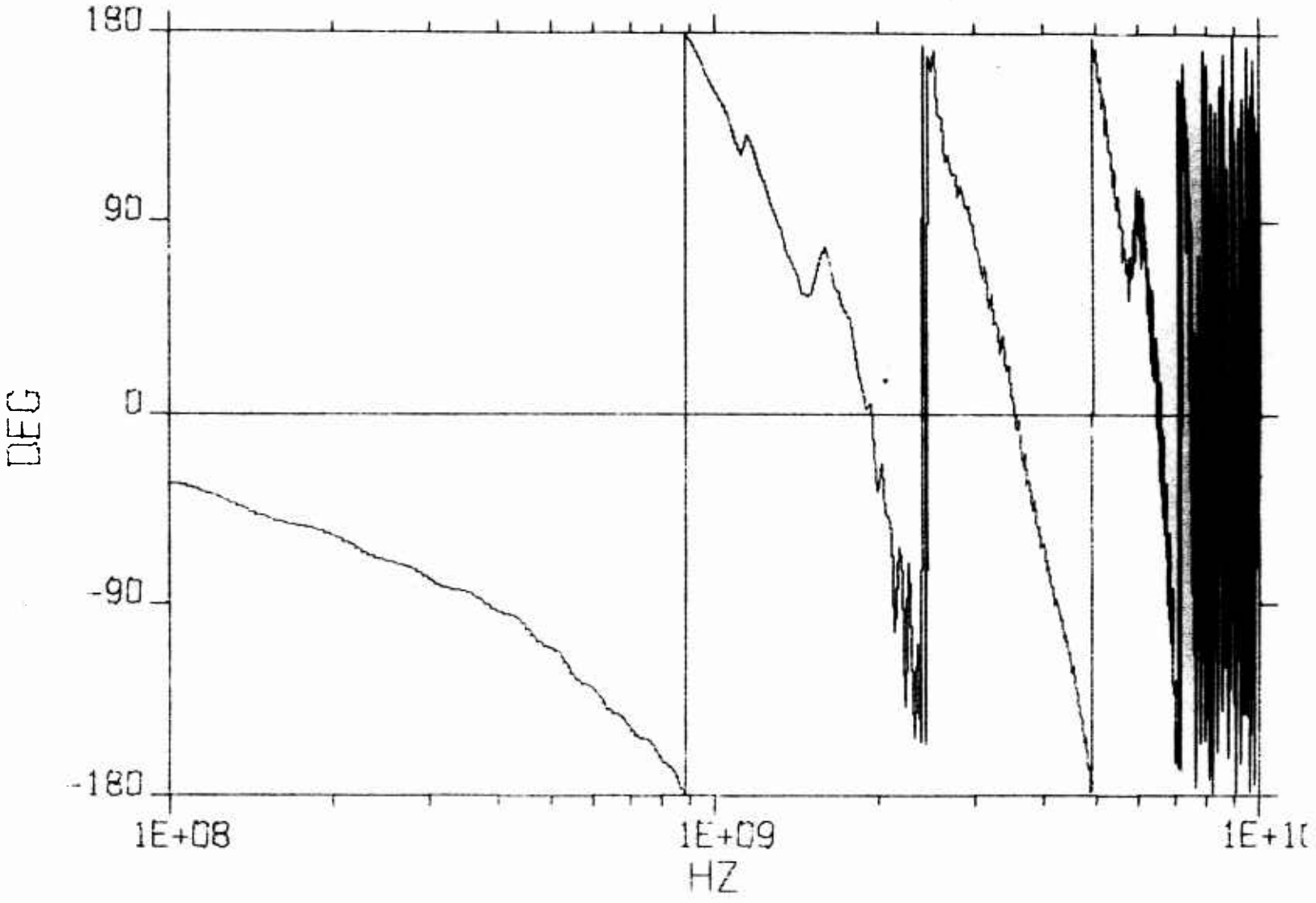


Figure C-5. Phase Angle Associated with the Spectrum of Figure C-4

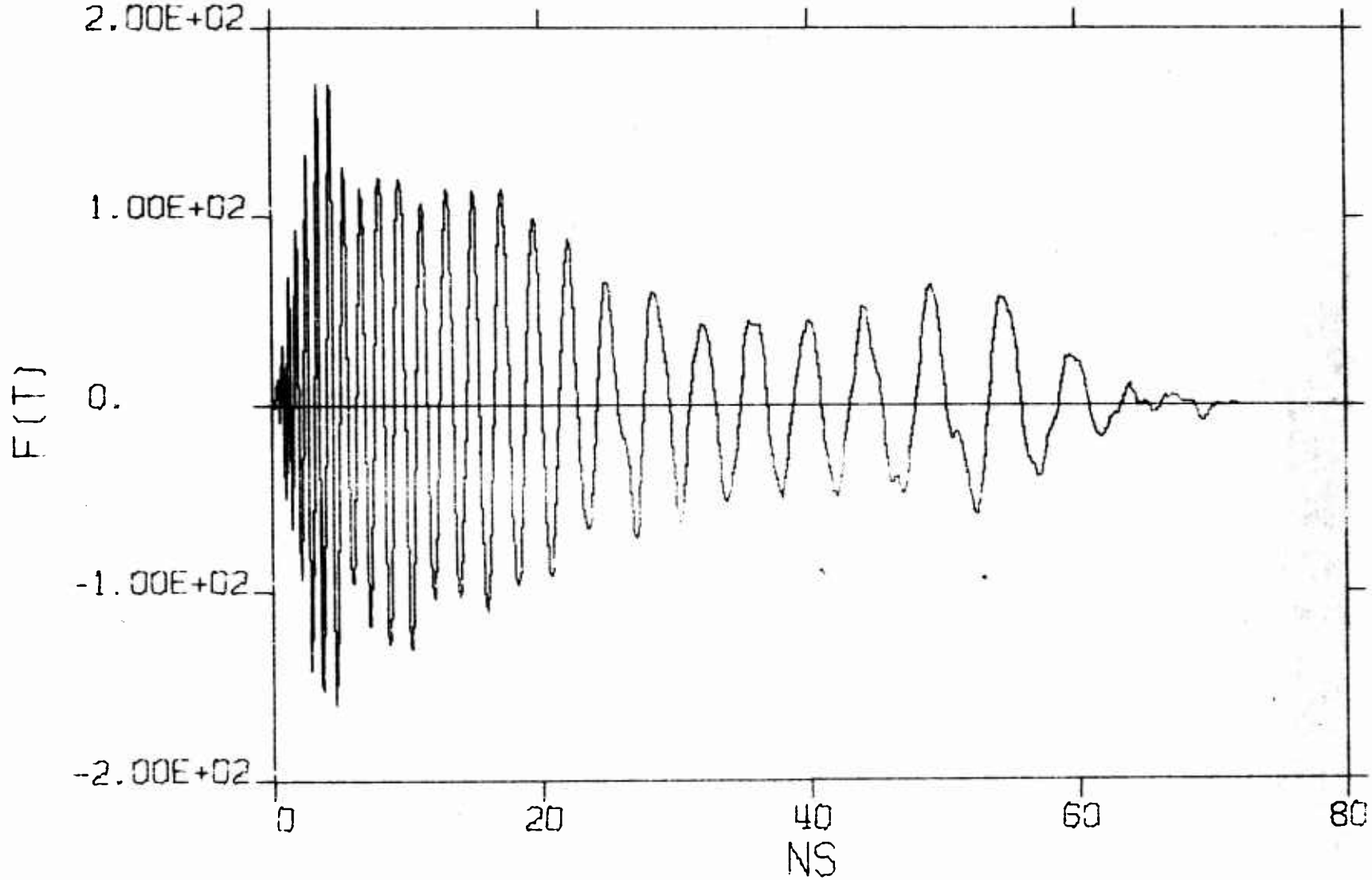


Figure C-6. The Dispersed Radiation $f_d(t)$ of ASN-1232A

$f_d(t)$ = Radiated dispersion when antenna is driven by the actual source (see Figure C-3 for ASN-1232A). (Eq. C-1)

the complex spectral density is defined as

$$F_d(f) = \int_{-\infty}^{\infty} f_d(t) \exp(-j2\pi ft)dt \qquad \text{(Eq. C-2)}$$

$$= |F_d(t)| \exp(j\phi_d(f))$$

where the amplitude of spectral density for the time function in Figure C-6 is shown in Figure C-7. With an amplitude reference at 0.2 GHz, the lowest CW-specified frequency 4.0 GHz is seen to have dropped to about -40 dB. Phase angle of the dispersed pulse spectrum is seen in Figure C-8 to have approximately log-periodic nature from 0.15 GHz to 0.9 GHz. Both spectral amplitude and phase of the dispersed pulse have indicated that this particular antenna radiates expected characteristics only from 0.15 to 0.9 GHz. Since the driving source (Figures C-4 and C-5) is affecting the dispersed pulse, it is desirable to eliminate its effects so that antenna characteristics can be obtained independent of the source. Let source function in the frequency domain be written as

$$S(f) = |S(f)| \exp(j\phi_s(f)) \qquad \text{(Eq. C-3)}$$

the antenna transfer function becomes

$$F_a(f) = F_d(f)/S(f) \qquad \text{(Eq. C-4)}$$

$$= |F_d(f)/S(f)| \exp(j(\phi_d(f) - \phi_s(f))$$

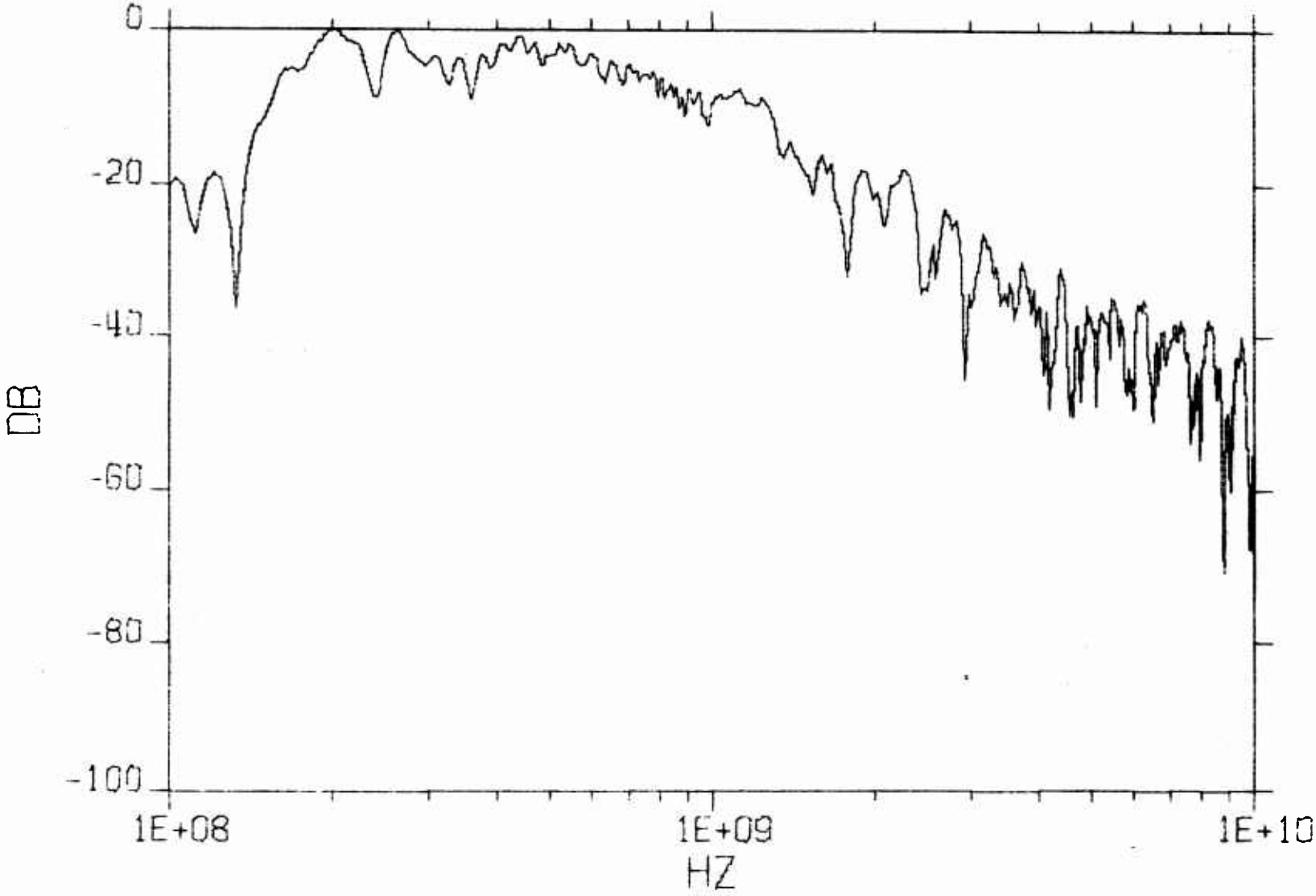


Figure C-7. Spectral Density Amplitude of $F_d(t)$ for Figure C-6

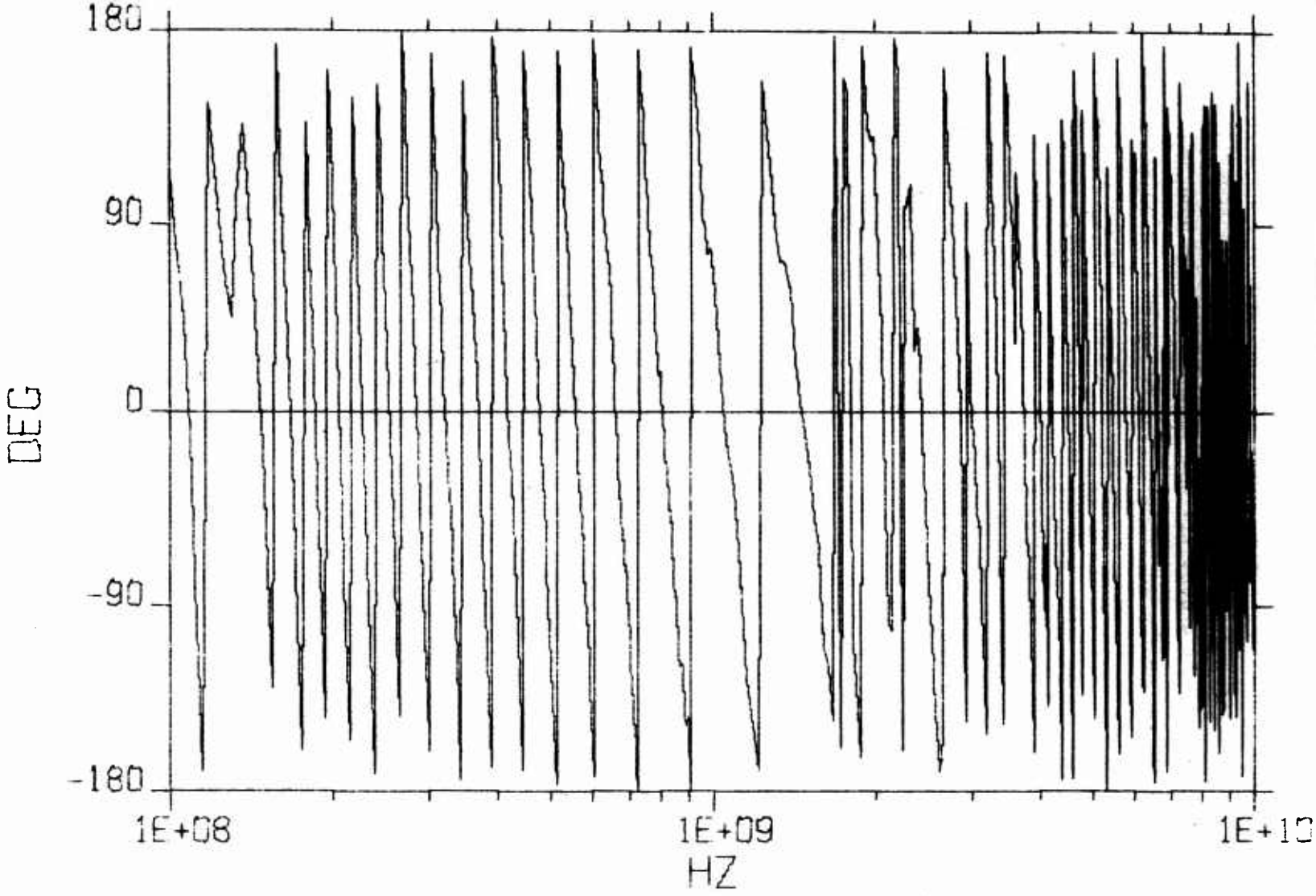


Figure C-8. Phase Angle $\phi_d(f)$ Associated with Figure C-7

Figure C-9 shows the amplitude of the ASN-1232A transfer function. The extremely high response around 2.1 GHz is caused by the deep null existing (Figure C-4) in the source and should be considered as a noise-induced result. The phase angle of the transfer function is shown in Figure C-10 where large deviations from log-periodic nature take place around 1.9 GHz and 3.0 GHz. Since deep nulls are also observed at 1.9 and 3.0 GHz in Figure C-9, it appears that the particular antenna used in the measurements has defects around the two frequency bands. Except for these two bands, the overall antenna transfer function is seen in Figures C-9 and C-10 to have a fairly flat amplitude and log-periodic phase from 0.15 GHz to 3.9 GHz.

4. TRANSFER FUNCTION OF CAVITY-BACKED SPIRAL ANTENNA ASN-117AA

Characteristics of this antenna were processed the same way as those of the previously discussed antenna. Figure C-11 shows the driving source with a truncation at about 6 ns. Its spectral amplitude and phase are shown in Figures C-12 and C-13. They show that the pulse has a (-20 dB) bandwidth of about 1.8 GHz. Significant spectral nulls occur about 2.7 GHz and 3.3 GHz. As a result, one anticipates that the transfer function of test antenna cannot be accurately evaluated near these nulls.

The radiated dispersion pulse is shown in Figure C-14 where the -10 dB duration is seen to be about 14 ns. The peak spectral component of the dispersed pulse is seen to be about 1 GHz in Figure C-15. Figure C-16 shows that log-periodic nature is maintained from 0.14 GHz to 3.6 GHz. By dividing the complex spectrum of a dispersed pulse by that of a driving source, the antenna transfer function amplitude and phase are given in Figures C-17 and C-18. Making use of the spectral amplitude at 2 GHz as a reference, the -10 dB bandwidth is approximately from 0.35 to 3.7 GHz.

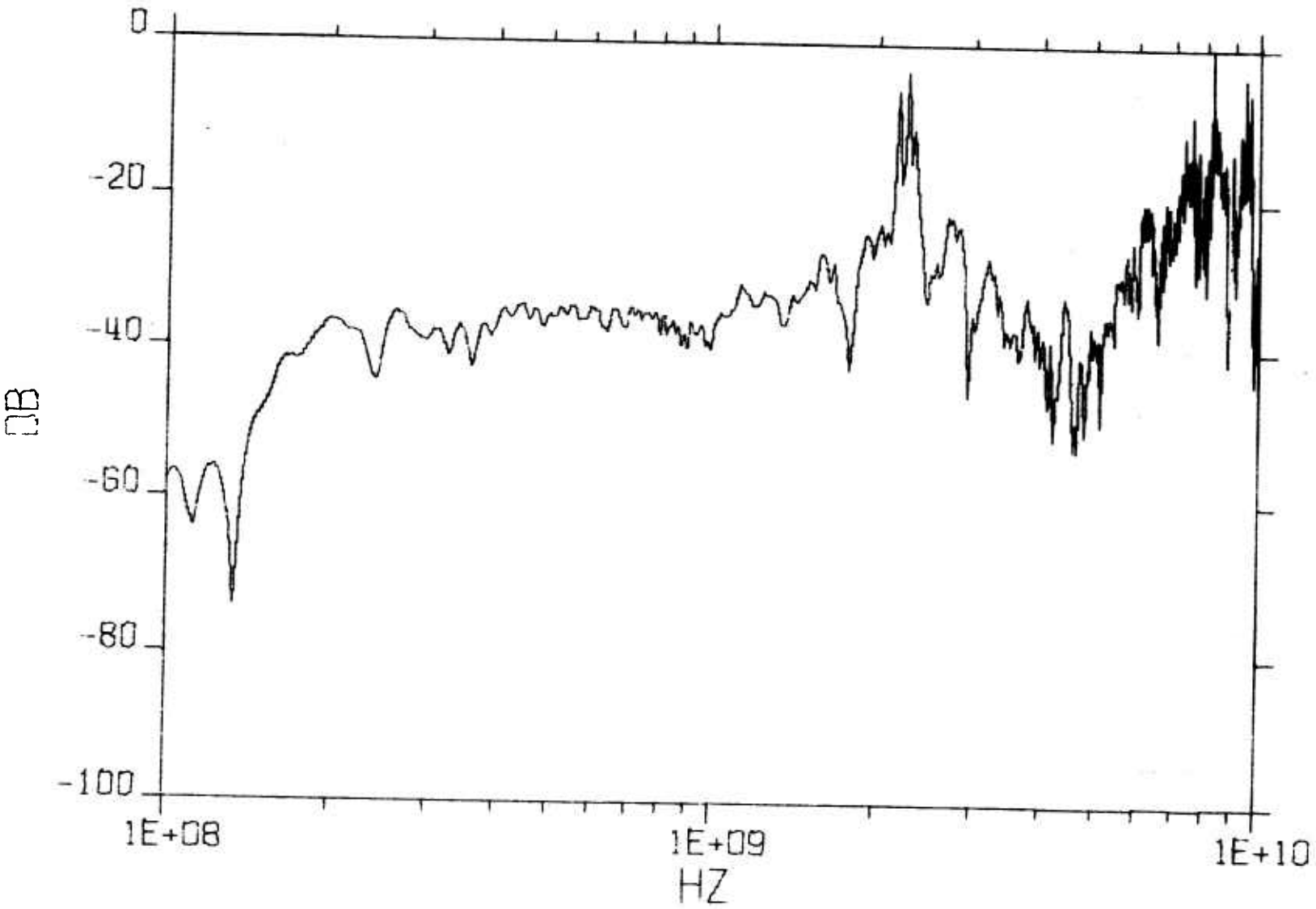


Figure C-9. Spectral Amplitude of $F_a(f)$ for ASN-1232A Transfer Function

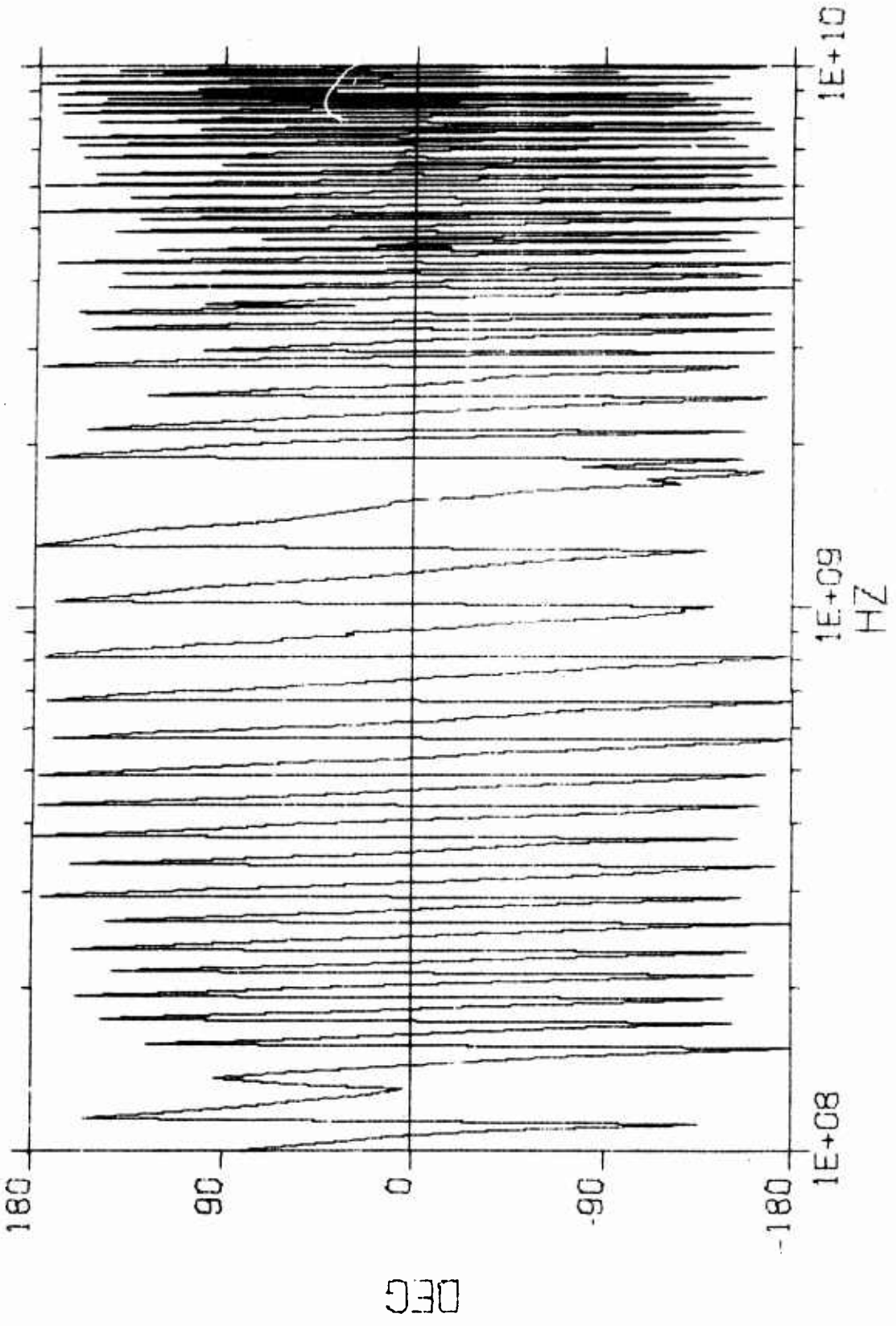


Figure C-10. Phase Angle of $F_a(f)$ for ASN-1232A Transfer Function

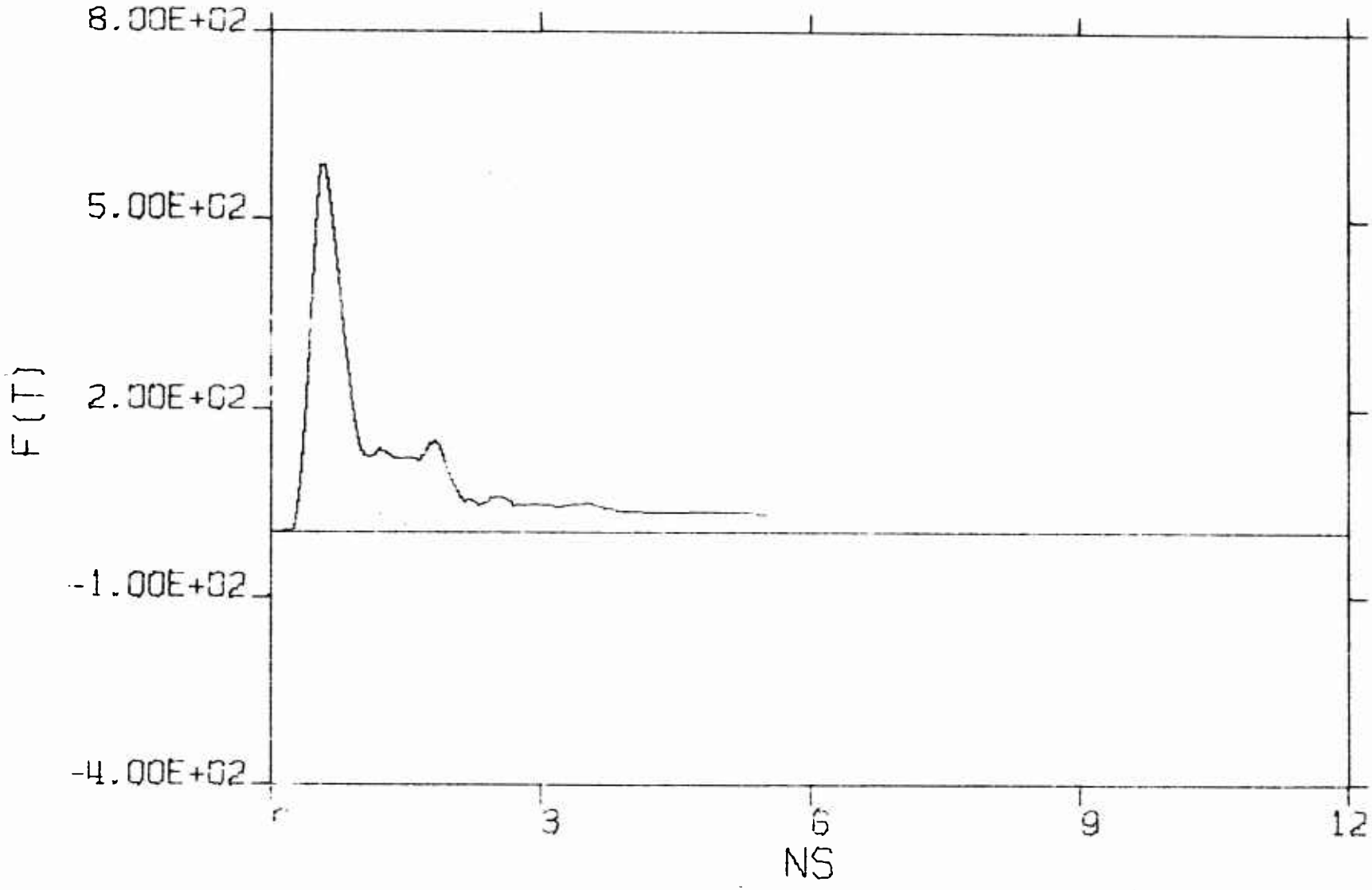


Figure C-11. Impulse Used to Drive Antenna ASN-117AA

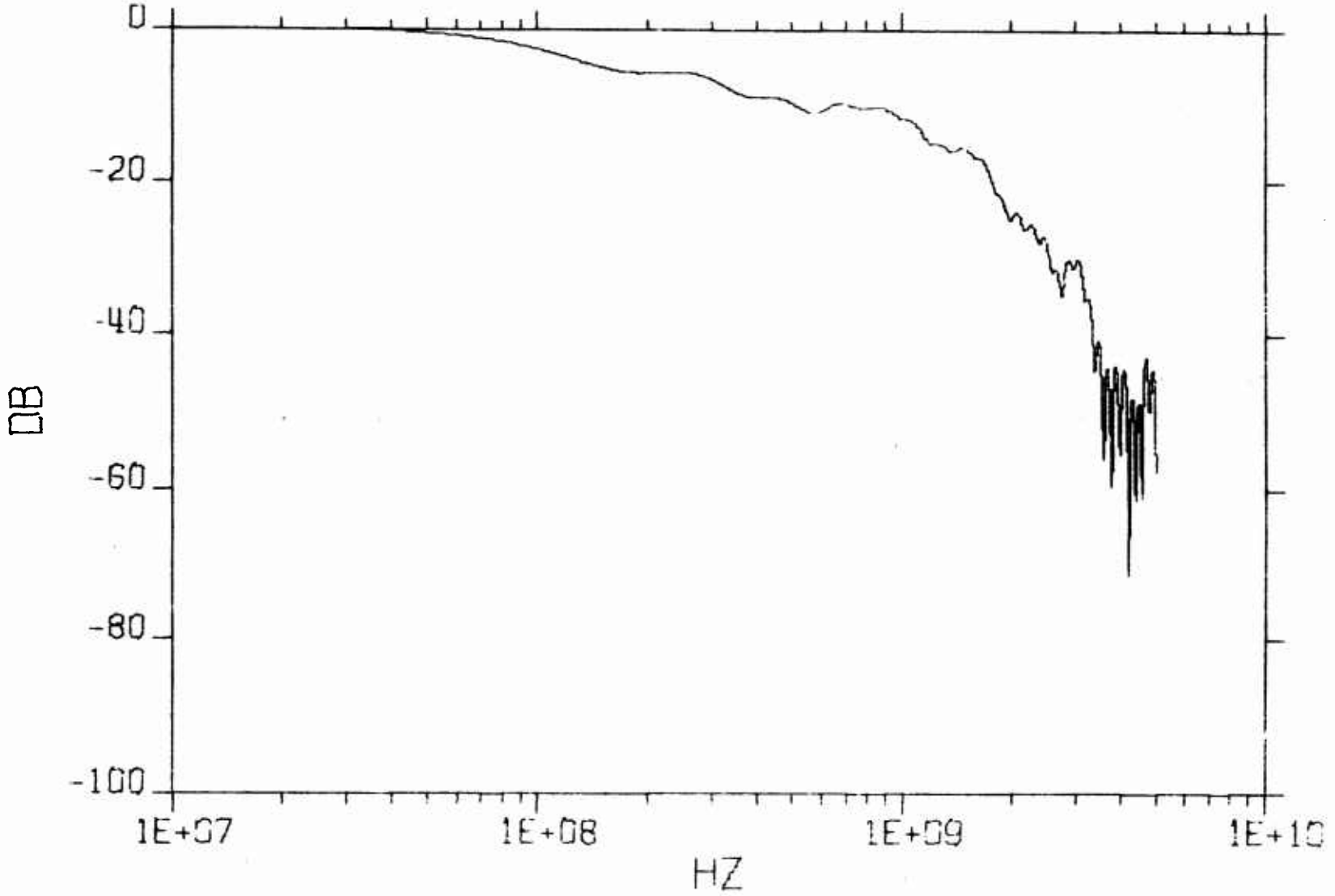


Figure C-12. Spectral Amplitude of the "Impulse" Used to Drive Antenna ASN-117AA

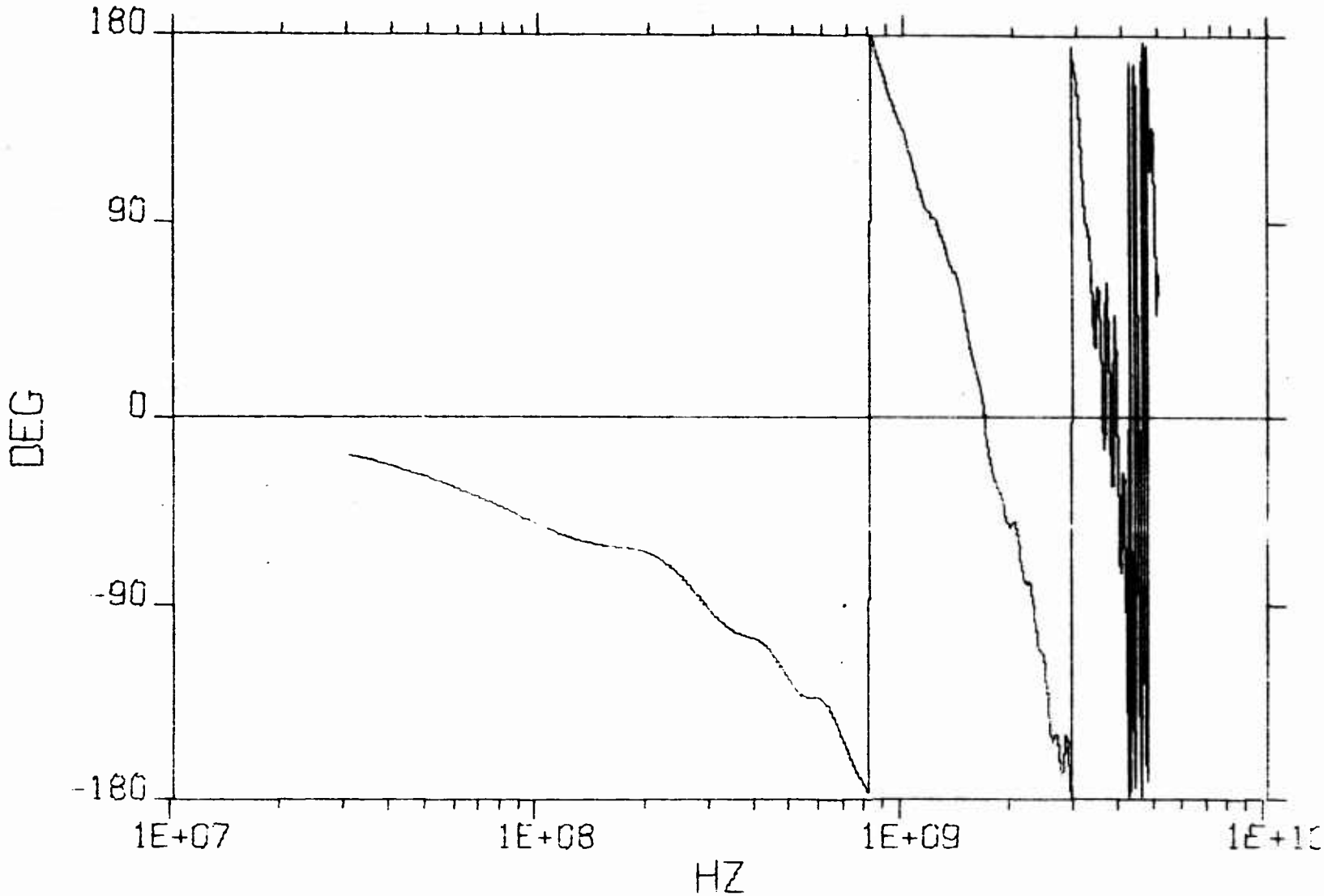


Figure C-13. Phase Angle Associated with the Spectrum of Figure C-12

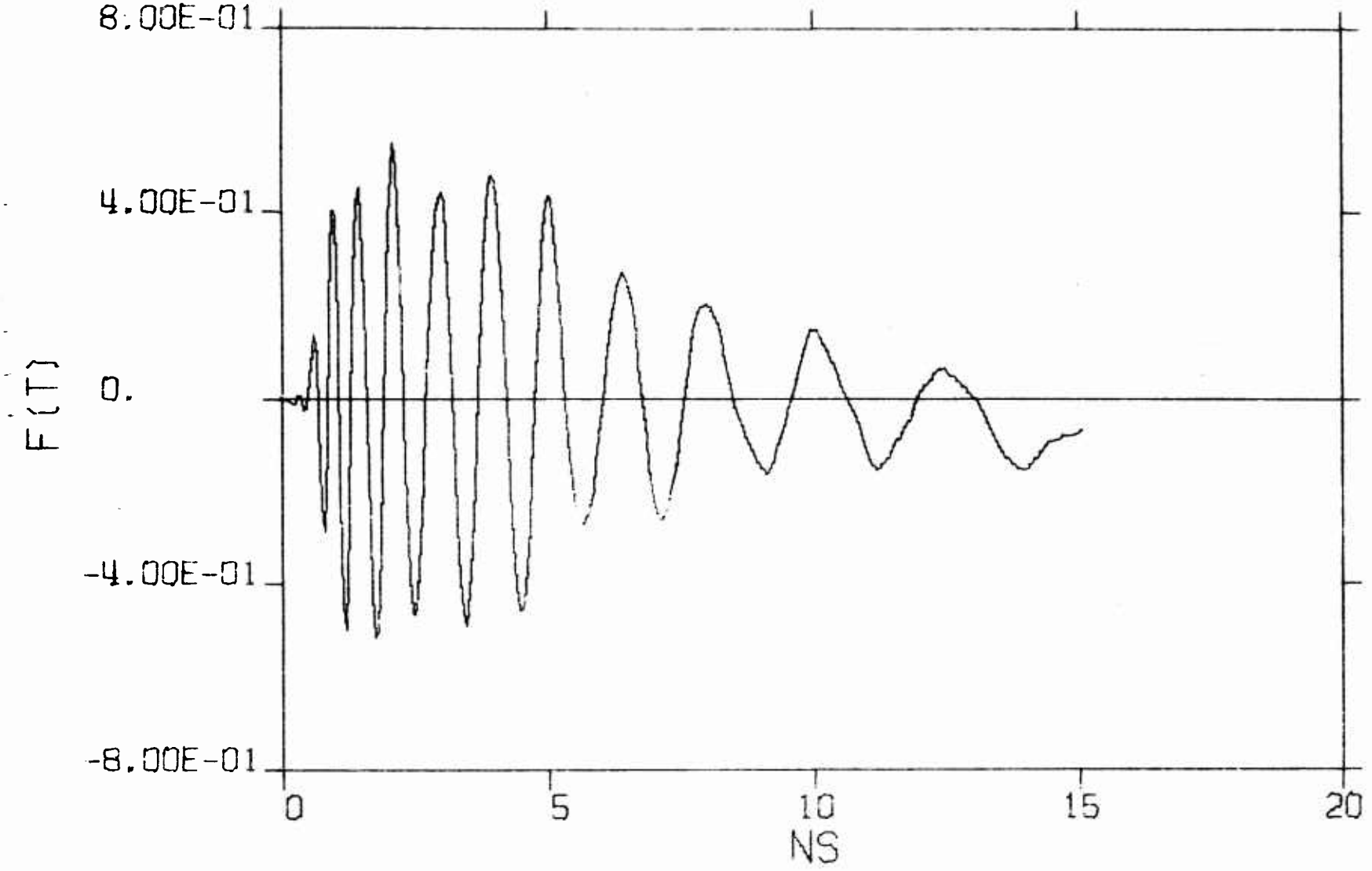


Figure C-14. The Dispersed Radiation $f_d(t)$ of ASN-117AA

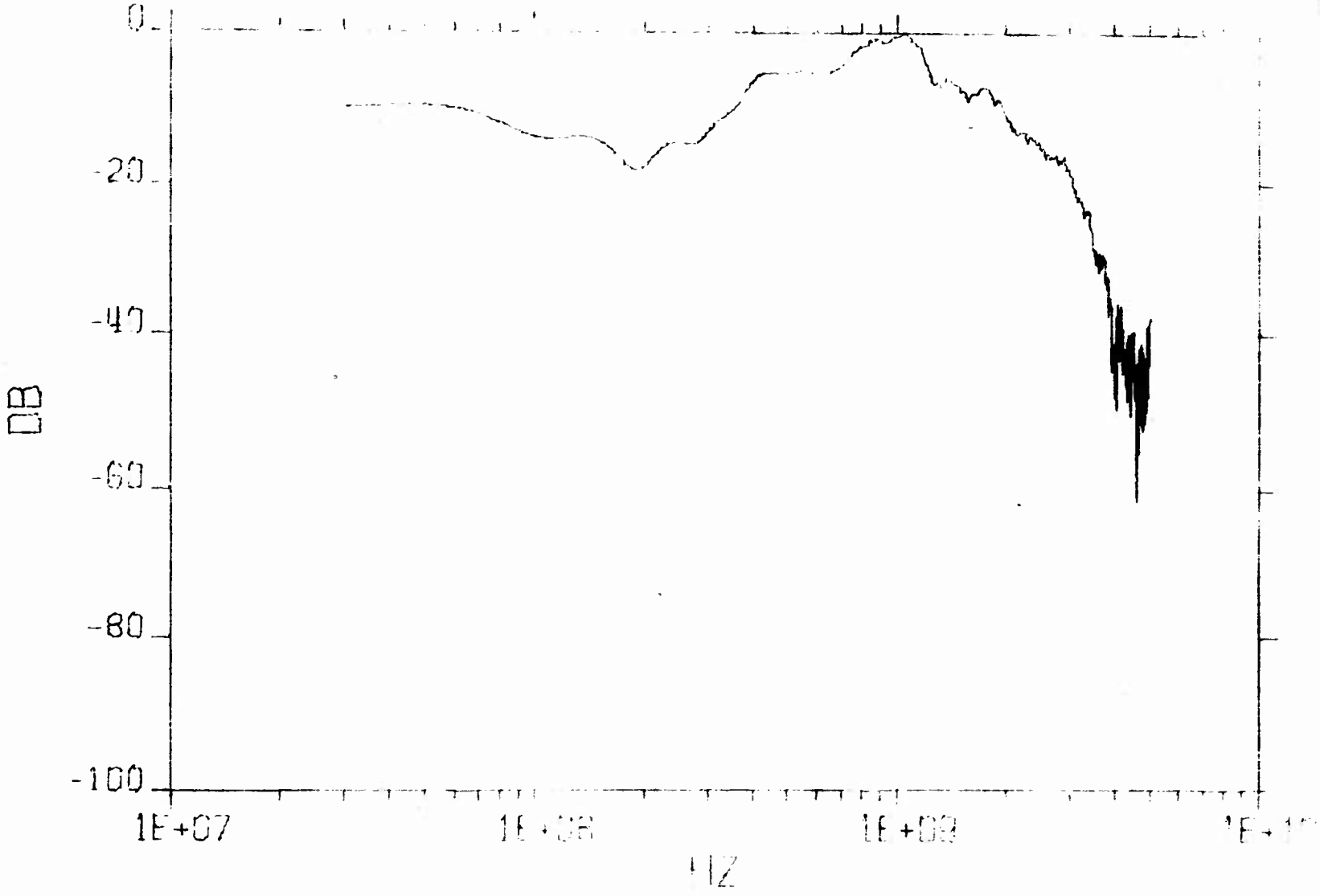


Figure C-15. Spectral Density Amplitude of $f_d(f)$ for Fig. C-14

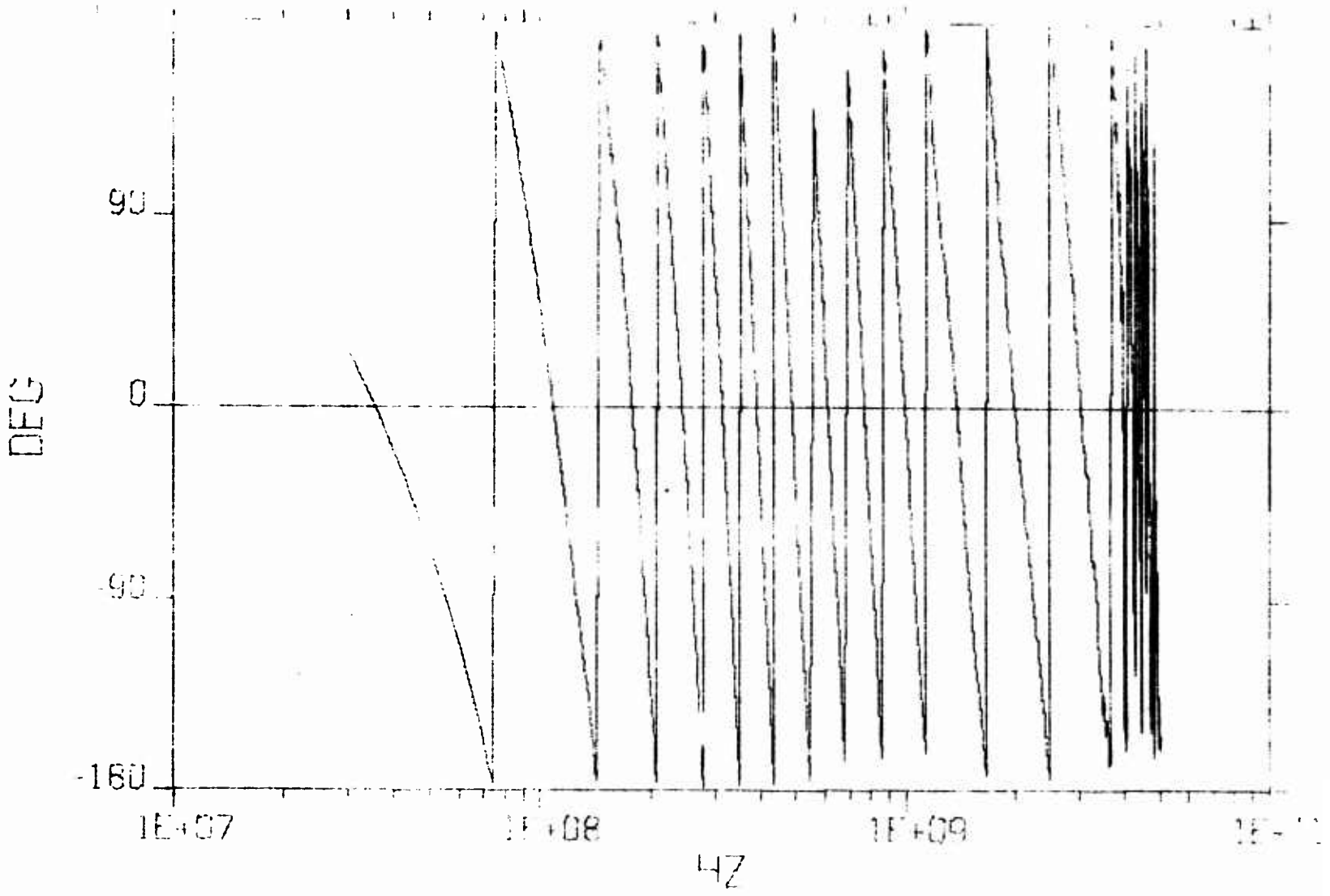


Figure C-16. Phase Angle $\phi_d(t)$ Associated with Figure C-15

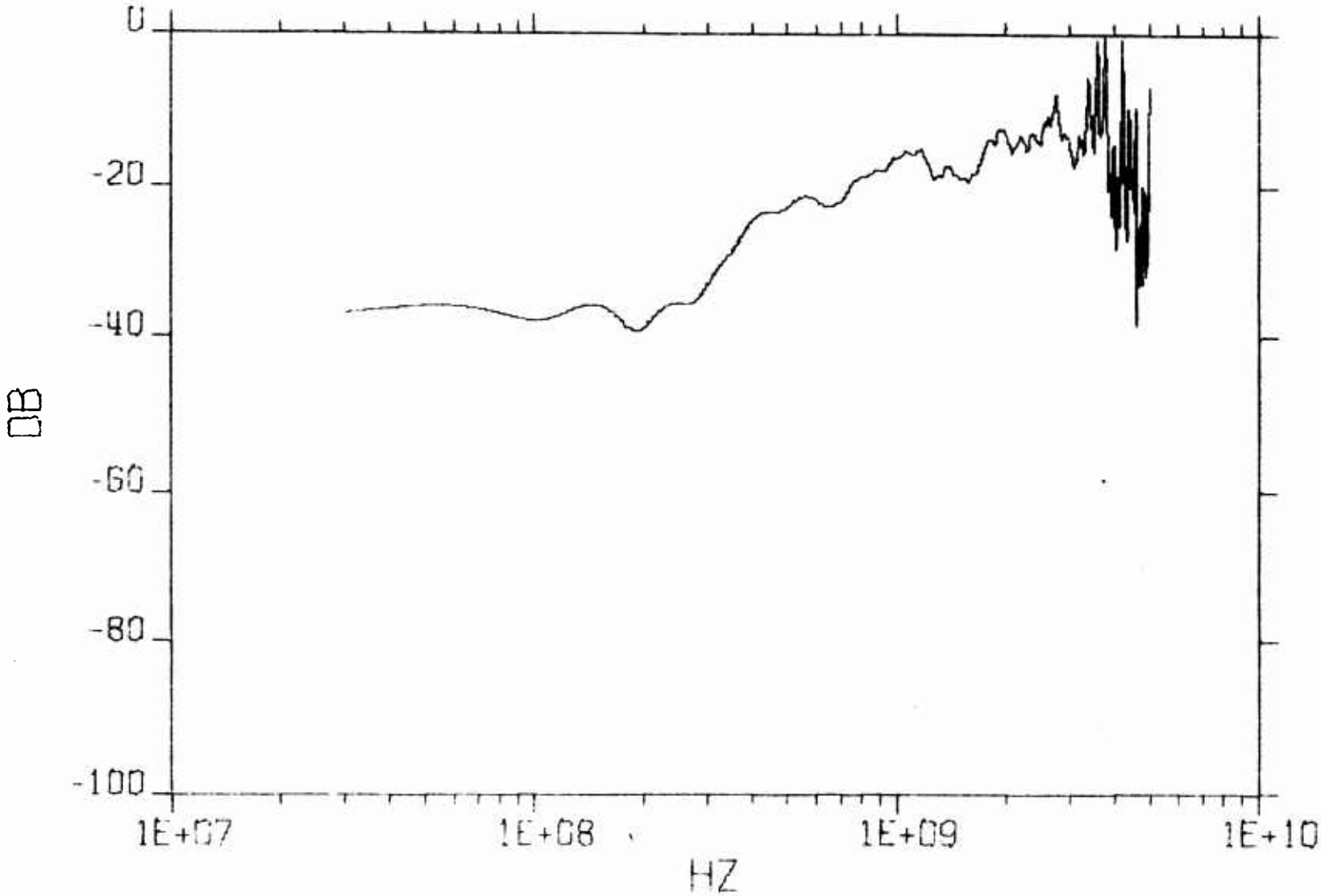


Figure C-17. Spectral Amplitude of $F_a(t)$ for ASN-117AA Transfer Function

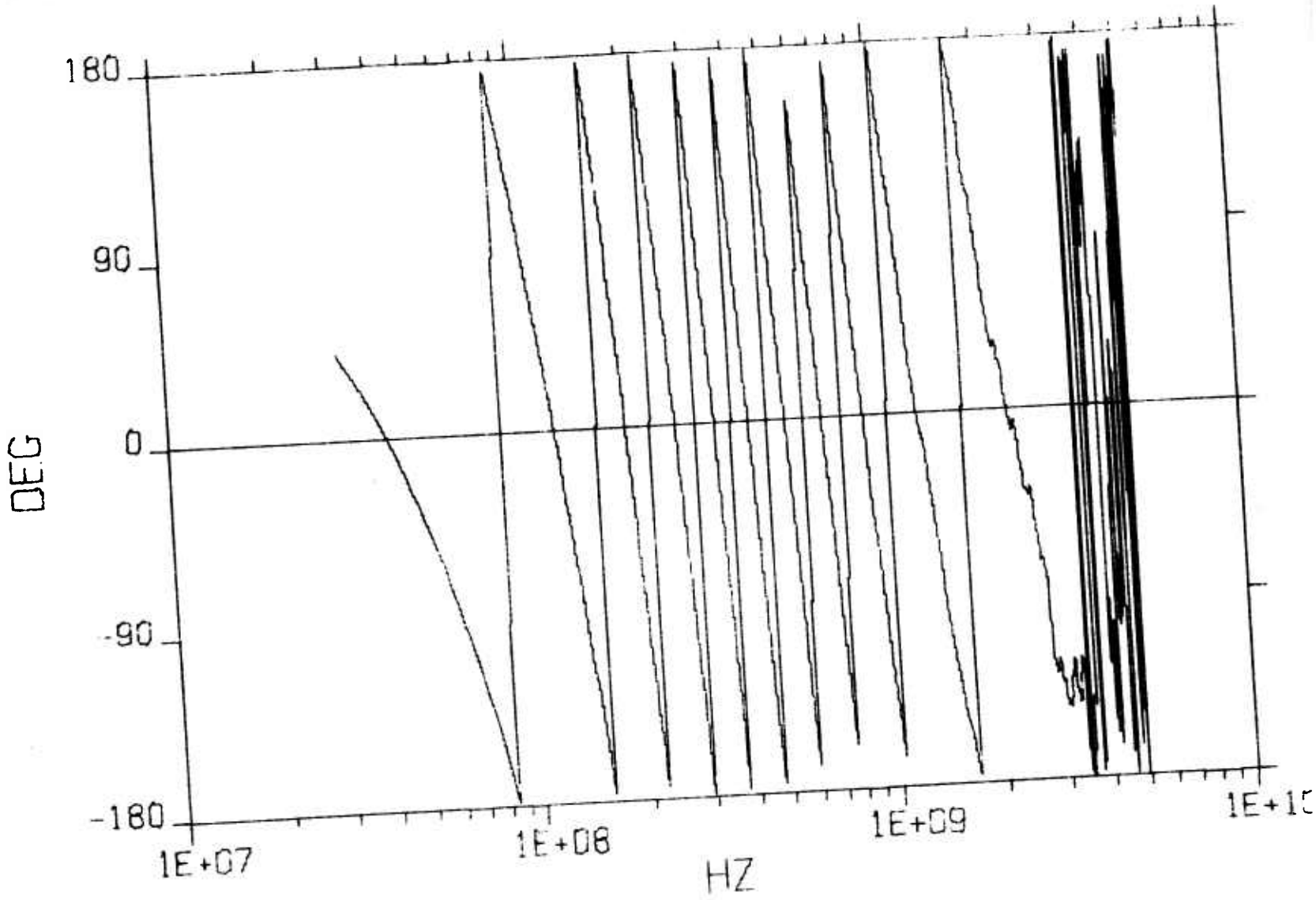


Figure C-18. Phase Angle of $F_a(t)$ for ASN-117AA Transfer Function

5. COMPRESSED PULSE OF CAVITY-BACKED SPIRAL ANTENNA ASN-116A

Two identical antennas ASN-116A were used for both transmission and reception. The transmitting antenna was driven by a step pulse which is approximately the same as the integrated pulse of the one shown in Figure C-3. The output of the receiving antenna is shown in Figure C-19. The light solid trace in Figure C-20 is the Fourier transform of the measured dispersion pulse. The heavy, solid trace is the two antenna response estimated by assuming a corresponding "impulse" was used. The dashed trace is the estimated response for a single antenna used in radiation only. (See Reference 8 for discussions on transfer functions.)

The phase angle for the two-antenna response using a step function is given in Figure C-21 from which the relative phase $4\phi(f)$ is shown in the solid curve of Figure C-22. The phase angle for single-antenna response to an "impulse" is also shown as $2\phi(f)$.

From the available response data by a "step function," the perfect-impulse response for a single-antenna reception is estimated as shown in Figure C-23. The -10 dB bandwidth is approximately from 0.67 GHz to 6.2 GHz. Assuming that antenna ASN-116A has spectral amplitude distributed as shown in Figure C-23, an application of conjugate-matched filter concepts would give a compressed pulse as shown in Figure C-24.

It is noted that the driving pulse for ASN-116A was not recorded for processing. Therefore, the antenna characteristics obtained here should be treated [illegible] being numerically rigorous.

6. TRANSFER FUNCTIONS OF CROSSED PLANAR LOG-PERIODIC DIPOLES APX-254A

Figures C-25 to C-27 give driving source characteristics associated with measurements for antenna APX-254A. The spectral components drop

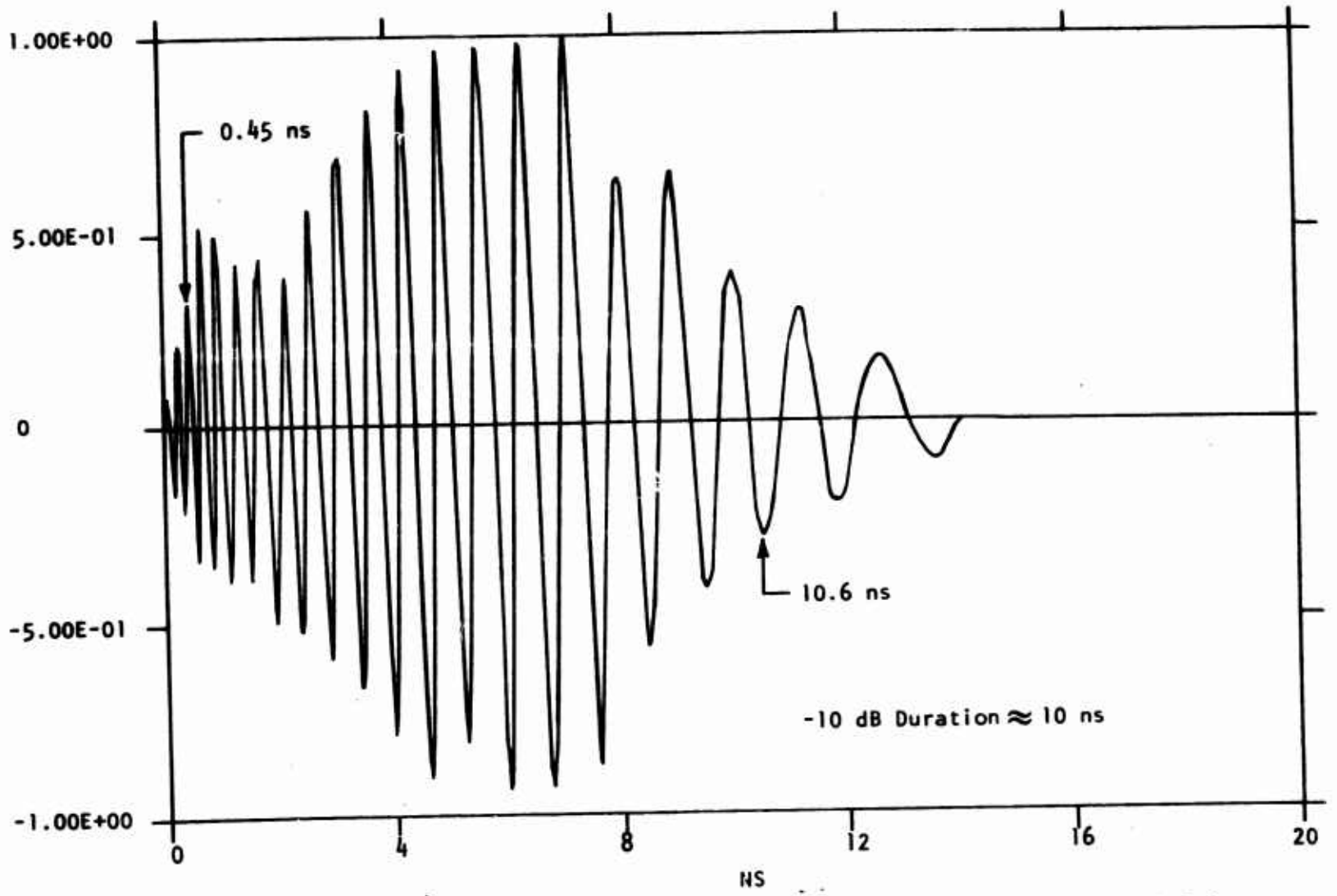


Figure C-19. Output of a Cavity-Backed Spiral Antenna AN-116A about 1.5 M Away from Another Identical Antenna Driven by Step Pulse

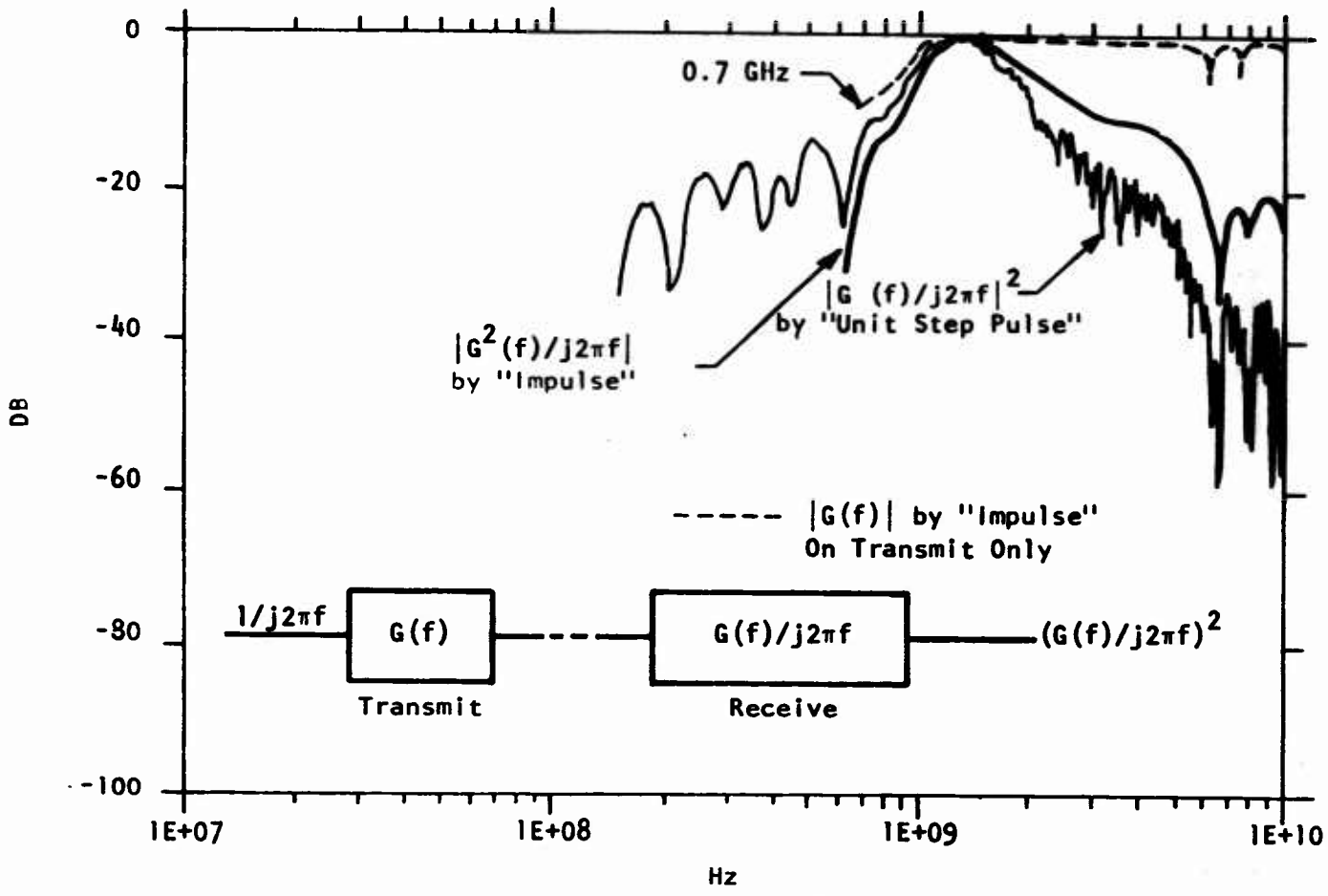


Figure C-20. Relative Spectral Distribution of the Response in Figure C-19

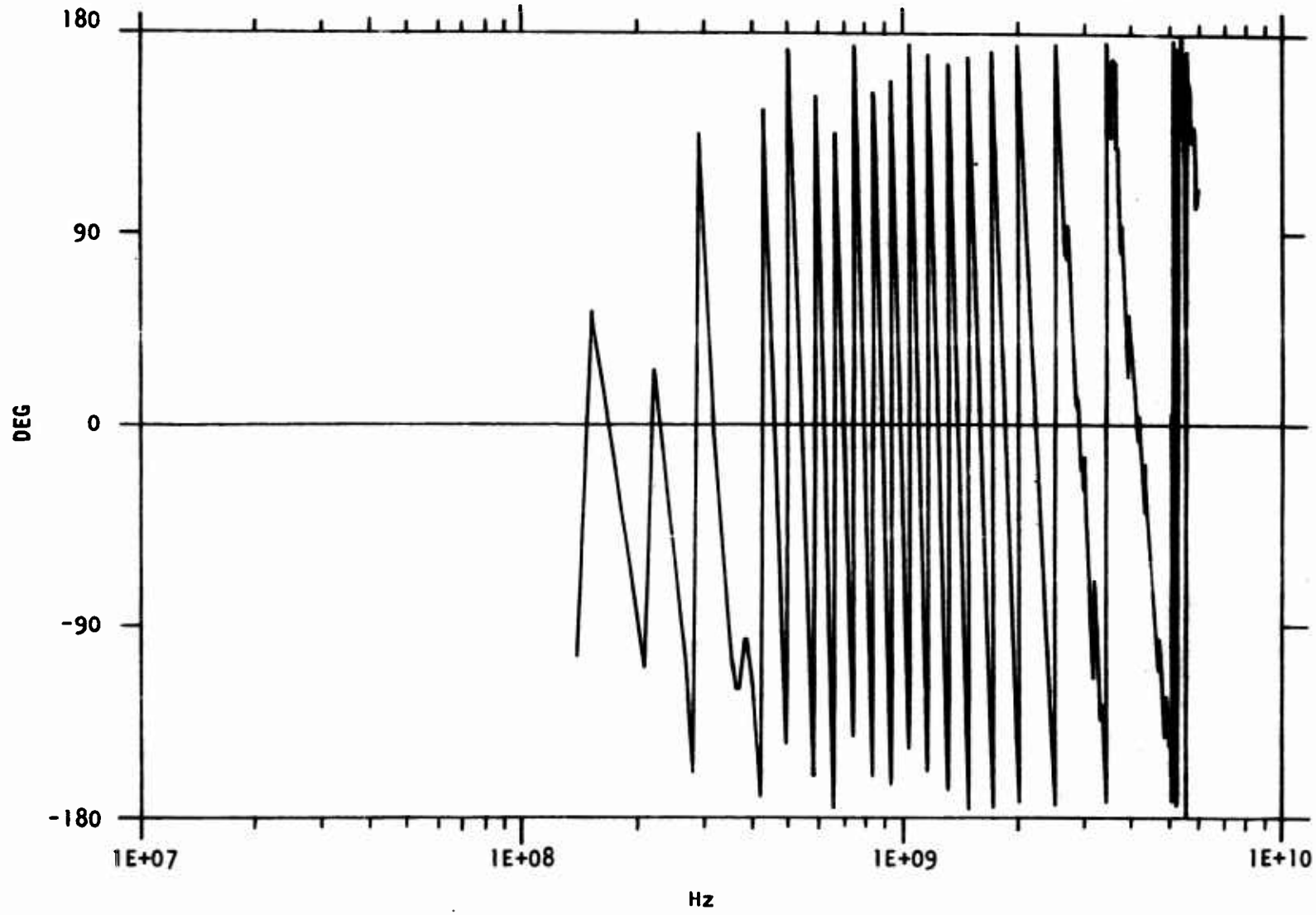


Figure C-21. Phase Angle Corresponding the "Unit Step Pulse" Response in Figure C-20

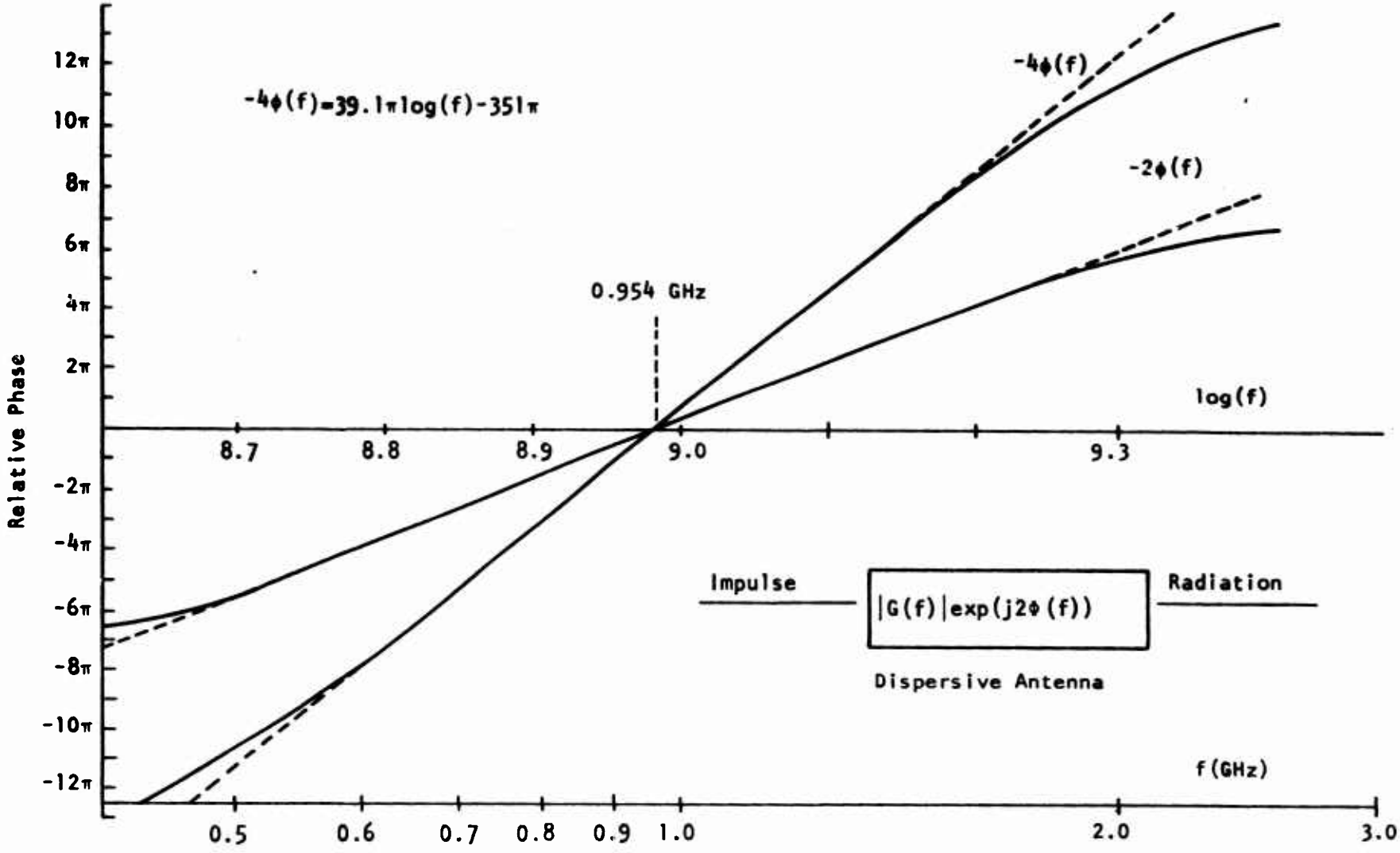


Figure C-22. Relative Phase Angles of the ASN-116A Cavity-Backed Spiral Antenna

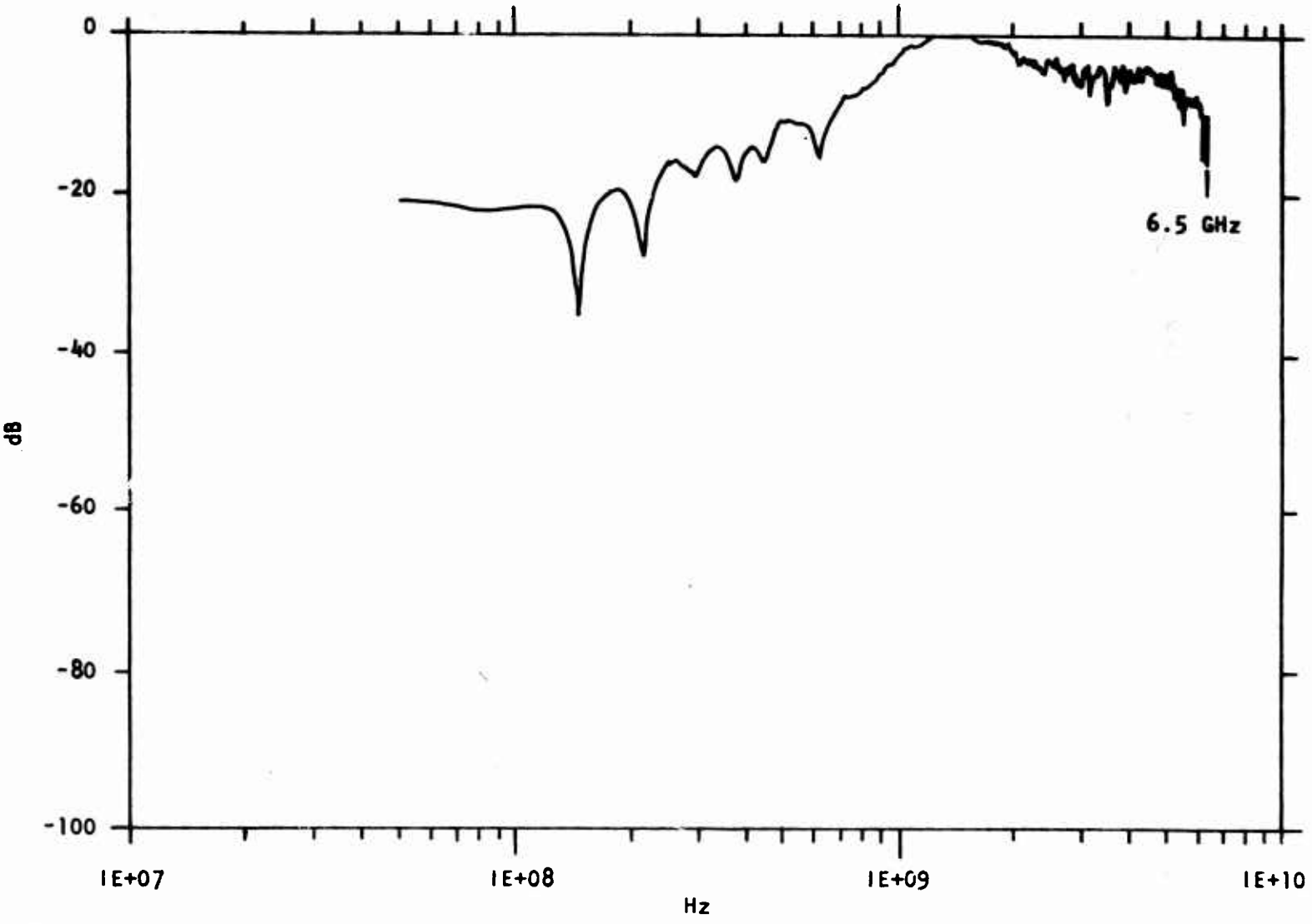


Figure C-23. Relative Spectral Distribution Estimated for the Reception of a Cavity-Backed Spiral Antenna ASN-116A

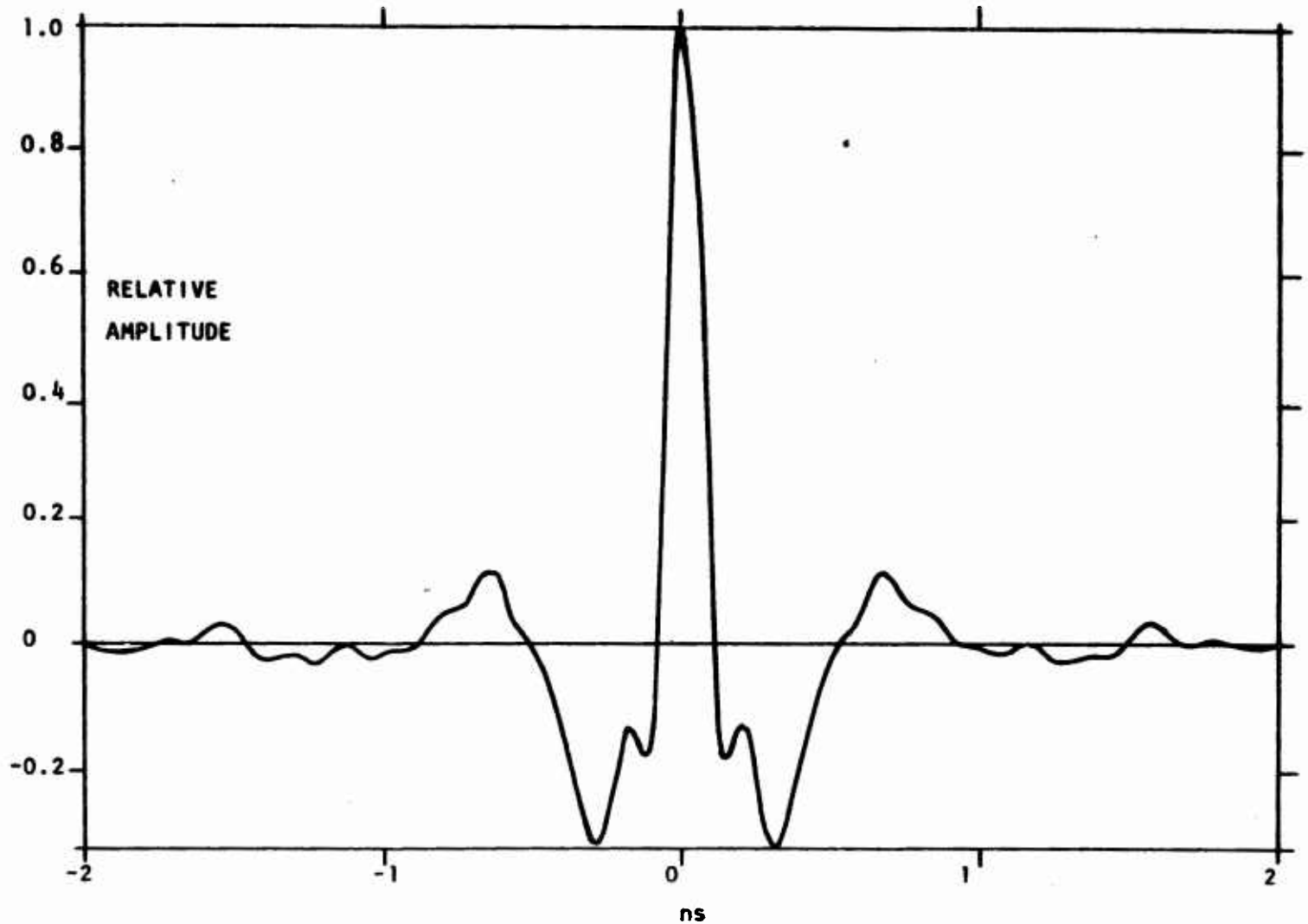


Figure C-24. Compressed Radiation Pulse of an Assumed Amplitude Distribution in Fig. C-23 (Under Matched-Filter Conditions)

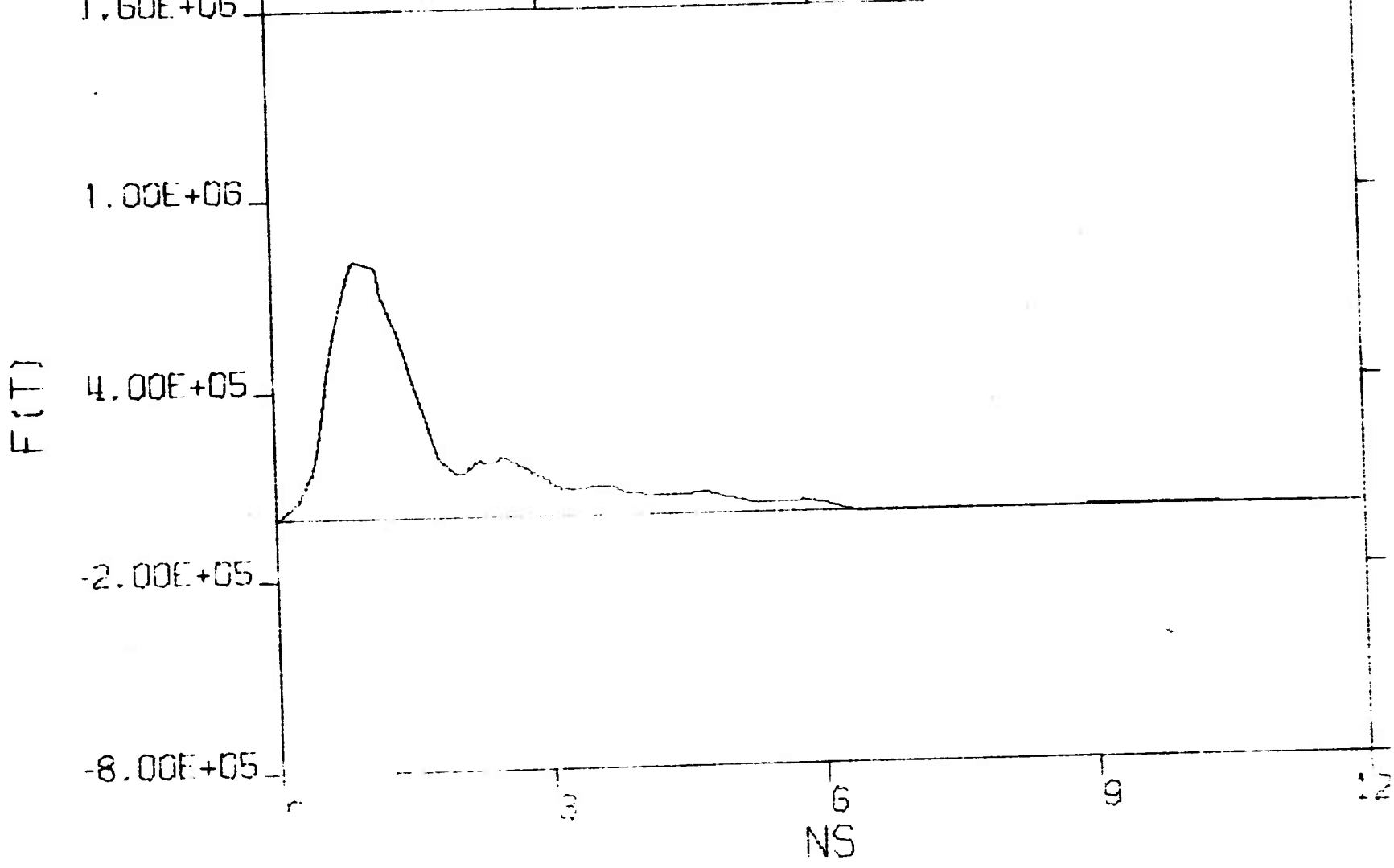


Figure C-25. "Impulse" Used to Drive Antenna APX-254A

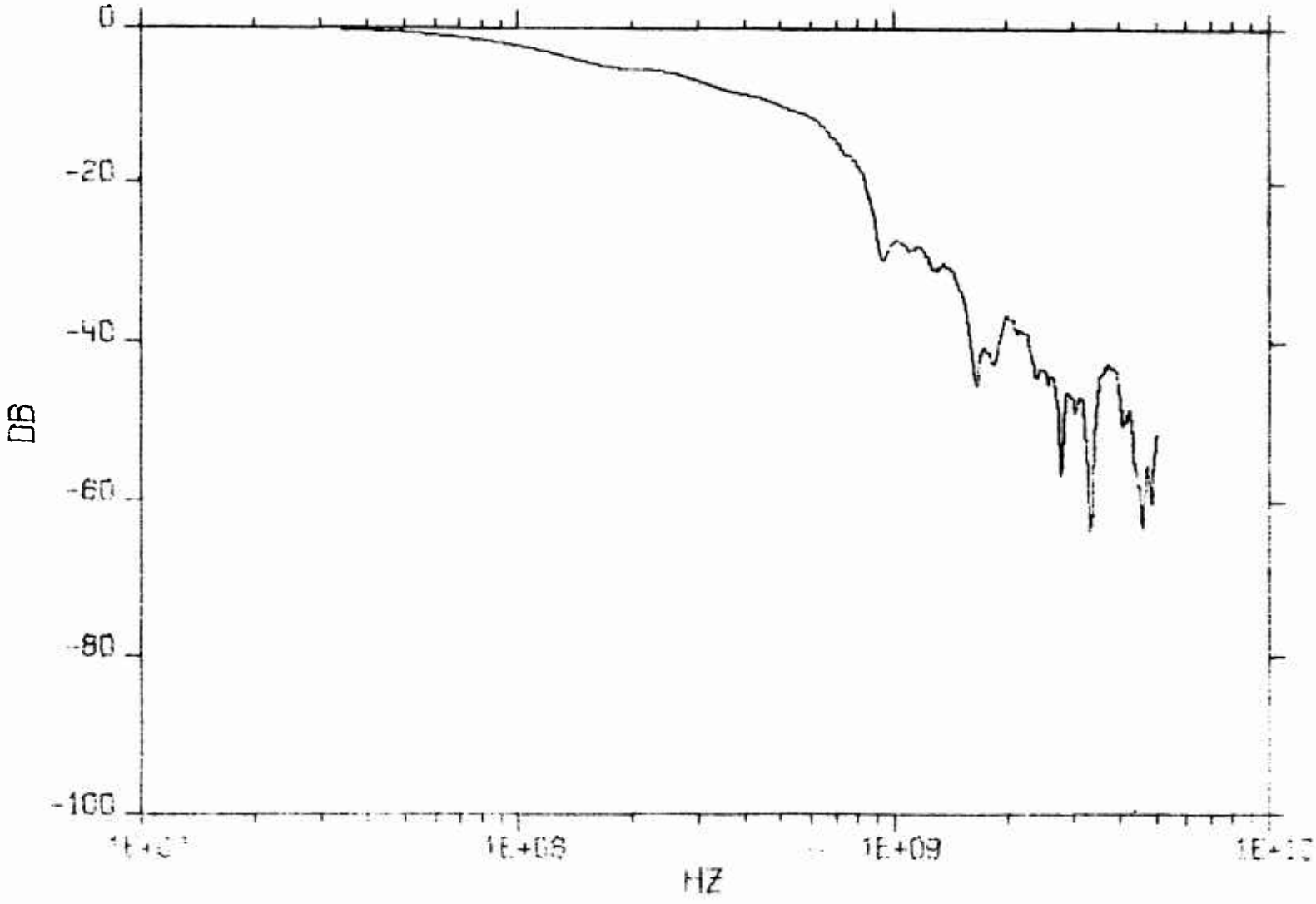


Figure C-26. Spectral Amplitude of the "Impulse" Used to Drive Antenna APX-254A

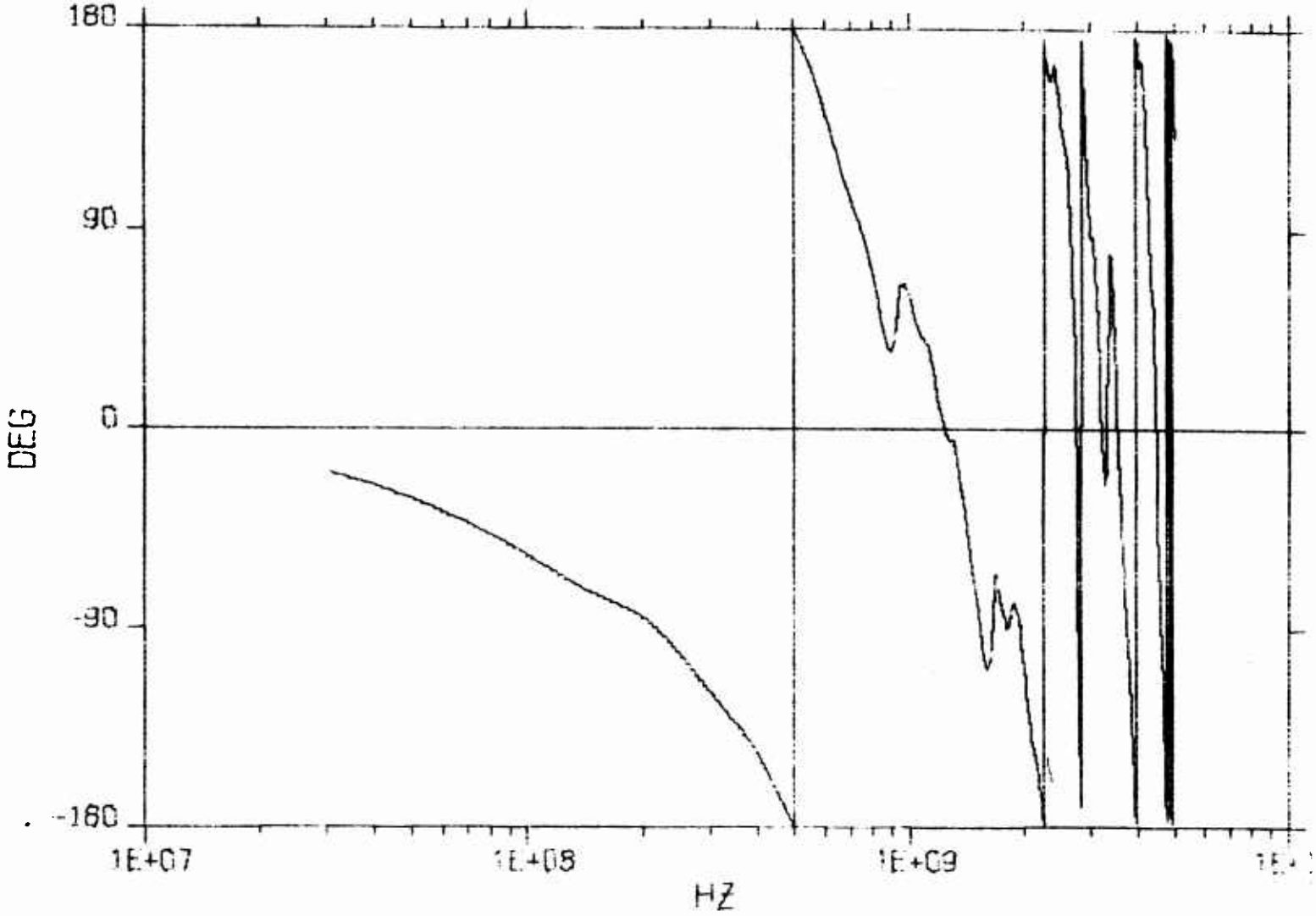


Figure C-27. Phase Angle Associated with the Spectrum of Figure C-26

below -20 dB for frequencies higher than 0.83 GHz and below -40 dB for frequencies higher than 1.5 GHz.. The dispersed pulse characteristics are given in Figures C-28 to C-30. Because of the extremely small amplitude for high frequencies in the driving source, it is not surprising to see that the dispersed pulse has meaningful spectral distribution only for frequencies less than 0.8 GHz. The transfer function shown in Figures C-31 and C-32 has not improved significantly by normalization with the driving source function. The -10 dB bandwidth of antenna APX-254A appears to be from 0.13 GHz to 1.08 GHz. The log-periodic phase is exhibited only from 0.14 GHz to 0.8 GHz.

The source used for this antenna should be considered inadequate for the test antenna whose CW-specified highest frequency is 4 GHz.

7. TRANSFER FUNCTION OF PLANAR LOG-PERIODIC DIPOLES APN-995B

The inadequacy of the driving pulse can be somewhat improved by taking a time derivative of the pulse similar to that shown in Figure C-3. Figures C-33 to C-35 give the driving source characteristics of a "doublet" used for APN-995B. The dispersed radiation characteristics are shown in Figures C-36 to C-38. The -10 dB dispersive response is about from 0.075 GHz to 1.1 GHz, and the log-periodic nature holds from 0.05 GHz to 1.1 GHz.

The transfer characteristics are shown in Figures C-39 and C-40. The -10 dB bandwidth referred to 2 GHz is approximately 0.03 GHz to 4.0 GHz and higher, except for those deep nulls caused by imperfect pulser and antenna. When the inverse Fourier transform is performed on the complex transfer function, the time-domain dispersion of Figure C-41 can be considered as approximately the response of a perfect impulse driving source. Strictly speaking, the "doublet" driving pulse is still inadequate for the test antenna. If the test antenna is of log-periodic and constant spectrum amplitude up to 4 GHz, it is expected that the early-time response of Figure C-41 would be altered.

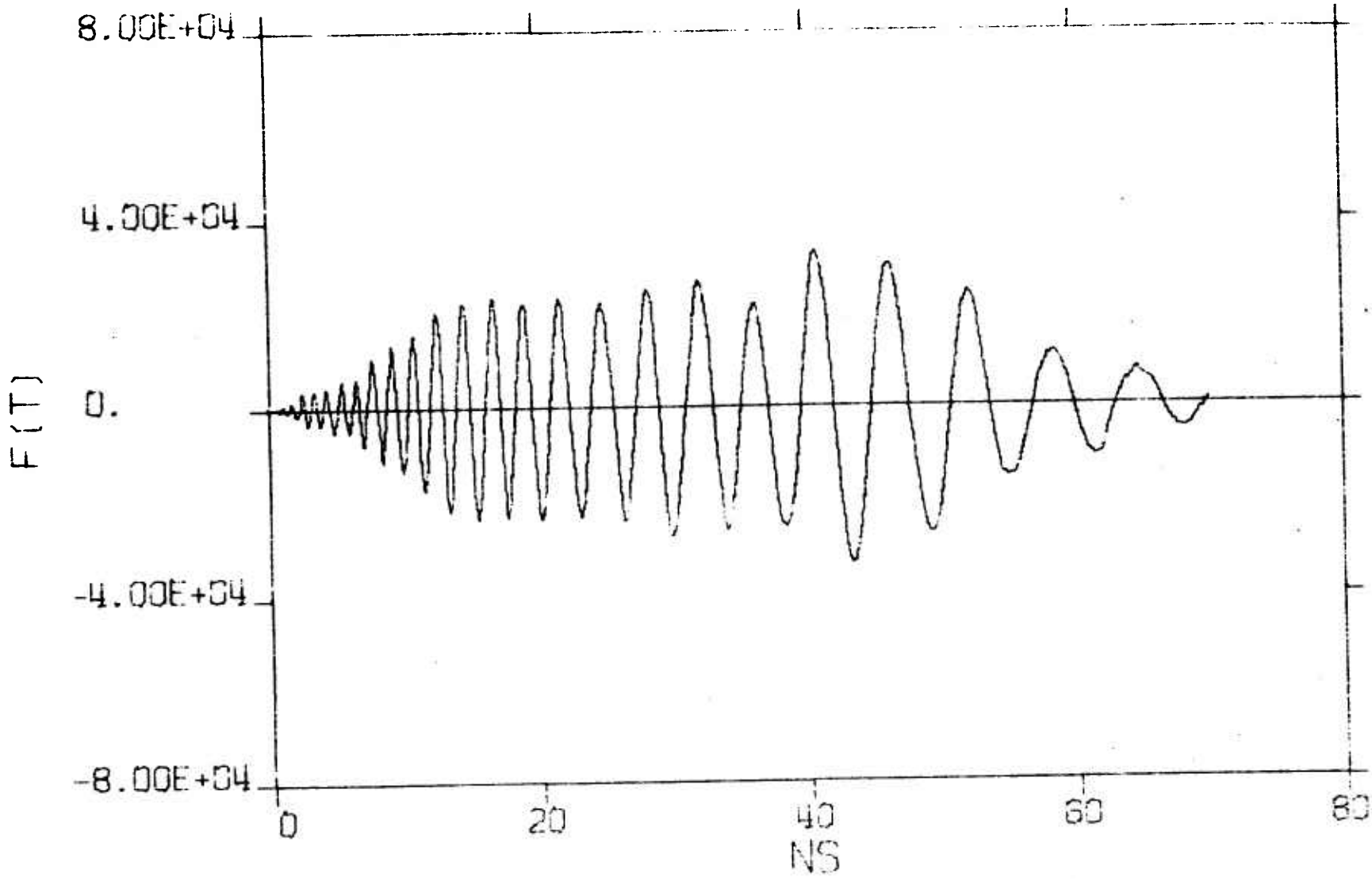


Figure C-28. The Dispersed Radiation $f_d(t)$ of APX-254A

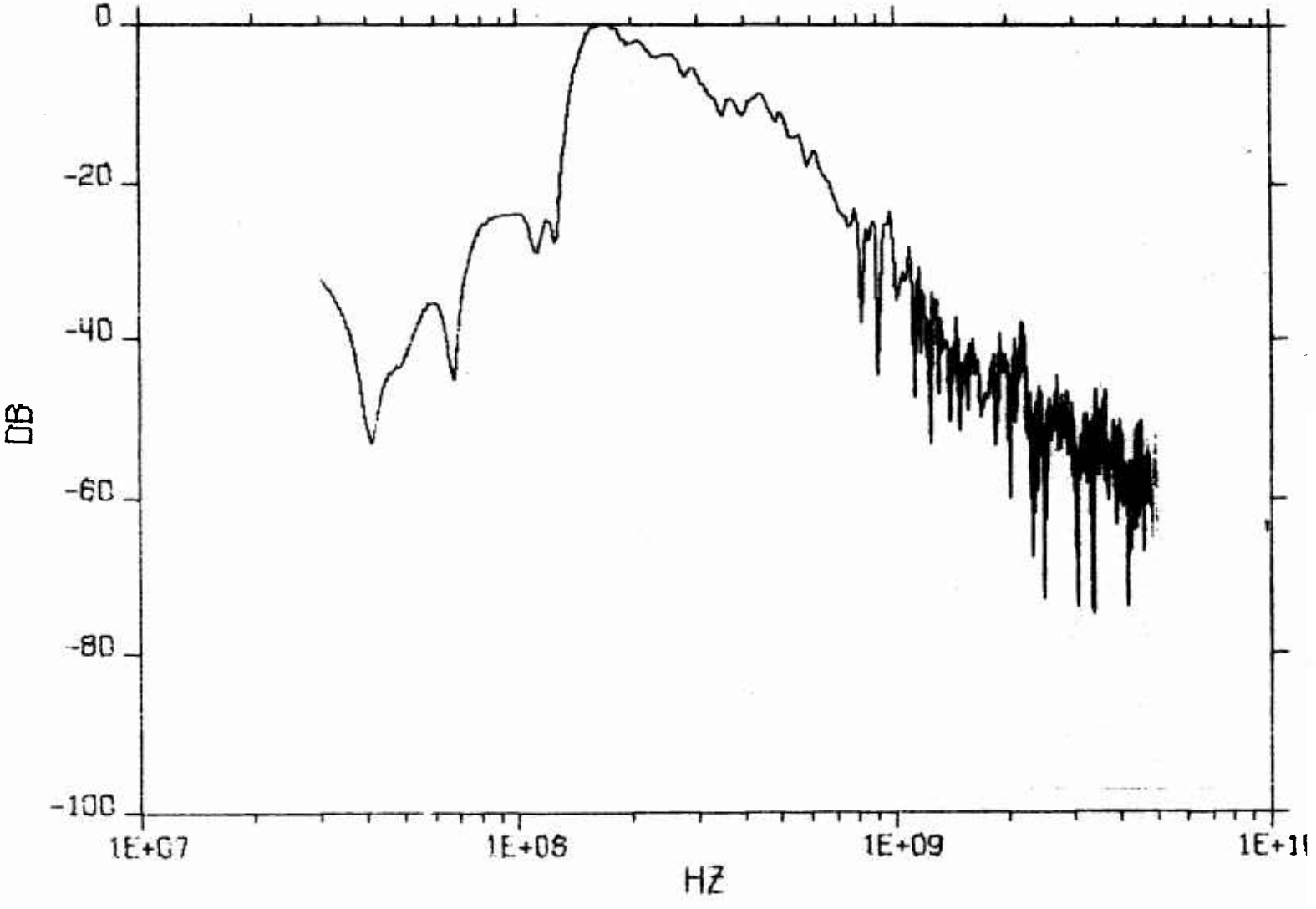


Figure C-29. Spectral Density Amplitude of $F_d(f)$ for Figure C-28

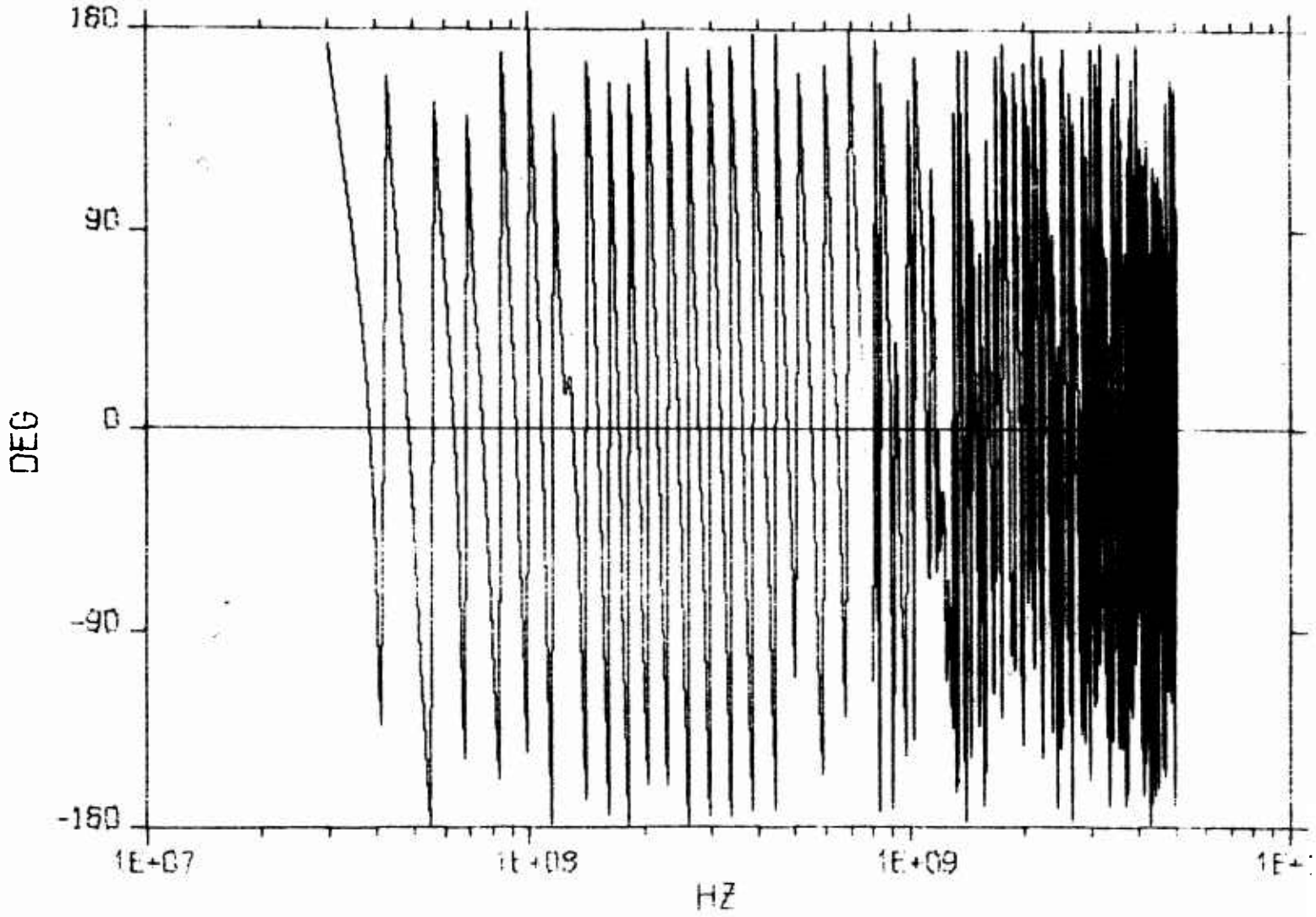


Figure C-30. Phase Angle $\phi_d(t)$ Associated with Figure C-29

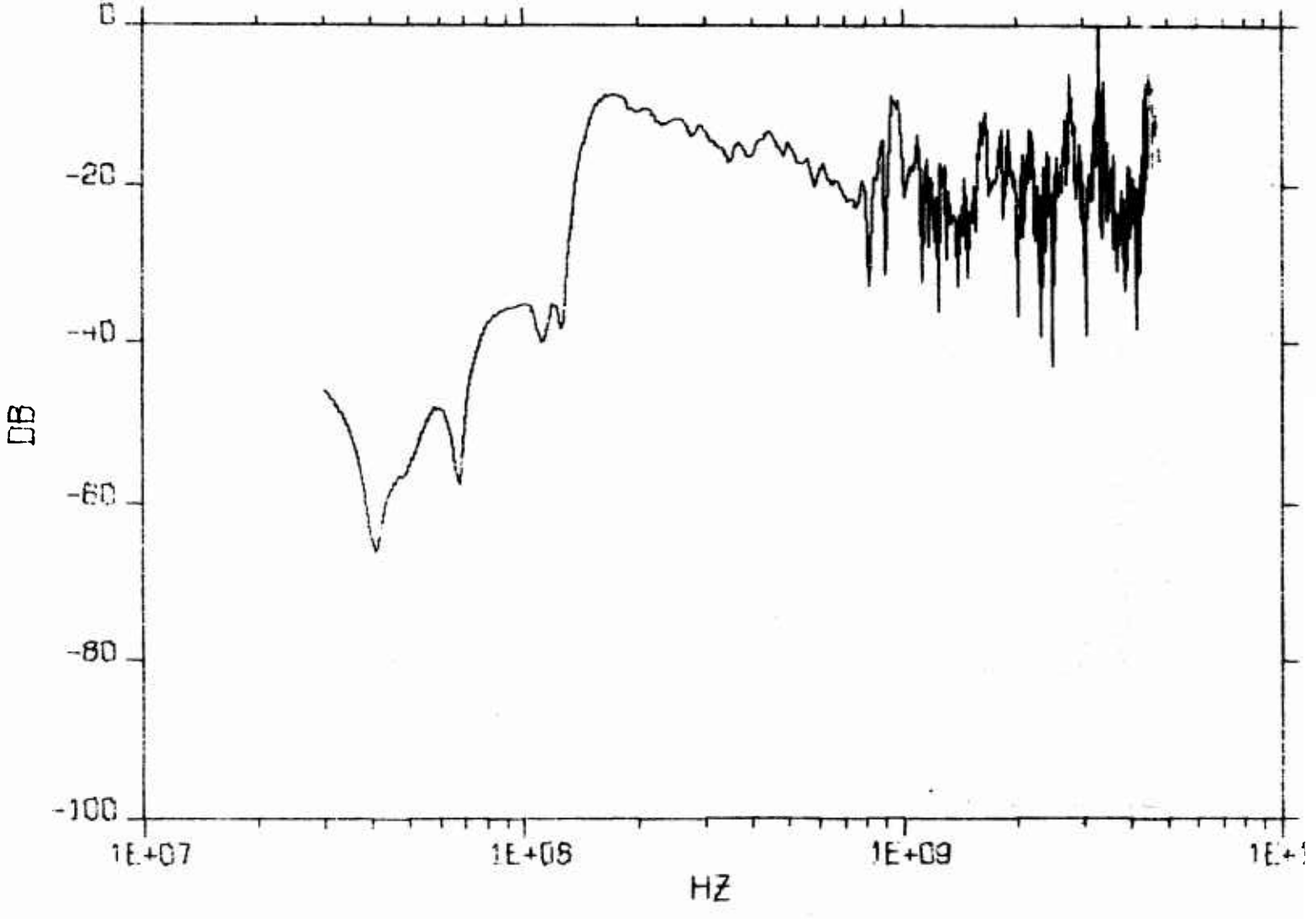


Figure C-31. Spectral Amplitude of $F_a(t)$ for APX-254A Transfer Function

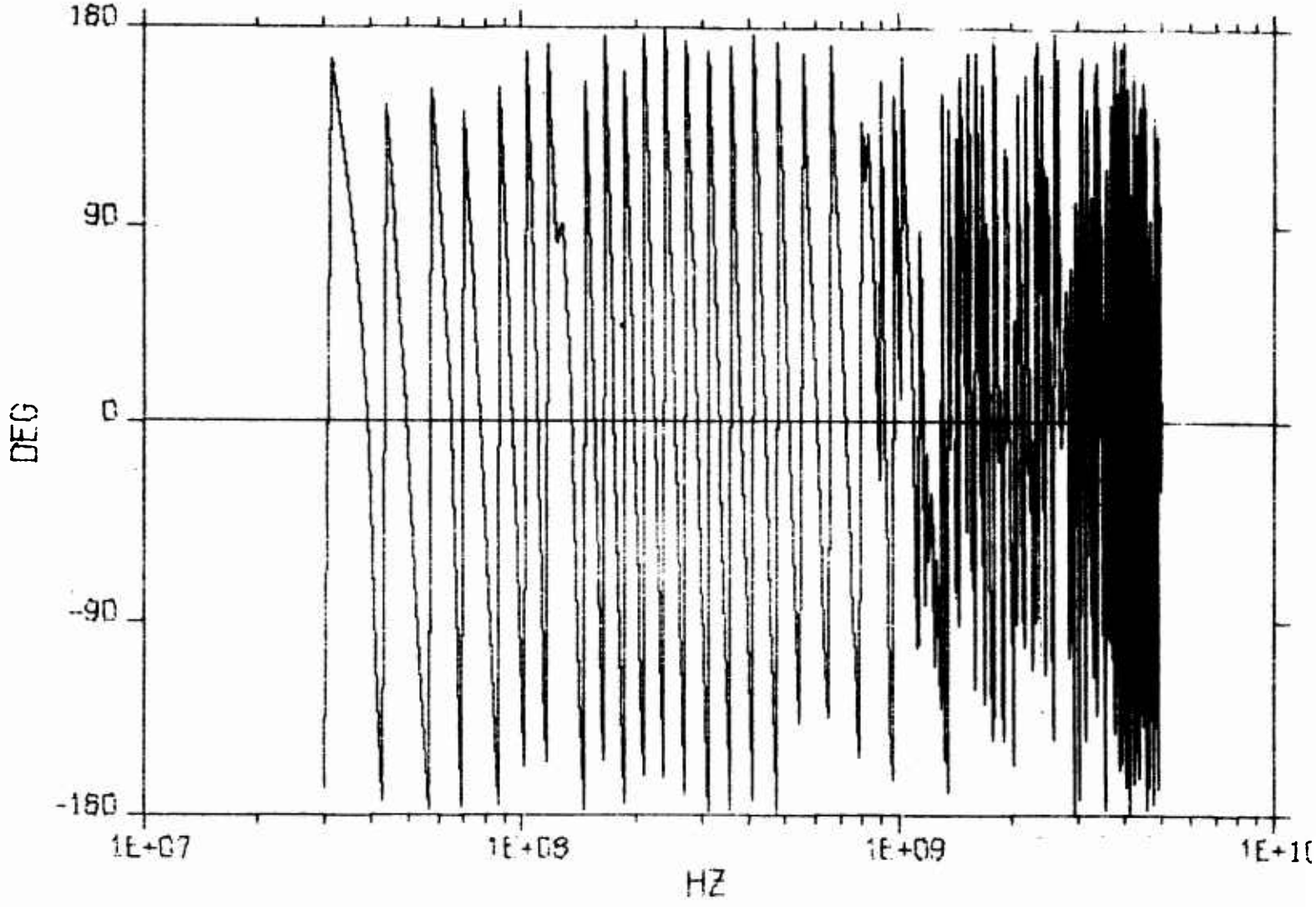


Figure C-32. Phase Angle of $F_a(f)$ for APX-254A Transfer Function

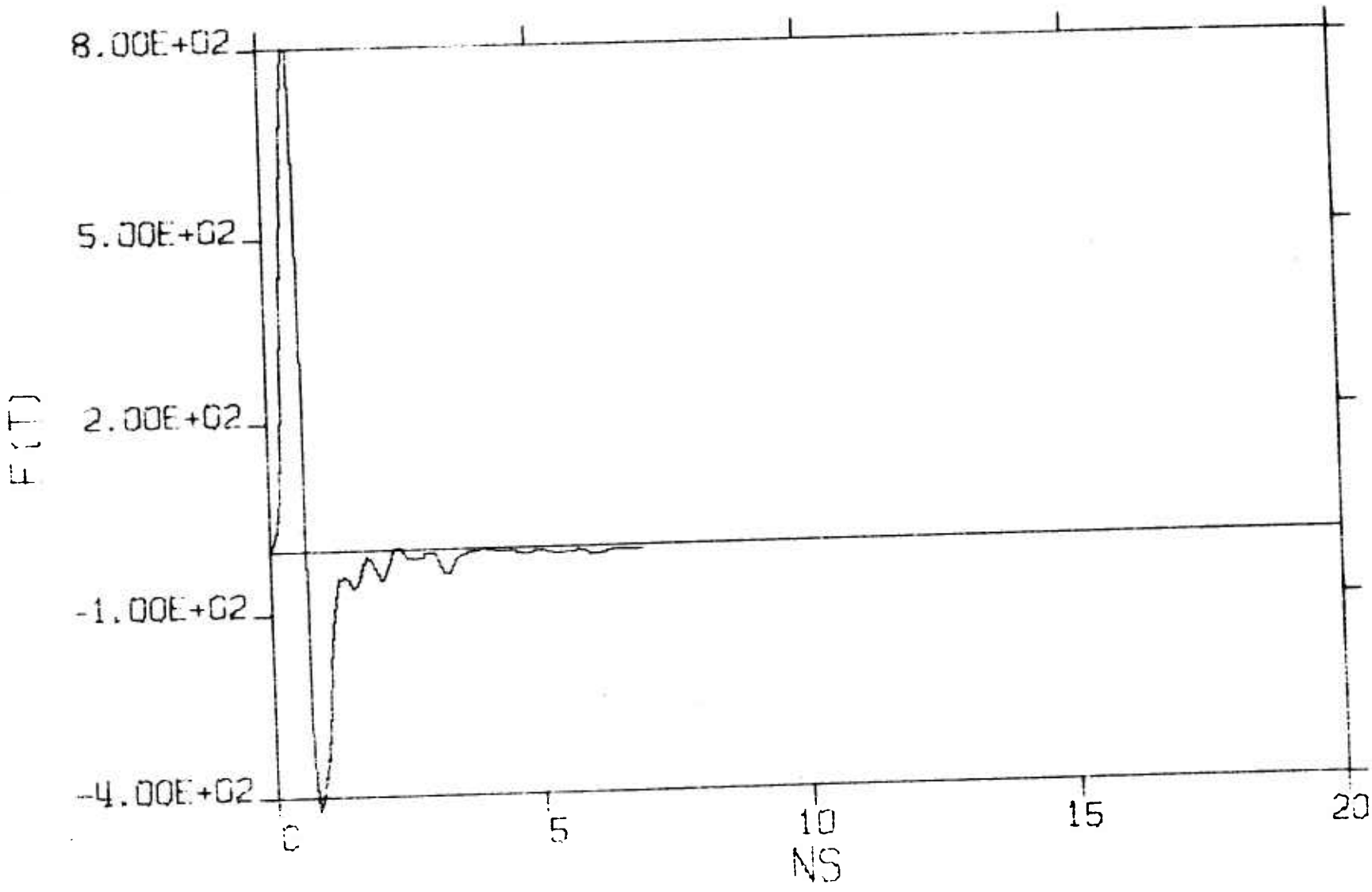


Figure C-33. "Doublet" Used to Drive Antenna APN-995B

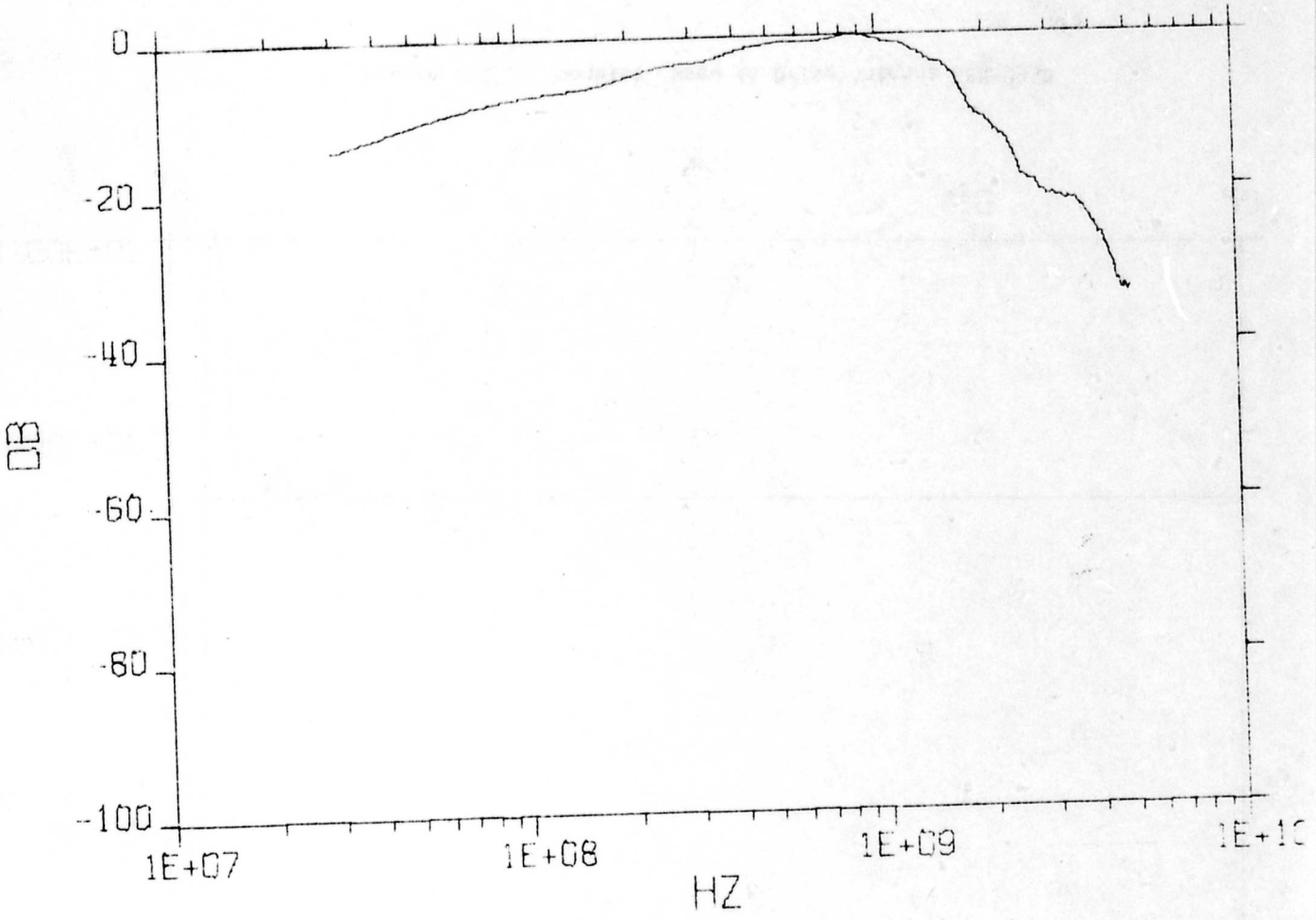


Figure C-34. Spectral Amplitude of the "Doublet" Used to Drive Antenna APN-995B

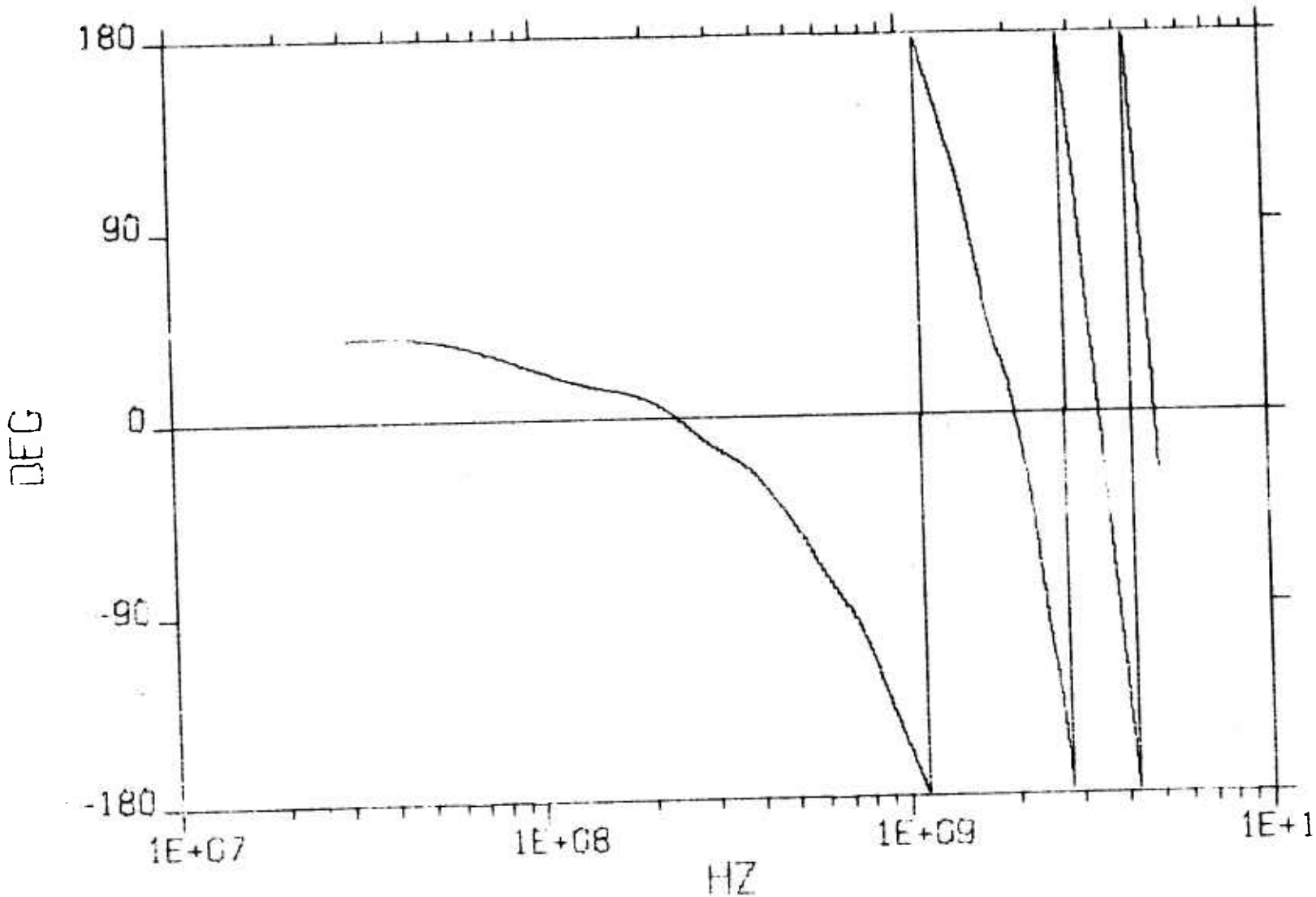


Figure C-35. Phase Angle Associated with the Spectrum of Figure C-34

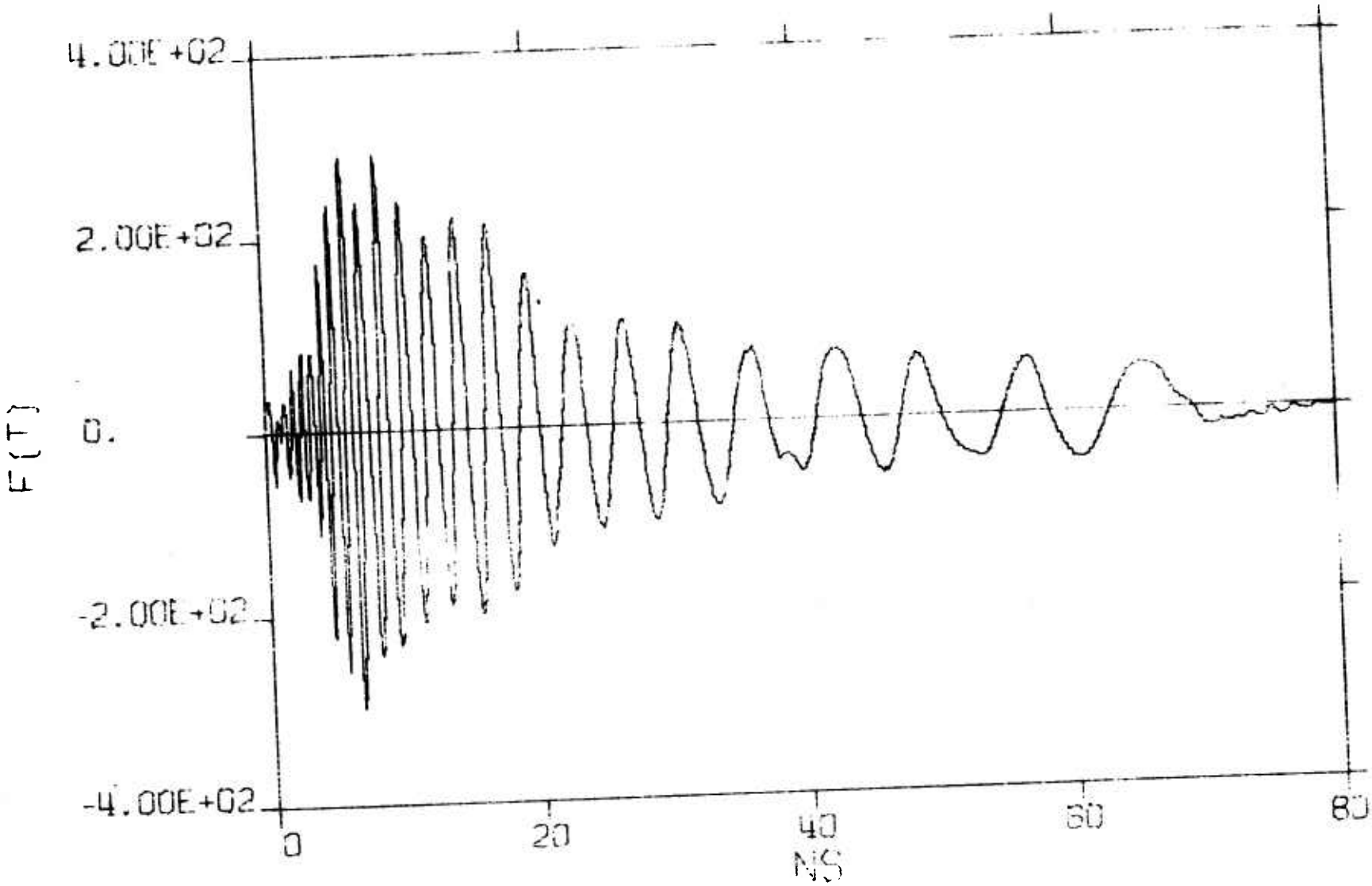


Figure C-36 The Dispersed Radiation $F_d(t)$ of APN-995B

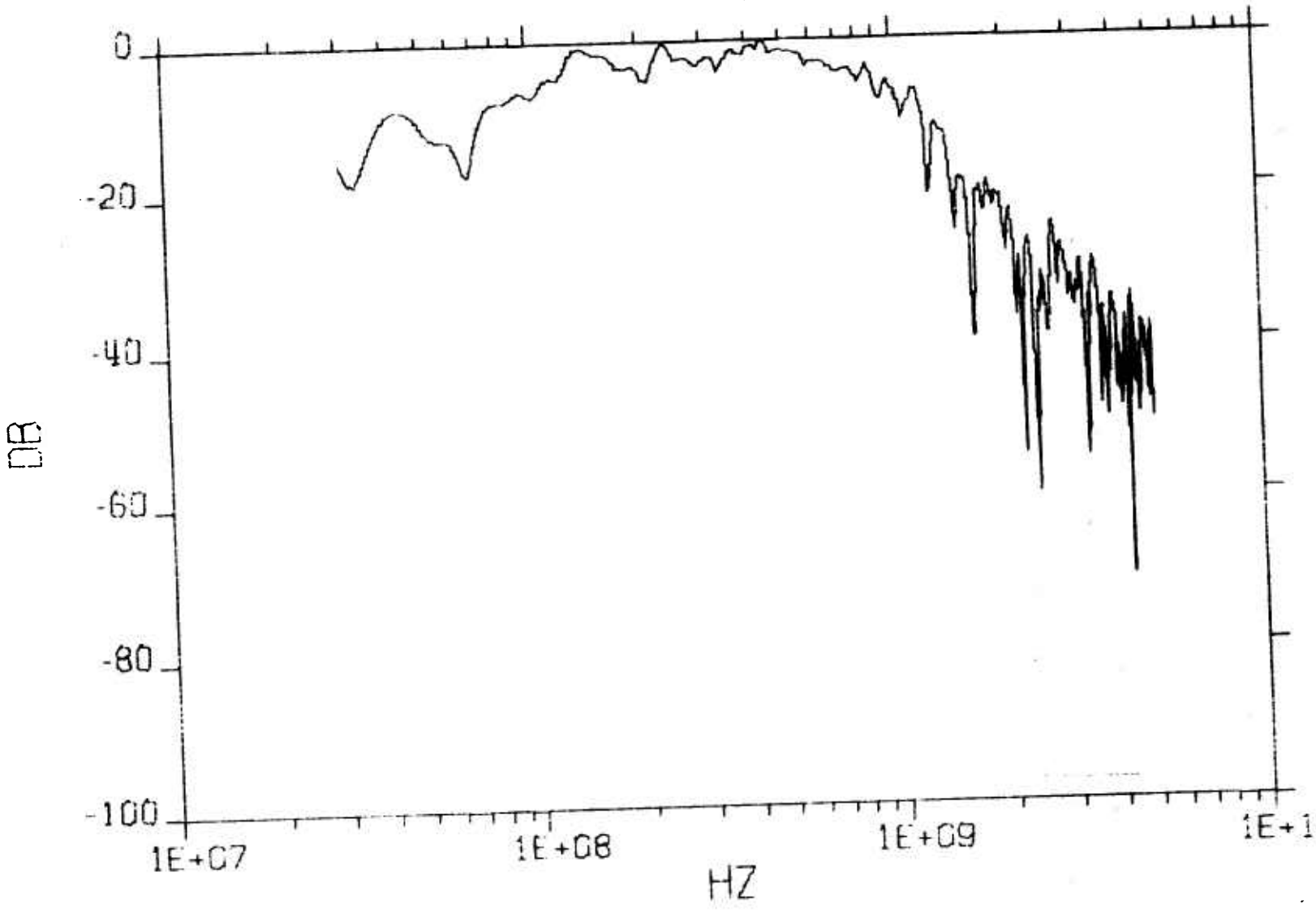


Figure C-37. Spectral Density Amplitude of $F_a(t)$ for Figure C-36

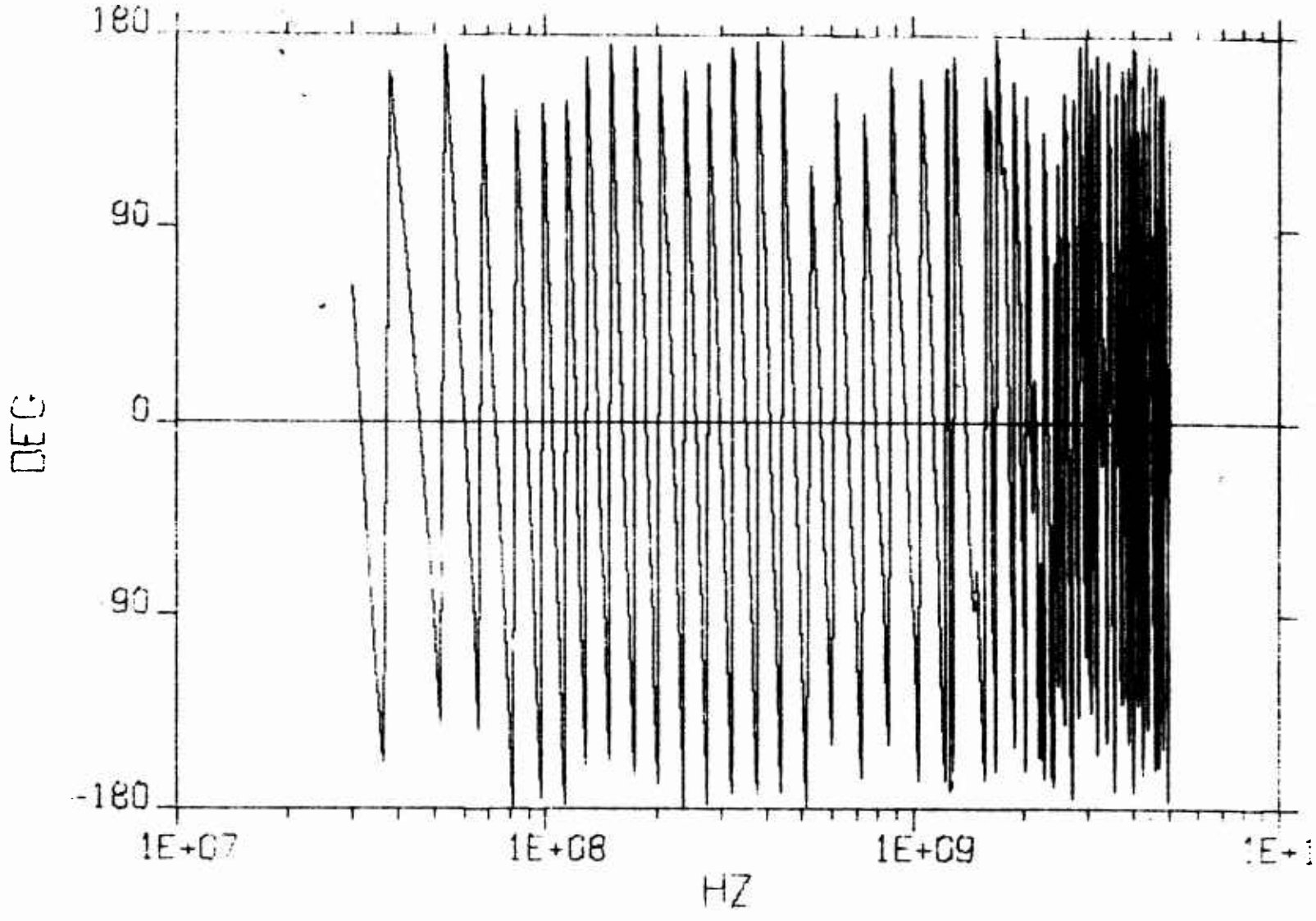


Figure C-38. Phase Angle $\phi_a(f)$ Associated with Figure C-37

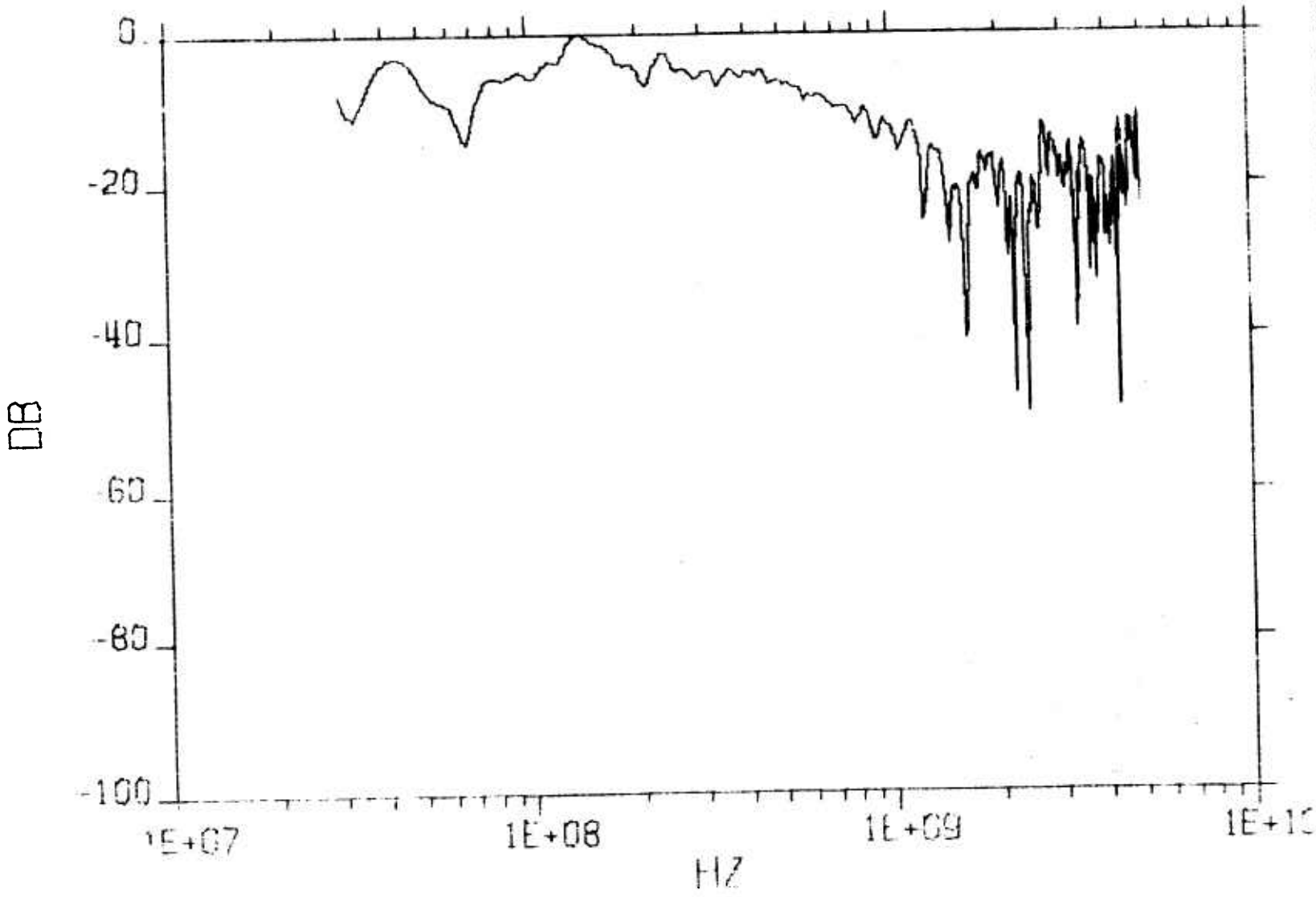


Figure C-39. Spectral Amplitude of $F_a(f)$ for APN-995B Transfer Function

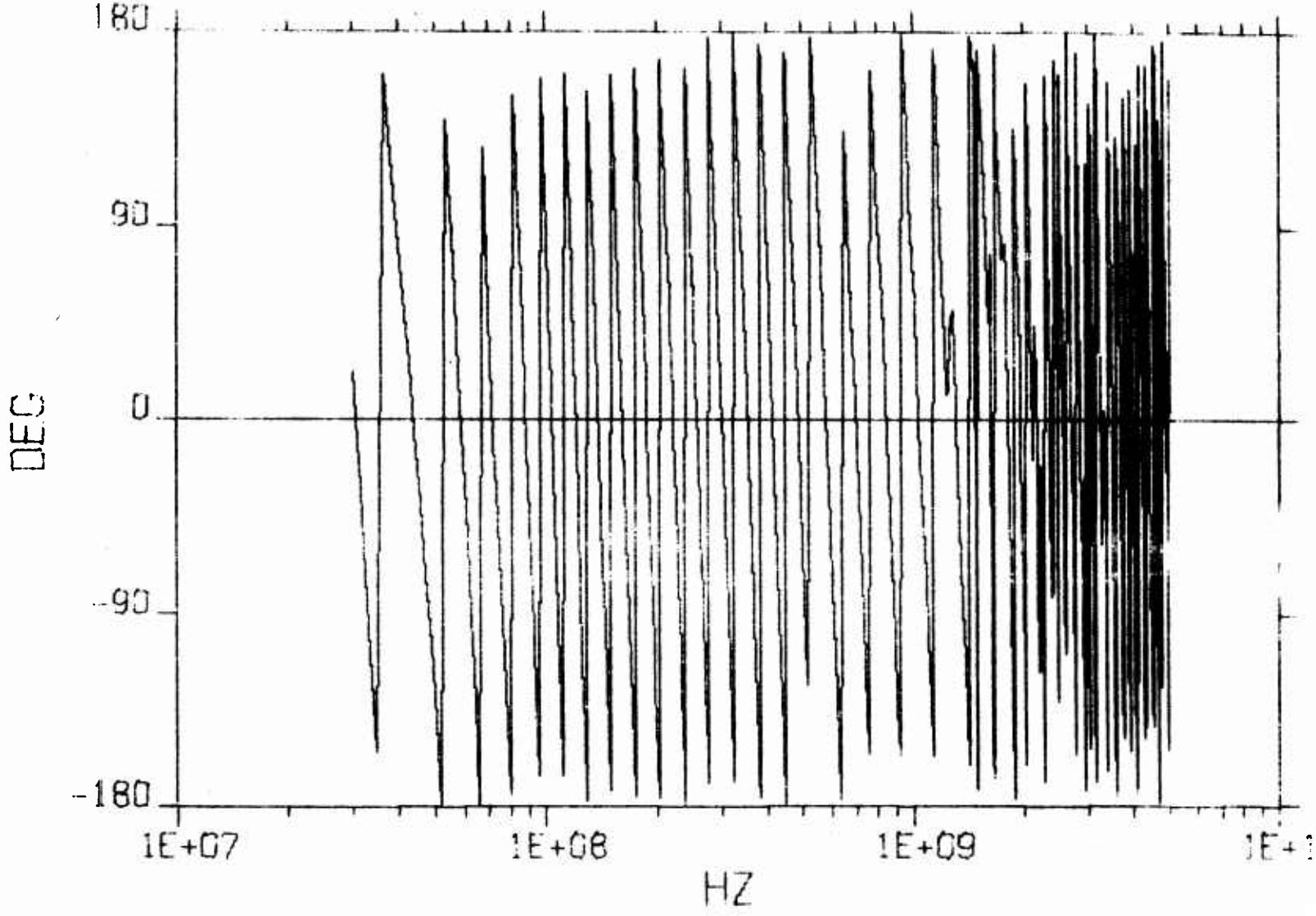


Figure C-40. Phase Angle of $F_a(t)$ for APN-995B Transfer Function

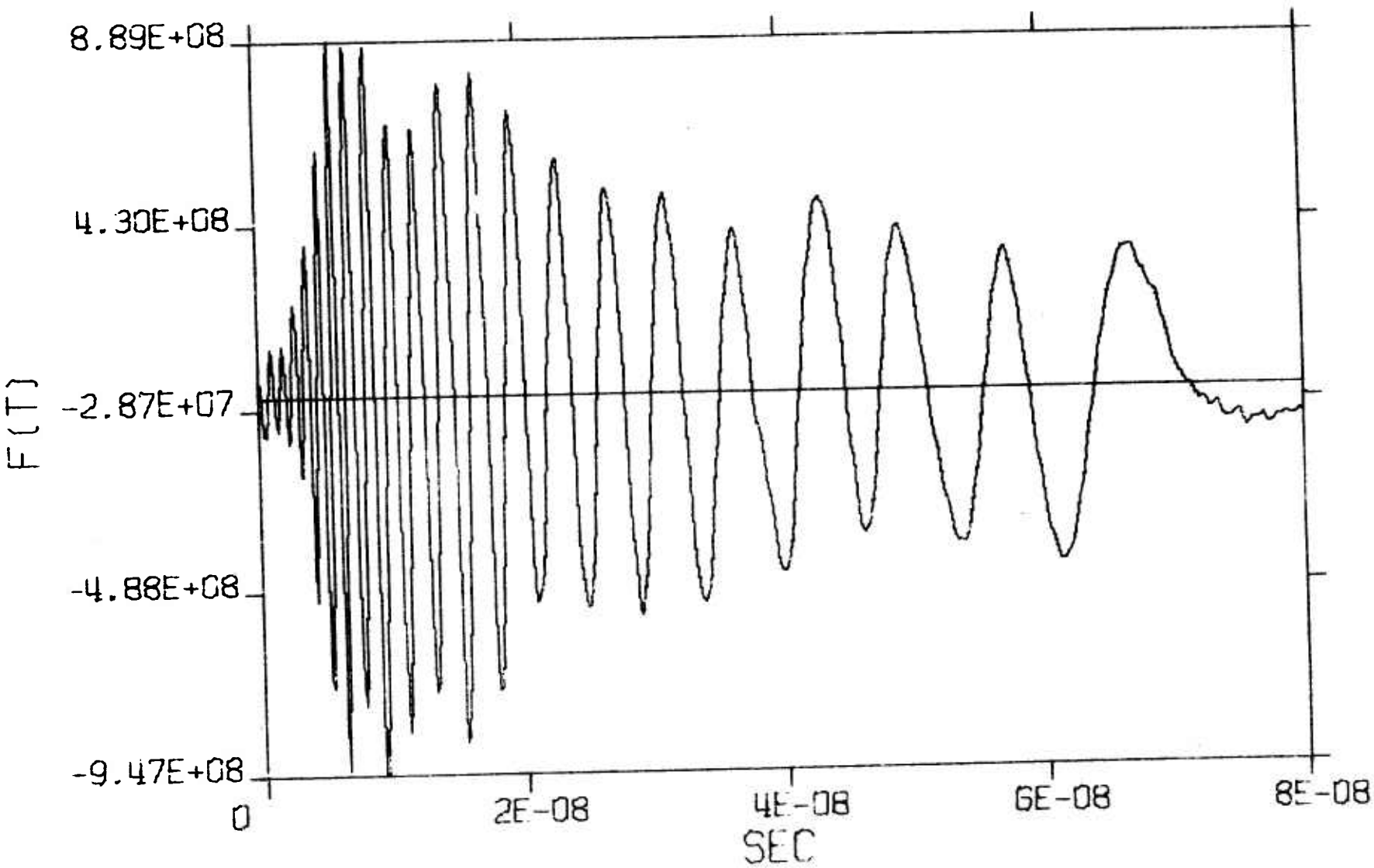


Figure C-41. Dispersion Pulse of APN-99B if it Were Driven by a Perfect Impulse

8. COMPRESSED PULSE OF PYRAMIDAL LOG-PERIODIC ANTENNA APN-502A

When APN-502A was driven by an "impulse" similar to that of Figure C-3, the dispersed radiation was measured as shown in Figure C-42. Assuming that the driving source was a perfect impulse, the -10 dB bandwidth of the antenna is 1.31 GHz as shown in Figures C-43 and C-44 for the dispersion characteristics. Considering the inadequacy of the driving source, the -10 dB bandwidth appears to cover 0.14 to 3.0 GHz, and the phase angle should be similar to the straight dashed line in Figure C-45 where the solid curve is the actual plot of the phase angle in Figure C-44.

If the distributions of Figures C-43 and C-44 were conjugate-matched by a dispersed pulse with the low frequencies arriving first and the high frequencies arriving last, the compressed pulse would be proportional to the pulse shown in Figure C-46.

9. ANALYSIS OF MEASUREMENT PROBE

Except for the cavity-backed spiral antenna ASN-116A, all the antennas described above are measured by a "monopole" stub for their radiated dispersion. The stub probe is described in Appendix B where a particular stub length of 2 cm was used extensively for the antenna ASN-117AA. The following gives a brief analysis of this type of probe.

Figure C-47 is an input impulse for a transmitting stub. The spectral amplitude and phase are shown in Figures C-48 and C-49. It was established in Appendix B that the transmitting stub produces a time derivative on its input pulse, and that an identical receiving probe receives a replica of the transmitted pulse as shown in Figure C-50. Let the probe's receiving function be $H(f)$, then the complex response of Figures C-51 and C-52 may be designated $R(f)$ as

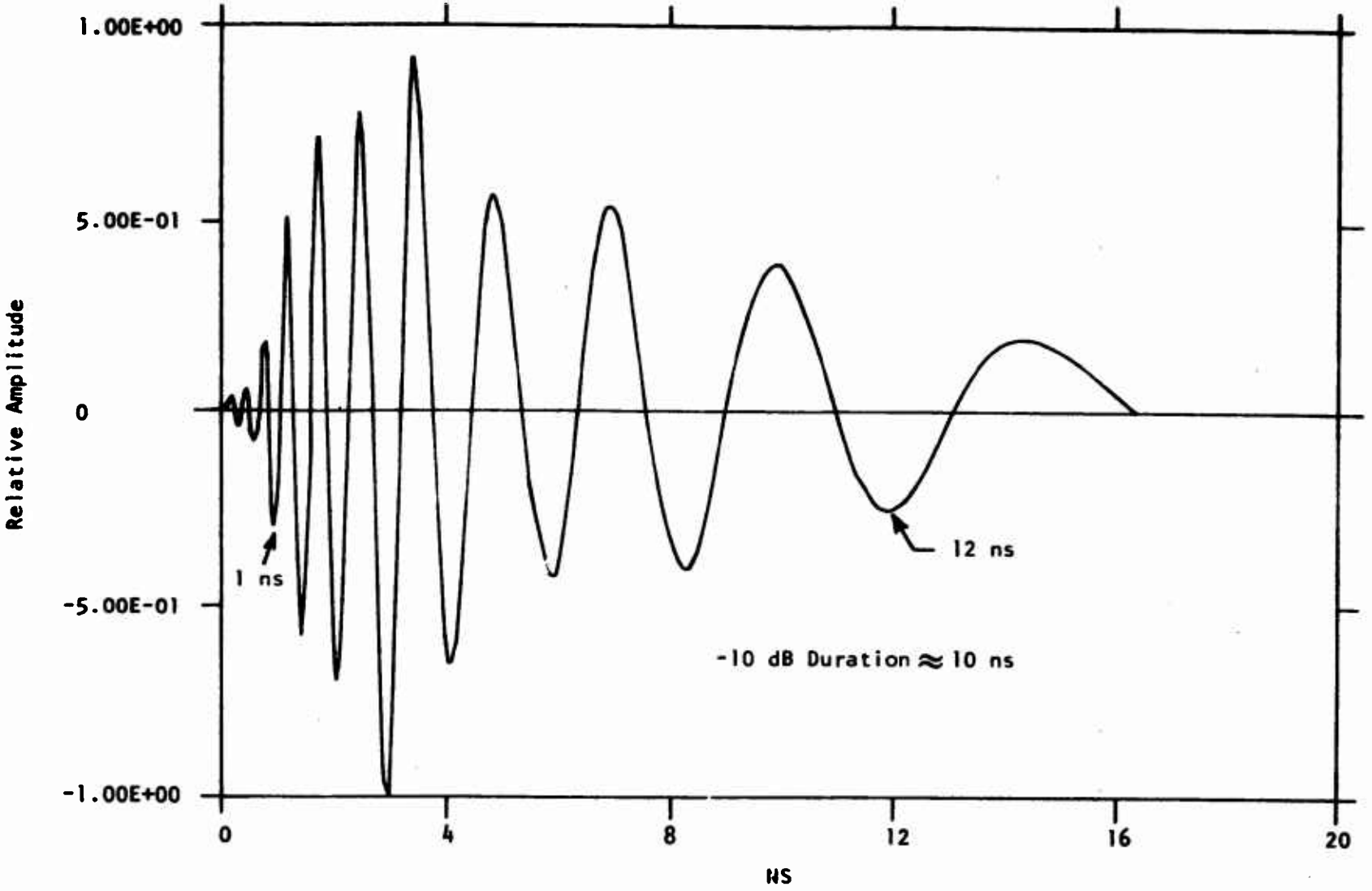


Figure C-42. Output of a 2.54 cm Monopole Sensing the Radiation of APN-502A Log Periodic Antenna Driven by an "Impulse"

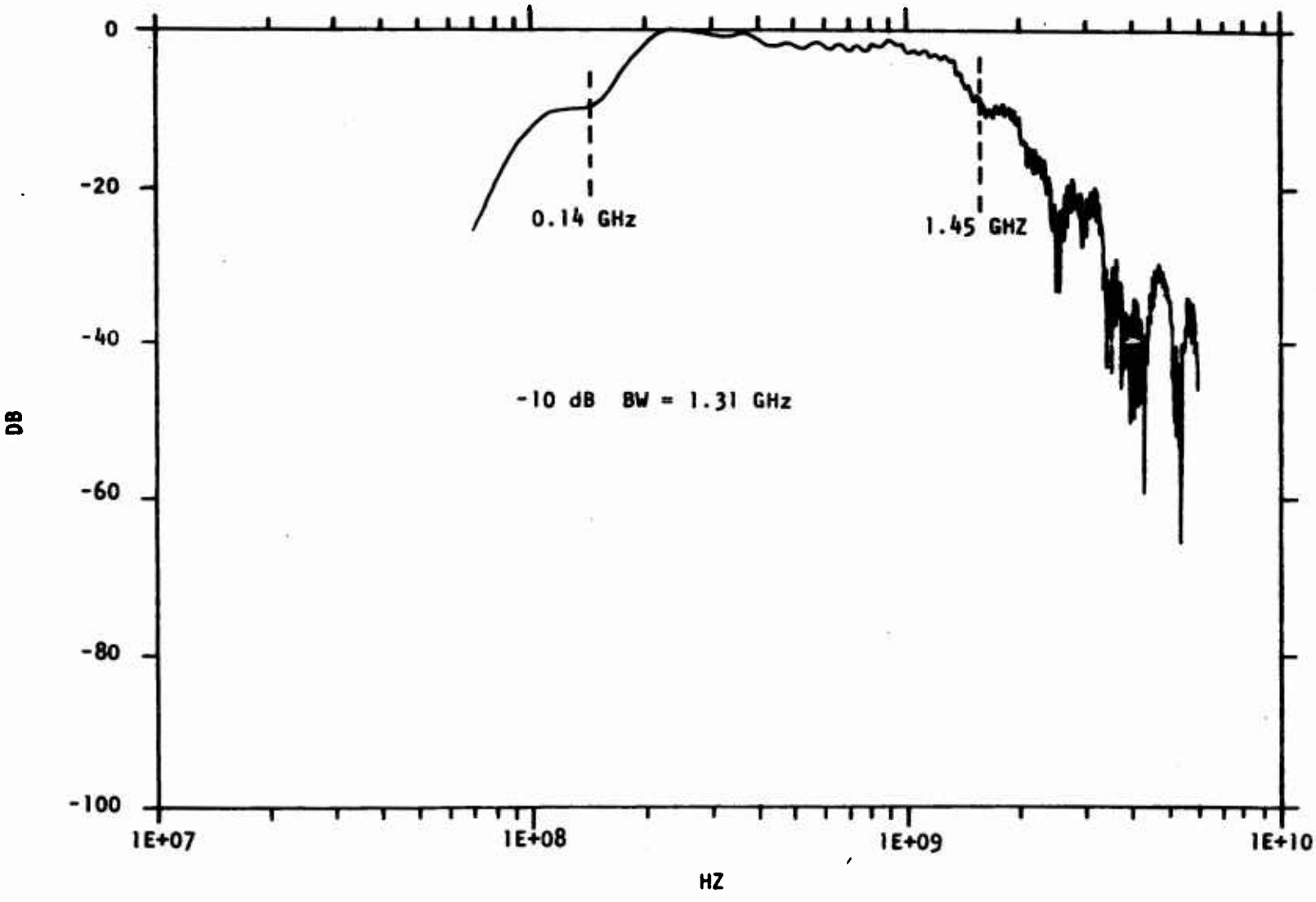


Figure C-43. Relative Spectral Distribution of the Response in Figure C-42

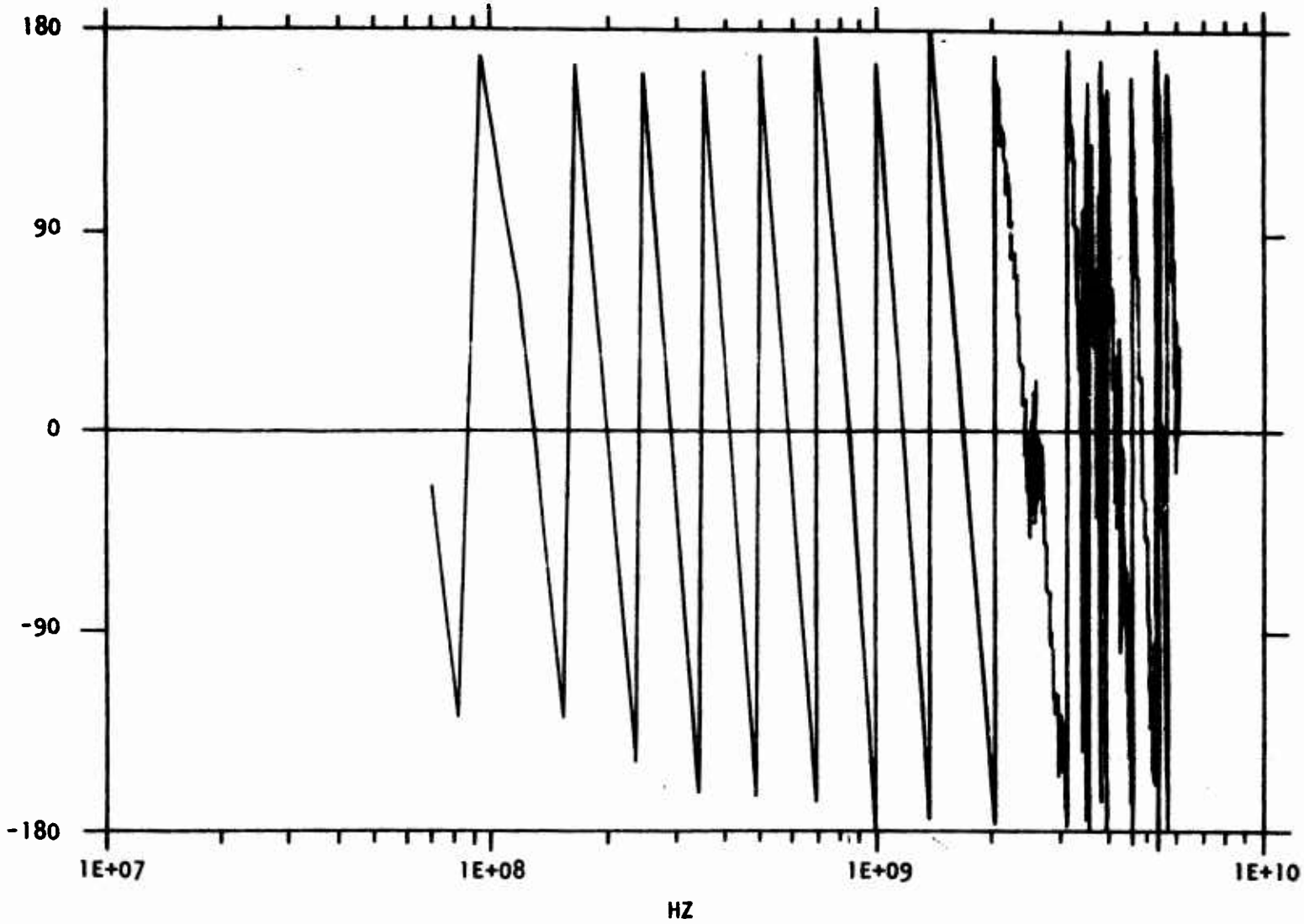


Figure C-44. Phase Angle Corresponding to the Relative Amplitude in Figure C-43

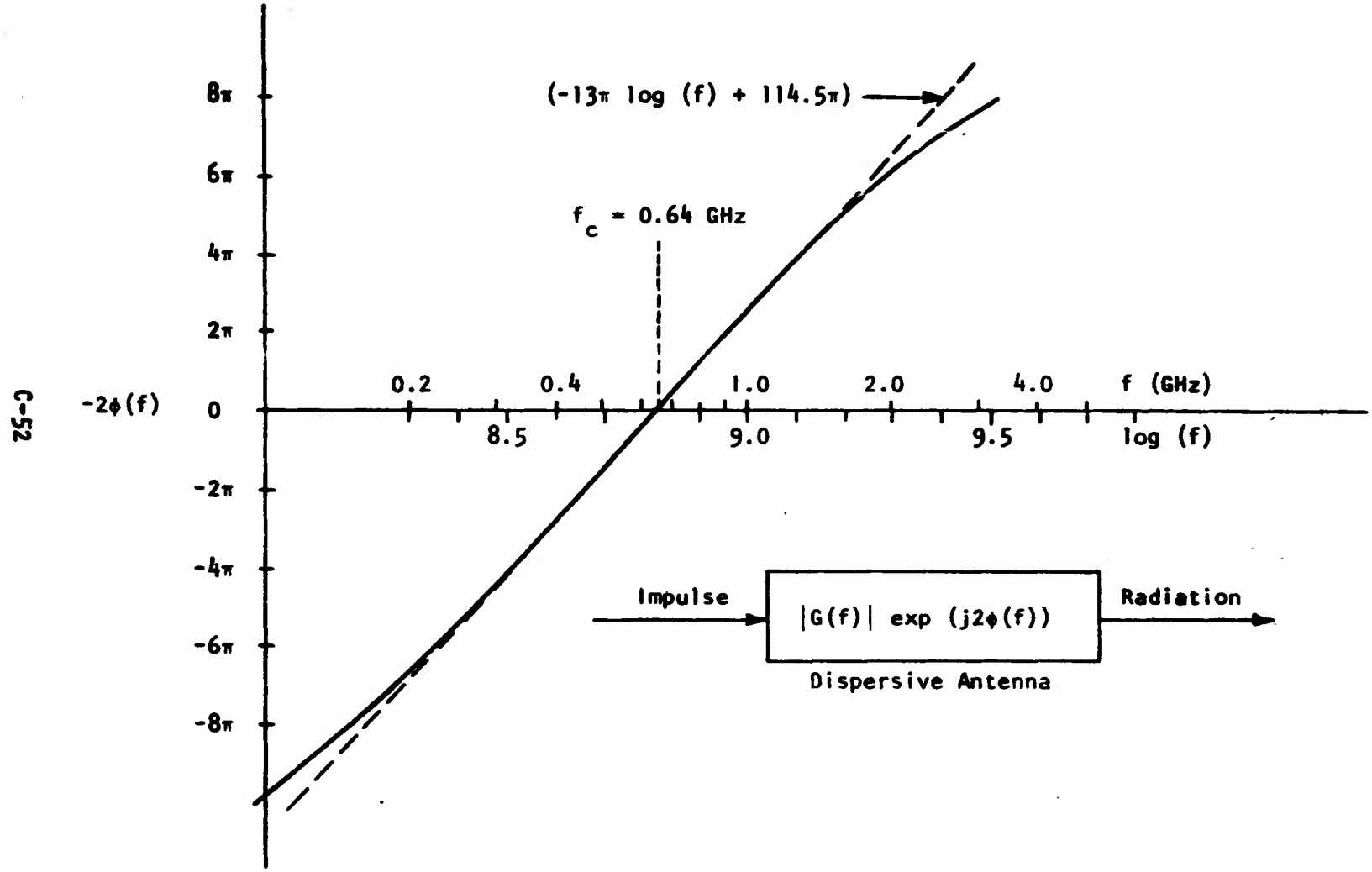


Figure C-45. Relative Phase Angle Obtained from Figure C-44

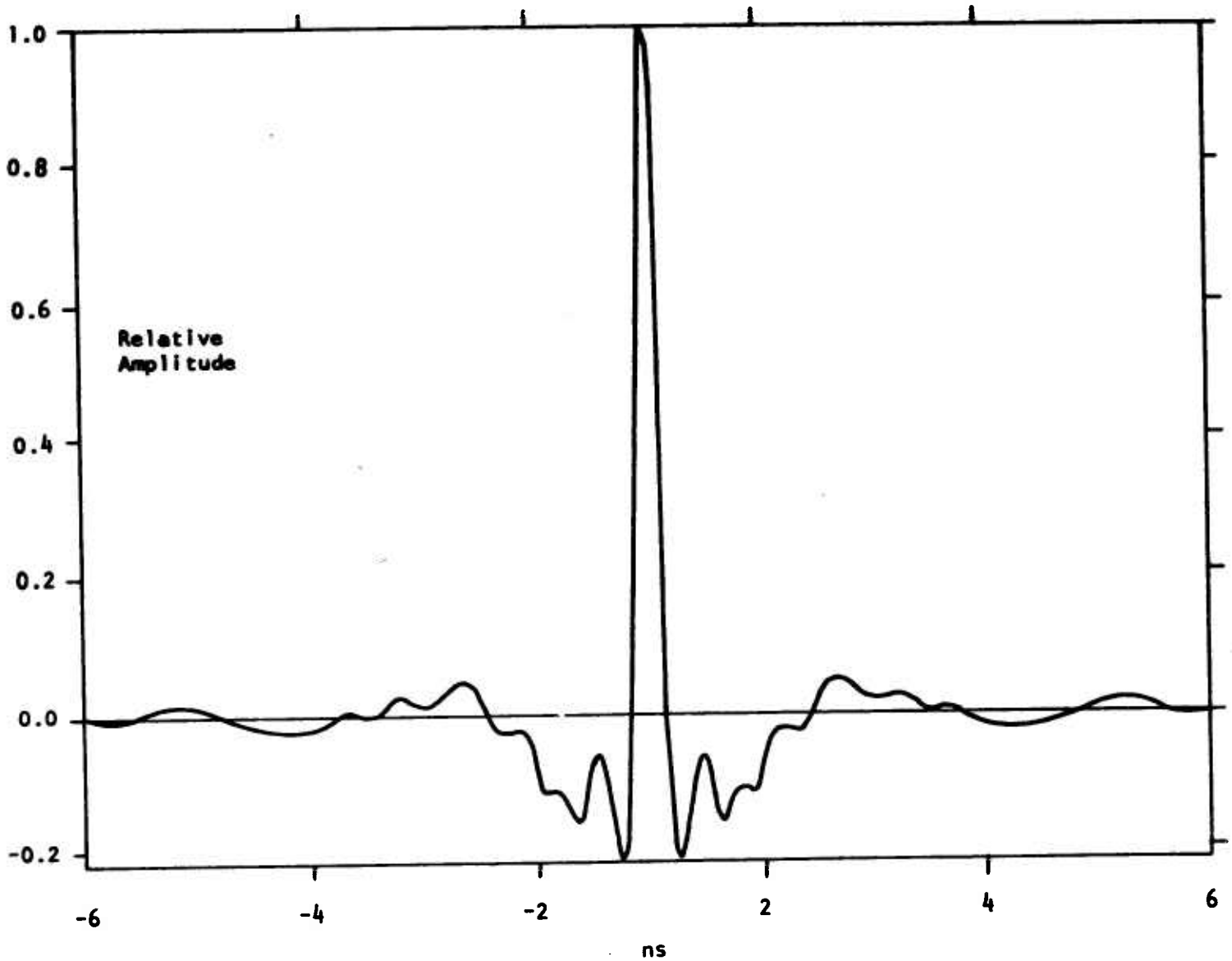


Figure C-46. Compressed Radiation Pulse Under Matched-Filter Conditions for the Characteristics Shown in Figures C-43 and C-44

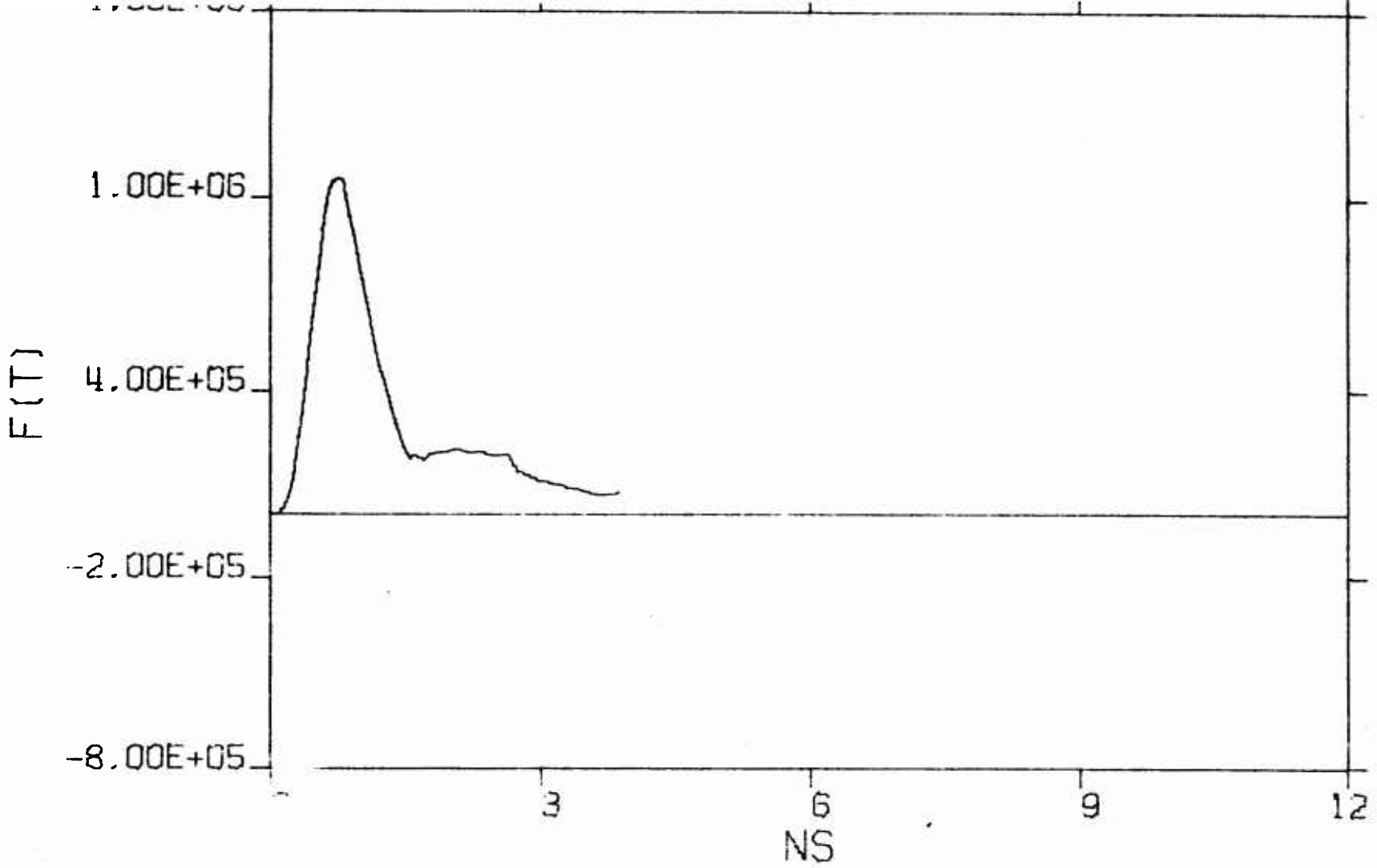


Figure C-47. Input Pulse of a Transmitting Test Probe with 2 cm Center-Conductor Stub

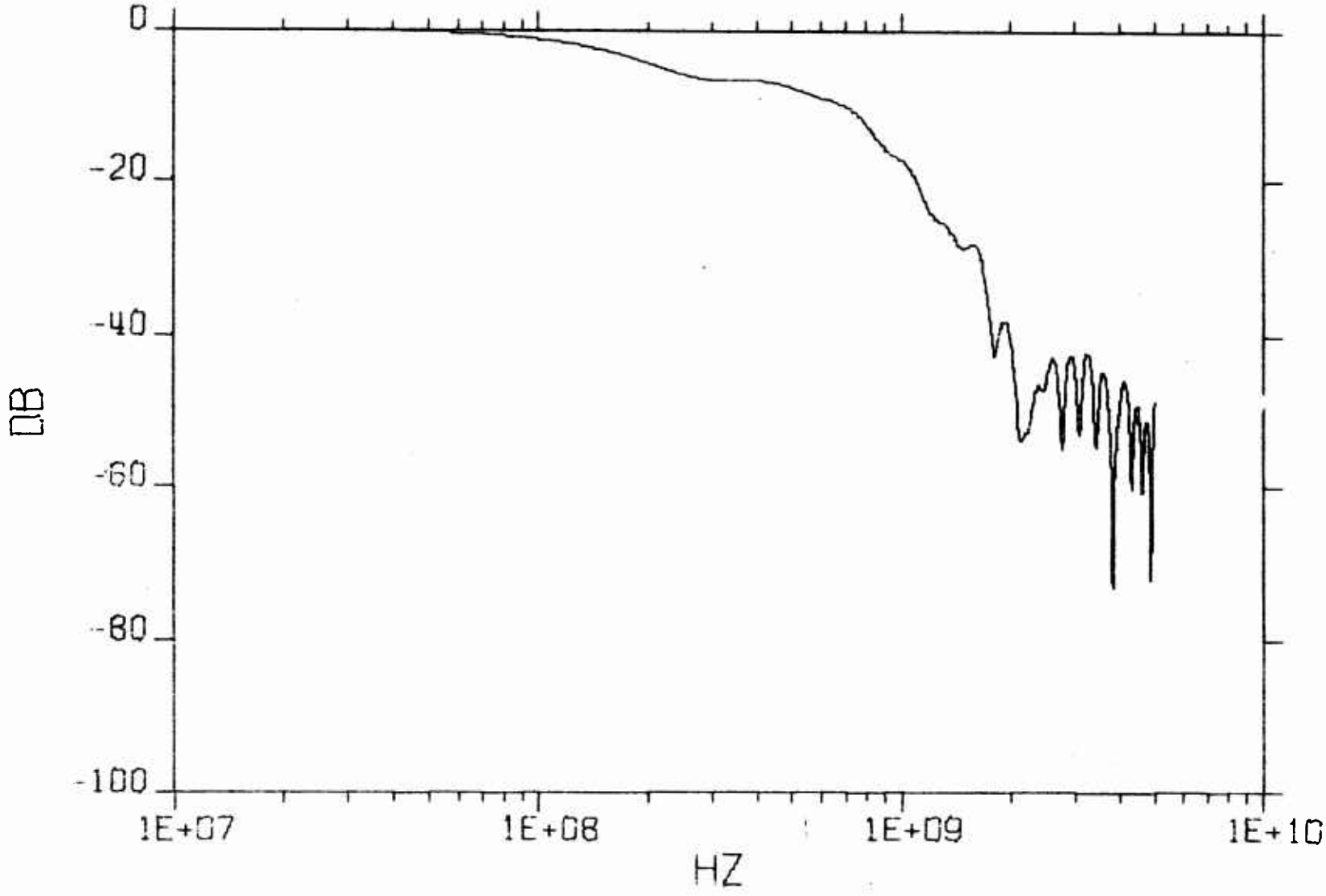


Figure C-48. Spectral Amplitude for the "Impulse" of Figure C-47

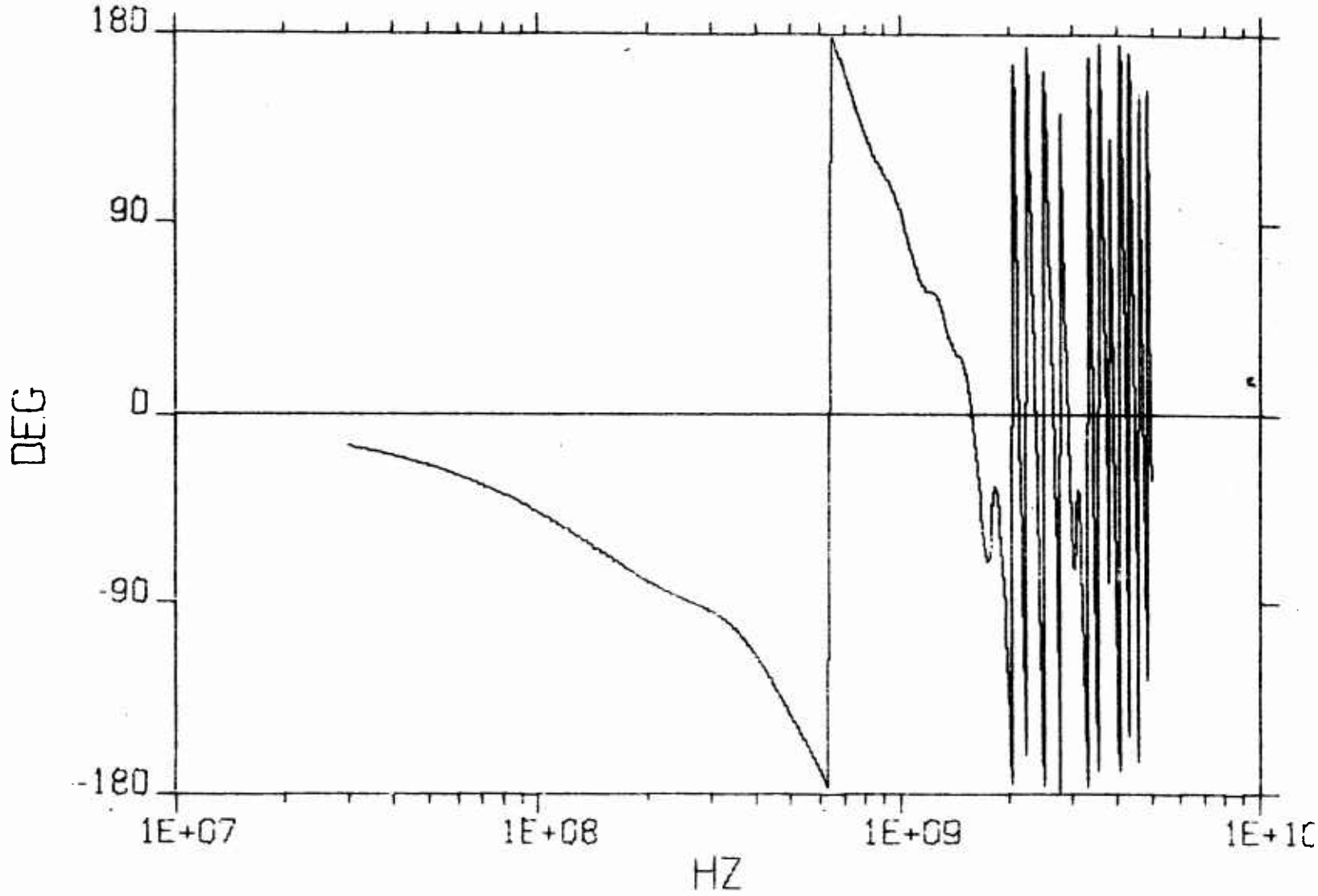


Figure C-49. Phase Angle Associated with the Spectral Amplitude in Figure C-48

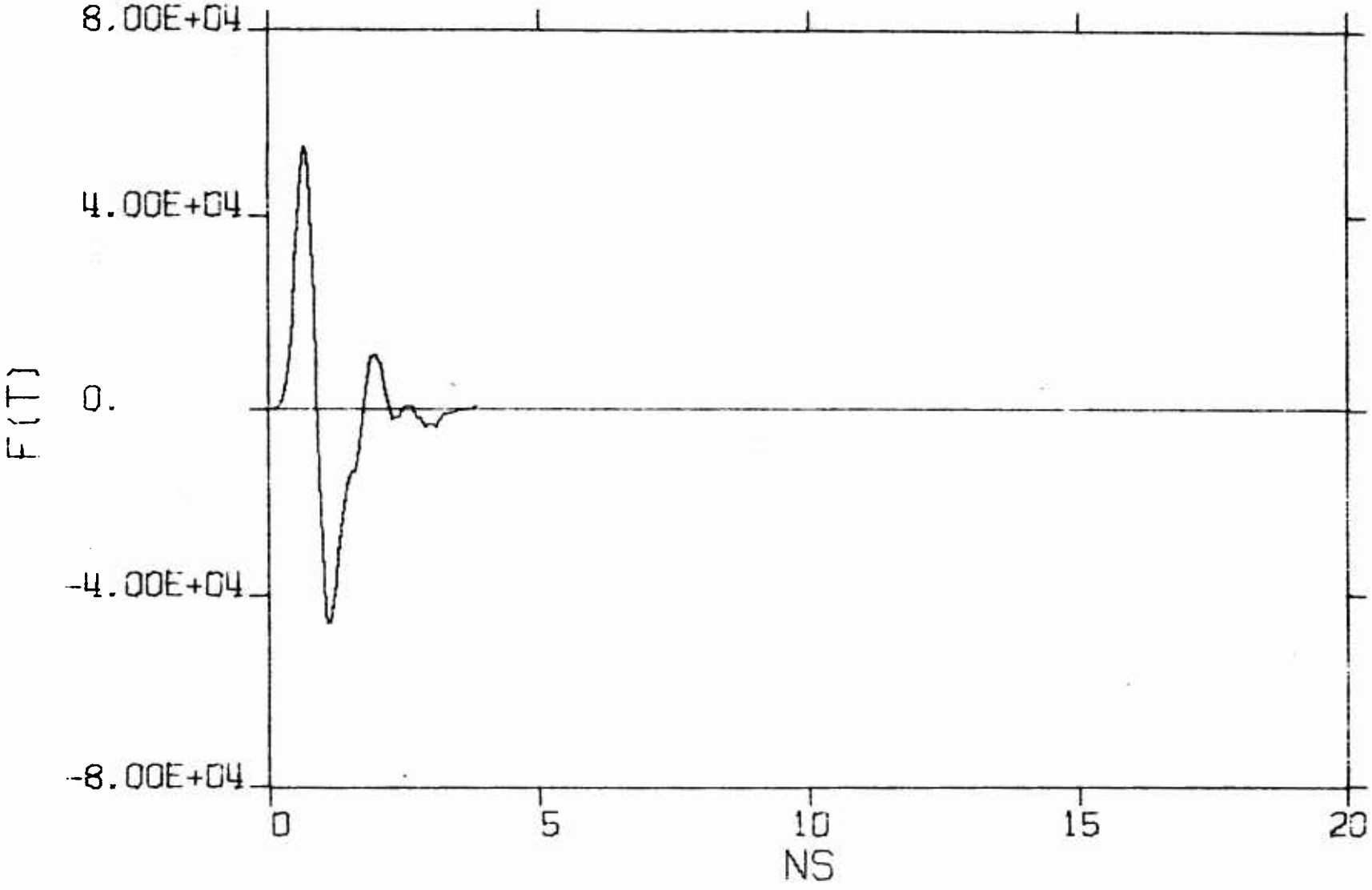


Figure C-50. Received Pulse of an Identical Probe Placed 1 m from the Transmitting Probe Driven by the Pulse in Figure C-47

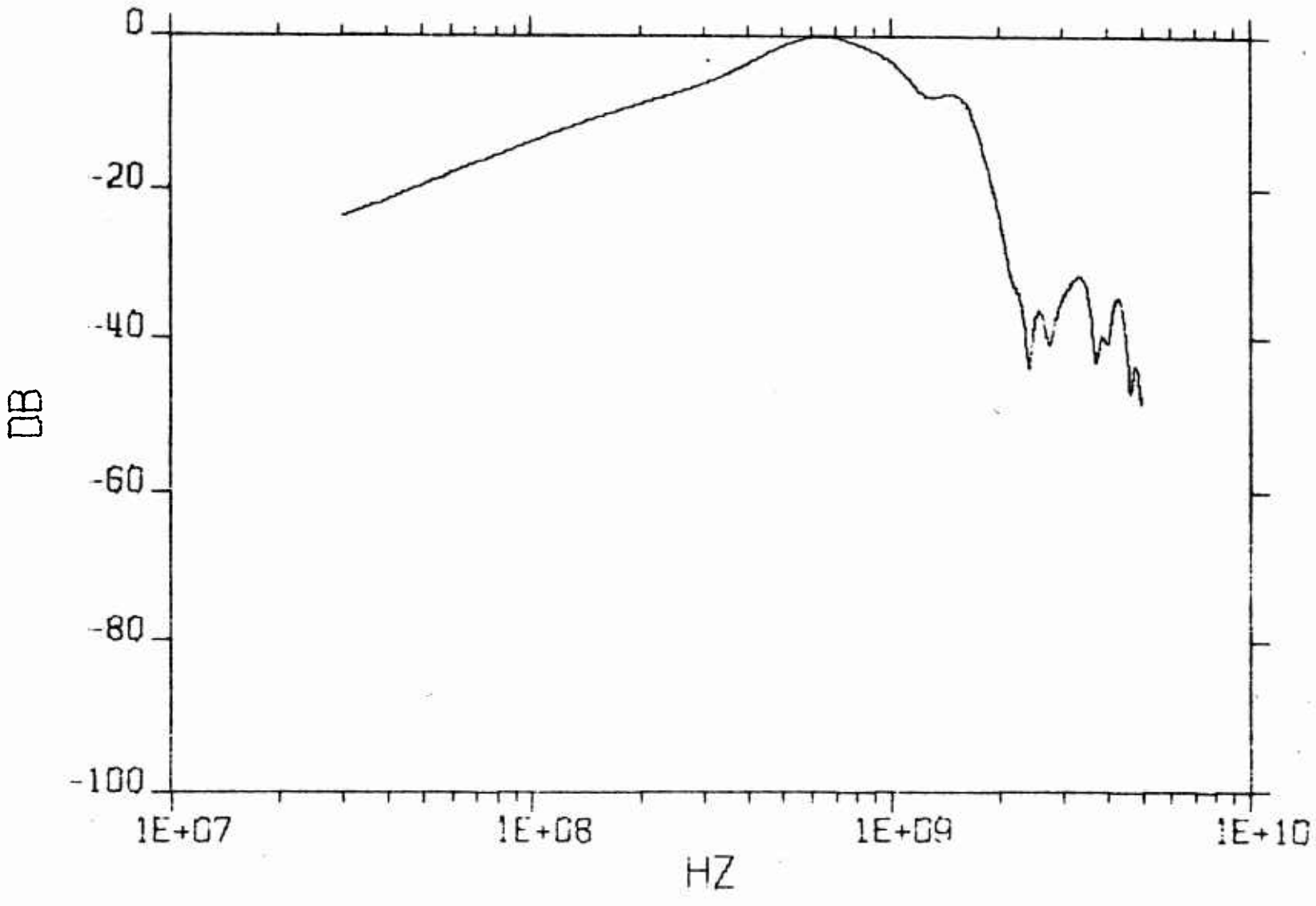


Figure C-51. Spectral Amplitude of Figure C-50

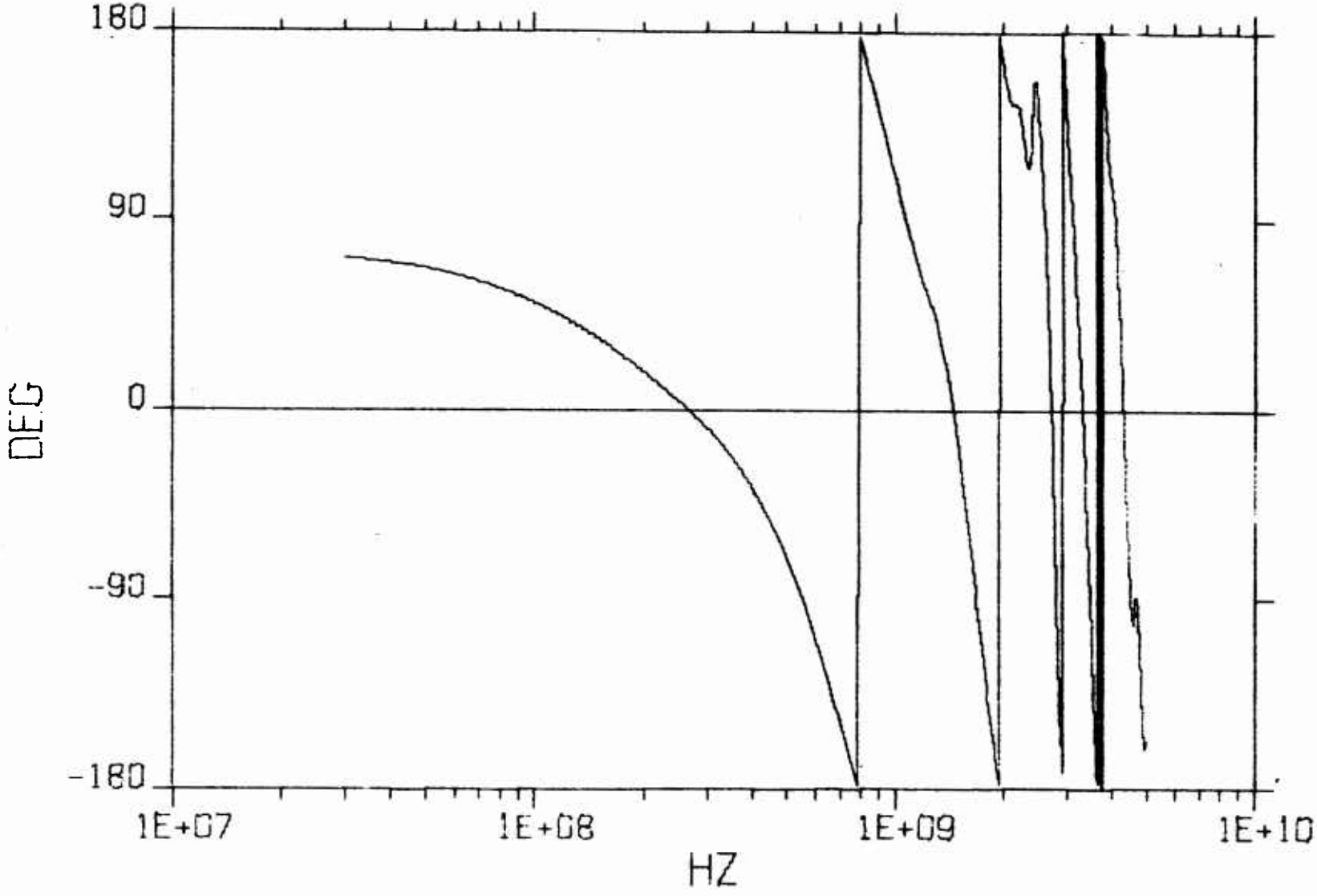


Figure C-52. Phase Angle Associated with the Spectral Amplitude in Figure C-51

$$R(f) = S(f)\ [j2\pi fH(f)]H(f) \qquad \text{(Eq. C-5)}$$

where S(f) is the impulse function given by Figures C-48 and C-49. The term $j2\pi fH(f)$ represent the probe's transmitting function. Since the function H(f) is of primary interest to characterize the receiving probe for dispersion measurements, Equation C-5 is rewritten as

$$j2\pi fH^2(f) = R(f)/S(f) \qquad \text{(Eq. C-6)}$$

The amplitude and phase of the above expression are shown in Figures C-53 and C-54. Well-behaved amplitude and phase for frequencies less than 1.6 GHz indicate that the probe is useful in this frequency range for the driving pulse used. For frequencies higher than 1.6 GHz, the probes' noisy responses are due to the lack of source energy as can be identified in Figure C-48.

Should an ideal impulse be used for the test probes, the response defined in Equation C-6 could produce useful data to as high as 7.5 GHz, because the probe's stub length of 2 cm corresponds to a resonance frequency of 7.5 GHz. These types of source-limited test results are the same as those data analyzed for the six test antennas discussed earlier. Thus, one is led to the conclusion that the probe used is adequate for the chosen source, although a satisfactory probe performance up to 7.5 GHz has not been established.

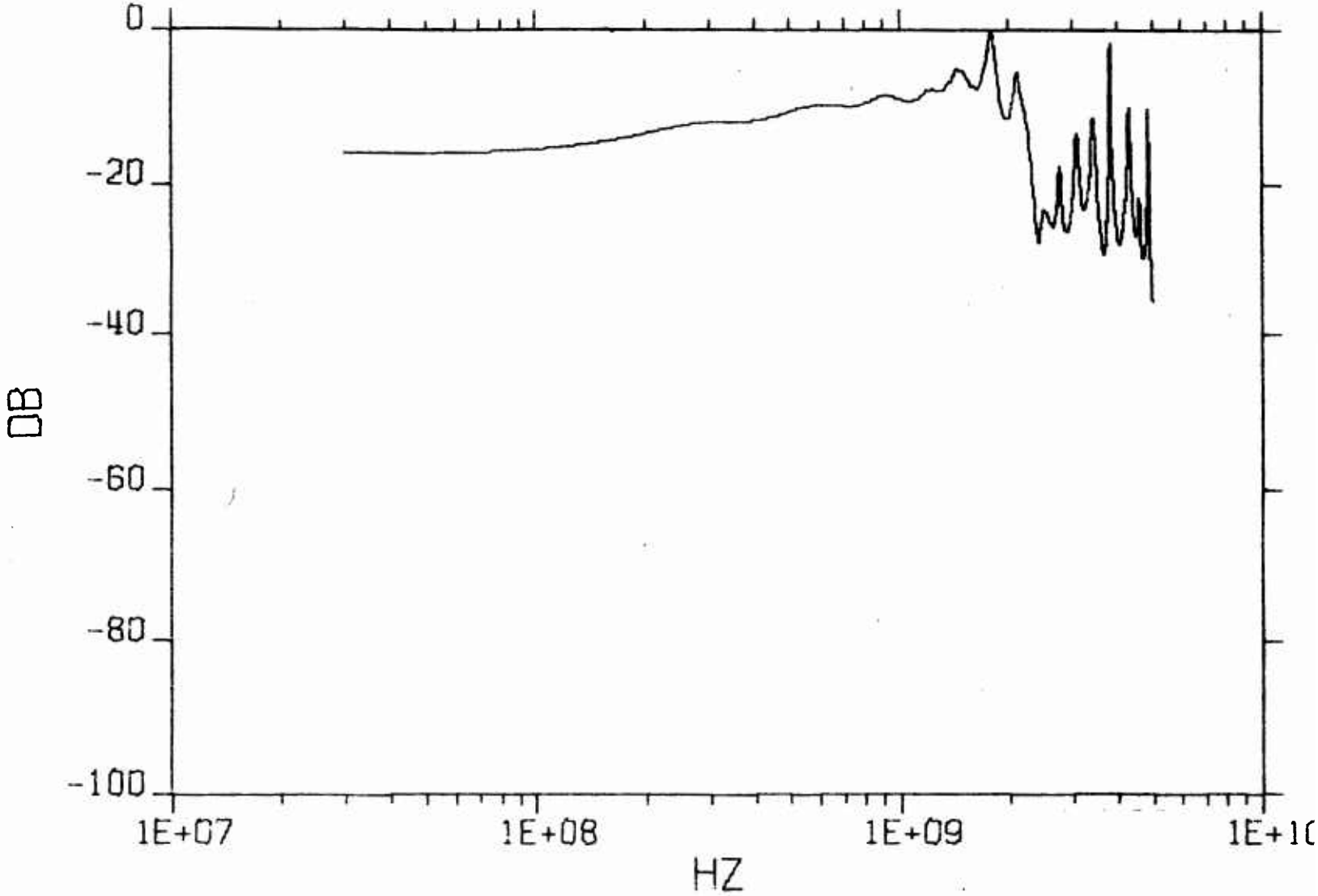


Figure C-53. Spectral Amplitude of $j2\pi f\ H^2(f)$ with H(f) As the Probe's Receiving Function

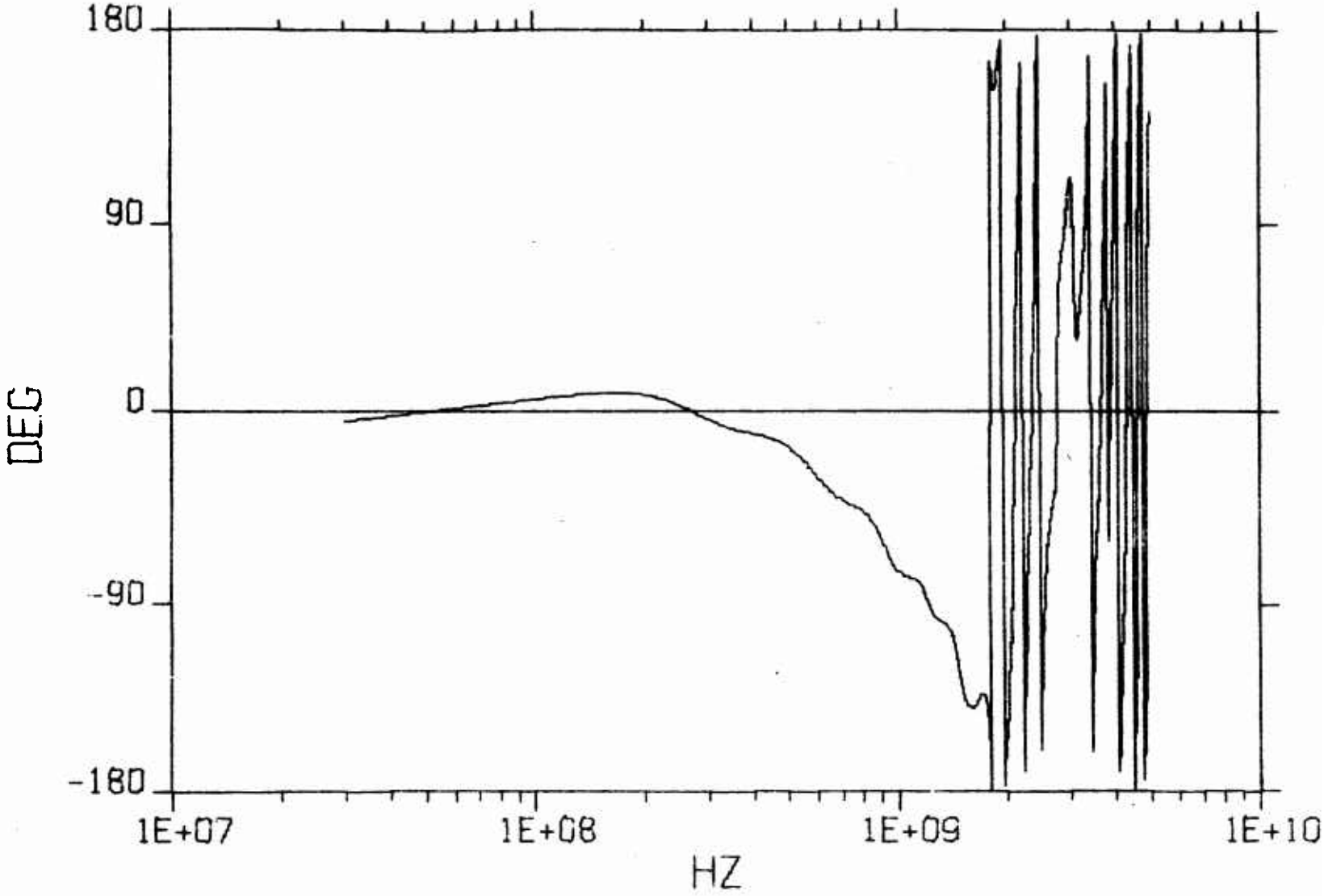


Figure C-54. Phase Angle Associated with the Spectral Amplitude of Figure C-53

APPENDIX D

ANALYTICAL FORMULATION OF RADIATION ELEMENTS

1. INTRODUCTION

Existing wide band or log-periodic antennas are known to radiate frequency spectra centered around elements of different lengths. Either geometrical locations or spectral locations from which radiations are centered are called radiation regions of an antenna. If the antenna was driven by an ideal impulse source, it would be analytically possible to describe radiations from each individual active region. The radiated pulse of each active region can be treated as a wave packet oscillating at the central frequency of the region. The pulse envelope will vary in width and be displaced in time depending on how active regions are relatively distributed.

The objectives of analyzing the dispersed pulses of various active regions are as follows:

(1) Analytically determine the complex frequency-domain distribution to approximate a realistic antenna.

(2) Analytically establish the bandwidth and phase angle of active regions to approximate the radiation mechanisms of antenna elements.

(3) Determine time-domain radiation characteristics and relative delay times of all antenna elements.

(4) Determine overall time-domain dispersed pulse of an antenna by superposing all dispersed pulses of active regions.

In relation to the above objectives, the purpose of this analysis can be stated as follows:

(1) To enable overall evaluation of a dispersive antenna on characteristics such as total effective bandwidth, total effective pulse duration phase velocity and group velocity of all frequency components.

(2) To enable analysis of each active region on characteristics such as percentage bandwidth and percentage duration of wave packets.

(3) To enable determination of relative delay times and relative efficiency in contributing to desired pulse compression.

(4) To enable characterization of overall dispersed pulse in terms of composite radiation from all active regions.

The following analysis will be restricted to the analytical model of log-periodic antennas and quadratic-phase antennas.

2. FREQUENCY-DOMAIN MODEL OF LOG-PERIODIC ANTENNAS

Let a log-periodic antenna have a total of N radiation elements or regions. Let the highest and the lowest frequencies of interest be f_h and f_ℓ, respectively. If a fractional cutoff bandwidth of each active region is assumed to be the same as 2δ, then the central frequency may be designated as f_{no} to relate the high-end and low-end cutoff frequencies as

$$f_{nh} = (1 + \delta) f_{no} \qquad \text{(Eq. D-1)}$$

$$f_{n\ell} = (1 - \delta) f_{no} \qquad \text{(Eq. D-2)}$$

f_{no} = the central frequency of the nth active region. (Eq. D-3)

By treating active regions in descending order of frequency, the first high-end frequency f_{1h} is the same as the highest cutoff frequency f_h of the whole antenna, i.e.,

$$f_{1h} = f_h = (1 + \delta)\, f_{1o} \qquad \text{(Eq. D-4)}$$

$$f_{1\ell} = (1 - \delta)\, f_{1o}. \qquad \text{(Eq. D-5)}$$

The nth central frequency of a log-periodic antenna is assigned in relation to f_h as

$$f_{no} = f_h\, (1 + \delta)^{-n} = f_{1o}\, (1 + \delta)^{-(n - 1)}. \qquad \text{(Eq. D-6)}$$

The last active region is at the lowest end of the frequency spectrum as

$$f_{No} = f_h\, (1 + \delta)^{-N} \qquad \text{(Eq. D-7)}$$

$$f_{Nh} = (1 + \delta)\, f_{No} = f_h\, (1 + \delta)^{-(N - 1)} \qquad \text{(Eq. D-8)}$$

$$f_{N\ell} = (1 - \delta)\, f_{No} = f_\ell. \qquad \text{(Eq. D-9)}$$

If the fractional bandwidth 2δ, the highest-end central frequency f_1, and the lowest-end central frequency f_{No} are known, the total number of active regions could be determined as

$$N = 1 + \ell n\, (f_{1o}/f_{No}) / \ell n\, (1 + \delta)$$

The complex spectral distribution of a log-periodic antenna is considered next. Assuming that the amplitude is fairly constant around the center of operating frequencies, it is realistic to assume that the amplitudes at both high- and low-end cut off frequencies are about 20 dB below that at the center. As for phase angles, the highest central frequency may be assumed to be the reference component with zero phase angle. Phase angles of other components are then assumed to be a logarithmic function of frequency. In approximating these assumptions, the complex spectral distributions of all active regions may be written for a radiated electric field as

$$E_n(r_o,f) = \frac{120k}{r_o}\left[0.54 + 0.46\cos\frac{\pi(f - f_o)}{f_h - f_o}\right]^{1/2} \cdot \qquad \text{(Eq. D-10)}$$

$$\cdot \left[0.54 + 0.46\cos\frac{\pi(f - f_{no})}{f_{nh} - f_{no}}\right]^{1/2}$$

$$\cdot \exp\left[j\pi\ell n(f/f_h)/\ell n(1 + \delta)\right], \quad f_{n\ell} \leq f \leq f_{nh}$$

$$f_o = (f_h + f_\ell)/2 \qquad \text{(Eq. D-11)}$$

where f_o is the center frequency of the antenna, r_o is the far-zone distance, and k is a constant dependent of the current on antenna. The electric field is written for a log-periodic antenna of pure dipole modes. For every n, the active region is restricted in the frequency ranges as shown.

The phase angle in Equation D-10 may be rewritten as

$$\phi(f) = j\pi \ell n(f/f_h)/\ell n(1+\delta)$$

$$= j\pi[\ell n(f/f_{No})/\ell n(1+\delta) - N]$$

$$= \phi'(f) - jN\pi \qquad \text{(Eq. D-12)}$$

where $\phi(f)$ is plotted in Figure D-1 for $\delta = 0.2$ and $N = 13$. For $f_h = f_{1h} = 2$ GHz and $f_\ell = f_{N\ell} = 0.1558$ GHz, the following table gives the center frequencies f_{no}, the high-cutoff frequencies f_{nh} and the low-cutoff frequencies f_n for 13 radiative regions

TABLE D-1

LIST OF RADIATIVE REGIONS

REGION	f_{no}	f_{nh}	$f_{n\ell}$
1	1.667E+09	2.000E+09	1.389E+09
2	1.389E+09	1.667E+09	1.157E+09
3	1.157E+09	1.389E+09	9.645E+08
4	9.645E+08	1.157E+09	8.038E+08
5	8.038E+08	9.645E+08	6.698E+08
6	6.698E+08	8.038E+08	5.582E+08
7	5.582E+08	6.698E+08	4.651E+08
8	4.651E+08	5.582E+08	3.876E+08
9	3.876E+08	4.651E+08	3.230E+08
10	3.230E+08	3.876E+08	2.692E+08
11	2.692E+08	3.230E+08	2.243E+08
12	2.243E+08	2.692E+08	1.869E+08
13	1.869E+08	2.243E+08	1.558E+08

Summing all the radiation regions in Equation D-10 gives the log-periodic antenna frequency-domain as

$$E(r_o,f) = \sum_{n=1}^{13} E_n(r_o,f) = |E(r_o,f)| \exp(-j\phi) \qquad \text{(Eq. D-13)}$$

The spectral amplitude and phase angle are plotted in Figures D-2 and D-3.

The analytical model for a log-periodic antenna is universally applicable to all practical log-periodic antennas such as log-periodic dipoles, pyramidal log-periodic dipoles, cavity-backed spirals and conical helix antennas. Most of these antennas have been measured and analyzed as given in Appendix B. Their phase angles maintain well behaved log-periodic natures depending on the elemental bandwidth δ. Because of source-limited measurements, most antennas did not show log-periodic phases for all their CW-specified bandwidth. However, the available measured data have confirmed that the analytical model developed here is accurate for all well-designed antennas. To use the model requires specifying the lowest and highest cutoff frequencies (f_ℓ, f_h) and the fractional elemental bandwidth δ as used in Equations D-10 and D-13.

3. LOG-PERIODIC PHASE ANGLE AND MODULATION

Phase angles are to be derived from a general form by assigning (f_ℓ, f_h, δ, N) for log-periodic antennas. Results will then be used to derive instantaneous frequency, group delay, total bandwidth and total duration of dispersion.

Let a log-periodic antenna have within its operating bandwidth a phase angle as

$$\phi(f) = a + b\,\ell n(f) \qquad \text{(Eq. D-14)}$$

where a and b are determined by the lowest cutoff frequency f_ℓ and the highest cutoff frequency f_h as

$$\phi(f_h) = o = a + b\ \ell n(f_h) \qquad \text{(Eq. D-15)}$$

$$\phi(f_\ell) = -(N + 1)\pi = a + b\ \ell n\ (f_\ell) \qquad \text{(Eq. D-16)}$$

The phase angle at f_ℓ is made log $(N + 1)\pi$ with respect to the f_h component. The number N designates total radiative regions of an antenna. When the cutoff fractional bandwidth of each radiative region is assigned 2δ around respective center frequencies, the solution of b can be obtained from the above two equations.

$$b = ((N + 1)\pi)/\ell n\ (f_h/f_\ell) = \frac{\pi}{\ell n\ (1 + \delta)} \qquad \text{(Eq. D-17)}$$

Consequently, the three parameters (f_h, f_ℓ, δ) specify the phase function

$$\phi(f) = (\pi \ell n(f/f_h))/\ell n\ (1 + \delta) \qquad \text{(Eq. D-18)}$$

Since the spectral group delay time is defined as

$$t = \frac{1}{2\pi}\frac{d\phi}{df} = \frac{1}{2\pi}\phi'(f) = \frac{1}{2f\ell n\ (1 + \delta)} \qquad \text{(Eq. D-19)}$$

The solution for instantaneous frequency is

$$f = \frac{1}{2t\ell n\ (1 + \delta)} \qquad \text{(Eq. D-20)}$$

This gives the phase-modulation function of the corresponding complex time function of a log-periodic antenna as

$$\theta(t) = 2\pi ft - \phi(f) \qquad \text{(Eq. D-21)}$$

$$= \frac{\pi}{\ell n\ (1+\delta)} - \frac{\pi \ell n(t f_h \ell n(1+\delta)^2)}{\ell n\ (1+\delta)}$$

For a highly dispersive antenna, its effective fractional bandwidth δ of a radiation region is in the neighborhood of 0.1 or less. Assuming δ is much less than 0.1, Equation D-20 would become

$$f = \frac{1}{2t\delta} \qquad \text{(Eq. D-22)}$$

$$= \frac{f_h}{2t(f_h\delta)} = \frac{f_h}{2t\ b_h}$$

$$= \frac{f_\ell}{2t(f_\ell\delta)} = \frac{f_\ell}{2t\ b_\ell}$$

where (b_ℓ, b_h) are the effective elemental bandwidth of the lowest and the highest radiation regions. Letting (t_h, t_ℓ) be the group delays of the (f_h, f_ℓ) components, Equation D-22 gives

$$1 = \frac{1}{2t_h\ b_h} \qquad \text{(Eq. D-23)}$$

$$1 = \frac{1}{2t_\ell\ b_\ell} = \frac{1}{2(T + t_h)b_\ell} \approx \frac{1}{2Tb_\ell} \qquad \text{(Eq. D-24)}$$

where the dispersion pulse duration is defined as

$$T = t_\ell - t_h \approx t_\ell \qquad \text{(Eq. D-25)}$$

if the group delay t_h is much smaller than t_ℓ. For the convenience of later discussions, the results of constant elemental bandwidth and group-delay time product are rewritten as

$$Tb_\ell \approx t_\ell\, b_\ell = t_h\, b_h = 1/2 \qquad \text{(Eq. D-26)}$$

4. TIME-DOMAIN MODEL OF LOG-PERIODIC ANTENNAS

For each active region in Equation D-10, there corresponds a wave packet modulated by the center frequency of the region. The phase angle can be locally linearized in each radiation region as

$$\phi_n(f) = \phi(f_{no}) + \phi'(f_{no})(f - f_{no}) - \frac{\phi''(f_{no})}{2!}(f - f_{no})^2 + \cdots$$

$$\approx \frac{\pi}{\ell n(1+\delta)} \left[\ell n(f_{no}/f_{lo}) + (f/f_{no}-1) + (f/f_{no}-1)^2/2 \right], \quad f_{n\ell} \le f \le f_{nh} \qquad \text{(Eq. D-27)}$$

where f_{no} are defined in Equation D-6. The phase delay for each spectral group of a radiative region is

$$\phi(f_{no}) = (\pi \ell n(f_{no}/f_h))/\ell n(1+\delta) \qquad \text{(Eq. D-28)}$$

$$= -n\pi$$

If the spectral amplitude is unity across the entire bandwidth, the radiated pulse from each radiative region is approximately

$$e_n(t) = f_{no}\delta \frac{\sin(\pi f_{no}\delta t - n\pi)}{\pi(f_{no}\delta t - n)} \exp(j2\pi f_{no}t) \qquad \text{(Eq. D-29)}$$

$$= \frac{\delta f_h}{(1+\delta)^n} \frac{\sin \pi(\frac{f_h \delta t}{(1+\delta)^n} - n)}{\pi(f_h t\delta(1+\delta)^{-n} - n)} \exp\ (j2\pi f_h(1+\delta)^{-n}t)$$

where $f_{no} = f_h/(1+\delta)^n$ is used with f_h as the highest cutoff frequency. The total radiated pulse from a log-periodic antenna with unity spectral density is obtained as

$$e(t) = \sum_{n=1}^{N} a_n \frac{\sin \pi(a_n t - n)}{\pi(a_n t - n)} \exp\ (j2\pi a_n t/\delta) \qquad \text{(Eq. D-30)}$$

$$a_n = \frac{\delta f_h}{(1+\delta)^n}$$

$$N = \frac{\ell n(f_h/f_{No})}{\ell n(1+\delta)}$$

where N is the nearest integer when the center frequency of the lowest radiative region is chosen to be f_{No}.

Instead of assuming a uniform spectral amplitude, the distribution as given in Equation D-13 and shown in Figures D-2 and D-3 is used to produce the total dispersed pulse of the antenna. Figure D-4 is the result of dispersive radiation due to 13 regions. When the 13 regions are treated separately, their radiated pulses are obtained as shown in Figure D-5 through D-17. Their envelope peaks are delayed by the amount of time obtainable from using Equation D-19 as

$$t_n = 1/2\ f_{no}\ \ell n(1 + \delta) \qquad \text{(Eq. D-31)}$$

where f_{no} are listed in Table D-1 and $\delta = 0.1$ is used.

It can be seen that, despite symmetrical weighting as shown in Figure D-2, the first region radiates a higher peak field than any of those radiated by Regions 4 to 13. If the antennas were driven by conjugate-matched current; its compressed peak-field intensity would have about 50 percent contributed by active Elements 2 and 3, and about 36 percent contributed by Elements 1 and 4. The remaining 14 percent of the field would be contributed by Elements 5 to 13. As a result; the first four elements occupying a very small fraction of antenna aperture would be contributing to 86 percent of the compressed field.

These results have indicated a need to redistribute complex spectra of future antenna designs for pulse compression purposes.

5. COMPLEX SPECTRUM OF QUADRATIC-PHASE ANTENNAS

Quadratic-phase antennas may be considered as the radiators that have instantaneous frequencies, changing linearly with time. Their radiation parameters are described in the following paragraphs although actual operational antennas are not known to exist.

Let (f_ℓ, f_h) be the cutoff limits of a bandwidth and f_o be the center frequency. Assume there are N radiation elements, each of which has an elemental bandwidth b, then the following relationships hold as

$$f_{no} = f_h - nb \qquad \text{(Eq. D-32)}$$

$$N + 1 = (f_h - f_\ell)/b \qquad \text{(Eq. D-33)}$$

$$f_o = (f_\ell + f_h)/2 \qquad \text{(Eq. D-34)}$$

Assuming an antenna that radiates a dispersed pulse centered at time t_o, and that its filter function has a unity spectral amplitude at frequency f_o, then the radiated dispersion spectrum can be written similar to Equation D-10 as

$$E_n(r_o, f) = \frac{120k}{r_o}\left[0.54 + 0.46\,\omega_o\,\frac{\pi(t - f_o)}{f_h - f_o}\right]^{1/2} \cdot \qquad \text{(Eq. D-35)}$$

$$\cdot \left[0.54 + 0.46\,\omega_o\,\frac{\pi(t - f_{no})}{f_{nh} - f_{no}}\right]^{1/2}$$

$$\cdot \exp\left[-j2\pi(f - f_o)t_o + j\pi(f - f_o)^2/\mu - j2\pi f_o t_o\right],$$

$$\text{for } f_{n\ell} \leq f \leq f_{nh}$$

The composite complex spectrum is the sum of all radiation regions

$$E(r_o, f) = \sum_{n=1}^{N} E_n(r_o, f) = |E(r_o, f)|\exp(-j\phi) \qquad \text{(Eq. D-36}$$

This quadratic phase characteristic has been widely discussed in many texts and papers concerning pulse compression. Essentially, the phase angle is a constant value centered at f_o and changes in quadratic form on both sides of f_o. The spectral amplitude distributions of individual region $f_\ell \leq f \leq f_h$ are assumed here to be of Hamming weighting. This assumption is realistic for many operational antennas and is particularly useful for pulse compression where inter-region coupling is desired to be as small as possible. Also, when conjugate-matched driving source is applied, the compressed pulse would concentrate its energy in a small duration with temporal sidelobe levels less than 40 dB of the pulse peak.

6. QUADRATIC-PHASE ANGLE AND MODULATION

Assume a quadratic-phase antenna with a general phase angle as

$$\phi(f) = k_o + k_1 (f - f_o) + k_2 (f - f_o)^2 \qquad \text{(Eq. D-37)}$$

where f_o is the center frequency of its operating bandwidth. Let the highest-frequency component f_h have zero group delay as

$$\frac{d\phi(f_h)}{df} = k_1 (f_h - f_o) + 2k_2 (f_h - f_o)^2 = 0 \qquad \text{(Eq. D-38)}$$

Substitution of the solution k_1 into $\phi(f)$ gives rise to

$$\phi(f) = k_o + k_2 \left[(f - f_o)^2 - 2(f_h - f_o)(f - f_o) \right] \qquad \text{(Eq. D-39)}$$

$$= k_o + k_2 \left[(f - f_o)^2 - Nb(f - f_o) \right]$$

where the total bandwidth is designated Nb with N as the number of total elements and b as the elemental bandwith. Let

$$\phi(f_h) = k_o + k_2 \left[N^2b^2/4 - N^2b^2/2 \right] = 0 \qquad \text{(Eq. D-40)}$$

$$\phi(f_\ell) = k_o + k_2 \left[N^2b^2/4 + N^2b^2/2 \right] = -(N + 1)\pi \qquad \text{(Eq. D-41)}$$

where (f_ℓ, f_h) are respectively the lowest and the highest cutoff frequencies. By assuming that $N + 1 \approx N$, the solution for ϕ is

$$\phi(f) = -\left[\frac{(f - f_o)^2}{Nb^2} - \frac{(f - f_o)}{b} + \frac{N}{2} \right] \pi \qquad \text{(Eq. D-42)}$$

The definition of group delay gives

$$t = \frac{1}{2\pi} \frac{d\phi}{df} = -\left(\frac{f - f_o}{Nb^2} - \frac{1}{2b} \right) \qquad \text{(Eq. D-43)}$$

which gives the instantaneous frequency as

$$f = f_o + \frac{Nb}{2} - Nb^2 t = f_h - Nb^2 t \qquad \text{(Eq. D-44)}$$

Since Nb is equal to the total bandwidth B, Equation D-44 may be written as

$$f = f_h - Bbt \qquad \text{(Eq. D-45)}$$

where Bb become the rate of frequency change. The dispersed pulse duration T may be defined by assuming that the highest frequency has zero group delay, i.e.,

$$T = (f_h - f_\ell)/Bb = 1/b \qquad \text{(Eq. D-46)}$$

In other words, the dispersed pulse duration can be uniquely determined by the elemental bandwidth b of the assumed N radiation regions.

By letting $2t_o = T$ in the phase angle of Equation D-35 and then comparing it with Equation D-42, the following useful identities are obtained:

$$Tb = 1 \qquad \text{(Eq. D-47)}$$

$$\mu = Nb^2 = Bb \qquad \text{(Eq. D-48)}$$

$$N = 2f_oD = (f_h + f_\ell)/b \approx (f_h - f_\ell)/b \approx f_h/b \qquad \text{(Eq. D-49)}$$

where the last expression implies that $f_h + f_\ell \approx f_h - f_\ell$ or $f_h \approx 2f_o$.

7. FOURIER TRANSFORM OF QUADRATIC-PHASE ANTENNAS

For f_ℓ/f_h approaching zero, or for an extremely large-bandwidth system, the time-domain amplitude of a quadratic-phase antenna remains essentially constant if a unity spectral amplitude existed in the entire bandwidth, i.e.,

$$\int_{-B/2}^{B/2} \exp\left(j\frac{\pi}{Bb}f^2 + j2\pi ft\right)df \approx \sqrt{jBb}\exp(-j\pi Bbt^2), \quad -\frac{T}{2} \le t \le \frac{T}{2} \qquad \text{(Eq. D-50)}$$

This transform pair holds for spectral distribution centered about $f = 0$ and dispersed pulse centered about $t = 0$. Making use of Equation D-47 for the transform pair, it can also be written

$$\int_{-T/2}^{T/2} \exp\left(-j2\pi ft - j\frac{\pi Bt^2}{T}\right)dt \approx \sqrt{\frac{T}{jB}}\exp\left(+j\frac{\pi Tf^2}{B}\right), \quad |f| \le B/2$$

$$\approx \sqrt{\frac{b}{j}} \qquad \text{(Eq. D-51)}$$

where, as has been defined earlier, B is the effective bandwidth and T is the effective duration of the dispersed pulse. Figure D-18 indicates the responses of a quadratic-phase filter driven by an impulse and conjugate-matched source. If the dispersion pulse is centered at T/2, and the frequencies are centered at f_o, the Fourier transform pair can be obtained by shiftings as

$$\int_{f_o - B/2}^{f_o + B/2} \exp(j2\pi ft - j\pi f_o T - j\pi D(f - f_o) + j\frac{\pi}{Bb}(f - f_o)^2) \qquad \text{(Eq. D-52)}$$

$$= \frac{jB}{D} \exp\left[j2\pi f_o(t - T/2) - j\pi Bb(t - T/2)^2\right]$$

8. REMARK ON BANDWIDTH-TIME PRODUCT

The duration of a dispersed pulse by a quadratic-phase filter can be obtained from Equation D-47 as

$$T = 1/b \qquad \text{(Eq. D-53)}$$

Application of a conjugate-matched driving source gives rise to a compressed pulse with a duration d which is related to the total effective bandwidth B as

$$B = 1/d \qquad \text{(Eq. D-54)}$$

Designating BT product as the power gain, the relationship below would result

$$\text{(Power Gain)(Compressed Duration)} = BTd = 1/b. \qquad \text{(Eq. D-55)}$$

This equation indicates that there exists a practical limit in making the elemental bandwidth extremely small. Usually the highest-frequency region centered at f_h would impose the smallest $b = f_h \delta_h$ where δ_h is the

fractional bandwidth of the region. Equation D-55 can now be written

$$(\text{Compressed Gain-Duration Product})_{\text{Quadratic}} = B_T df_h = \frac{1}{\delta_h} \qquad \text{(Eq. D-56)}$$

This is for a quadratic-phase dispersive antenna. Similar equation for a log-periodic antenna can be obtained from Equation D-26 as

$$(\text{Compressed Gain-Duration Product})_{\text{Log-Periodic}} = \frac{1}{2\delta_\ell}$$

where δ_ℓ is the fractional bandwidth of the lowest radiation region.

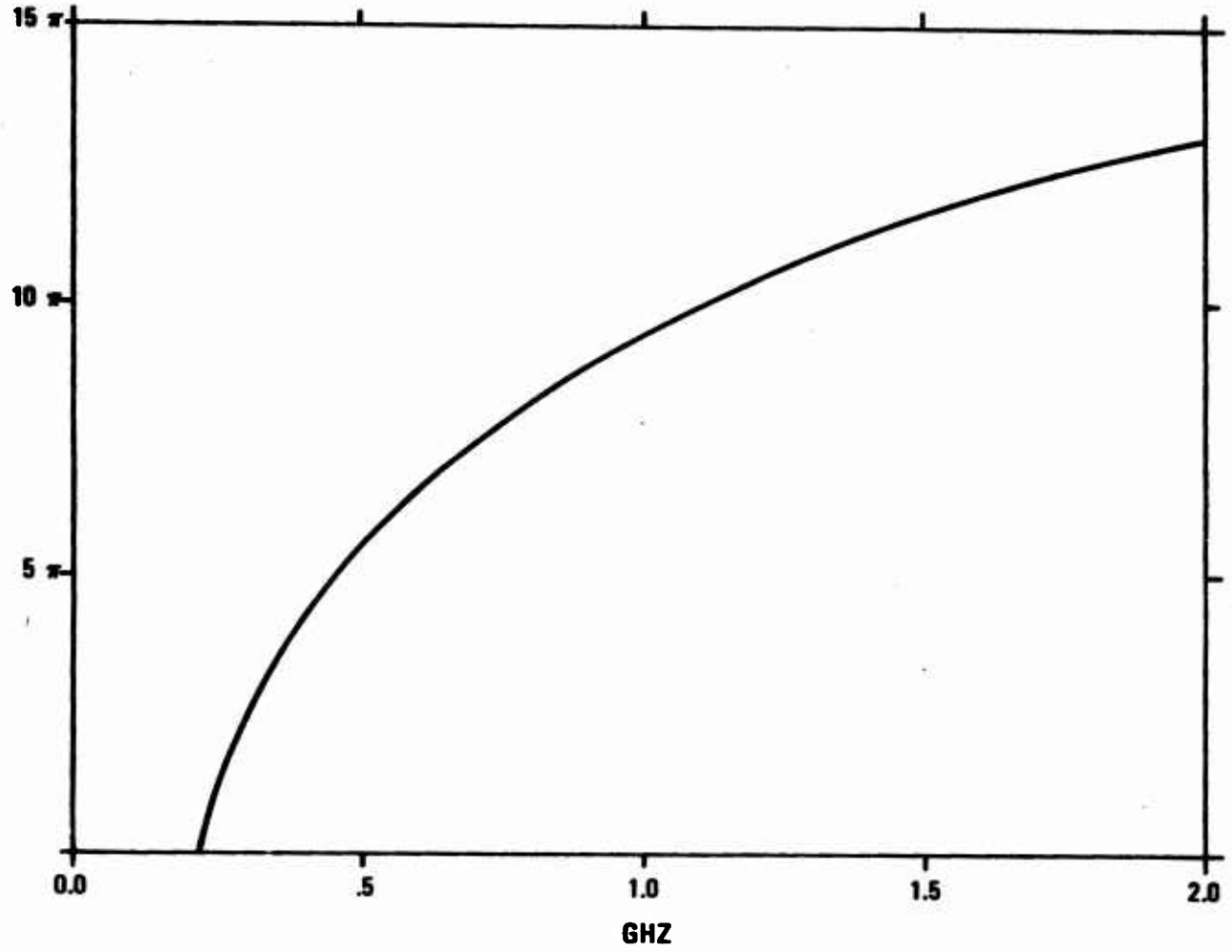


Figure D-1. Log-Periodic Phase Angle Plotted Against Linear Frequency

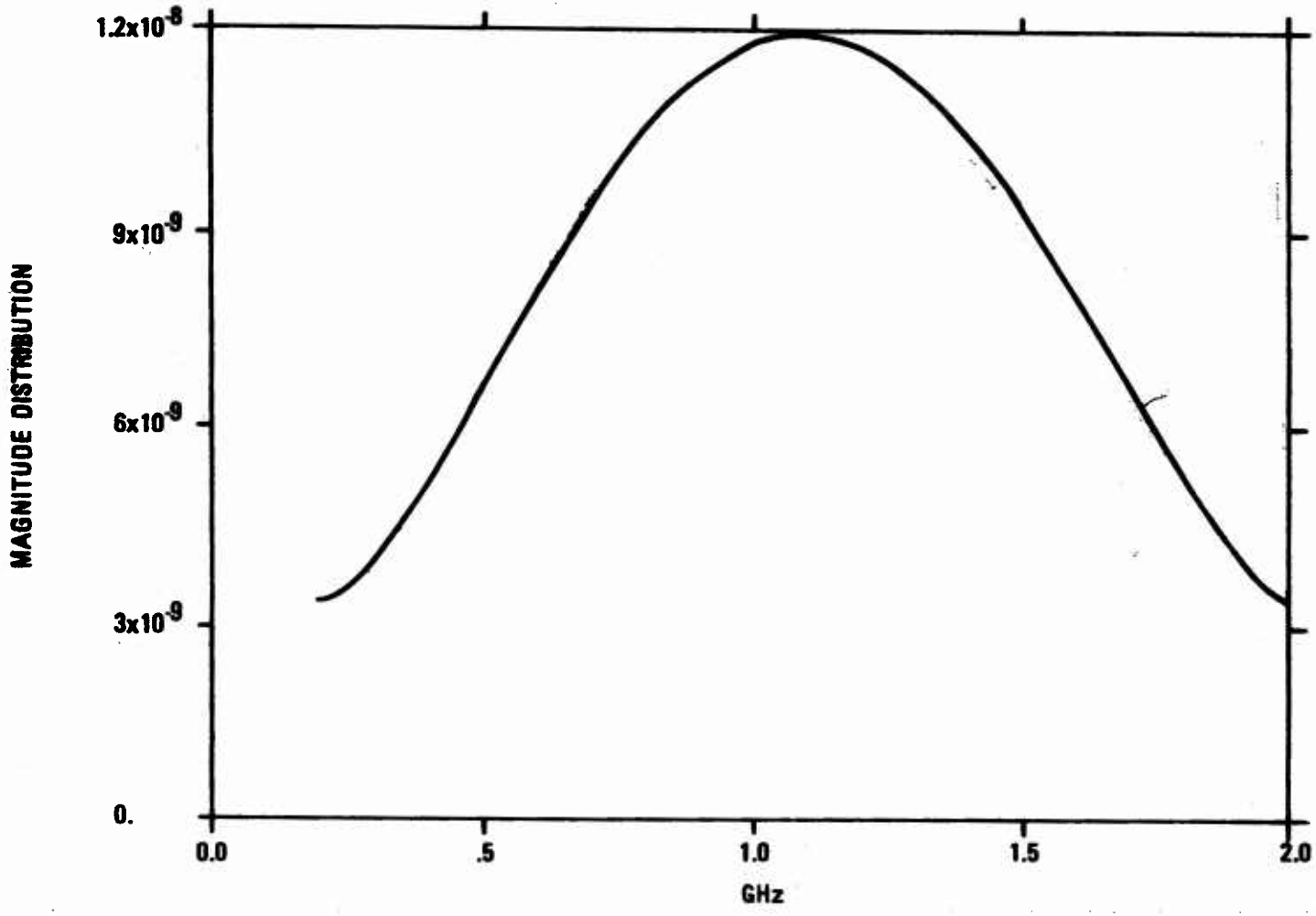


Figure D-2. Spectral Amplitude Assigned to a Log-Periodic Antenna

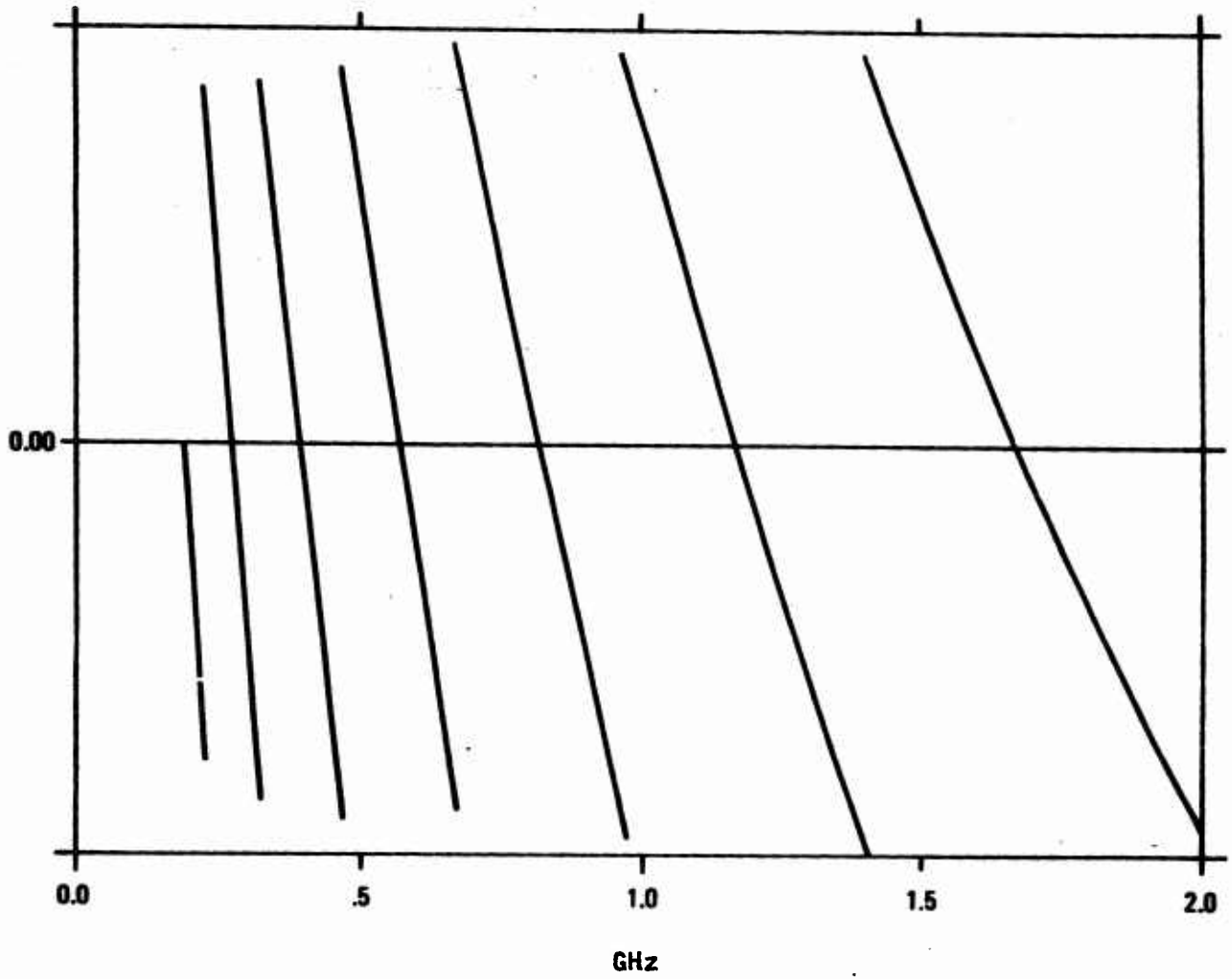


Figure D-3. Phase Angle Assigned Corresponding to the Spectrum in Figure D-3

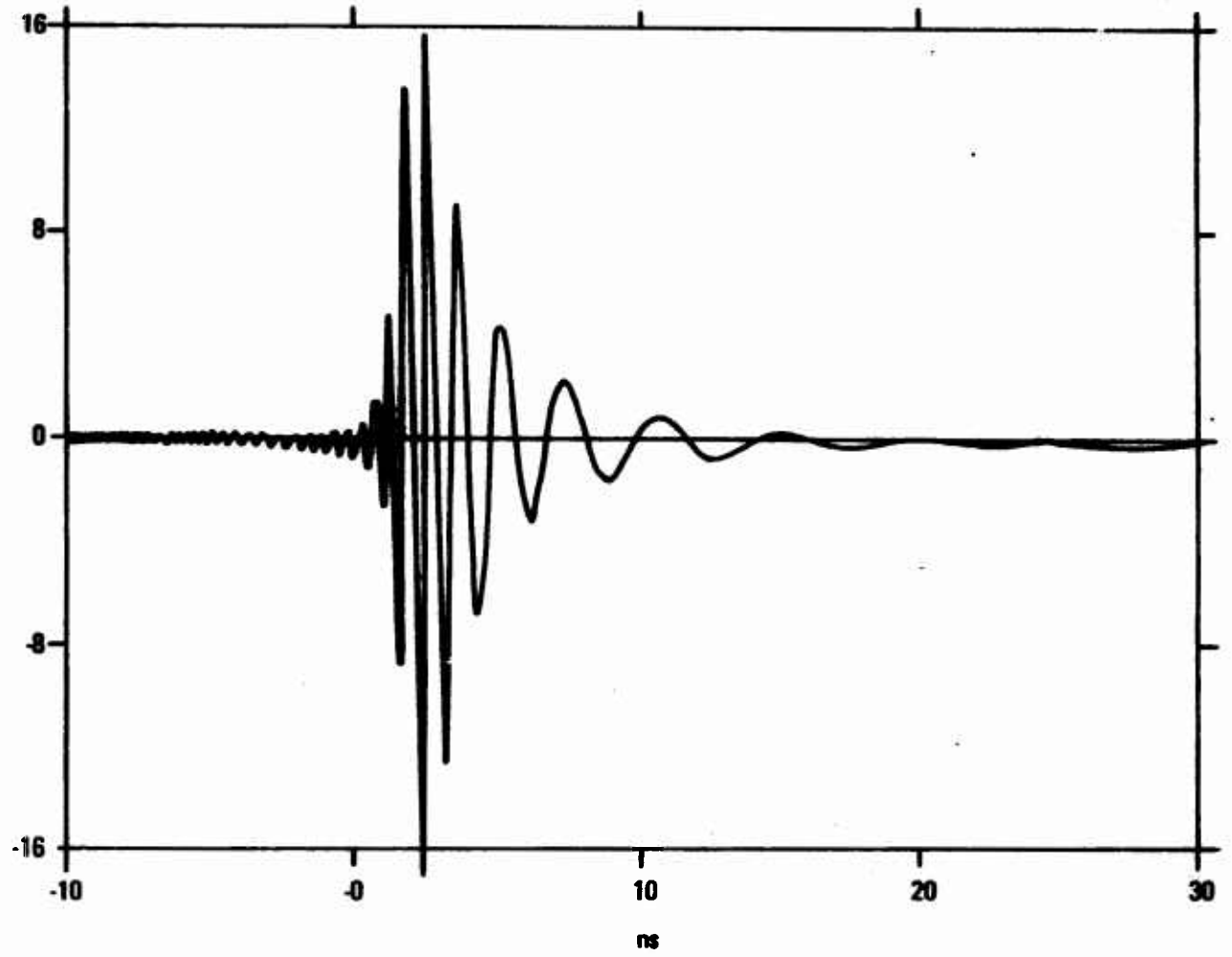


Figure D-4. Dispersed Pulse Resulting From Complex Distribution of Figures D-3 and D-4

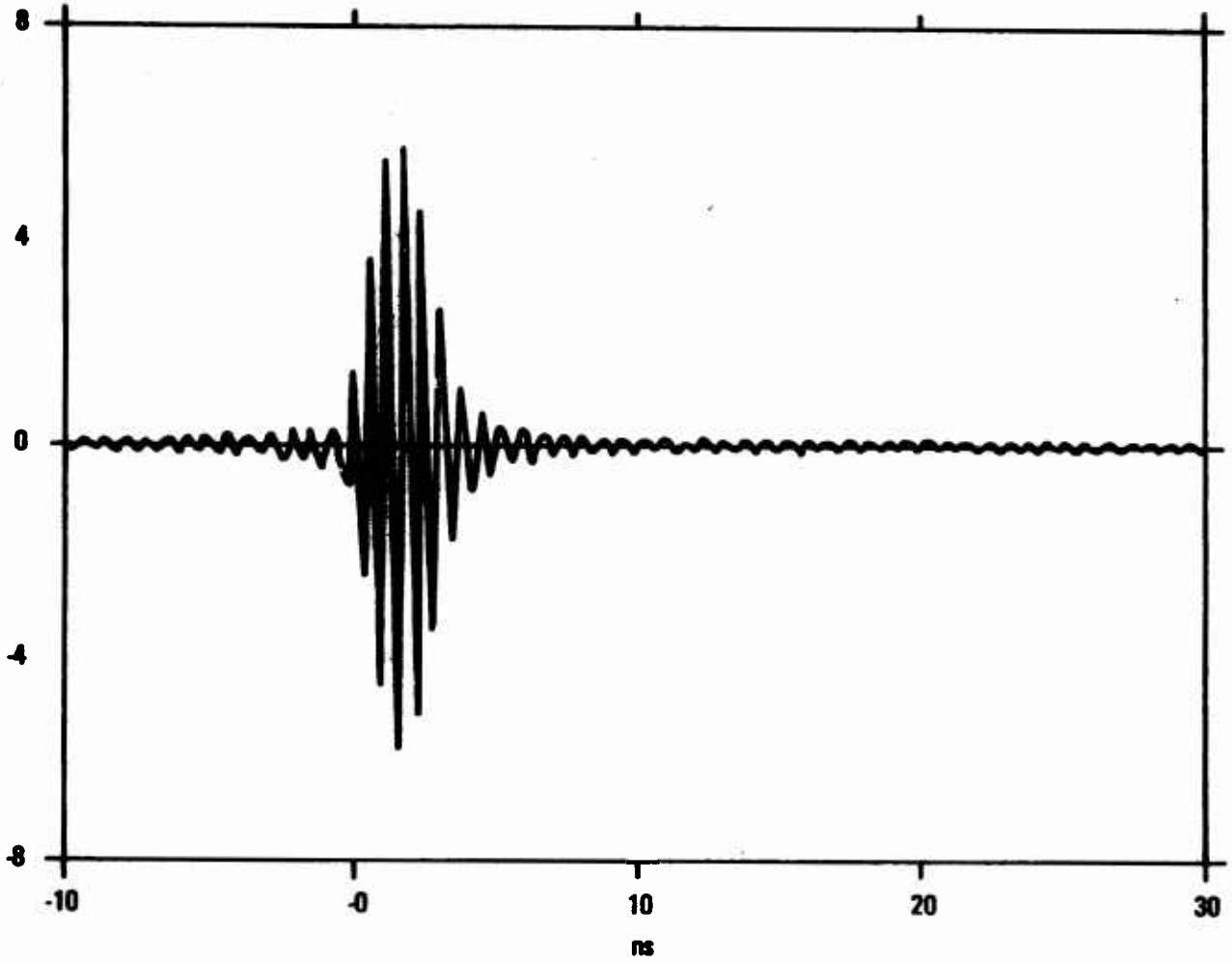


Figure D-5. Radiated Pulse of the First Region Assigned to Figures D-2 and D-3

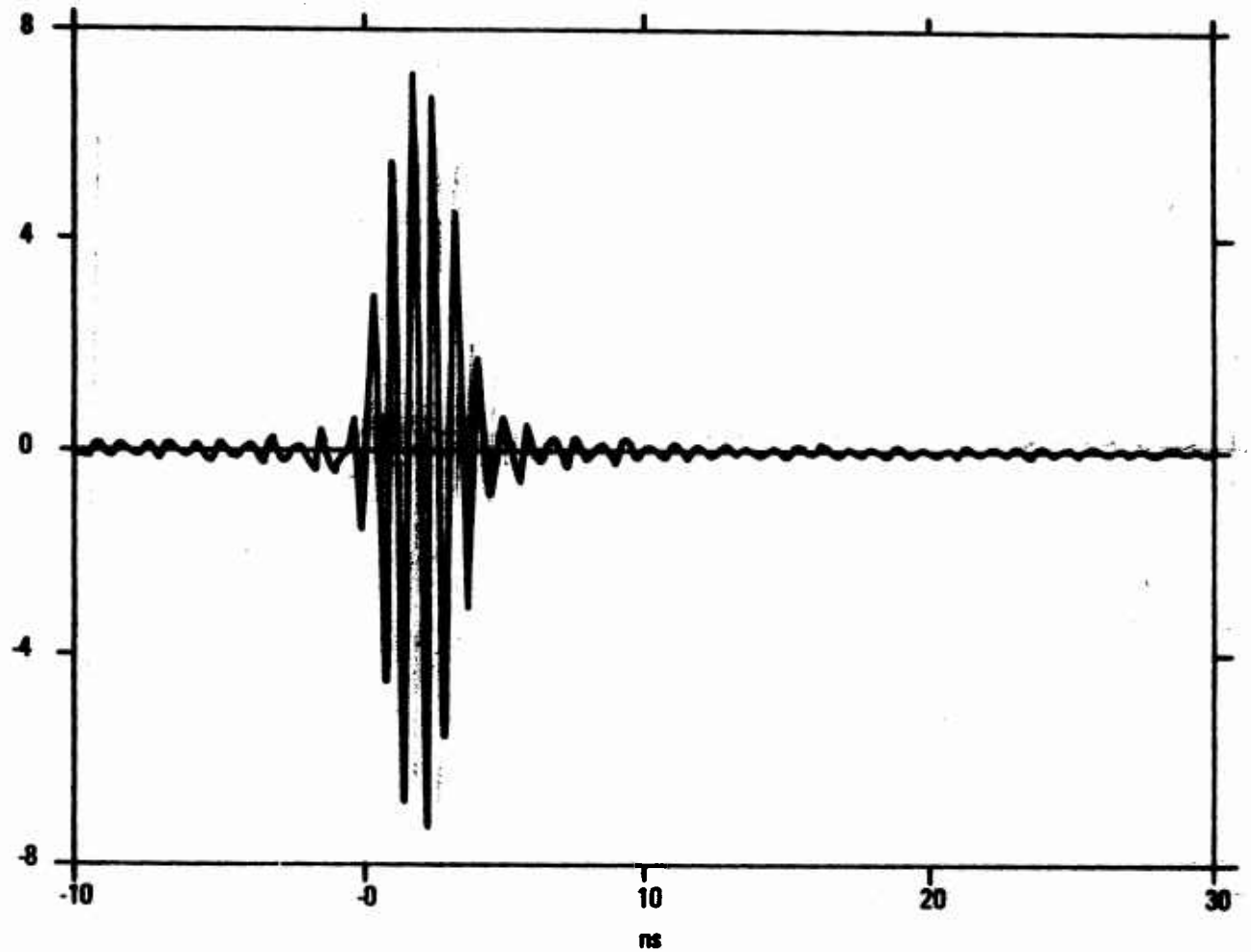


Figure D-6. Radiated Pulse of the Second Region Assigned to Figures D-2 and D-3

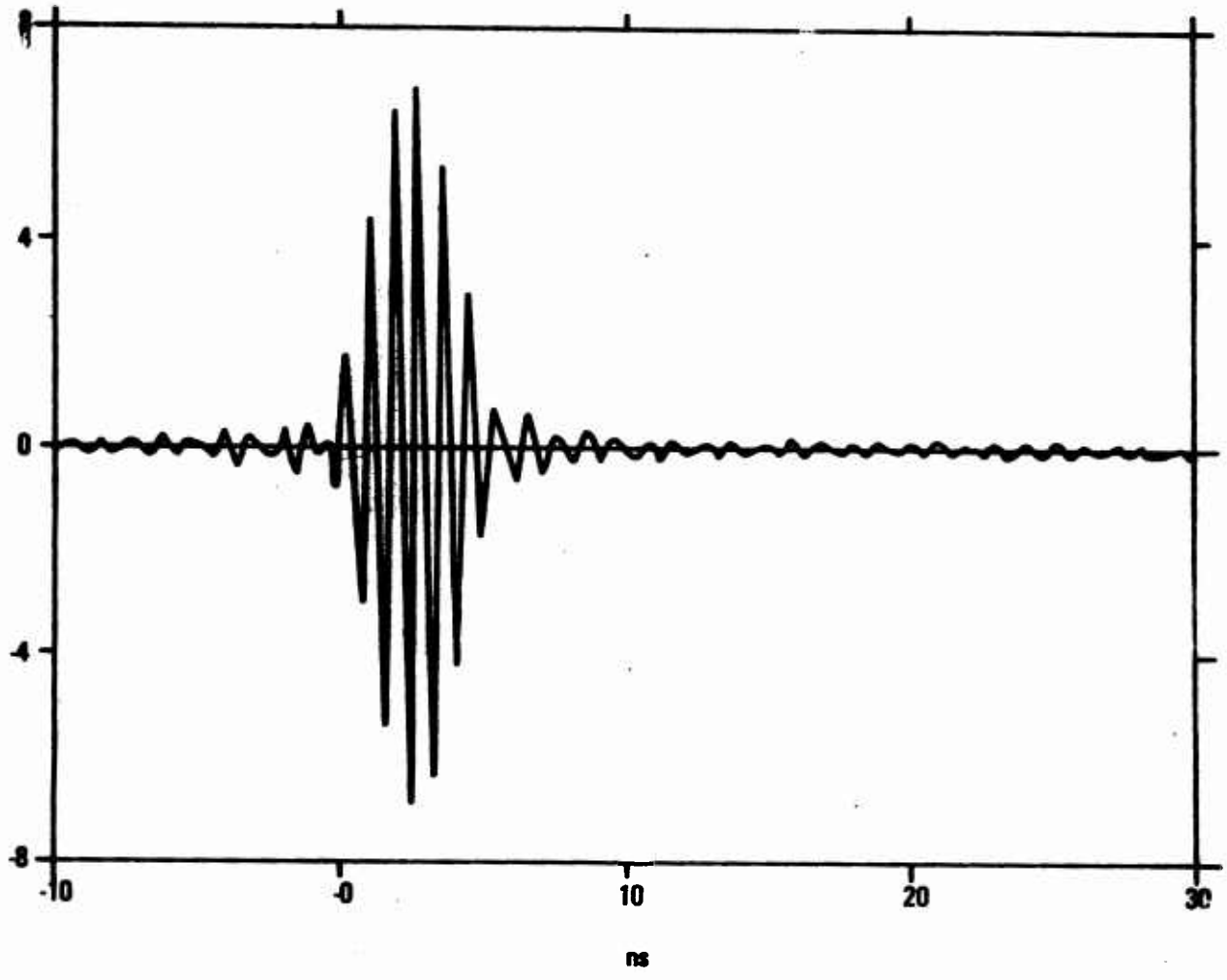


Figure D-7. Radiated Pulse of the Third Region Assigned to Figures D-2 and D-3

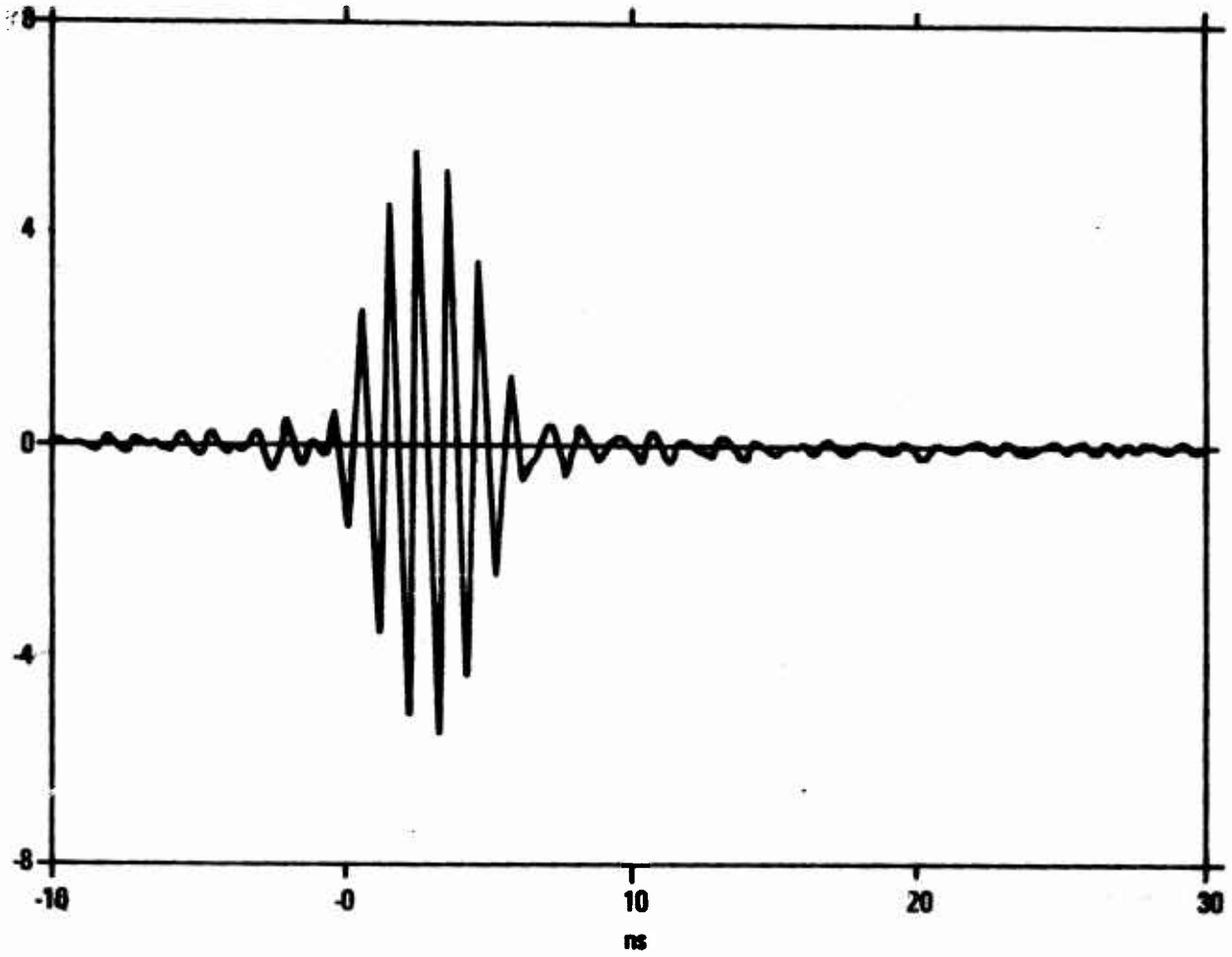


Figure D-8. Radiated Pulse of the Fourth Region Assigned to Figures D-2 and D-3

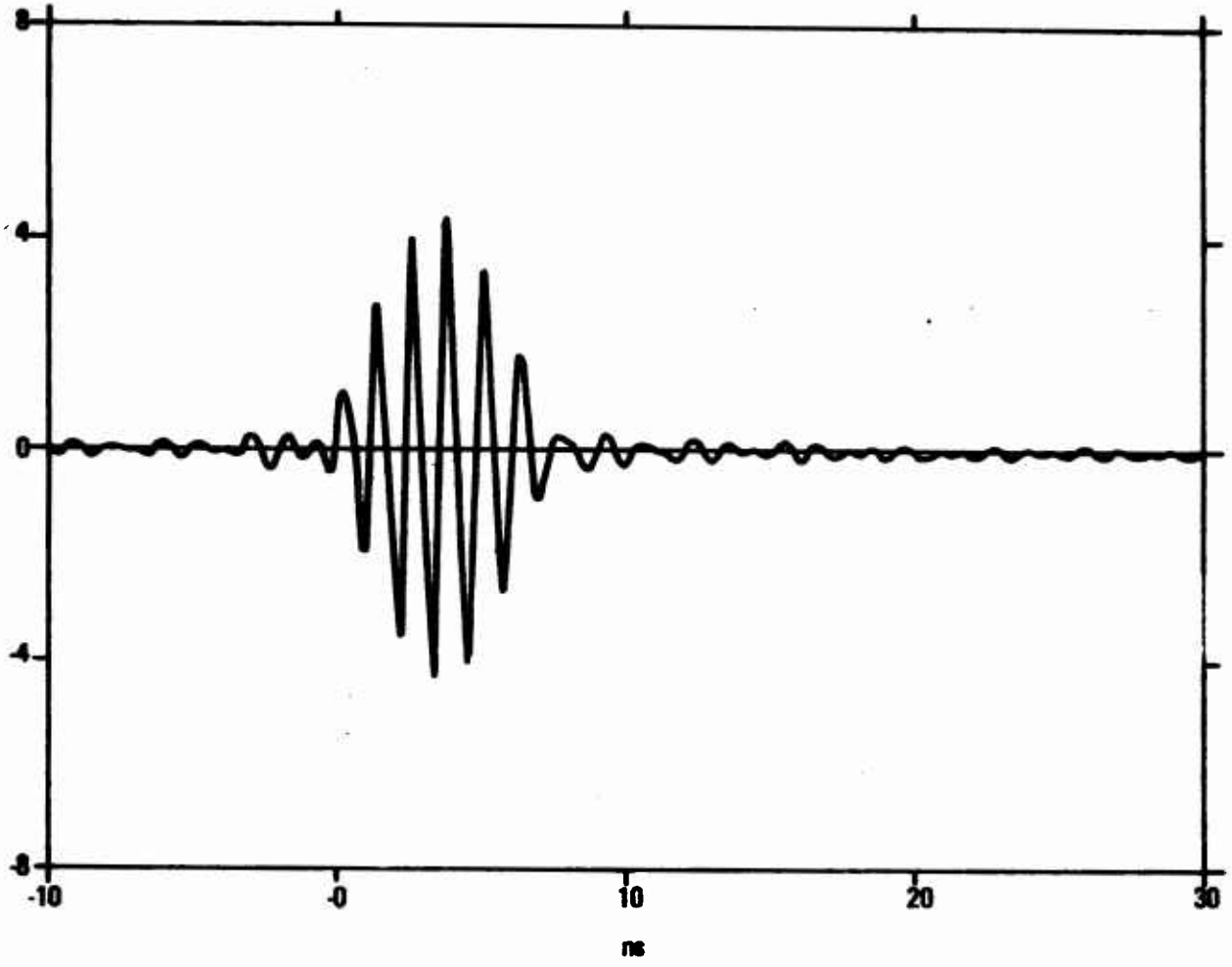


Figure D-9. Radiated Pulse of the Fifth Region Assigned to Figures D-2 and D-3

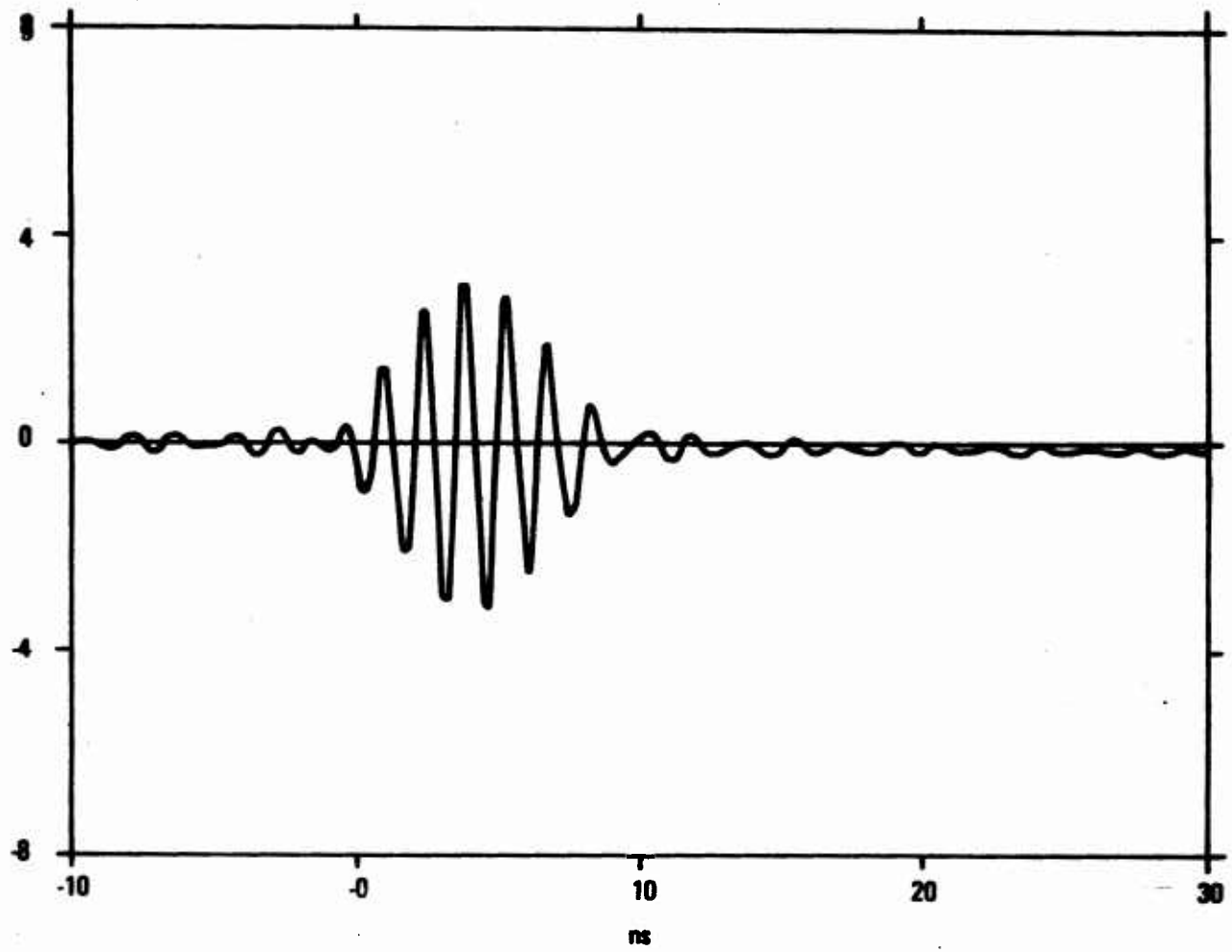


Figure D-10. Radiated Pulse of the Sixth Region Assigned to Figures D-2 and D-3

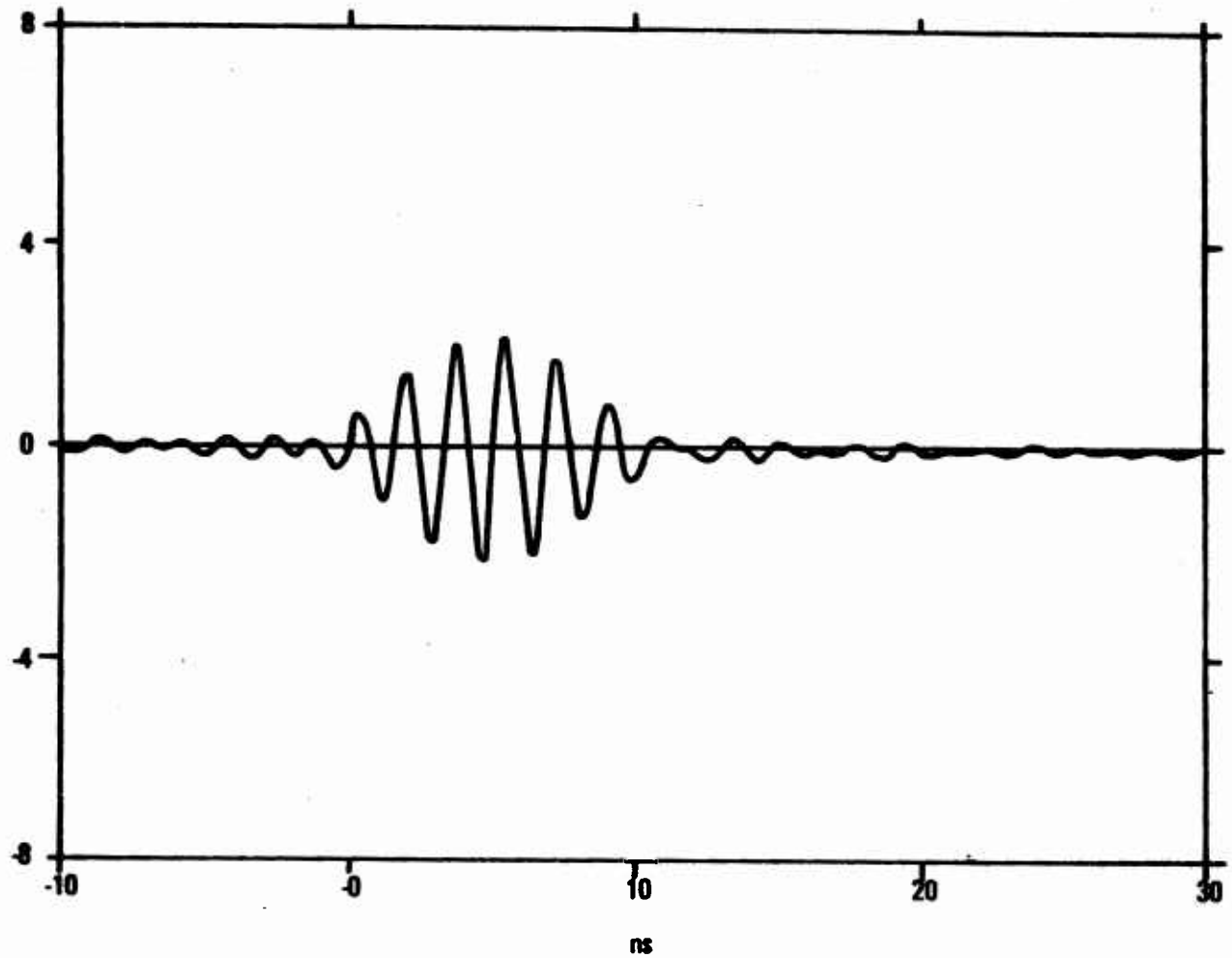


Figure D-11. Radiated Pulse of the Seventh Region Assigned to Figures D-2 and D-3

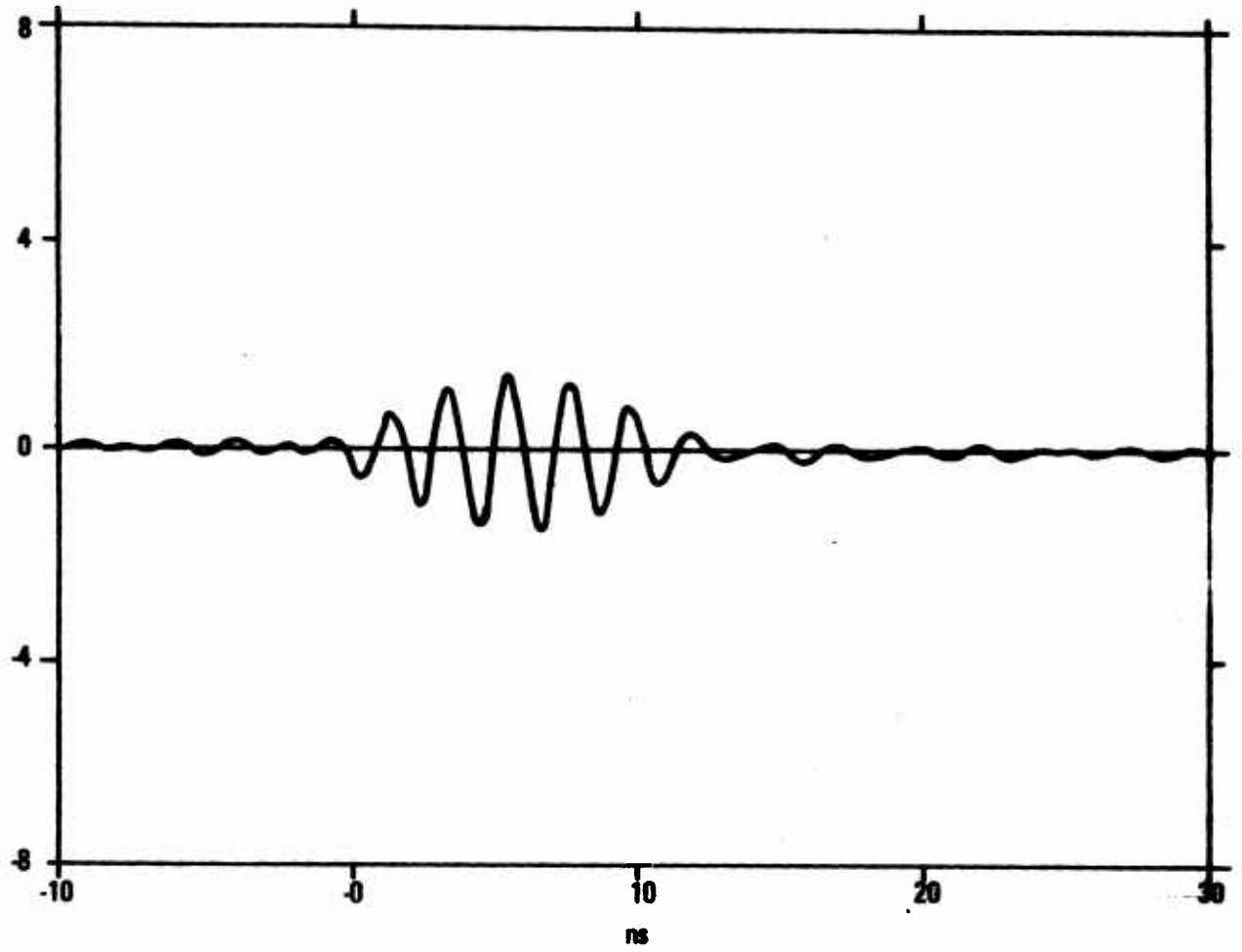


Figure D-12. Radiated Pulse of the Eighth Region Assigned to Figures D-2 and D-3

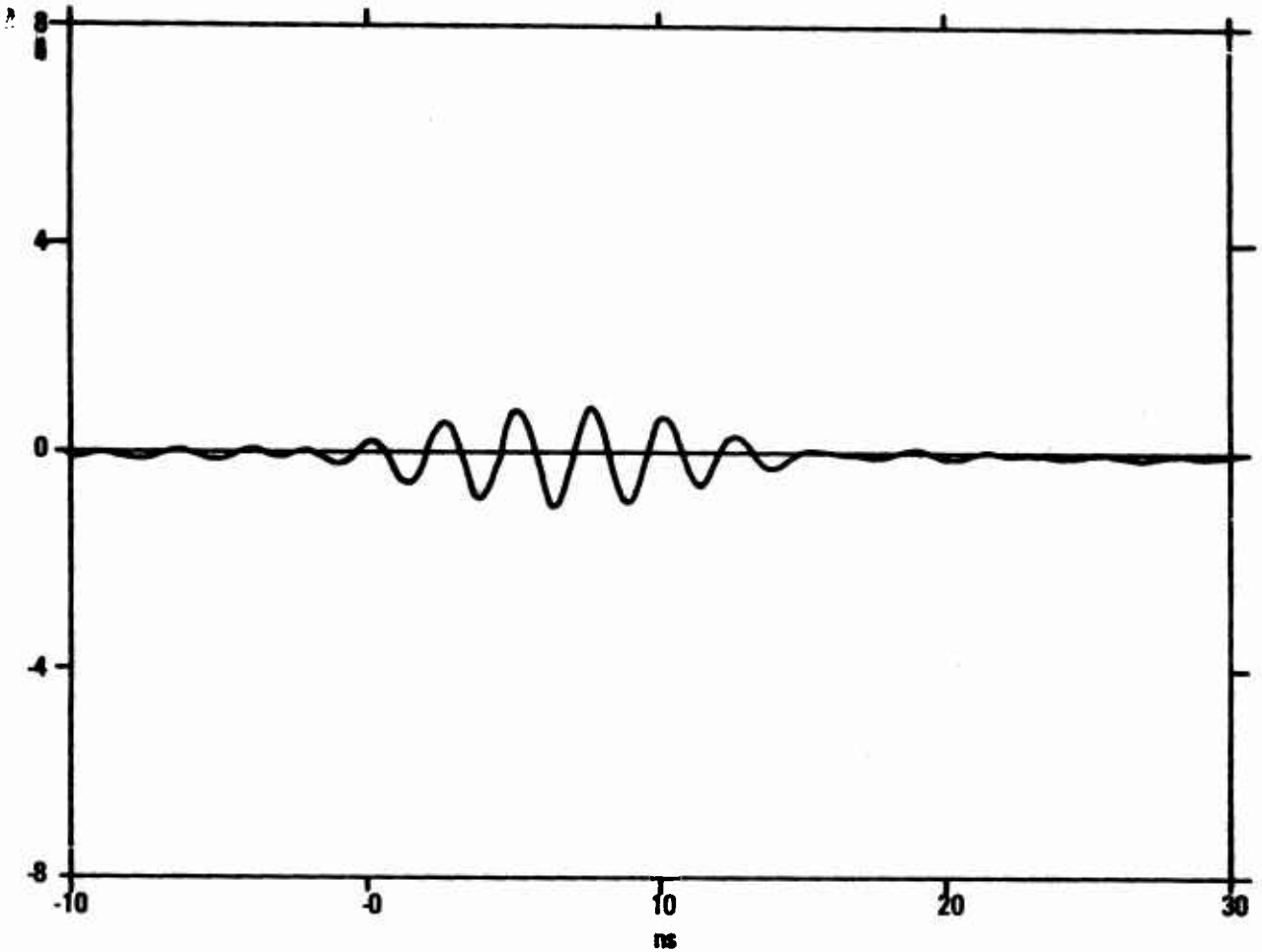


Figure D-13. Radiated Pulse of the Ninth Region Assigned to Figures D-2 and D-3

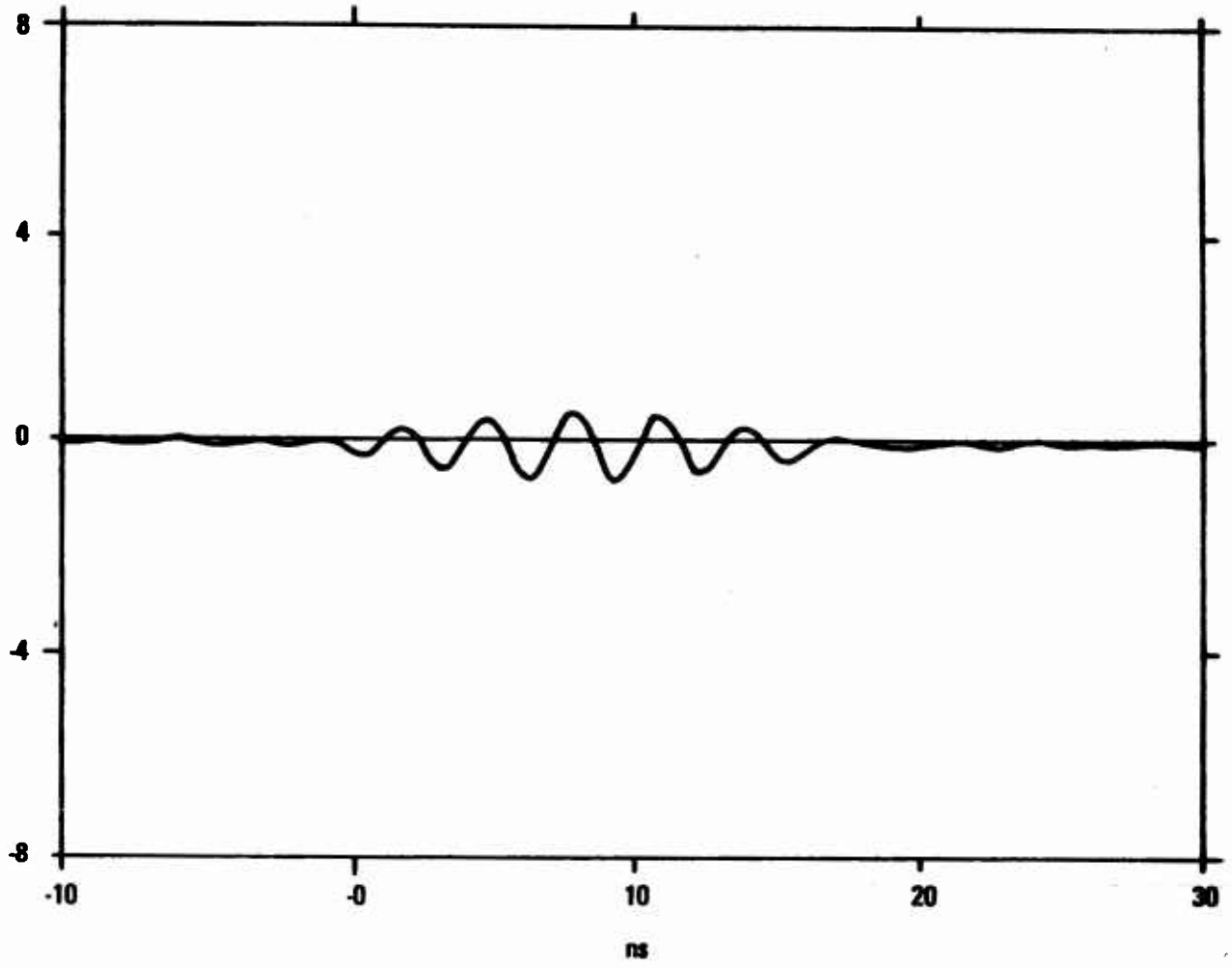


Figure D-14. Radiated Pulse of the Tenth Region Assigned to Figures D-2 and D-3

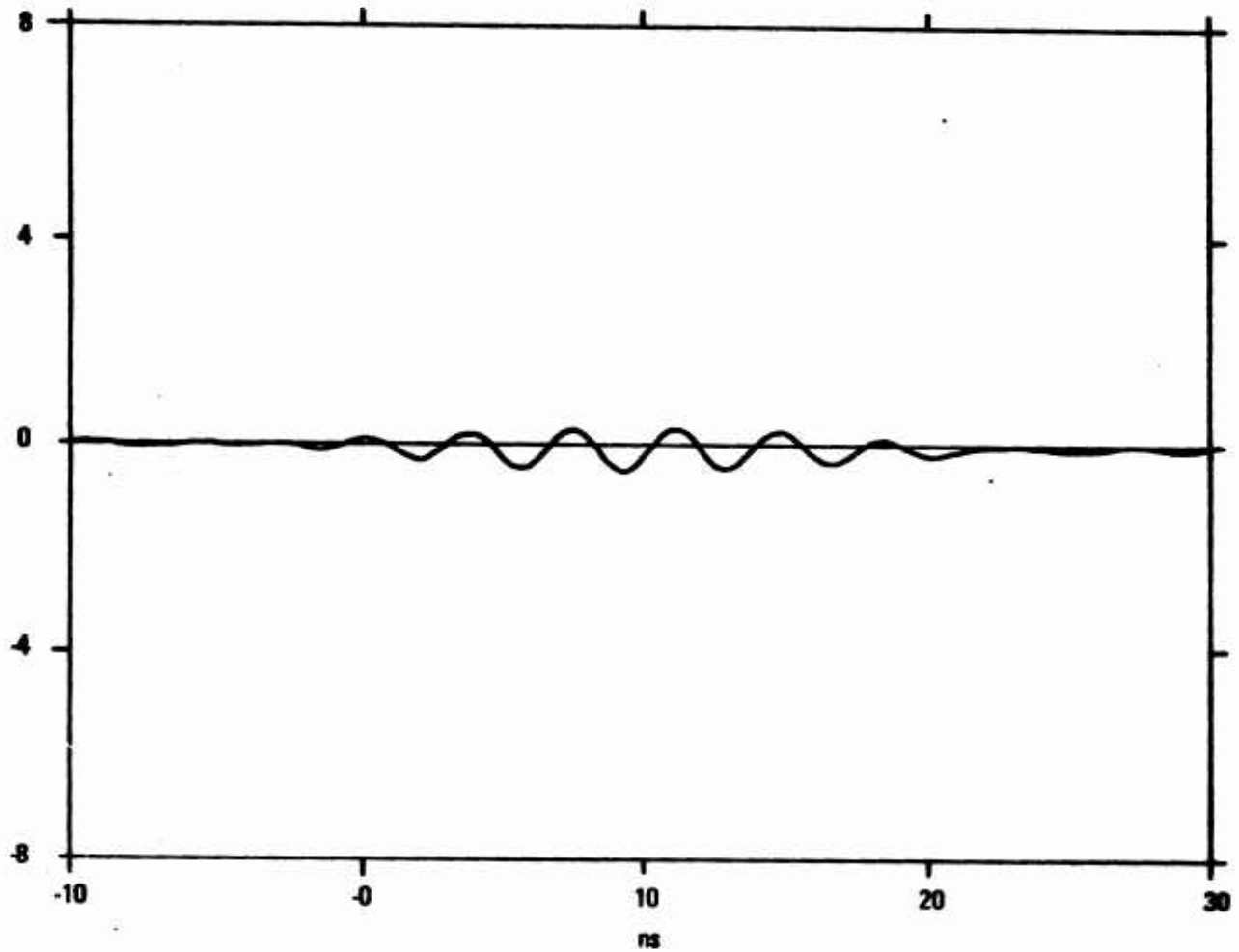


Figure D-15. Radiated Pulse of the Eleventh Region Assigned to Figures D-2 and D-3

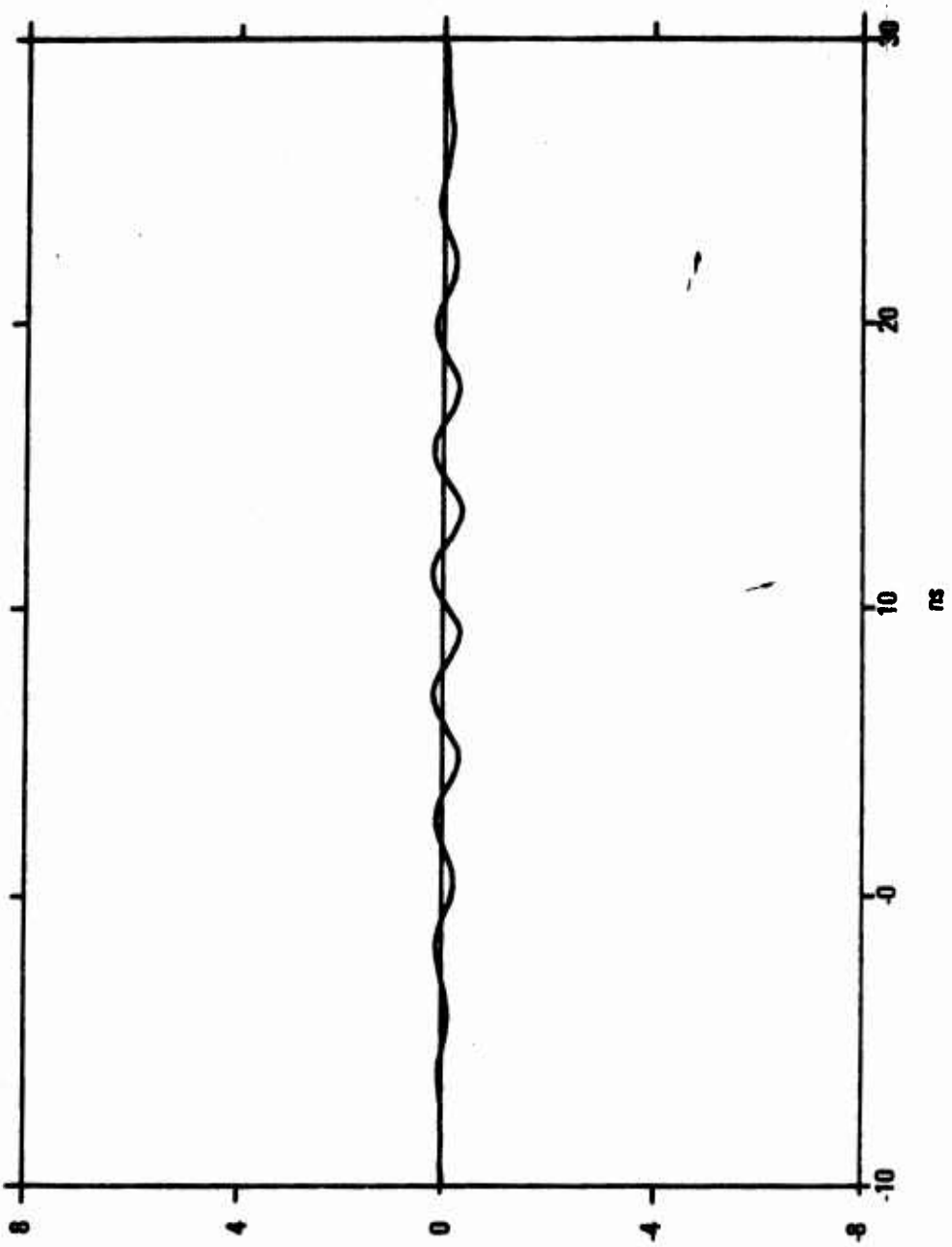


Figure D-16. Radiated Pulse of the Twelfth Region Assigned to Figures D-2 and D-3

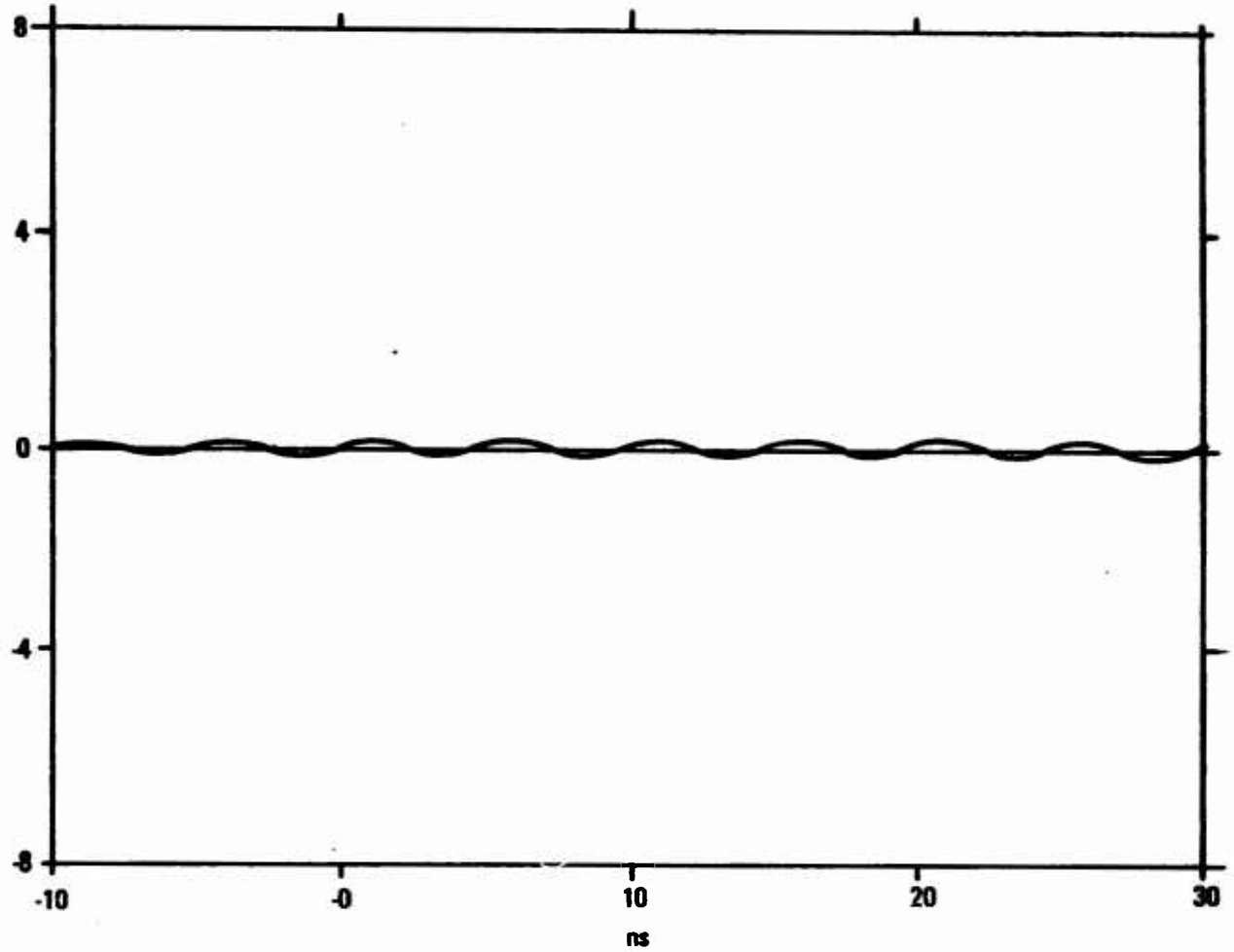
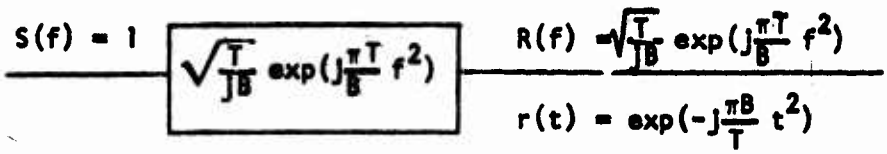
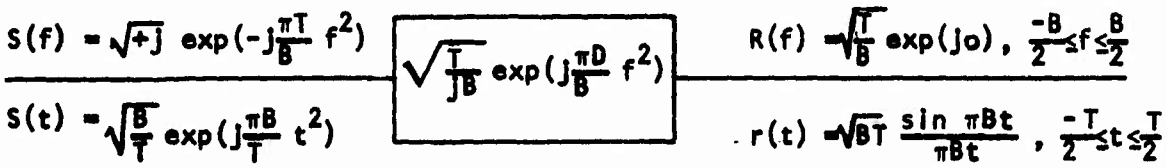


Figure D-17. Radiated Pulse of the Thirteenth Region Assigned to Figures D-2 and D-3



(a) Dispersive Quadratic-Phase Filter Driven By an Impulse



(b) Conjugate-Matched Driving Source and the Filter Responses

Figure D-18. Quadractic-Phase Filter Characteristics and Responses

APPENDIX E

WAVE PROPAGATION ALONG PERIODICALLY LOADED STRUCTURES

1. INTRODUCTION

All known types of frequency-independent antennas possess a structure geometry which scales log-periodically. When the logarithmic expansion rate is slow enough, departure from uniform periodicity is very slight over several spatial periods. Under this condition, the structure is said to be locally periodic. A locally periodic portion of the antenna is equivalent to an active region, that is, a region which determines the radiation characteristics over a particular frequency interval comprising only a small portion of the overall antenna bandwidth. It follows, therefore, that the physical behavior of waves traveling through an active region of the antenna may be adequately described by the theory for wave propagation along uniformly periodic structures. This theory, as it is presented here, generally follows the description given by Hessel.[1]

Frequency-independent antenna operation is best understood in terms of traveling-wave propagation along periodically loaded structures. In general, such a structure can be open or closed, depending on whether it will radiate or not. In the former case, the structure is an antenna, while in the latter, it is essentially a waveguide. Besides this distinction, periodically loaded structures may be further broken down into three types, depending on the propagation velocities of the waves which they support: basically slow waves, basically TEM waves traveling at approximately the speed of light,

---

[1] A. Hessel, "General Characteristics of Traveling-Wave Antennas," Chapter 19, Antenna Theory, Pt. 2, Edited by R.E. Collin and F. J. Zucker, McGraw-Hill, 1969.

and basically fast waves. However, it should be cautioned that this distinction is only approximate: it is possible for a given structure to support waves of more than one type.

The analysis of periodic loaded structures is carried out in terms of the modal characteristics of the structure. In the most general case for open structures, the fields are represented by a discrete spectrum of modes which are due to the finiteness of the structure and by a continuous spectrum of modes which the structure exhibits because of its ability to radiate energy. Because of certain instabilities which violate the radiation condition that fields must vanish at infinity, some modes are considered to be improper with respect to the surface waves supported by the structure. When these modes are deleted, the remaining ones, termed proper, form a complete set in terms of which the fields on an open structure may be expanded, at least in principle. In practice, all modes are obtained from the characteristic dispersion relation of the structure which cannot be evaluated in closed form. Despite these shortcomings, the modal analysis still provides the greatest insight as to the operation of antennas characterized by periodically loaded traveling-wave structures.

A characteristic of traveling waves on open, periodic structures, that is very important for frequency-independent antenna operation, is the following. When the spatial period of the structure approaches one-half of the free-space wavelength at a given frequency of operation, a slow wave can no longer be supported by a periodically loaded, basically TEM traveling wave structure; consequently a complex guided wave appears, accompanied by radiation at some angle between backfire and endfire.

2. PROPERTIES OF FIELDS ON OPEN, PERIODICALLY-LOADED, TRAVELING-WAVE STRUCTURES

To understand the radiation mechanism of traveling wave antennas requires a thorough knowledge of the manner in which the phase of the

feed wave changes as it travels down the structure. This can be described in terms of the dispersive properties of the structure. Some of these properties, leading to the creation of spatial harmonics, arise solely because of structure periodicity. Certain other dispersion properties involve resonant growth of spatial harmonics, or the coupling of modes, and are associated with energy transfer between modes. These processes will be described in the following sections.

a. Floquet's Theorem

The form of waves traveling on a periodic structure can be conveniently described by a theorem due to Floquet. Consider a structure which is axially periodic in the Z-direction with period d. The theorem states that: a time-harmonic electromagnetic field $\psi(x,y,z)$ of a normal mode traveling along an axially periodic structure possesses the property

$$\Psi(x,y,z+d) = e^{ik_{zo}d}\,\Psi(x,y,z) \qquad \text{(Eq. E-1)}$$

where

$$k_{zo} \equiv \beta_o + i\alpha \qquad \text{(Eq. E-2)}$$

is known as the fundamental (complex) propagation constant. β_o and α represent the corresponding phase and attenuation constants, respectively. If one defines a periodic vector field $\vec{P}(x,y,z)$ by

$$\vec{P}(x,y,t) = e^{-ik_{zo}z}\,\vec{\Psi}(x,y,z) \qquad \text{(Eq. E-3)}$$

then it follows from Equation E-1 that

$$\vec{P}(x,y,z+d) = \vec{P}(x,y,z) \qquad \text{(Eq. E-4)}$$

Fields satisfying Equations E-3 and E-4 are often referred to as Bloch waves. They imply that, upon sampling a traveling wave along an axially periodic structure at points with constant transverse value (x, y) spaced a period d apart, one may observe only the macroscopic field of the form $e^{ik_{zo}z}$. The periodic function $\vec{P}(x,y,z)$ describes the microscopic field structure within a period. Thus, if the field distribution is known within a single period, then it is uniquely determined at any point on an infinite structure.

b. Spatial Harmonics

The periodic vector function $\vec{P}(x,y,z)$ may be expanded in a Fourier series

$$\vec{P}(x,y,z) = \sum_{n=-\infty}^{\infty} \vec{a}_n(\vec{q})e^{i(2\pi/d)nz}, \quad \vec{q} = (x,y) \qquad \text{(Eq. E-5)}$$

which when substituted into Equation E-3 yields

$$\vec{\psi}(x,y,z) = \sum_{n=-\infty}^{\infty} \vec{a}_n(\vec{q})e^{ik_{zn}z} \qquad \text{(Eq. E-6)}$$

where

$$k_{zn} = k_{zo} + \frac{2\pi n}{d}, \quad n = 0, \pm 1, \pm 2, \cdots \qquad \text{(Eq. E-7)}$$

$$k_{zn} = \beta_n + i\alpha = \beta_o + \frac{2\pi n}{d} + i\alpha \qquad \text{(Eq. E-8)}$$

Thus, the field of a normal mode of an axially periodic structure can be expressed in terms of an infinite number of traveling waves of the form $a_n(\vec{q})e^{-jk_{zn}z}$, called spatial harmonics. The wave numbers k_{zn} represent the various spatial harmonic axial propagation constants, and the $a_n(\vec{q})$ are the corresponding spatial harmonic amplitudes.

c. The $k_o d - \beta d$ Diagram

The graphical representation of dispersion is based on the $k_o d - \beta d$ diagram where k_o and β are the wave numbers in free space and in the medium, respectively, and d is the period of the structure. The use of these diagrams to describe log-periodic antenna behavior ultimately requires three distinct levels of interpretation: (1) the $k_o - \beta$ diagram for uniform structures (i.e., structures which are non-periodic); (2) the $k_o d - \beta d$ diagram for strictly periodic structures; (3) the $k_o d - \beta d$ diagrams for slightly aperiodic structures, in particular those which taper log-periodically. First, consider a uniform (non-periodic) space filled with a non-magnetic ($\mu = \mu_o$), lossless dielectric of permittivity $\varepsilon > \varepsilon_o$. The dispersion relation of a wave propagation in such a medium is given by

$$v_p^2 \beta^2 = \omega^2 \qquad \text{(Eq. E-9)}$$

where

$$v_p \equiv \frac{1}{\pm\sqrt{\varepsilon\mu_o}} \qquad \text{(Eq. E-10)}$$

In free space the dispersion would be given by

$$c^2 k_o^2 = \omega^2 \qquad \text{(Eq. E-11)}$$

where

$$c \equiv \frac{1}{\pm\sqrt{\varepsilon_o \mu_o}} \qquad \text{(Eq. E-12)}$$

It is convenient to consider the relative dispersion denoted by the velocity ratio

$$\frac{v_p}{c} = \frac{k_o}{\beta} = \frac{1}{\sqrt{\varepsilon_r}} \qquad \text{(Eq. E-13)}$$

where $\varepsilon_r = \varepsilon/\varepsilon_o > 1$, the relative permittivity. Equation E-13 now denotes the dispersion of the system and it is equivalent to a dielectric-loaded uniform TEM line. A plot of Equation E-13 for some ε_r sets the slowness, or load line, of the uniform structure and is shown in Figure E-1. The straight lines with slopes $\pm \pi/4$ separate the slow and fast wave regions. Forward traveling waves or backward traveling waves are associated with positive or negative slopes, respectively.

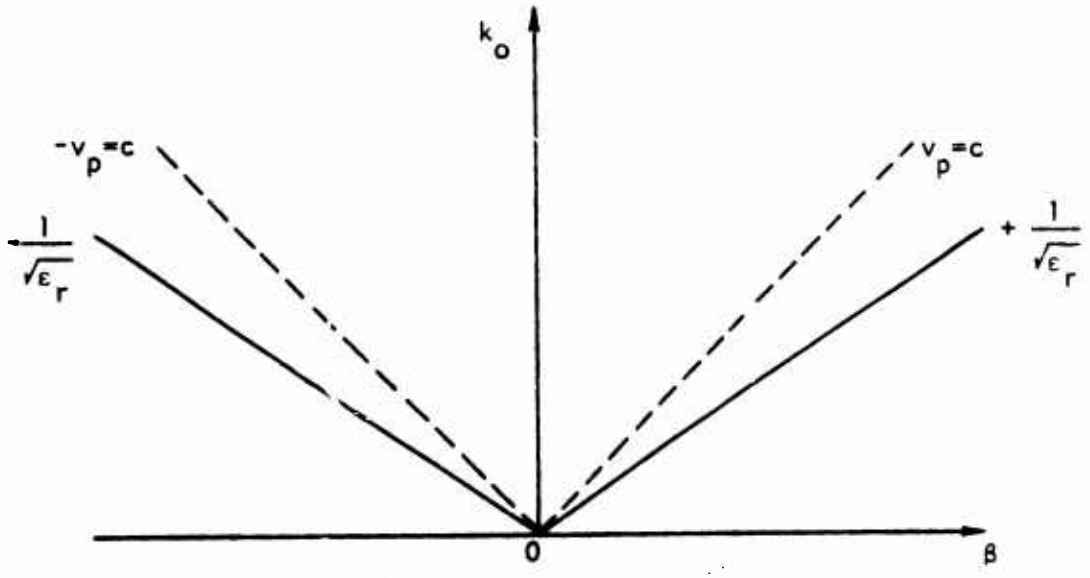


Figure E-1. The k_o-β Diagram Corresponding to a Uniform Lossless Dielectric of Relative Permittivity $\varepsilon_r > 1$ (i.e., Basically a Slow-Wave Structure).

This type of structure does not lead to spatial harmonic waves involving resonant growth since the structure is not periodic. It will admit the usual set of waveguide solutions.

When the dielectric medium is periodically loaded, the dispersion is modified and, hence, the curve in Figure E-1 is changed. In the most general case, periodic loading may be expressed in terms of a spatially periodic permittivity and can be represented by

$$\epsilon(z) = \epsilon_0 \left[1 + M F\left(\frac{2\pi}{d} z\right)\right] \qquad \text{(Eq. E-14)}$$

where M is a modulation index, usually less than or equal to unity, F is a periodic function of z, and d is the spatial period of the structure. A consequence of periodic structures is that a single wave will not propagate because the medium is no longer homogeneous. Instead, wave solutions will consist of an infinite set of spatial harmonic solutions when boundary conditions are considered:

$$\Psi(x,y,z) = \sum_{n=-\infty}^{\infty} a_n(\vec{q}) e^{ik_{zn}z} \qquad \text{(Eq. E-15)}$$

where

$$\vec{q} = (x,y), \qquad \text{(Eq. E-16)}$$

a vector transverse to the axial direction, and

$$k_{zn} = \beta_n + i\alpha = \beta_0 + \frac{2\pi n}{d} + i\alpha \qquad \text{(Eq. E-17)}$$

The $a_n(\vec{q})$ are the spatial harmonic amplitudes and k_{zn} represent their wave numbers. The β_n, where

$$\beta_n = \beta_o + \frac{2\pi n}{d}, \quad n=0, \pm 1, \pm 2, \ldots \qquad \text{(Eq. E-18)}$$

are the spatial harmonic phase constants. β_o is the phase constant of the fundamental wave feeding the structure. α is an attenuation constant associated with the fundamental.

These types of waves arise because the spatial variations arising from the periodic structure cause the medium to be represented by an inhomogeneous wave equation, and this requires the presence of spatial harmonic waves.

Each spatial harmonic has an axial phase velocity, v_{pn} given by

$$v_{pn} = \omega/\beta_n \qquad \text{(Eq. E-19)}$$

When $|n|$ is sufficiently large, such that $\beta_n > k_o$ (or $v_p < c$), all spatial harmonics are slow waves. Taking $\beta_o > o$, spatial harmonics for $n \geq 0$, are considered forward traveling and those for $n < 0$ and either $|n| >> 1$ or $d<<\lambda$ have negative phase velocities and are associated with backward waves. It should be noted that a backward wave spatial harmonic with $n=-1$ is allowed provided $d<<\lambda$. It will be argued later that radiation involves predominately this spatial harmonic. Since this requires $d<<\lambda$, it follows that the structure must basically support slow waves.

Waves of the form given in Equation E-6 will satisfy Maxwell's equations and the constitutive relations, including Equation E-14, provided

$$D\ (k_{zn}, k_o) = 0, \quad n = 0, \pm 1, \pm 2, \cdots \qquad \text{(Eq. E-20)}$$

Equation E-20 gives an infinite set of dispersion relations for the axially periodic traveling wave structure. Closed form solutions to this set of equations are not generally possible. Usually, a perturbation technique, which assumes that spatial harmonic amplitudes become vanishingly small when n is very large, is used to obtain approximate solutions.

In the limit of infinitesimal loading, i.e., $M \ll 1$ and $\epsilon(z) \sim \epsilon_r$, then

$$\beta_o d \cong \sqrt{\epsilon_r}\ k_o d \qquad \text{(Eq. E-21)}$$

When $k_o d$-βd diagram for this structure now consists of a grid of straight lines of slope $1/\sqrt{\epsilon_r}$ given by

$$k_o d = \pm \frac{1}{\sqrt{\epsilon_r}} (\beta_n d - 2\pi n) \qquad \text{(Eq. E-22)}$$

The introduction of spatial periodicity to the structure, therefore, changes the $k_o d - \beta d$ diagram from that of Figure E-1 to that given by Figure E-2.

Using Figure E-2 as a basis, the qualitative effect of increasing the loading which leads to mode coupling may be discussed. The mode coupling principle, based on the case of lossless coupling between two normal modes of a passive, unloaded, traveling wave structure, asserts that the qualitative form of the dispersion curve of a loaded structure may be obtained from the dispersion curves of the two interacting modes of the unloaded structure. If the group velocities of both modes have the same sign at the point of intersection, then the coupling is termed codirectional. This is shown in Figure E-3a. If the group velocities have opposite signs, the coupling is contradirectional and a stop band appears. This is shown in Figure E-3b. The group velocities $v_{gn} = \partial\omega/\partial\beta_n$ of the individual spatial harmonics are identical, when k_{zo} is real, and are equal to the group velocity $v_g = \partial\omega/\partial\beta_o$ of the entire normal mode, Equation E-6.

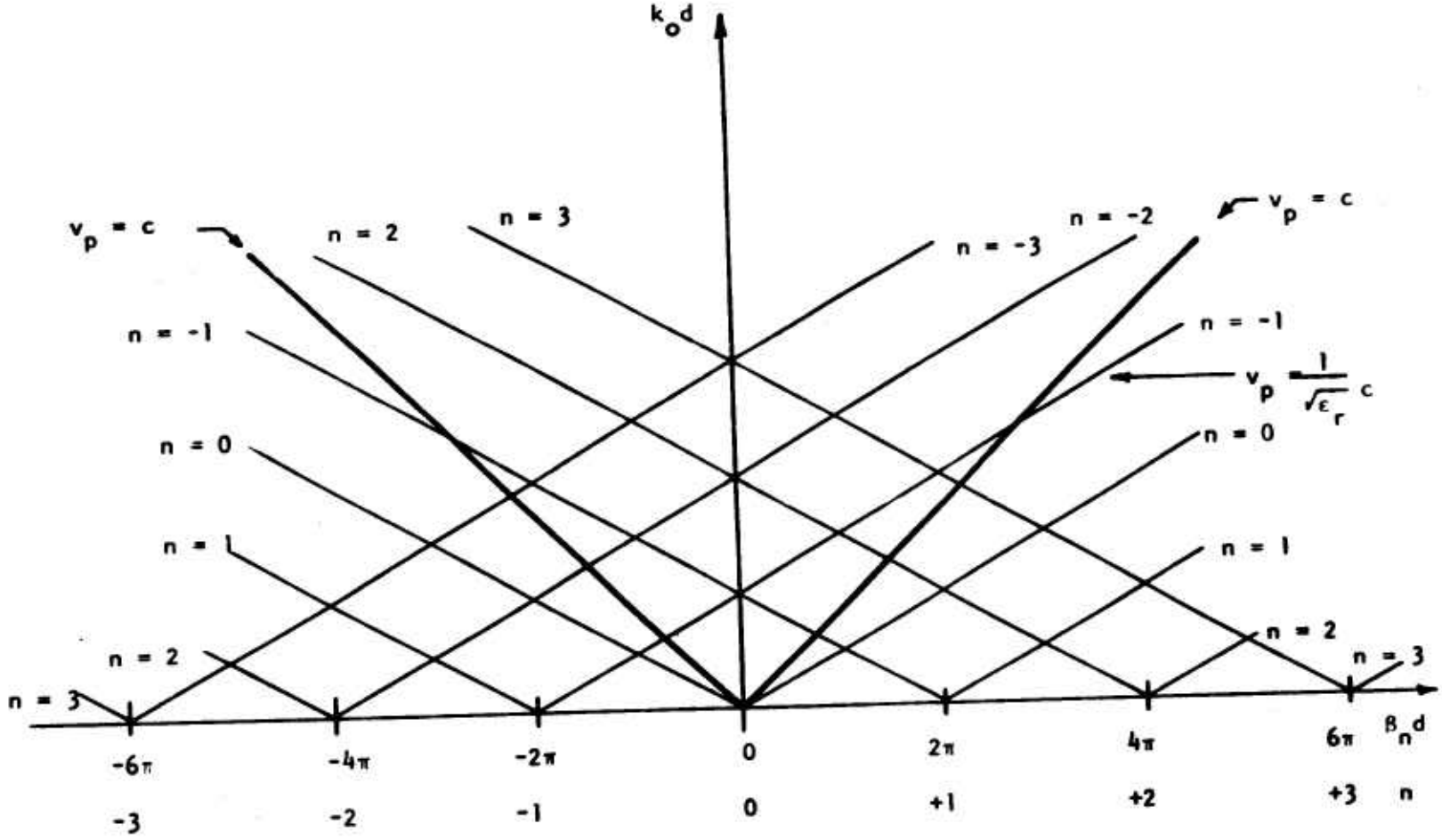
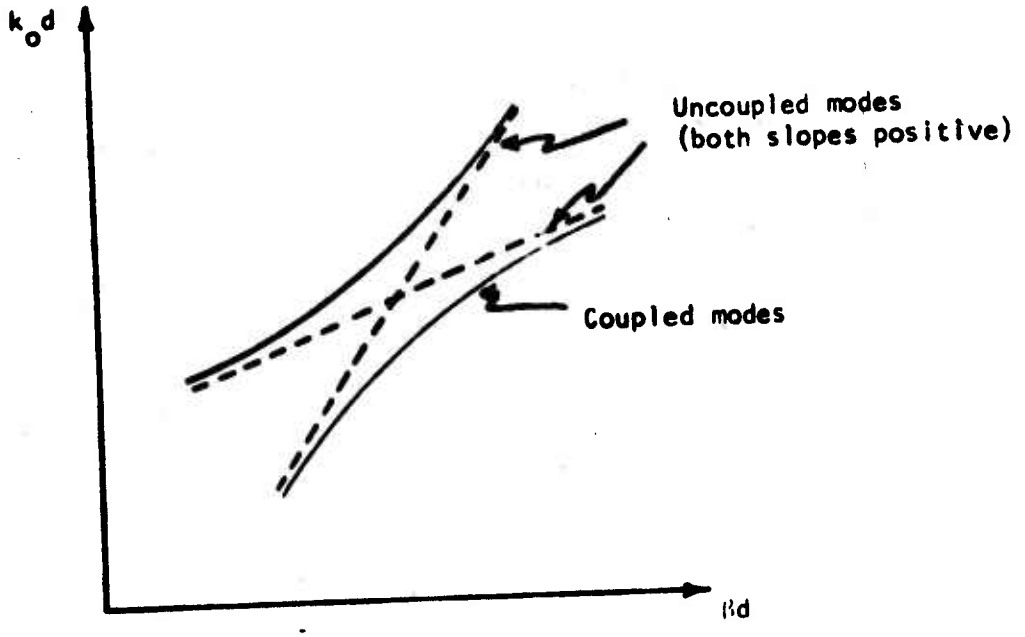
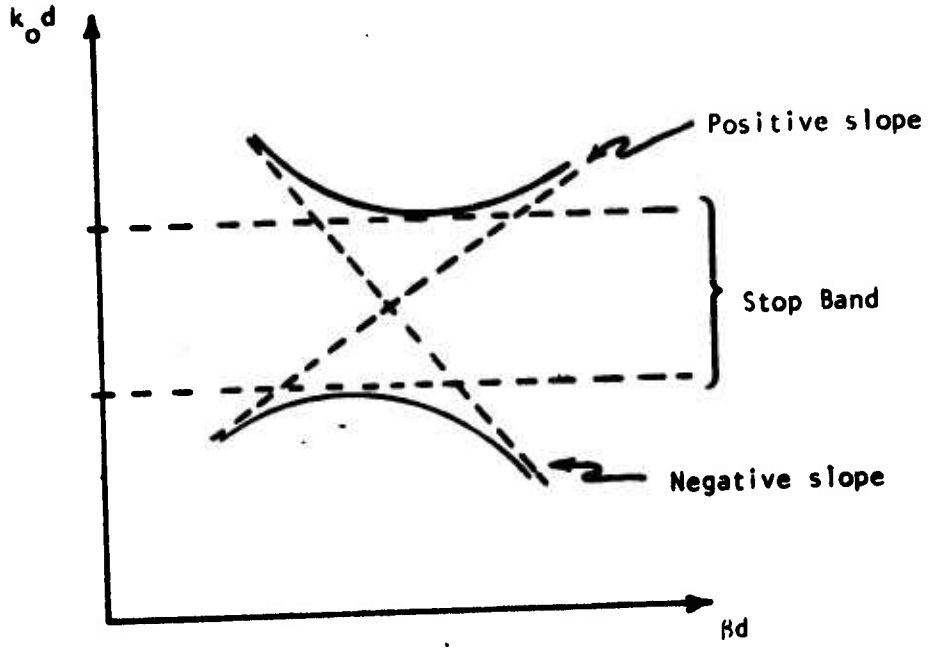


Figure E-2. The $k_o d - \beta d$ Diagram for a Periodic Structure of Period d for Small Loading (i.e., Uncoupled Modes. The Grid is Obtained by Plotting $k_o d = \pm \frac{1}{\sqrt{\epsilon_r}} (\beta_n d - 2\pi n)$ for $n = 0, \pm 1, \pm 2, \ldots, \epsilon_r > 1$ and Therefore Corresponds to a Slow-Wave Structure



(a)



(b)

Figure E-3. The Two Types of Mode Coupling: (a) Codirectional Coupling Occurs When Tangents at Point of Intersection Have Same Signs; (b) Contradirectional Coupling Occurs When Tangents Have Opposite Signs

If mode coupling is applied to Figure E-2, it is seen that, qualitatively, the coupling is contradirectional and stop bands would be expected to appear at points where $\beta d = n\pi$, n an integer. However, an important distinction must be made between open and closed periodically loaded structures. In a closed structure complex, solutions of the dispersion relation, Equation E-20, always are associated with stop bands and the absence of real axial power flow. In contrast, however, such attenuation ($\alpha \neq 0$ in Equation E-9) in open periodic structures may be associated either with a stop band or with loss of energy along the structure due to radiation. Combinations of both effects may appear: it is found that, on open structures, stop bands analogous to those in closed waveguides may occur only in the slow wave region, while attenuation due to energy radiation only occurs in or near the boundaries of fast-wave regions. These regions are defined in Figure E-4. It should be remembered that for open periodic structures, the features of Figures E-2 and E-4 are combined and the mode coupling features added to give the complete $k_o d - \beta d$ diagram. This complete picture for specific antennas does not exist, but some progress toward understanding the operating mechanisms is possible. For the sake of completeness, it should be mentioned that there is one additional qualification on the use of these diagrams for the analysis of log-periodic antennas which will be discussed later.

It should also be mentioned that the actual dynamics of traveling wave interactions on periodic structures (i.e., the analytical treatment of mode coupling) has not been presented here. There are two reasons for this: first, the available analysis for coupling between modes in unloaded periodic structures is rather lengthy; and second, no complete mode-coupling formalism has yet been developed for radiating structures which is, of course, the primary interest here. Basically, the problem of treating mode-coupling involves the solution of the dispersion relation represented by Equation E-20 in what may be termed the resonance regime.

3. GENERAL RADIATION CHARACTERISTICS OF LOG-PERIODIC ANTENNAS USING $k_o d - \beta d$ DIAGRAMS

The relevance of the $k_o d - \beta d$ diagram to the understanding of operation and to the design of log-periodic antennas is based on a perturbation argument according to which the antenna structure may be considered as locally periodic for a gradual expansion of antenna geometry. For a fixed value of k_o and a slowly varying local period d, there corresponds a slowly varying local axial propagation constant $k_z(k_o d)$ which is obtained from the $k_o d - \beta d$ diagram of a uniformly periodic structure with parameters equal to those of the local geometry. The usual design procedure requires the knowledge, either from theory or experiment, of the $k_o d - \beta d$ diagram of a matching, periodic structure, to which the log-periodic tapering is then applied. The uniformly periodic configuration is considered to be a basically slow, traveling-wave structure, which is modulated with a log-periodic taper. The $k_o d - \beta d$ diagram which represents a suitable dispersion curve of the unmodulated structure is shown in Figure E-5. It can be seen that, at a fixed value of k_o and for a slowly expanding log-periodic structure, d is gradually and monotonically increasing, so that $k_o d$ will increase steadily away from the feed. As a result, the line (n=o) will be traversed from low toward increasing values of $k_o d$ and the $k_o d - \beta d$ diagram may be regarded as a plot of the propagation constant along the log-periodic array as a function of variable element spacing. Near the feed, the element spacing and therefore the values $k_o d$ are sufficiently small that the structure operates in its bound-wave region and the traveling wave is guided along the structure as a proper surface wave. (In the following discussion it will be helpful to refer to Figures E-2 - E-4.) On log periodic dipole arrays the stop band at $\beta d = \pi$ can be eliminated by mechanically reversing the phase between adjacent elements. This is unnecessary on the other log-periodic structures. The wave progresses away from the feed until the point 2 on the boundary of the backfire radiation region is reached. There the traveling wave becomes complex with $\beta_{-1} d = -k_o d$ and backfire radiation of the n = -1

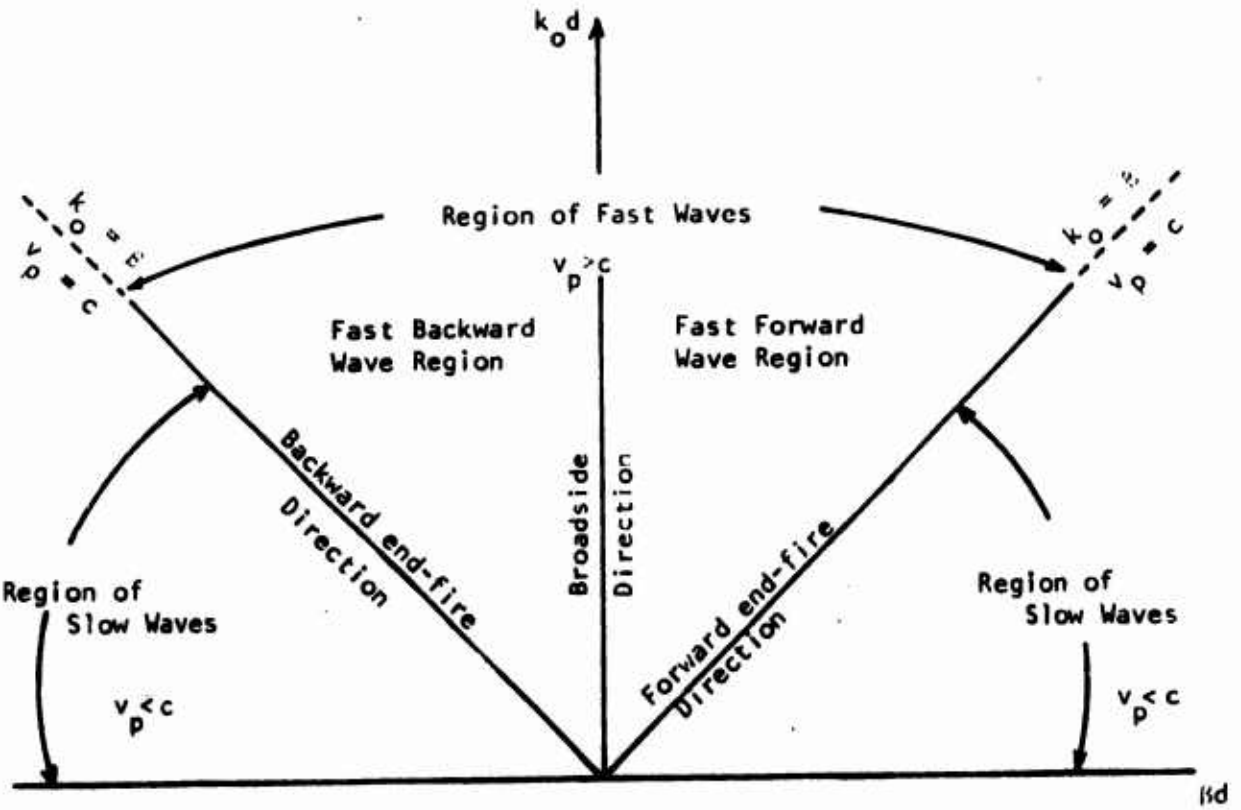


Figure E-4. Wave Propagation Characteristics in the $k_o d - \beta d$ plane

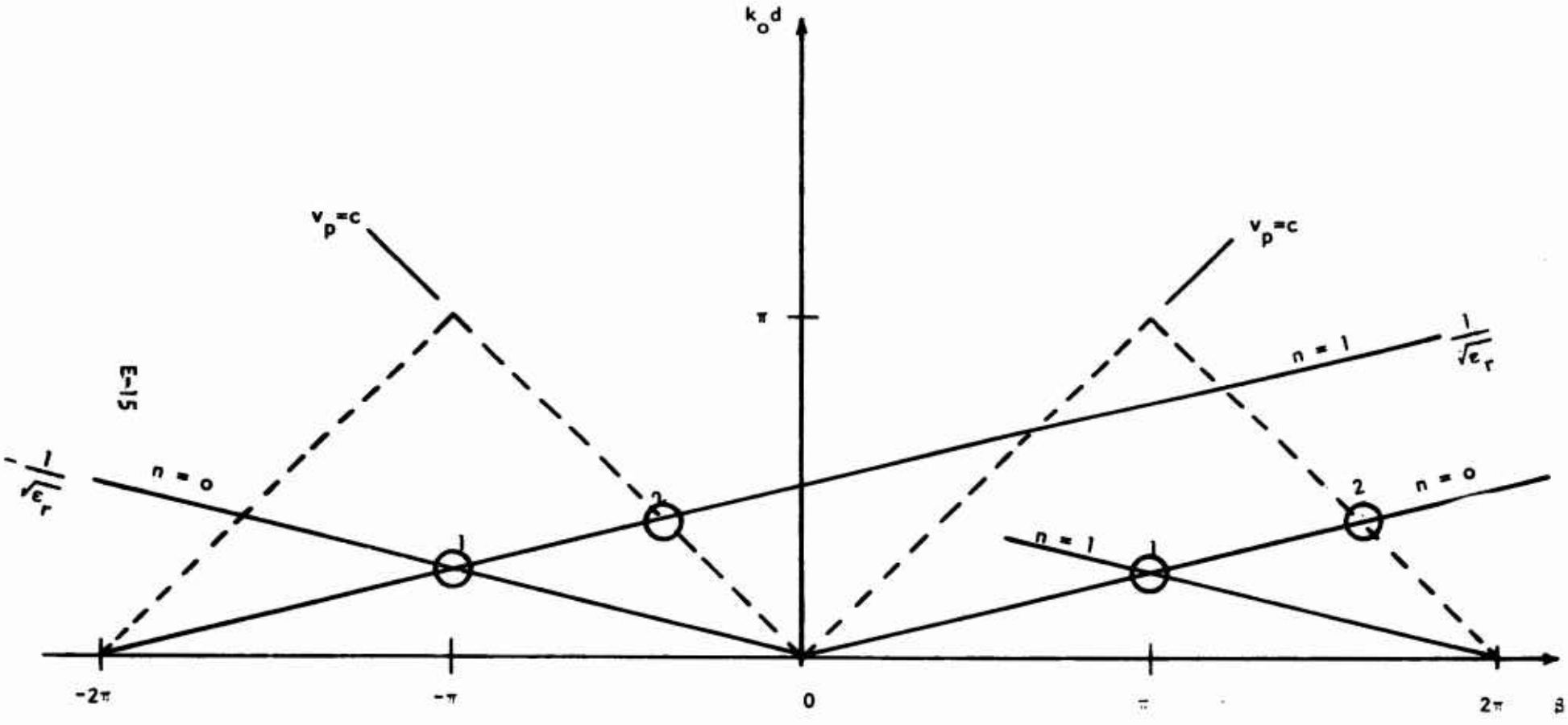


Figure E-5. Brillouin ($k_o d - \beta d$) Diagram for a Basically Slow-Wave ($\epsilon_r > \epsilon_o$), Periodically Loaded Structure Which Also Supports Fast Waves. When the Phase of the Slow Fundamental (M = o) Wave Reaches Point 2, it Becomes Complex; the n = -1 Harmonic Simultaneously Grows Into a Dominant Fast Wave

spatial harmonic occurs. To enhance this backward radiation, the elements in region 2 are designed to one-half the wavelength at the operating frequency. This defines the active region of the antenna.

To understand the dispersive properties of log-periodic structures, consider the following argument. The active region in these antennas moves in response to a frequency modulated (FM) signal in order to satisfy the scaling condition. As the FM pulse travels down the structure, the various components spread out such that the high frequencies radiate off from regions close to the apex, whereas the low frequency components have to travel farther down the structure to their active region before they radiate. This delay in transit time down the structure plus an additional delay, on radiation, for the waves to travel back towards the apex causes the input FM pulse to spread out in time. Thus, the dispersive behavior of frequency independent antennas is a direct consequence of the scaling condition.

APPENDIX F

COMPARISON OF KNOWN FREQUENCY INDEPENDENT ANTENNAS

In this section, frequency independent antennas of the log-periodic class are compared. Virtually all known antenna structures which exhibit bandwidths on the order of 10:1 or greater, belong to this single class because they all satisfy the same scaling condition. Members of this class include the conical log-spiral, the planar log-periodic dipole array, the equiangular or planar log-spiral and several other variants, such as the bent zig-zag, cavity-backed spiral and multiarm spirals.

By virtue of the fact that the equiangular or planar spiral and the log-periodic dipole array are limiting forms of the more general conical log-spiral geometry, these types exhibit many common features such as bandwidth, impedance, and method of operation. There are also some notable differences. For example, all spiral type antennas have circular polarization, while the log-periodic dipole array is linearly polarized. The only antenna that does not have axially periodic structure is the equiangular or planar spiral; instead, it is log-periodic in the radial direction in terms of an active region which scales with frequency. The $k_o d - \beta d$ diagram has been used as an aid in understanding the principle of operation in the case of any antenna of the log-periodic class having axial periodicity. Several of these antennas will now be discussed separately.

1. EQUIANGULAR OR PLANAR SPIRAL ANTENNA

This antenna is presented first partly for historial reasons: it was the first frequency independent antenna discovered[1]. The design of

[1] J. D. Dyson, "The Equiangular Spiral Antenna," IRE Trans. on Antennas and Propagation, Vol. AP-7, pp. 181-187; April, 1959.

this antenna is based upon the simple fundamental principle that if the shape of the antenna were such that it would be specified entirely by angles, its performance would be independent of wavelength. Since all such shapes extend to infinity, it is always necessary to truncate the structure by specifying at least one length. This length, the spiral arm length, need only be on the order of one wavelength at the lowest frequency for which the antenna is designed to operate. The highest operating frequency is determined more by physical construction limitations than anything else. The geometry of the antenna allows the arm length to be spiraled into a maximum diameter of one-half wavelength (of the lowest operating frequency) or less. Antennas of this type have been constructed that have essentially constant radiation patterns and input impedances over bandwidths greater than 20:1.

The equiangular or logarithmic spiral of Figure F-1 is a plane curve defined by the equation

$$\rho = ke^{a\phi} \qquad \text{(Eq. F-1)}$$

where ρ and ϕ are the conventional polar coordinates and a and k are positive constants. If ϕ increases by 2π, one complete turn, then ρ increases by $e^{2\pi a}$, thus each turn of the spiral is a repetition of every other turn except for a constant multiplier. The length of the spiral arm may be calculated from

$$L = \left[1 + \frac{1}{a^2}\right]^{\frac{1}{2}} \left(\rho_{max} - \rho_{min}\right) \qquad \text{(Eq. F-2)}$$

An antenna is constructed by considering two conductors with edges defined by the two curves

$$\rho_1 = ke^{a\phi} \quad \text{and} \quad \rho_2 = ke^{a(\phi-\delta)} = \kappa\rho_1 \qquad \text{(Eq. F-3)}$$



Figure F-1. Equiangular (or Logarithmic) Spiral Antenna Geometry

and $$\rho_3 = ke^{a(\phi-\pi)} \quad \text{and} \quad \rho_4 = ke^{a(\phi-\pi-\delta)} = \kappa\rho_3 \qquad \text{(Eq. F-4)}$$

This defines two balanced conductors, spiraling in opposite directions. each having a finite width δ.

The behavior of the radiation pattern can be obtained by scaling the radial coordinate ρ in terms of wavelength. From Equation F-1 we have

$$\rho' = \frac{\rho}{\lambda} = ke^{a(\phi-\phi_o)} \qquad \text{(Eq. F-5)}$$

where $$\phi_o = \frac{1}{a} \ln \lambda \qquad \text{(Eq. F-6)}$$

Equation (F-6) indicates that the effect of changing the wavelength is equivalent to changing the angle ϕ_o. Thus, except for a rotation, the radiation pattern would be independent of wavelength or frequency within the designed bandwidth. This radiation is bidirectional with equal beams radiated from the front and the back of the antenna. The pattern is circularly polarized over the design bandwidth. However, for frequencies such that the spiral arms are very short compared to wavelength, the radiated field tends to become linearly polarized. As the arm length is increased in terms of wavelength, the field on the axis perpendicular to the plane of the antenna becomes elliptically and then circularly polarized. This change in field polarization is a useful criterion for specifying the cutoff of the pattern bandwidth.

It has been found that the antenna should be spiraled tightly (i.e., made physically small) if the maximum bandwidth is to be obtained for a given diameter antenna.

The average beamwidth is relatively insensitive to antenna parameters, but the tightly spiraled antennas tend to exhibit smaller variations. Typically, beamwidths are on the order of 70°.

The input impedance converges rapidly with increasing frequency to a nearly constant value: these antennas are rarely mismatched and VSWR is better than 3:1 into a 50-ohm line and are usually better than 2:1 over the bandwidth.

The efficiency of the basic antenna (i.e., the metal spiral arms in free space without dielectric material or any type of cavity-backing), has been found to be approximately 98 percent for antennas with arm lengths of one wavelength or more. For arm lengths shorter than one wavelength, the efficiency decreases rapidly.

Much of the emphasis toward analysis of equiangular planar spirals has been placed on sheath or multiarm versions rather than the two arm structure considered above. Generally, as the number of spiral arms is increased, the radiation pattern breaks up into more and narrower lobes.

At present there appears to be no comprehensive treatment of the movement of the active region in terms of the spatial harmonic analysis which would incorporate the use of the $k_o d - \beta d$ diagram, however, there seems to be no reason to suspect that the radiation mechanism could not be at least qualitatively described in this manner.

2. CONICAL LOG-SPIRAL ANTENNA

The balanced conical logarithmic-spiral antenna is treated as a basically slow-wave, locally periodic structure which has a slowly-varying period. A conical bifilar helix is used as the basic structure to generate the $k_o d - \beta d$ diagram.

The basic design equation for the conical log-spiral is given by[1]

$$\rho = \rho_o e^{b(\phi-\delta)}$$

[1] J. D. Dyson, "The Characteristics and Design of the Conical Log-Spiral Antenna," IEEE Trans. on Antenna and Propagation, Vol. Ap-13, July 1965, pp. 488-499.

where

$$b = \frac{\sin \phi_o}{\tan \alpha}$$

These parameters are defined in Figure F-2. The cone half-angle is ϕ_o, α is the rate of wrap of the spiral arms, and δ is the angular width of the arms.

The variation of the propagation constant on this structure can be studied using Figure E-5 and the ensuing discussion. As the frequency of operation is scaled, the active radiation region moves along the structure, with the highest frequencies being radiated near the apex and the lowest frequencies being radiated near the truncated base. As explained previously, all radiation is by the predominant mode of n = -1 spatial harmonic in the backfire direction. It is observed that no appreciable radiation occurs for angles other than backfire. This so because once the wave is phased for backfire wave radiation, most of the energy is released, hence, there is very little left to radiate at the same frequency, as the phase angle continues to increase.

The directivity of the conical spiral generally increases as the cone angle $2\theta_o$ decreases. The radiating efficiency increases as the spiral wrap rate angle, α, increases and is circularly polarized. The half-power beamwidth can be as small as 40° for $\alpha = 85°$ and $2\theta_o = 2°$. However, as directionality is increased, the structure must be physically longer in order to maintain the bandwidth. As the cone angle increases to make the antenna dimensions more compact, directivity is lost, and proper phasing for backfire radiation cannot be maintained. This should be intuitively clear since for $2\theta_o = 180°$ the conical spiral degenerates into a planar spiral for which the phasing is for broadside radiation.

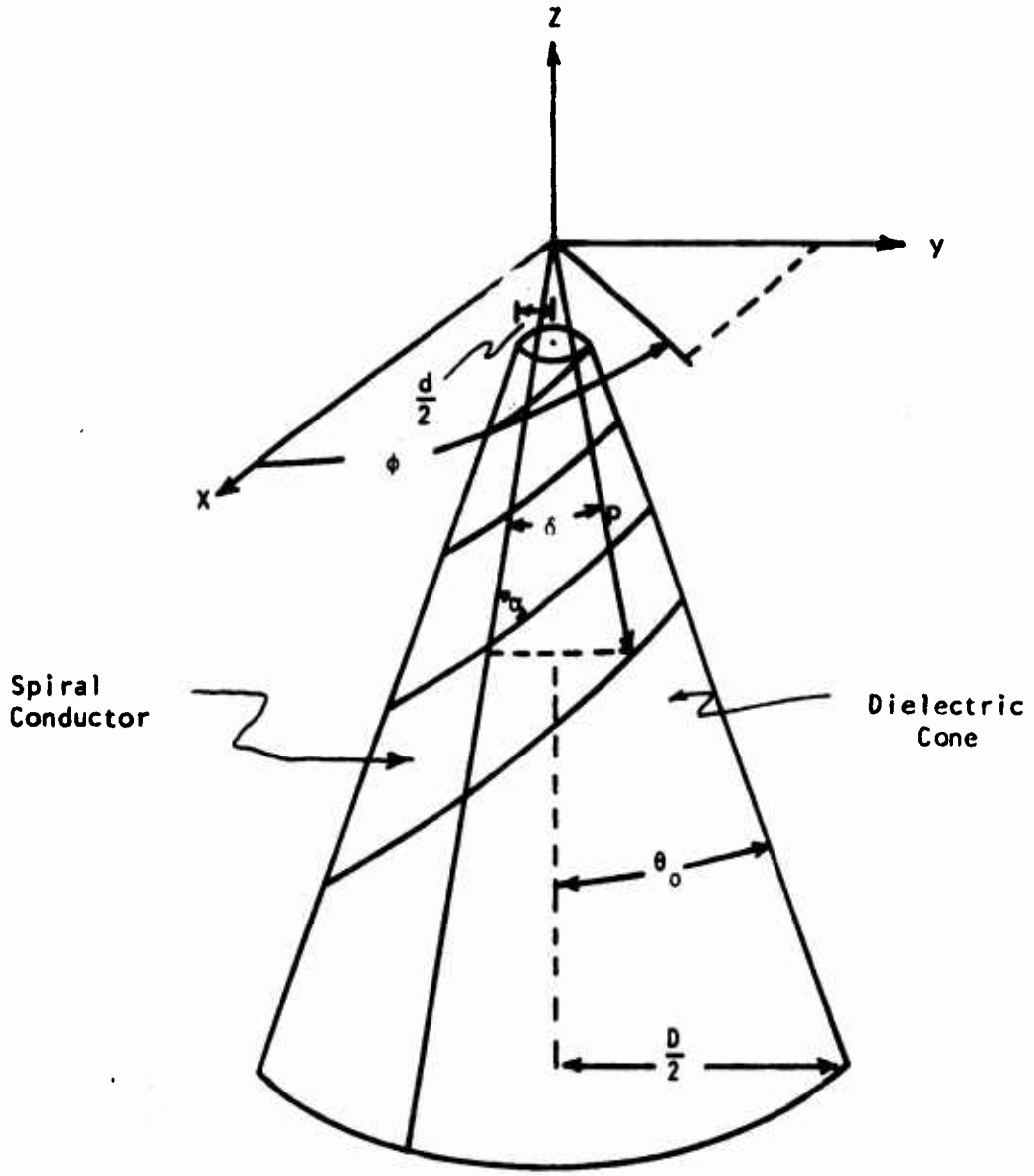


Figure F-2. Conical Log-Spiral Antenna Geometry

Measured VSWR is typically 1.3:1. The input impedance of the antenna is primarily controlled by the spiral arm width, varying from about 320 ohms for narrow arms, to about 80 ohms for very wide arms. The impedance increases as the cone angle increases and approaches the theoretical value of 189 ohms for $2\theta_0 = 180^\circ$. The impedance variation with change in the spiral angle is slight. The impedance bandwidth is consistently greater than the radiation pattern bandwidth.

The characteristics, design and operation of the other frequency independent antennas, such as the log-periodic dipole array, log periodic zig-zag, and conical helix, all differ very little from those already presented above. This is because they are all derived forms of the conical-log spiral.[1,2,3] Discussions of these types may be found in the literature.

---

1 E. Hudock and P. E. Mayes, "Near-Field Investigation of Uniform Periodic Monopole Arrays," IEEE Trans. on Ant. and Prop., AP-13, pp. 488-499, July, 1965

2 J. W. Greiser and P. E. Mayes, "The Bent Backfire ZIGzap - A Vertically-Polarized Frequency Independent Antenna," IEEE Trans. on Ant. and Prop., pgs. 281-290, May, 1964.

3 E. C. Jordan, et.al., "Developments in Broadband Antennas," IEEE Spectrum, pgs. 58-71, April, 1964.

APPENDIX G

NUMERICAL AND ASYMPTOTIC EVALUATION OF BT PRODUCTS

1. INTRODUCTION

The general expression for the BT product of a conical log-spiral antenna, derived in Appendix H, will now be analyzed by varying antenna parameters. An asymptotic expression for this product will also be derived.

2. BD PRODUCT ANALYSIS BY VARIATION OF PARAMETERS

Using the derived result of Equation H-68, the BT product of the conical log-spiral antenna is:

$$BT(A_N, L, \theta_o, \alpha) = \left(\frac{L \tan\theta_o}{A_N}\right)\left[\frac{1}{2\pi\left(1 + \frac{A_N}{L \tan\theta_o}\right)} \frac{\tan\alpha}{\tan\theta_o}\right.$$

$$\left. - \frac{1}{\pi \tan\theta_o}\left(\frac{\sin\alpha \cos\theta_o}{1 + \cos\alpha \cos\theta_o}\right) \sinh\left(\frac{\pi \sin\theta_o}{\tan\alpha}\right)\right] \quad \text{(Eq. G-1)}$$

The BT product depends, in general, upon four independent parameters:

(1) A_N - The cone radius at the highest frequency active region.

(2) L - The axial length of the conical antenna.

(3) θ_o - The half-cone angle.

(4) α - The spiral wrap rate or pitch angle.

In practice, the number of independent variables will be less because of geometrical constraints on the size of the antenna structure. A useful equation of constraint is given by

$$L = \frac{A_1 - A_N}{\tan \theta_o} \qquad \text{(Eq. G-2)}$$

where A_1 is the truncated cone base radius. If the maximum antenna aperture is fixed, thus fixing A_1, then L can be expressed in terms of A_N and θ_o, reducing the number of independent variables to three. For most design applications, however, both A_1 and A_N would be fixed. A_1 is fixed because of maximum aperture size allowed and A_N fixed because of the physical size of the feed input cable for a given power application. In this case

$$L \tan \theta_o = \text{constant}$$

The BT product for this case has been analyzed for half-cone angles ranging from $\theta_o = 40°$ to $\theta_o = 2°$ and for wrap rate angles $\alpha = 60°$ to $\alpha = 89°$. In all cases, $A_1 = 1$ meter and $A_N = .00284$ meters. These results are shown in Figure G-1.

3. ASYMPTOTIC BT PRODUCT LIMIT

Here an asymptotic expression for the BT product is obtained in the limit of small θ_o and large α. Let

$$\alpha = \frac{\pi}{2} - \delta \qquad \theta_o = \delta \qquad \text{(Eq. G-3)}$$

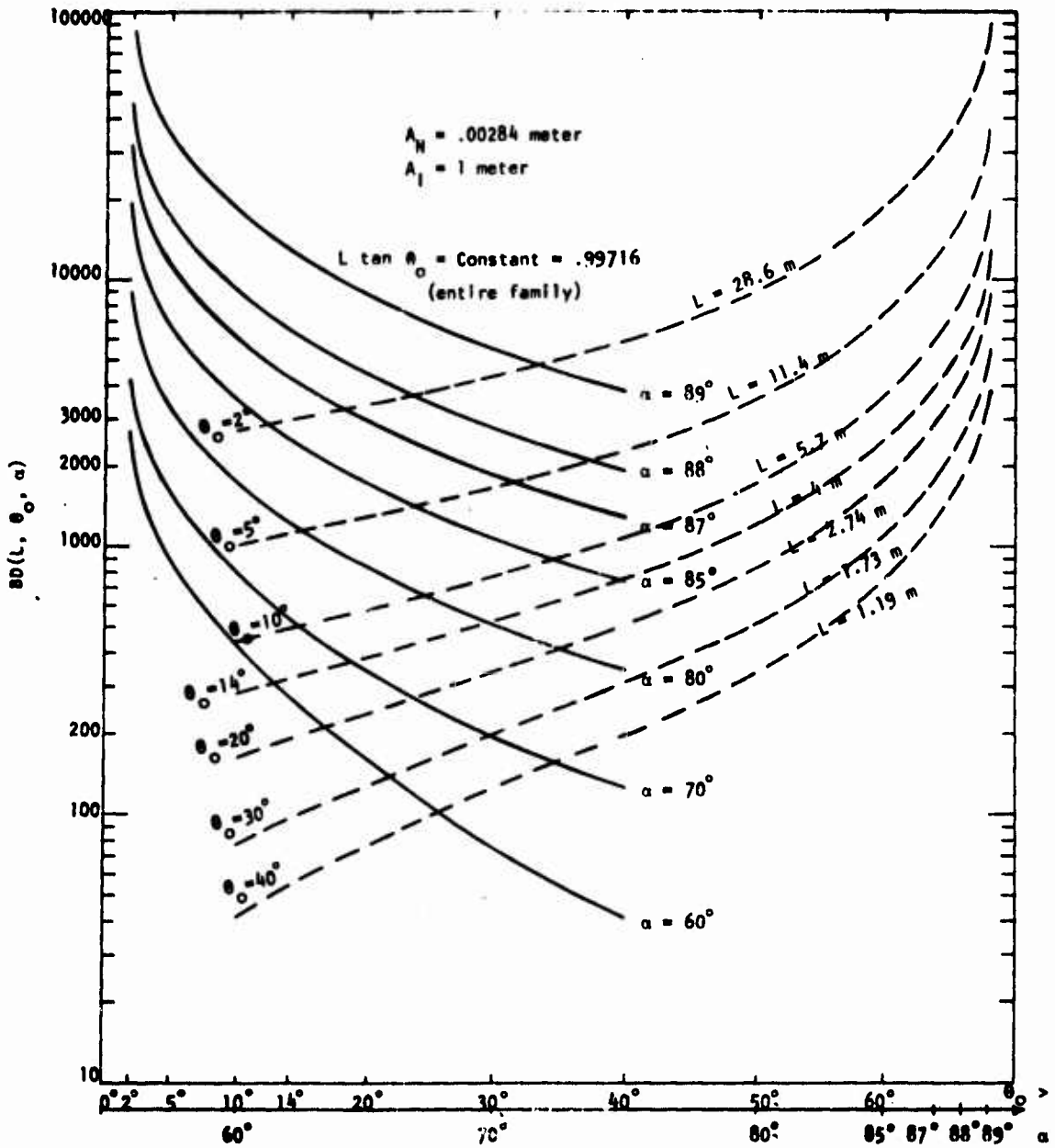


Figure G-1. Parametric Curves for BT Versus θ_o and BT Versus α for A_N = .00284 Meter and A_1 = 1 Meter for a Conical Spiral Antenna

The following relations hold for any δ:

$$\frac{L \tan \theta_o}{A_N} = \frac{L \tan \delta}{A_N} \qquad \text{(Eq. G-4)}$$

$$\frac{\tan \alpha}{\tan \theta} = \frac{\sin(\alpha + \theta_o) + \sin(\alpha - \theta_o)}{\sin(\alpha + \theta_o) - \sin(\alpha - \theta_o)} = \frac{1 + \cos 2\delta}{1 - \cos 2\delta} \qquad \text{(Eq. G-5)}$$

$$\frac{\sin \alpha \cos\theta_o}{1 + \cos \alpha \cos\theta_o} = \frac{\frac{1}{2}\left[\sin(\alpha + \theta_o) + \sin(\alpha - \theta_o)\right]}{1 + \frac{1}{2}\left[\cos(\alpha + \theta_o) + \cos(\alpha - \theta_o)\right]} = \frac{\frac{1}{2}\left[1 + \cos 2\delta\right]}{1 + \frac{1}{2}\sin 2\delta} \qquad \text{(Eq. G-6)}$$

$$\frac{\sin\theta_o}{\tan \alpha} = \frac{\frac{1}{2}\left[\sin(\alpha + \theta_o) - \sin(\alpha - \theta_o)\right]}{\sin \alpha} = \frac{\frac{1}{2}\left[1 - \cos 2\delta\right]}{\cos\delta} \qquad \text{(Eq. G-7)}$$

Equation G-1 may be expressed now as

$$BT(A_N, L, \delta) = \frac{1}{2\pi} \frac{\left(\frac{L \tan \delta}{A_N}\right)^2}{\left(\frac{L \tan \delta}{A_N} + 1\right)} \left(\frac{1 + \cos 2\delta}{1 - \cos 2\delta}\right) - \frac{L}{\pi A_N} \left(\frac{\frac{1}{2}(1 + \cos 2\delta)}{1 + \frac{1}{2}\sin 2\delta}\right) \cdot \sinh\left(\frac{\frac{\pi}{2}(1 - \cos 2\delta)}{\cos\delta}\right) \qquad \text{(Eq. G-8)}$$

Equation G-8 expresses a BT product which is now dependent upon only one angle, δ, the axial length L of the antenna, and the radius A_N of the smallest end of the cone.

Now consider the case where $0 < \delta << 1$. Small angle approximations are valid, thus

$$\frac{L \tan \theta_o}{A_N} \sim \frac{L\delta}{A_N} \qquad \text{(Eq. G-9)}$$

$$\frac{\tan \alpha}{\tan \theta_o} \sim \frac{1}{\delta^2} \qquad \text{(Eq. G-10)}$$

$$\frac{\sin \alpha \cos\theta_o}{1 + \cos \alpha \cos\theta_o} \sim 1 - \delta \approx 1 \qquad \text{(Eq. G-11)}$$

$$\sinh\left(\frac{\pi \sin\theta_o}{\tan \alpha}\right) = \sinh\left(\frac{\pi \delta^2}{1 - \frac{\delta^2}{2}}\right) \cong \frac{\pi \delta^2}{1 - \frac{\delta^2}{2}} \cong \pi \delta^2 \qquad \text{(Eq. G-12)}$$

Substituting Equation G-9 - G-12 into Equation G-8, we obtain

$$\lim_{\substack{\theta_o \to \delta \\ \alpha \to \frac{\pi}{2} - \delta \\ \delta << 1}} BT(A_N, L, \theta_o, \alpha) = BT(\delta, A_N, L) \qquad \text{(Eq. G-13)}$$

$$BT(\delta, A_N, L) = \frac{1}{2\pi} \frac{\left(\frac{L}{A_N}\right)^2}{\left(1 + \frac{L\delta}{A_N}\right)} - \frac{L\delta^2}{A_N} \qquad \text{(Eq. G-14)}$$

There are two special cases under which Equation G-14 must be evaluated since $\delta << 1$ does not exclude either $\delta << A_N/L$ or $\delta >> A_N/L$.

(1) Case A

$$\delta << A_N/L$$

In this case Equation (G-14) reduces to

$$BT(A_N, L) = \frac{1}{2\pi}\left(\frac{L}{A_N}\right)^2 \qquad \text{(Eq. G-15)}$$

(2) Case B

$$\delta >> A_N/L$$

In this case, Equation (G-14) reduces to

$$BT(\delta, L, A_N) = \left(\frac{L}{A_N}\right)\left[\frac{1}{2\pi\delta} - \delta^2\right]$$

or

$$BT(\delta, L, A_N) = \frac{1}{2\pi}\left(\frac{L}{A_N\delta}\right) \qquad \text{(Eq. G-16)}$$

Given δ, A_N, and L, the maximum theoretical BT product may be obtained either from Equations G-15 or G-16. It is obvious that BT can, in principle, be made as large as desired, but for a given set of design parameters δ, A_N, and L, there will be a definite upper limit as indicated by Cases A and B.

APPENDIX H

MAXIMUM BANDWIDTH-TIME PRODUCTS OF FREQUENCY INDEPENDENT ANTENNAS

1. INTRODUCTION

Pratical limits for maximum bandwidth-time products (BT products) for three types of frequency independent antennas will now be derived. These antennas, the planar log-periodic dipole array (LPDA), the conical spiral, and the cavity-backed spiral, represent the most divergent types of the log-periodic class; therefore, their individual maximum BT products may be directly compared to yield the overall maximum BT product as well as providing insight to show how antenna parameters affect this result. This comparison will allow the various trade-offs among antenna parameters, such as axial length, aperture size and directivity, which affect the BT product, to be evaluated in terms of specific antenna requirements.

Since there are no analytical limitations on the bandwidth of any of these antennas, then the bandwidth is determined on the basis of physically realizable or practical considerations. These limitations will be discussed first in Paragraph 2, since they will not differ essentially among antenna types. Analyses for the LPDA, conical spiral, and cavity-backed spiral will follow in Paragraphs 3, 4, and 5, respectively. Finally, some conclusions for maximum BT products will be drawn in Paragraph 6.

2. BANDWIDTH

Even though it has already been shown, it should again be emphasized that a perfect frequency independent antenna would possess infinite bandwidth and would also have infinite dimensiors. The limitation on the bandwidth for a properly designed log-periodic antenna is the requirement

that it be a finite structure having finite dimensions. Besides this overall limitation, there are other factors which will affect bandwidth. These factors relate, in general, to the apex region or the smallest scaled antenna dimension, and hence, limit the high frequency response. This can be stated another way: choosing fixed axial and transverse dimensions is sufficient in order to obtain an antenna structure of finite spatial extent, but because the apex region of any of these antennas scales to a geometrical point (i.e., zero spatial dimension), the structure is still undefined. What then limits the high frequency response of a finite antenna? In practice, it is the dimensions of the antenna feed cable. Furthermore, feed dimensions also depend upon the maximum currents and voltages the feed cable is capable of supporting. Therefore, the larger the input power to the antenna, the larger the feed must become, and a larger feed means lowering the highest operating frequency.

Therefore, in order to obtain estimates of maximum bandwidth, it is necessary to establish some criteria on the feed dimensions. It will be assumed that the smallest feed cable for a practical antenna to accept a reasonable amount of input power is one which has an outside diameter of 0.358 cm (.141 inch). Such a cable typically would be capable of delivering an average power ranging from 100 watts at 15 GHz to about 3000 watts at 50 MHz into a 50-ohm load. For fast pulse applications, such as pulse compression, the instantaneous peak power would be a more useful parameter and these values could easily be several orders of magnitude greater than those for average power.

The feed cable diameter will determine the highest operating frequency. The diameter of the first or highest active region should be several times larger than the feed diameter for efficient radiation, that is, radiation which does not interfere significantly with the feed cable. When this condition is imposed, the highest operating frequency

will turn out to be approximately 15 GHz. The manner in which the value is established will be discussed separately for each antenna type in the following paragraphs.

The low frequency limit of a given antenna depends upon both the maximum diameter and the specific structure geometry. For the LPDA, the longest element is approximately one-half wavelength. For both the conical spiral and cavity-backed spiral, the lowest frequency is more dependent upon turn spacing and spiral length than on the maximum structure diameter. For these latter types, the longest radiated wavelength may be several times this diameter. Generally, the spiral type antennas exhibit good low frequency response as long as the spiral length is long compared to wavelength. For the conical spiral,[1] the low frequency limit can be determined from the expressions[2]

$$\lambda_1 = \pi T \left[\frac{1 + S}{\sin \alpha \cos \theta_o}\right] \qquad \text{(Eq. H-1)}$$

and

$$S = \frac{k}{\beta} = \frac{v}{C} = \cos \alpha \cos \theta_o \qquad \text{(Eq. H-2)}$$

where λ_1 is the wavelength corresponding to the lowest frequency, D is the maximum diameter, S is the slowness factor obtained from the k-β diagram, α is the pitch angle of the spiral turns and θ_o is the cone half angle. Equation H-2 relates the slowness factor of the representative k - β diagram for the strictly periodic helix to the parameters α and θ_o of the tapered periodic structure (i.e., the conical spiral). Since the slowness factor of the helix is S = cos α, the difference between these two expressions is given by (1 - cos θ_o). For cone angles up to $2\theta_o = 20^\circ$, this difference is less than 1.5 percent, whereas for a cone angle of $2\theta_o = 80^\circ$ the difference is 23 percent. The low frequency limit for the

---

1 For conical spiral geometry, please refer to Appendix F; also see the following reference.

2 Dyson, J. D., "The Characteristics and Design of the Conical Log-Spiral Antenna," IEEE Trans. on Antennas and Propagation, Vol. AP-13, July 1965, pp. 488-499.

cavity-backed spiral is somewhat more arbitrary. Usually, it is defined in terms of the axial ratio of the polarizations (i.e., generally the radiation is circularly polarized but as the frequency decreases, the pattern tends to become first elliptically and finally linearly polarized). The lowest frequency is commonly taken as that frequency at which the axial ratio of the polarization ellipse is 2 or 3 to 1.

There is some variation in the low frequency limit of these three antennas when all have the same maximum physical aperture of 2 meters. However, this variation is slight and does not affect practical bandwidths significantly when the highest frequency is several orders of magnitude greater than the lowest as will certainly be the case here. Since the maximum antenna diameter need only be on the order of one-half wavelength, it follows that the lowest operating frequency will be about 75 MHz.

Therefore, the maximum practical bandwidth for an antenna designed to handle appreciable power (viz., 100 watts at 15 GHz) can be expected to be of the order

$$B = 15 \text{ GHz} - 75 \text{ MHz} = 14.93 \text{ GHz} \qquad \text{(Eq. H-3)}$$

This value is intended only as a rough estimate, but, as the following discussions will show, in all cases it will be within 1 percent of the values calculated for the individual antennas.

The three antennas will now be studied individually under the overall geometrical constraints:

(1) Maximum axial length = 4 meters

(2) Maximum transverse length = 2 meters

3. LOG-PERIODIC DIPOLE ARRAY

The LPDA is defined in Figure H-1 by the relations

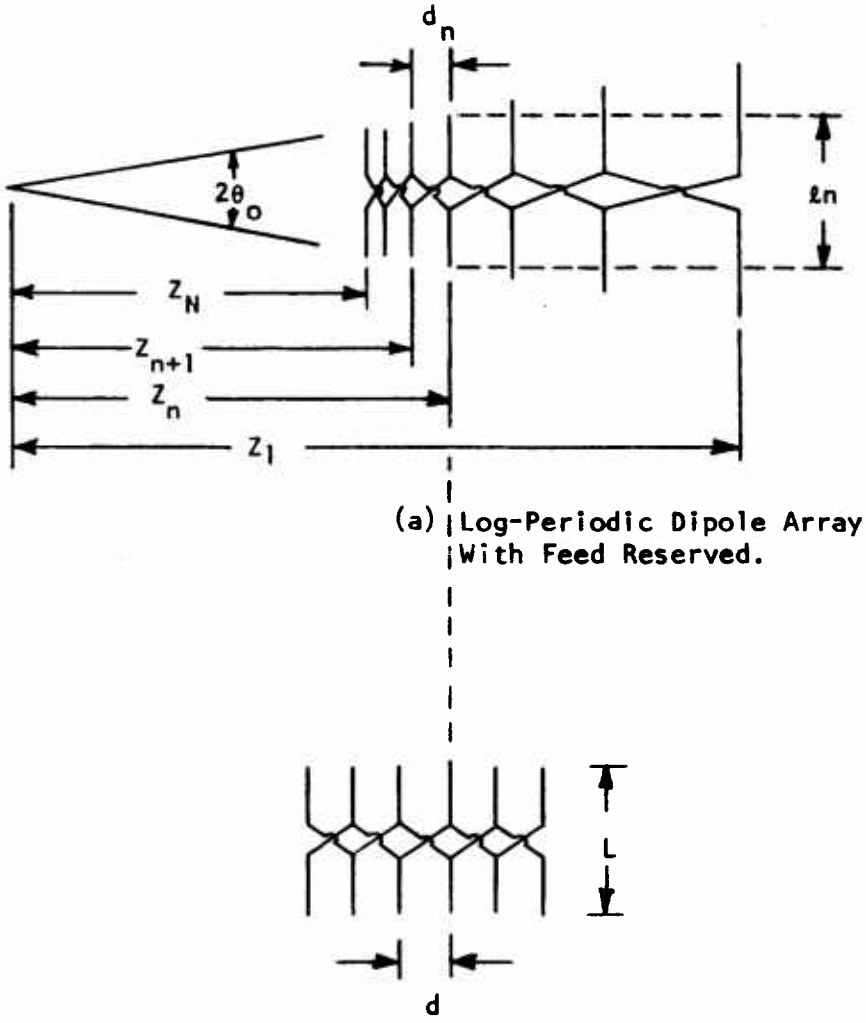
$$\frac{Z_{n+1}}{Z_n} = \tau \qquad \text{(Eq. H-4)}$$

$$\frac{d_{n+1}}{d_n} = \tau \qquad \text{(Eq. H-5)}$$

$$\frac{\ell_{n+1}}{\ell_n} = \tau \qquad \text{(Eq. H-6)}$$

$$\frac{d_n}{\ell_n} = \sigma \qquad \text{(Eq. H-7)}$$

The parameter τ determines the logarithmic growth in periodicity along the structure and usually is slightly less than unity. The ratio of element length to element spacing, denoted by σ in Equation H-7, is related to the slowness of wave propagation along the structure. Generally, for maximum time duration and bandwidth, σ should be as small as possible, certainly less than 0.5. However, as will be seen presently, antenna efficiency for pulse compression is greatly reduced when σ is too small. Allowable lower limits on σ vary among different LPDA designs because it turns out that σ and τ are not independent, but are related through the cone half-angle, θ_o, of the antenna. This relationship will be demonstrated in the following discussion.



(a) Log-Periodic Dipole Array With Feed Reserved.

(b) Uniformly Periodic Slow-Wave Structure That is Complementary to the Nth Active Region of the LPDA.

Figure H-1. Log-Periodic Dipole Array Definition

Radiation at the highest frequency, f_N, occurs in the active region centered about the element ℓ_N. The distance from the apex to this element is

$$Z_N = \frac{\ell_N}{2 \tan \theta_o} \qquad \text{(Eq. H-8)}$$

To insure that there is a slow wave feed geometry at Z_N, it is assumed that there is one additional element at Z_{N+1} located in front of ℓ_N such that

$$Z_N - Z_{N+1} = d_N \qquad \text{(Eq. H-9)}$$

The position of the element ℓ_{N+1} is at

$$Z_{N+1} = \frac{\ell_{N+1}}{2 \tan \theta_o} \qquad \text{(Eq. H-10)}$$

where

$$\ell_{N+1} = \tau \ell_N \qquad \text{(Eq. H-11)}$$

This locates one end of the LPDA. Assuming a resonant half wavelength, the highest frequency element ℓ_N is resonant at

$$f_N = \frac{c}{\lambda_N} = \frac{c}{2\ell_N} \qquad \text{(Eq. H-12)}$$

Assuming that ℓ_N should be several times larger than the cable diameter of 0.358 cm, the value ℓ_N = 1 cm has been chosen. In this case, the highest operating frequency would be f_N = 15 GHz. The bandwidth would be approximately doubled if ℓ_N were halved, but these would likely be increased interference with the feed on radiation. It should be understood, therefore, that there is some arbitrariness in taking ℓ_N = 1 cm.

The other end of the antenna will depend upon the location of the lowest frequency element

$$\ell_1 = \frac{c}{2f_1} \qquad \text{(Eq. H-13)}$$

This element would be approximately equal to the maximum allowable structure diameter, namely 2 meters, in order to provide maximum bandwidth. With respect to the apex, the position of element ℓ_1 is

$$Z_1 = \frac{Z_{N+1}}{\tau^N} \qquad \text{(Eq. H-14)}$$

The total length of the antenna, L, is found by subtracting Equations H-10 and H-14

$$L = Z_1 - Z_{N+1} = \left(\frac{1}{\tau^N} - 1\right)\frac{\ell_{N+1}}{2\tan\theta_o} \qquad \text{(Eq. H-15)}$$

Equation H-15 may be written in terms of the highest and lowest operating frequencies

$$L = \frac{c}{4\tan\theta_o}\left[\frac{1}{f_1} - \frac{\tau}{f_N}\right] \qquad \text{(Eq. H-16)}$$

Since, as will now be shown, θ_o and τ are not independent variables, Equations H-15 and H-16 should not be used indiscriminately. The reason is that neither of these equations explicitly show dependence on the slowness factor σ.

Consider the nth element of the LPDA. Its location with respect to the apex may be obtained using

$$Z_n - Z_{n+1} = d_n \qquad \text{(Eq. H-17)}$$

Recalling Equation H-4, Equation H-17 may be written

$$Z_n = \frac{d_n}{(1 - \tau)} \qquad \text{(Eq. H-18)}$$

However, Z_n is also given by

$$Z_n = \frac{\ell_n}{2 \tan \theta_o} \qquad \text{(Eq. H-19)}$$

Equating Equations H-18 and H-19, and using Equation H-7 gives

$$\tau = 1 - 2\sigma \tan \theta_o \qquad \text{(Eq. H-20)}$$

The importance of Equation H-20 is that it relates the three most important design parameters for the LPDA. Substituting Equation H-20 into Equation H-16 to eliminate τ and solving the resulting expression for the cone angle θ_o gives

$$\theta_o = \tan^{-1}\left[\frac{\left(1 - \frac{1}{B_R}\right)}{2\left(\frac{L}{\ell_1} - \frac{\sigma}{B_R}\right)}\right] \qquad \text{(Eq. H-21)}$$

where the bandwidth ratio, B_R, is

$$B_R = \frac{f_N}{f_1} \qquad \text{(Eq. H-22)}$$

To use Equation H-21 σ must be specified. In general, σ must lie in the range

$$0 < \sigma \lesssim .5 \qquad \text{(Eq. H-23)}$$

If the structure is to support slow waves. σ can be related to the slowness factor as follows:

$$k_n d_n = \pi\sigma \qquad \text{(Eq. H-24)}$$

For the structure to be properly phased for backfire radiation at a particular value of $k_n d_n$, βd must change by at least $\pi/2$. When $k_n d_n = \pi/2$, then backfire phasing will occur for $dn = \lambda_n/4$. Since $\ell_n = \lambda_n/2$, it follows that $\sigma = .5$. In this case

$$S = \frac{kd}{\beta d} = \frac{v}{c} = 2\sigma = 1$$

which is the limiting value of the slow wave structure. As σ decreases, $\beta d > \pi/2$ in order to maintain backfire phasing, thereby increasing the slowness ($S < 1$). Therefore, in practice, σ should be made as small as possible to maximize the time delay. However, as can be seen from any $k_o d - \beta d$ diagrams, when σ approaches zero, backfire phasing becomes indistinguishable from broadside and forward radiation phasing. Thus, radiation tends first to become isotropic for very small σ and then ceases completely as $\sigma \to 0$.

Once σ has been chosen for a slow wave structure, Equation H-21 may be solved for θ_o. Then σ and θ_o can be used in Equation H-20 to obtain τ. Once τ and σ are known, the LPDA can be built by applying Equations H-4 to H-7.

An analytic expression for the BT product of an LPDA will now be obtained. The bandwidth of an LPDA is defined as

$$B = f_N - f_1 \qquad \text{(Eq. H-25)}$$

Since the center frequency of the nth active region is

$$f_n = \frac{c}{4 Z_n \tan \theta_o},$$

Equation H-25 becomes

$$B = \frac{c}{4 \tan \theta_o Z_1} \left(\frac{Z_1}{Z_N} - 1 \right)$$

Recalling Equations H-4 and H-14, the last equation may be written

$$B = f_1 \left(\frac{1}{\tau^{N-1}} - 1 \right) \qquad \text{(Eq. H-26)}$$

Also, using Equations H-22 and H-25, we have

$$B = f_1 (B_R - 1) \qquad \text{(Eq. H-27)}$$

and

$$B_R = \frac{1}{\tau^{N-1}} \qquad \text{(Eq. H-28)}$$

Equation H-28 may be used to determine the number of elements of the LPDA:

$$N = 1 - \frac{\ln B_R}{\ln \tau} \qquad \text{(Eq. H-29)}$$

The bandwidth of the active region, B_A, is defined as the frequency difference between two consecutive elements of the array when $\sigma = 0.5$. In this case, there will be a total phase change of π radians (neglecting the mechanical π phase shift because of cross feeding) between the elements. Thus,

$$B_A^{(n)} = f_{n+1} - f \qquad \text{(Eq. H-30)}$$

It is convenient to introduce the active region bandwidth ratio, B_{AR}, as

$$B_{AR} \equiv \frac{f_{n+1}}{f_n} = \frac{1}{\tau} \qquad \text{(Eq. H-31)}$$

Then

$$B_A^{(n)} = f_n (B_{AR} - 1) \qquad \text{(Eq. H-32)}$$

It is seen in Equation H-32 that the active region bandwidth increases as the frequency increases.

Since the phase angle varies linearly with the natural logarithm of frequency, i.e.,

$$\phi(\omega) = K(\ln\omega - \ln\omega_o), \qquad \text{(Eq. H-33)}$$

where

$$K = \frac{\pi}{\ln B_{AR}}, \qquad \text{(Eq. H-34)}$$

the time delay of radiation at frequency f is given by

$$t_f = \frac{d\,\phi(\omega)}{d\omega} = \frac{K}{\omega} = \left(\frac{1}{2 \ln B_{AR}}\right)\frac{1}{f} \qquad \text{(Eq. H-35)}$$

or

$$t_f = -\left(\frac{1}{2 \ln \tau}\right)\frac{1}{f} \qquad \text{(Eq. H-36)}$$

The maximum delay occurs for radiation at the lowest frequency

$$t_1 = -\left(\frac{1}{2 \ln \tau}\right)\frac{1}{f_1} \qquad \text{(Eq. H-37)}$$

Besides the feed delay in exciting the lowest frequency, there is an additional delay due to the spatial displacement between the first and last active regions of the antenna. This delay is

$$t_2 = \frac{L - d_1}{c} = \frac{\sigma}{2 f_1}\left[\frac{\left(1 - \frac{1}{B_R}\right)}{\left(\frac{1}{\tau} - 1\right)}\right] \qquad \text{(Eq. H-38)}$$

The total dispersion, or time delay, is the sum of Equations H-37 and H-38:

$$T = t_1 + t_2 = \frac{1}{2 f_1}\left[\frac{1}{\ln \tau} + \frac{\sigma\left(1 - \frac{1}{B_R}\right)}{\left(\frac{1}{\tau} - 1\right)}\right] \qquad \text{(Eq. H-39)}$$

Thus, the BD product for the LPDA may be written:

$$BT(\theta_o, \sigma; B_R) = \frac{1}{2} (B_R - 1) \left[\frac{1}{\ln (1 - 2\sigma \tan \theta_o)} + \left(\frac{\cot \theta_o}{2} - \sigma \right) \left(1 - \frac{1}{B_R} \right) \right]$$

(Eq. H-40)

In order to evaluate Equation H-40 for the maximum BT product, σ must be specified. Since a value for maximum bandwidth has already been obtained, it is only necessary to maximize D. By far the greatest contribution to T comes from t_1 which depends strongly on τ. In turn, τ also depends strongly on σ. As σ becomes smaller, τ approaches unity and t_1 gets larger for fixed θ_o. Therefore, to maximize BT, one must minimize σ. Slow wave LPDA structures have been investigated for values as small as $\sigma = 0.1$.[1] Taking this value for σ and

$$B = f_N - f_1 = (15 - .075) \text{ GHz} = 14.925 \text{ GHz},$$

and

$$L = 4 \text{ meters},$$

one solves Equation H-21 for θ_o:

$$\theta_o = 14^\circ$$

From Equation H-20:

$$\tau = .95$$

Equation H-39 yields:

$$T = 142.4 \text{ ns} \qquad \text{(Eq. H-41)}$$

---

[1] Kieburtz, R. B., "Analysis and Synthesis of Aperture Fields of Log-Periodic Antennas," Electromagnetic Wave Theory, Pt 2, Pergamon Press, 1967, p. 767.

Finally, one obtains the maximum BT product for an LPDA:

$$BT = (14.93 \text{ GHz})\ (142.4 \text{ ns}) = 2126 \qquad \text{(Eq. H-42)}$$

Let us examine the effect of varying the parameters θ_o, σ, and B_R on the value of the BT product. If we take $\sigma = .25$, we find $\theta_o = 14^o3'$ and $B_R = 200$, which are approximately the same as the preceding case. However, we now find that $\tau = .875$ and that duration is significantly reduced:

$$BT = (14.93)\ (66.4 \text{ ns}) = 991 \qquad \text{(Eq. H-43)}$$

If we take $\sigma = .25$ and $f_1 = .150$ GHz so that $B_R = 100$, we find $\theta_o = 7^o3'$ and $\tau = .938$. Thus

$$BT = (14.85 \text{ GHz})\ (64.5 \text{ ns}) = 958 \qquad \text{(Eq. H-44)}$$

As the cone angle decreases, leading to increased directivity, the BT product decreases. As σ increases, leading to increased phase velocity along the structure, the delay time decreases, lowering the BT product as expected.

4. CONICAL SPIRAL ANTENNA

The conical spiral antenna comprises the most general case of log-periodic antennas: the LPDA and the cavity-backed spiral may be considered as special cases of this geometry. The time delay between excitation of the highest and lowest frequencies on the conical spiral is

$$t_1 = \frac{L}{c\ S} \qquad \text{(Eq. H-45)}$$

where L is the allowed axial length of the structure, c is the speed of light, and

$$S = \cos \alpha \cos \theta_o \qquad \text{(Eq. H-46)}$$

is the slowness factor. The angles α and θ_o are the pitch and cone angles, respectively, of the conical spiral. Clearly, for a given L, t will be maximum for smallest S. The slowness factor is related to the ratio of cone radius to wavelength as

$$\frac{A}{\lambda} = \frac{1}{2\pi} \frac{\sin \alpha \cos \theta_o}{1 + S} \qquad \text{(Eq. H-47)}$$

since

$$S \equiv \cos \alpha \cos \theta_o = \frac{k}{\beta} = \frac{v}{c} , \qquad \text{(Eq. H-48)}$$

it is observed that S will be minimum when either α or θ_o is 90°. However, as θ_o is increased, the ratio A/λ becomes smaller. For a fixed minimum radius A_N at the antenna apex this would cause the high frequency limit to become lower thereby decreasing the bandwidth. For this reason α should be made as large as possible while keeping θ_o relatively small. The cone angle cannot be made too small if maximum bandwidth is desired for a given axial antenna length L.

This procedure is as follows. The radii of the cone ends A_N and A_1 are determined. Then for a given L, θ_o may be determined from

$$\theta_o = \tan^{-1} \left(\frac{A_1 - A_N}{L} \right) \qquad \text{(Eq. H-49)}$$

A realizable spiral wrap rate is determined: this fixes α. Next S and A/λ may be found using Equations H-47 and H-48. The highest and lowest frequencies of operation f_N and f_1 may then be determined.

The diameter of the feed cable is again taken to be 0.358 cm. Allowing for some taper in the apex region of the antenna to guarantee a slow wave structure prior to the onset of the highest frequency radiation, the minimum radius at the apex corresponding to this frequency is taken to be

$$A_N = 0.28 \text{ cm} \qquad \text{(Eq. H-50)}$$

The radius of the truncated cone base is determined by the maximum allowed aperture diameter. Since a diameter of 2 meters has been assumed, then

$$A_1 = 1 \text{ meter} \qquad \text{(Eq. H-51)}$$

For a maximum allowable axial antenna length of L = 4 meters the half-cone angle is found from Equation H-49:

$$\theta_o = 14^o \qquad \text{(Eq. H-52)}$$

The wrap rate angle α is taken to be 85°. This choice is somewhat arbitrary and it should be pointed out that a difference of several degrees in the value taken for α will affect the slowness factor and, hence, the BD product, greatly. However, it can be argued that on the basis of the $k_o d - \beta d$ diagram for slow wave structures (see Figure E-2) S can become so small that backfire phasing cannot be maintained. For S = 0, this diagram shows that the backward, broadside, and forward radiation regions become coincident. The antenna radiation, therefore, becomes isotropic in this limit which would tend to make any further increase in the BT product less meaningful.

It follows that

$$S = .084 \qquad \text{(Eq. H-53)}$$

and

$$\frac{A}{\lambda} = .14 \qquad \text{(Eq. H-54)}$$

The highest and lowest operating frequencies are, therefore,

$$f_N = \frac{c}{\lambda_N} = \frac{.14c}{A_N} = 15 \text{ GHz} \qquad \text{(Eq. H-55)}$$

and

$$f_1 = \frac{c}{\lambda_1} = \frac{.14c}{A_1} = .042 \text{ GHz} \qquad \text{(Eq. H-56)}$$

respectively.

The delay time t_1 may be evaluated using Equation H-45,

$$t_1 = 158 \text{ ns} \qquad \text{(Eq. H-57)}$$

There will be an additional time delay, t_2, upon radiation from the last active region due to the finite propagation velocity of electromagnetic waves in free space. This is given by

$$t_2 = \frac{L - P_1}{c} \qquad \text{(Eq. H-58)}$$

where P_1 is the pitch distance of the last spiral turn[1]

$$P_1 = \frac{2A_1}{\tan \theta_o} \sinh\left(\frac{\pi \sin \theta_o}{\tan \alpha}\right) \qquad \text{(Eq. H-59)}$$

Then

$$t_2 = 11.6 \text{ ns} \qquad \text{(Eq. H-60)}$$

[1]See footnote 2, page H-3.

The total time delay is, therefore,

$$T = t_1 + t_2 = 169.6 \text{ ns} \qquad \text{(Eq. H-61)}$$

Since the bandwidth of this antenna is 14.96 GHz, we obtain a BT product of

$$BT = (14.96 \text{ GHz})\ (169.6 \text{ ns}) = 2537 \qquad \text{(Eq. H-62)}$$

Because of approximations involved in setting A_N and α, the value given by Equation H-62 could possibly be several times greater, but it is considered realistic.

In general, one can express the bandwidth and time duration in terms of the antenna parameters as follows. Bandwidth can be written

$$B = f_1\ (B_R - 1) \qquad \text{(Eq. H-63)}$$

Since

$$f_1 = \frac{c}{\lambda_1} = \frac{c}{2\pi A_1}\left[\frac{\sin\alpha\cos\theta_o}{1 + \cos\alpha\cos\theta_o}\right] \qquad \text{(Eq. H-64)}$$

and

$$B_R = \frac{A_1}{A_N} = \frac{L\tan\theta_o + A_N}{A_N}\ , \qquad \text{(Eq. H-65)}$$

where Equations H-47 and H-49 have been used, B can be expressed as

$$B(A_N, L, \theta_o, \alpha) = \frac{c\left(\frac{L\tan\theta_o}{A_N}\right)}{2\pi L\tan\theta_o\left(1 + \frac{A_N}{L\tan\theta_o}\right)}\left[\frac{\sin\alpha\cos\theta_o}{1 + \cos\alpha\cos\theta_o}\right] \qquad \text{(Eq. H-66)}$$

Recalling Equations H-57, H-58, and H-59, the time delay can be expressed

$$T(A_N, L, \theta_o, \alpha) = \frac{L}{c}\left[\frac{1 + \cos\alpha\cos\theta_o}{\cos\alpha\cos\theta_o} - 2\left(1 + \frac{A_N}{L\tan\theta_o}\right)\sinh\left(\frac{\pi\sin\theta_o}{\tan\alpha}\right)\right]$$

(Eq. H-67)

Finally, the product BT is

$$BT(A_N, L, \theta_o, \alpha) = \left(\frac{L\tan\theta_o}{A_N}\right)\left[\frac{1}{2\pi\left(1 + \frac{A_N}{L\tan\theta_o}\right)}\frac{\tan\alpha}{\tan\theta_o} - \frac{1}{\pi\tan\theta_o}\left(\frac{\sin\alpha\cos\theta_o}{1 + \cos\alpha\cos\theta_o}\right)\sinh\left(\frac{\pi\sin\theta_o}{\tan\alpha}\right)\right] \quad \text{(Eq. H-68)}$$

5. CAVITY-BACKED SPIRAL ANTENNA

The geometry[1] of the center of the spiral is the same as the conical spiral, therefore, the high frequency is also the same

$$f_N = 15\ \text{GHz} \quad \text{(Eq. H-69)}$$

The ratio of spiral diameter to wavelength is approximately[2]

$$\frac{D}{\lambda} = .28 \quad \text{(Eq. H-70)}$$

[1] See Appendix F for a discussion of the geometry and some of the properties of the antenna.

[2] This value is based on Equation H-54 to provide maximum slowness. (This D should not be confused with the pulse duration D.)

Using Equation H-70, an estimate of the lowest frequency of operation can be obtained by setting D = 2 meters:

$$f_1 = \frac{c}{\lambda_1} = \frac{.28c}{D} \qquad \text{(Eq. H-71)}$$

$$f_1 = .042 \text{ GHz} \qquad \text{(Eq. H-72)}$$

Therefore, the maximum bandwidth is taken as

$$B = (15 - .042) \text{ GHz} = 14.96 \text{ GHz} \qquad \text{(Eq. H-73)}$$

The time delay between excitation of the lowest and highest frequencies is related to the length, T, of the spiral

$$T = \frac{T}{c} = \frac{R_{MAX} - R_{MIN} \sec \phi}{c} \qquad \text{(Eq. H-74)}$$

where R_{MAX} and R_{MIN} are the maximum and minimum spiral radii and the angle ϕ is related to the tightness with which the spiral is wound, i.e.,

$$\phi = \cot^{-1} (\ln \mu) \qquad \text{(Eq. H-75)}$$

where

$$\mu = \frac{R_{\theta'}}{R_\theta} \qquad \text{(Eq. H-76)}$$

with $\theta' = \theta + \Delta\theta$; $\Delta\theta = 1$ radian. It is seen that sec ϕ increases as $\mu \to 1$, therefore, maximum time delay will be obtained when the spiral is tightly wound. Inherent in Equation H-76 is the spiral arm width, δ, which must be kept small. For very tightly wound spirals, ϕ can approach

$$\phi = 88^\circ\ 51' \qquad \text{(Eq. H-77)}$$

which corresponds to a spiral arm radius increase of about .02 cm over 1 radian. For these values, the spiral length wound over a 2 meter aperture would be

$$T = 49.3 \text{ meters} \qquad \text{(Eq. H-78)}$$

yielding a time delay

$$T = 164 \text{ ns} \qquad \text{(Eq. H-79)}$$

The maximum BT product for the cavity-backed spiral is, therefore,

$$BD = (14.96 \text{ GHz})\ (164 \text{ ns}) = 2453 \qquad \text{(Eq. H-80)}$$

6. SUMMARY

Maximum BT products for each of the three antennas show some variation as expected. However, it is somewhat surprising that the variation is as slight as has been found here. It can be seen that for a given set of antenna parameters the BT product may be increased in two ways. B can only be significantly increased by raising the highest operating frequency: lowering the lowest operating frequency does not significantly change the bandwidth if it has already been maximized for a given volume. However, the duration T will be increased if the lowest frequency is lowered further: raising the highest frequency does not significantly increase the duration when antenna parameters are fixed. A thorough evaluation of BT product variation is given in Appendix G.

APPENDIX I

A NEAR-ZONE EVALUATION PROCEDURE AND SOME OF ITS RESULTS

1. INTRODUCTION

The objective of electromagnetic pulse compression in the present study is to intensify radiated power density in the far-zone radiation. Angular compressions of a radiated field are usually accomplished by appropriate source distributions on a large antenna aperture. Since the angular compressions are presently of no immediate concern, antennas of large apertures will not be discussed. Instead, only antennas of predominantly dipole modes are chosen for pulse compression in the radiation direction. The antenna element used for this study is an electromagnetic dipole* that has an axially symmetric cardioid pattern with peak field intensity twice the value of a corresponding electric dipole in free-space.

The desired pulse compression is produced by a number of electromagnetic dipoles covering a specified bandwidth of the pulse. Radiations from these dipoles are delayed in an appropriate manner so that their fields in the far zone would produce an intensified short pulse. In other words, these dipoles are arranged to give rise to a dispersive antenna which can be treated as a spatial filter. When such a dispersive filter is driven by an appropriate pulse of long duration, matched-filter techniques can be employed to produce an intensified pulse of extremely short duration depending on the total dispersion duration and antenna bandwidth.

---

*Yu, Jiunn S. and H. A. Morimoto, "Electromagnetic Dipole," Tech. Infor. Series No. R71 EMH3, G.E. Co., Jan. 1971; or IEEE Symposium Digest of 1971 IEEE G-AP International Symposium at Los Angeles, California.

Assuming that optimal pulse compression is achieved in the far-zone of radiation, there arises a question as to what would be the corresponding near-zone pulse shape and peak intensity. The following outlines certain formulations of near-zone compressed fields at various distances from the antenna. Numerical results are to be extensively given first. Conclusions will be drawn after all cases are treated.

2. A NEAR-ZONE FORMULATION OF DIPOLE ARRAY

It is well known that near-zone radiations depend on antenna configurations. The dipole array to be used here approximates closely a log-periodic antenna that is fed from a common terminal. The phase centers of radiating elements are presently assumed at the common feedpoint.

For a short electric dipole, the general expression of maximum electric field induced by a given current I is

$$E(r,f) = -j(d/2\lambda_o)(\mu_o Ic/r)[1-(2\pi fr/c)^{-2} - j(2\pi fr/c)^{-1}]\exp(-j2\pi fr/c) \quad \text{(Eq. I-1)}$$

$$\mu_o c \approx 120\,\pi \text{ Ohms} \quad \text{(Eq. I-2)}$$

where r is the distance between point of observation and point of radiation. The minus sign designates the sense of electric field referred to that of the current. For a half-wave dipole of consinusoidal current distribution, the average dipole length can be assumed to be $2/\pi$, and the fields due to half-wave dipole are approximated as

$$E(r,f) = -j\,60(I/r)[1-(2\pi fr/c)^{-2}\; j(2\pi fr/c)^{-1}]\exp(-j2\pi fr/c),\ V/m \quad \text{(Eq. I-3)}$$

where I now stands for the maximum value of consinusoidal distribution.

It is noted that an electric dipole radiates omnidirectionally in the plane perpendicular to the dipole, but most broad band antennas in practice radiate unidirectionally. To approximate the radiation elements of these antennas, a balanced electromagnetic dipole radiating an axially symmetric cardioid pattern is used. The maximum electric field of this antenna is known to be approximately

$$E(r,f) = -j(120(I/r)[1-0.5(2\pi fr/c)^{-2} - j(2\pi fr/c)^{-1}] \exp(-j2\pi fr/c) \quad \text{(Eq. I-4)}$$

Assuming I has a zero phase, this field in the far-zone ($r \to \infty$) would be $-j120(I/r)\exp(-j2\pi fr/c)$. Neglecting the time-delay r/c, the phase angle of the electric field lags $\pi/2$ in phase when referred to that of I. Since this phase angle is the same for all active elements, it can be neglected without loss in generality.

Let the spectral density I of a dispersive antenna be

$$I(f) = \left(0.54 + 0.46 \cos\frac{\pi(f-f_o)}{(f_h-f_o)}\right)^p \exp(j\phi(f)) \quad \text{(Eq. I-5)}$$

where the exponent p is used to alter the relative distribution of current within the bandwidth to which the center frequency is designated, and the total bandwidth is $2(f_h-f_o)$ where f_h is the high-end cutoff frequency. If the antenna can be driven by an impulse, the radiated dispersive pulse at a far-zone point r_o can be written as

$$E(r_o,f,p) = -j(120/r_o)\left[0.54 + 0.46 \cos\frac{\pi(f-f_o)}{(f_h-f_o)}\right]^p \exp(j\phi(f)) \cdot [1-0.5(2\pi fr_o/c)^{-2} - j(2\pi fr_o/c)^{-1}] \exp(-j2\pi fr_o/c) \quad \text{(Eq. I-6)}$$

If the antenna is driven by matched filter techniques, the compressed pulse at the far-zone point r_o is proportional to

$$|E(r_o,f,p)| = (120/r_o)\ [0.54 + 0.46\ \cos\frac{\pi(f-f_o)}{(f_h-f_o)}\ ]^{2p}\ .$$

$$\cdot[\{1-0.5\ (2\pi f r_o/c)^{-2}\}^2 + (2\pi f r_o/c)^{-2}] \qquad \text{(Eq. I-7)}$$

Finally, the compressed pulse at an arbitrary field point r can be written as

$$E(r,f,r_o,p,k) = k\ |E(r_o,f)|^2\ E(r,f)/E(r_o,f) \qquad \text{(Eq. I-8)}$$

3. COMPRESSED PULSES OF A DIPOLE ARRAY

Making use of $k = 10^{-8}$, $r_o = 100$ m, and $0.2 \leq f\ (GHz) \leq 10.2$ for Equation I-8, the compressed pulse spectral density (volt·sec/m) in the far-zone is shown in Figure I-1 for r = 100 m and p = 1/2. The corresponding time-domain pulse (volt/m) is given in Figure I-2. When p = 1, the positive time-sidelobes in Figure I-4 become higher than those in Figure I-2. For p = 1/4 in Figure I-6, the negative time-sidelobes decay gradually. It is from the comparison among Figures I-2, I-4, and I-6 that one considers the compressed pulse in Figure I-2 as an optimal case.

Figures I-8, I-10, and I-12 are compressed pulses at a field point r = 1 m from the dispersive antenna apex. Comparisons of these pulses with those in Figures I-2, I-4, and I-6 demonstrate that r = 1 m can be adequately considered as a far-zone point, because no great distortions of pulses have taken place. In CW considerations, the lowest frequency 0.2 GHz can be used to establish the well known far-zone criterion $2D^2/\lambda$. Let the aperture dimension be $D = \lambda/2$, the result is $\lambda/2$ or 0.75 m as the minimum far-zone criterion for the frequency range of interest. Therefore, the transient far-zone criterion can be established by choosing the lowest frequency component and then applying the formula $2D^2/\lambda$.

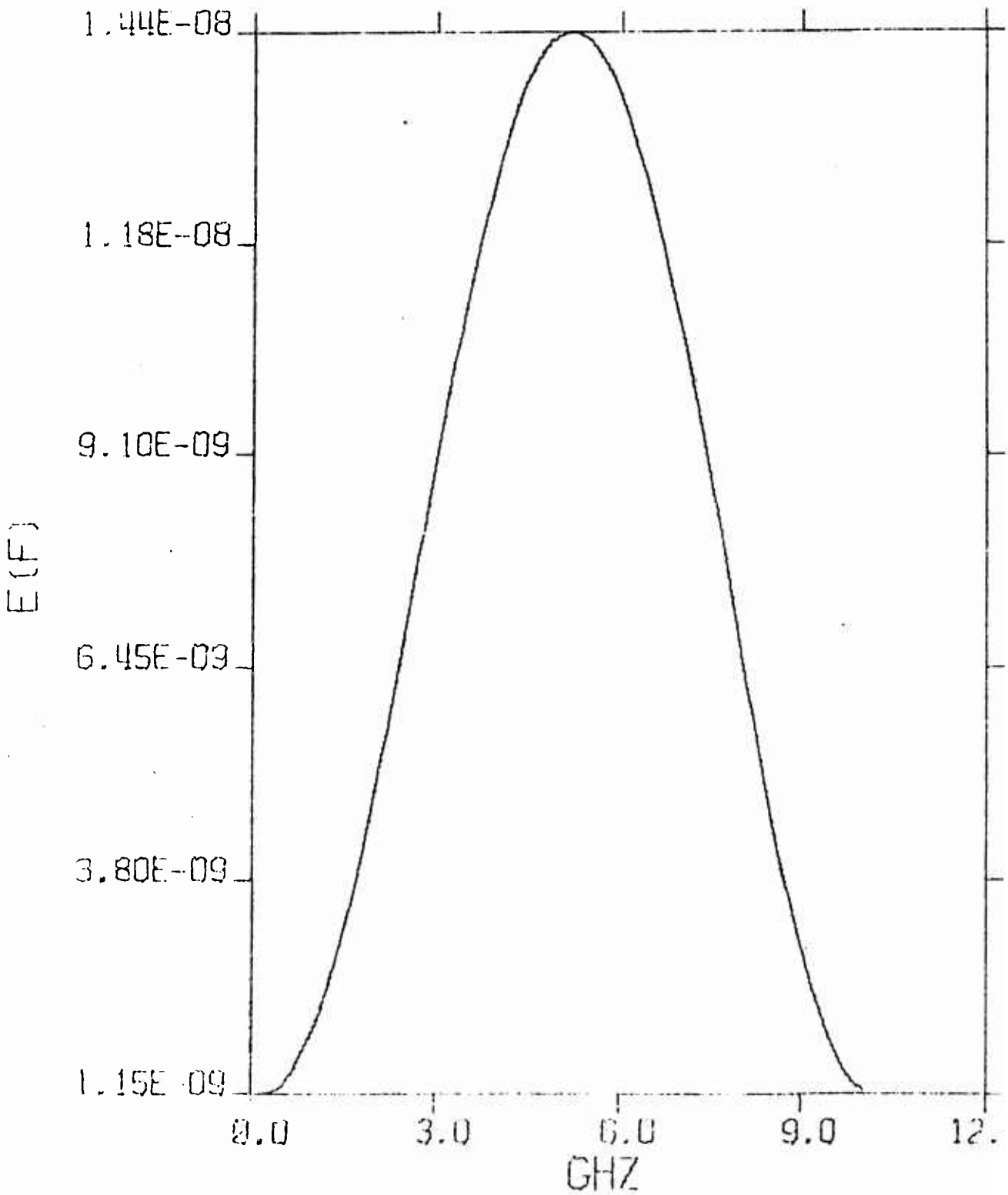


Figure I-1. Spectral Density E(r, f, r_o, p, k) X 1.2 with r = 100 m, and p = 1/2

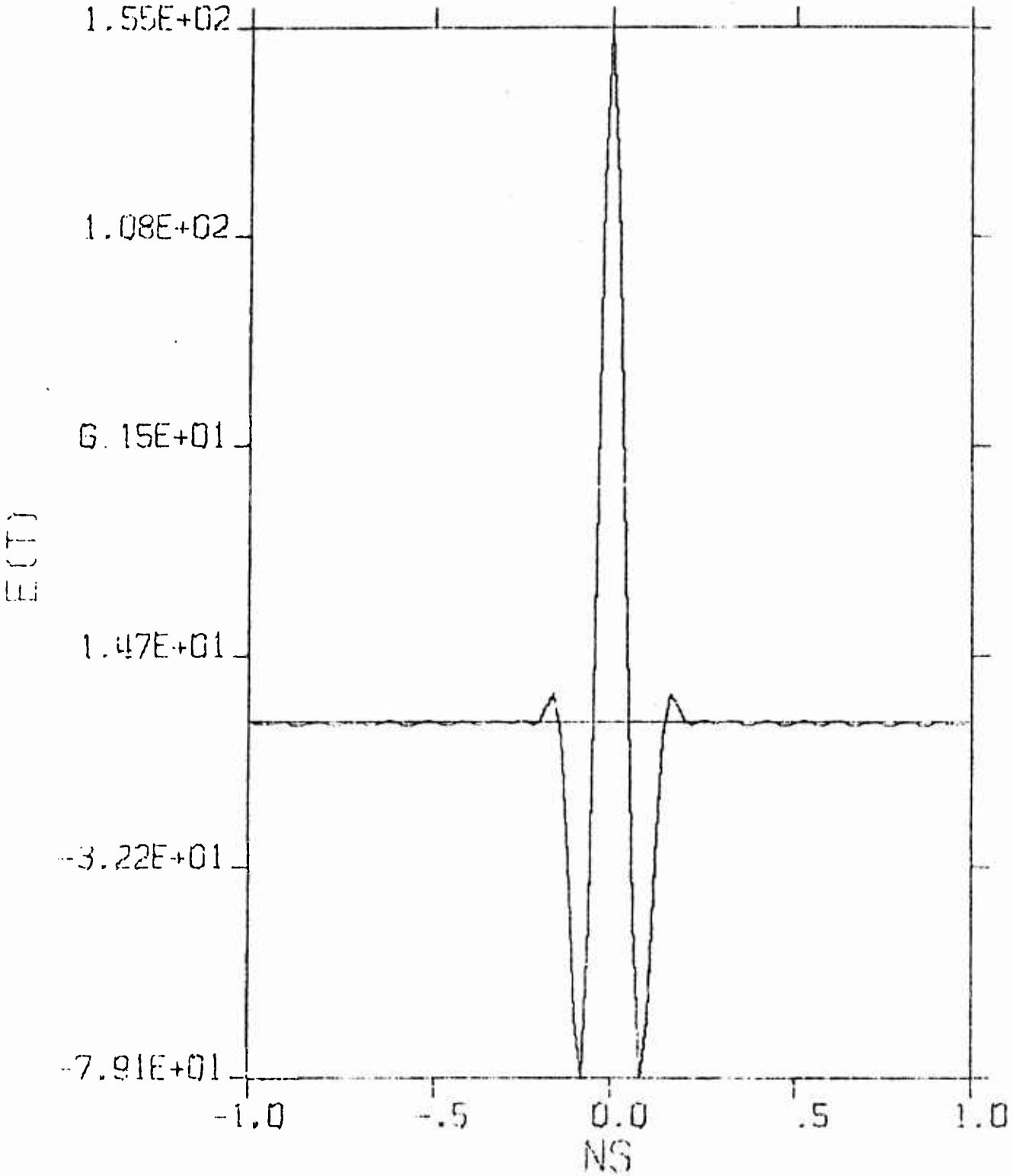


Figure I-2. Compressed Pulse of Spectrum in Figure I-1

Figures I-14, I-16, and I-18 are compressed pulses at r = 0.1 m which can no longer be considered in the far zone, because it is less than $2D^2/\lambda$ for lower frequencies. Clearly, the pulses are distorted as a result.

Greater distortions can be observed in Figures I-19 through I-36 where the field point r approaches closer to the antenna apex. Not only the pulses are more widely dispersed than those in the far-zone, the amplitudes increase with reversals in polarity.

Figures I-37 and I-38 summarize the near-zone compressed pulses from r = 0.015 m to 1.00 m.

4. PULSE COMPRESSION INCLUDING HIGHER-ORDER MODES

Pulse compression has been treated in the previous sections with dipole modes alone. The results have been recognized to be a good approximation only at distances greater than one-half wavelength. In order to formulate the near-zone field more accurately, two techniques can be used. One is the well known Fresnel's approximation technique that assumes current distributions on an antenna. The other is using spherical modes that include dipoles, quadrapoles, and octupoles, etc. Presently, the latter techniques are chosen for the near-zone field formulation.

A pair of balanced electric and magnetic currents is shown in Figure I-39. Only the electric field perpendicular to the y-z plane is discussed here. By following the conventional coordinates systems, this corresponds to the x component of the electric field that can be obtained as

$$E_x = \frac{-2I\eta_o}{3b_1^c(\rho_c)\lambda_o s_o} \sum_{n=1}^{3} \left[b_n^c(\rho_o)\zeta_n(s_o)q_n(\theta) + jb_n^c(\rho_o)\zeta_n'(s_o)p_n(\theta) \right] \quad \text{(Eq. I-9)}$$

$$\rho_o = 2\pi a/\lambda_o \qquad \text{(Eq. I-10)}$$

$$s_o = 2\pi r/\lambda_o \qquad \text{(Eq. I-11)}$$

$$b_n^c(\rho_o) = \frac{-\psi_n'(\rho_o)}{\zeta_n'(\rho_o)} \qquad \text{(Eq. I-12)}$$

$$\zeta_n'(\rho) = \frac{d}{d\rho}\{\rho[j_n(\rho) - jy_n(\rho)]\} \qquad \text{(Eq. I-13)}$$

$$\psi_n'(\rho) = \frac{d}{d\rho}\{\rho j_n(\rho)\} \qquad \text{(Eq. I-14)}$$

$$p_n(\theta) = \frac{(2n+1)\, P_n'(\cos\theta)}{n(n+1)\sin\theta} \qquad \text{(Eq. I-15)}$$

$$q_n(\theta) = \frac{(2n+1)}{n(n+1)} \frac{d}{d\theta} P_n'(\cos\theta) \qquad \text{(Eq. I-16)}$$

where η_o and λ_o are free-space wave impedance and wavelength, 2a is the length of the current elements, r is the distance of the field point, and b_n^c are electric modal coefficients of orders 1 to 3. Corresponding magnetic model coefficients are set equal to b_n^c by assuming balanced radiation of axially symmetric cardioid. The function j_n and y_n are spherical Bessel functions, and P_n' are associated Legendre functions. The current I is used for peak value under the assumption that each resonant dipole has an average length of λ_o/π.

By including only the dipole mode b_1^c in Equation I-9, the amplitude and phase of the E-field is shown in Figure I-40. This complex spectral distribution is used to obtain the compressed pulses shown in Figures I-1 through I-36. If all the modes (b_1^c, b_2^c, b_3^c) are included, the electric field of Equation I-9 in the near-zone has a considerably higher amplitude than that of using b_1^c alone. A comparison of these two results is given in Figure I-41. Since the difference is about a constant ratio for r/λ_o larger than 0.25, it is considered a good approximation when

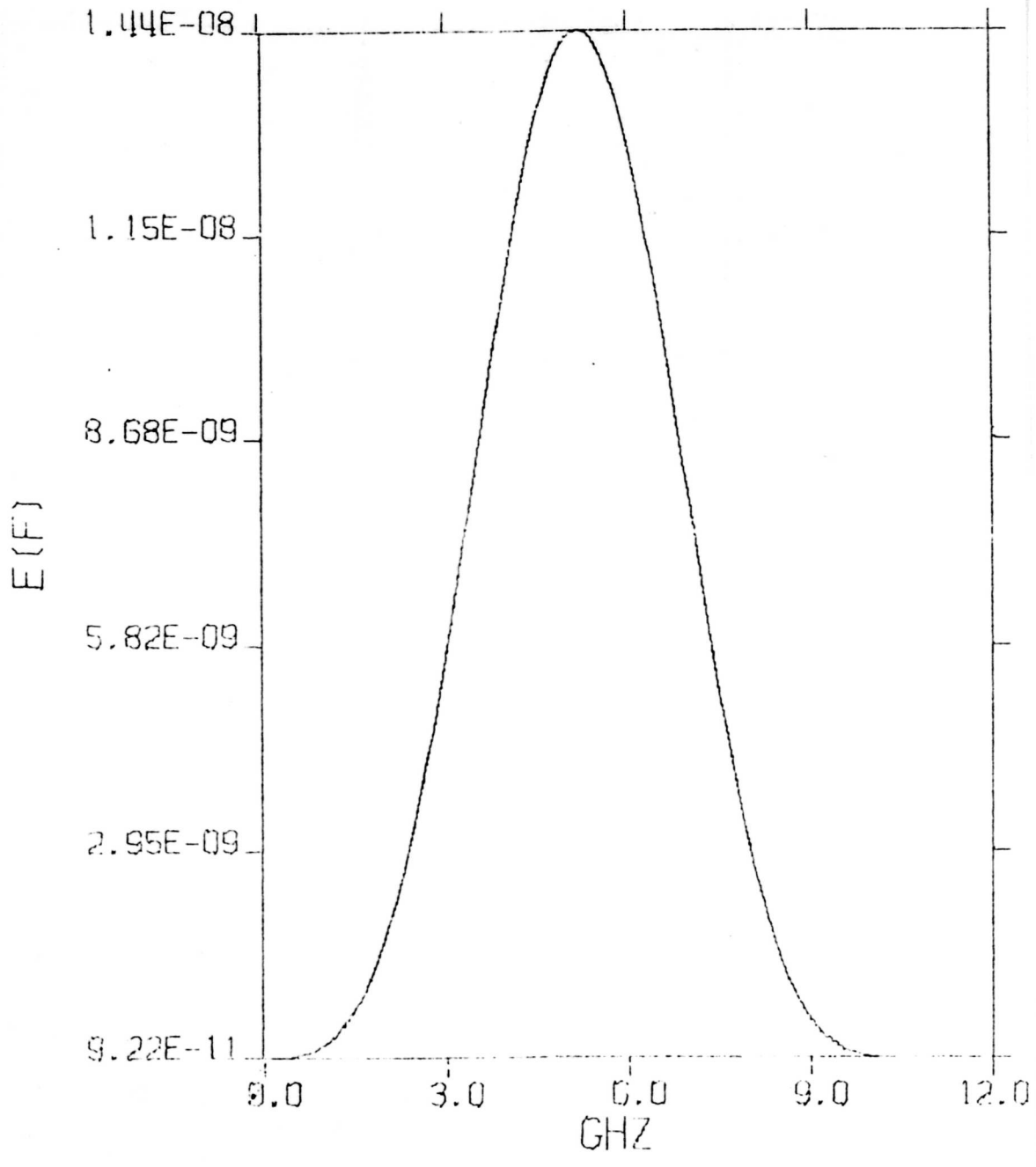


Figure I-3. Spectral Density E(r, f, r_o, p, k) X 1.2
With r = 100 m, and p = 1

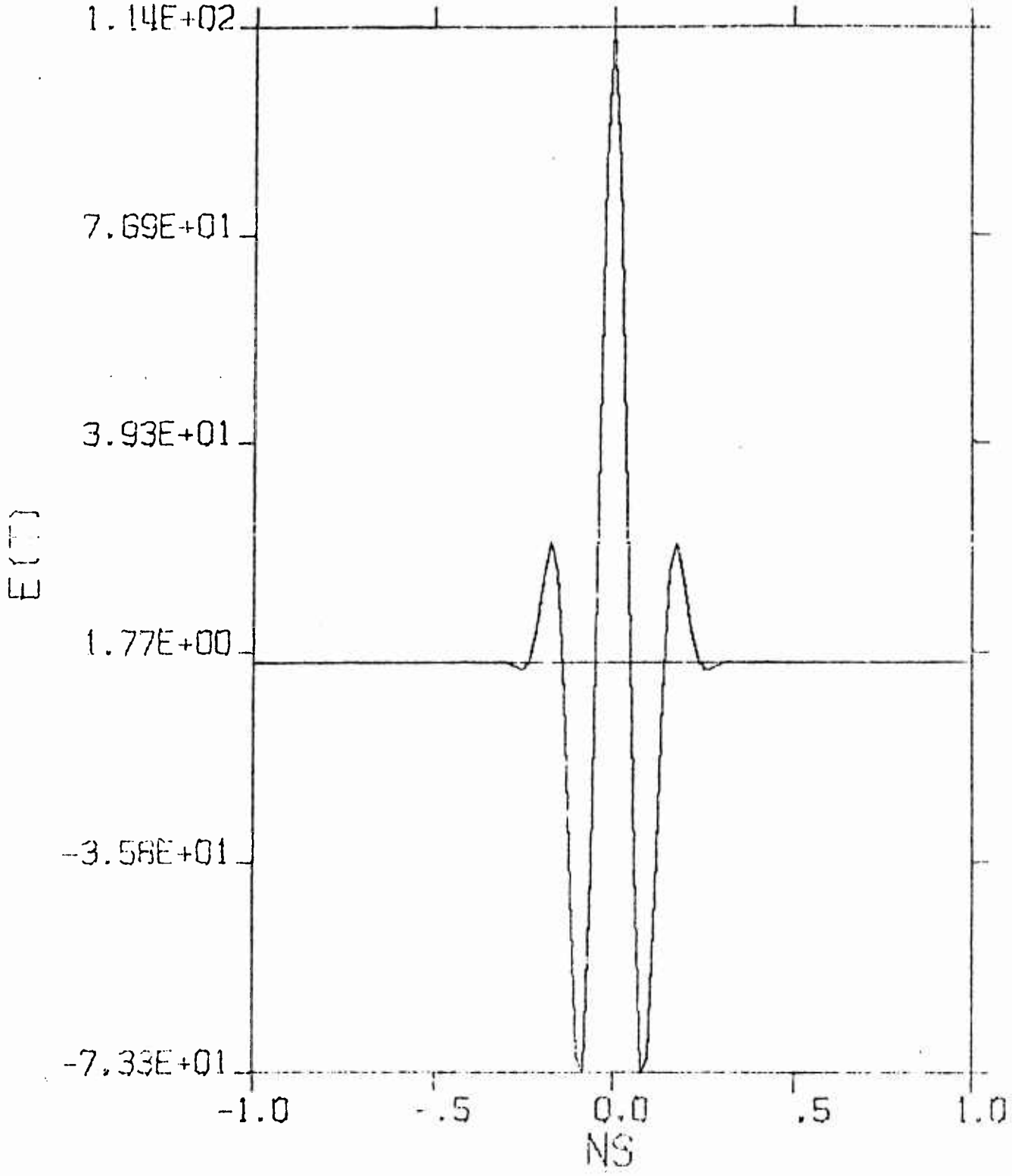


Figure 1-4. Compressed Pulse of Spectrum in Figure 1-3

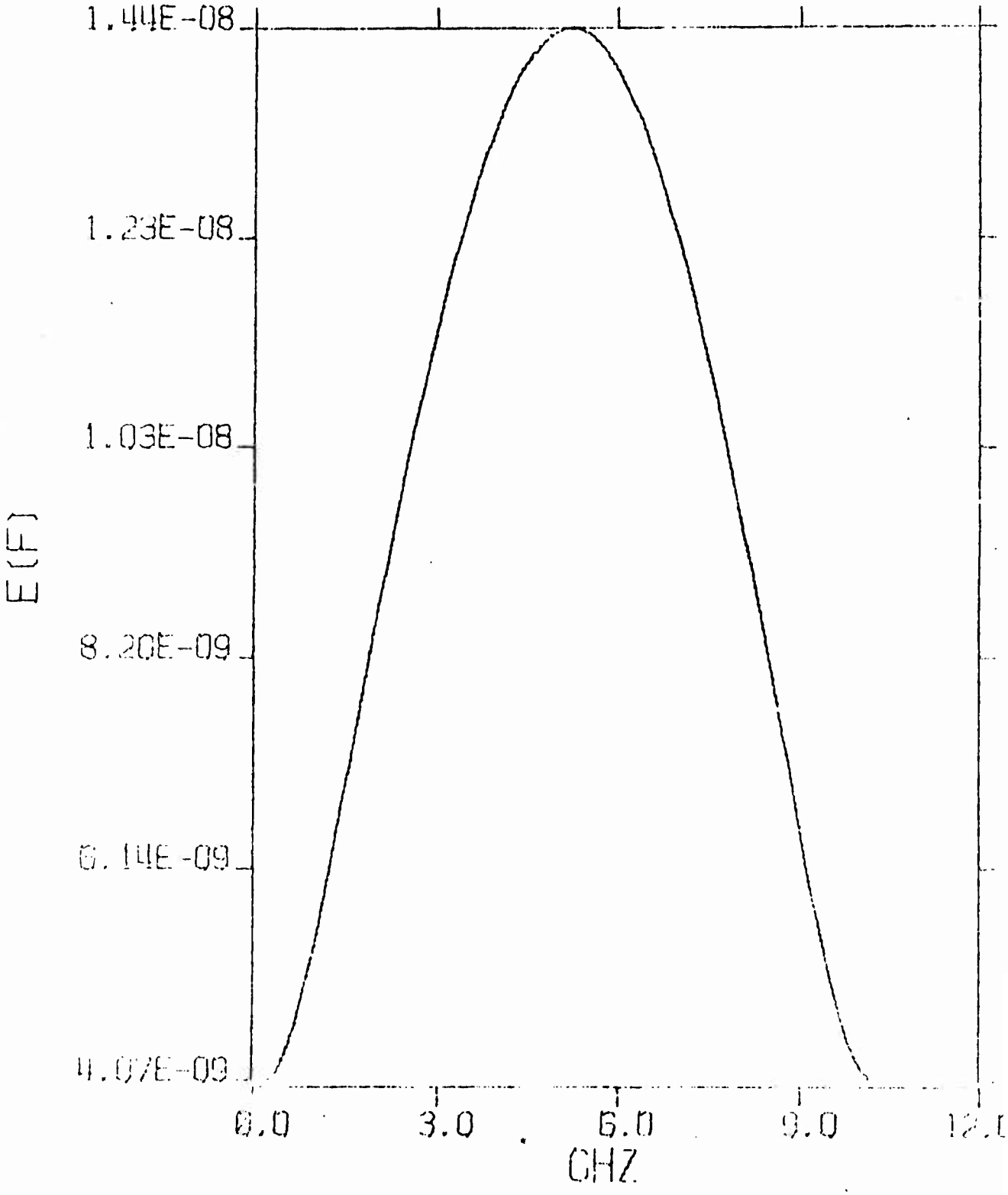


Figure I-5. Spectral Density E(r, f, r_o, p, k) X 1.2
With r = 100 m, and p = 1/4

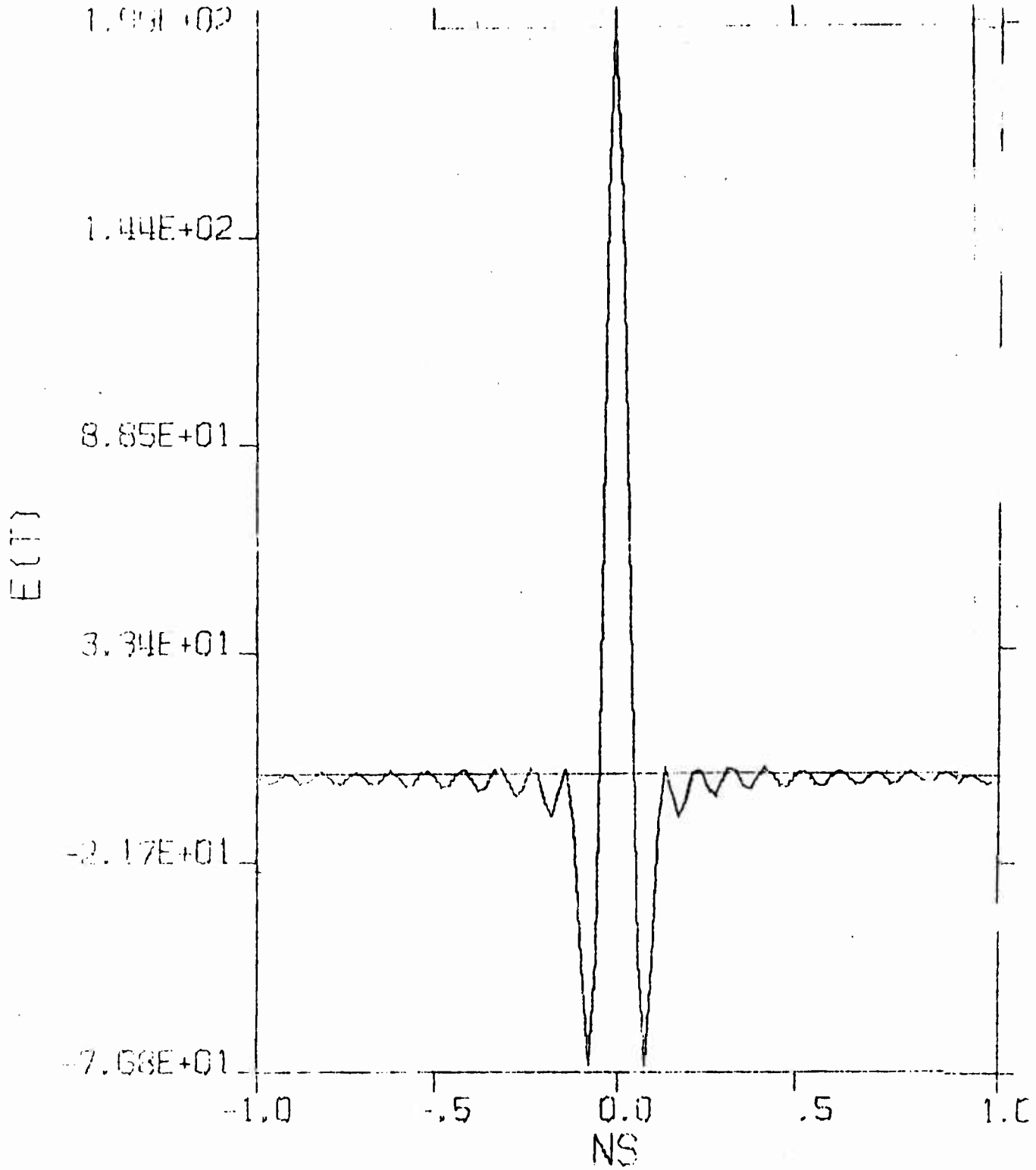


Figure 1-6. Compressed Pulse of Spectrum in Figure 1-5

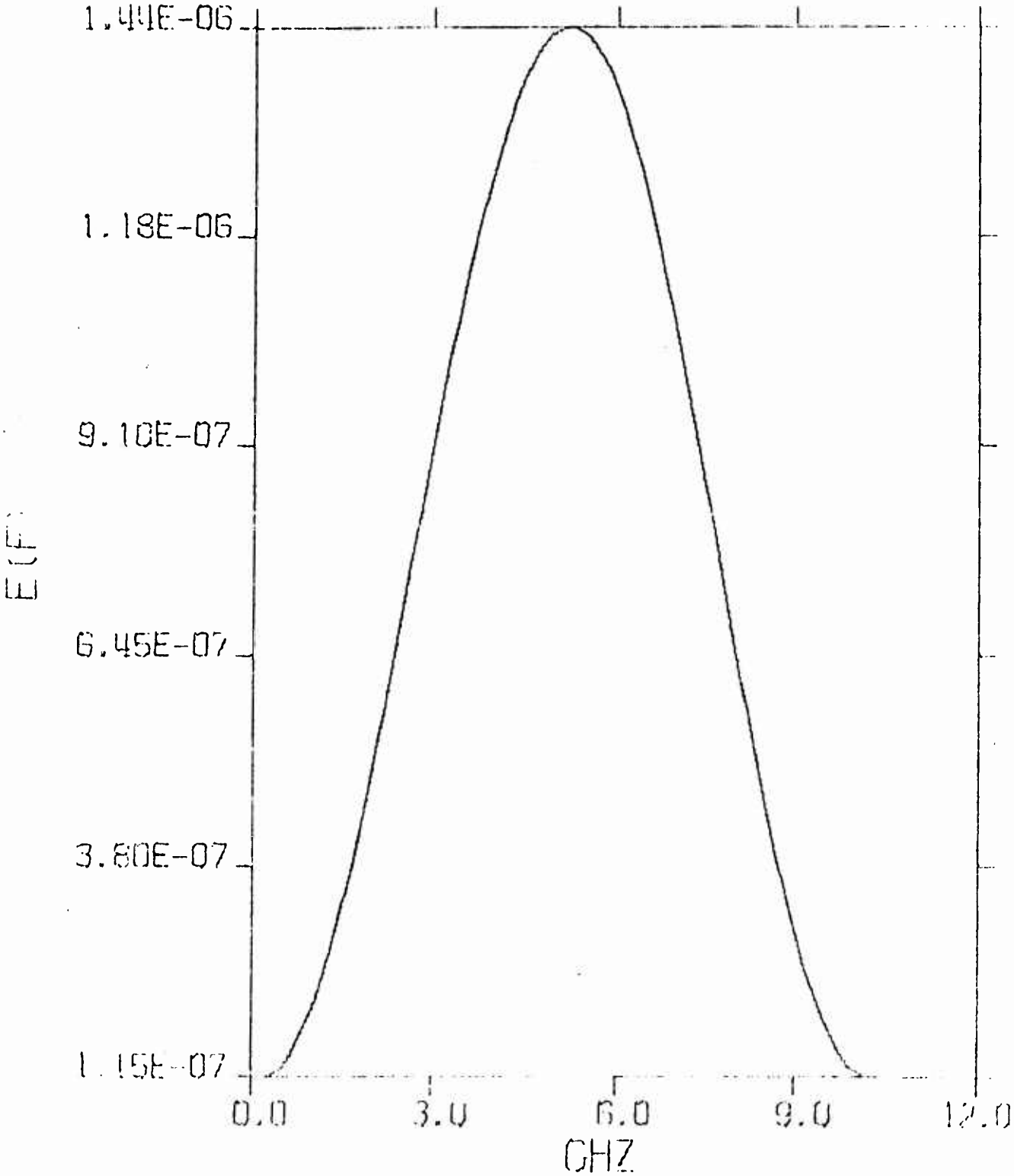


Figure I-7. Spectral Density E(r, f, r_o, p, k) X 1.2
With r = 1 m, and p = 1/2

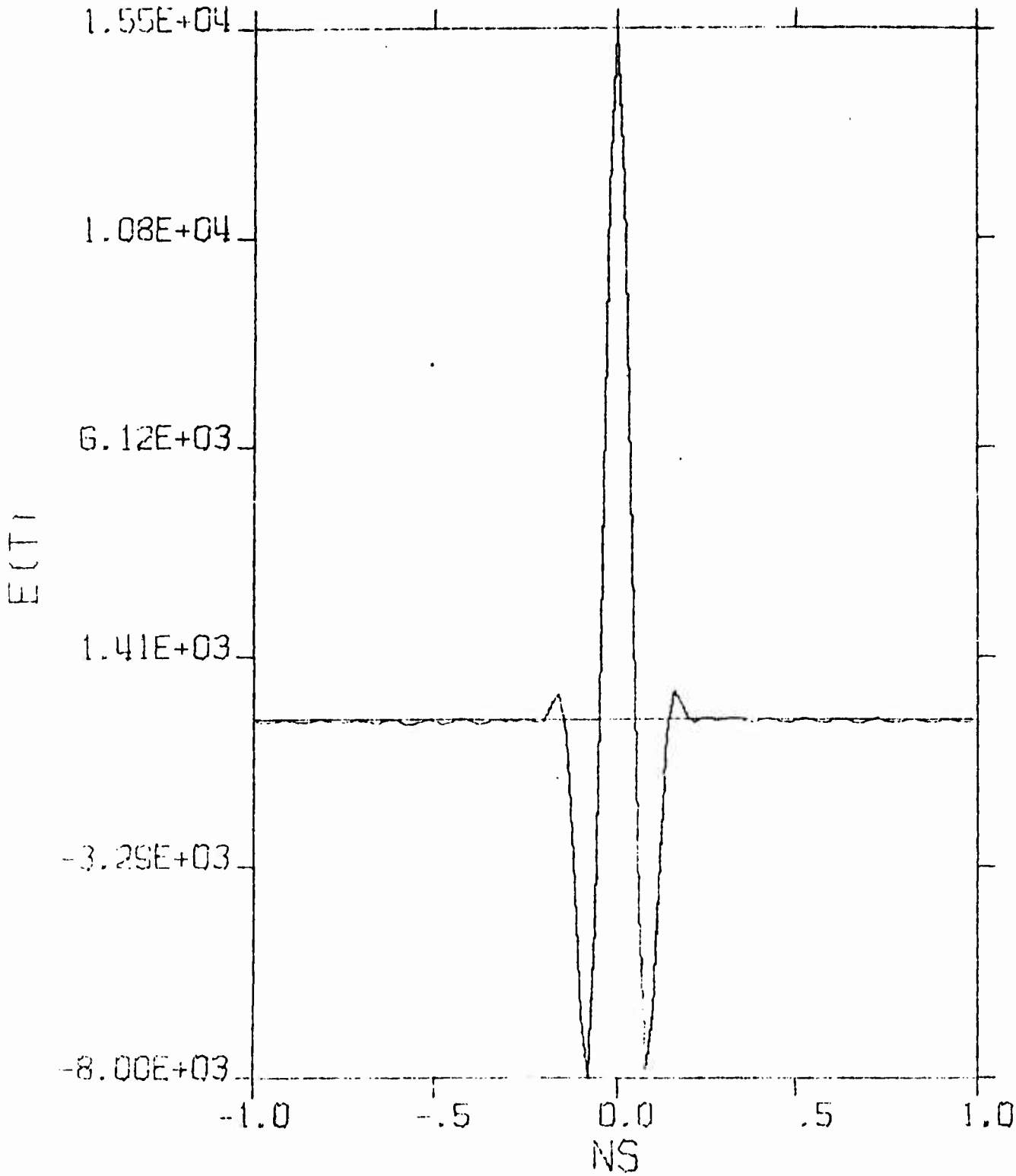


Figure 1-8. Compressed Pulse of Spectrum in Figure 1-7

Reproduced from best available copy.

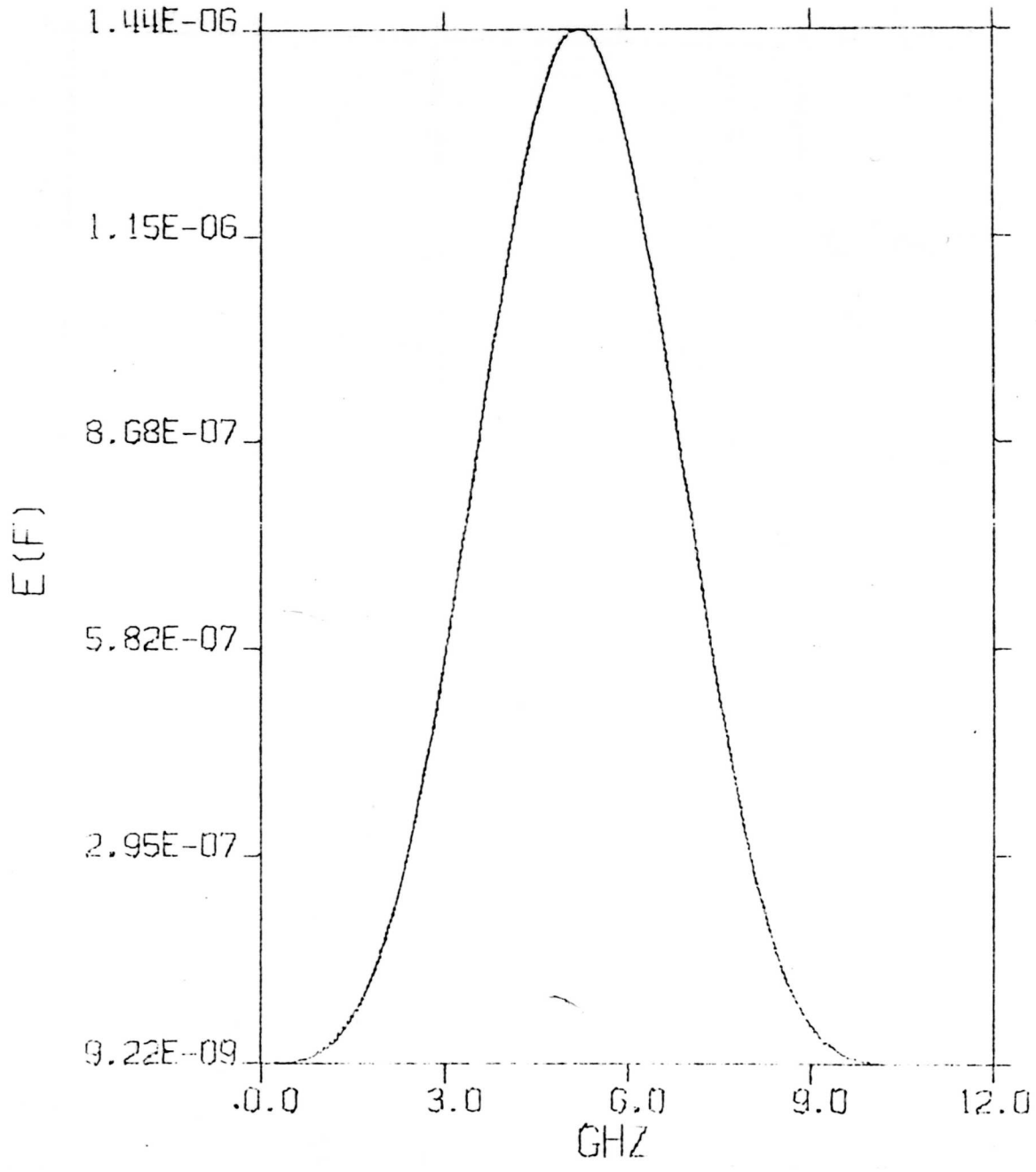


Figure I-9. Spectral Density E(r, f, r_o, p, k) X 1.2 With r = 1 m, and p = 1

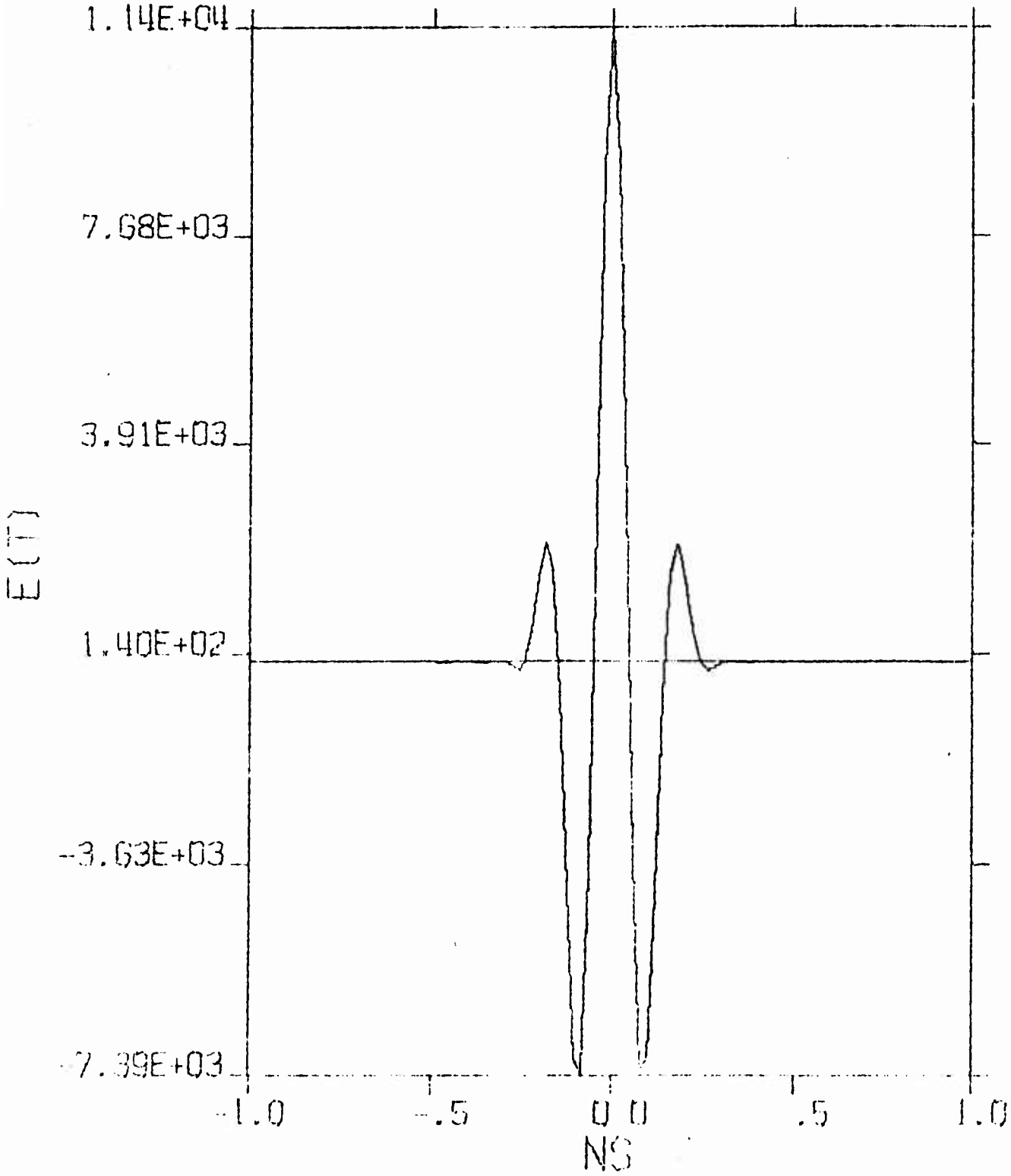


Figure I-10. Compressed Pulse of Spectrum in Figure I-9

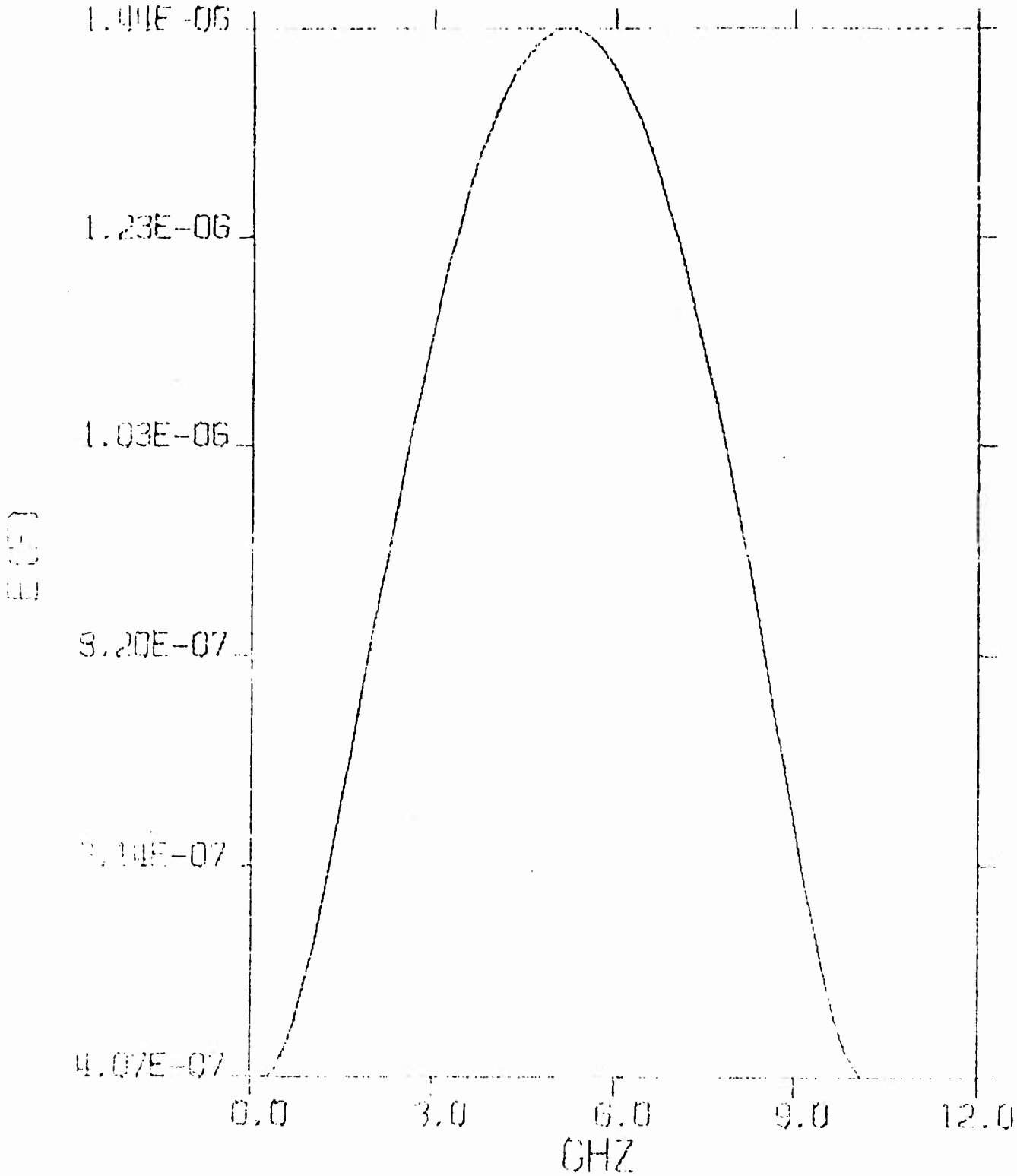


Figure 1-11. Spectral Density E(r, f, r_o, p, k) X 1.2
With r = 1 m, and p = 1/4

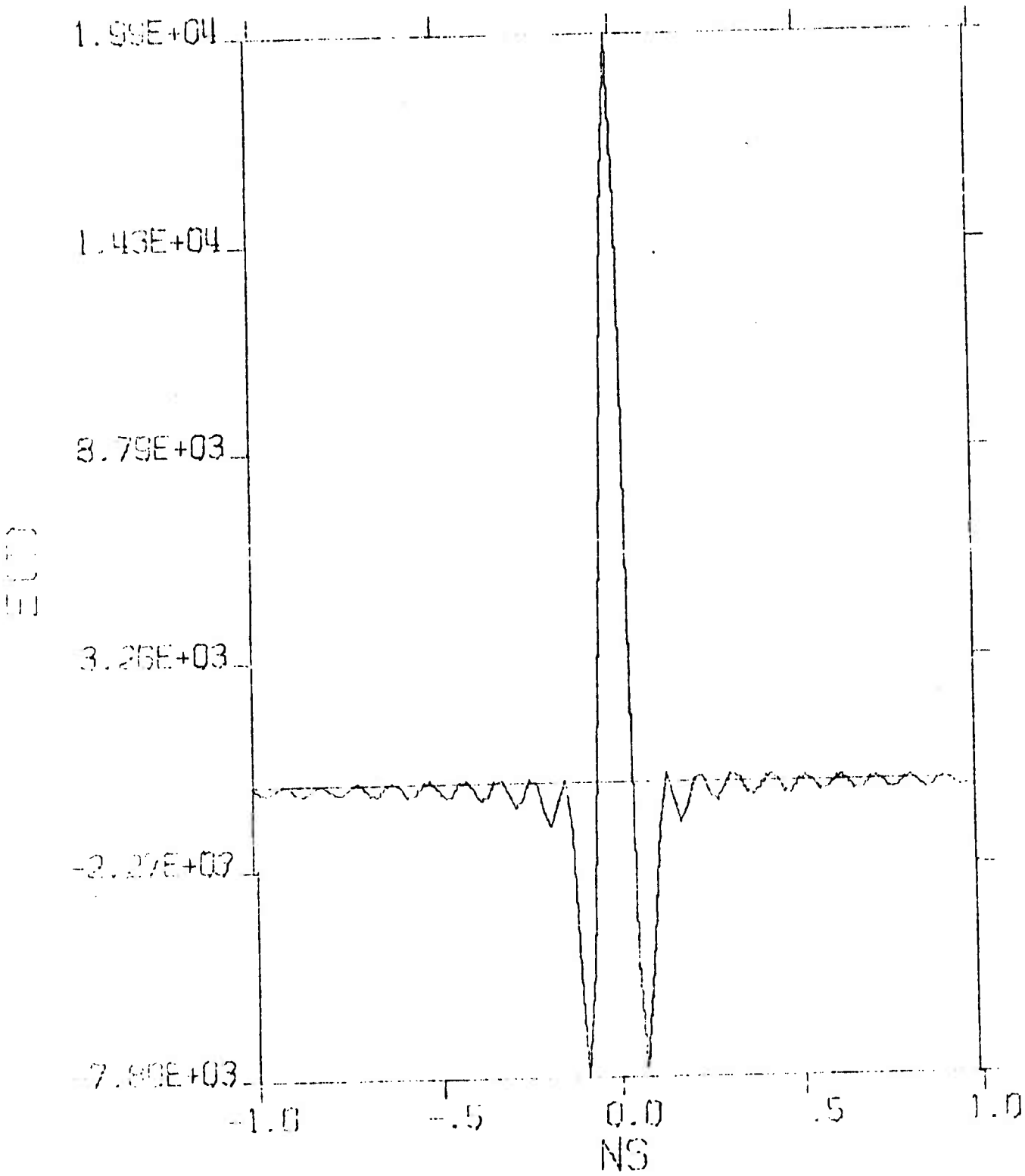


Figure I-12. Compressed Pulse of Spectrum in Figure I-11

Reproduced from best available copy.

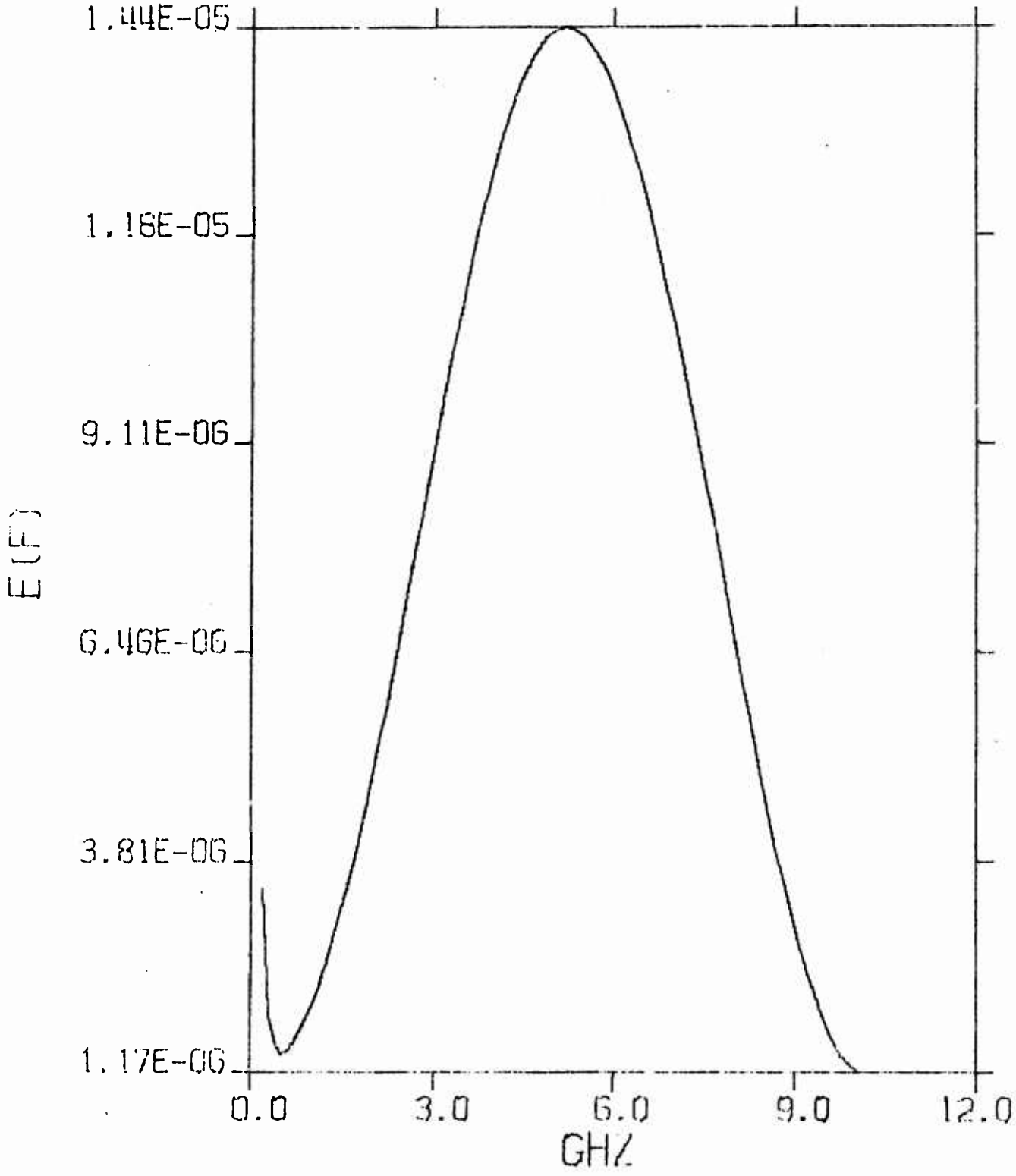


Figure I-13. Spectral Density E(r, f, r_o, p, k) X 1.2
With r = 0.1 m, and p = 1/2

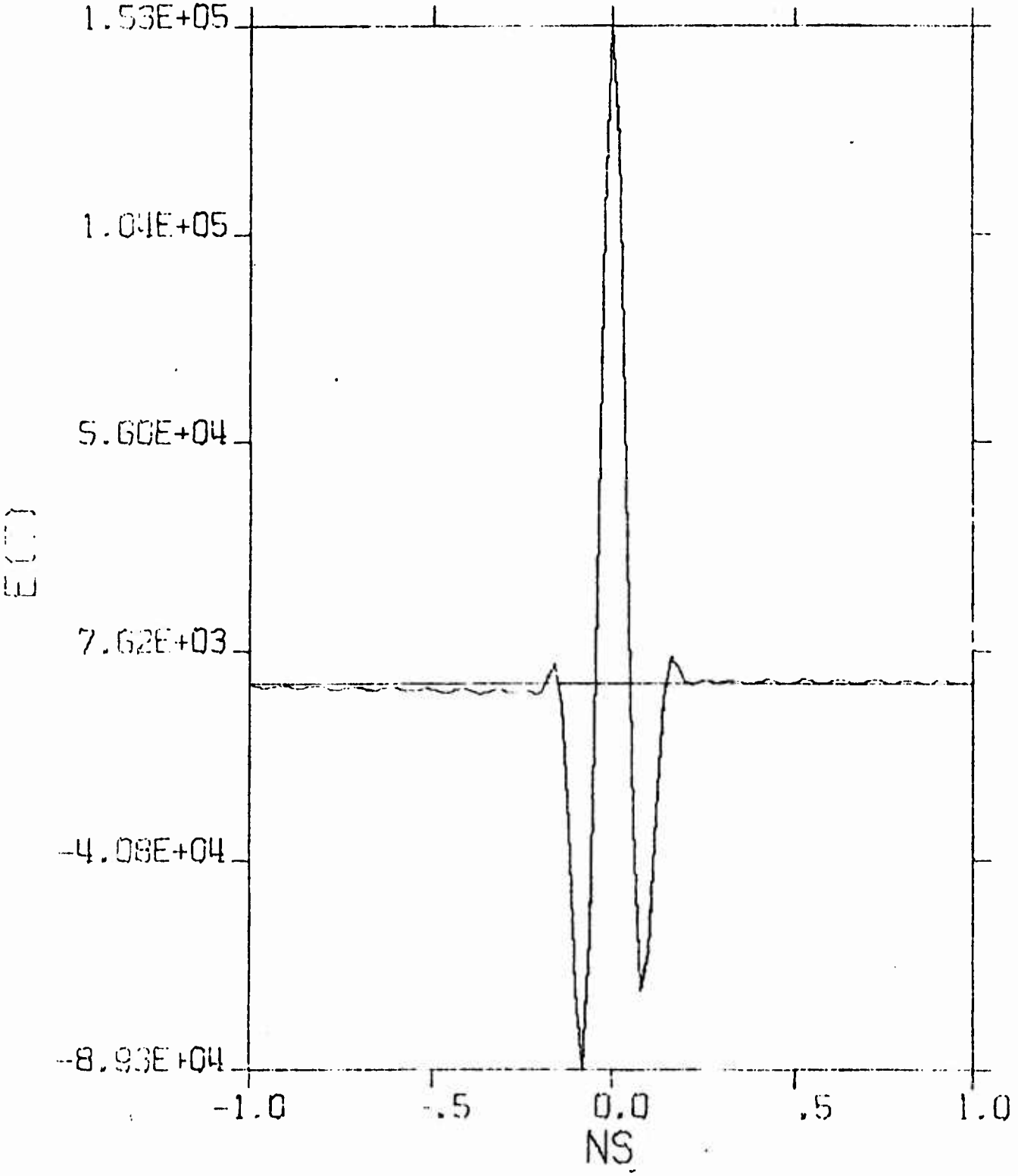


Figure 1-14. Compressed Pulse of Spectrum in Figure 1-13

Reproduced from best available copy.

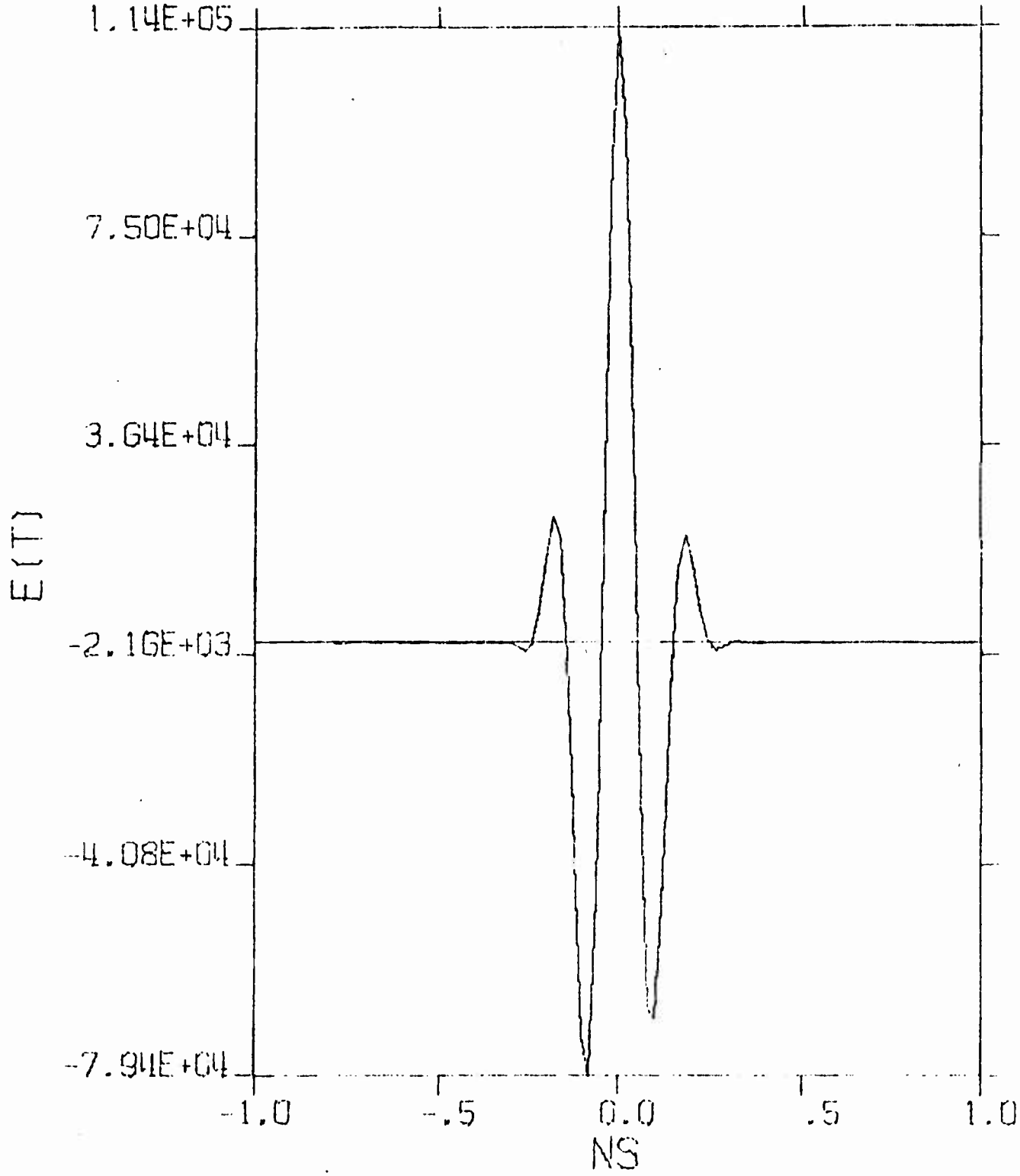


Figure I-15. Spectral Density E(r, f, r_o, p, k) X 1.2
With r = 0.1 m, and p = 1

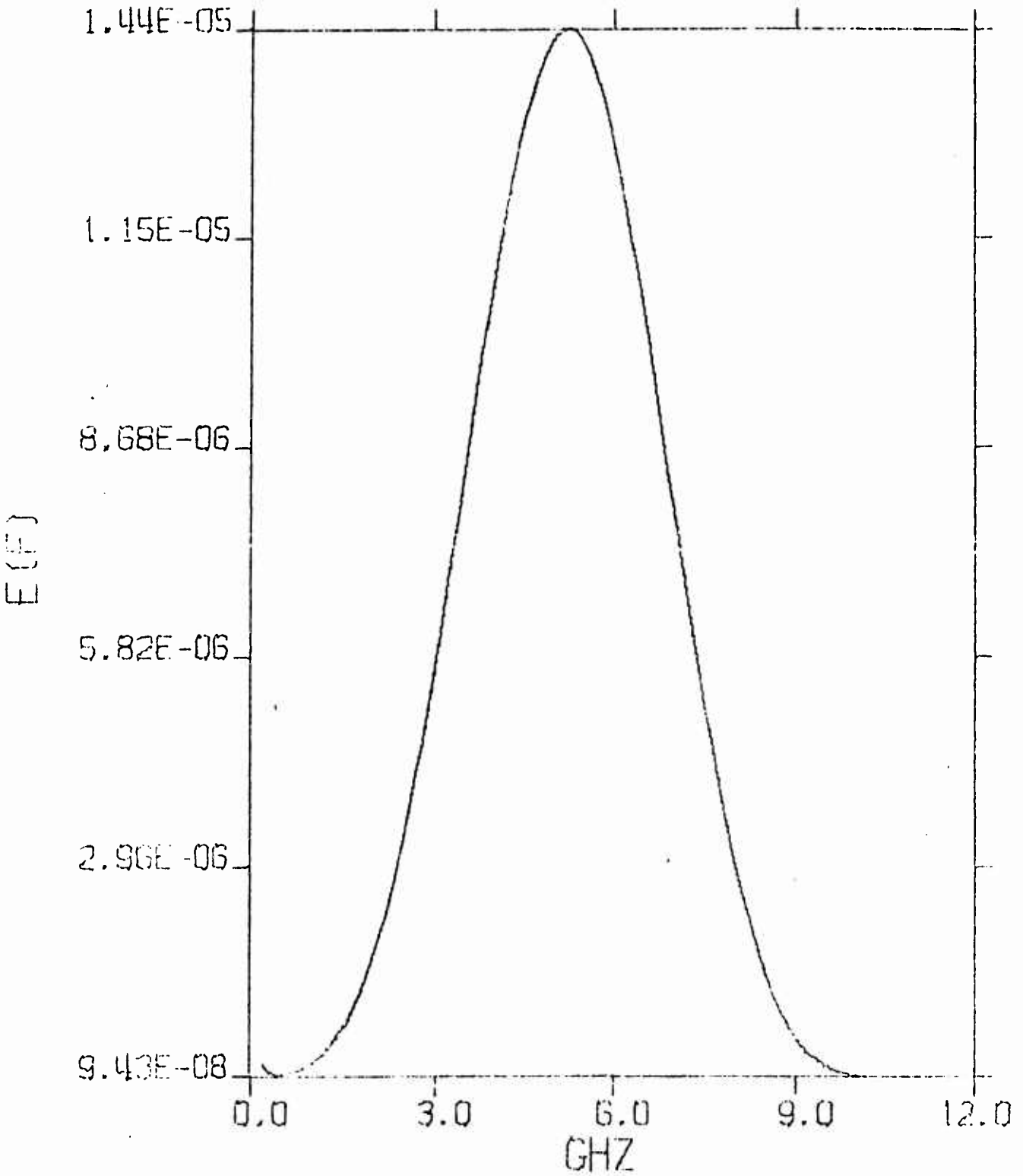


Figure 1-16. Compressed Pulse of Spectrum in Figure 1-15

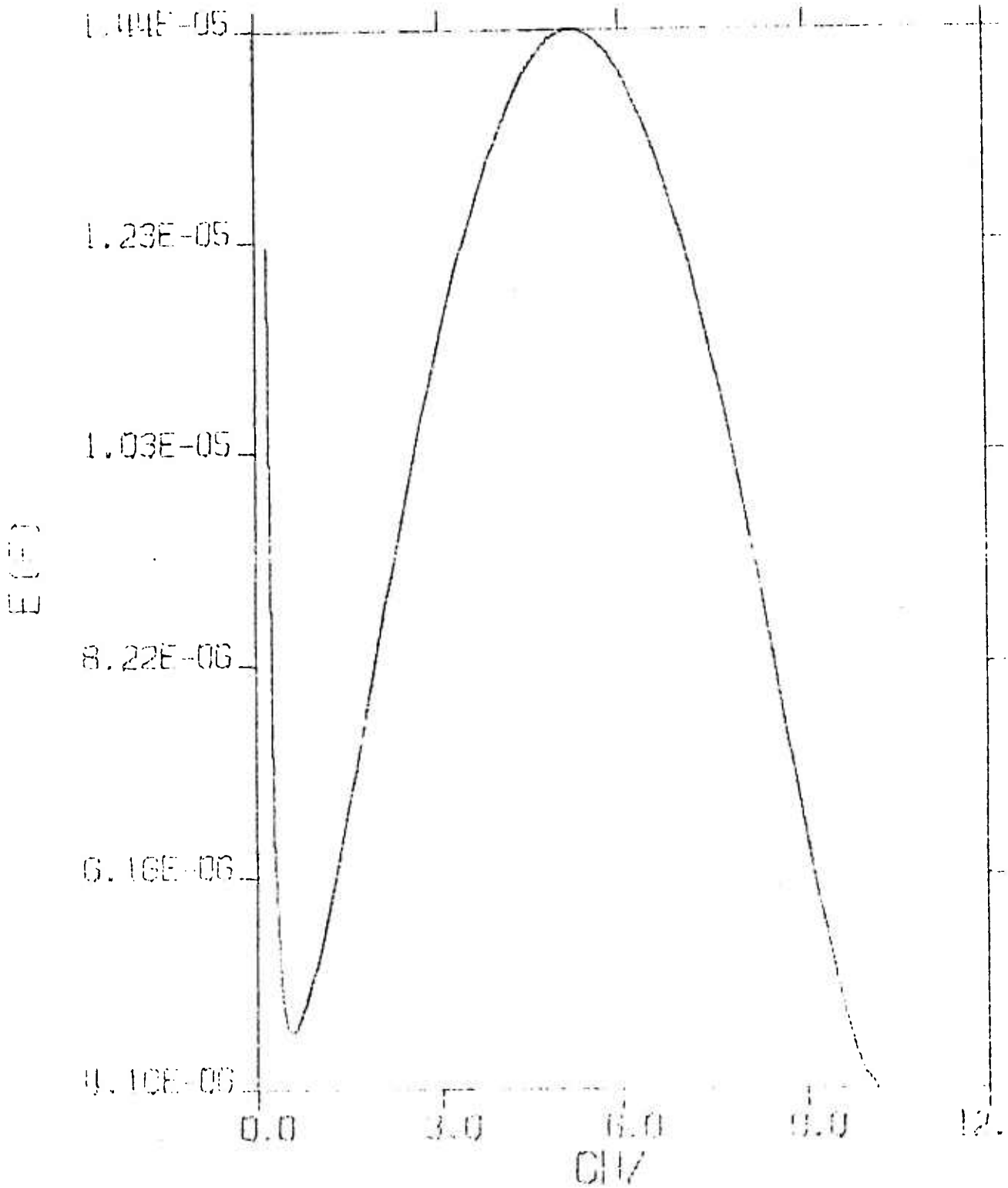


Figure I-17. Spectral Density E(r, f, r_o, p, k) X 1.2
With r = 0.1 m, and p = 1/4

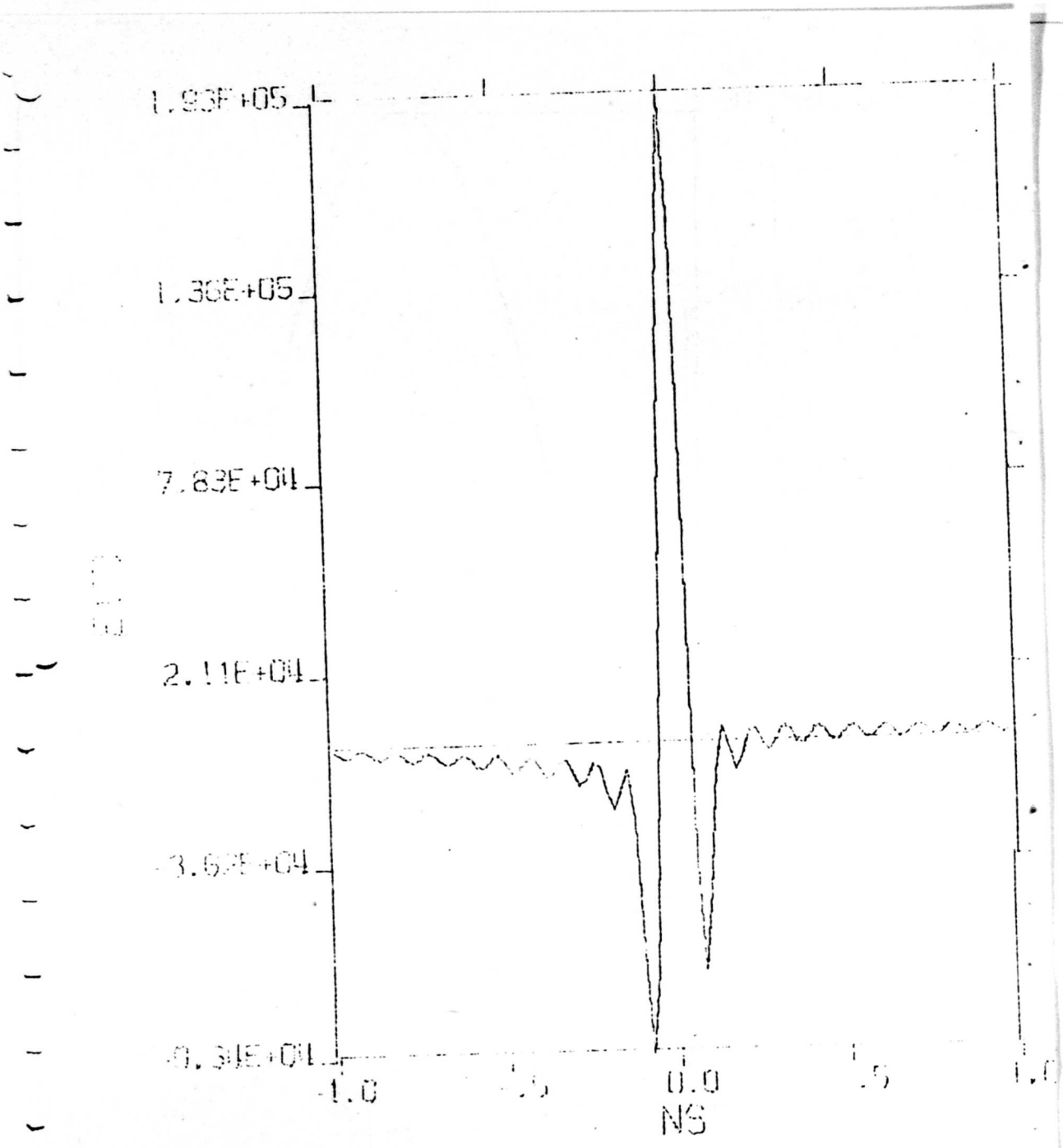


Figure I-18. Compressed Pulse of Spectrum in Figure I-17

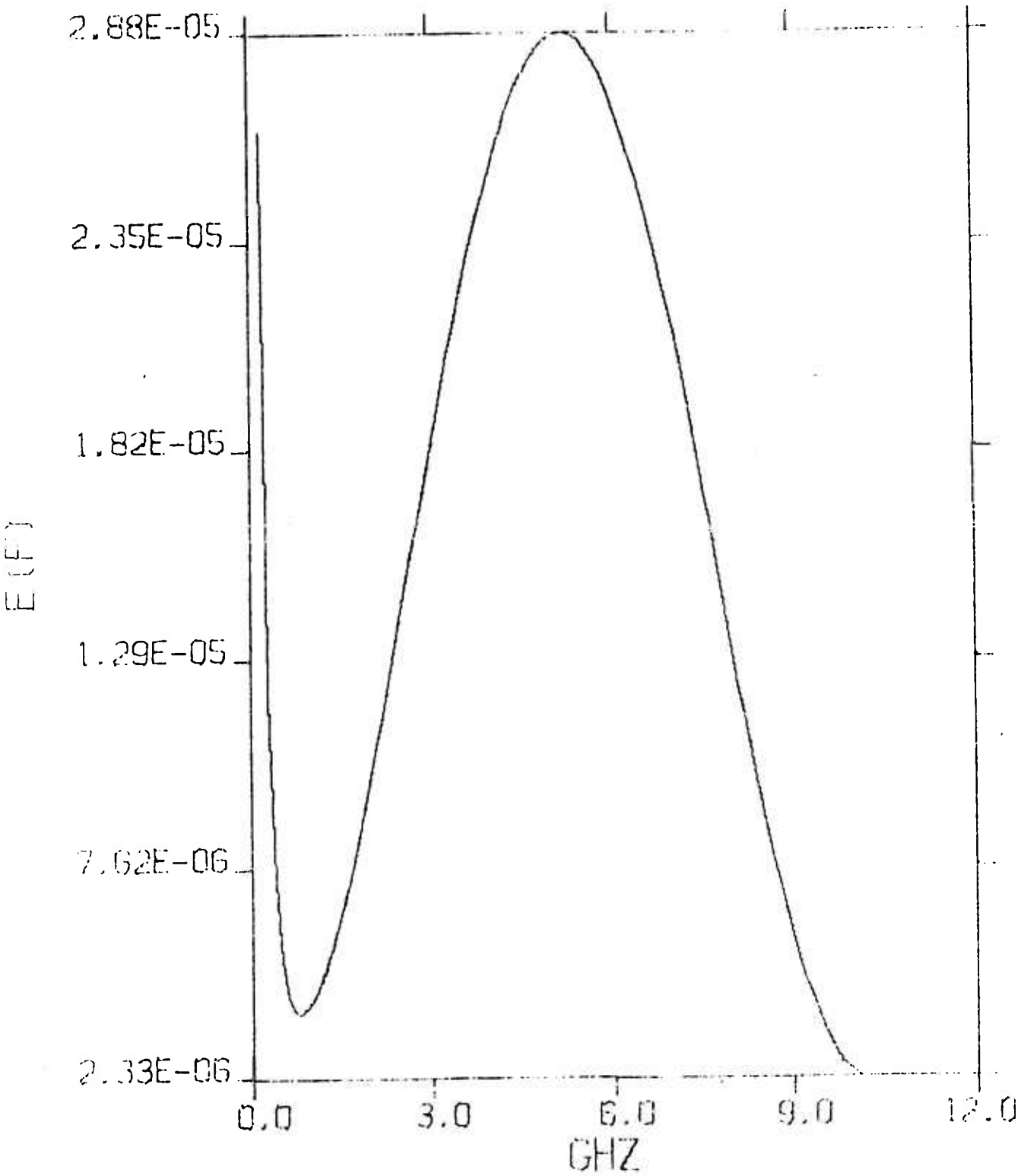


Figure I-19. Spectral Density $E(r, f, r_o, p, k)$ X 1.2
With r = 0.05 m, and p = 1/2

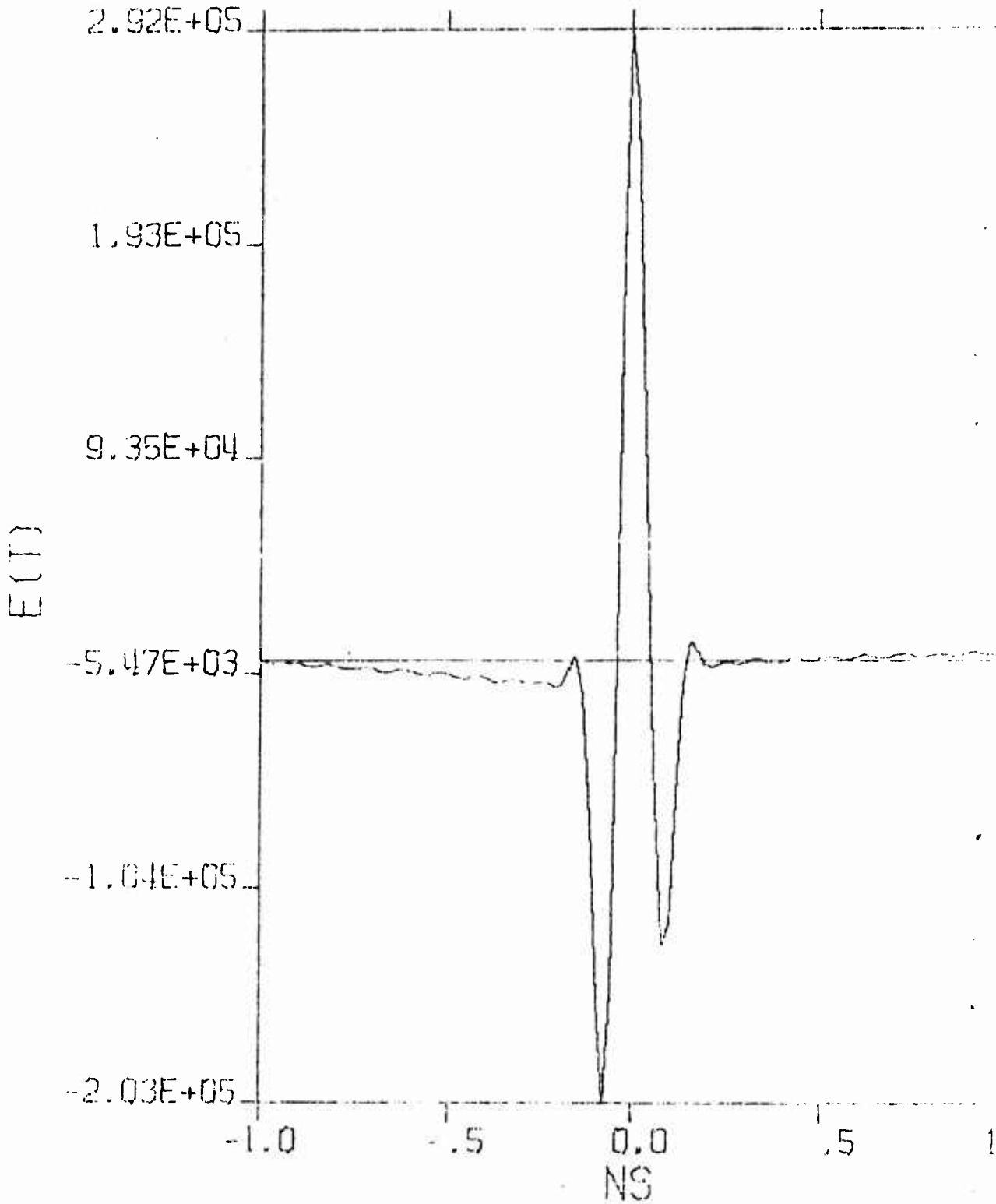


Figure I-20. Compressed Pulse of Spectrum in Figure I-19

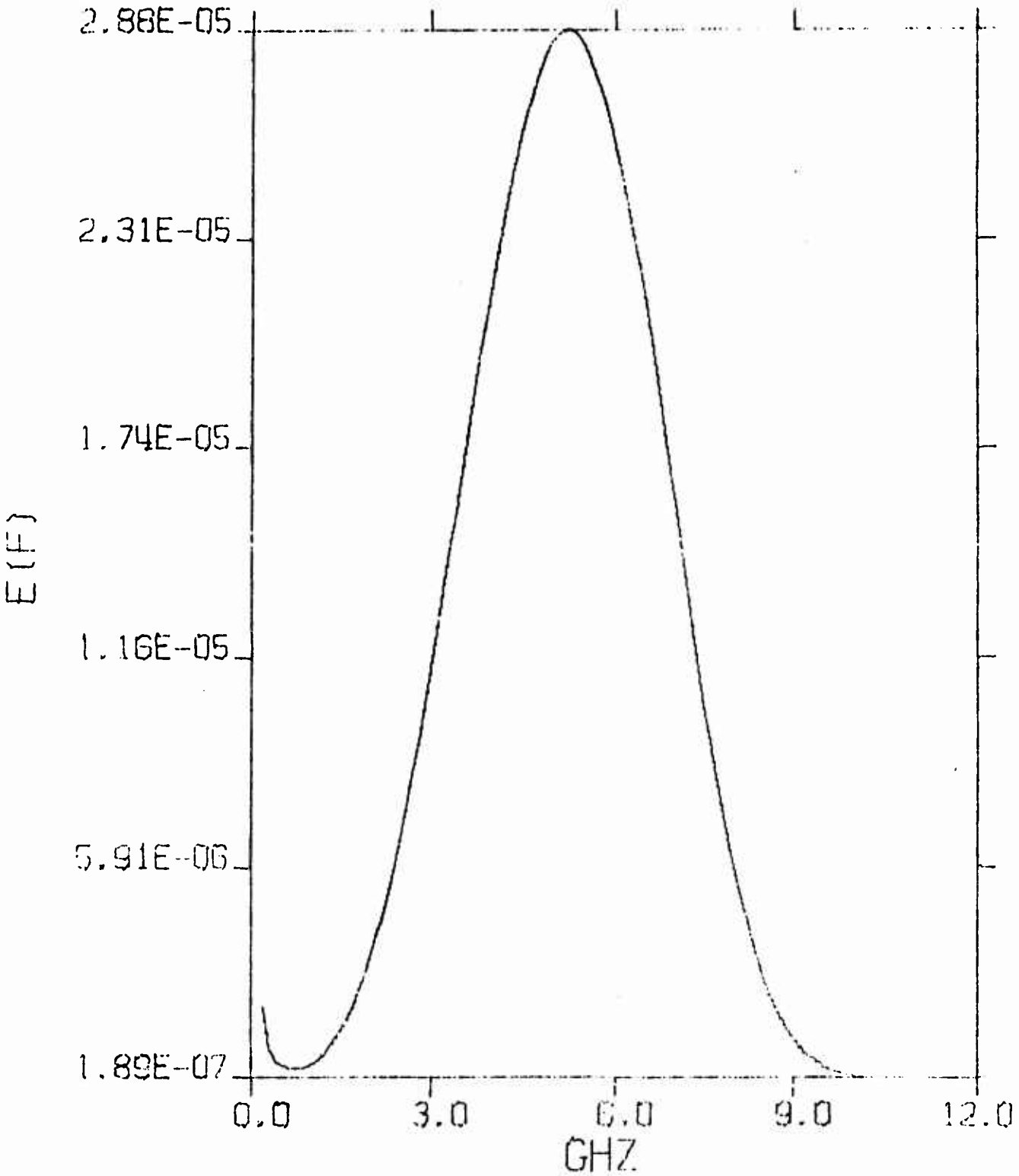


Figure I-21. Spectral Density E(r, f, r_o, p, k) X 1.2
With r = 0.05 m, and p = 1

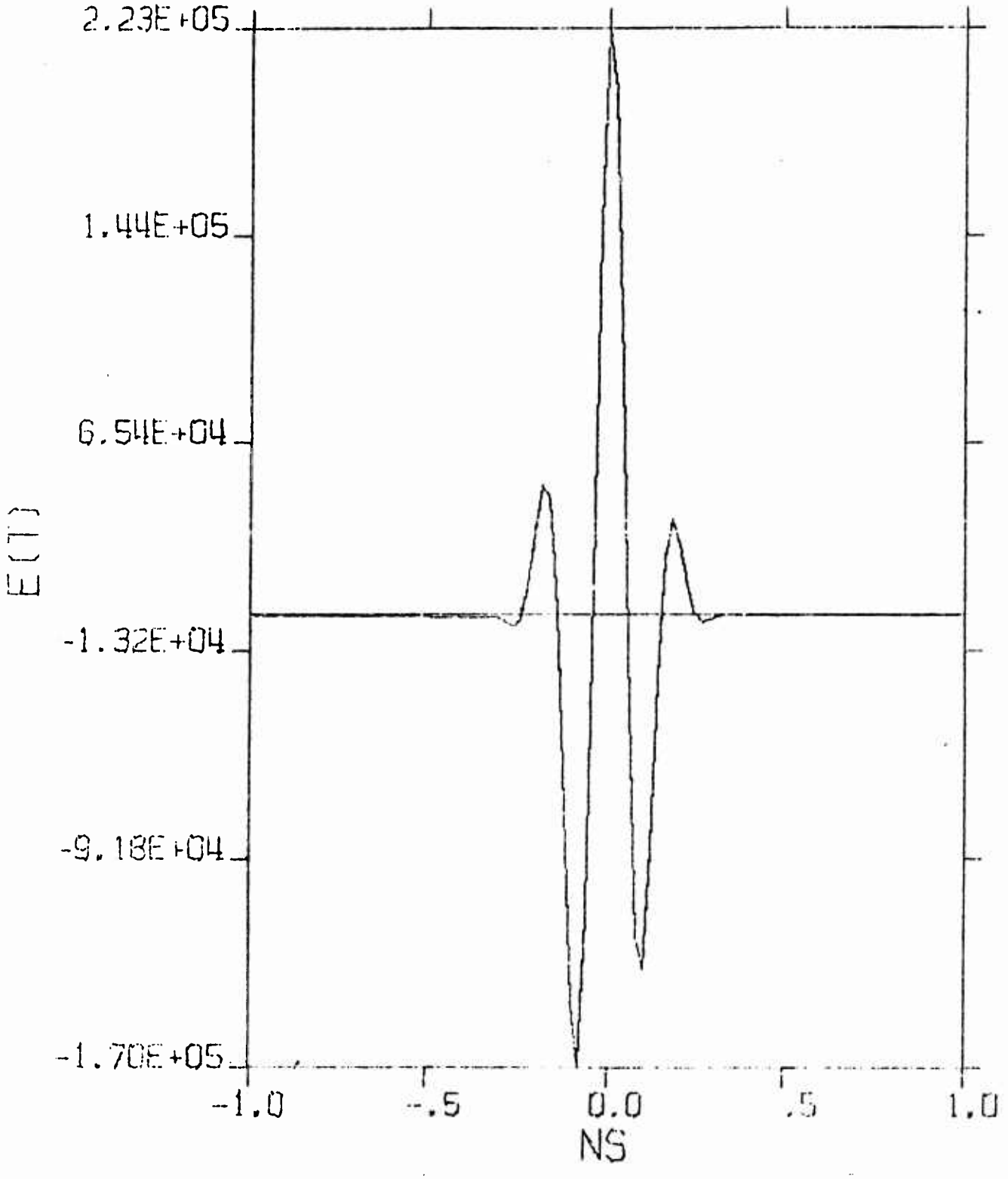


Figure I-22. Compressed Pulse of Spectrum in Figure I-21

Reproduced from best available copy.

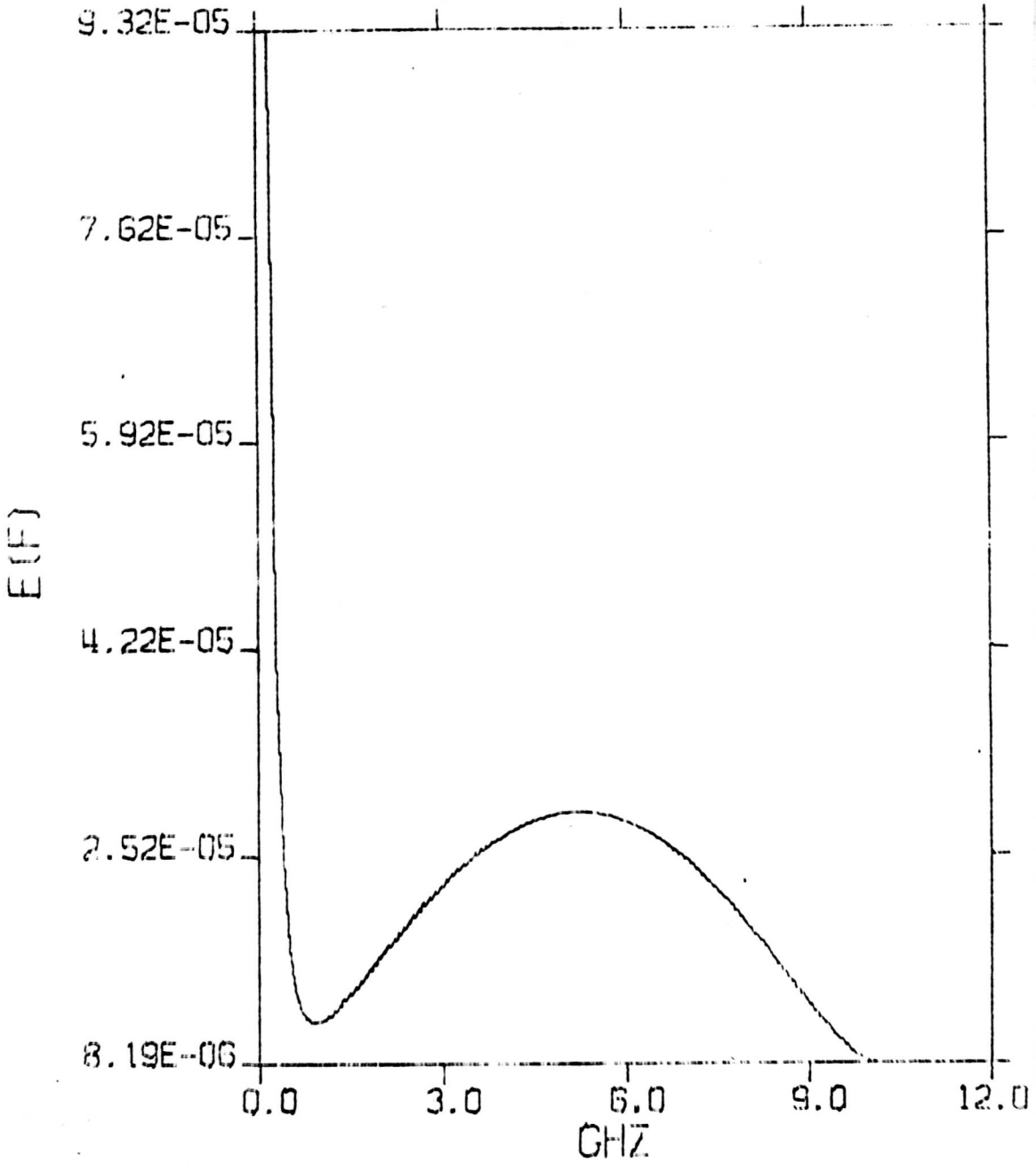


Figure I-23. Spectral Density E(r, f, r_o, p, k) X 1.2 With r = 0.05 m, and p = 1/4

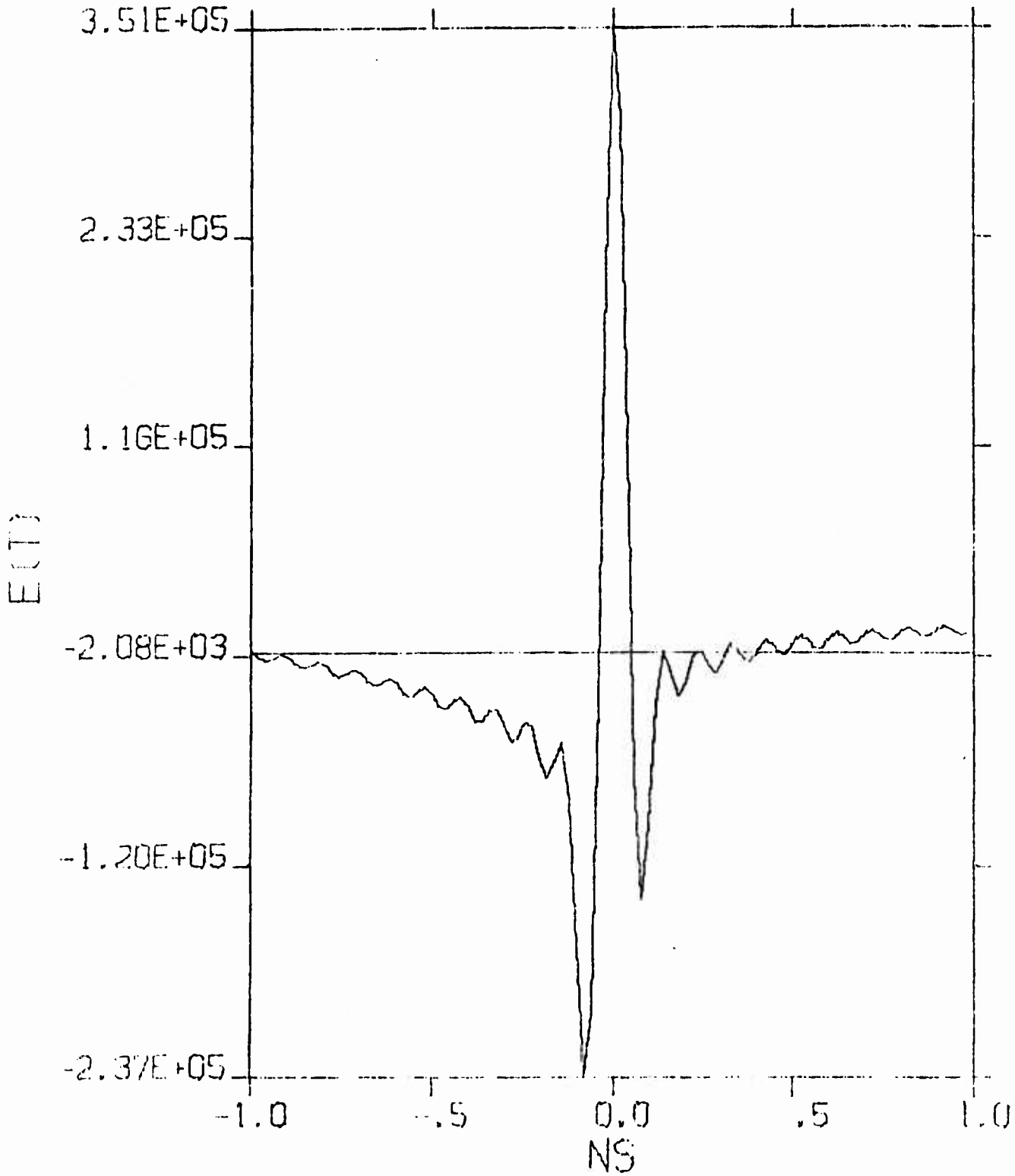


Figure I-24. Compressed Pulse of Spectrum in Figure I-23

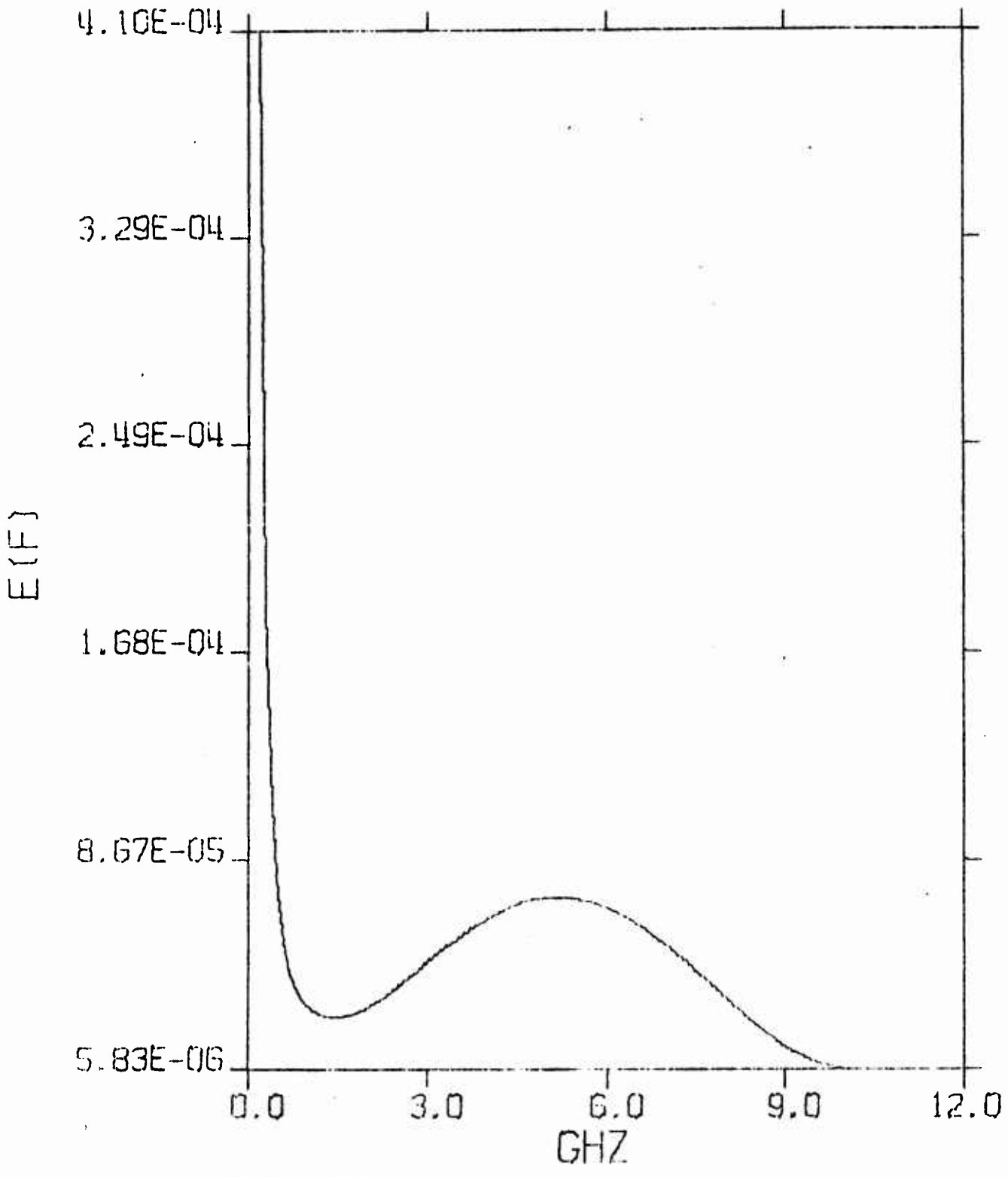


Figure I-25. Spectral Density E(r, f, r_o, p, k) X 1.2
With r = 0.02 m, and p = 1/2

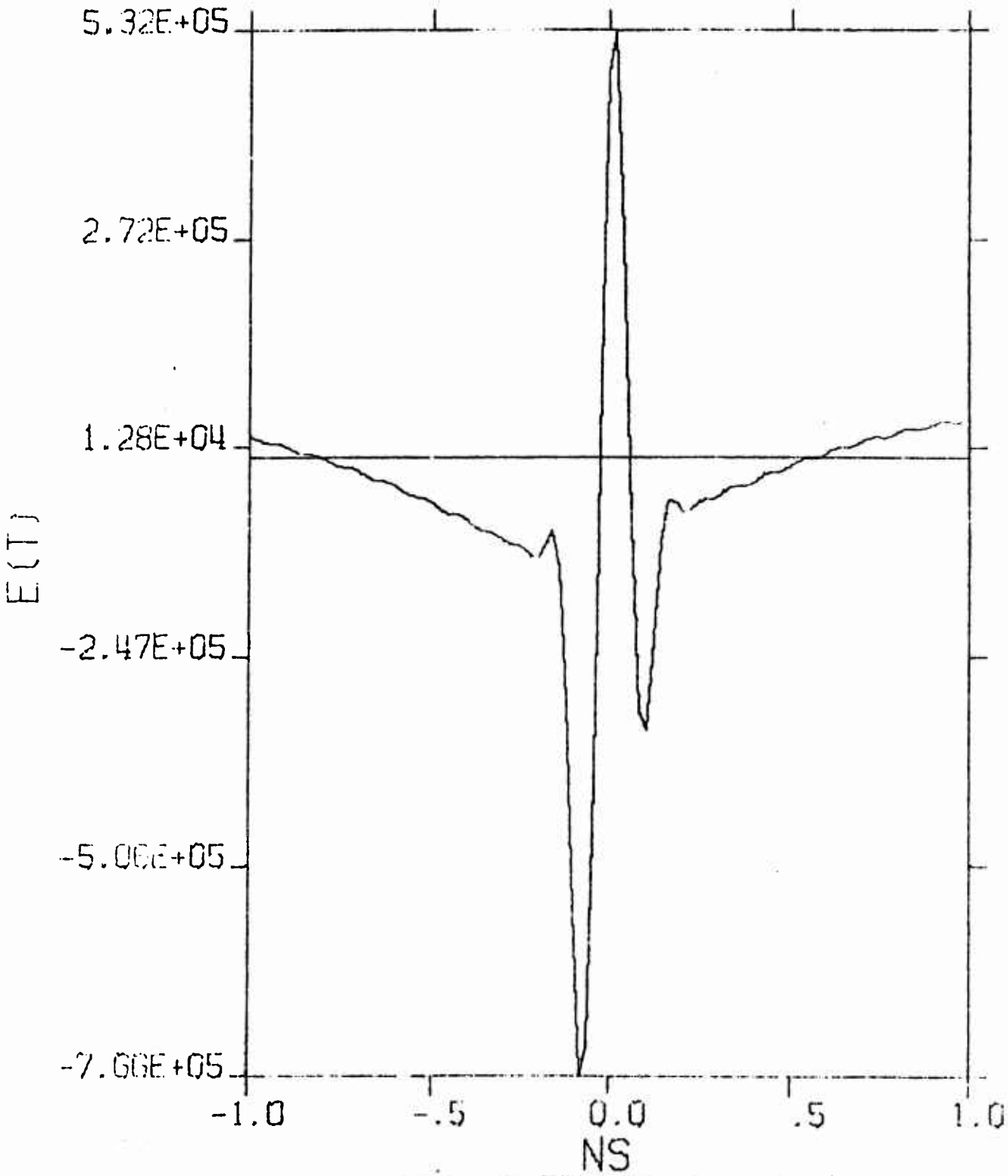


Figure 1-26. Compressed Pulse of Spectrum in Figure 1-25

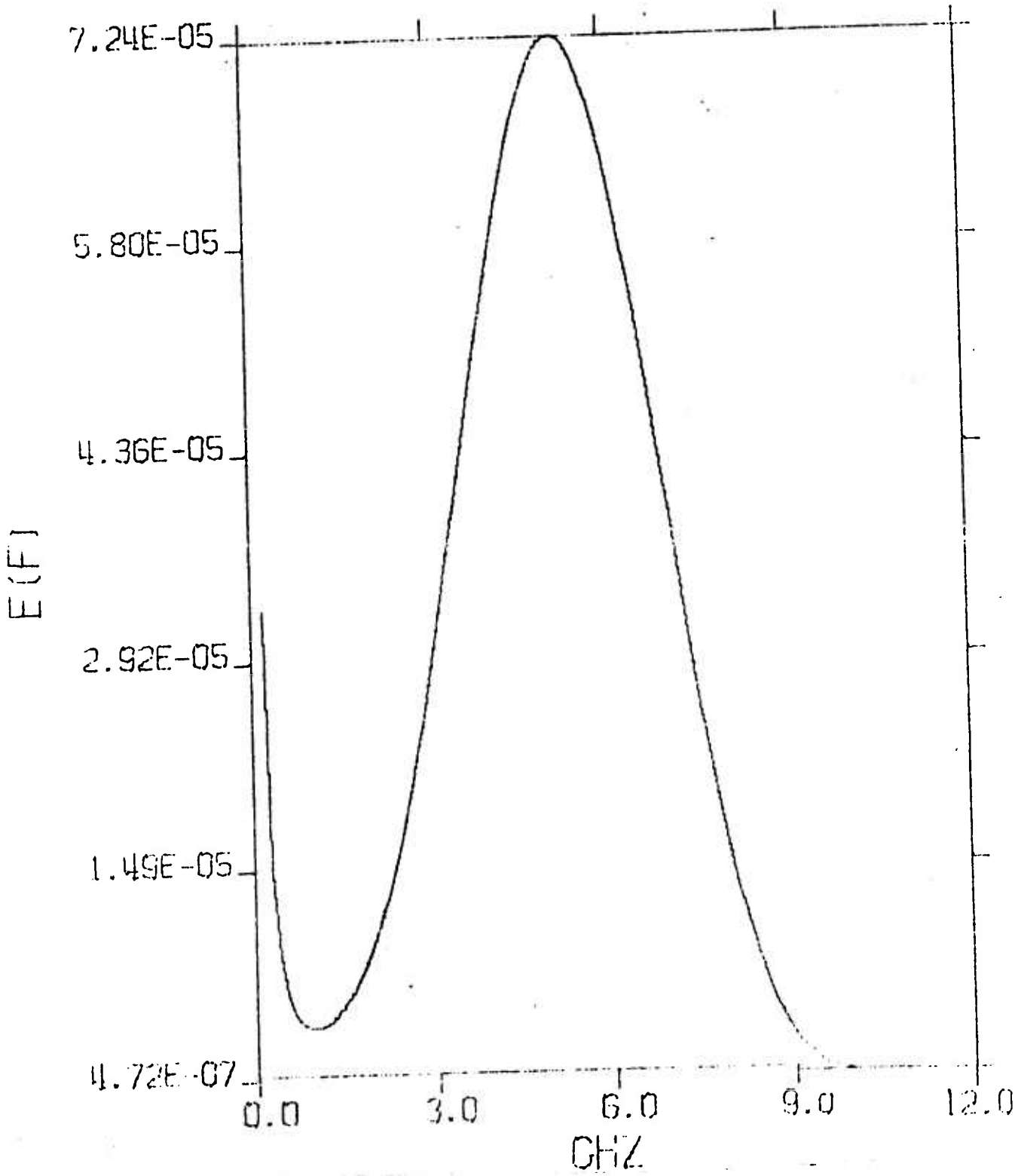


Figure I-27. Spectral Density E(r, f, r_o, p, k) X 1.2
With r = 0.02 m, and p = 1

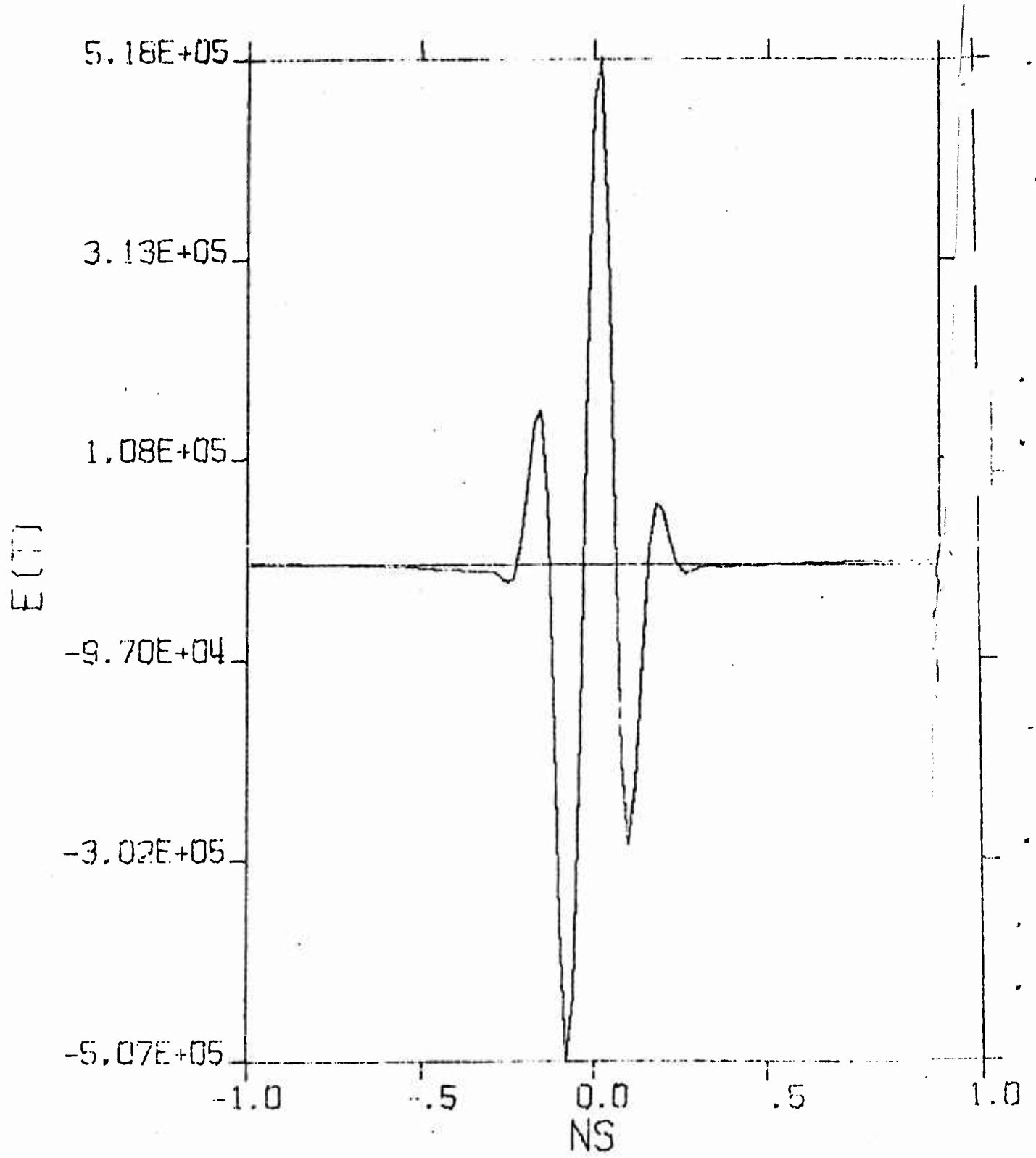


Figure I-28. Compressed Pulse of Spectrum in Figure I-27

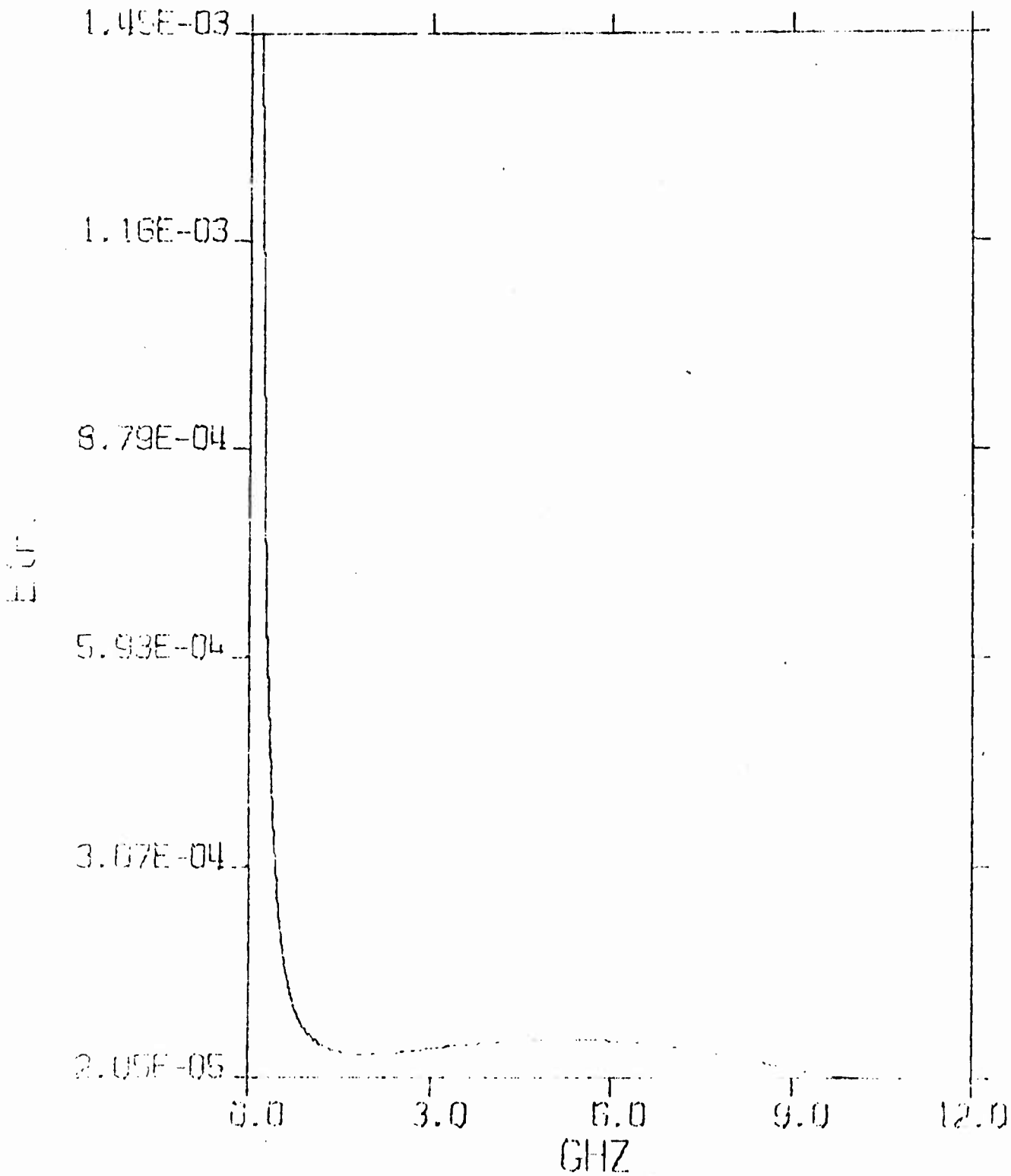


Figure I-29. Spectral Density E(r, f, r_o, p, k) X 1.2
With r = 0.02 m, and p = 1/4

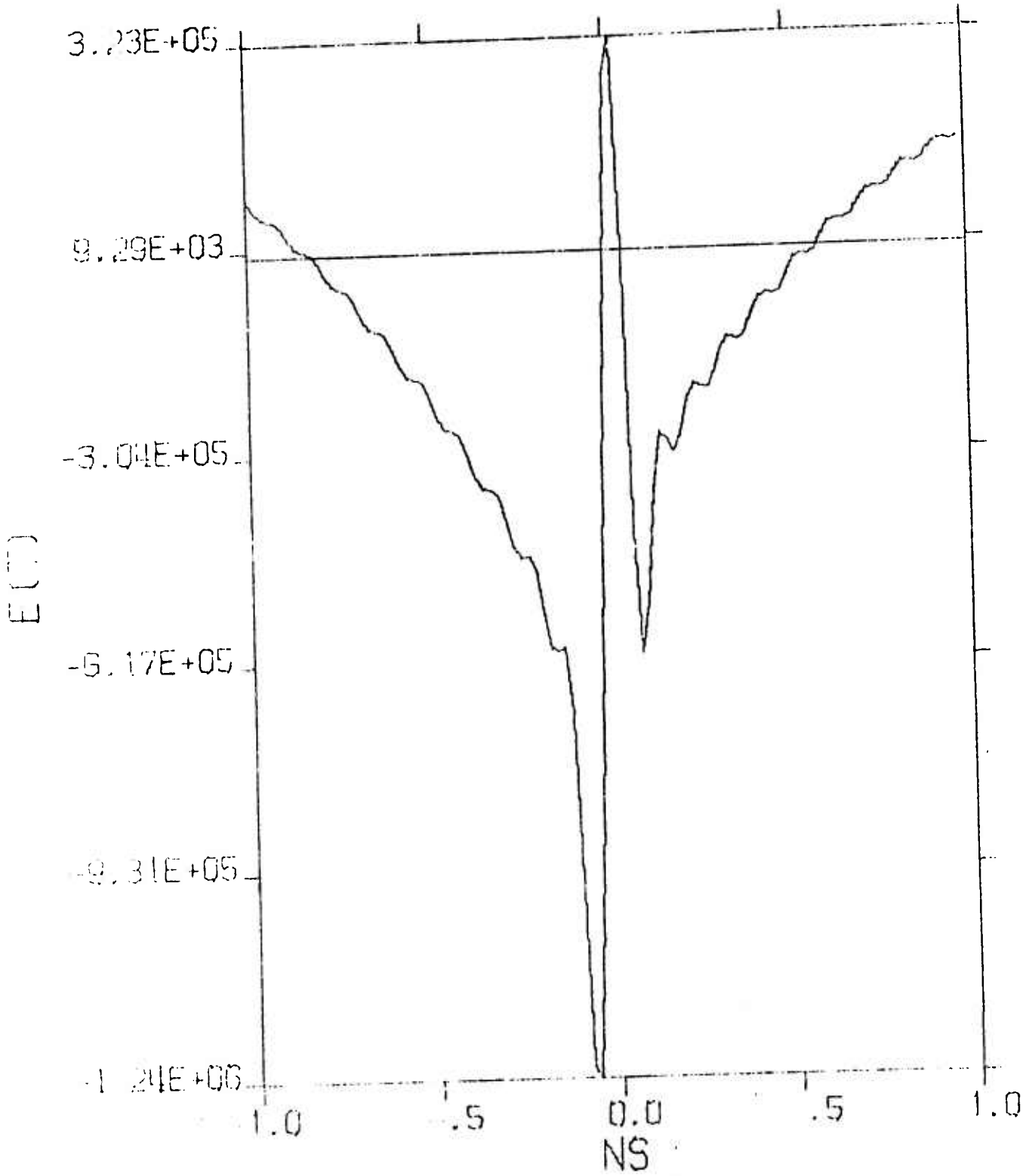


Figure 1-30. Compressed Pulse of Spectrum in Figure 1-29

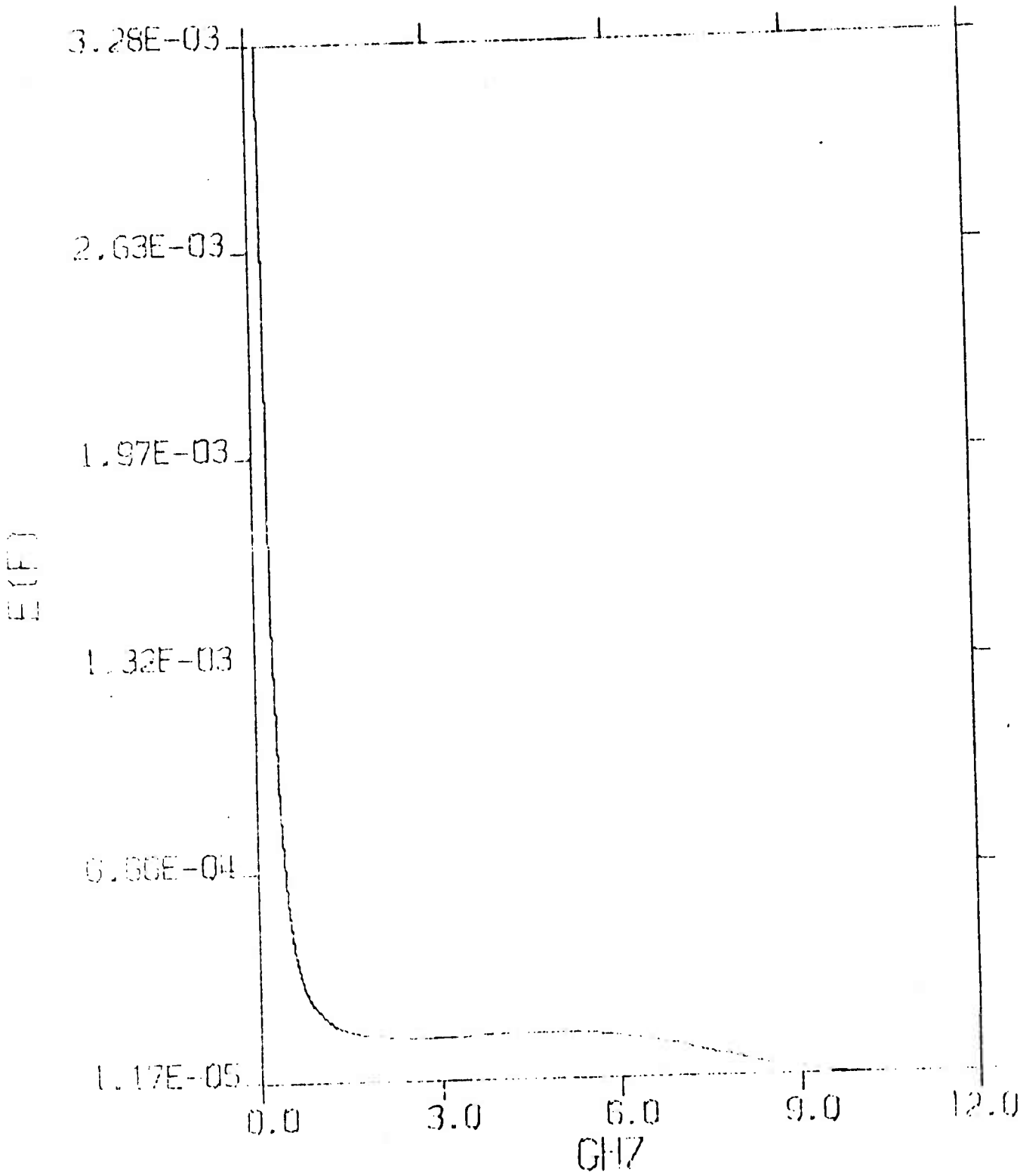


Figure I-31. Spectral Density $E(r, f, r_o, p, k)$ X 1.2
With r = 0.01 m, and p = 1/2

Reproduced from best available copy.

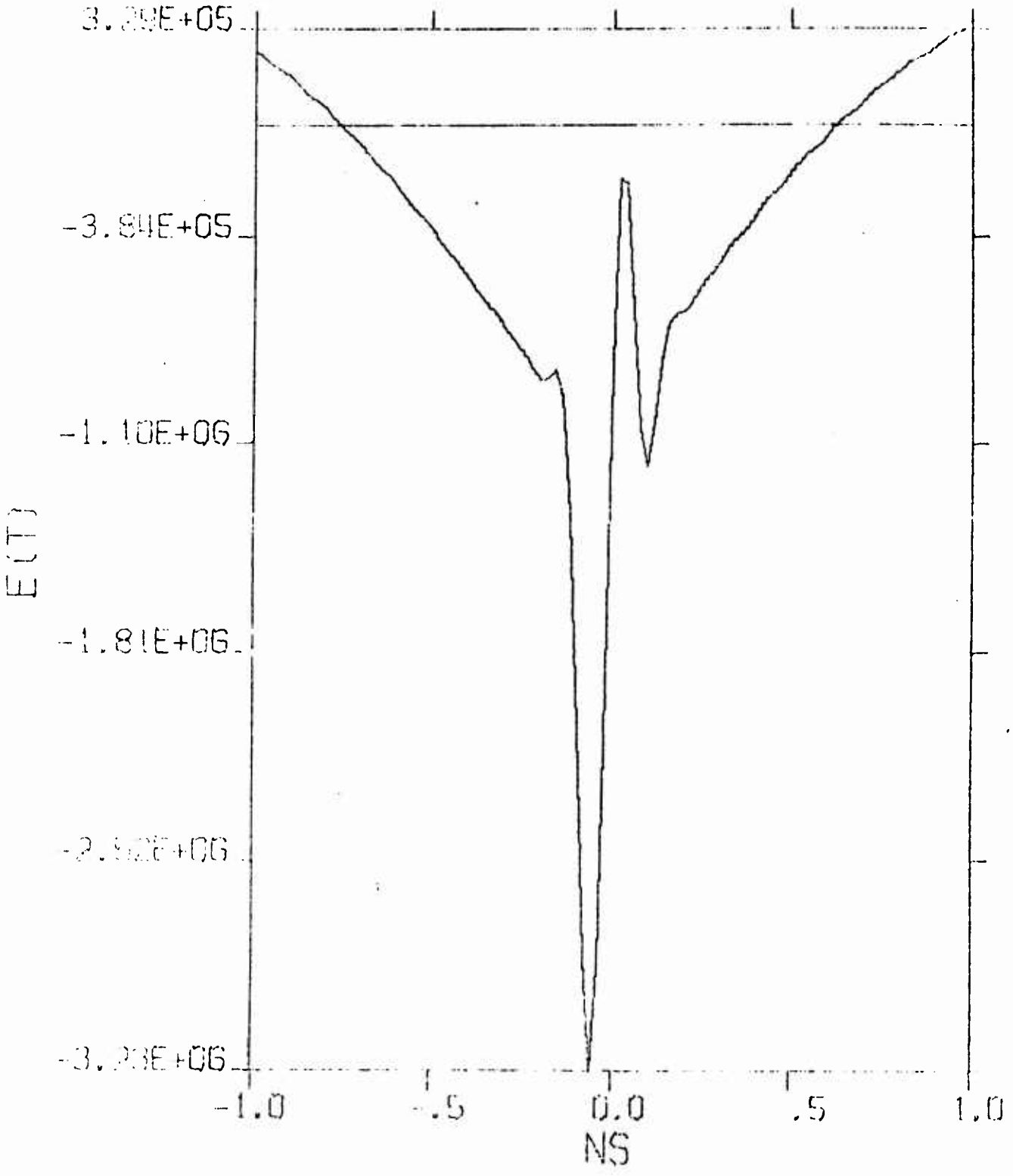


Figure I-32. Compressed Pulse of Spectrum in Figure I-31

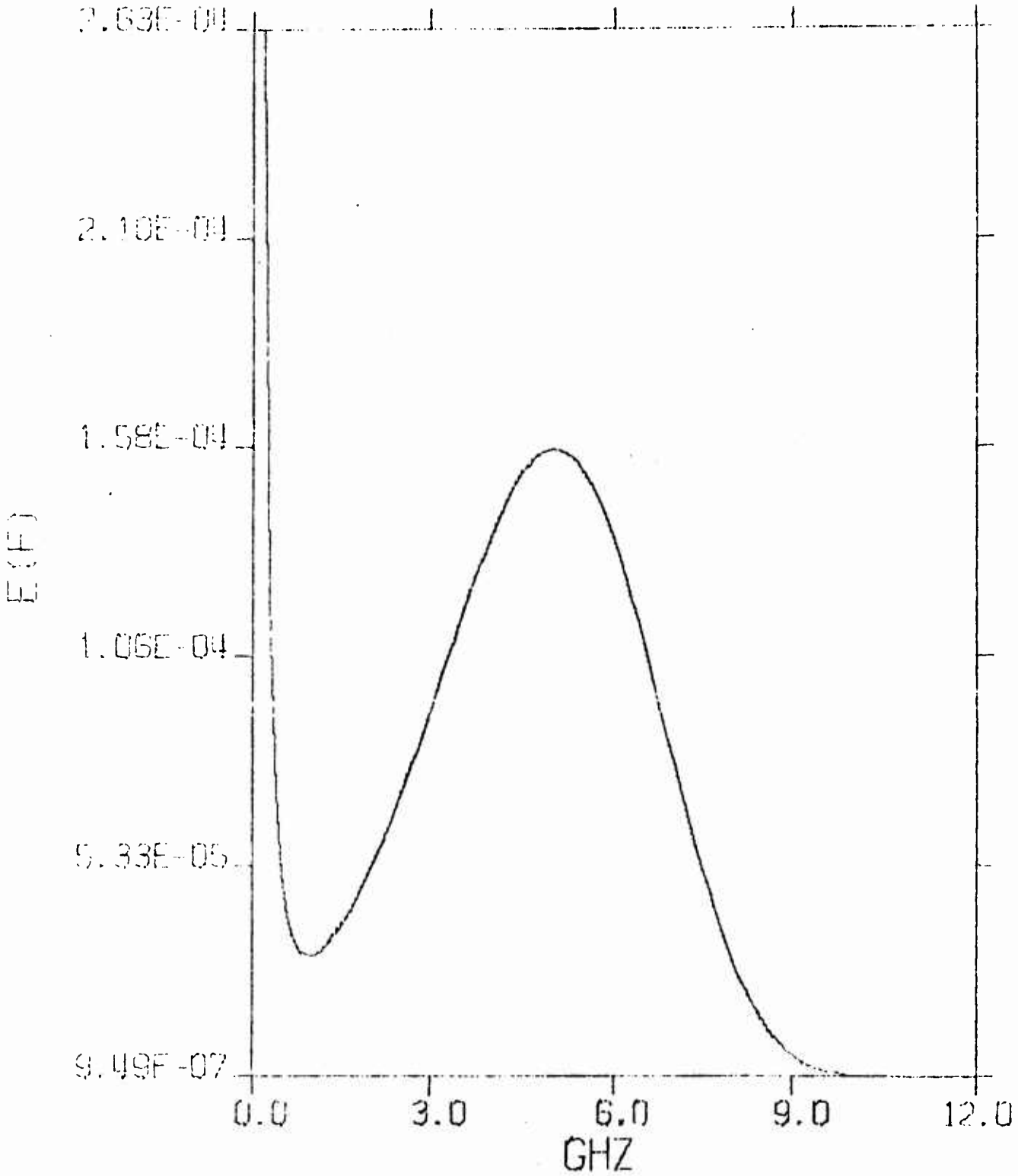


Figure I-33. Spectral Density E(r, f, r_o, p, k) X 1.2
With r = 0.01 m, and p = 1

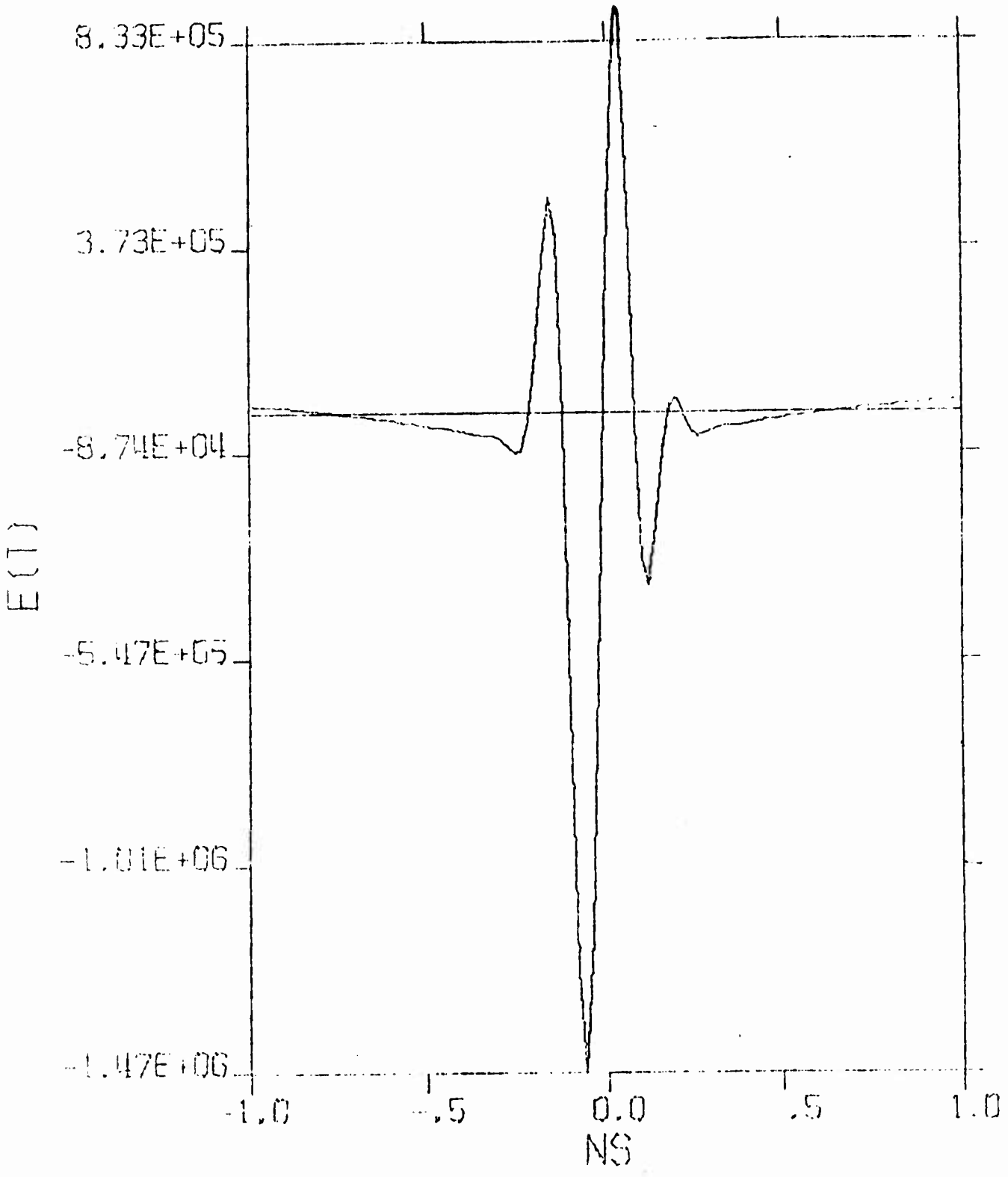


Figure 1-34. Compressed Pulse of Spectrum in Figure 1-33

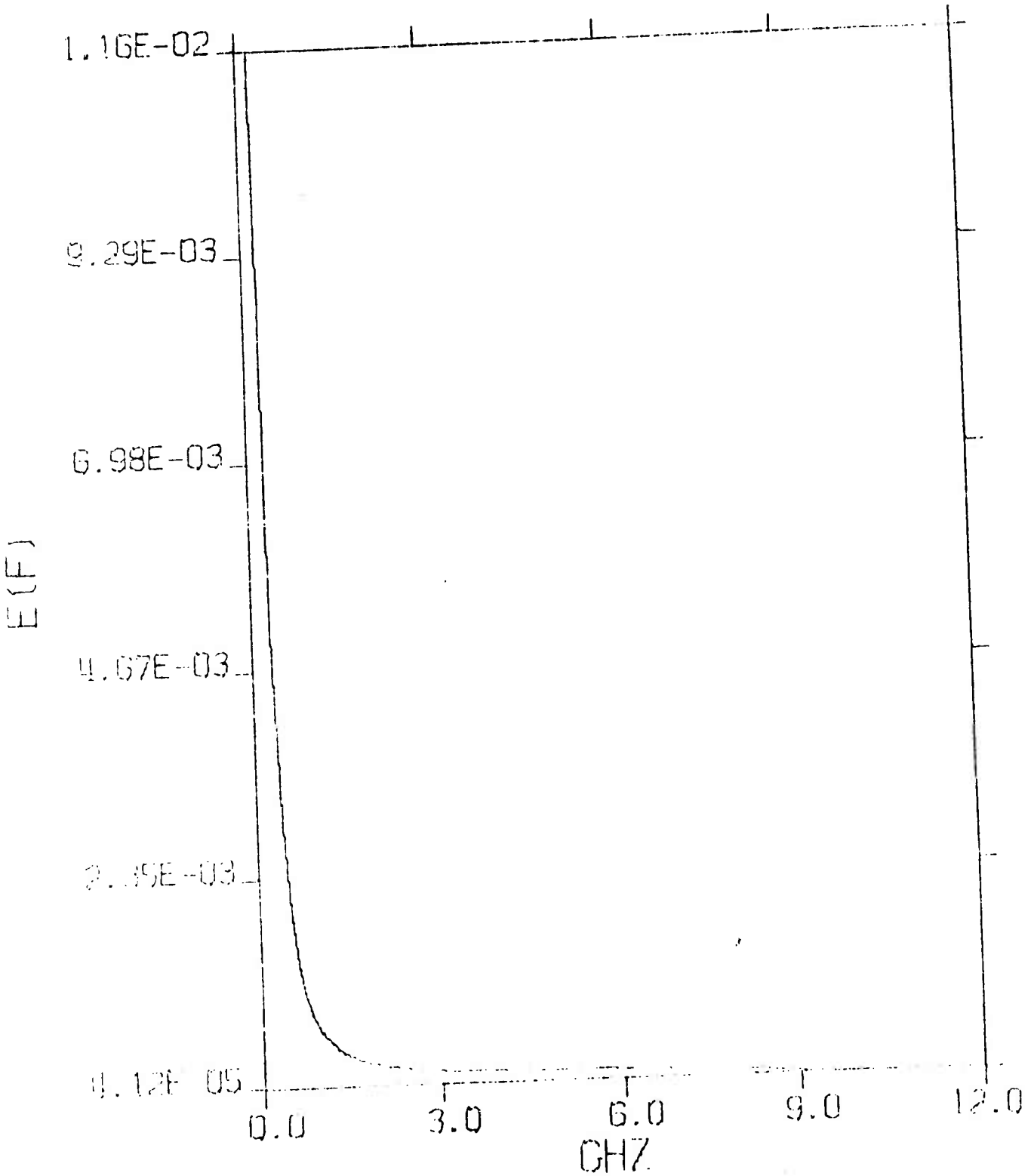


Figure 1-35. Spectral Density E(r, f, r_o, p, k) X 1.2
With r = 0.01 m, and p = 1.4

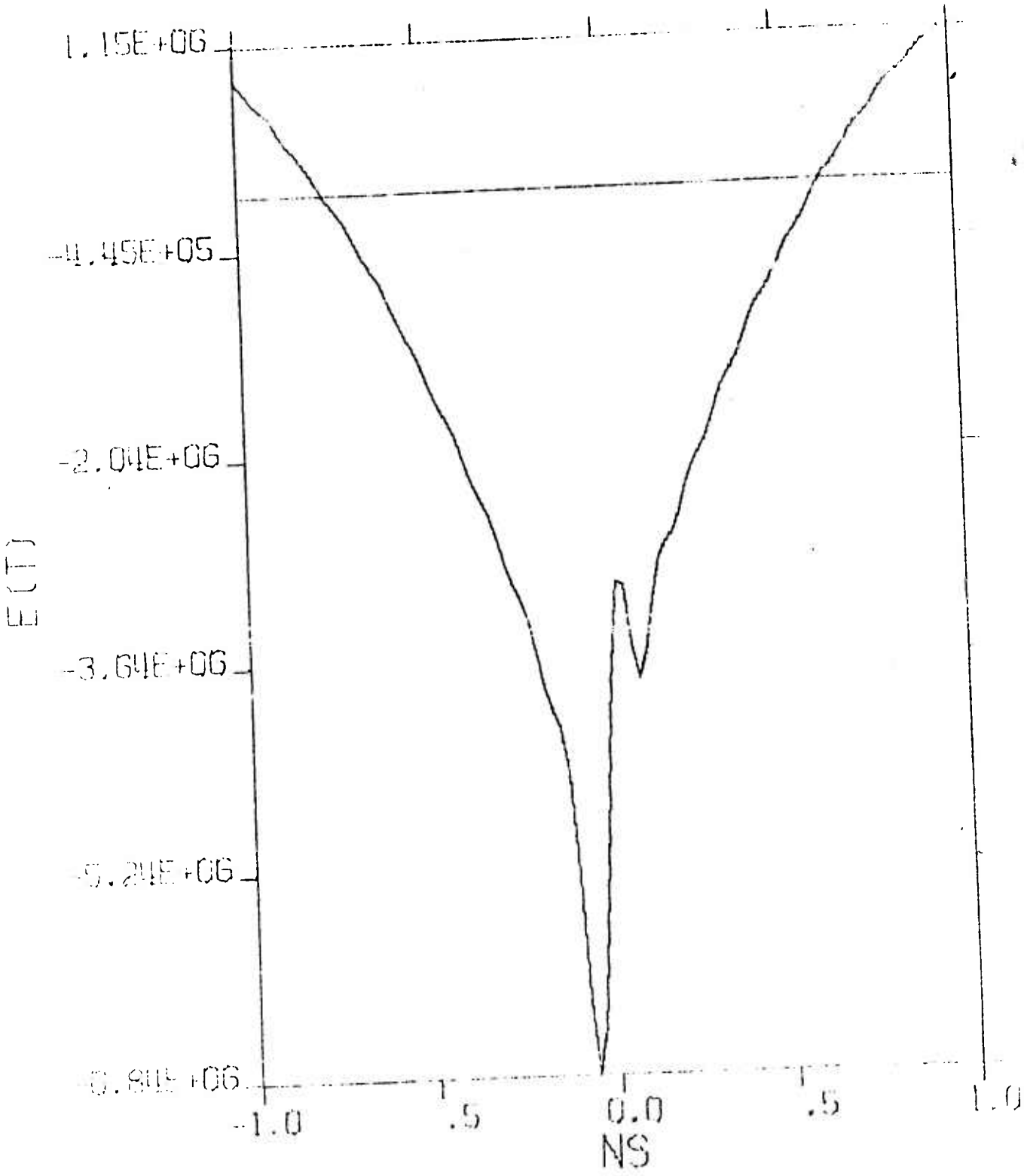


Figure 1-36. Compressed Pulse of Spectrum in Figure 1-35

only the dipole mode is used for pulse compression computations. Inclusion of higher-order modes has, in effect, increased compressed pulses by approximately a constant factor of less than 1.3 in the far zone.

5. BACKWARD RADIATION ARRAYS

A log-periodic dipole array model is shown in Figure I-42. It is a backward radiator because radiation takes place in the direction opposite to that of feeding currents. The field at point P is a superposition of the fields due to all elements. Assuming that all the elements are in resonance lengths, then the quantity defined in Equation I-16 is a constant for all elements. Consequently, all the modal coefficients defined in Equation I-12 also remain constants for all radiating elements. With the radiation distance r in Equation I-11 being subscripted for each element in Figure I-42, the electric fields at point P are

$$E_x(s_k,\ \theta = 0) = \frac{-2I\eta_o}{3b_1^c(\rho_o)\lambda_o s_k} \sum_{n=1}^{3} \frac{2n+1}{2} \left[\zeta_n(s_k) + j\zeta_n'(s_k) \right] b_n^c(\rho_o) \qquad \text{(Eq. I-17)}$$

$$s_k = 2\pi r_k/\lambda_o \qquad \text{(Eq. I-18)}$$

where $p_n(\theta = 0) = qn(\theta = 0) = (2n + 1)/2$ is used in Equation I-9 to obtain Equation I-17. The value of r_k can be determined by referring to Figure I-42.

The total field from all elements is the sum

$$E_x = \sum_{k=1}^{K} E_x(s_k,\ \theta = 0). \qquad \text{(Eq. I-19)}$$

Evaluation of this field will give a more accurate description than the previous results in both near and far zones for pulse compression purposes, provided the field is not evaluated for $z_1/\lambda_o < 0.25$ where the field expression would involve source singularities for all elements concerned.

Should source singularities be excluded from considerations, the near-zone compressed pulses for the antenna in Figure I-42 would be smaller than those shown in Figures I-7 through I-36. This is so because the low-frequency regions would contribute decreasingly at a given field point. Although this antenna has less severe near-zone compression problems, it is not the type that has the least severe near-zone problem. The broadside array to be treated next will show that substantial reduction will take place in the amplitudes near-zone compressed pulses.

6. BROADSIDE RADIATION ARRAY

A conical spiral antenna can be approximated for one component of its circularly-polarized field as the array shown in Figure I-43. Complete circularly-polarized radiation is presently not treated. The compressed electric field component E_x can be calculated for the nth component contribution by use of Figure I-44 as

$$E_n(r,r_n,f) = \frac{120 \times 10^{-8}}{r_n}\left[0.54 + 0.46\cos\left(\frac{\pi(f-f_o)}{(f_h-f_\ell)}\right)\right]\cdot \qquad \text{(Eq. I-20)}$$

$$\cdot\left[0.54 + 0.46\cos\left(\frac{\pi(f-f_{no})}{(f_{nh}-f_{no})}\right)\right]\cdot$$

$$\cdot\left[1 - 0.5(2\pi f_{no}r_n/c)^{-2} - j(2\pi f_{no}r_n/c)^{-1}\right]\cdot$$

$$\cdot \exp\left[-j2\pi f_{no}(r_n-r)/c\right]$$

$$\cdot \cos\theta_n, \text{ for } f_{n\ell} \le f \le f_{nh}$$

where the definition of each radiation region, the high and low cutoff frequencies, and the complex spectral distribution of the antennas are referred to in Section 2 of Appendix D. When all the radiation regions are summed for their compressed pulses, the resultant contribution is

$$E(r,f) = \sum_{n=1}^{N} E_n(r,r_n,f), \text{ for } f_\ell \leq f \leq f_h \qquad \text{(Eq. I-21)}$$

where the cutoff frequencies ($f_\ell f_h$) are chosen to be (0.2, 10.2) GHz, the same as those used to compute for Figures I-10 through I-36. The effective elemental fractional bandwidth is chosen as $\delta = 0.111$, and the total number of elements is N = 37 as can be determined from Section 2 of Appendix D.

All the 37-region parameters (Region Number, nth High Cutoff Frequency, nth Center Frequency, nth Low Cutoff Frequency, Number of Frequency Increment in 0.04 GHz, nth Element Height $h_{n(m)}$ in Figure I-44) are given in Table I-1 for reference purposes. Complex spectra of compressed pulses by the antenna model are shown in Figure I-45 for three near-zone distances. The spectral amplitudes are smoothed curves representing average values of superimposed spectra due to 37 radiation regions. The manner by which sampling has been done in Equations I-20 and I-21 constitutes a spectral amplitude of 1.16 of the original values at the centers of radiation regions and a spectral amplitude of 1.08 of the original values between two radiation regions. Therefore, on the average, the spectral amplitudes sketched in Figure I-45 are about 12 percent higher than the original values before sampling was made for the 37 radiation regions. It is clear that symmetrical amplitude distribution exists at 100 cm range and its associated phase variation becomes extremely small.

Figures I-46 through I-54 give numerical results of compressed pulses at various distances. At 1.5 cm range the compressed pulse in Figure I-46 appears to be symmetrical about the pulse peak, even though its spectral amplitude appears to be asymmetric about 5 GHz in Figure I-45. This property is in sharp contrast with the compressed pulse at 5 cm range shown in Figure I-20. When the pulses are compressed in the far zone (Figures I-53 and I-54) the peak values are respectively 13 kV/m

TABLE I-1

PARAMETERS USED IN NEAR-ZONE COMPRESSED PULSES OF BROADSIDE ARRAY

n	f_{nh} (Hz)	f_{no} (Hz)	$f_{n\ell}$ (Hz)	$(f_{nh}-f_{n\ell})/4\times10^6$	h_n (m)
1	10.20E+09	91.81E+08	81.62E+08	50.95E+00	81.69E-04
2	91.81E+08	82.64E+08	73.46E+08	45.86E+00	90.76E-04
3	82.64E+08	74.38E+08	66.12E+08	41.28E+00	10.08E-03
4	74.38E+08	66.95E+08	59.52E+08	37.16E+00	11.20E-03
5	66.95E+08	60.26E+08	53.57E+08	33.44E+00	12.45E-03
6	60.26E+08	54.24E+08	48.22E+08	30.10E+00	13.83E-03
7	54.24E+08	48.82E+08	43.40E+08	27.10E+00	15.36E-03
8	48.82E+08	43.94E+08	39.07E+08	24.39E+00	17.07E-03
9	43.94E+08	39.55E+08	35.16E+08	21.95E+00	18.96E-03
10	39.55E+08	35.60E+08	31.65E+08	19.76E+00	21.07E-03
11	35.60E+08	32.04E+08	28.49E+08	17.78E+00	23.41E-03
12	32.04E+08	28.84E+08	25.64E+08	16.01E+00	26.00E-03
13	28.84E+08	25.96E+08	23.08E+08	14.41E+00	28.89E-03
14	25.96E+08	23.37E+08	20.77E+08	12.97E+00	32.10E-03
15	23.37E+08	21.03E+08	18.70E+08	11.67E+00	35.66E-03
16	21.03E+08	18.93E+08	16.83E+08	10.51E+00	39.62E-03
17	18.93E+08	17.04E+08	15.15E+08	94.57E-01	44.01E-03
18	17.04E+08	15.34E+08	13.63E+08	85.12E-01	48.90E-03
19	15.34E+08	13.80E+08	12.27E+08	76.62E-01	54.33E-03
20	13.80E+08	12.43E+08	11.05E+08	68.96E-01	60.36E-03
21	12.43E+08	11.18E+08	99.43E+07	62.07E-01	67.06E-03
22	11.18E+08	10.07E+08	89.49E+07	55.87E-01	74.50E-03
23	10.07E+08	90.61E+07	80.55E+07	50.29E-01	82.77E-03
24	90.61E+07	81.56E+07	72.50E+07	45.26E-01	91.96E-03
25	81.56E+07	73.41E+07	65.26E+07	40.74E-01	10.22E-02
26	73.41E+07	66.07E+07	58.74E+07	36.67E-01	11.35E-02
27	66.07E+07	59.47E+07	52.87E+07	33.01E-01	12.61E-02
28	59.47E+07	53.53E+07	47.59E+07	29.71E-01	14.01E-02
29	53.53E+07	48.18E+07	42.85E+07	26.74E-01	15.57E-02
30	48.18E+07	43.37E+07	38.55E+07	24.07E-01	17.29E-02
31	43.37E+07	39.04E+07	34.70E+07	21.66E-01	19.21E-02
32	39.04E+07	35.14E+07	31.24E+07	19.50E-01	21.35E-02
33	35.14E+07	31.63E+07	28.11E+07	17.55E-01	23.72E-02
34	31.63E+07	28.47E+07	25.31E+07	15.80E-01	26.35E-02
35	28.47E+07	25.62E+07	22.78E+07	14.22E-01	29.27E-02
36	25.62E+07	23.06E+07	20.50E+07	12.80E-01	32.52E-02
37	23.06E+07	20.76E+07	18.45E+07	11.52E-01	36.13E-02

and 0.13 kV/m when the over-densed sampling factor of 1.12 is used to divide those computed values. These peak field intensities are in agreement with those shown in Figures I-7 and I-2 if their computed values are divided by a factor of 1.2 as shown in Figures I-6 and I-1.

To summarize the near-zone compression mechanism, Figure I-55 shows a series of pulses. These pulses are clearly much lower in their peak values if comparison is made against those plotted in Figure I-37. The most significant result of broadside array radiation is that its compressed pulses do not have the tendency to diverge rapidly toward the aperture plane. Instead, the pulse peak takes place with a smaller value at 1.5 cm range and reaches a maximum at 3.5 cm range. This desirable range variation is shown in Figure I-56.

7. CONCLUDING REMARKS

Pulse compressions in the near zone have been formulated here for both longitudinal delay and transversal delay. The former case resembles log-periodic dipole arrays while the latter resembles cavity-backed spiral antennas. Choosing an operating bandwidth of 0.2 to 10.2 GHz as an example, and setting the compressed spectral distribution in the far-zone as a Hamming weighted function, the "worst" case and the "best" case compressions are summarized in Figure I-57 for their peak values. The choice of having all radiation regions coincident in phase centers is simply a way of establishing an upper bound to which all log-periodic antennas are limited for possible compression peaks. Providing that all log-periodic antennas are conjugate-matched to produce the same compressed spectrum as discussed above, their peak compressed value should be confined within the two curves shown in Figure I-57.

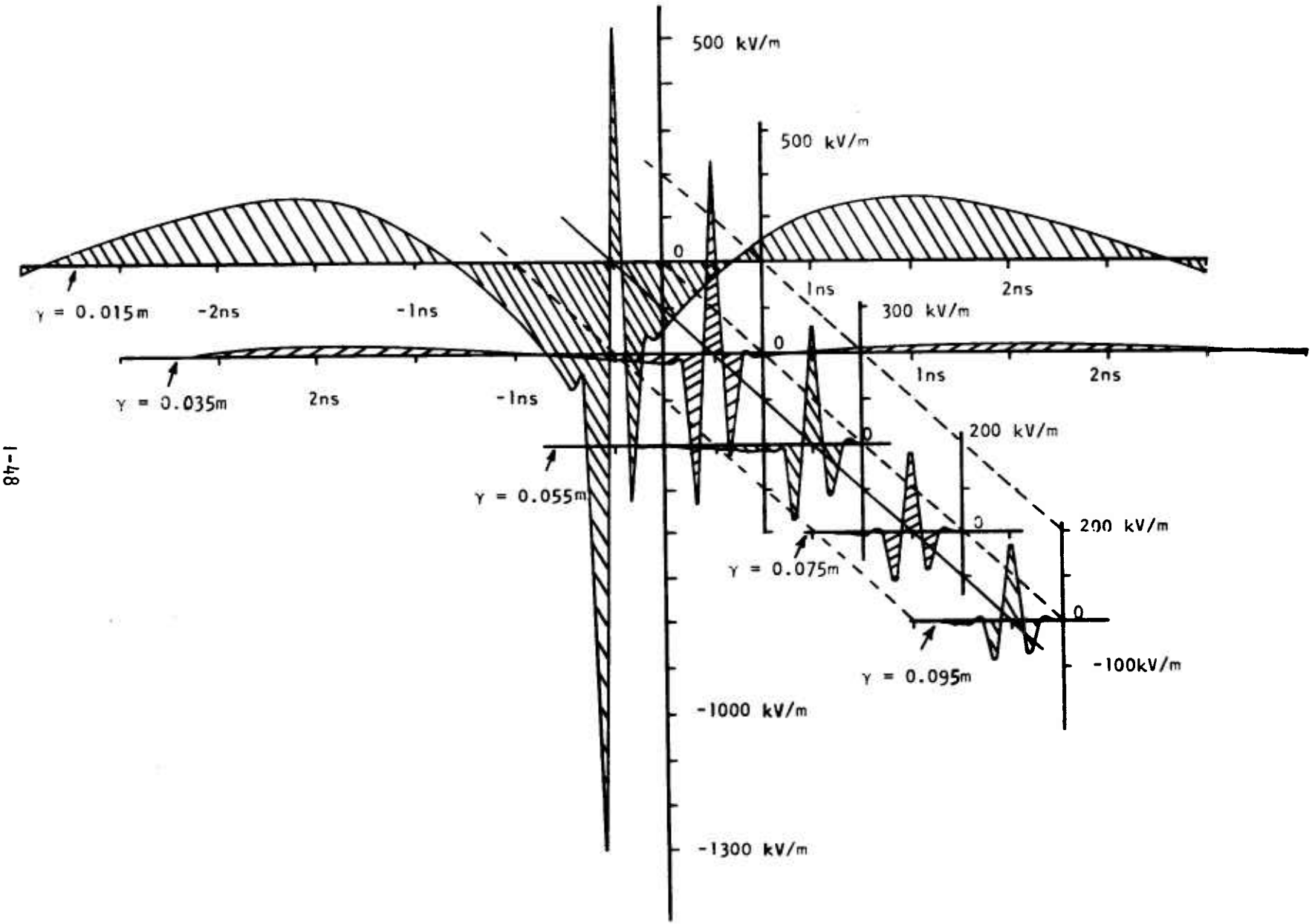


Figure I-37. Pulse compressions in the Near-Zone

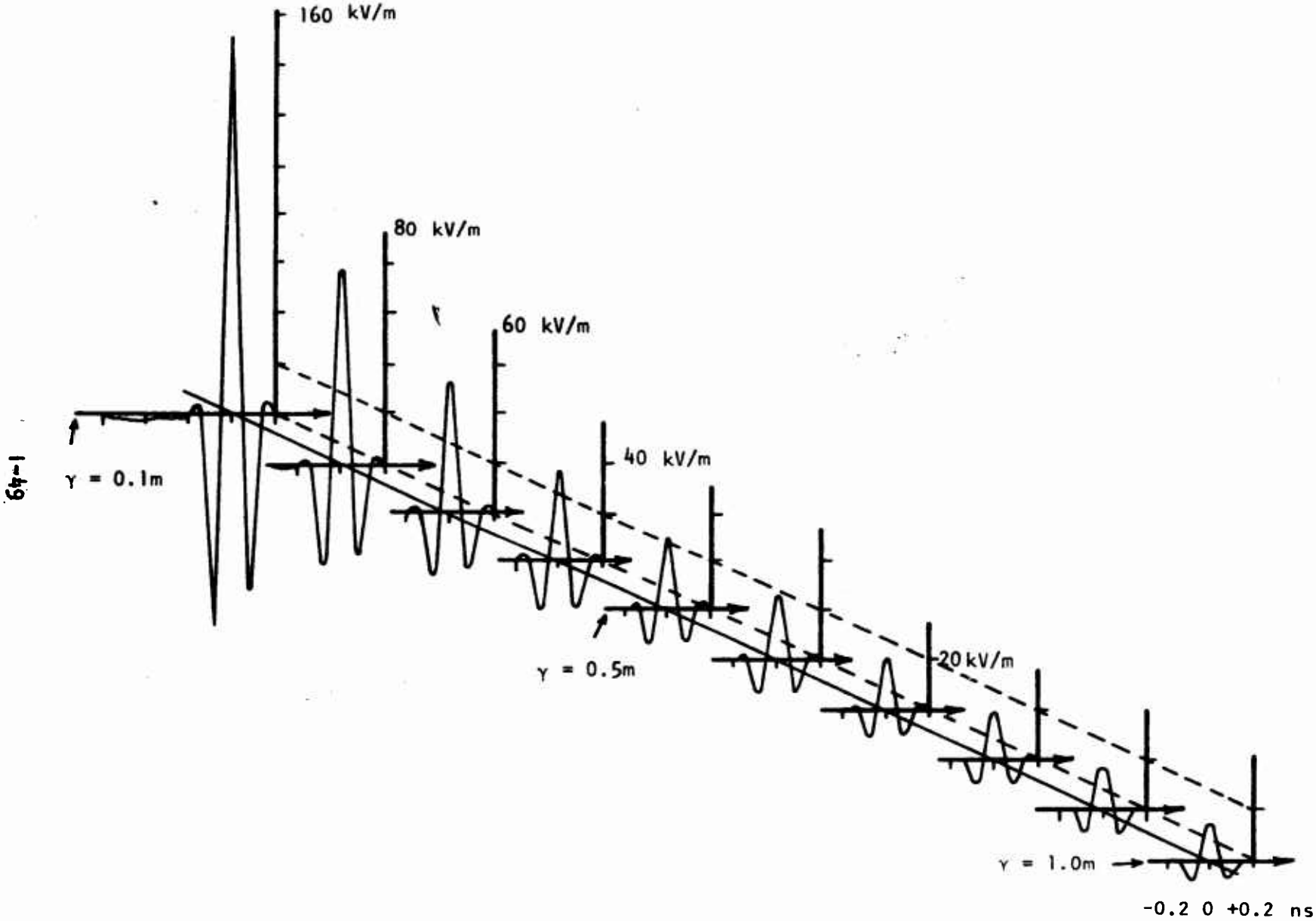


Figure I-38. Pulse Compression in the Far-Zone ($\gamma > 0.75$ m)

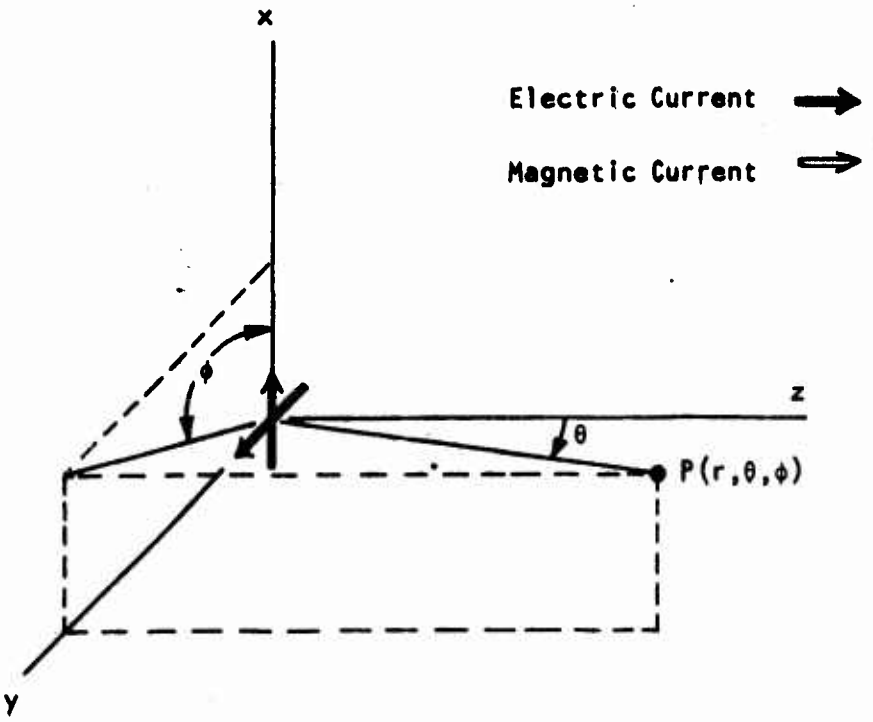


Figure I-39. Balanced Electric and Magnetic Currents for Axially Symmetric Cardioid Radiation Around the Z-Axis

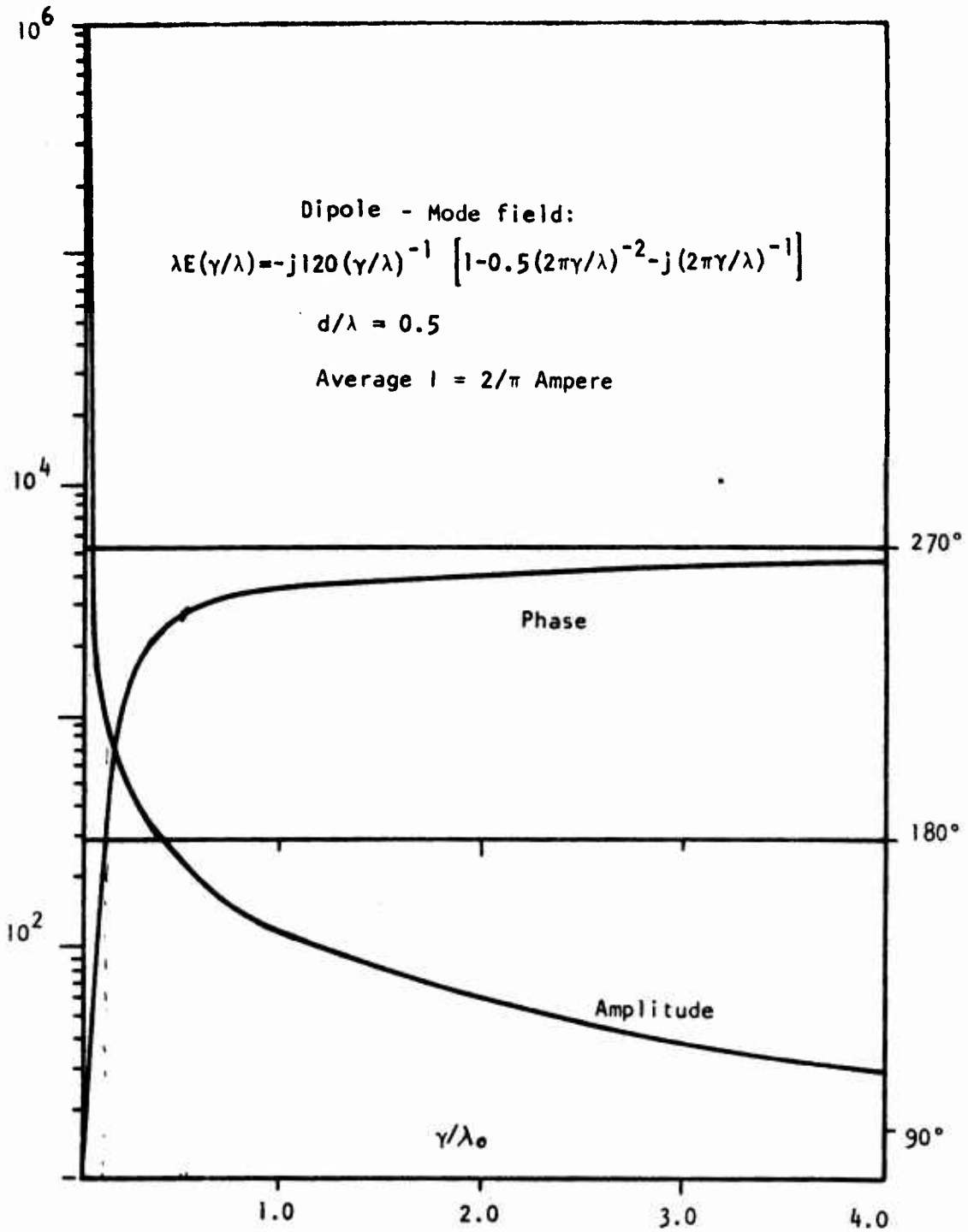


Figure I-40. Pure Dipole-Modes Spectral Density as a Function of Distance in Wavelength λ

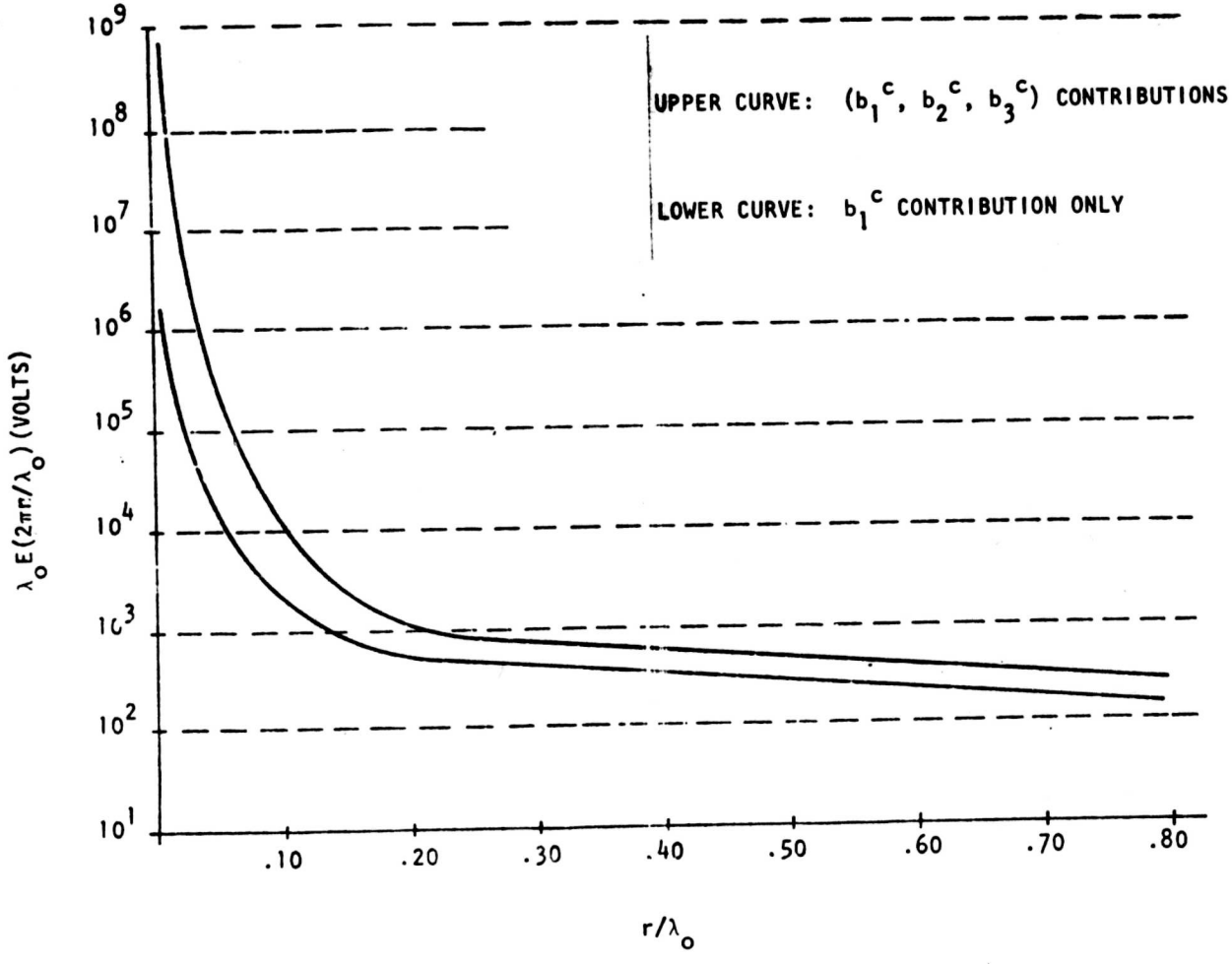
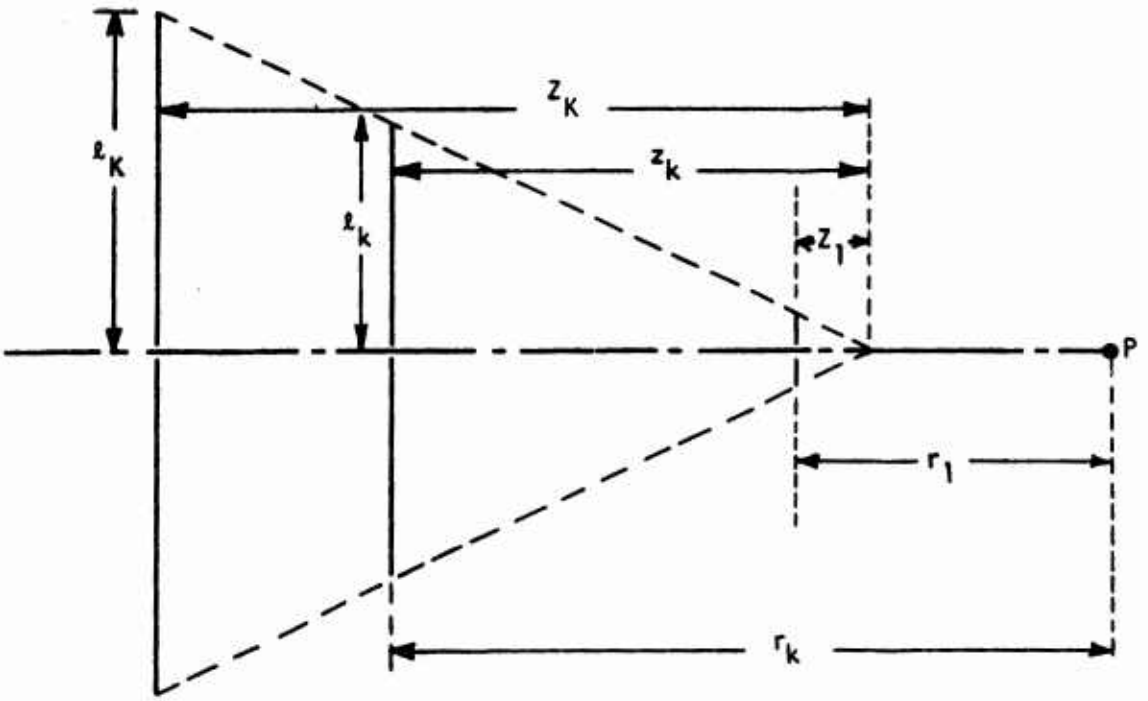


Figure I-41. Spectral Amplitudes of Eq. (I-9)



$$\tau = \frac{\ell_{k-1}}{\ell_k} = \frac{z_{k-1}}{3k}$$

$$r_k = r_{k-1} + (z_k - z_{k-1})$$

Figure 1-42. Linear Log-Periodic Dipole Array Model

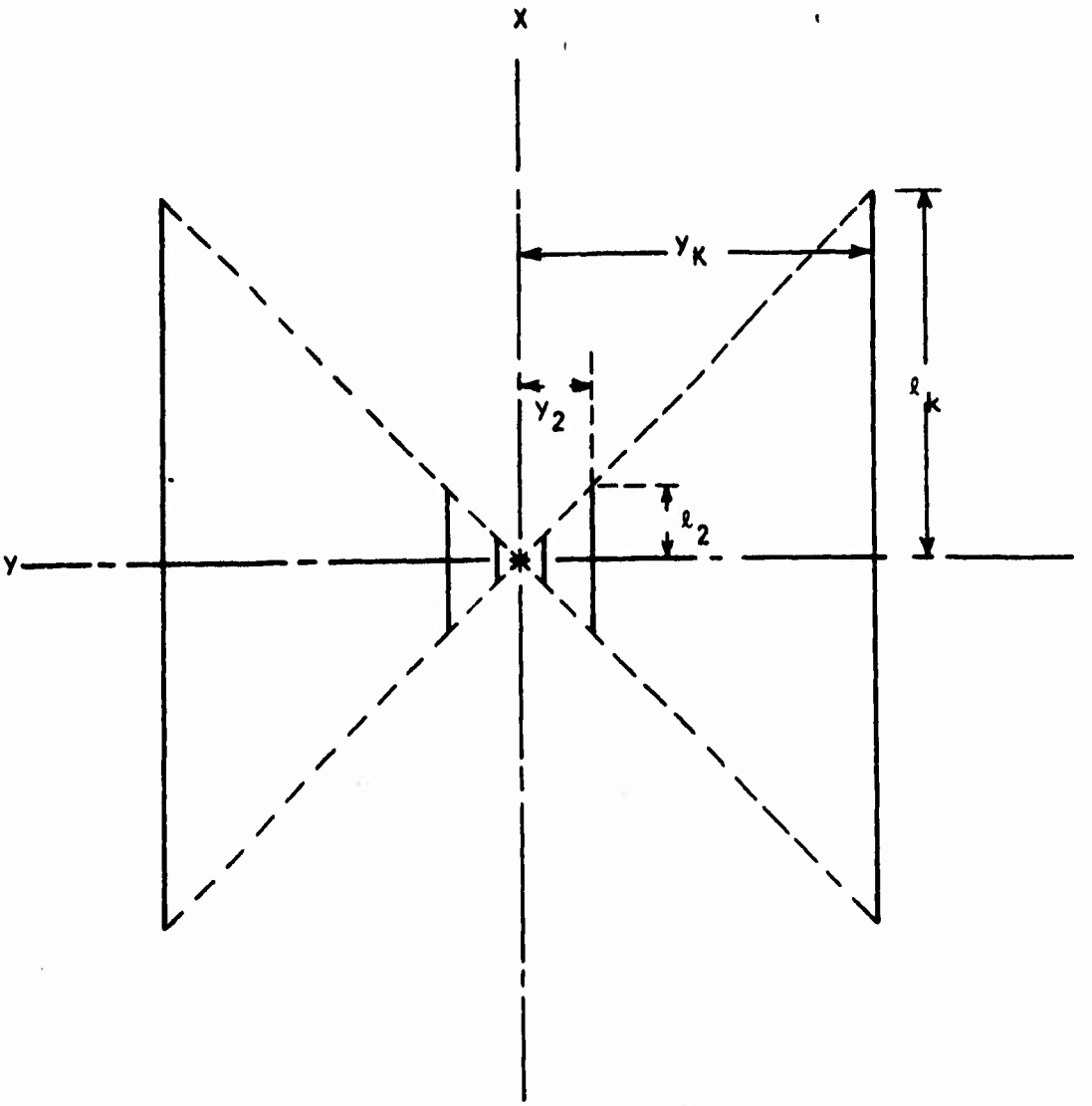
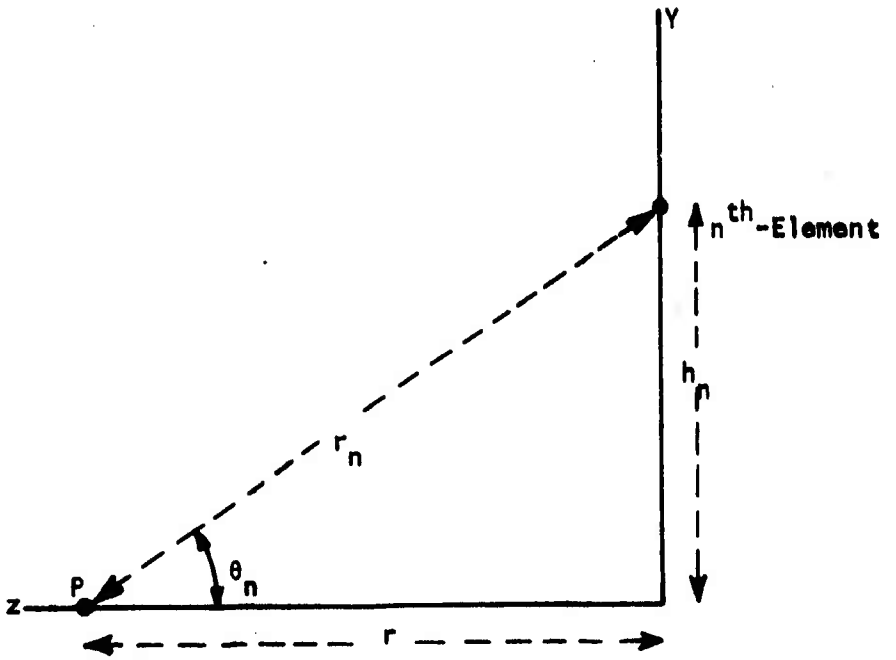


Figure I-43. Linearly Polarized Planar Array with Broadside Radiation



$$r_n = (r^2 + h_n^2)^{1/2}$$

$$\cos \theta_n = r/r_n$$

Figure I-44. Coordinates of Field Point P and the nth Element

SMOOTHED SPECTRAL DISTRIBUTION OF THEORETICAL MODEL APPROXIMATING A CAVITY-BACKED SPIRAL ANTENNA WHICH COMPRESSES PULSES AT r = 1.5 cm, 3.5 cm and 100 cm

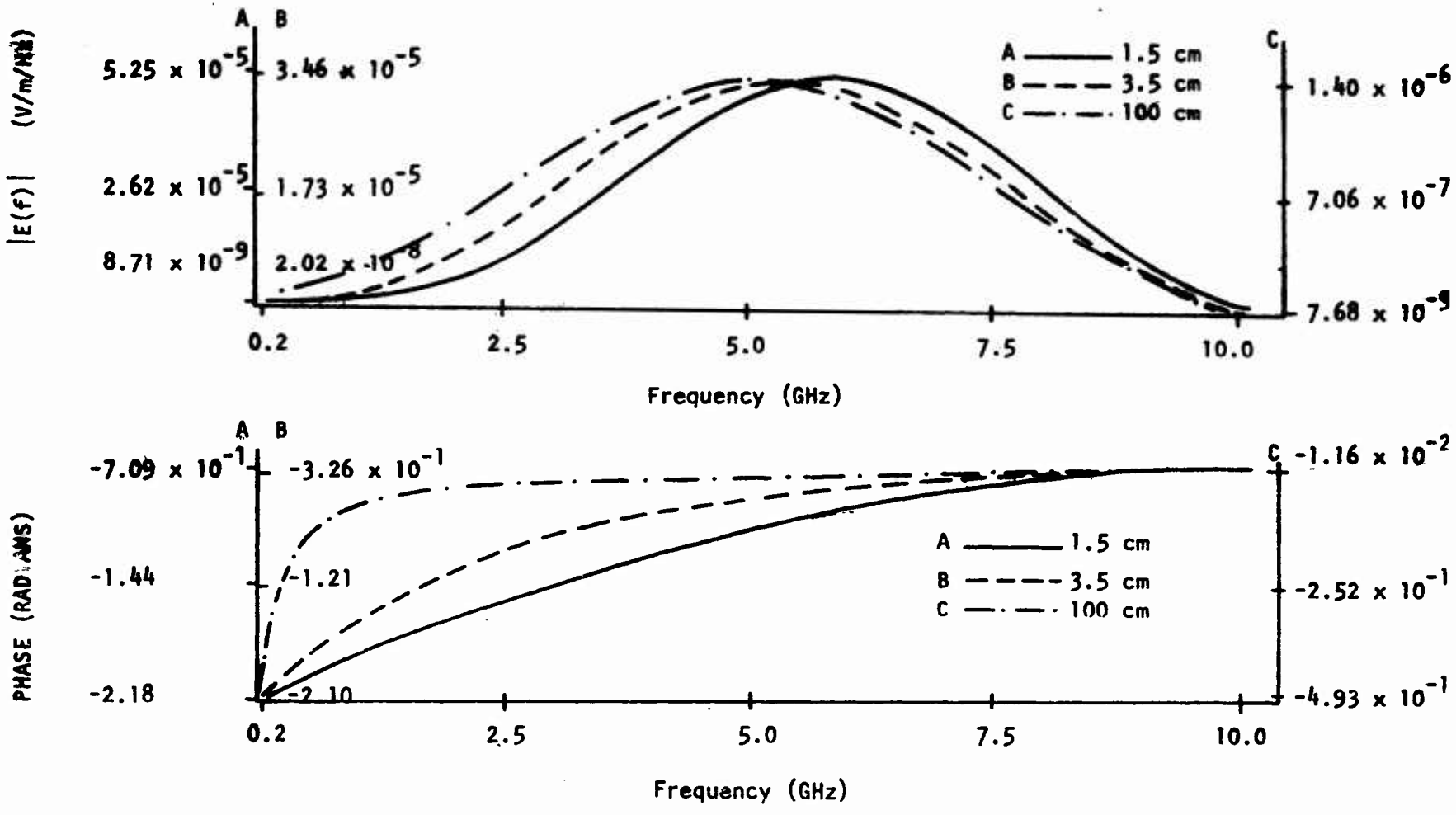


Figure I-45. Smoothed Spectral Distribution of Theoretical Model Approximating a Cavity-Backed Spiral Antenna Which Compresses Pulses at r = 1.5 cm, 3.5 cm and 100 cm

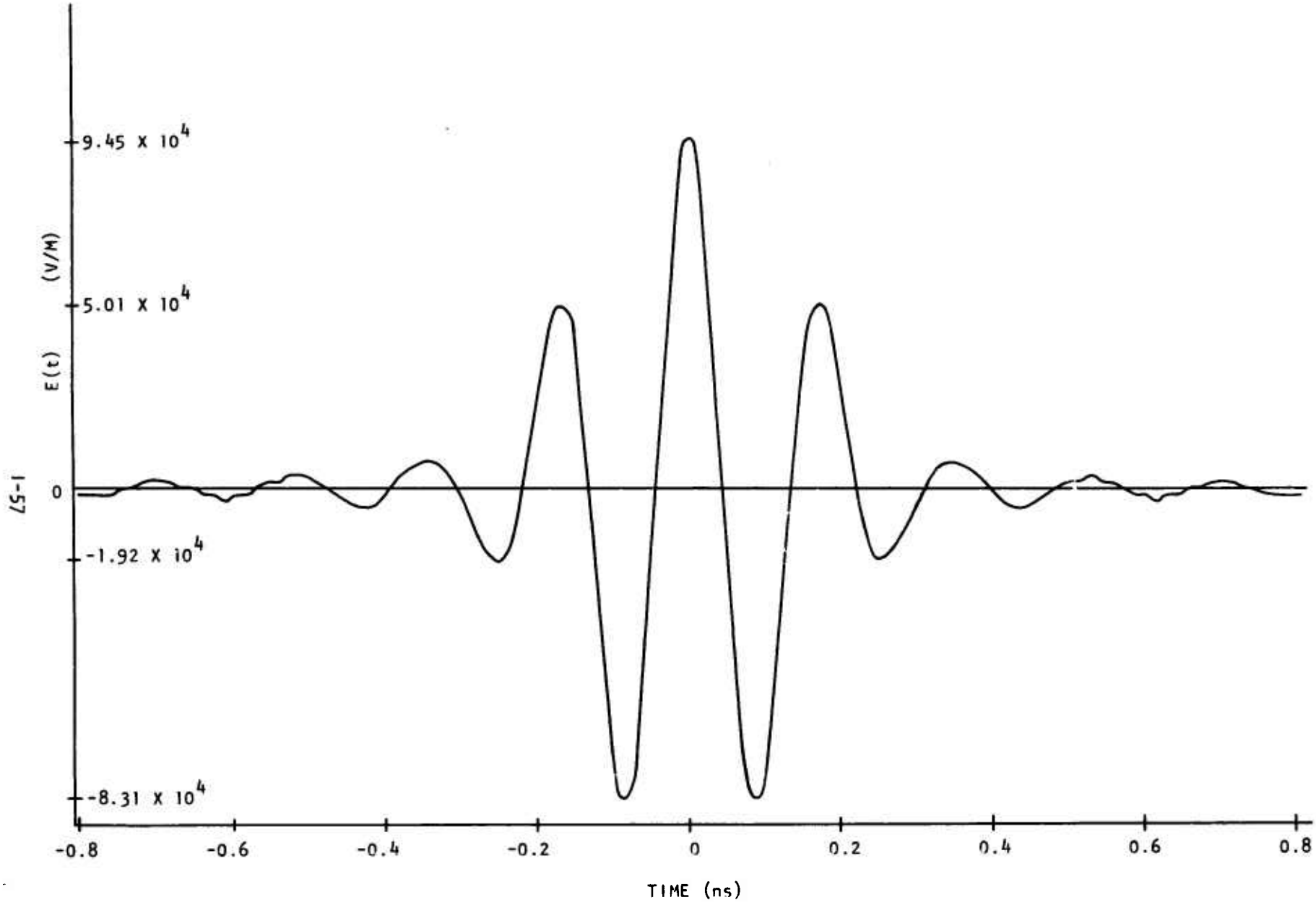


Figure I-46. Compressed Pulse at 1.5 Centimeters from Antenna Aperture on Boresight

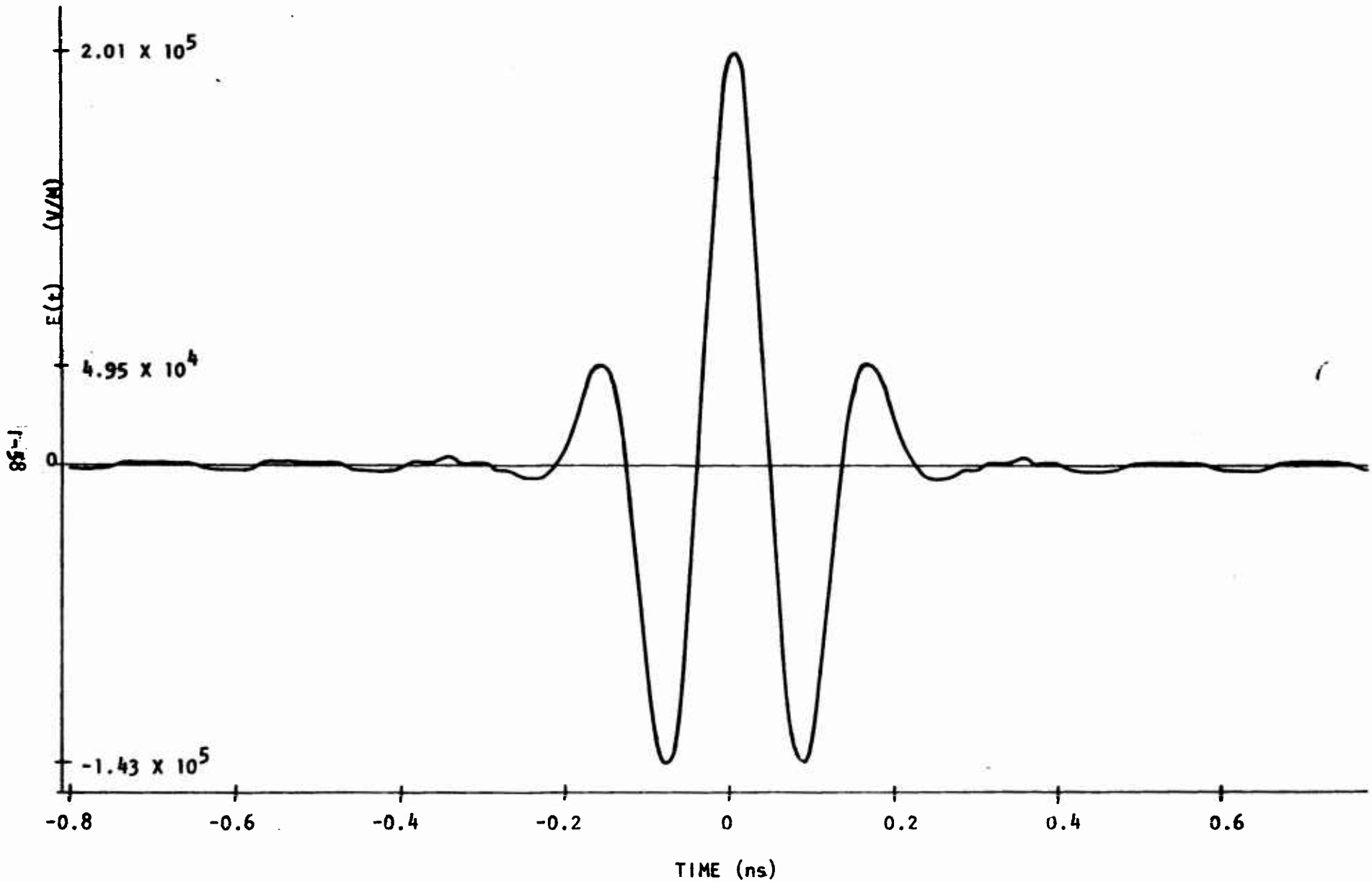


Figure I-47. Compressed Pulse at 3.0 Centimeters from Aperture Plane on Boresight

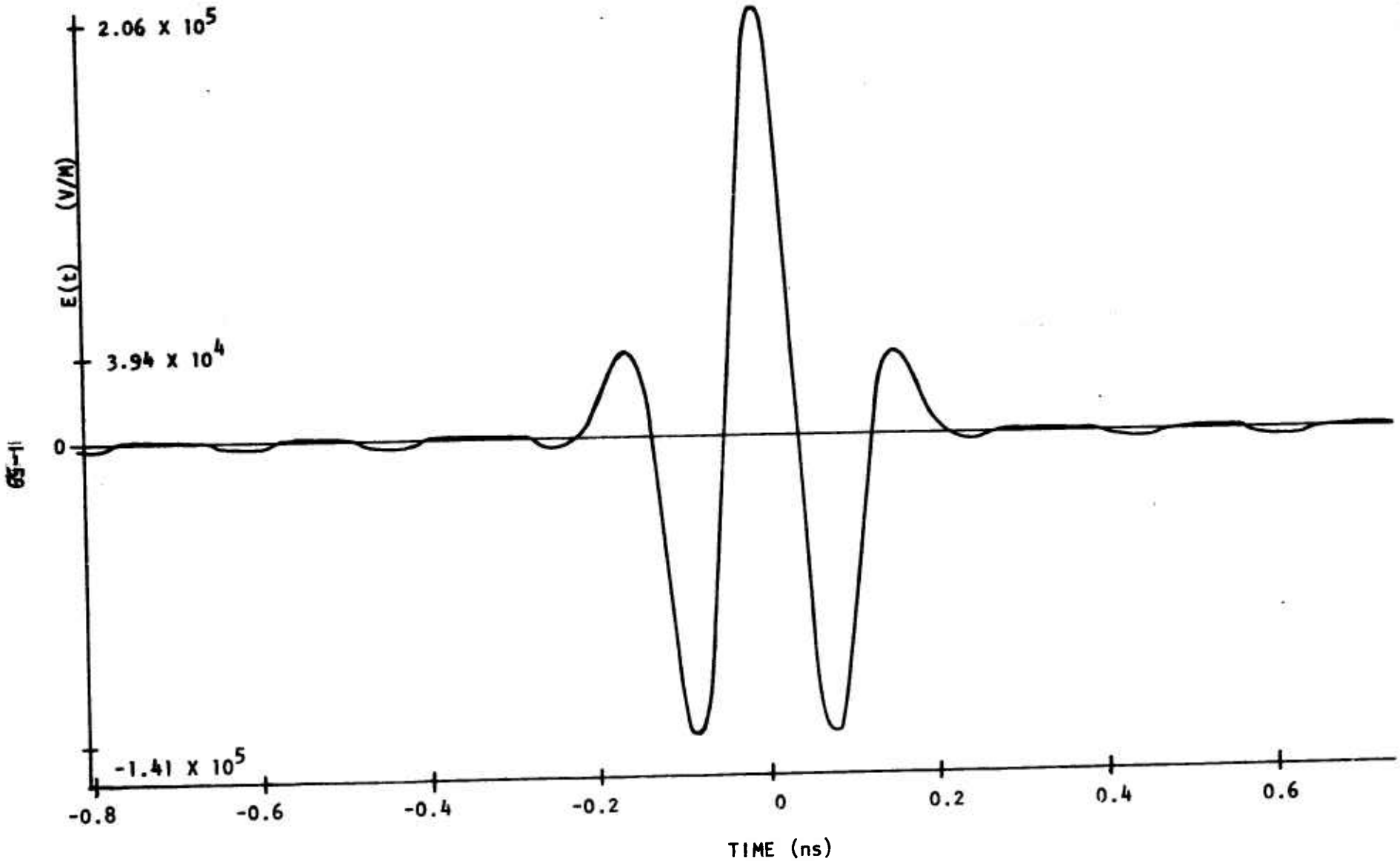


Figure I-48. Compressed Pulse at 3.5 Centimeters from Aperture Plane on Boresight

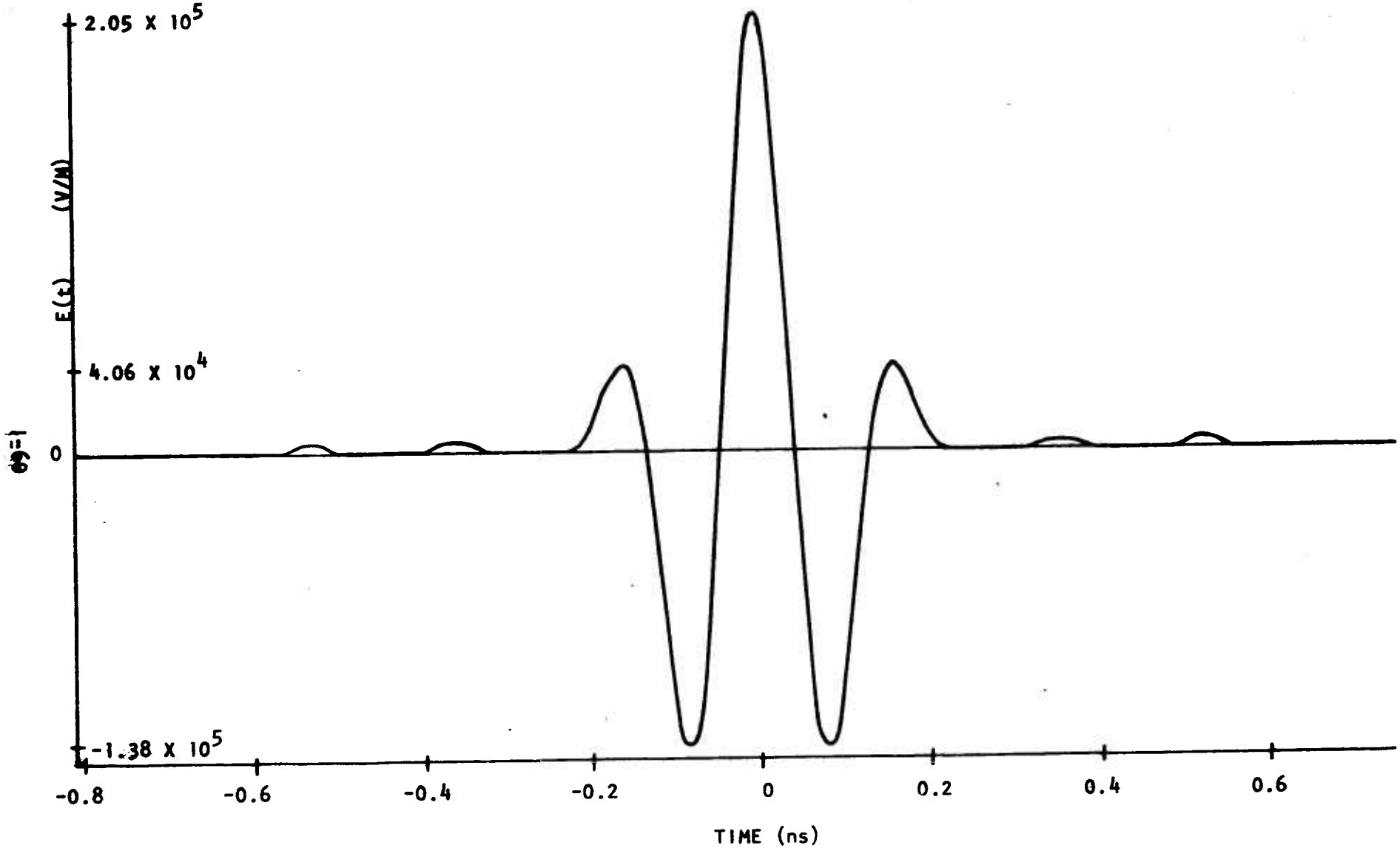


Figure I-49. Compressed Pulse at 3.75 Centimeters from Aperture Plane on Boresight

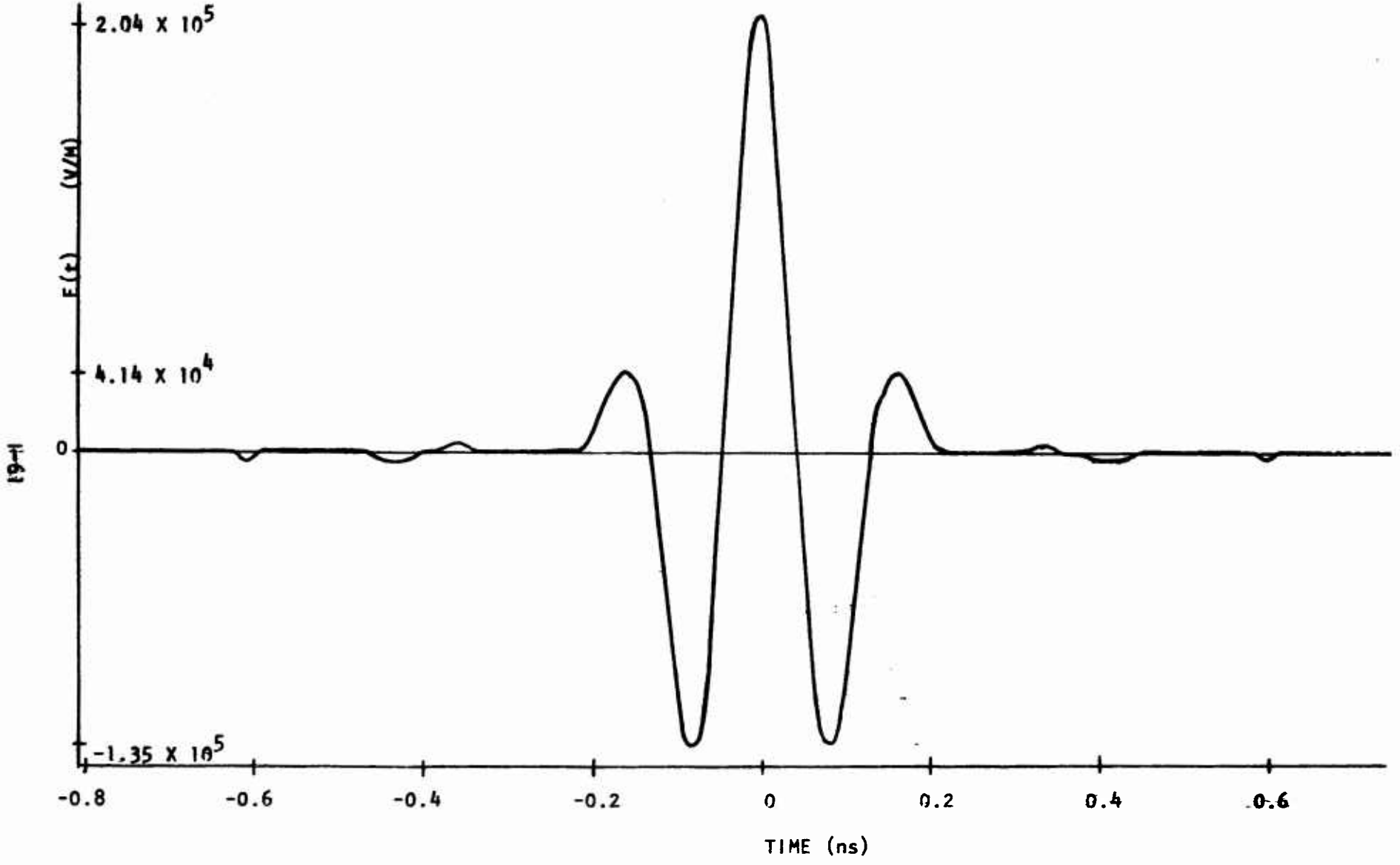


Figure I-50. Compressed Pulse at 4.0 Centimeters from Aperture Plane on Boresight

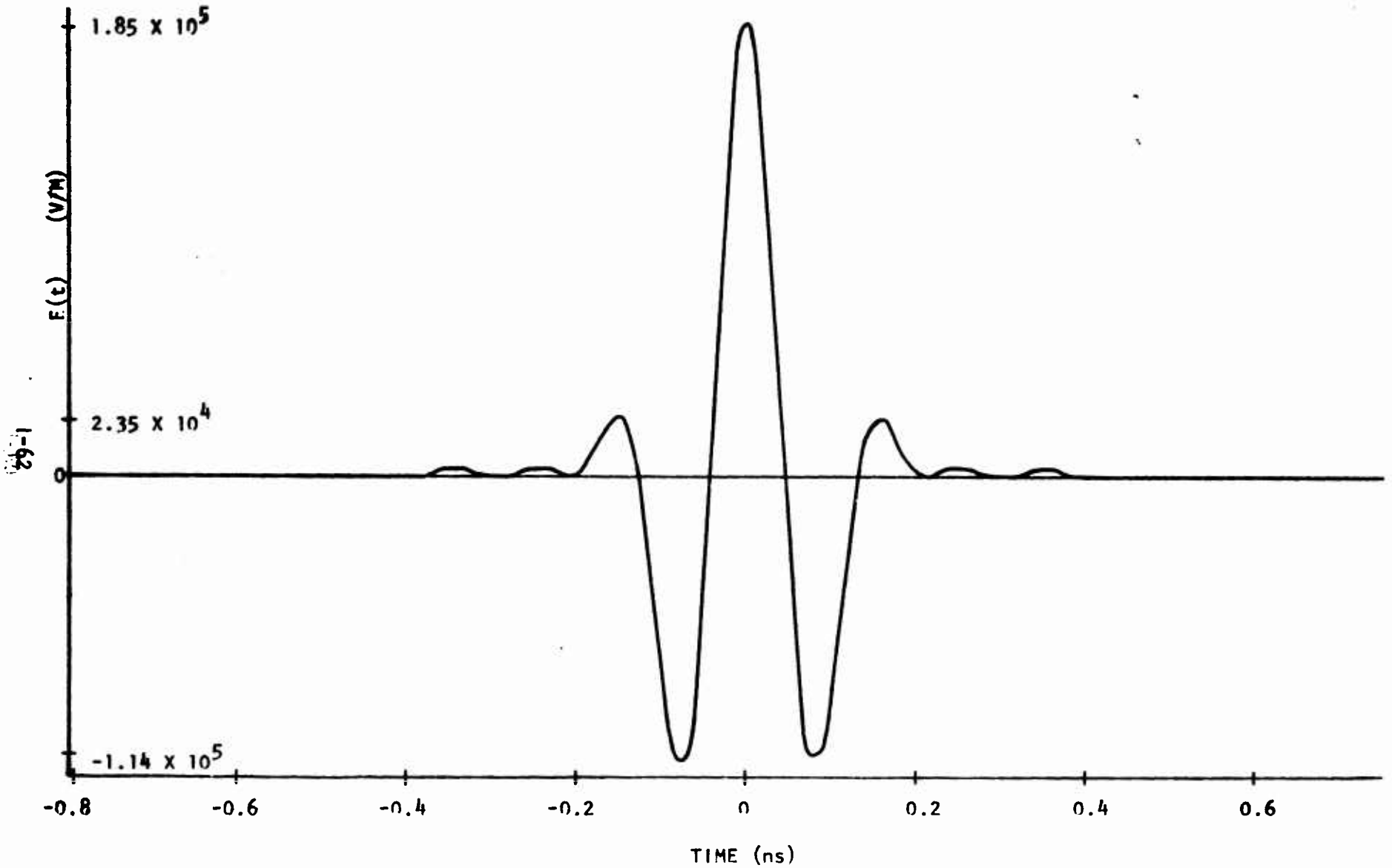


Figure I-51. Compressed Pulse at 5.5 Centimeters from Aperture Plane on Boresight

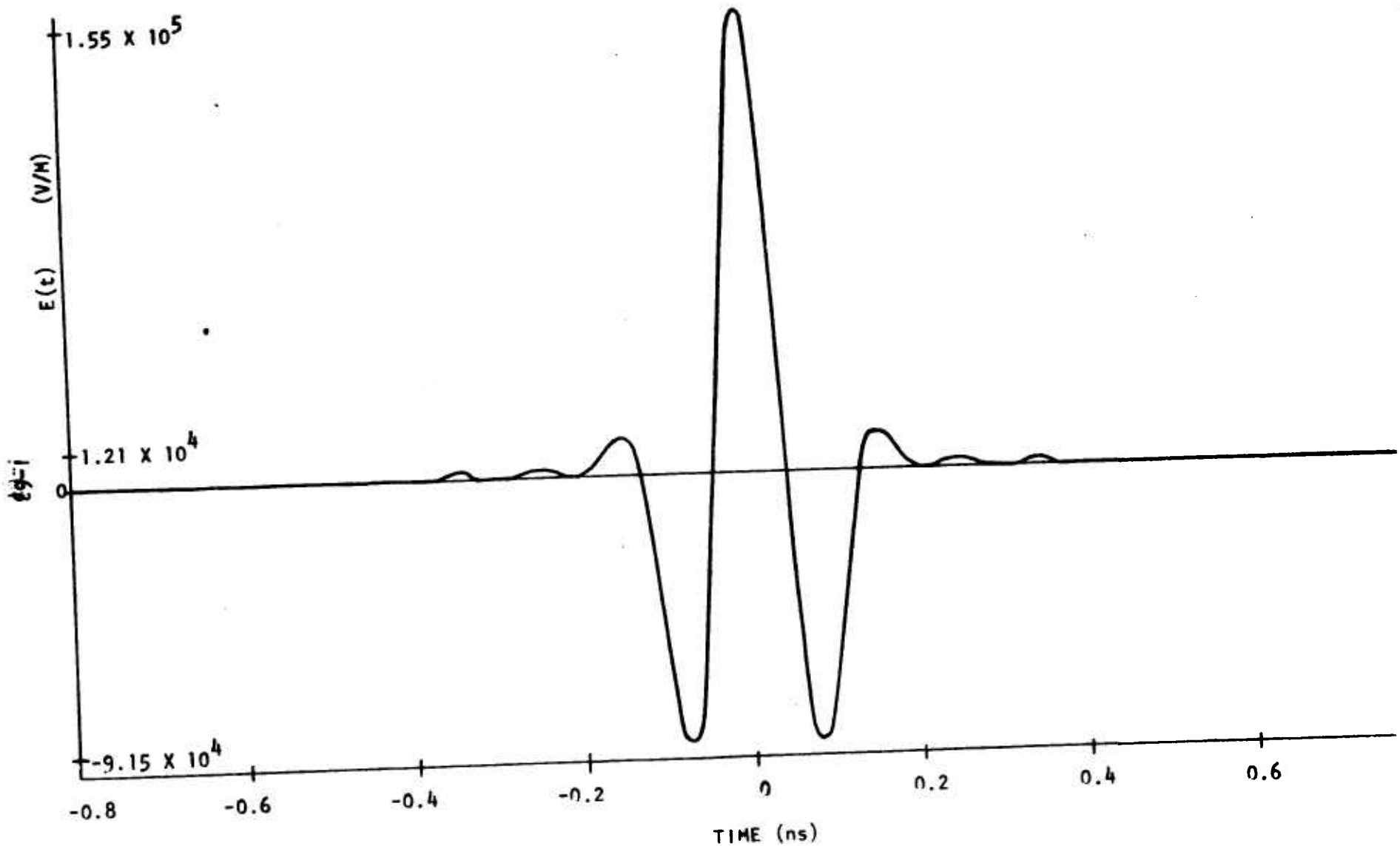


Figure 1-52. Compressed Pulse at 7.5 Centimeters from Aperture Plane on Boresight

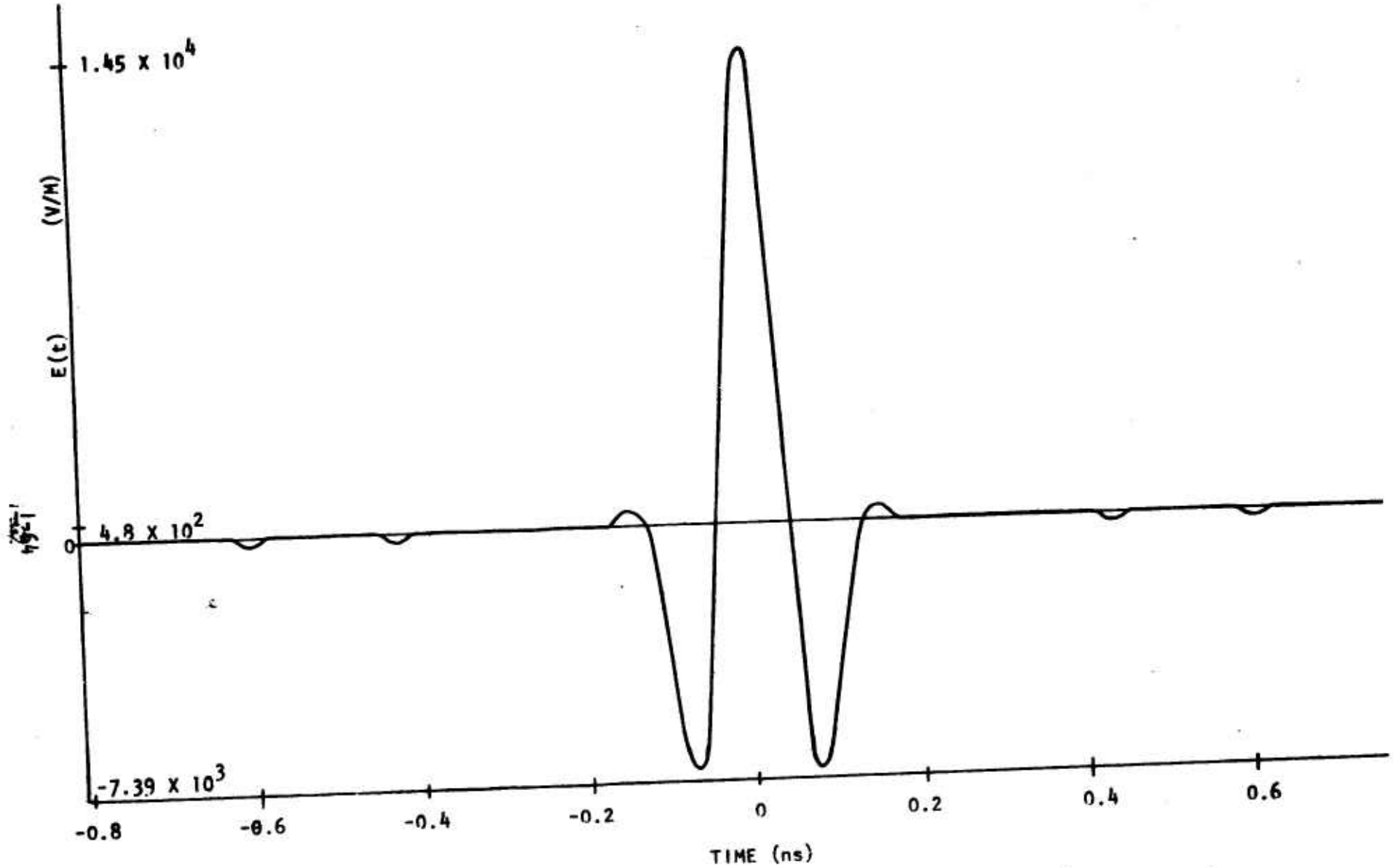


Figure I-53. Compressed Pulse at 1.0 Meter from Aperture Plane on Boresight

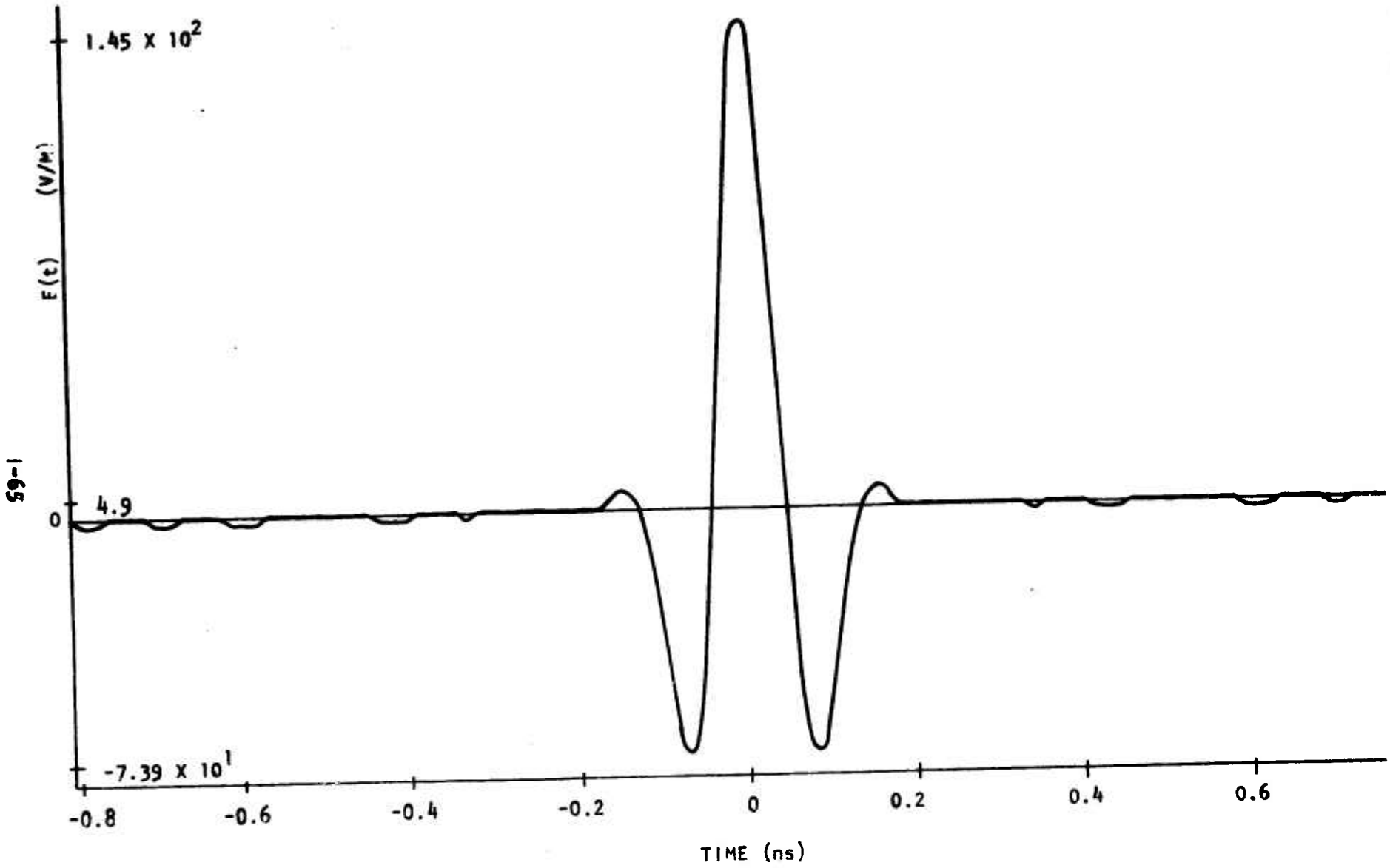


Figure I-54. Compressed Pulse at 100 Meters from Aperture Plane on Boresight

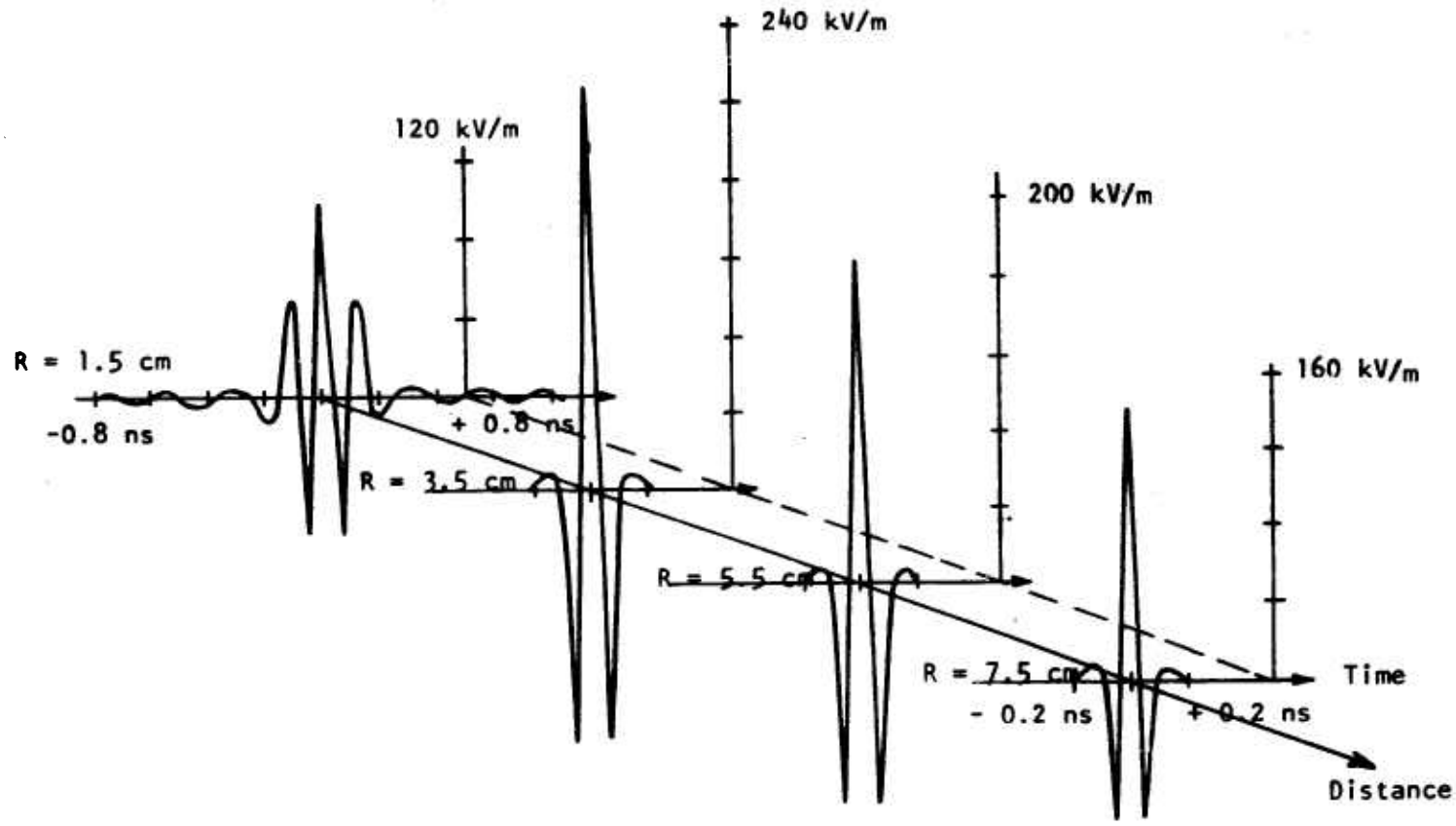


Figure I-55. Near-Field Space-Time Pulse Compression for an Antenna Model Possessing a Transverse Time Delay Characteristic

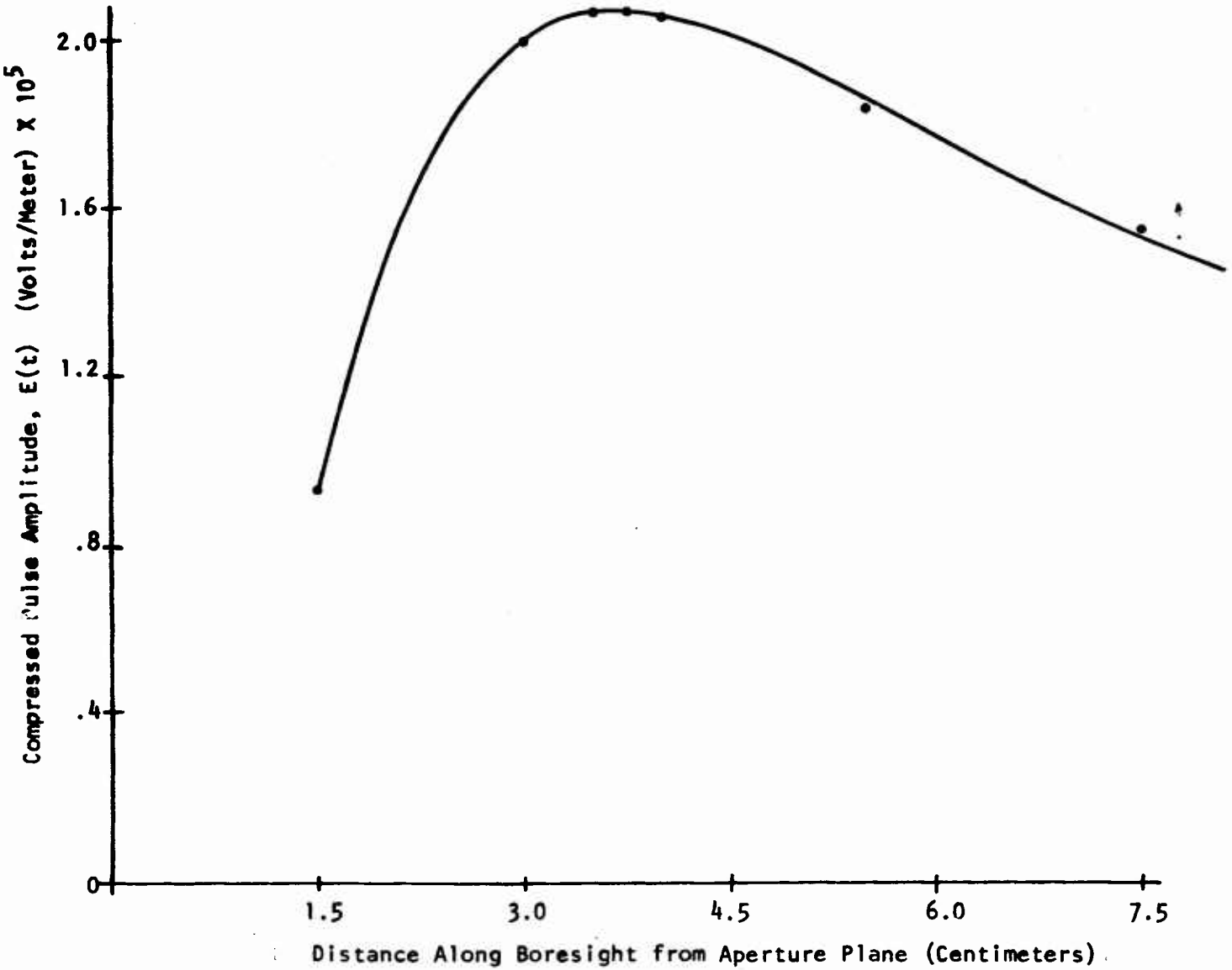


Figure 1-56. An Advantage of Pulse Compression Antennas Possessing Transverse Time Delay Characteristics, Such as the Cavity-Backed Spiral, is that Peak Pulse Amplitud Occurs at Distances Away from the Aperture Plane

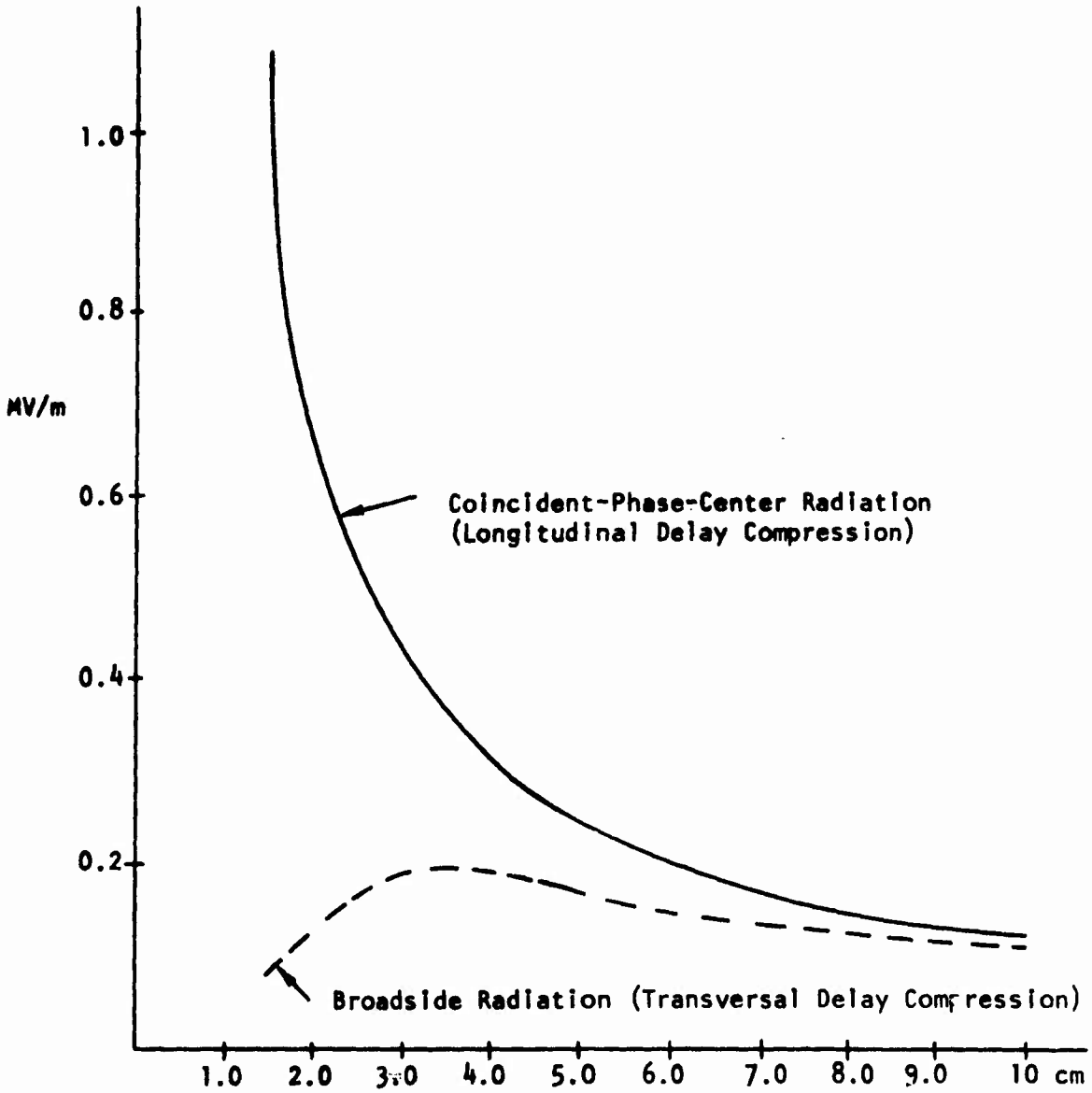


Figure I-57. Compressed Pulse Peaks as Functions of Radiation Distance r(cm)

APPENDIX J

AIR-BREAKDOWN BY COMPRESSED PULSES AND BREAKDOWN LAG TIME

1. INTRODUCTION

It has been recognized that compressed pulses may possess field intensities above the dielectric strength of the surrounding medium. Such a situation would be expected to lead to quenching of the compressed pulse. However, as will be seen, when an overvoltage condition is created, this does not cause instantaneous breakdown; it is possible to exceed the breakdown voltages of dielectric media by several orders of magnitude because of the finite amount of time required for breakdown to occur after the overvoltage condition has been established.

2. BREAKDOWN LAG TIME

It is known[1,2] that pulse breakdown in gases involves electron avalanche processes which require a certain minimum amount of time to develop. After peak overvoltage has been established, there is a formative or delay time before breakdown commences. In general, this delay time is composed of two parts: a statistical time and a breakdown lag time. The statistical time consists of a random sequence of intervals which occur statistically. Even though electron avalanche is initiated, an arbitrary number of quenches will precede the avalanche that finally culminates in actual breakdown. Breakdown lag time is a time associated with that avalanche which does not quench. It is the time difference between the onset of avalanche and the time at which the avalanche has grown to a critical value where the growth rate has changed from exponential to a nonlinear one that is much faster. In the limit of zero statistical lag time, the total time delay between the onset of peak field strength and the commencement of breakdown would just equal the breakdown lag time.

This would therefore represent the minimum time necessary for breakdown to occur for a given overvoltage condition. It has been shown[2] that this breakdown lag time is a function of the field strength, E, the pressure, p, several other constants which characterize the type of dielectric and the various mechanisms leading to electron avalanche, and geometrical factors such as electrode shape and separation. A curve which shows electric field strength as a function of breakdown lag time in air at a pressure of one atmosphere is shown in Figure J-1. An expanded scale in Figure J-2 gives field strengths for breakdown lag times as short as 0.01 ns. Both of these curves represent averages over geometrical factors and therefore are insensitive to electrode shape and separation.

3. ALLOWABLE OVERVOLTAGE IN PULSE COMPRESSION

The interpretation of Figures J-1 and J-2 is as follows. It is recalled that pulse compression is a dynamic process. At the instant the pulse reaches maximum compression, and hence, maximum field strength, it is traveling at the speed of electromagnetic waves in air, essentially c. Assuming that the electric field strength of the compressed pulse does exceed the breakdown strength of air (approximately three megavolts/meter), the curve gives the breakdown lag time necessary before breakdown can occur. If the transit time (i.e., the time necessary for the pulse to travel a distance equal to its width divided by c) is greater than the breakdown lag time, then breakdown does not occur. Some ionization of the air molecules will take place in the unit volume in which electron avalanche is initiated, but the avalanche process itself is expected to quench if the pulse moves into an adjacent unit volume in a time faster than the breakdown lag time. For example, if the pulse has been compressed to a duration of 0.1 ns, then the largest field strength which can be radiated without causing breakdown is that which corresponds to a breakdown lag time that just equals 0.1 ns, or about 18 megavolts/meter.

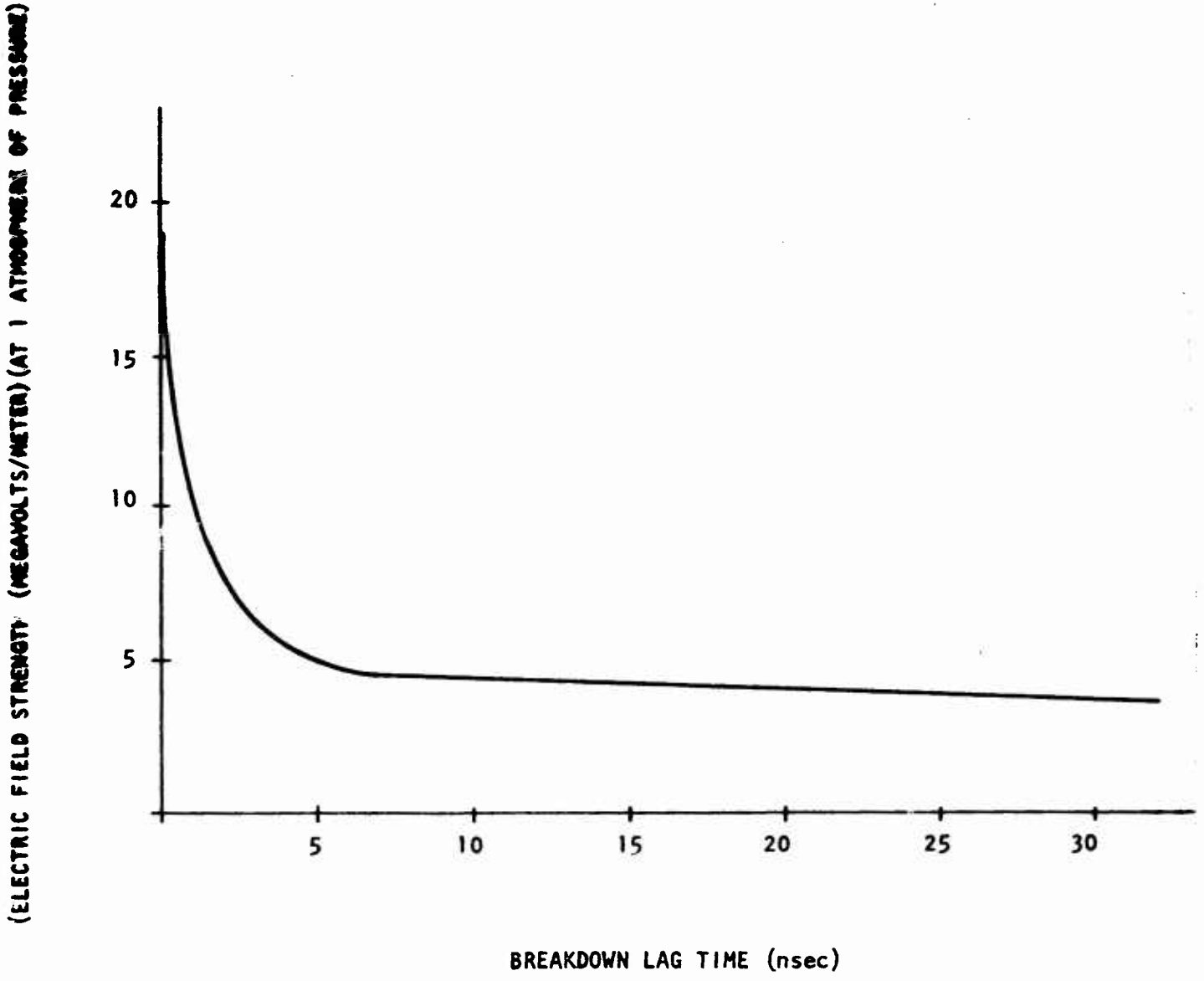


Figure J-1. When Field Strengths Exceed the Dielectric Strength of Air at a Given Pressure, a Minimum Time is Required Before Breakdown Occurs

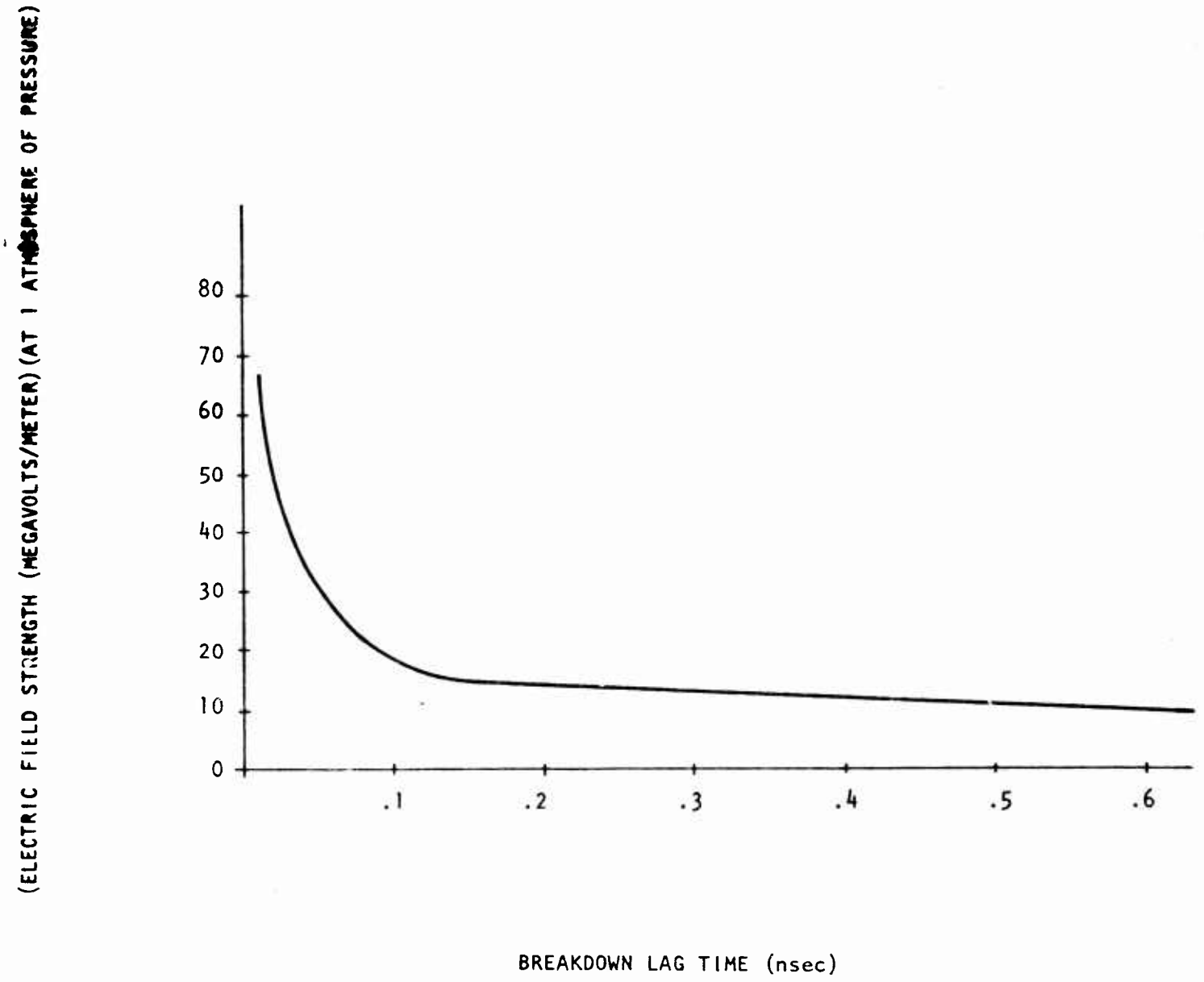


Figure J-2. Expansion of Figure J-1 Showing Breakdown Lag Times for Field Strengths in the High Megavolt/Meter Range

The conclusion to be drawn from this discussion is that even when an overvoltage condition exists as the result of pulse compression, breakdown will not occur provided the pulse can move out of the avalanche region within the breakdown lag time. It should again be noted that the breakdown lag time actually represents the worst case, or shortest possible breakdown time, since the statistical time has been ignored. Inclusion of statistical time would tend to increase the overall time necessary for breakdown to occur.

We interpret breakdown lag time to represent the maximum allowable compressed pulse duration at a given electric field strength. Table J-1 provides some data on allowable pulse durations for various field strengths above air breakdown.

TABLE J-1

MAXIMUM ALLOWED COMPRESSED PULSE DURATIONS FOR VARIOUS FIELD STRENGTHS

ELECTRIC FIELD STRENGTH (MV/M)	MAXIMUM ALLOWED COMPRESSED PULSE DURATION (ns)
49	.02
34	.04
26	.06
22	.08
18	.1
15	.2
13	.4
11	.6
9.8	1
7.6	2
6.3	3
5.5	4
5.1	5
3.8	30
3 (Air Breakdown)	∞